frontiers | Research Topics

Translational medicine in the diagnosis and treatment of cancer based on oncogenetics: From bench to bedside

Edited by
Changjing Cai, Rui Cao, Jiao Hu, Ying Han and Changsheng Xing

Published in
Frontiers in Genetics

ISSN 1664-8714
ISBN 978-2-8325-4012-1
DOI 10.3389/978-2-8325-4012-1

About Frontiers

Frontiers is more than just an open access publisher of scholarly articles: it is a pioneering approach to the world of academia, radically improving the way scholarly research is managed. The grand vision of Frontiers is a world where all people have an equal opportunity to seek, share and generate knowledge. Frontiers provides immediate and permanent online open access to all its publications, but this alone is not enough to realize our grand goals.

Frontiers journal series

The Frontiers journal series is a multi-tier and interdisciplinary set of open-access, online journals, promising a paradigm shift from the current review, selection and dissemination processes in academic publishing. All Frontiers journals are driven by researchers for researchers; therefore, they constitute a service to the scholarly community. At the same time, the *Frontiers journal series* operates on a revolutionary invention, the tiered publishing system, initially addressing specific communities of scholars, and gradually climbing up to broader public understanding, thus serving the interests of the lay society, too.

Dedication to quality

Each Frontiers article is a landmark of the highest quality, thanks to genuinely collaborative interactions between authors and review editors, who include some of the world's best academicians. Research must be certified by peers before entering a stream of knowledge that may eventually reach the public - and shape society; therefore, Frontiers only applies the most rigorous and unbiased reviews. Frontiers revolutionizes research publishing by freely delivering the most outstanding research, evaluated with no bias from both the academic and social point of view. By applying the most advanced information technologies, Frontiers is catapulting scholarly publishing into a new generation.

What are Frontiers Research Topics?

Frontiers Research Topics are very popular trademarks of the *Frontiers journals series*: they are collections of at least ten articles, all centered on a particular subject. With their unique mix of varied contributions from Original Research to Review Articles, Frontiers Research Topics unify the most influential researchers, the latest key findings and historical advances in a hot research area.

Find out more on how to host your own Frontiers Research Topic or contribute to one as an author by contacting the Frontiers editorial office: frontiersin.org/about/contact

Translational medicine in the diagnosis and treatment of cancer based on oncogenetics: From bench to bedside

Topic editors

Changjing Cai — Central South University, China
Rui Cao — Capital Medical University, China
Jiao Hu — Central South University, China
Ying Han — Central South University, China
Changsheng Xing — University of Southern California, United States

Citation

Cai, C., Cao, R., Hu, J., Han, Y., Xing, C., eds. (2023). *Translational medicine in the diagnosis and treatment of cancer based on oncogenetics: From bench to bedside*. Lausanne: Frontiers Media SA. doi: 10.3389/978-2-8325-4012-1

Table of contents

frontiers | Frontiers in Genetics

TYPE Editorial
PUBLISHED 13 November 2023
DOI 10.3389/fgene.2023.1210094

OPEN ACCESS

EDITED AND REVIEWED BY
Anton A. Buzdin,
European Organisation for Research and Treatment of Cancer, Belgium

*CORRESPONDENCE
Changjing Cai,
vccj07@csu.edu.cn
Jiao Hu,
hujiao@csu.edu.cn
Changsheng Xing,
cxing999@usc.edu

RECEIVED 21 April 2023
ACCEPTED 02 November 2023
PUBLISHED 13 November 2023

CITATION
Cao R, Han Y, Cai C, Hu J and Xing C (2023), Editorial: Translational medicine in the diagnosis and treatment of cancer based on oncogenetics: from bench to bedside.
Front. Genet. 14:1210094.
doi: 10.3389/fgene.2023.1210094

Editorial: Translational medicine in the diagnosis and treatment of cancer based on oncogenetics: from bench to bedside

Rui Cao[1], Ying Han[2], Changjing Cai[3]*, Jiao Hu[4]* and Changsheng Xing[5]*

[1]Department of Urology, Beijing Friendship Hospital, Capital Medical University, Beijing, China, [2]Department of Oncology, Xiangya Hospital, Central South University, Changsha, China, [3]National Clinical Research Center for Geriatric Disorders, Xiangya Hospital, Central South University, Changsha, China, [4]Department of Urology, Xiangya Hospital, Xiangya School of Medicine, Central South University, Changsha, China, [5]Department of Medicine, Keck School of Medicine, University of Southern California, Los Angeles, CA, United States

KEYWORDS

translation medicine, bench to bedside, diagnosis, treatments, cancer

Editorial on the Research Topic
Translational medicine in the diagnosis and treatment of cancer based on oncogenetics: from bench to bedside

Cancer is a major public health problem worldwide. Clarifying cancer etiology and pathogenesis is of great significance to its prevention, diagnosis, and treatment. The concept of translational medicine, which was first mentioned as "bench to bedside" (B to B) pattern by Choi (1992), can be a useful method for cancer-related studies. Thus, in this Research Topic, we aim to highlight the emerging role of onco-genetics in cancer and discuss the potential challenges of cancer diagnoses and treatments, from the bench to the bedside.

In this Research Topic, Xiao et al. demonstrated the involvement of HOXC-4 in pan-cancer. They investigated the relationship between the expression level of HOXC-4 and prognosis, and additionally, the correlation between HOXC4 and clinical outcome of immunotherapy, together with anti-cancer drug sensitivity. This research provided a new potential biomarker in clinical process and shed new light on the anti-tumor immunotherapy (Xiao et al.).

Furthermore, the research of Cheng et al. indicated the advanced lung cancer inflammation index (ALI), which was a powerful prognostic and predictive biomarker in multiple myeloma (MM) patients and maintained the function of predicting the chemotherapy efficacy in MM patients receiving induction therapy. AMI was a promising biomarker in predicting the clinical outcome of immune checkpoint inhibitor efficacy in advanced non-small-cell lung cancer (Mountzios et al., 2021). In colorectal cancer patients, the preoperative ALI acted as a role in predicting the compositions and recurrence after curative resection (Horino et al., 2022). ALI also takes part in predicting the elderly patients with heart failure, which serves as an effective nutritional biomarker to predict the patient with better prognosis with higher ALI (Yuan et al., 2022). ALI exerted prognosis value in various kinds of cancers and immune therapy responses, together with heart disease.

In the future, ALI may provide new therapy for cancer or cardiovascular diseases in the aspect of nutrition.

Neoadjuvant chemotherapy (NAC) is the standard treatment for muscle-invasive bladder cancer (MIBC), while the response of the NAC is still unclear for part of the MIBC patients (Hermans et al., 2018). The research by Li et al. constructed a signature to predict the prognosis of the patient and the clinical outcome and treatment of NAC with the help of bioinformatic analysis. The five-gene-based risk score predicted the NAC response with high accuracy, which might provide individualized treatment for each of different stage or pathological types of patients with more dawn.

RNA modification writer is widespread on all nucleotides and the modification is at the RNA level (Chen et al., 2021a). RNA modifying proteins may serve as a series of antitumor targets for drug discovery. The process of tumor formation also includes epi-transcriptome, which has been a hot Research Topic recently (He et al., 2019). The research of Cheng and Yi established a new signature which was associated with the distinct RNA modification clusters to test and verify the relationship between the signature and the related biological process, which was related to the tumor signaling pathway, tumor microenvironment, and clinical outcome. This research has provided new insight into the early diagnoses and treatment of cancer.

Ferroptosis is an advanced type of programmed cell death and is intensively connected to maintaining homeostasis and the development of detrimental diseases, especially tumorigenesis (Chen et al., 2021b). In recent years, researchers have found the role of lipid and mitochondria metabolism regulates ferroptosis in head and neck cancer drug-resistant (Wu et al., 2020). In the research of our Research Topic, Wei et al.conclude 47 genes related to ferroptosis and obtain the relation to the prognosis as well as immune signatures of head and neck squamous cancer (HNSCC) patients. The authors also assessed their conclusion in different clinical cohorts constructed by the FPRS scoring system. Thus, it provides a new prediction target and a therapeutic implication in clinical practice. Meanwhile, Yao et al. found that another cell death type, cuproptosis, has a close relationship with the prognosis of kidney renal clear cell carcinoma.

Interferon-γ (IFN-γ) plays a critical role in signaling pathway alterations in cancers (Jorgovanovic et al., 2020). At present, researchers have reported the inhibition of ER stress obviously prevents IFN-γ-triggered apoptosis, causing IFN-γ-mediated anticancer responses in lung cancers (Fang et al., 2021). As for Deng et al. research, an IFN-γ-related signature was found for its remarkable roles in the regulation of tumor progression, immune response, mutation, and tumor microenvironment in bladder cancer. The enhanced understanding of the IFN-γ-related signature would be expected to apply in clinic in the near future and be validated in more clinical cohorts.

Alkaline ceramidase 2 (ACER2) is an enzyme located in the Golgi complex participating in sphingolipid metabolizing, which is upregulated in most types of cancer (Xu et al., 2018). Liu et al. revealed that the expression level of ACER2 was correlated with bladder cancer in various aspects. Tumor microenvironment and immune checkpoint were hot research topics in cancer that correlate with ACER2 expression level significantly. Furthermore, ACER2 predicted the molecular subtypes to further estimate the immunotherapy response obliquely. Additionally, the ACER2 also obtained the ability to predict the clinical outcome of chemotherapy and immune therapy directly and accurately. The study also revealed that the ACER2 is significantly upregulated in other types of cancers, which may provide new insight into cancer treatment or new cancer biomarkers in the future.

In bone vascular endothelial cells, the immunolabeling of PECAM1 was revealed to show the vascular network (Wang et al., 2019). However, the tumor premetastatic environment can be formed before dissemination due to the tumor-derived factors released from primary tumors, including several growth factors associated with vascular networks (Wang et al., 2020). Thus we should attach importance to PECAM1 and bone metastases. In the research of Liang et al., they analyze the association and find that PECAM1 could be recognized as the potential biomarker that signifies the diagnosis and treatment of bone metastases and verified in bone metastatic tumor tissues. But there is also a limitation because the tissues in need were difficult to harvest. Thus, the authors believed the enlargement of the sample size was necessary and would continue collecting as many tissue samples as possible.

The PTPN family genes are promising prognostic biomarkers and therapeutic targets for various cancers. But the distinct roles of the PTPN family in acute myeloid leukemia (AML) have not yet been explored entirely. Liu et al. performed a comprehensive analysis which focused on the PTPN family expression profile and prognostic significance in AML. They screened out several differentially expressed PTPN family genes in AML. Especially, PTPN6 was one of these members and may be used as an AML diagnostic and prognostic marker (Liu et al.).

ZNF281 (zinc finger protein 281) plays critical roles in regulating embryonic stem cell (ESC) differentiation and maintaining cellular stemness. Hou et al. performed a pan-cancer analysis and indicated that ZNF281 was overexpressed in various cancers and related to shorter survival. Then, they correlated the ZNF281 with immune characters in tumor microenvironment. Overall, they provided new insights into the dual role of ZNF281 and approved that it was a potential biomarker for regeneration and tumor prognosis. Similarly, Guo et al. performed a pan-cancer analysis focused on Methyl methanesulfonate-sensitivity protein 22-like (MMS22L). They revealed the essential role of MMS22L as a tumor-regulating gene in human cancers while further emphasizing its feasibility as a novel molecular marker in hepatocellular carcinoma. Their findings provide an essential reference for the study of MMS22L in tumors. Meanwhile, Bao et al. found that overexpression of SPAG6 and low expression of NM23 are negatively related to the pathological grade, metastasis, and enneking stage and prognosis of osteosarcoma patients. This suggested that SPAG6 and NM23 should be considered candidate prognostic biomarkers for patients with osteosarcoma. Tang et al. confirmed FN1 is the potential novel biomarker for predicting poor prognosis and radio-resistance in HNSCC patients. Overexpression of FN1 plays an important role in the tumorigenesis, prognosis, and radio-resistance of HNSCC.

Taking advantage of novel computational approaches, publicly available datasets can be utilized to provide new scientific

hypotheses. In this Research Topic, Ma and Yu identified the ADAM family as novel pan-cancer biomarkers for patient prognosis and potential clinical responses, using bioinformatics analyses and experimental approaches. The authors comprehensively analyzed the differential expression levels of ADAMs in multiple types of cancers, and explored the correlations between ADAMs and tumor microenvironment, stemness, immune subtype, and sensitivities to chemotherapy and immunotherapy. Since cancer immunotherapy shows impressive efficacy but limited responses in majority of cancer patients, the identification of new therapeutic targets will surely benefit the therapeutic decision-making and prediction of clinical outcomes.

In conclusion, it is our great honor to successfully recruit and attract numerous researchers to this Research Topic, who have contributed plenty of advanced, fascinating, and important works. However, limited by the present situation, we can only publish part of these articles which we believe are more applicable to our Research Topic. We believe with the progression of "B to B" studies, cancer treatments will be enormously improved, and eventually, future cancer patients will benefit from these research works.

Author contributions

RC, CC, CX, and JH wrote the article. YH and CX edited and revised the manuscript. All authors contributed to the article and approved the submitted version.

Conflict of interest

The authors declare that the research was conducted in the absence of any commercial or financial relationships that could be construed as a potential conflict of interest.

Publisher's note

References

Chen, H., Yao, J., Bao, R., Dong, Y., Zhang, T., Du, Y., et al. (2021a). Cross-talk of four types of RNA modification writers defines tumor microenvironment and pharmacogenomic landscape in colorectal cancer. *Mol. Cancer* 20, 29. doi:10.1186/s12943-021-01322-w

Chen, X., Kang, R., Kroemer, G., and Tang, D. (2021b). Broadening horizons: the role of ferroptosis in cancer. *Nat. Rev. Clin. Oncol.* 18, 280–296. doi:10.1038/s41571-020-00462-0

Choi, D. W. (1992). Bench to bedside: the glutamate connection. *Science* 258, 241–243. doi:10.1126/science.1357748

Fang, C., Weng, T., Hu, S., Yuan, Z., Xiong, H., Huang, B., et al. (2021). IFN-γ-induced ER stress impairs autophagy and triggers apoptosis in lung cancer cells. *Oncoimmunology* 10, 1962591. doi:10.1080/2162402X.2021.1962591

He, L., Li, H., Wu, A., Peng, Y., Shu, G., and Yin, G. (2019). Functions of N6-methyladenosine and its role in cancer. *Mol. Cancer* 18, 176. doi:10.1186/s12943-019-1109-9

Hermans, T. J. N., Voskuilen, C. S., Van Der Heijden, M. S., Schmitz-Dräger, B. J., Kassouf, W., Seiler, R., et al. (2018). Neoadjuvant treatment for muscle-invasive bladder cancer: the past, the present, and the future. *Urol. Oncol.* 36, 413–422. doi:10.1016/j.urolonc.2017.10.014

Horino, T., Tokunaga, R., Miyamoto, Y., Hiyoshi, Y., Akiyama, T., Daitoku, N., et al. (2022). The advanced lung cancer inflammation index is a novel independent prognosticator in colorectal cancer patients after curative resection. *Ann. Gastroenterol. Surg.* 6, 83–91. doi:10.1002/ags3.12499

Jorgovanovic, D., Song, M., Wang, L., and Zhang, Y. (2020). Roles of IFN-γ in tumor progression and regression: a review. *Biomark. Res.* 8, 49. doi:10.1186/s40364-020-00228-x

Mountzios, G., Samantas, E., Senghas, K., Zervas, E., Krisam, J., Samitas, K., et al. (2021). Association of the advanced lung cancer inflammation index (ALI) with immune checkpoint inhibitor efficacy in patients with advanced non-small-cell lung cancer. *ESMO Open* 6, 100254. doi:10.1016/j.esmoop.2021.100254

Wang, Q., Liu, K., Yang, L., Wang, H., and Yang, J. (2019). BoneClear: whole-tissue immunolabeling of the intact mouse bones for 3D imaging of neural anatomy and pathology. *Cell Res.* 29, 870–872. doi:10.1038/s41422-019-0217-9

Wang, M., Xia, F., Wei, Y., and Wei, X. (2020). Molecular mechanisms and clinical management of cancer bone metastasis. *Bone Res.* 8, 30. doi:10.1038/s41413-020-00105-1

Wu, Y., Yu, C., Luo, M., Cen, C., Qiu, J., Zhang, S., et al. (2020). Ferroptosis in cancer treatment: another way to rome. *Front. Oncol.* 10, 571127. doi:10.3389/fonc.2020.571127

Xu, R., Garcia-Barros, M., Wen, S., Li, F., Lin, C. L., Hannun, Y. A., et al. (2018). Tumor suppressor p53 links ceramide metabolism to DNA damage response through alkaline ceramidase 2. *Cell Death Differ.* 25, 841–856. doi:10.1038/s41418-017-0018-y

Yuan, X., Huang, B., Wang, R., Tie, H., and Luo, S. (2022). The prognostic value of advanced lung cancer inflammation index (ALI) in elderly patients with heart failure. *Front. Cardiovasc Med.* 9, 934551. doi:10.3389/fcvm.2022.934551

frontiers | Frontiers in Genetics

TYPE Original Research
PUBLISHED 19 September 2022
DOI 10.3389/fgene.2022.1012548

OPEN ACCESS

EDITED BY
Changjing Cai,
Xiangya Hospital, Central South University, China

REVIEWED BY
Haibo Wu,
University of Science and Technology of China, China
Aimin Jiang,
The First Affiliated Hospital of Xi'an Jiaotong University, China

*CORRESPONDENCE
Zhengqi Bao,
baozhengqi@163.com
Tian Li,
fmmult@foxmail.com
Damin Chai,
0100155@bbmc.edu.cn

†These authors have contributed equally to this work

SPECIALTY SECTION
This article was submitted to Cancer Genetics and Oncogenomics, a section of the journal Frontiers in Genetics

RECEIVED 05 August 2022
ACCEPTED 30 August 2022
PUBLISHED 19 September 2022

CITATION
Bao Z, Zhu R, Fan H, Ye Y, Li T and Chai D (2022), Aberrant expression of SPAG6 and NM23 predicts poor prognosis of human osteosarcoma. *Front. Genet.* 13:1012548. doi: 10.3389/fgene.2022.1012548

Aberrant expression of SPAG6 and NM23 predicts poor prognosis of human osteosarcoma

Zhengqi Bao[1,2*†], Ruizhi Zhu[1†], Huagang Fan[1], Yuchen Ye[1], Tian Li[3*] and Damin Chai[4*]

[1]Department of Orthopedics, The First Affiliated Hospital of Bengbu Medical University, Bengbu, China, [2]Anhui Province Key Laboratory of Tissue Transplantation, Bengbu Medical University, Bengbu, China, [3]School of Basic Medicine, Fourth Military Medical University, Xi'an, China, [4]Department of Pathology, The First Affiliated Hospital of Bengbu Medical University, Bengbu, China

Objective: To investigate the expression and clinical significance of sperm-associated antigen 6 and NM23 proteins in human osteosarcoma.

Methods: The specimens of conventional osteosarcoma with follow-up from 42 Chinese patients were analyzed in this study, and 12 cases of osteochondroma were considered controls. The expression of SPAG6 and NM23 was inspected using immunohistochemical staining, qRT-PCR, and Western blotting methods.

Results: The positive expression rate of SPAG6 protein (71.43%) in 42 cases of osteosarcoma tissue was significantly higher than that (33.33%) in 12 cases of osteochondroma tissues ($p < 0.05$), while the positive rate of NM23 protein (35.71%) in osteosarcoma tissue was lower than that (58.33%) in osteochondroma tissue ($p < 0.05$). The mRNA and protein levels of SPAG6 were significantly higher than those of the adjacent normal tissues, while the expression of NM23 was lower in osteosarcoma tissues than that in the controls ($p < 0.05$ for all). There was a positive relationship between the expression of SPAG6 and pathological grade, metastasis, and Enneking stage ($p < 0.05$ for all). The overall survival rate of osteosarcoma patients with SPAG6 positive expression was significantly lower than that with SPAG6 negative expression. The relationship between the expression of NM23 and pathological grade, metastasis, and Enneking stage was negative ($p < 0.05$ for all). The overall survival rate of the osteosarcoma patients with NM23 positive expression was higher than that of the patients with NM23 negative expression ($p < 0.05$).

Conclusion: Overexpression of SPAG6 and low expression of NM23 are negatively related to pathological grade, metastasis, and Enneking stage and prognosis of osteosarcoma patients. This suggested that SPAG6 and NM23 should be considered candidate prognostic biomarkers for patients with osteosarcoma.

KEYWORDS
osteosarcoma, SPAG6, NM23, prognosis, overall survival

Introduction

Osteosarcoma (OS), also referred to as osteogenic sarcoma, is the most popular malignant tumor originating in the bones and is more prevalent in males than in females (Mirabello et al., 2009a; Mirabello et al., 2009b; Biermann et al., 2013). The worldwide incidence of osteosarcoma is about 3–4 cases per million each year, about 800 new cases are diagnosed, and half of these are reported in adolescents (Rickel et al., 2017; Assi et al., 2021). Patients with osteosarcoma often have high cancer-related mortality, especially once metastasis to the lungs begins, the 5-year survival rate becomes less than 20% (EESNW Group, 2012; Luetke et al., 2014). In addition to surgery, the use of neoadjuvant chemotherapy and immunotherapy significantly increases the 5-year survival of non-metastasis osteosarcoma patients to approximately 58–75% (Bacci et al., 2005). However, there have been only minimal improvements in the prognosis of metastasis osteosarcoma patients in the last 2 decades (EESNW Group, 2012). Therefore, it is necessary to research novel molecular markers of metastasis and to identify the underlying molecular mechanism of OS evolvement and progression, which will identify a novel therapeutic strategy for patients with OS.

Sperm-associated antigen 6 (SPAG6) gene, first identified in human testicular tissue, also named CT141 and pf16, is considered a cancer-testis antigen (CTA) and involved in many cancers (Abe et al., 2008; Silina et al., 2011; Coan et al., 2018; Jiang et al., 2019). Many studies' results have shown that SPAG6 plays a critical role in tumor involvement and progression, especially in myelodysplastic syndrome (MDSC), the common hematological malignancies, and SPAG6 levels were significantly higher than those in solid tumors (Barretina et al., 2019). The aberrant expression of SPAG6 has been found in neuroblastoma (NBL) cell lines, serous ovarian cancer (HGSOC) samples, myeloid SKM-1 and K562 cell lines, breast cancer tissues, bladder cancer tissues, and non-small-cell lung cancer (NSCLC) samples (Abe et al., 2008; Kitchen et al., 2015; Altenberger et al., 2017; Coan et al., 2018; Jiang et al., 2019). Non-metastasis 23 (NM23) plays a suppressive role in tumor metastasis (Carotenuto et al., 2015). Studies have confirmed that the low expression of NM23 is positively related to metastasis and irradiation (Xi et al., 2019; Wang et al., 2021). Until now, there are few reports about the association of the expression of SPAG6 and NM23 with the metastasis and prognosis of osteosarcoma, and the precise role of SPAG6 is unclear.

In this study, we detected the association between SPAG6 and NM23 and the clinicopathological parameters of metastasis and prognosis of osteosarcoma using immunohistochemical staining, qRT-PCR, and Western blotting methods.

Materials and methods

Ethics statement and human osteosarcoma tissue sample collection

Ethical approval for the overall study was agreed upon by the Ethics Committee of The First Affiliated Hospital of Bengbu Medical College, and all the patients consented to the study. A total of 42 cases of paraffin-embedded paired conventional human osteosarcoma tissues were collected for this retrospective review, during the time of surgery from January 2005 to December 2016 at The First Affiliated Hospital of Bengbu Medical College. A total of 12 osteochondroma samples were obtained as controls for the study. Also, from six cases of human osteosarcoma, fresh osteosarcoma specimens and adjacent normal muscle tissues (control) for qRT-PCR and Western blotting (Table 1) were immediately put in liquid nitrogen, frozen, and stored at −80°C. All the human osteosarcoma patients in this study were managed with surgery but did not manage with chemotherapy or radiotherapy. Relevant clinicopathological parameters were obtained by retrospectively reviewing the patients' medical records. The survival time of the patients with osteosarcoma in this study was predicted by the follow-up through phone or through out-patient visiting or through consulting local police stations, and the time interval was 3 months until the patients died or Jun 2022.

Immunohistochemical analysis and interpretation

Immunohistochemical staining methods were performed to detect the expression of SPAG6 in specimens of the 42 human osteosarcoma and control tissues as described previously according to the procedure of the Elivision TM Plus detection kit (Lab Vision, United States) (Yang et al., 2014; Bao et al., 2016). Fixed in 10% buffered formalin, all of the tissues were paraffin-embedded and sliced into 3–4-μm-thick tissue sections. The expression of SPAG6 (dilution: 1:200, Catalog No. Ab155653, Abcam, United States) and NM23 (dilution: 1:100, Catalog No. 3338, Cell Signaling Technology, Inc., Danvers, MA, United States) was predominantly localized in the cytoplasm. Upon immunohistochemical staining, the immunoreaction was scored based on the percentage of positively stained tumor cells: 1 (<10%); 2 (11%–50%); 3 (51%–75%); and 4 (>75%). The intensity was scored as follows: 0 (negative); 1 (weak); 1 (moderate); and 1 (strong). The final score was decided by multiplying the staining percentage by the intensity, which commonly ranges from 0 to 12. The score was interpreted as >2, which is a positive expression.

TABLE 1 Clinicopathological data of the human conventional osteosarcoma patients with their lesions detected using qRT-PCR and Western blotting (n = 6).

Patient code	Gender	Age (years)	Site	Histological type	Metastasis	Diameter (cm)	Pathological degree	Enneking stage
1	Female	6	Femur	Osteoblast	No	3.5	G1	I
2	Male	21	Humerus	Osteoblast	Lung	5.4	G2	III
3	Male	28	Thurl	Fibroblast	Lung	6.3	G2	III
4	Female	36	Femur	Osteoblast	Lung	4.5	G2	III
5	Male	48	Jaw	Fibroblast	No	2.5	G1	I
6	Male	22	Femur	Mixed	Lung	5.5	G2	III

Real-time PCR

The total RNA of fresh osteosarcoma tissues and cells in the test and control group was obtained using TRIzol (Invitrogen, Carlsbad) and then reverse-transcribed to cDNA using the reverse transcription system (Bao et al., 2019). The expression of SPAG6 was determined using the SYBR Green RT-PCR Assay (Takara, Dalian, China) and normalized to GAPDH (glyceraldehyde 3-phosphate dehydrogenase) as described previously (Ma et al., 2019). Quantitative real-time PCR was implemented on an ABI 7900 System with SYBR Green (Takara, Dalian, China). The primers used in the PCR are as follows: SPAG6, forward primer, 5′-AGC AAT GGC AGT CAT CAT TTC-3′ and reverse primer, 5′-GGA TGA ATG GTC GGG AAC TT- 3′; NM23, forward primer, 5′-ACGCTTGCTCTGTTTGTG G-3′ and reverse primer, 5′-CTGGAAGGCACACCATCC-3’; and GAPDH, forward primer, 5-CAG CCT CAA GAT CAGCA-30 and reverse primer, 5′-TGT GGT CAT GAG TCC TTC CA-3′.

Western blot analyses

Western blot analyses were performed as reported previously (Du et al., 2015; Bao et al., 2016). Briefly, human osteosarcoma and normal adjacent soft tissues were rinsed two times with ice-cold phosphate-buffered saline (PBS, pH 7.4) and lysed with RIPA buffer supplemented with protease inhibitors. Then, the lysates were boiled for 10 min in a water bath and centrifuged at 12,000 g at 4°C for about 10 min. The protein concentrations in the supernatant were surveyed by bicinchoninic acid (BCA) protein assay (Pierce, United States). Equal amounts of proteins were loaded on 10% sodium dodecyl sulfate-polyacrylamide gel electrophoresis (SDS-PAGE) and transferred to nitrocellulose membranes (Hybond ECL, GE Healthcare Bio-Sciences Corp., United States). The membranes were then blocked with 5% non-fat milk, and protein expression was measured as described previously (Chai et al., 2019; Ma et al., 2019).

Statistical analysis

Statistical analysis was performed using SPSS version 19.0 software (SPSS Inc., United States) and GraphPad Prism version 5 for Windows (GraphPad Software, San Diego, California, United States). All data were presented as mean ± SD. Comparisons between groups were implemented by one-way ANOVA followed by Tukey's *post hoc* test. The correlation between SPAG6 and NM23 was analyzed using Spearman correlation analysis. The relationship between SPAG6 and overall survival time of patients with human osteosarcoma was performed using the Kaplan–Meier method and log-rank test. Multivariate prognosis analysis was carried out using the Cox regression method. The error bars represent SD. $p < 0.05$ was considered statistically significant.

Results

Aberrant expression of SPAG6 and NM23 in osteosarcoma tissue

The positive expression rate of SPAG6 protein was 71.43% (30/42) in 42 cases of osteosarcoma tissues and 33.33% (4/12) in 12 cases of osteochondroma tissues, with $p < 0.05$ for all. The staining of SPAG6 was located in the cytoplasm and nucleus of osteosarcoma and control tissues (Figure 1A, B). The positive expression rate of NM23 protein was 35.71% (15/42) in 42 cases of osteosarcoma tissues and 58.33% (7/12) in 12 cases of osteochondroma tissues, with $p < 0.05$ for all. The staining of NM23 was located in the cytoplasm of osteosarcoma and control tissues (Figures 1C, D). To further validate our results, the mRNA and protein expression levels of SPAG6 and NM23 were detected by RT-PCR and Western blot analyses in six cases of osteosarcoma and adjacent normal tissues. We found that mRNA and protein levels of SPAG6 were significantly higher than those of the adjacent normal tissues (Figure 2A), while the expression of NM23 was lower in osteosarcoma tissues than in controls (Figure 2A). As shown in Figures 2B,C, the results of the Western blot analysis indicated that the relative intensity of SPAG6 and NM23 protein blots was 1.80- and 0.78-fold greater in osteosarcoma tissues than in control tissues, with $p < 0.05$ for all.

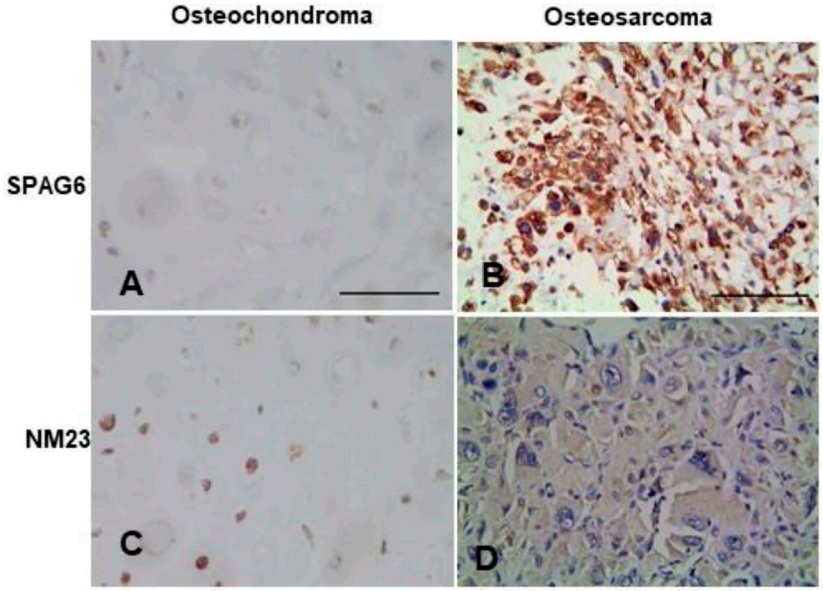

FIGURE 1
Representation micrographs showing SPAG6 and NM23 proteins in osteochondroma and osteosarcoma tissues (Elivision). **(A,B)** SPAG6 staining is predominantly localized in the cytoplasm in the osteochondroma tissue and osteosarcoma tissue. **(C,D)** NM23 staining is predominantly localized in the cytoplasm in the osteochondroma tissue and osteosarcoma tissue. Scale bar = 50 μm.

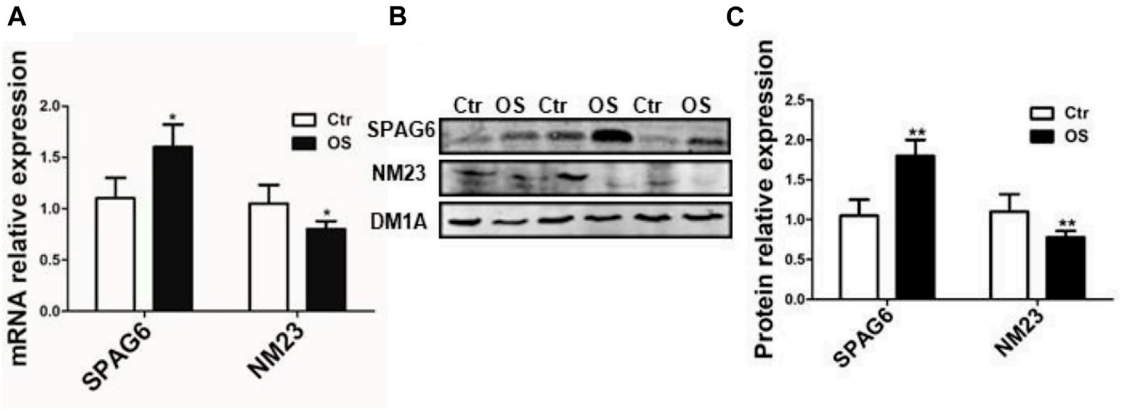

FIGURE 2
qRT-PCR and Western blot analysis of SPAG6 and NM23 in osteosarcoma and adjacent normal muscle tissues (control). **(A)** SPAG6 and NM23 mRNAs were detected by qRT-PCR. **(B)** SPAG6 and NM23 proteins were detected by Western blotting in osteosarcoma and adjacent normal tissues. **(C)** Quantitative analysis was conducted, and the results were normalized against the levels of α-tubulin (DM1A). The data were presented with ±s (n = 6). OS: osteosarcoma; Ctr: control (adjacent normal muscle tissues). *p < 0.05 *vs.* control group.

The association between aberrant expression of SPAG6 and NM23 and clinicopathological features in human osteosarcoma patients

Among the 42 patients with human osteosarcoma, 25 were males and 17 were females; the age ranged from 6 to 75 years, and the average age was 19.35 years. A total of 22 patients were younger and 20 patients were older than 25 years. There were 19 lesions in adjacent knees, 8 in the humerus, 7 in jaws, and 8 in other bones. According to multiple distinct histological subtypes, human osteosarcoma is classified as conventional (osteoblastic), chondroblastic, fibroblastic, telangiectatic, small cell, surface, and secondary subtypes (Assi et al.,

TABLE 2 Expression of SPAG6 in OS and the relationship with clinicopathological parameters (n = 42).

Parameter	Case	SPAG6		*p*-value	NM23		*p*-value
		+	-		+	-	
Gender							
Male	25	19	6	0.43	8	17	0.54
Female	17	11	6		7	10	
Age (year)							
<19	22	16	6	0.85	8	14	0.93
≥19	20	14	6		7	13	
Location							
Knee	19	13	6	0.74	7	12	0.67
Humerus	8	6	2		2	6	
Jaw	7	5	2		2	5	
Others	8	6	2		4	4	
Histological type							
Osteoblast	19	14	5	0.81	6	13	0.18
Fibroblast	10	8	2		2	8	
Chondroblast	10	6	4		6	5	
Others	3	2	1		2	1	
Diameter (cm)							
<5.0	25	19	6	0.49	8	17	0.54
≥5.0	17	11	6		7	10	
Distant metastasis							
Yes	31	27	4	<0.01	8	23	0.02
No	11	3	8		7	4	
Pathological grade							
G1	6	2	4	0.03	5	1	<0.01
G2	36	28	8		10	26	
Enneking stage							
I	8	2	6	<0.01	6	2	<0.01
II	14	10	4		6	8	
III	20	18	2		3	17	

2021). In this study, there were osteoblastic subtype (n = 19), fibroblastic subtype (n = 10), chondroblastic subtype (n = 10), and others subtypes (n = 3). The diameter of the lesions was longer than 5.0 cm in 25 cases and shorter than 5.0 cm in 17 cases. About metastasis, especially to lungs, 31 cases were found metastasized. A total of six cases were low-potential malignancy (G1) and 36 cases were high-potential malignancy (G2). With regard to Enneking surgery stages, 8 cases were stage Ⅰ, 14 cases were stage Ⅱ, and 20 cases were stage Ⅲ. As for the 12 osteochondroma patients, 7 were males and 5 were females, and the age ranged from 8 to 42 years with a mean age of 18.5 years.

To further study the clinical significance of the aberrant expression of SPAG6 and NM23 proteins, the relationship between the expression of SPAG6 and NM23 and clinicopathological features in human osteosarcoma patients was analyzed. The expression of SPAG6 protein was positive while that of NM23 was negative, associated with distant metastasis, pathological grade, and Enneking stage of osteosarcoma patients, with $p < 0.05$ for all. But the expression of SPAG6 and NM23 proteins was not associated with patient's gender, age, tumor location, histological types, and diameter ($p > 0.05$) (Table 2).

Prognosis and multivariate analysis

Our results showed that the overall mean survival time of osteosarcoma patients with positive expression of SPAG6 (35.08 ± 2.58 months) was significantly shorter than that

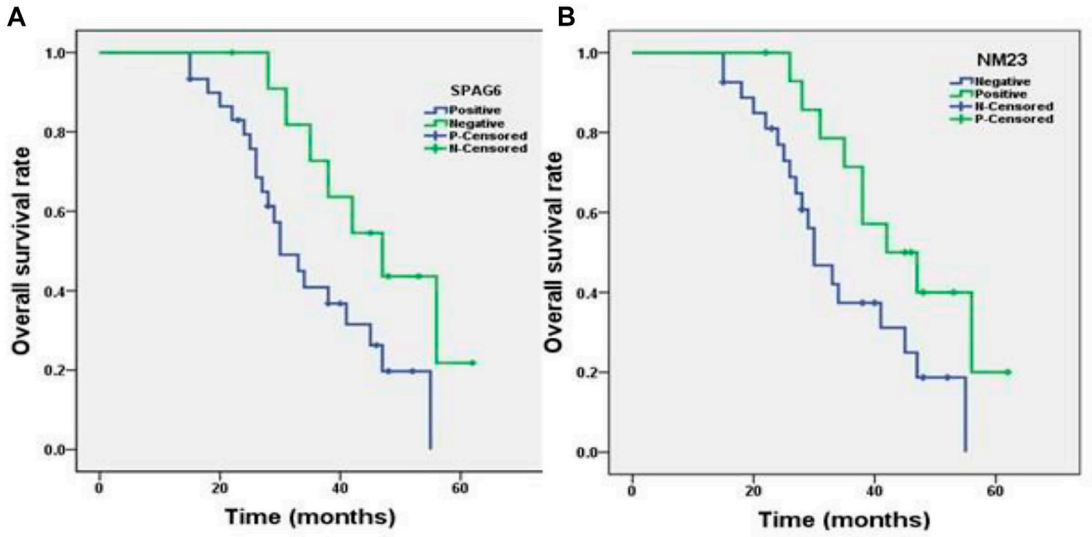

FIGURE 3
Kaplan–Meier survival analysis of patients with osteosarcoma (n = 42). **(A)** Correlation of the SPAG6 protein expression level with the overall survival time of patients with osteosarcoma. The y-axis represents the percentage of patients, the x-axis represents their survival in months, and the green line represents SPAG6$^+$ patients with a worse survival trend than the blue line representing SPAG6$^-$ ($p < 0.05$). **(B)** Correlation of the NM23 protein expression level with the overall survival time of patients with osteosarcoma, and the green line represents NM23$^+$ patients with a better survival trend than the blue line representing NM23$^-$ patients ($p < 0.05$).

TABLE 3 Multivariate survival analysis of 42 patients with osteosarcoma.

Covariate	B	SE	Sig	HR	HR 95%CI
Pathological degree	−39.695	18.928	0.036	0.000	0.000–0.075
Distant metastasis	−42.559	18.993	0.025	0.000	0.000–0.005
Enneking stage	0.897	0.395	0.023	1.131	1.131–5.320
SPAG6	1.971	0.873	0.024	1.298	1.298–39.727
NM23	2.502	1.175	0.033	1.221	1.221–122.076

with negative expression of SPAG6 (46.69 ± 2.35 months), while the overall mean survival time (45.30 ± 3.47 months) of the NM23 positive expression group was longer than that of the NM23 negative expression group (34.56 ± 2.77 months), with $p < 0.05$ for all. The Kaplan–Meier curve analysis (log-rank test) results showed that the overall survival rate of osteosarcoma patients with SPAG6 positive expression was significantly less than that with SPAG6 negative expression (Figure 3A), while the rate was adverse in NM23 expression (Figure 3B) with $p < 0.05$ for all.

The expression of SPAG6 and NM23, distant metastasis, pathological grade, and Enneking stages were found to be independent prognostic factors of osteosarcoma using the Cox multivariate analysis method ($p < 0.05$ for all, Table 3).

Correlation of SPAG6 and NM23 in human osteosarcoma

In thirty cases of the SPAG6 positive expression group, there were only six cases of NM23 positive expression in human osteosarcoma tissues. But in the twelve cases of the SPAG6 negative expression group, there were nine cases of NM23 positive expression in human osteosarcoma tissues. The negative correlation between SPAG6 and NM23 proteins was found (r = 0.519 and $p < 0.01$).

Discussion

Osteosarcoma displays a bimodal distribution, with the first peak at the age of 10–19 years and the second peak at 70–79 years (Savage and Mirabello, 2011). In teenage, it is often distributed in the metaphysis of the long bones nearby the knee joints, and the second region is the vicinity of the shoulder joints (distal femur > proximal tibia > proximal humerus) (Damron et al., 2007; Sasaki et al., 2019). In the elderly, it is often distributed in the axial skeleton and skull (Rickel et al., 2017). According to pathological subtypes, osteosarcoma is classified as osteoblastic, and the most popular subtypes are chondroblastic, fibroblastic, telangiectatic, small cell, surface, and secondary subtypes (Assi et al., 2021). Relapsing or metastatic patients with osteosarcoma have a dismal prognosis with a median overall survival of less than 8 months

(Lagmay et al., 2016). NM23 plays a suppressing role in tumor metastasis (Carotenuto et al., 2015; Kim and Lee, 2021). It inhibits bone-specific metastasis by upregulating miR-660-5p in lung cancer and represses metastasis *via* redox regulation in breast cancer (Ai et al., 2020; Kim and Lee, 2021). In this study, we found NM23 was downregulated more in osteosarcoma tissues than the controls in mRNA and protein levels. Furthermore, it was negatively related to the pathological grade, distant metastasis, Enneking stage, and worst prognosis of patients with osteosarcoma.

SPAG6 was first inspected in human testicular tissue and is mainly expressed in the sperm, lungs, central nervous system, and inner ear (Hu et al., 2016; Liu et al., 2019). Functionally, SPAG6 is predominately involved in sperm maturation and nervous system development under normal physiological conditions in mammals (Li et al., 2017; Liu et al., 2019). Accumulating evidence has demonstrated that SPAG6 was identified as a novel cancer-testis antigen (Silina et al., 2011). Aberrant expression of SPAG6 in hematological malignancies, Burkitt lymphoma, and breast and non-small cell lung cancers may serve an important role in the occurrence and development of different human cancers by regulating the growth, apoptosis, invasion, and metastasis of tumor cells *via* AKT/FOXO, PTEN/PI3K/AKT, and other pathways (Jiang et al., 2019; Mijnes et al., 2019; Zheng et al., 2019; Zhang et al., 2020). So far, there are no reports about the clinical significance and correlation between SPAG6 expression and NM23 in osteosarcoma.

In the present study, we reported that SPAG6 was upregulated more in osteosarcoma tissues than the controls in mRNA and protein levels. Furthermore, research showed that the expression of SPAG6 was positively related to the pathological grade, distant metastasis, Enneking stage, and worst prognosis of patients with osteosarcoma. Also, the positive expression of SPAG6 indicated a shorter mean overall survival time (35.08 months) than SPAG6 negative expression (45.30 months). For children, where recurrent/refractory osteosarcoma was uniformly poor, there have been few new chemotherapy drugs, small-molecule targeted medicine, or immunotherapeutic agents found to treat osteosarcoma (Meyers et al., 2005; Lagmay et al., 2016). Our research also showed that SPAG6 and NM23 were positively correlated with each other. We deduced that SPAG6 may promote distant metastasis by suppressing NM23 and lead to worse prognosis in osteosarcoma. Some studies found that SPAG6 is also a promising anti-cancer therapeutic candidate (Li et al., 2017; Yin et al., 2018).

Our results suggest that SPAG6 may provide a potential tumor marker and a promising antitumor therapeutic target. To some extent, combined detection of SPAG6 and NM23 can indicate the biological behavior of osteosarcoma cells, thus giving a selection of targeted therapies. However, our study only detected mRNA and proteins in human osteosarcoma tissues; the molecular mechanism of SPAG6 regulating NM23 will be studied in our future research.

Data availability statement

The original contributions presented in the study are included in the article/Supplementary Material; further inquiries can be directed to the corresponding authors.

Ethics statement

The studies involving human participants were reviewed and approved by the Ethics Committee of The First Affiliated Hospital of Bengbu Medical College. Written informed consent to participate in this study was provided by the participants' legal guardian/next of kin.

Author contributions

ZB and DC studied the concept and design. RZ and HF acquired the data. RZ and HF analyzed the data. HF and YY drafted the manuscript. TL revised the manuscript. RZ and HF provided acquisition, analysis, and interpretation of data and statistical analysis. All authors read and approved the final manuscript.

Funding

This work was supported in part by the Nature Science Major and Key Program of College and University of Anhui Province (KJ2020A0559 and KJ2021A0684) and 512 Talents Development Project of Bengbu Medical College (BY51201304).

Acknowledgments

The authors thank Freescience for language editing services.

Conflict of interest

The authors declare that the research was conducted in the absence of any commercial or financial relationships that could be construed as a potential conflict of interest.

Publisher's note

All claims expressed in this article are solely those of the authors and do not necessarily represent those of their

affiliated organizations, or those of the publisher, the editors, and the reviewers. Any product that may be evaluated in this article, or claim that may be made by its manufacturer, is not guaranteed or endorsed by the publisher.

Supplementary material

The Supplementary Material for this article can be found online at: https://www.frontiersin.org/articles/10.3389/fgene.2022.1012548/full#supplementary-material

References

Abe, M., Watanabe, N., McDonell, N., Takato, T., Ohira, M., Nakagawara, A., et al. (2008). Identification of genes targeted by CpG island methylator phenotype in neuroblastomas, and their possible integrative involvement in poor prognosis. *Oncology* 74 (1-2), 50–60. doi:10.1159/000139124

Ai, C., Ma, G., Deng, Y., Zheng, Q., Gen, Y., Li, W., et al. (2020). Nm23-H1 inhibits lung cancer bone-specific metastasis by upregulating miR-660-5p targeted SMARCA5. *Thorac. Cancer* 11 (3), 640–650. doi:10.1111/1759-7714.13308

Altenberger, C., Heller, G., Ziegler, B., Tomasich, E., Marhold, M., Topakian, T., et al. (2017). SPAG6 and L1TD1 are transcriptionally regulated by DNA methylation in non-small cell lung cancers. *Mol. Cancer* 16 (1), 1. doi:10.1186/s12943-016-0568-5

Assi, T., Watson, S., Samra, B., Rassy, E., Le Cesne, A., Italiano, A., et al. (2021). Targeting the VEGF pathway in osteosarcoma. *Cells* 10 (5), 1240. doi:10.3390/cells10051240

Bacci, G., Longhi, A., Fagioli, F., Briccoli, A., Versari, M., and Picci, P. (2005). Adjuvant and neoadjuvant chemotherapy for osteosarcoma of the extremities: 27 year experience at rizzoli institute, Italy. *Eur. J. Cancer* 41 (18), 2836–2845. doi:10.1016/j.ejca.2005.08.026

Bao, Z., Dai, X., Wang, P., Tao, Y., and Chai, D. (2019). Capsaicin induces cytotoxicity in human osteosarcoma MG63 cells through TRPV1-dependent and -independent pathways. *Cell cycle* 18 (12), 1379–1392. doi:10.1080/15384101.2019.1618119

Bao, Z. Q., Zhang, C. C., Xiao, Y. Z., Zhou, J. S., Tao, Y. S., and Chai, D. M. (2016). Over-expression of Sox4 and beta-catenin is associated with a less favorable prognosis of osteosarcoma. *J. Huazhong Univ. Sci. Technol. Med. Sci.* 36 (2), 193–199. doi:10.1007/s11596-016-1565-z

Barretina, J., Caponigro, G., Stransky, N., Venkatesan, K., Margolin, A. A., Kim, S., et al. (2019). Addendum: The Cancer Cell Line Encyclopedia enables predictive modelling of anticancer drug sensitivity. *Nature* 565 (7738), E5–E6. doi:10.1038/s41586-018-0722-x

Biermann, J. S., Adkins, D. R., Agulnik, M., Benjamin, R. S., Brigman, B., Butrynski, J. E., et al. (2013). Bone cancer. *J. Natl. Compr. Canc. Netw.* 11 (6), 688–723. doi:10.6004/jnccn.2013.0088

Carotenuto, M., de Antonellis, P., Chiarolla, C. M., Attanasio, C., Damiani, V., Boffa, I., et al. (2015). A therapeutic approach to treat prostate cancer by targeting Nm23-H1/h-Prune interaction. *Naunyn. Schmiedeb. Arch. Pharmacol.* 388 (2), 257–269. doi:10.1007/s00210-014-1035-8

Chai, D. M., Qin, Y. Z., Wu, S. W., Ma, L., Tan, Y. Y., Yong, X., et al. (2019). WISP2 exhibits its potential antitumor activity via targeting ERK and E-cadherin pathways in esophageal cancer cells. *J. Exp. Clin. Cancer Res.* 38 (1), 102. doi:10.1186/s13046-019-1108-0

Coan, M., Rampioni Vinciguerra, G. L., Cesaratto, L., Gardenal, E., Bianchet, R., Dassi, E., et al. (2018). Exploring the role of fallopian ciliated cells in the pathogenesis of high-grade serous ovarian cancer. *Int. J. Mol. Sci.* 19 (9), E2512. doi:10.3390/ijms19092512

Damron, T. A., Ward, W. G., and Stewart, A. (2007). Osteosarcoma, chondrosarcoma, and ewing's sarcoma: National cancer data base report. *Clin. Orthop. Relat. Res.* 459, 40–47. doi:10.1097/BLO.0b013e318059b8c9

Du, L. L., Chai, D. M., Zhao, L. N., Li, X. H., Zhang, F. C., Zhang, H. B., et al. (2015). AMPK activation ameliorates Alzheimer's disease-like pathology and spatial memory impairment in a streptozotocin-induced Alzheimer's disease model in rats. *J. Alzheimers Dis.* 43 (3), 775–784. doi:10.3233/JAD-140564

EESNW Group (2012). Bone sarcomas: ESMO clinical practice guidelines for diagnosis, treatment and follow-up. *Ann. Oncol.* 23 (7), vii100–9. doi:10.1093/annonc/mds254

Hu, X., Yan, R., Cheng, X., Song, L., Zhang, W., Li, K., et al. (2016). The function of sperm-associated antigen 6 in neuronal proliferation and differentiation. *J. Mol. Histol.* 47 (6), 531–540. doi:10.1007/s10735-016-9694-z

Jiang, M., Chen, Y., Deng, L., Luo, X., Wang, L., and Liu, L. (2019). Upregulation of SPAG6 in myelodysplastic syndrome: Knockdown inhibits cell proliferation via AKT/FOXO signaling pathway. *DNA Cell Biol.* 38 (5), 476–484. doi:10.1089/dna.2018.4521

Kim, B., and Lee, K. J. (2021). Activation of Nm23-H1 to suppress breast cancer metastasis via redox regulation. *Exp. Mol. Med.* 53 (3), 346–357. doi:10.1038/s12276-021-00575-1

Kitchen, M. O., Bryan, R. T., Haworth, K. E., Emes, R. D., Luscombe, C., Gommersall, L., et al. (2015). Methylation of HOXA9 and ISL1 predicts patient outcome in high-grade non-invasive bladder cancer. *PloS one* 10 (9), e0137003. doi:10.1371/journal.pone.0137003

Lagmay, J. P., Krailo, M. D., Dang, H., Kim, A., Hawkins, D. S., Beaty, O., 3rd, et al. (2016). Outcome of patients with recurrent osteosarcoma enrolled in seven phase II trials through children's cancer group, pediatric Oncology group, and children's Oncology group: Learning from the past to move forward. *J. Clin. Oncol.* 34 (25), 3031–3038. doi:10.1200/JCO.2015.65.5381

Li, X., Xu, L., Sun, G., Wu, X., Bai, X., Li, J., et al. (2017). Spag6 mutant mice have defects in development and function of spiral ganglion neurons, apoptosis, and higher sensitivity to paclitaxel. *Sci. Rep.* 7 (1), 8638. doi:10.1038/s41598-017-08739-8

Liu, Y., Zhang, L., Li, W., Huang, Q., Yuan, S., Li, Y., et al. (2019). The sperm-associated antigen 6 interactome and its role in spermatogenesis. *Reproduction* 158 (2), 181–197. doi:10.1530/REP-18-0522

Luetke, A., Meyers, P. A., Lewis, I., and Juergens, H. (2014). Osteosarcoma treatment - where do we stand? A state of the art review. *Cancer Treat. Rev.* 40 (4), 523–532. doi:10.1016/j.ctrv.2013.11.006

Ma, J., Cui, Y., Cao, T., Xu, H., Shi, Y., Xia, J., et al. (2019). PDS5B regulates cell proliferation and motility via upregulation of Ptch2 in pancreatic cancer cells. *Cancer Lett.* 460, 65–74. doi:10.1016/j.canlet.2019.06.014

Meyers, P. A., Schwartz, C. L., Krailo, M., Kleinerman, E. S., Betcher, D., Bernstein, M. L., et al. (2005). Osteosarcoma: A randomized, prospective trial of the addition of ifosfamide and/or muramyl tripeptide to cisplatin, doxorubicin, and high-dose methotrexate. *J. Clin. Oncol.* 23 (9), 2004–2011. doi:10.1200/JCO.2005.06.031

Mijnes, J., Tiedemann, J., Eschenbruch, J., Gasthaus, J., Bringezu, S., Bauerschlag, D., et al. (2019). SNiPER: A novel hypermethylation biomarker panel for liquid biopsy based early breast cancer detection. *Oncotarget* 10 (60), 6494–6508. doi:10.18632/oncotarget.27303

Mirabello, L., Troisi, R. J., and Savage, S. A. (2009). International osteosarcoma incidence patterns in children and adolescents, middle ages and elderly persons. *Int. J. Cancer* 125 (1), 229–234. doi:10.1002/ijc.24320

Mirabello, L., Troisi, R. J., and Savage, S. A. (2009). Osteosarcoma incidence and survival rates from 1973 to 2004: Data from the surveillance, epidemiology, and end results Program. *Cancer* 115 (7), 1531–1543. doi:10.1002/cncr.24121

Rickel, K., Fang, F., and Tao, J. (2017). Molecular genetics of osteosarcoma. *Bone* 102, 69–79. doi:10.1016/j.bone.2016.10.017

Sasaki, R., Osaki, M., and Okada, F. (2019). MicroRNA-based diagnosis and treatment of metastatic human osteosarcoma. *Cancers* 11 (4), E553. doi:10.3390/cancers11040553

Savage, S. A., and Mirabello, L. (2011). Using epidemiology and genomics to understand osteosarcoma etiology. *Sarcoma* 2011, 548151. doi:10.1155/2011/548151

Silina, K., Zayakin, P., Kalnina, Z., Ivanova, L., Meistere, I., Endzelins, E., et al. (2011). Sperm-associated antigens as targets for cancer immunotherapy: Expression pattern and humoral immune response in cancer patients. *J. Immunother.* 34 (1), 28–44. doi:10.1097/CJI.0b013e3181fb64fa

Wang, Y. F., Lin, Y. K., Lin, C. P., Chen, Y. J., and Chang, C. J. (2021). NM23-H1 expression of head and neck squamous cell carcinoma in association with the response to irradiation. *Front. Oncol.* 11, 646167. doi:10.3389/fonc.2021.646167

Xi, M., Wan, S., Hua, W., Zhou, Y., Jiang, W., and Hu, J. (2019). Correlation of SOX9 and NM23 genes with the incidence and prognosis of prostate cancer. *Oncol. Lett.* 17 (2), 2296–2302. doi:10.3892/ol.2018.9828

Yang, Q., Zhang, F., Ding, Y., Huang, J., Chen, S., Wu, Q., et al. (2014). Antitumour activity of the recombination polypeptide GST-NT21MP is mediated by inhibition of CXCR4 pathway in breast cancer. *Br. J. Cancer* 110 (5), 1288–1297. doi:10.1038/bjc.2014.1

Yin, J., Li, X., Zhang, Z., Luo, X., Wang, L., and Liu, L. (2018). SPAG6 silencing induces apoptosis in the myelodysplastic syndrome cell line SKM1 via the PTEN/PI3K/AKT signaling pathway *in vitro* and *in vivo*. *Int. J. Oncol.* 53 (1), 297–306. doi:10.3892/ijo.2018.4390

Zhang, R., Zhu, H., Yuan, Y., Wang, Y., and Tian, Z. (2020). SPAG6 promotes cell proliferation and inhibits apoptosis through the PTEN/PI3K/AKT pathway in Burkitt lymphoma. *Oncol. Rep.* 44 (5), 2021–2030. doi:10.3892/or.2020.7776

Zheng, D. F., Wang, Q., Wang, J. P., Bao, Z. Q., Wu, S. W., Ma, L., et al. (2019). The emerging role of sperm-associated antigen 6 gene in the microtubule function of cells and cancer. *Mol. Ther. Oncolytics* 15, 101–107. doi:10.1016/j.omto.2019.08.011

frontiers | Frontiers in Genetics

TYPE Original Research
PUBLISHED 21 September 2022
DOI 10.3389/fgene.2022.1017762

OPEN ACCESS

EDITED BY
Changjing Cai,
Central South University, China

REVIEWED BY
Xiaoyong Ren,
Department of Otorhinolaryngology, Second Affiliated Hospital of Xi'an Jiaotong University, China
Ping-An WU,
The University of HongKong-Shenzhen Hospital, China
Yuanteng Xu,
Fujian Medical University, China

*CORRESPONDENCE
Ying Zhang,
zyebyh@csu.edu.cn
Shisheng Li,
lissdoctor@csu.edu.cn

SPECIALTY SECTION
This article was submitted to Cancer Genetics and Oncogenomics, a section of the journal Frontiers in Genetics

RECEIVED 12 August 2022
ACCEPTED 29 August 2022
PUBLISHED 21 September 2022

CITATION
Tang X, Tang Q, Yang X, Xiao Z-A, Zhu G, Yang T, Yang Q, Zhang Y and Li S (2022), FN1 promotes prognosis and radioresistance in head and neck squamous cell carcinoma: From radioresistant HNSCC cell line to integrated bioinformatics methods. *Front. Genet.* 13:1017762. doi: 10.3389/fgene.2022.1017762

FN1 promotes prognosis and radioresistance in head and neck squamous cell carcinoma: From radioresistant HNSCC cell line to integrated bioinformatics methods

Xiaojun Tang, Qinglai Tang, Xinming Yang, Zi-An Xiao, Gangcai Zhu, Tao Yang, Qian Yang, Ying Zhang* and Shisheng Li*

Department of Otolaryngology Head and Neck Surgery, The Second Xiangya Hospital of Central South University, Changsha, China

Background: Radioresistance in head and neck squamous cell carcinoma (HNSCC) patients means response failure to current treatment. In order to screen radioresistant biomarkers and mechanisms associated with HNSCC, differentially expressed genes (DEGs) associated with radioresistance in HNSCC were investigated.

Methods: The HNSCC cell line with radioresistance, Hep2-R, was established and detected the radiosensitivity using MTT, colony formation assay and flow cytometry analysis. Clariom™ D chip was applied to compare DEGs between Hep2 and Hep2-R groups and build the differential gene expression profiles associated with radioresistance in HNSCC. Bioinformatic analysis were used to find biological functions and pathways that related to radioresistance in HNSCC, including cell adhesion, cytochrome P450 and drug metabolism. Gene Expression Omnibus (GEO) datasets were selected to verify DEGs between HNSCC radioresistant cells and tissues. The representation of DEGs were validated between HNSCC patients with complete response and post-operative radiation therapy failure. In addition, we evaluated the clinical prognosis of DEGs using The Cancer Genome Atlas (TCGA) database.

Results: 2,360 DEGs (|Fold Change|>1.5, $p < 0.05$) were identified between Hep2 and Hep2-R, including 1,144 upregulated DEGs and 1,216 downregulated DEGs. They were further verified by HNSCC radioresistant cells and tissues in GEO. 13 radioresistant DEGs showed same difference in expression level between cells and tissues. By comparing 13 DEGs with HNSCC patients, upregulations of FN1, SOX4 and ETV5 were found identical with above results. Only FN1 was a prognostic indicator of HNSCC in TCGA.

Conclusion: FN1 is the potential novel biomarker for predicting poor prognosis and radioresistance in HNSCC patients. Overexpression of FN1 plays an important role in the tumorigenesis, prognosis and radioresistance of HNSCC.

KEYWORDS
head and neck squamous cell carcinoma, radioresistance, bioinformatics methods, radioresistant HNSCC cell line, prognosis

Introduction

Head and neck squamous cell carcinoma (HNSCC) is seventh malignancies globally, which develops from mucosal epithelium in the nasal cavity, oral cavity, pharynx and larynx (Castellanos and Pan, 2016; Johnson et al., 2020; Pei et al., 2020). Over 60% patients with HNSCC are diagnosed at an advanced stage resulting in poor prognosis. Treatments including surgery, radiotherapy, chemotherapy and targeted therapy can reduce recurrence and prolong survival, while resistance to radiotherapy restricts the 5-year survival rate of HNSCC patients (Porcheri and Mitsiadis, 2021).

For HNSCC patients who are not suitable for surgery (advanced stage or co-existing diseases that cannot tolerate surgery), radiotherapy is a more suitable treatment (Jones et al., 2016; Kerawala et al., 2016; Mehanna et al., 2016; Pracy et al., 2016). Tumor tissues are more sensitive to radiation comparing with normal tissues because unable to repair damaged DNA quickly, while the biological complexity and heterogeneity of cancer result in inherent radioresistance (Mendenhall et al., 2001). The survival of HNSCC patients is restricted by existence of inherent radioresistant tumor cells and radioresistance after fractional radiotherapy, which leading to local recurrence and distant metastasis. When surgery is performed as a salvage method after radiotherapy failure, the rate of complications increase (Aarts et al., 2011). Therefore, radioresistance of HNSCC has become an important factor restricting the clinical efficacy of HNSCC and prolonging the survival of patients.

The mechanism of radioresistance in HNSCC has also become a recent research hotspot. The disruption of proliferation, apoptosis, DNA damage response and repair, angiogenesis, epithelial-mesenchymal transition and cancer stem cells are known as contributors to radioresistance in HNSCC (Chang et al., 2013; Brown, 2014; Barker et al., 2015; Ahmad et al., 2017). TP53 mutations were associated with apoptosis and increased radioresistance in HNSCC (Skinner et al., 2012). The most frequently mentioned pathways leading to the development of HNSCC radioresistance are EGFR, PI3K/AKT, and RAS Pathways (Zimmermann et al., 2006; Chang et al., 2013; Perri et al., 2015). Although there have been studies to explore the mechanism of radioresistance, the exact mechanism of radioresistance in HNSCC is still not completely clear up to now.

The clinical efficiency of HNSCC is greatly restricted by radioresistance. For exploring the characteristics and mechanism of radioresistant HNSCC, differentially expressed genes (DEGs) association with radioresistance were investigated in HNSCC using transcriptome analysis and public databases. The present study provides new markers for predicting radioresistance or targets for improving radiosensitivity.

Materials and methods

Cell culture and establishment of radioresistant HNSCC cells

Human laryngeal squamous carcinoma cell line, Hep2 was purchased from the Institute of Biochemistry and Cell Biology of the Chinese Academy of Sciences, Shanghai, China. The cells were cultured with RPMI medium 1,640(Corning, United States) containing 10% fetal bovine serum (Corning, United States) and 1% antibiotics (Gibco-BRL, Gaithersburg, MD, United States), and incubated at 37 °C with saturated humidity and 5% CO2. Radioresistant Hep2 (termed Hep2-R) was established by exposure repeated radiation of Hep2 with 8 Gy for 6 times (Zhou et al., 2020). For Hep2-R the D0 was 2.512 Gy, n was 2.52, Dq was 2.322 Gy, and D37 was 4.83 Gy, which compared to 1.879 Gy, 2.003,1.305 Gy, and 3.185 Gy for Hep2.

Viability of radioresistant HNSCC cells

The viability and proliferation of above cells were verified by MTT assay, colony formation assay and flow cytometry. All experiments were carried out in five samples.

Cell proliferation was monitored by use of 2-(4,5-dimethyltriazol-2-yl)-2,5-diphenyl tetrazolium bromide (MTT, Sigma) assay. Briefly, Hep2 and Hep2-R were re-seeded into 96-well plate with 2×10^3 cells per well and culture for 6 h. Exposed to 8 Gy and indicated for 72 h, 20 μL of MTT was added to each well and incubated at 37 °C with 5% CO2 for 4 h. After adding 150 μL of dimethyl sulfoxide, the optical density at 450 nm was measured for each sample using a Bio-rad 550 Microplate Reader.

In the colony formation assay, Hep2 and Hep2-R were re-seeded in 6-well plates at a density of 1×10^3 cells per well and exposed to 8 Gy. The cells were cultured for 14 days then washed twice with PBS, fixed with methanol for 15 min, and stained with 0.1% crystal violet solution for another 20 min at room temperature. Five randomly chosen fields were taken by an inverted microscope to count the number of colonies, and the mean was taken.

An apoptosis assay was detected by AnnexinV-FITC/PI kit, and flow cytometry analysis was conducted using a BD LSR II flow cytometer. After exposing to 8 Gy and indicating for 72 h, Cells were collected and resuspended. The process was performed according to the manufacturer's instructions.

DEGs identification using microarray

According to the manufacturer's protocol, total RNA was extracted from HNSCC radioresistant cell line Hep2-R and

parental cell line Hep2 using TRIzol (Invitrogen, Carlsbad, CA, United States). Total RNA was tested integrity and construction by Agilent 2,100 Bioanalyzer (RIN≥7.0 and 28S/18S>0.7) and Thermo NanoDrop 2000 (1.7 < A260/A280 < 2.2). After constructing a RNA library for sequencing, cDNA was prepared by GeneChip WT PLUS Kit. The cDNA was purified and segmented, and hybridized with the chip probe. The chip was washed and dyed, and images and original data were obtained by scanning After the hybridization.

Identifying DEGs using databases

In Gene Expression Omnibus (GEO) database (https://www.ncbi.nlm.nih.gov/geo), GSE9712, GSE9713 and GSE9714 are based on the platform of GPL 96, detecting DEGs in radioresistant and radiosensitive tumors and cell lines in HNSCC. GSE9712, GSE9713 and GSE9714 belong to SuperSeries GSE9716. GSE9712 detected DEGs in radioresistant tumors, GSE9713 Detected DEGs in radioresistant and radiosensitive tumors before and after irradiation, and GSE9714 explored DEGs in radioresistant and radiosensitive human head and neck tumor cell lines. Radiosensitive human head and neck tumor cell lines is SCC-61. Nu61, a radioresistant human head and neck tumor cell lines, was selected from a parental radiosensitive tumor SCC-61 by eight serial cycles of passage in athymic nude mice and *in vivo* irradiation. Obtained tumors were established as xenografts in nude mice using SCC-61 and Nu61 (Khodarev et al., 2004; Khodarev et al., 2007). GSE67614 was used to validate the findings, containing 102 HNSCC specimens from surgically excised tumors. These specimens are from patients treated by post-operative radiation therapy and are being used to develop gene signatures for therapeutic response. For identifying DEGs, both R and GEO2R were used (https://www.ncbi.nlm.nih.gov/geo/geo2r/). Genes with $|\log FC| \geq 1$ and $p < 0.05$ were regarded as DEGs.

The prognostic value and protein expression of FN1

The prognostic value of FN1 was obtained from the gene expression profiling interactive analysis (GEPIA) database (http://gepia.cancer-pku.cn/index.html). The protein location of FN1 was detected using human protein atlas (HPA).

Statistical analysis

All statistical analyses were analyzed using a SPSS (version 24.0; SPSS Inc., Chicago,IL). Data are presented as the mean ± standard deviation. Student's t-test was used to compare the differences between the two groups. Statistical significance was set at $p < 0.05$.

Results

Hep2-R was successfully established by intermittent and repeated sub-lethal dose X-ray radiation

To explore cell proliferation and radioresistant capacity after exposure to radiation, MTT assay and colony formation assay were applied. As shown in Figure 1A, the proliferation rate of Hep2-R was higher than that of the control group ($p < 0.05$). As shown in Figure 1C, after explosion under the same conditions, the clone formation rate of Hep2-R was higher than that of the control group ($p < 0.05$). Furthermore, Hep2 showed significant apoptosis compared to Hep2-R (Figure 1B). These results indicated that Hep2-R decreased the sensitivity of Hep2 to X-ray irradiation.

Radioresistance causes a differential gene expression profile

To identify radioresistant differentially expressed genes (DEGs), RNA sequencing (RNA-seq) technology was used. 2,360 DEGs were identified (absolute average fold change >1.5 and $p < 0.05$), of which 1,144 were upregulated and 1,216 were downregulated. The names of these 2,360 DEGs and their average fold change are shown in Supplementary Table S1 and volcano plot was showed in Figure 2A.

Hierarchical clustering, gene-ontology and kyoto encyclopedia of genes and genomes pathways analysis of the differential expressed genes

To get more insight on the biological significance of the radioresistant DEGs, hierarchical clustering was performed. All DEGs were hierarchically grouped into four groups (Figure 2B). The genes within the same cluster are coregulated genes, and may have similar biological functions during bronchial epithelial carcinogenesis. GO analysis revealed that DEGs are enriched with the genes of different functions, such as tissue development, regulation of cell proliferation (Figure 2C). KEGG pathway analysis showed that DEGs involved in 10 signaling pathways (Figure 2D). The DEGs may play a role in radioresistance by these signaling pathways. The DEGs were enriched in pathways including "steroid hormone biosynthesi", "ascorbate and aldarate metabolism", "pentose and glucuronate interconversions", "drug metabolism—other enzymes", "focal adhesion", "starch and sucrose metabolism", "porphyrin and chlorophyll metabolism",

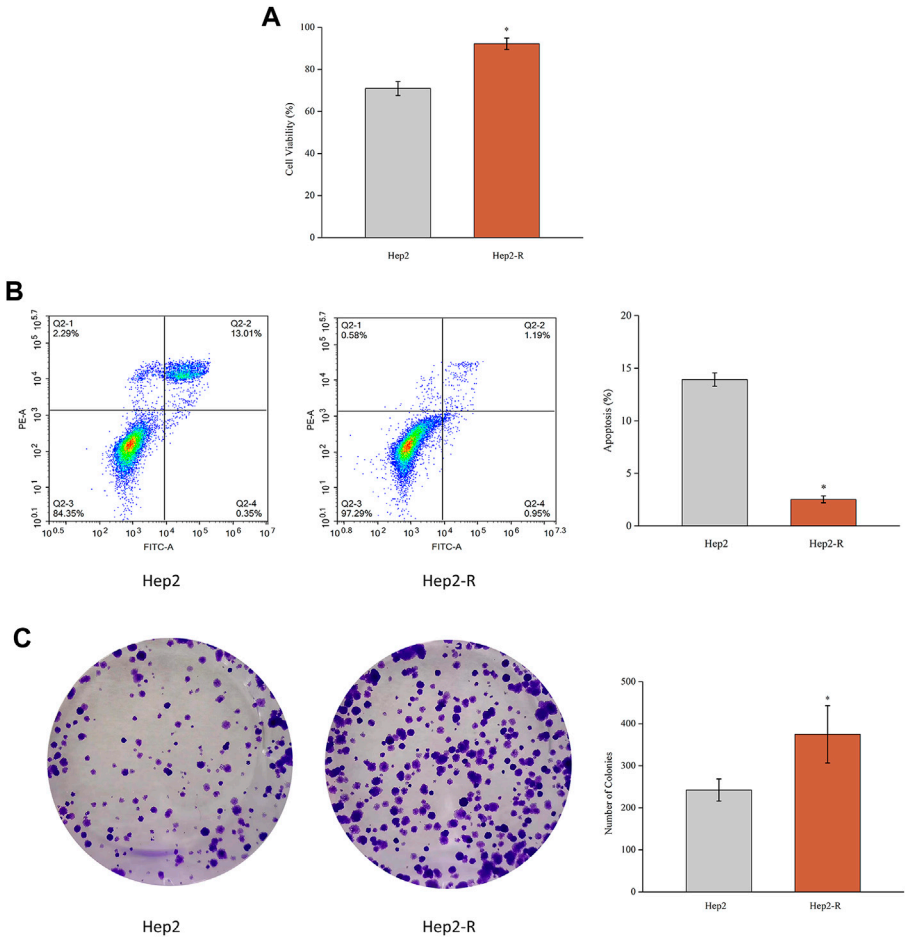

FIGURE 1
(A) MTT assay was performed to measure the viability of Hep2 and Hep2-R. **(B)** Apoptosis of Hep2 and Hep2-R were detected on flow cytometry. **(C)** The clone formation rate of Hep2-R was higher than Hep2. *$p < 0.05$.

"metabolism of xenobiotics by cytochrome P450", "drug metabolism—cytochrome P450", and "retinol metabolism".

Identifying biomarkers in radioresistant HNSCC cells and tissues

We previously constructed HNSCC radioresistant cell line, Hep2-R, by repeated X-ray irradiation on Hep2. In addition, we also analyzed the DEGs between radioresistant HNSCC cells and tissues using GEO dataset SuperSeries GSE9716, including GSE9712, GSE9713 and GSE9714. In GSE9714, two radioresistant and two radiosensitive HNSCC cell lines were selected. All tumor samples between GSE9712 and GSE9713 were divided into four subsets according to irradiation: Subset 1 (six radiosensitive tumors versus six radioresistant tumors without irradiation, Figure 3A), Subset 2 (three radiosensitive tumors versus three radioresistant tumosr with irradiation, Figure 3B), Subset 3 (three radiosensitive tumors versus three radioresistant tumors 5 h after irradiation, Figure 3C), Subset 4 (three radiosensitive tumors versus three radioresistant tumors 24 h after irradiation, Figure 3D). The Venn diagram revealed that a total of 13 DEGs were found when our data (Hep2 versus Hep2-R) and GSE9714 compared with above four subsets. Six genes were overexpressed and seven genes were lowly expressed in radioresistant cells and tissues in comparison with the normal with absolute average fold change >1 and $p < 0.05$ (Figure 3).

Upregulation of FN1, SOX4 and ETV5 contributes to the radioresistance of HNSCC

To verify this deduction, we also analyzed the 13 DEGs in surgically excised tumor tissues between radiosensitive and

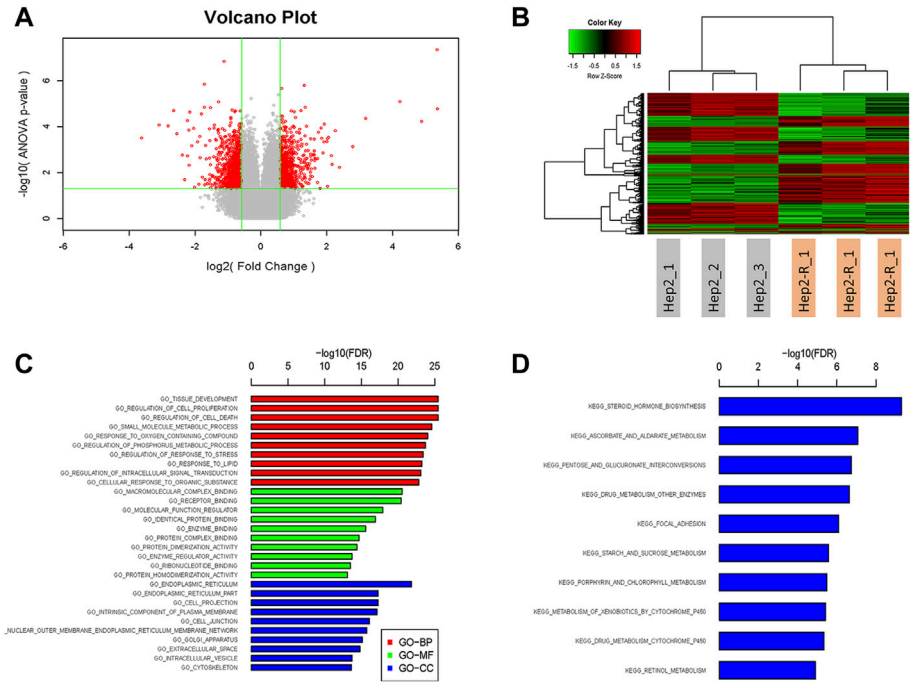

FIGURE 2
Volcano plot **(A)**, Hierarchical clustering **(B)**, GO analysis **(C)** and KEGG pathway analysis **(D)** of 2,360 differentially expressed genes.

radioresistant patients in GEO dataset in GSE67614. Except U2SURP, 12 DEGs were identified in GSE67614.50 tumor tissues from HNSCC radiosensitive patients and 52 from radioresistant HNSCC patients were selected. All HNSCC patients had surgery and post-operative radiation therapy. Figure 4A showed that tumor tissues with post-operative radiation therapy failure had higher expression of upregulated radioresistant genes FN1, SOX4 and ETV5, while none of the downregulated radioresistant genes were downregulated simultaneously (Figure 4B). Therefore, we speculated that high expression of FN1, SOX4 and ETV5 might be important biomarkers of HNSCC radioresistance. The above three proteins affected the radiosensitivity of HNSCC *in vivo*.

High level of FN1 is a prognostic indicator of HNSCC

Aiming to understand the association of above DEGs (FN1, SOX4 and ETV5) with HNSCC prognosis, the alterations of them were explored through HNSCC TCGA dataset. Overexpression of FN1, SOX4 and ETV5 were found in 43 paired samples between paracancerous tissues and tumor tissues of HNSCC (Figure 5A). While only FN1 was associated with prognosis when all HNSCC samples in TCGA dataset were included (Figure 5B). As a risk factor, FN1 not only affected the prognosis of patients with HNSCC, but also affects other types of squamous cell carcinomas (lung squamous cell carcinoma and cervical squamous cell carcinoma) or other types of carcinomas in TCGA dataset (Figure 6). Figure 5C showed that FN1 overexpressed in HNSCC, meaning protein expression was consistent with mRNA expression in HNSCC tissues.

Discussion

Radioresistance restricts the prognosis of HNSCC, therefore it is crucial to find biomarkers and therapeutic targets associated with radiosensitivity. In the present study, differential expression profile of genes associated with radioresistance in HNSCC was established using transcriptome analysis. Based on DEG analysis of the HNSCC radioresistant cells and tissues in public databases, 13 DEGs were identified. FN1, SOX4 and ETV5 were further validated in HNSCC patients' tumor tissues with irradiated failures, which is novel radioresistance biomarkers in HNSCC. Furthermore, a comprehensive database analysis showed that FN1 had a high expression level between HNSCC patients with post-operative radiation therapy failure and tumor tissues of HNSCC from the GEO and TCGA. From GEPIA, patients harboring an increased expression of FN1 not only have a poor prognosis in HNSCC, but also in other 2 types of squamous cell carcinomas, such as lung squamous cell

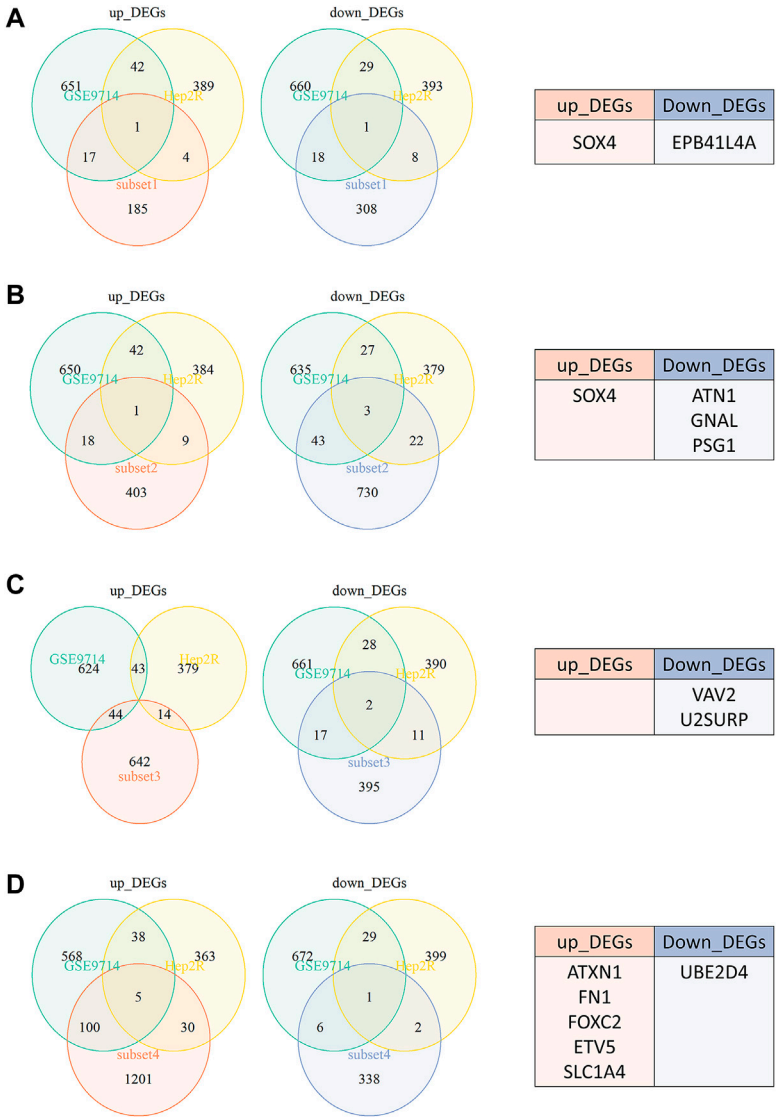

FIGURE 3
The Venn diagram revealed that a total of 13 DEGs were found when our data (Hep2 versus Hep2-R) and GSE9714 compared with four subsets. **(A)** Subset 1-six radiosensitive tumors versus six radioresistant tumors without irradiation. **(B)** Subset 2-three radiosensitive tumors versus three radioresistant tumosr with irradiation. **(C)** Subset 3-three radiosensitive tumors versus three radioresistant tumors 5 h after irradiation. **(D)** Subset 4-three radiosensitive tumors versus three radioresistant tumors 24 h after irradiation.

carcinoma and cervical squamous cell carcinoma. Considering the level of FN1 under different conditions, it is rational that FN1 affects the prognosis of HNSCC, and radiation could enhance the transcriptional level of FN1.

KEGG, as an integrated database, provides networks of generic molecular and understanding of disease mechanisms (Kanehisa et al., 2021). The mechanisms underlying HNSCC radioresistance not yet been fully elucidated. In our study, mechanism was analyzed with KEGG. The DEGs were enriched in pathways including "steroid hormone biosynthesi", "ascorbate and aldarate metabolism", "pentose and glucuronate interconversions", "drug metabolism—other enzymes", "focal adhesion", "starch and sucrose metabolism", "porphyrin and chlorophyll metabolism", "metabolism of xenobiotics by cytochrome P450", "drug metabolism—cytochrome P450", and "retinol metabolism". These results suggested that cell adhesion, cytochrome P450 and drug metabolism were associated with HNSCC radioresistance. Focal adhesion signaling includes integrins and epidermal growth factor receptors (EGFR), several kinases and adapter molecules, which impacted on contact and connection between cell and extracellular matrix (ECM) and contributed to tumor development and progression (Eke and

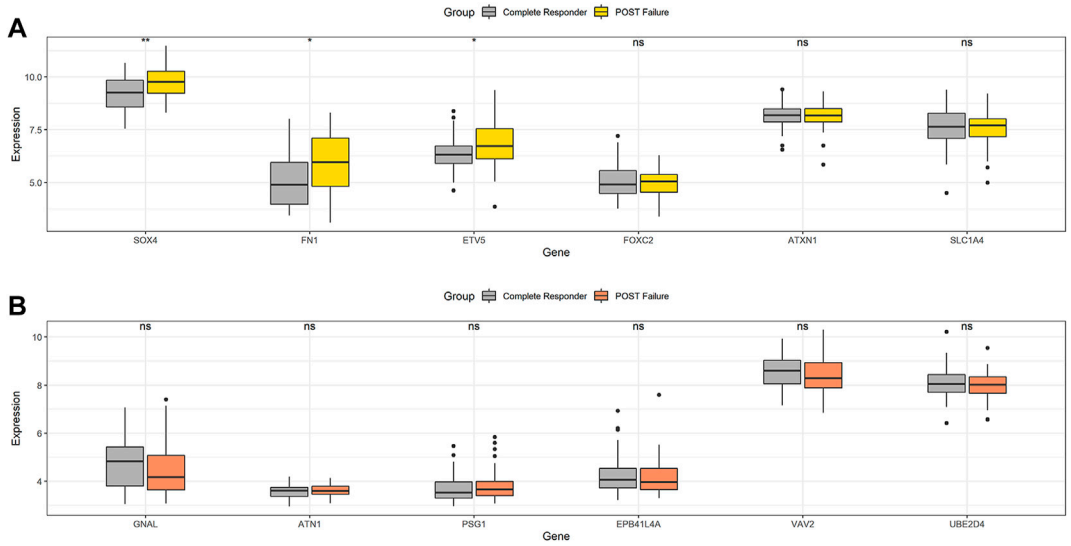

FIGURE 4
In GSE67614, tumor tissues with post-operative radiation therapy failure had higher expression of upregulated radioresistant genes FN1, SOX4 and ETV5 **(A)**, while none of the downregulated radioresistant genes were downregulated simultaneously **(B)**. *$p < 0.05$, **$p < 0.01$.

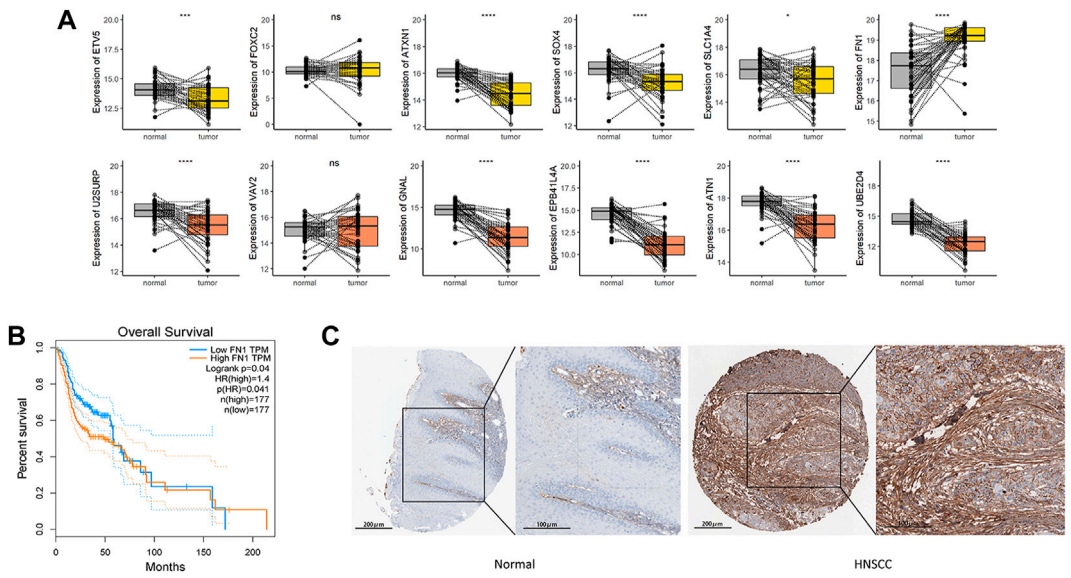

FIGURE 5
(A) In HNSCC TCGA dataset, overexpression of FN1, SOX4 and ETV5 were found in 43 paired samples between paracancerous tissues and tumor tissues. **(B)** While only FN1 was associated with prognosis when all HNSCC samples in TCGA dataset were included. **(C)** FN1 overexpressed in HNSCC tissues, meaning protein expression was consistent with mRNA expression. ***$p < 0.001$, ****$p < 0.0001$.

Cordes, 2015). Integrins and EGFR not only regulate tumorigenesis and metastasis but also modulate radioresistance. Recent studies illustrate β1 integrin inhibition enhanced radiosensitivity in HNSCC, mainly impacting on β1 Integrin/FAK/cortactin signaling (Eke et al., 2012a; Eke et al., 2012b). αV integrin enhances radioresistance in human nasopharyngeal carcinoma *via* SAPK/JNK pathway (Ou et al., 2012). Overexpression of EGFR indicates poor prognosis, and targeted agents of EGFR enhanced radiosensitivity (Bonner et al., 2006; Cohen, 2014). The Molecular interplays between integrin and

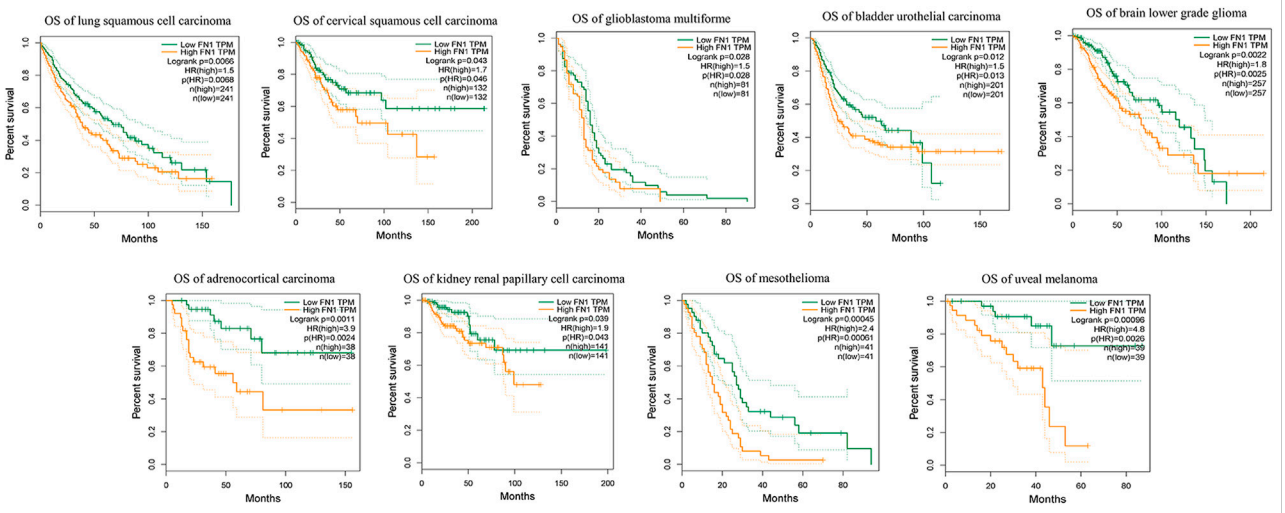

FIGURE 6
As a risk factor, FN1 not only affected the prognosis of patients with HNSCC, but also affects other types of squamous cell carcinomas or other types of carcinomas in TCGA dataset.

EGFR cannot be ignored. EGFR and integrin in astrocytoma frozen sections predict clinical outcome and correlate with radioresistance *in vitro* (Petras et al., 2013). The efficacy of EGFR inhibition in HNSCC cells can be enhanced by joint targeting of EGFR and β1 integrin (Eke and Cordes, 2011; Eke et al., 2013).

Our study revealed 19 DEGs enriched in focal adhesion, including Fibronectin 1 (FN1). FN1 locates in both cell surface and extracellular matrix of multiple cell types, linking matrices and cells. As a member of the fibronectin family, FN1 involves in embryologic development, wound healing, hematopoiesis (Wang and Ni, 2016) and infections (Speziale et al., 2019). FN1 in the tumor cells is called cancerous fibronectin, and related to malignancy, metastasis or poor prognosis of tumor (Steffens et al., 2012; Lin et al., 2020; Sun et al., 2020). FN1 interacted with binding partner ITGA5 and promoted viability, invasion, and migration in colorectal cancer through suppressing apoptosis (Sun et al., 2020). FN1 was bound by miR-1271 in neuroglioma (Gong et al., 2017). In HNSCC, several studies have proved FN1 was potential diagnostic indicators and involved in focal adhesion signaling pathway (Li et al., 2019) using integrated bioinformatics methods (Kuang et al., 2016). However, the importance of FN1 on the HNSCC radiation resistance is still unclear. Our study identified FN1 was an up-regulated genes related to worse prognosis and radioresistance, and enriched in focal adhesion pathway. These results suggested that FN1 overexpression is an indicator for poor prognosis and radioresistance, and focal adhesion may be associated with radioresistance in HNSCC.

In this study, SOX4 and ETV5 showed association with radioresistance in HNSCC. SOX4 belongs to the C subgroup of the SOX family, which involve in many developmental processes. High-expressed SOX4 affected tumor development (Fang et al., 2012; Zhang et al., 2012; Wang et al., 2013) or radioresistance (Xue et al., 2021) in many cancers. In HNSCC, Study from Yoon et al. (Yoon et al., 2015) proved that SOX4 may serve as an oncogene and causes radioresistance. E26 transformation-specific (ETS) transcription factors including ETV5, play important roles in tumor cell invasion, differentiation and angiogenesis (de Sousa et al., 2014). It has been reported that high levels of ETV5 facilitate tumor cell proliferation, epithelial-mesenchymal transition, and metastasis in ovarian and colorectal cancers (Llauradó et al., 2012; Cheng et al., 2019). The relation between ETV5 and radioresistant HNSCC is unclear, but ETV5 can overcome cetuximab resistance. Park et al. found that knockdown of ETV5 can increase cetuximab sensitivity in colon cancer cell lines (Park et al., 2019).

The important aspect of this study proved that overexpressed FN1 is correlated with radioresistance in HNSCC and enriched in focal adhesion pathway. Nevertheless, our study has limitations. The mechanisms underlying HNSCC radioresistance not yet been fully elucidated, additional studies *in vivo* and *in vitro* are needed to verify the actual value of the FN1. The present study provides important insights into novel prognostic indicators for patients with HNSCC radioresistance.

Conclusion

In summary, we established an expression profile of genes associated with radioresistance in HNSCC cells and tissues, and

found that FN1 was overexpressed in the HNSCC patients with radiation failure, suggesting that FN1 may contribute to tumorigenesis and radioresistance the in HNSCC. FN1 most likely involved in focal adhesion to regulate radiosensitivity. FN1 is an indicator for prognostic and radioresistamce in HNSCC patients.

Data availability statement

The datasets presented in this study can be found in online repositories. The names of the repository/repositories and accession number(s) can be found in the article/Supplementary Material.

Author contributions

XT: Conceptualization, Methodology, Investigation, Formal analysis, Writing—Original Draft. QT: Verification, Writing—Review and Editing, Funding acquisition. XY: Verification, Writing—Review and Editing. Z-AX: Verification, Writing—Review and Editing. GZ: Resources, Funding. TY: Formal analysis, Funding. QY: Formal analysis. YZ and SL: Conceptualization, Resources, Writing—Review and Editing, Supervision, Funding.

Funding

This work was supported by the National Natural Science Foundation of China (No. 81870711, No. 82002895 and No. 82173341) and the Natural Science Foundation of Hunan Province (No. 2020JJ4791).

Acknowledgments

The authors wish to acknowledge National Natural Science Foundation of China and Natural Science Foundation of Hunan Province for their financial supports.

Conflict of interest

The handling editor CC declared a shared parent affiliation with the authors at the time of the review.

The authors declare that the research was conducted in the absence of any commercial or financial relationships that could be construed as a potential conflict of interest.

Publisher's note

All claims expressed in this article are solely those of the authors and do not necessarily represent those of their affiliated organizations, or those of the publisher, the editors and the reviewers. Any product that may be evaluated in this article, or claim that may be made by its manufacturer, is not guaranteed or endorsed by the publisher.

Supplementary material

The Supplementary Material for this article can be found online at: https://www.frontiersin.org/articles/10.3389/fgene.2022.1017762/full#supplementary-material

References

Aarts, M. C., Rovers, M. M., Grau, C., Grolman, W., and Gj, V. D. H. (2011). Salvage laryngectomy after primary radiotherapy: What are prognostic factors for the development of pharyngocutaneous fistulae? Otolaryngology--head and neck surgery. *Otolaryngol. Head. Neck Surg.* 144, 5–9. doi:10.1177/0194599810390914

Ahmad, P., Sana, J., Slavik, M., Slampa, P., Smilek, P., and Slaby, O. (2017). MicroRNAs involvement in radioresistance of head and neck cancer. *Dis. Markers* 2017, 8245345. doi:10.1155/2017/8245345

Barker, H. E., Paget, J. T., Khan, A. A., and Harrington, K. J. (2015). The tumour microenvironment after radiotherapy: Mechanisms of resistance and recurrence. *Nat. Rev. Cancer* 15, 409–425. doi:10.1038/nrc3958

Bonner, J. A., Harari, P. M., Giralt, J., Azarnia, N., Ang, K. K., Cohen, R. B., et al. (2006). Radiotherapy plus cetuximab for squamous-cell carcinoma of the head and neck. *N. Engl. J. Med. Overseas. Ed.* 354, 567–578. doi:10.1056/nejmoa053422

Brown, J. M. (2014). Vasculogenesis: A crucial player in the resistance of solid tumours to radiotherapy. *Br. J. Radiol.* 87, 20130686. doi:10.1259/bjr.20130686

Castellanos, M. R., and Pan, Q. (2016). Novel p53 therapies for head and neck cancer. *World J. Otorhinolaryngol. Head. Neck Surg.* 2, 68–75. doi:10.1016/j.wjorl.2016.05.005

Chang, L., Graham, P. H., Hao, J., Ni, J., Bucci, J., Cozzi, P. J., et al. (2013). Acquisition of epithelial-mesenchymal transition and cancer stem cell phenotypes is associated with activation of the PI3K/Akt/mTOR pathway in prostate cancer radioresistance. *Cell. Death Dis.* 4, e875. doi:10.1038/cddis.2013.407

Cheng, X., Jin, Z., Ji, X., Shen, X., Feng, H., Morgenlander, W., et al. (2019). ETS variant 5 promotes colorectal cancer angiogenesis by targeting platelet-derived growth factor BB. *Int. J. Cancer* 145, 179–191. doi:10.1002/ijc.32071

Cohen, R. B. (2014). Current challenges and clinical investigations of epidermal growth factor receptor (EGFR)- and ErbB family-targeted agents in the treatment of head and neck squamous cell carcinoma (HNSCC). *Cancer Treat. Rev.* 40, 567–577. doi:10.1016/j.ctrv.2013.10.002

de Sousa, V. P., Chaves, C. B., Huguenin, J. F., Moreira, F. C., de Reis, B. S., Chimelli, L., et al. (2014). ERM/ETV5 and RUNX1/AML1 expression in endometrioid adenocarcinomas of endometrium and association with neoplastic progression. *Cancer Biol. Ther.* 15, 888–894. doi:10.4161/cbt.28879

Eke, I., and Cordes, N. (2011). Dual targeting of EGFR and focal adhesion kinase in 3D grown HNSCC cell cultures. *Radiother. Oncol.* 99, 279–286. doi:10.1016/j.radonc.2011.06.006

Eke, I., and Cordes, N. (2015). Focal adhesion signaling and therapy resistance in cancer. *Semin. Cancer Biol.* 31, 65–75. doi:10.1016/j.semcancer.2014.07.009

Eke, I., Deuse, Y., Hehlgans, S., Gurtner, K., Cordes, N., Baumann, M., et al. (2012). β_1Integrin/FAK/cortactin signaling is essential for human head and neck cancer resistance to radiotherapy. *J. Clin. Invest.* 122, 1529–1540. doi:10.1172/JCI61350

Eke, I., Dickreuter, E., and Cor De S, N. (2012). Enhanced radiosensitivity of head and neck squamous cell carcinoma cells by β1 integrin inhibition. *Radiother. Oncol.* 104, 235–242. doi:10.1016/j.radonc.2012.05.009

Eke, I., Storch, K., Krause, M., and Cordes, N. (2013). Cetuximab attenuates its cytotoxic and radiosensitizing potential by inducing fibronectin biosynthesis. *Cancer Res.* 73, 5869–5879. doi:10.1158/0008-5472.CAN-13-0344

Fang, C. L., Hseu, Y. C., Lin, Y. F., Hung, S. T., Tai, C., Uen, Y. H., et al. (2012). Clinical and prognostic association of transcription factor SOX4 in gastric cancer. *PLoS One* 7, e52804. doi:10.1371/journal.pone.0052804

Gong, J., Wang, Z. X., and Liu, Z. Y. (2017). miRNA-1271 inhibits cell proliferation in neuroglioma by targeting fibronectin 1. *Mol. Med. Rep.* 16, 143–150. doi:10.3892/mmr.2017.6610

Johnson, D. E., Burtness, B., Leemans, C. R., Lui, V. W. Y., Bauman, J. E., and Grandis, J. R. (2020). Head and neck squamous cell carcinoma. *Nat. Rev. Dis. Prim.* 6, 92. doi:10.1038/s41572-020-00224-3

Jones, T. M., De, M., Foran, B., Harrington, K., and Mortimore, S. (2016). Laryngeal cancer: United Kingdom national multidisciplinary guidelines. *J. Laryngol. Otol.* 130, S75–s82. doi:10.1017/S0022215116000487

Kanehisa, M., Furumichi, M., Sato, Y., Ishiguro-Watanabe, M., and Tanabe, M. (2021). Kegg: Integrating viruses and cellular organisms. *Nucleic Acids Res.* 49, D545–d551. doi:10.1093/nar/gkaa970

Kerawala, C., Roques, T., Jeannon, J. P., and Bisase, B. (2016). Oral cavity and lip cancer: United Kingdom national multidisciplinary guidelines. *J. Laryngol. Otol.* 130, S83–s89. doi:10.1017/S0022215116000499

Khodarev, N. N., Beckett, M., Labay, E., Darga, T., Roizman, B., and Weichselbaum, R. R. (2004). STAT1 is overexpressed in tumors selected for radioresistance and confers protection from radiation in transduced sensitive cells. *Proc. Natl. Acad. Sci. U. S. A.* 101, 1714–1719. doi:10.1073/pnas.0308102100

Khodarev, N. N., Minn, A. J., Efimova, E. V., Darga, T. E., Labay, E., Beckett, M., et al. (2007). Signal transducer and activator of transcription 1 regulates both cytotoxic and prosurvival functions in tumor cells. *Cancer Res.* 67, 9214–9220. doi:10.1158/0008-5472.CAN-07-1019

Kuang, J., Zhao, M., Li, H., Dang, W., and Li, W. (2016). Identification of potential therapeutic target genes and mechanisms in head and neck squamous cell carcinoma by bioinformatics analysis. *Oncol. Lett.* 11, 3009–3014. doi:10.3892/ol.2016.4358

Li, B., Shen, W., Peng, H., Li, Y., Jia, L., Zheng, L., et al. (2019). Fibronectin 1 promotes melanoma proliferation and metastasis by inhibiting apoptosis and regulating EMT. *Onco. Targets. Ther.* 12, 3207–3221. doi:10.2147/OTT.S195703

Lin, T.-C., Yang, C.-H., Cheng, L.-H., Chang, W.-T., Lin, Y.-R., and Cheng, H.-C. (2020). Fibronectin in cancer: Friend or foe. *Cells* 9, E27. doi:10.3390/cells9010027

Llauradó, M., Abal, M., Castellví, J., Cabrera, S., Gil-Moreno, A., Pérez-Benavente, A., et al. (2012). ETV5 transcription factor is overexpressed in ovarian cancer and regulates cell adhesion in ovarian cancer cells. *Int. J. Cancer* 130, 1532–1543. doi:10.1002/ijc.26148

Mehanna, H., Evans, M., Beasley, M., Chatterjee, S., Dilkes, M., Homer, J., et al. (2016). Oropharyngeal cancer: United Kingdom national multidisciplinary guidelines. *J. Laryngol. Otol.* 130, S90–s96. doi:10.1017/S0022215116000505

Mendenhall, W. M., Amdur, R. J., Morris, C. G., and Hinerman, R. W. (2001). T1-T2N0 squamous cell carcinoma of the glottic larynx treated with radiation therapy. *J. Clin. Oncol.* 19, 4029–4036. doi:10.1200/JCO.2001.19.20.4029

Ou, J., Wei, L., Deng, J., Sa, R., and Liang, H. (2012). αV integrin induces multicellular radioresistance in human nasopharyngeal carcinoma via activating SAPK/JNK pathway. *Plos One* 7, e38737. doi:10.1371/journal.pone.0038737

Park, S. M., Hwang, C. Y., Cho, S. H., Lee, D., Gong, J. R., Lee, S., et al. (2019). Systems analysis identifies potential target genes to overcome cetuximab resistance in colorectal cancer cells. *FEBS J.* 286, 1305–1318. doi:10.1111/febs.14773

Pei, S., Chen, L., Yang, Y., and Zhu, X. (2020). Identification of genes associated with cancer stem cell characteristics in head and neck squamous cell carcinoma through co-expression network analysis. *Head. Neck* 42, 2460–2472. doi:10.1002/hed.26266

Perri, F., Pacelli, R., Della Vittoria Scarpati, G., Cella, L., Giuliano, M., Caponigro, F., et al. (2015). Radioresistance in head and neck squamous cell carcinoma: Biological bases and therapeutic implications. *Head. Neck* 37, 763–770. doi:10.1002/hed.23837

Petras, M., Lajtos, T., Friedlaender, E., Klekner, A., Pinty, E., Feuerstein, B. G., et al. (2013). Molecular interactions of ErbB1 (EGFR) and integrin-β1 in astrocytoma frozen sections predict clinical outcome and correlate with Akt-mediated *in vitro* radioresistance. *Neuro. Oncol.* 15, 1027–1040. doi:10.1093/neuonc/not046

Porcheri, C., and Mitsiadis, T. A. (2021). New scenarios in pharmacological treatments of head and neck squamous cell carcinomas. *Cancers* 13, 5515. doi:10.3390/cancers13215515

Pracy, P., Loughran, S., Good, J., Parmar, S., and Goranova, R. (2016). Hypopharyngeal cancer: United Kingdom national multidisciplinary guidelines. *J. Laryngol. Otol.* 130, S104–s110. doi:10.1017/S0022215116000529

Skinner, H. D., Sandulache, V. C., Ow, T. J., Meyn, R. E., Yordy, J. S., Beadle, B. M., et al. (2012). TP53 disruptive mutations lead to head and neck cancer treatment failure through inhibition of radiation-induced senescence. *Clin. Cancer Res.* 18, 290–300. doi:10.1158/1078-0432.CCR-11-2260

Speziale, P., iola, C. A. r., and Pietrocola, G. (2019). Fibronectin and its role in human infective diseases. *Cells* 8, 1516. doi:10.3390/cells8121516

Steffens, S., Schrader, A. J., Vetter, G., Eggers, H., Blasig, H., Becker, J., et al. (2012). Fibronectin 1 protein expression in clear cell renal cell carcinoma. *Oncol. Lett.* 3, 787–790. doi:10.3892/ol.2012.566

Sun, Y., Zhao, C., Ye, Y., Wang, Z., He, Y., Li, Y., et al. (2020). High expression of fibronectin 1 indicates poor prognosis in gastric cancer. *Oncol. Lett.* 19, 93–102. doi:10.3892/ol.2019.11088

Wang, L., Zhang, J., Yang, X., Chang, Y. W., Qi, M., Zhou, Z., et al. (2013). SOX4 is associated with poor prognosis in prostate cancer and promotes epithelial-mesenchymal transition *in vitro*. *Prostate Cancer Prostatic Dis.* 16, 301–307. doi:10.1038/pcan.2013.25

Wang, Y., and Ni, H. (2016). Fibronectin maintains the balance between hemostasis and thrombosis. *Cell. Mol. Life Sci.* 73, 3265–3277. doi:10.1007/s00018-016-2225-y

Xue, T., Yin, G., Yang, W., Chen, X., Liu, C., Yang, W., et al. (2021). MiR-129-5p promotes radio-sensitivity of NSCLC cells by targeting SOX4 and RUNX1. *Curr. Cancer Drug Targets* 21, 702–712. doi:10.2174/1568009621666210415094350

Yoon, T. M., Kim, S. A., Cho, W. S., Lee, D. H., Lee, J. K., Park, Y. L., et al. (2015). SOX4 expression is associated with treatment failure and chemoradioresistance in oral squamous cell carcinoma. *BMC cancer* 15, 888. doi:10.1186/s12885-015-1875-8

Zhang, J., Liang, Q., Lei, Y., Yao, M., Li, L., Gao, X., et al. (2012). SOX4 induces epithelial-mesenchymal transition and contributes to breast cancer progression. *Cancer Res.* 72, 4597–4608. doi:10.1158/0008-5472.CAN-12-1045

Zhou, Z. R., Wang, X. Y., Yu, X. L., Mei, X., Chen, X. X., Hu, Q. C., et al. (2020). Building radiation-resistant model in triple-negative breast cancer to screen radioresistance-related molecular markers. *Ann. Transl. Med.* 8, 108. doi:10.21037/atm.2019.12.114

Zimmermann, M., Zouhair, A., Azria, D., and Ozsahin, M. (2006). The epidermal growth factor receptor (EGFR) in head and neck cancer: Its role and treatment implications. *Radiat. Oncol.* 1, 11. doi:10.1186/1748-717X-1-11

frontiers | Frontiers in Genetics

TYPE Original Research
PUBLISHED 05 October 2022
DOI 10.3389/fgene.2022.1021473

OPEN ACCESS

EDITED BY
Rui Cao,
Capital Medical University, China

REVIEWED BY
Hailong Ma,
Shanghai Jiao Tong University, China
Qiang Wang,
Chinese Academy of Medical Sciences and Peking Union Medical College, China
Xizhe Liu,
Sun Yat-sen University, China

*CORRESPONDENCE
Shifang Peng,
sfp1988@csu.edu.cn
Yani Yin,
yinyani@csu.edu.cn

†These authors have contributed equally to this work

SPECIALTY SECTION
This article was submitted to Cancer Genetics and Oncogenomics, a section of the journal Frontiers in Genetics

RECEIVED 17 August 2022
ACCEPTED 22 September 2022
PUBLISHED 05 October 2022

CITATION
Xiao J, Li Y, Liu Y, Chen Y, He Z, Peng S and Yin Y (2022), The involvement of homeobox-C 4 in predicting prognosis and unraveling immune landscape across multiple cancers via integrated analysis.
Front. Genet. 13:1021473.
doi: 10.3389/fgene.2022.1021473

The involvement of homeobox-C 4 in predicting prognosis and unraveling immune landscape across multiple cancers *via* integrated analysis

Junbo Xiao[1,2,3†], Ying Li[4†], Yajun Liu[5], Yiqian Chen[6], Zixuan He[6], Shifang Peng[4*] and Yani Yin[1,2,3*]

[1]Department of Gastroenterology, Xiangya Hospital, Central South University, Changsha, Hunan, China, [2]Hunan International Scientific and Technological Cooperation Base of Artificial Intelligence Computer Aided Diagnosis and Treatment for Digestive Disease, Xiangya Hospital, Central South University, Changsha, China, [3]National Clinical Research Center for Geriatric Disorders, Xiangya Hospital, Central South University, Changsha, Hunan, China, [4]Department of Infectious Diseases, Xiangya Hospital, Central South University, Hunan Key Laboratory of Viral Hepatitis, Changsha, Hunan, China, [5]Department of Gastroenterology, Hunan Provincial People's Hospital, Hunan Normal University, Changsha, Hunan, China, [6]University of South China, HengYang Medical School, HengYang, Hunan, China

Background: There has been growing evidence that the aberrantly expressed Homeobox-C 4 (HOXC4) plays crucial roles in the development of some cancer types. However, it remains unclear as far as its expression patterns and prognostic significance are concerned, as is tumor immunity.

Methods: To investigate the expression levels and prognostic implications of HOXC4, multiple data sources were used in conjunction with quantitative real-time polymerase chain reaction (qRT-PCR) verification. Afterward, diverse immunological-related analyses, along with anti-cancer drug sensitivity, were performed in a number of cancer types. A further exploration of the underlying mechanisms of HOXC4 in tumorigenesis and immunity was carried out using the Gene Set Enrichment Analysis (GSEA) and the Gene Set Variation Analysis (GSVA).

Results: Based on extensive database mining, HOXC4 was ubiquitously expressed across 21 tumor cell lines and significantly higher than that of normal tissues in 21 tumor types. The outcome of survival analysis including overall survival (OS), disease-free interval (DFI), disease-specific survival (DSS) and progression-free interval (PFI) revealed that upregulation of HOXC4 expression in several cancers was associated with worse prognosis. Additionally, HOXC4 was observed to correlate closely with colon adenocarcinoma (COAD), head and neck squamous cell carcinoma (HNSC), lower grade glioma (LGG), liver hepatocellular carcinoma (LIHC), rectum adenocarcinoma (READ), and thyroid carcinoma (THCA) in terms of tumor immune cells infiltration. As a result of our comprehensive pan-cancer study, we have identified a significant link between the expression of HOXC4 and the efficacy of immunotherapy-related treatments, together with anti-cancer drug

sensitivity. As a final note, HOXC4 was found to modulate multiple signaling pathways involved in tumorigenesis and immunity.

Conclusion: HOXC4 has been implicated in our study for the first time as an oncogene in cancers with a poor prognosis, potentially laying the groundwork for promising clinical biomarkers and immunotherapy approaches.

KEYWORDS

HOXC4, pan-cancer, immune modulation, immunotherapy-related analysis, bioinformatic analysis

Introduction

As a worldwide health concern, cancer has gradually imposed a disheartening detriment to society's well-being and clinical practice (Siegel et al., 2021; Sung et al., 2021). The progress in diagnosing, assessing, and treating cancer continues to advance; however, the disease remains a major financial burden around the world (Bragazzi and Sellami, 2021). As of today, there are not any definite cures. Lack of early diagnosis, local recurrence, distant metastasis, and chemotherapeutic resistance are considered to be the major barriers to poor survival for cancer patients. In light of this, it is imperative that novel methods be explored in order to screen potential diagnostic biomarkers and accordingly to develop corresponding cancer therapy.

Homeobox (HOX) genes, originally associated with developmental process (Gehring and Hiromi, 1986), encode transcription factors that play essential roles for maintaining morphogenesis in multicellular organisms (Arnold et al., 2020). As evidence accumulates over recent decades, dysregulation of HOX genes is implicated in carcinogenesis, the cluster of which Homeobox-C (HOXC) 4 is included (Luo and Farnham, 2020). It has been proved that aberrant expression of HOXC4 contributes to the occurrence and progression of multiple cancers, including prostate cancer, colon cancer, bladder cancer, lung cancer, etc. (Omatu, 1999; Cantile et al., 2003; Leyten et al., 2015). Recently, evidence was presented that HOXC4 can be used to detect prostate cancer at an early stage and predict recurrence, thus indicating its potential as an oncogenic promoter (Miller et al., 2003; Luo and Farnham, 2020). As yet, little is known about the critical role of HOXC4 in pan-cancer.

A great deal of attention has hitherto been paid to immunity-related mechanisms and immunotherapeutics, including determining how immunity interacts with cancer and identifying novel biomarkers for immunotherapy (Gravitz, 2013). It has been established that the tumor microenvironment (TME), especially the tumor immune microenvironment (TIME), is an integral factor of tumor prognosis (Locy et al., 2018). A dramatic shift has occurred from complicated mechanistic protocols to first-line regimens in immunotherapy, which targets microsatellite instability (MSI) and tumor mutational burden (TMB) as well as TME. (Frankel et al., 2017; Chang et al., 2018; Chan et al., 2019; Kalantari Khandani et al., 2020). In recent decades, immunotherapy has shown impressive effectiveness against cancer. There are a number of emerging therapeutic strategies, including PD-1/PD-L1 inhibitors, being used for the treatment of several types of cancer, including colon and lung cancer (Li et al., 2019). However, current checkpoint immunotherapy can only benefit a small number of patients with cancer. To the best of our knowledge, there is still a lack of clarity regarding HOXC4-associated immunotherapy and its underlying mechanisms and functions.

Data for the present study were analyzed from several databases, including the Cancer Genome Atlas (TCGA), Cancer Cell Line Encyclopedia (CCLE), and Genotype Tissue-Expression (GTEx). An in-depth analysis of HOXC4 expression in multiple types of malignancies and its relationship with survival outcomes was performed. In the following analysis, immunological correlations were systematically performed, focusing on HOXC4 expression in different tumor types in relation to TME, immune cell infiltration, MSI, and TMB. Co-expression analysis was then carried out with the mismatch repair (MMR) genes, DNA methylation, and immune-related genes. In addition, Gene Set Enrichment Analysis (GSEA) and Gene Set Variation Analysis (GSVA) were conducted to further explore how HOXC4 might contribute to tumorigenesis. Additionally, various compounds were analyzed in different cell lines to determine the likelihood of resistance to chemotherapy drugs. The findings of this study suggest that HOXC4 may serve as a latent candidate for therapeutic target associated with immunological strategies in a wide variety of cancer types, apart from serving as a prognostic biomarker. HOXC4-associated tumor immunotherapy may yield new insights into personalized treatment and shed new light on HOXC4-associated tumorigenesis.

Materials and methods

Data on HOXC4 expression and sample information

Data were obtained from TCGA database on the differential expression of HOXC4, as well as clinical and prognostic outcomes across numerous cancer types (https://portal.gdc.cancer.gov/) (Wang et al., 2016). Data showing insufficient information were excluded (survival time, for example) from a large amount of collected samples. Data from GTEx database was used to analyze HOXC4 expression in 31 normal tissues (https://commonfund.nih.gov/GTEx). HOXC4 gene expression was analyzed in 21 tumor cell lines using the CCLE database (https://portals.broadinstitute.org/ccle/). Our analysis included integration of TCGA and GTEx data to examine the expression differences of HOXC4 between cancer and normal tissues. A log2 (TPM+1) normalization was applied to the whole expression data. This study was conducted according to the flowchart of Supplementary Figure S1.

Tissue culture, RNA extraction and quantitative real-time polymerase chain reaction

Liver cancer patients with adjacent normal tissue samples (n = 8), colon cancer patients with adjacent normal tissue samples (n = 4) and breast cancer patients with adjacent normal tissue samples (n = 3) were collected from the Pathology Department of Xiangya Hospital, Central South University between December 2021 and March 2022,in which the tissue specimen was obtained in the process of diagnosis and treatment of patients after resection of tumor tissues, and is in full assurance of pathological diagnosis after being apart from the patients, in order to further verify HOXC4 expression (supplementary material of ethic approval).

Briefly, total RNAs (1 ug) were transcribed into cDNAs using the SuperScript III Reverse Transcriptase kit (Invitrogen, Carlsbad, CA, USA). RT-qPCR was performed using Geneseed® qPCR SYBR® Green Master Mix and monitored using the ABI PRISM 7500 Sequence Detection System (Applied Biosystems, Life Technologies). Primers were synthesized by Qiagen (Valencia, CA, USA). GAPDH was used as an endogenous control gene. The RT-qPCR reaction conditions were as follows: hot start at 95°C for 5 min, 40 cycles at 95°C for 10 s, 60°C for 34 s, melting curve stage at 95°C for 15 s, 60°C for 60 s, and 95°C for 15 s. All of the reactions were carried out in triplicate. The experimental data were analyzed using the $2^{-\triangle\triangle Ct}$ method. The qRT-PCR primer sequences of HOXC4 were as follows: forward: GCCAGC AAGCAACCCATAGT, Reverse: CCTTCTCCTTCGGGT CAGGT; GAPDH, forward GGAGCGAGATCCCTCCAA AAT and reverse GGCTGTTGTCATACTTCTCATGG. The result was shown in supplementary material of HOCX4 qPCR results.

Prognosis analysis

Among the aspects of survival analysis, overall survival (OS), disease-specific survival (DSS), disease-free intervals (DFI), and progression-free intervals (PFI) were used to systematically examine the relationship between HOXC4 expression and survival in pan-cancer. Forest plots and Kaplan–Meier curves were used to illustrate the results. By utilizing univariate survival analysis, we calculated the hazard ratio (HR) with 95% confidence interval and log-rank P-value.

Analysis of HOXC4 expression with TMB, MSI, mismatch repair gene mutation and DNA methyltransferases

The TMB feature in tumor cells promotes immune recognition and correlates with immunotherapy effectiveness (Fusco et al., 2021). An MSI occurs when new alleles are inserted into a tumor as a result of an alteration in microsatellites and is considered one of the hallmarks of immune-checkpoint-related therapy (O'Connell et al., 2020). These scores were computed from somatic mutation data obtained from TCGA. Two radar legends were generated to illustrate the relationship between HOXC4 expression and TMB and MSI, based on Spearman's rank correlation analysis.

As well, MMR is a process of DNA repair in which unrepairable errors in DNA replication may occur, resulting in a higher incidence of somatic mutations (Armaghany et al., 2012). DNA methylation is a DNA modification mechanism, whose methyltransferases are capable of modulating gene expression and chemical chromatin structure (Szigeti et al., 2018). An evaluation of Pearson correlation analysis between HOXC4 expression levels and mutation levels in five MMR genes (MLH1, MSH2, MSH6, PMS2, and EPCAM) and four methyltransferases' genes (DNMT1, DNMT2, DNMT3A, and DNMT3B) was conducted.

Immunological analysis with HOXC4

A database named Tumor Immune Evaluation Resource (TIMER) is intended to provide systematic and integrative data on immune infiltrations in cancer, such as scores for immune cell infiltration. A relationship was estimated between HOXC4 expression and six immune cell infiltration scores,

including macrophages, CD8 + T cells, dendritic cells, B cells, CD4 + T cells and neutrophils (Linnebacher and Maletzki, 2012; Yoshihara et al., 2013; Aran et al., 2015; Newman et al., 2015).

Additionally, co-expression analyses were performed on HOXC4 and immune-related genes, including genes encoding MHC, immune activation, immunosuppression, chemokine and chemokine receptor proteins, ferroptosis, m6A and immune checkpoint genes.

In 809 cancer cell lines, GDSC2 datasets (https://www.cancerrxgene.org/) were used to analyze the relationship between HOXC4 expression and half-maximal inhibitory concentration (IC50) values (Yang et al., 2013). To determine IC50 differences of each drug in different gene expression groups, median HOXC4 gene expression was used; then plots concerning IC50 differences and gene expression correlation were generated.

The biological significance analysis

GSEA and GSVA were performed using normalized RNA-Seq data from TCGA database to examine HOXC4's underlying functions (Subramanian et al., 2005). As part of the GSEA, GO terms, KEGG pathways, and Reactome data are included. As compared with KEGG analysis, where HOXC4 pathway enrichment was observed, GO analysis concentrated on 3 aspects of regulatory features, namely biology process (BP), cell component (CM) and molecular function (MF). Over 20,000 gene sets are contained in the MSigDB database (version 7.1, updated March 2020; https://www.gsea-msigdb.org/gsea/msigdb/index.jsp), which has been used to determine GSVA scores for cancers (Liberzon et al., 2011). 15 functional pathways were visualized for each tumor showing the most significant correlations with HOXC4 expression.

CancerSEA (http://biocc.hrbmu.edu.cn/CancerSEA/) is the first integrated database that identifies cellular functions at the single-cell level in cancer, covering nearly 41,900 tumor cells, depicting different functional states (such as stemness, invasion, metastasis, proliferation, EMT, angiogenesis, apoptosis, cell cycle, differentiation, DNA damage, DNA repair, hypoxia, inflammation, and quiescence) (Yuan et al., 2019).

Statistical analysis

Statistic analysis was performed using R software (Version 3.5.3) and GraphPad Prism (version 7.0; GraphPad Software, La Jolla, CA, USA). The Kruskal–Wallis test was used to analyze the differences in HOXC4 expression between tumor cell lines and different normal tissues. For comparing tumor and normal HOXC4 expression, the T-test was used. For correlation analysis, Spearman and Pearson tests were used. It was determined that a statistically significant difference existed at a P-value of <0.05.

Results

Pan-cancer with abnormal expression of HOXC4

Based on the GTEx dataset, Figure 1A shows the pattern of HOXC4 expression in 31 normal tissues. It was found that HOXC4 is extensively expressed in normal tissues, with the fallopian tube showing the highest levels. HOXC4 expression levels were then evaluated according to the CCLE database in Figure 1B, indicating that HOXC4 was expressed ubiquitously across 21 types of tumor cells. As shown in Figure 1C, we compared HOXC4 mRNA levels using the TCGA database to further determine whether HOXC4 was differentially expressed between tumors and normal tissues. A number of cancer tissues, including BLCA, BRCA, CHOL, ESCA, GBM, HNSC, KICH, KIRC, LGG, LIHC, LUAD, LUSC and PRAD, expressed HOXC4 at significantly higher levels than normal tissues. Since TCGA samples of normal tissues were limited, GTEx and TCGA data were then integrated to estimate the HOXC4 expression difference across different cancer types. As a result, higher expression of HOXC4 was observed in 21 tumors, including ACC, BLCA, BRCA, CESC, CHOL, ESCA, GBM, HNSC, KICH, KIRP, LGG, LIHC, LUAD, LUSC, OV, PAAD, PRAD, STAD, TGCT and UCS (Figure 1D). Also, we selected liver cancercolon cancer and breast cancer tissues compared to their adjacent normal ones for qRT-PCR verification due to the limited number of pathological samples available, confirming significant HOXC4 expression upregulation, which was also consistent with our bioinformatic analysis (Figure 1E). Overall, a combined analysis of pan-cancer results reveals that HOXC4 is aberrantly expressed across a variety of cancer types.

The prognostic significance of HOXC4 expression in various cancer types

As yet, no prognostic value has been determined for HOXC4 expression in cancer patients. Thus, Data from TCGA were used to assess the association between HOXC4 expression level and patients' survival (e.g., DFI, DSS, OS, and PFI). As far as HOXC4 expression is concerned with DFI, univariate survival analysis was conducted, as in Figure 2A. It has been shown that HOXC4 expression is significantly correlated with DFI for patients with four types of cancer, including ACC (p = 0.021, HR = 1.2), LGG (p = 0.029, HR = 1.13), PRAD (p = 0.0048, HR = 1.04) and STAD (p = 0.037, HR = 1.03). Additionally, Kaplan-Meier curves comparing DFI for these four tumors (Figure 2B) have shown that patients who express more HOXC4 were more likely to have a worse outcome. In relation to patients' DSS, HOXC4 expression showed a significant correlation with seven cancer types, including ACC (p = 2.3e-03, HR = 1.16), COAD (p = 1.6e-02, HR = 1.08), LGG

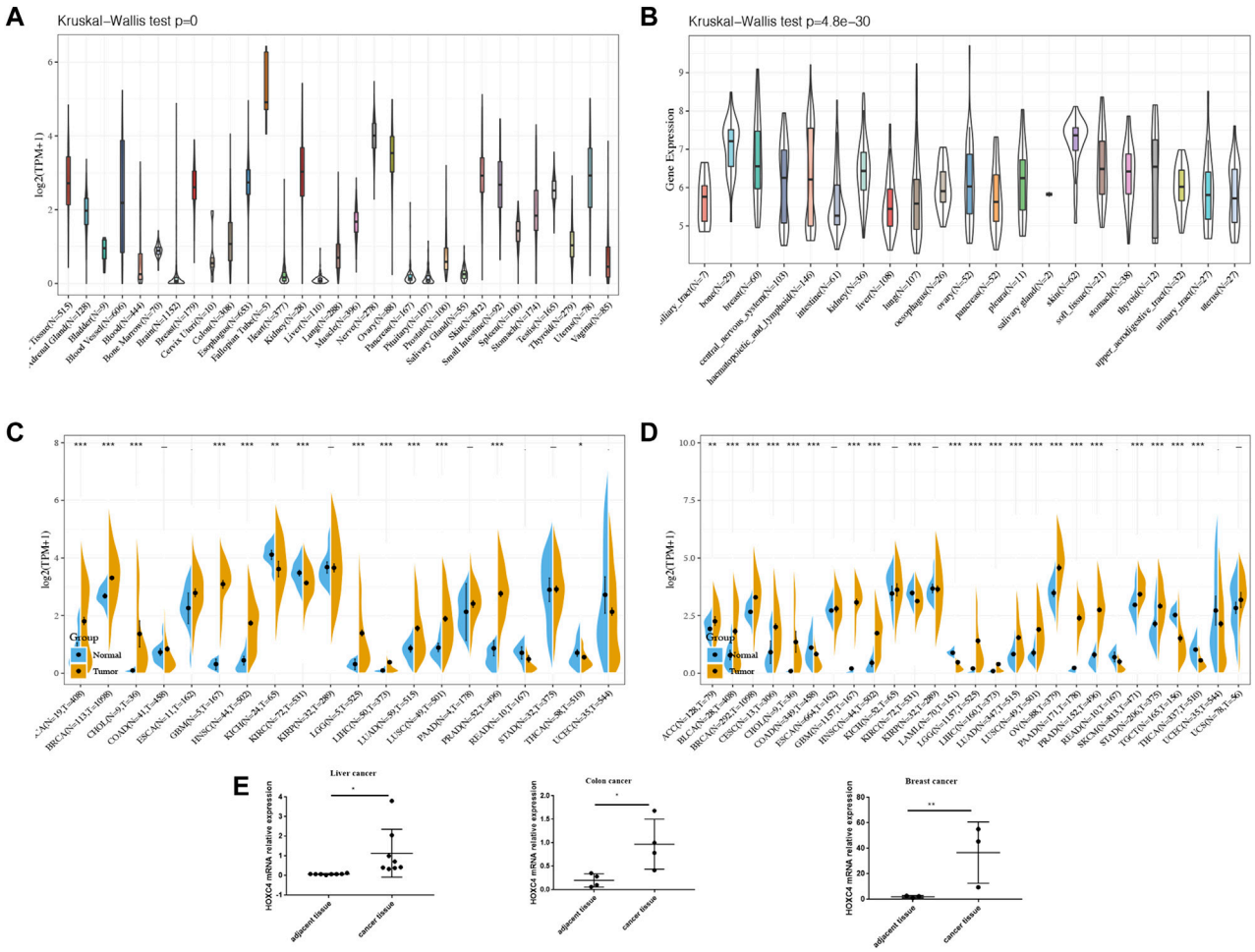

FIGURE 1
HOXC4 expression in pan-cancer. **(A)** Expression levels of HOXC4 in GTEx dataset. **(B)** Expression levels of HOXC4 the CCLE base. **(C)** Expression levels of HOXC4 in TCGA database. **(D)** HOXC4 expression difference in tumors combined with data of normal tissues I GTEx database and data of TCGA tumor tissues.**(E)** qRT-PCR validation of HOXC4. Cancer vs. adjacent tissue samples from liver cancer, colon cancer and breast cancer patients respectively.*$p < 0.05$, *"$p < 0.01$, *"*$p < 0.001$.

(p = 1.1e-12, HR = 1.09), LUSC (p = 3.8e-02, HR = 1.02), PAAD (p = 3.8e-03, HR = 1.11), READ (p = 5.3e-03, HR = 1.14), and UVM (p = 1.5e-02, HR = 1.3) in Figure 2C. Kaplan-Meier curves of DSS for these seven tumors also showed increases in HOXC4 expression to be associated with unsatisfactory outcomes (Figure 2D). HOXC4 expression was also associated with patients' OS in the Forest plot shown in Figure 3A. It was found that HOXC4 expression correlated with patient OS in six cancer types, including ACC (p = 3.4e-03, HR = 1.16), COAD (p = 4.2e-02, HR = 1.06), LGG (p = 1.1e-14, HR = 1.09), PAAD (p = 8.6e-03, HR = 1.08), READ (p = 2.3e-02, HR = 1.1), and UVM (p = 1.8e-02, HR = 1.29). On the other hand, Kaplan–Meier curves comparing OS in these six cancers (Figure 3B) suggested an association between increased HOXC4 expression and a worse prognosis. Further, significant correlation between HOXC4 and patients' PFI (Figure 3C) was observed in four types of cancer, including ACC (p = 1.1e-14, HR = 1.09), LGG (p = 3.1e-18, HR = 1.09), LIHC (p = 1.5e-2, HR = 1.11), and PRAD (p = 5.1e-04, HR = 1.03). Moreover, Kaplan-Meier PFI curves for these four tumors (Figure 3D) showed HOXC4 expression led to a poorer prognosis. Therefore, HOXC4 expression may play an integral role in determining patients' prognoses across a variety of cancer types.

Infiltrated immune cells and HOXC4 expression in cancers

TME contains tumor cells and non-tumor elements, the latter of which include stromal and immune cell components

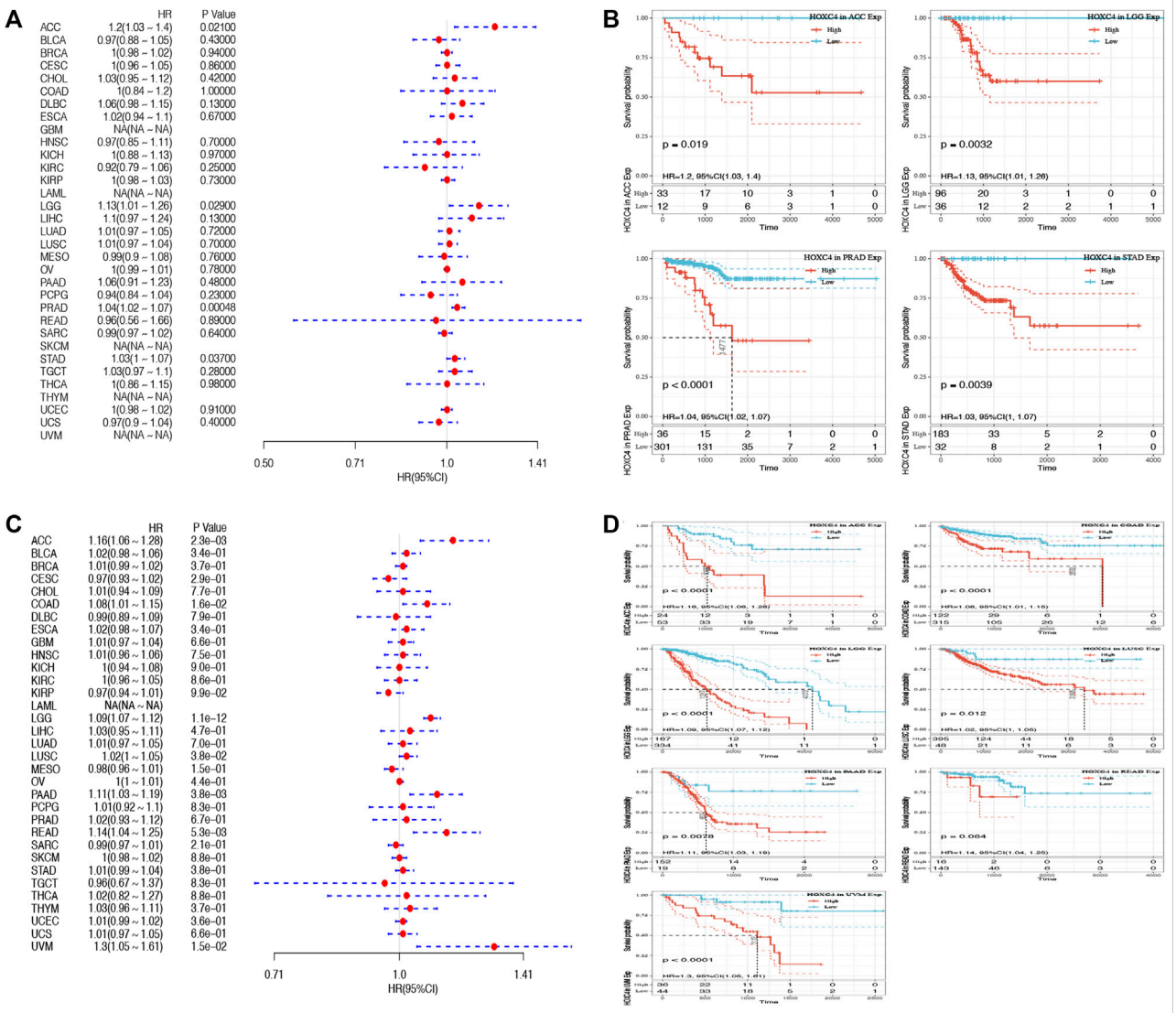

FIGURE 2
Forest plot and Kaplan-Meier curves of the relationship between HOXC4 expression and DFI and DSS in various types of tumors **(A,B)** HOXC4 expression is associated with DFI analysis in ACC, LGG, PRAD and STAD; **(C,D)** HOXC4 expression is associated with DSS analysis in ACC, COAD, LGG, LUSC, PAAD, READ and UVM.

(Bolouri, 2015). Although the evaluation of immune cell infiltration has been implicated in various cancers of prognostic significance and cancer-targeted immunotherapy potential, the critical role of HOXC4 expression in TME warrants further investigation. As a result of data provided by TIMER, the relationship between HOXC4 expression and immune cell infiltration was first determined by calculating the score of six immune cells, including B cells, $CD4^+$ T cells, $CD8^+$ T cells, neutrophils, macrophages, and dendritic cells. Consequently, increased infiltration of macrophages was correlated with an increased expression level of HOXC4 in BLCA, COAD, GBM, HNSC, KIRC, LGG, LIHC, OV, PRAD, READ, SKCM, STAD, TGCT, THCA, and UCEC. As for B cells, $CD4^+$ T cells, $CD8^+$ T cells, neutrophils, and dendritic cells, their infiltration levels were significantly linked with HOXC4 expression in BLCA, BRAC, CESC, CHOL, COAD, GBM, HNSC, KIRC, KIRP, LGG, LIHC, LUAD, LUSC, MESO, OV, PAAD, PCPG, PRAD, READ, SARC, SKCM, STAD, TGCT, THCA, THYM, UCEC, UCS and UVM. As shown in Figure 4A, infiltration of all six immune cell types exerted significant correlations with HOXC4 expression in COAD, HNSC, LGG, LIHC, READ, and THCA, which provides a solid basis for analyzing immune-related factors. In contrast, no significant correlation was found between immune cell infiltration in

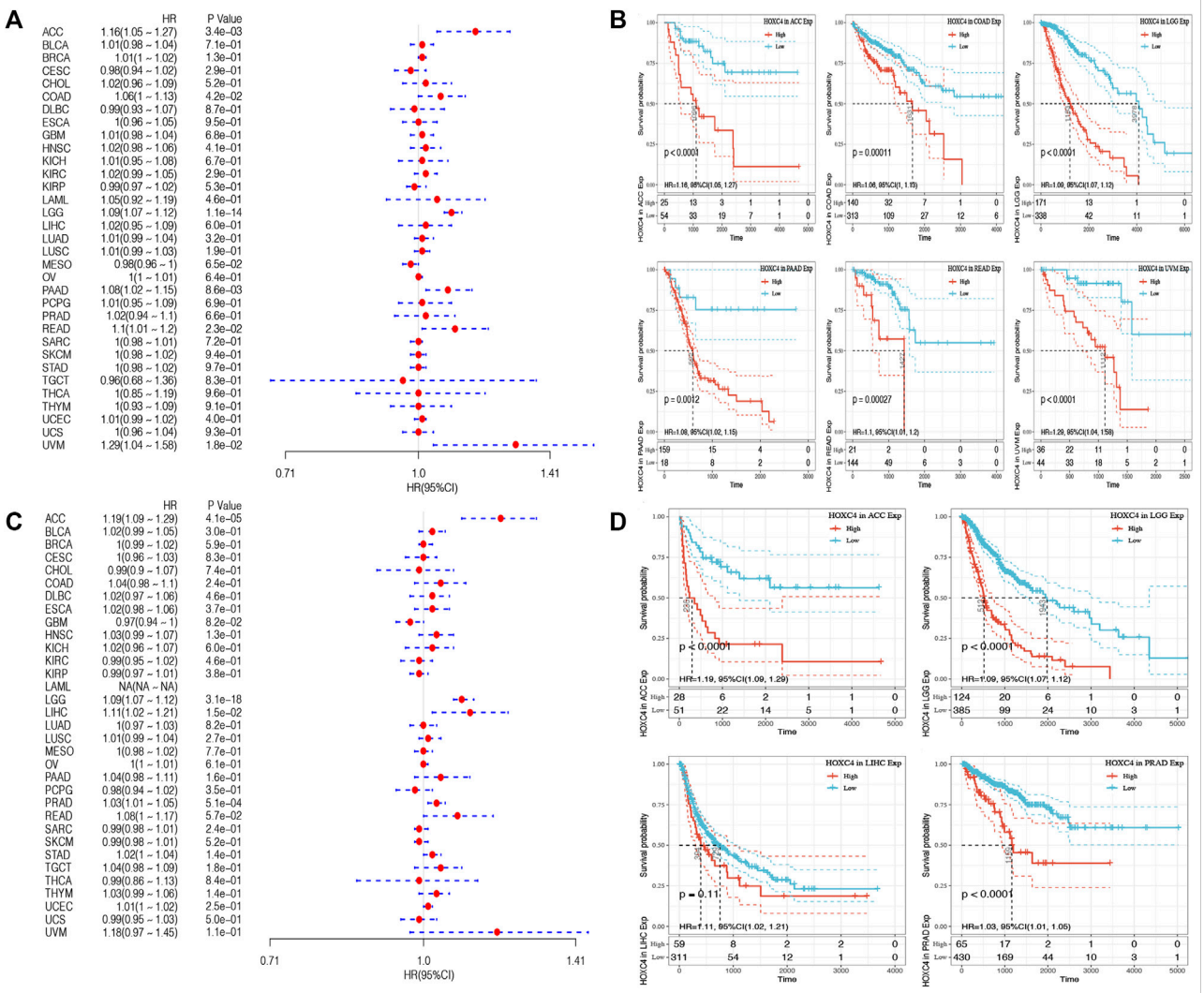

FIGURE 3
Forest plot and Kaplan-Meier curves of the relationship between HOXC4 expression and OS and PFI in 33 types of tumors **(A,B)** HOXC4 expression is associated with DFI analysis in ACC, COAD, LGG, PAAD, READ and UVM; **(C,D)** HOXC4 expression is associated with PFI analysis in ACC, LGG, LIHC and PRAD.

ACC, DBLC, KICH, ESCA, or LAML. Detailed information can be found in Supplementary Figure S2. These findings, therefore, suggest that HOXC4 expression was significantly related to immune cell infiltrations and the recruitments of immune cells in various tumor types.

Expression of HOXC4 with respect to TMB, MSI, MMR gene mutation, DNA methylation, and immune markers

TMB is a marker of genomic alterations that promotes immune recognition, which could induce and accelerate immune recognition associated with the preliminary assessment of immunotherapy response (Sabari et al., 2018). Nonetheless, no relevant reports have been found regarding HOXC4 expression with TMB. BLCA, COAD, ESCA, LGG, LUAD, MESO, PAAD, PRAD, and STAD showed significant correlations between HOXC4 expression and TMB based on Spearman correlation analysis. As illustrated in a radar legend of Figure 4B, its expression in COAD exhibited the strongest correlation with TMB (P = 6e-11).

The MSI was originally seen as a marker of hypermutability in DNA and a potential treatment target for immuno-checkpoint blockade therapy (Hause et al., 2016). Also, few studies have detected the association between HOXC4 and MSI in cancers. We analyzed the

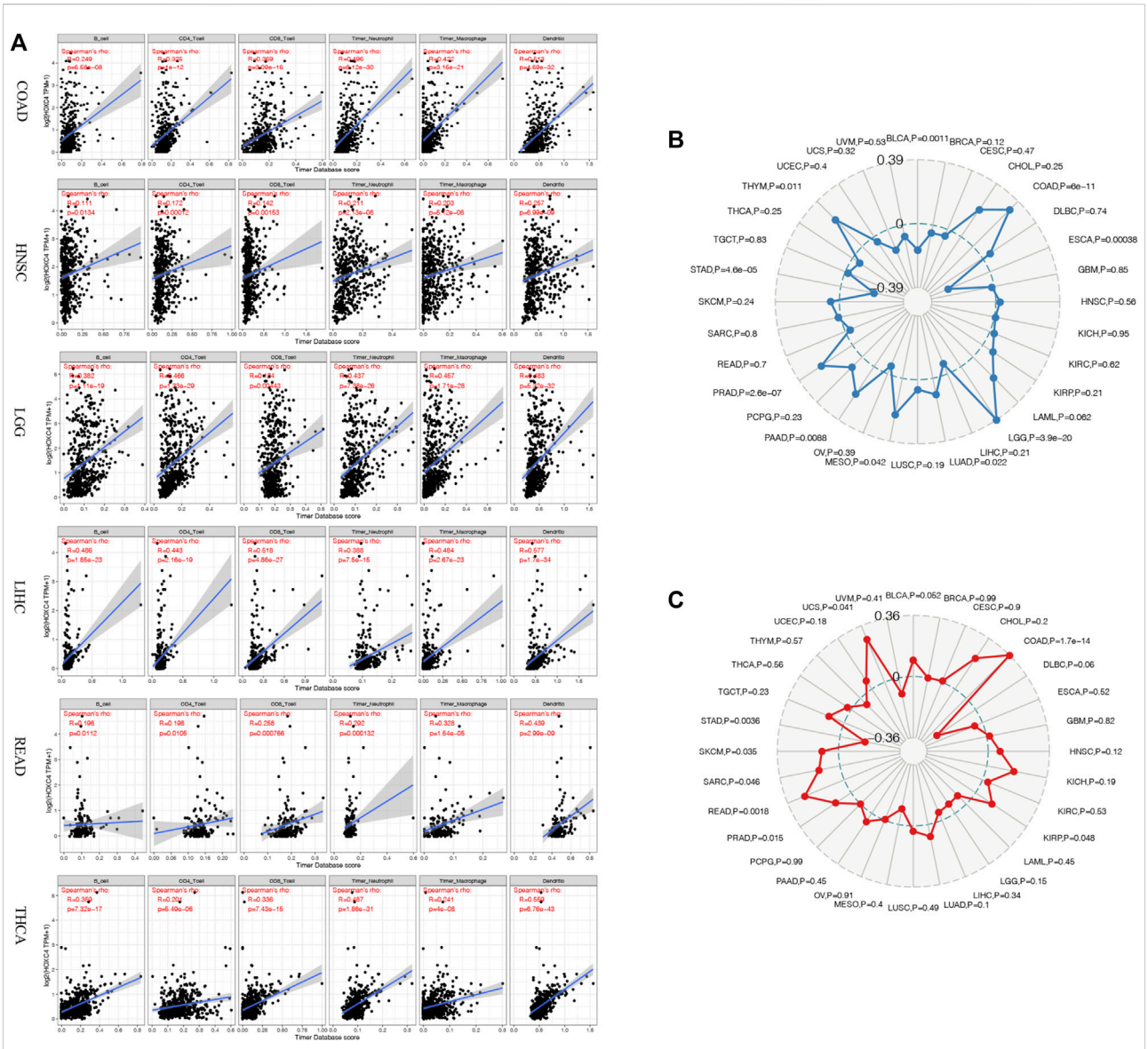

FIGURE 4
(A) Correlation analysis between HOXC4 expression and immune cell infiltration in COAD, HNSC, LGG, LIHC, READ, and THCA. **(B)** Correlation analysis between HOXC4 expression and TMB. **(C)** Correlation analysis between HOXC4 expression and MSI.

relationship between MSI and HOXC4 expression across multiple cancer types using MSI data downloaded from TCGA database. Figure 4C shows that expression of this gene is significantly correlated with MSI in COAD, KIRP, PRAD, READ, SARC, SKCM, STAD, and UCS, with the most significant correlation seen in COAD (p = 1.7e-14).

DNA mismatch errors are repaired by MMR, and failure to correct them can result in more somatic mutations and cancer (McKinney et al., 2020). Therefore, we detected the association between HOXC4 expression and five MMR genes mutation levels (MLH1, MSH2, MSH6, PMS2 and EPCAM). In Figure 5A, HOXC4 expression in ACC, BRCA, CESC, COAD, ESCA, GBM, HNSC, KIRC, KIRP, LGG, LIHC, LUAD, MESO, PAAD, PCPG, PRAD, READ, SKCM, STAD, TGCT, UCEC and UCS correlates with these five MMR genes. As a result, HOXC4 may be able to regulate genes involved in the repair-related genes regarding DNA replication errors to improve survival capability of cancer cells.

Additionally, DNA methylation is another mechanism of methyltransferases that can play a crucial role in DNA modification, the change of which could act as a crucial factor in tumorigenesis (Tiffen et al., 2020). The purpose of this study was to further examine the differential expression

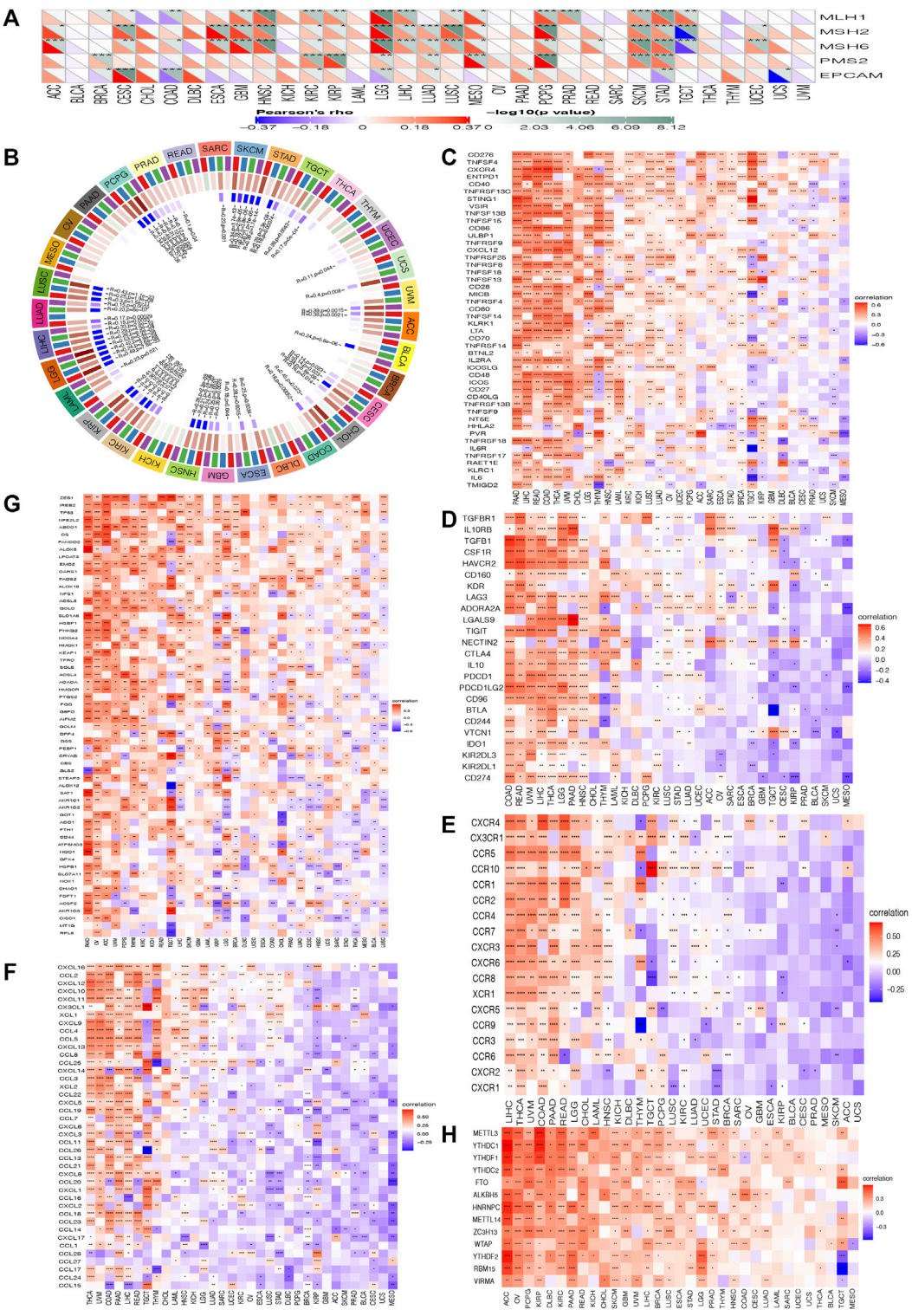

FIGURE 5
Correlation analysis between the expression of HOXC4 and **(A)** MMR mutation genes **(B)** DNA methyltransferases **(C)** immune activation **(D)** immunosuppressive **(E)** chemokine receptor gene **(F)** chemokine **(G)** ferroptosis **(H)** m6A; ***$p < 0.001$, **$p < 0.01$, *$p < 0.05$, no *$p > 0.05$.

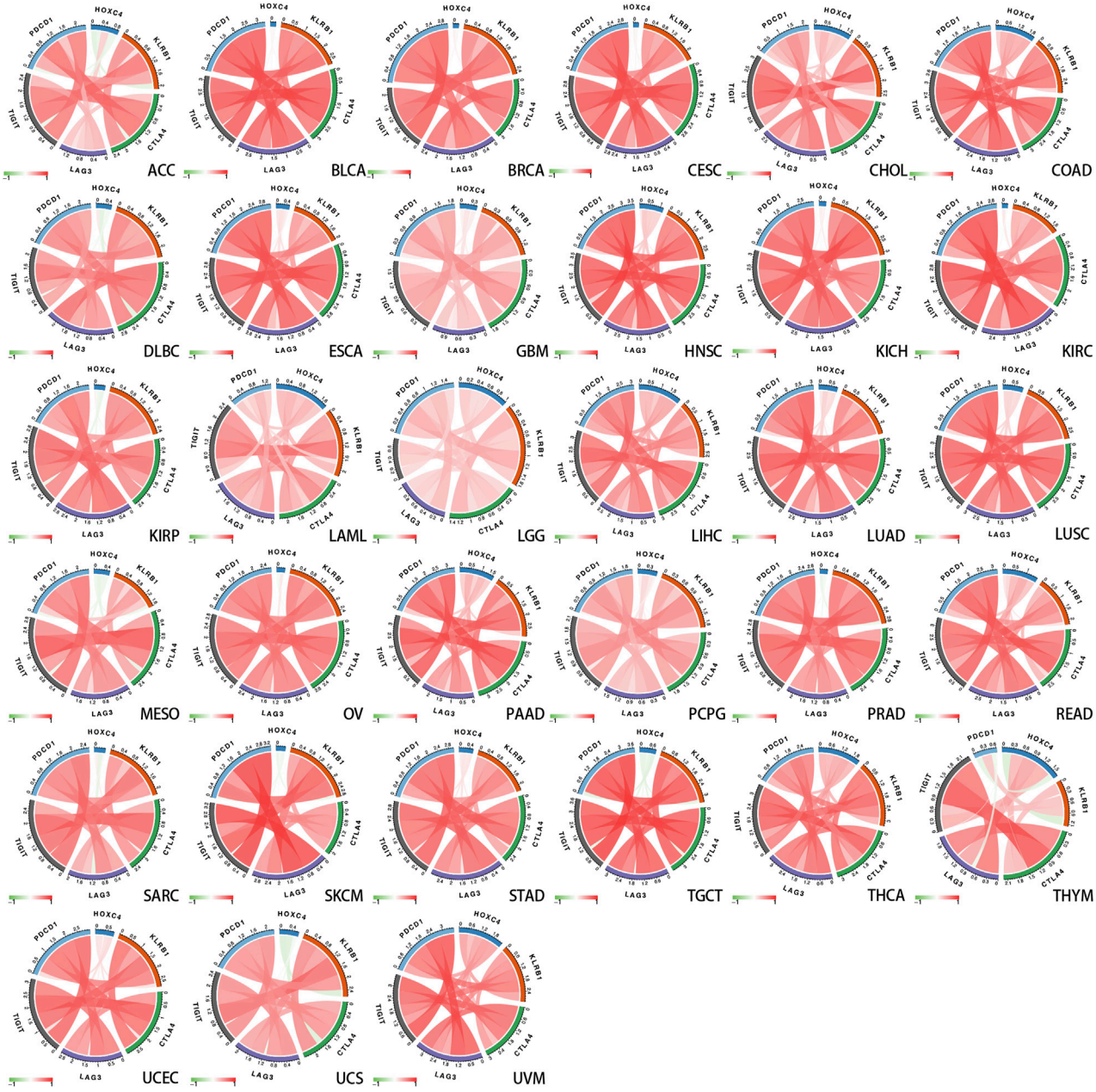

FIGURE 6
Correlation between HOXC4 expression and five main immune checkpoint genes from TCGA database.

of HOXC4 with four DNA methyltransferases, namely DNMT1, DNMT2, DNMT3A and DNMT3B. Figure 5B indicates that HOXC4 expression was significantly correlated with the expression of four DNA methyltransferase genes other than BRCA, DLBC, KICH, MESO, OV, PAAD and THYM, suggesting that HOXC4 may be involved in tumorigenesis of pan-cancer by modifying epigenetic DNA methylation.

Additionally, it is acknowledged that immune modulation and immune surveillance play vital roles in cancer patients' prognosis. Co-expression analysis of HOXC4 expression was thus performed with seven immune-related marker gene sets including immune activation, immunosuppression, chemokine receptor proteins, chemokine, ferroptosis, m6A, and immune checkpoint markers. As shown in Figures 5C–F, HOXC4 expression was extensively significantly correlated with immune-activation,

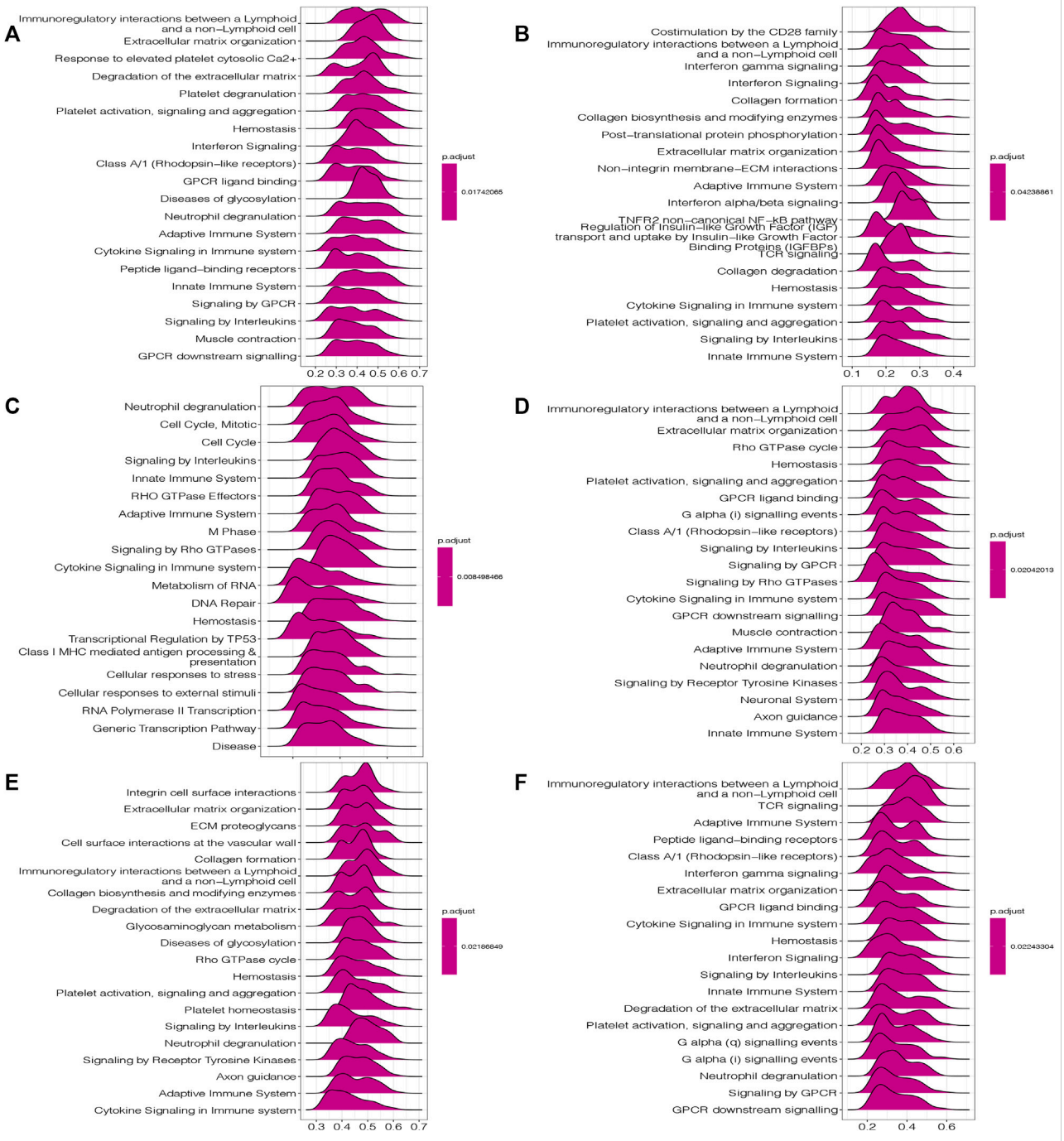

FIGURE 7
GSEA results of HOXC4 expression involved in Reactome pathways **(A)** COAD; **(B)** HNSC; **(C)** LGG; **(D)** LIHC; **(E)** READ; **(F)** THCA.

immunosuppression, chemokine receptor genes, and chemokine in COAD, HNSC, LGG, LIHC, THCA, etc. Moreover, ferroptosis and m6A gene markers (Figures 5G,H) also exhibited co-expression with HOXC4 in all types of tumors, except UCS. Simultaneous exploration was made concerning the relationship between HOXC4 and five immune checkpoint genes, including LAG3, TIGIT, PDCD1(PD-1), KLRB1 and CTLA4. HOXC4 expression was in close correlation with immune checkpoint genes in BRCA, COAD, HNSC, LGG, LIHC, LUSC, STAD, THYM, etc. (Figure 6). Collectively, the expression level of HOXC4 may be involved significantly in immune regulation and immunological events across pan-cancer.

FIGURE 8
GSVA results of HOXC4 expression involved in **(A)** COAD; **(B)** HNSC; **(C)** I,GG; **(D)** LIHC; **(E)** READ; **(F)** THCA.

GSEA, GSVA and CancerSEA analyses

In view of the significant correlation of HOXC4 expression with immune infiltrations in COAD, HNSC, LGG, LIHC, READ and THCA, GSEA and GSVA analyses were performed to further explore the biological significance of HOXC4 expression in these cancers.

GSEA analysis includes GO terms, KEGG pathways and Reactome database. According to Reactome analysis in Figure 7, HOXC4 might be involved in immune-related

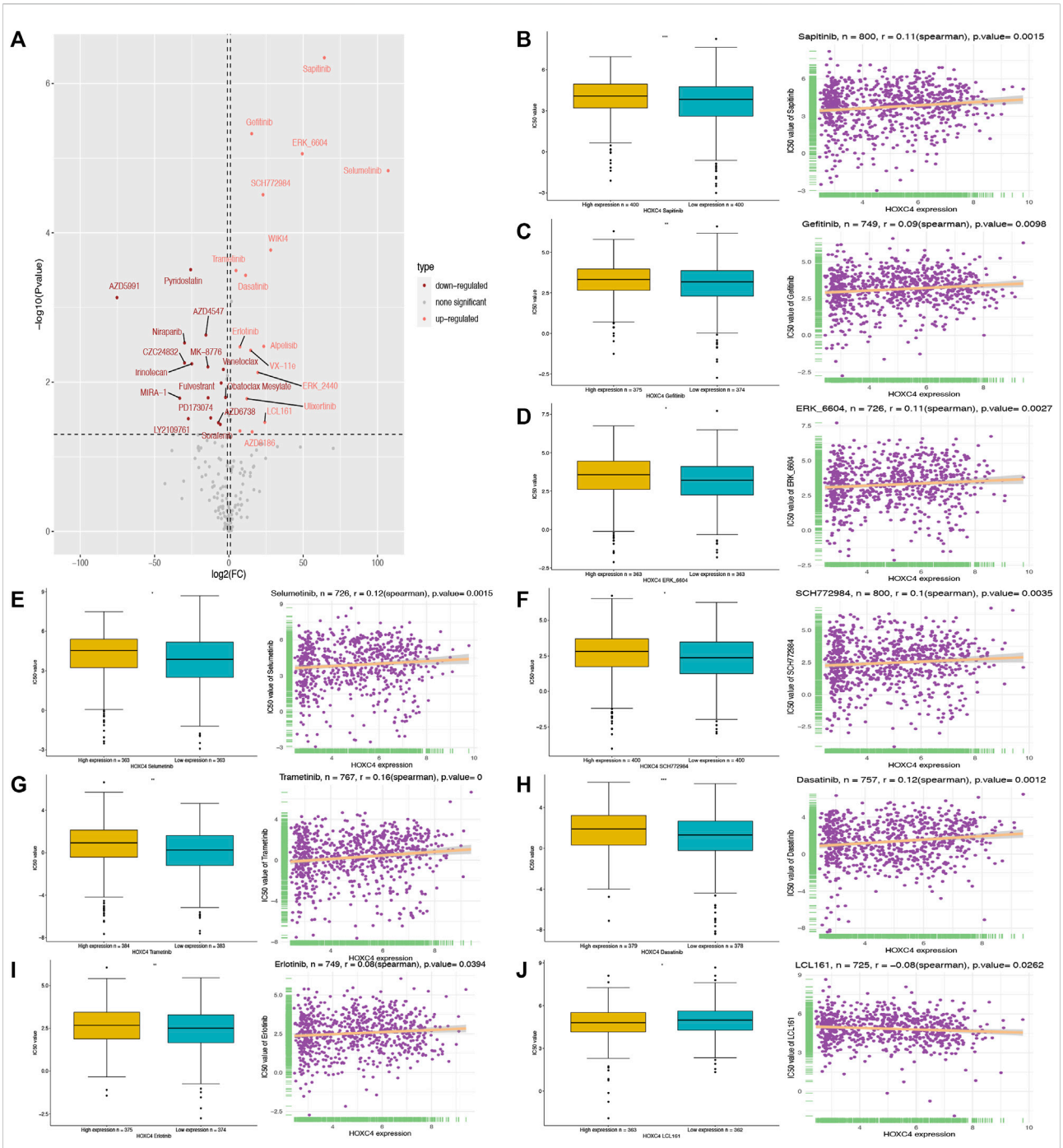

FIGURE 9
Correlation analysis between HOXC4 expression and anti-cancer drug sensitivity from GSDC2 dataset **(A)** volcano plot visualizes the correlation bewteen high-/low- HOXC4 expression group and different 1,050 values; **(B–J)** 1,050 values of 9 chemotherapy drugs show significant correlation with upregulated expression of HOXC4.

functions, cell cycle and tumor metabolism in multiple cancers, including the modulation of innate/adaptive immune system, cytokine/interferon/interleukins signaling in the immune system, neutrophil degranulation, B cell receptors, immunoregulatory interactions, class I MHC mediated antigen processing and presentation and several immune-related signaling pathways. As for the potential of HOXC4 in cancer metabolic issues, its expression in

LGG, READ, etc. Impacted cellular metabolic process, glycosaminoglycan metabolism, metabolism of RNA, and some metabolic pathways. GSEA results of GO analysis and KEGG pathways was shown in Supplementary Figure S3.

GSVA analysis was also conducted to further investigate the underlying biological functions and mechanisms of HOXC4 expression, presented by 15 pathways of the most positive and negative association with HOXC4 in these 6 tumors. The results in Figure 8 illustrated that the expression of HOXC4 was positively related to some immune-related signaling pathways, including B, $CD4^+$ T, and CD8 T cells, signal transduction by P53 class mediator, SMAD, STAT3, and PTPIB pathways. In contrast, HOXC4 expression was negatively correlated with cell cycle-related pathways and specific metabolic pathways, such as disease of DNA repair, peroxisomal lipid metabolism, cellular lipid catabolic process, epithelial to mesenchymal transition, etc. Taken these results together, HOXC4 expression may be linked with a variety of biological functions and signaling pathways, especially concerning tumor immunity, cell cycle and metabolic issues.

CancerSEA database contains multitudinous functional states at the cancer single-cell level. To unearth more potential mechanisms, further exploration was performed focusing on the functional state of HOXC4 across 4 types of cancer in CancerSEA database, including brain, skin, breast, and ovary (Supplementary Figure S4). For example, in breast cancer, HOXC4 expression was negatively associated with cell cycle, DNA damage, DNA repair and invasion. Moreover, apoptosis and cell cycle were found to be positively involved in OV, and negatively correlated with DNA repair, hypoxia, proliferation, and stemness, greatly broadening our vision of HOXC4 functional states in cancers.

Prediction of HOXC4 expression with drug resistance

To our knowledge, no study has exploited GDSC data to predict anti-cancer drug sensitivity systematically by comparing the expression of HOXC4 in cancer cell lines and IC50 measurements in drugs. Therefore, Spearman correlation analysis was employed to analyze the association between HOXC4 expression and the IC50 values of 198 drugs in 809 cell lines. Then, we carried out evaluations of drug response prediction in GDSC dataset with their corresponding IC50 values as drug response measurement in comparison between high-/low- HOXC4 expression groups, with corresponding results plotted. As shown in Figure 9, 15 drugs presented significant IC50 differences in high-expression groups, of which only 9 showed a significant correlation between HOXC4 and IC50, including Sapitinib, Gefitinib, ERK_6604, Selumetinib, SCH772984, Trametinib, Dasatinib, Erlotinib, and LCL161. Accordingly, the positive correlation of higher HOXC4 expression with IC50 values may indicate that elevated HOXC4 expression may result in anti-cancer drug resistance and lower chemosensitivity.

Discussion

Identifications of critical biomarkers with involvement in tumor initiation and progression have sparked great interest in tumorigenesis research. An integrative pan-cancer study of a single gene is by far endowed with significant implications towards early diagnosis, therapeutic regimen and cancer prevention (Qureshi et al., 2020; Srivastava and Hanash, 2020). In the meantime, comprehensive and systematic studies have been undertaken concerning tumor immunity and its influence on immunotherapy (Jiang et al., 2020; Passaro et al., 2020). According to our previous description, HOXC4 plays a vital role during embryonic development and in the development of cancer. However, HOXC4 is not well understood as a molecular biomarker in pan-cancer, nor its expression level. Here, our study uncovers new insights into how aberrant HOXC4 expression plays an important role in tumor immunology and as a potential biomarker for malignancy development.

Based on a comprehensive analysis of the expression of HOXC4 in pan-cancer, the present study found that HOXC4 was widely expressed in 31 normal tissues as well as 21 tumor cell lines, with the highest expression of HOXC4 occurring in the fallopian tube and ovary, respectively. In the meantime, the combined TCGA and GTEx databases revealed abnormal overexpression of HOXC4 in 21 types of cancer, including ACC, BLCA, BRCA, CESC, CHOL, ESCA, GBM, HNSC, KICH, KIRP, LGG, LIHC, LUAD, LUSC, OV, PAAD, PRAD, STAD, TGCT and UCS, which suggests that HOXC4 may function in carcinogenesis as an oncogene. Moreover, a clarification of the relationship between HOXC4 expression and survival outcomes revealed that higher levels of HOXC4 were associated with suboptimal survival outcomes, regardless of OS, DSS, DFI and PFI. Thus, abnormally high levels of HOXC4 expression appear to be crucial for multiple cancers to form and develop.

The TME, which includes the tumor immune microenvironment (TIME), in which immune cells infiltrate, is considered to be one of the "seventh marker feature" of a tumor, comprising an indispensable component of the immune response and tumor progression, along with assessing therapeutic effectiveness and survival outcomes (Junttila and de Sauvage, 2013). There is still uncertainty, however, as to

whether the expression of HOXC4 is pivotal to TME. In our study, we observed a significant correlation between HOXC4 expression and 6 immune infiltrating cells: B cells, $CD4^+$ T cells, $CD8^+$ T cells, dendritic cells, macrophages, and neutrophils in COAD, HNSC, LGG, LIHC, READ, and THCA(41). Several studies have found that dendritic cells and macrophages play an important role in antitumor immunity, which can lead to detrimental tumor immunity escape in the presence of excessive chemotactic factors (Ohtani, 2007). In this manner, infiltration of these immune cells may contribute to impaired immunity and may be closely related to cancers of the six types. Hence, infiltrating immune cells can be regulated by HOXC4 expression during different types of cancer development and immune escape can be influenced.

Previously, we have discussed the significant role that TMB and MSI play in immunotherapy (Gajewski and Schumacher, 2013; Goodman et al., 2017). This study indicates that HOXC4 expression was strongly correlated with TMB in BLCA, COAD, ESCA, LGG, LUAD, MESO, PAAD, PRAD, and STAD, suggesting that HOXC4 is probably responsible for mutation-driven tumorigenesis. Additionally, studies suggest that immunotherapeutic outcomes may be improved with HOXC4 expression in tumors with higher TMB, suggesting that HOXC4 expression may be warranted in tumors with higher TMB. For MSI, significant associations with HOXC4 expression were found in COAD, KIRP, PRAD, READ, SARC, SKCM, STAD, and UCS, which indicates that HOXC4 may serve as a hall marker for patients undergoing immune-checkpoint-blockade therapy. Furthermore, HOXC4 can play a crucial role in determining the oncogenic validity of immune cells and immune-related genes in various cancers, particularly through their co-expression analyses. A mutation in MMR genes or an alteration in DNA methylation markers can lead to a cumulative increase in genetic or epigenetic errors, which can contribute to tumor occurrence (Butler et al., 2020; Georgakopoulos-Soares et al., 2020). A significant correlation was also found between the expression of HOXC4 and the MMR mutation genes in this study, with the exception of BLCA, CHOL, DLBC, KICH, LAML, OV, SARC, THCA, THYM and UVM. Aside from BRCA, DLBC, KICH, MESO, OV, PAAD, and THYM, HOXC4 expression is significantly associated with DNA methyltransferase genes expression. In turn, these results substantiate and support our previous findings. It was further clarified that HOXC4 expression is correlated with immune-related genes, particularly immunosuppressive genes such as PD-1 and PD-L1. As a result of their strongly positive correlation, it is likely that HOXC4 regulates the tumor immunosuppressive microenvironment and functions as a novel target for immunotherapy against related tumors. In conclusion, HOXC4 expression is intimately correlated with tumorigenesis and genes involved in immunity in pan-cancer, supporting the importance of HOXC4 in immune modulation and immunotherapy.

It is well known that ineffective chemotherapy can increase mortality and decrease quality of life in cancer patients. Personalized chemotherapy continues to be a challenging endeavor (Chen et al., 2013; Kim et al., 2016). In our study, to test the significance of HOXC4 expression in chemotherapeutic drug application, tumor cell lines with similar responses to a drug were simulated in a manner similar to that of tumor patients. To date, GDSC is the largest project that evaluates anticancer drug sensitivity and identifies biomarkers for drug response in cancer cell lines. Among the drugs examined in our study, Sapitinib, Gefitinib, ERK_6604, Selumetinib, SCH772984, Trametinib, Dasatinib, Erlotinib, and LCL161 showed significant correlations between upregulated HOXC4 expression and their corresponding IC50 values. Hence, by assessing different anti-cancer drug responses in various patients based on their HOXC4 expression levels, we may eventually be able to improve our individual therapeutic treatment.

Last but not least, we investigated the biological significance of HOXC4 expression. In this study it was discovered that HOXC4 could play a role in cancer pathogenesis through its involvement in a variety of immunological pathways, including *via* immune response, PD-L1 expression and PD-1 checkpoint pathway in cancers, PI3K-AKT signaling pathway, NK-κB signaling, and several metabolic pathways, consistent with previously published studies (Rouce et al., 2016; Yang et al., 2017; Pham et al., 2020). Collectively, HOXC4 plays an important oncogenic role in the development and progression of cancers, as well as in the regulation of these signaling pathways.

In summary, we found that HOXC4 expression differs significantly among tissue types, and that overexpression of HOXC4 is significantly associated with poorer clinical outcomes in pan-cancer. Furthermore, our findings suggest that HOXC4 strongly correlates with TME, including an increase in the level of infiltration of six immune cells across a variety of cancers. It is also noteworthy that the expression of HOXC4 is strongly related to the expression of TMB, MSI, MMR mutation genes, DNA methyltransferases, immune-related markers, and immune checkpoint markers across a broad spectrum of cancer types, all of which affect immunotherapy-related treatment. Further, differential chemosensitivity responses of different cancers could be reflected by upregulation of HOXC4 expression, which

could facilitate better tailoring of anticancer therapies. Nevertheless, our results mostly relied on comprehensive and systematic data analysis. We will conduct further basic experimental verification in our subsequent research and HOXC4's biological activity in different cancer cells will then be explored, such as proliferation and/or migration. Also, we did not analyze the association between HOXC4 expression and immunotherapy cohort, which could be potential indicators of patients' immunotherapy response. So, the predictive value of HOXC4 regarding the immunotherapy response remains to be well-documented in the future. We hope that our research will provide novel insights into precision medicine for more individualized immunotherapy advancement in the future by elucidating the multifaceted roles HOXC4 plays in tumorigenesis and tumor immunity.

Data availability statement

The original contributions presented in the study are included in the article/Supplementary Material, further inquiries can be directed to the corresponding authors.

Ethics statement

The studies involving human participants were reviewed and approved by the Ethic Committee of Xiangya Hospital of Central South University.

Author contributions

JX and YiL designed and wrote the article; YaL, YC, and ZH assisted in construction of tables and figures and revision of the literature. SP and YY supervised the whole process.

Funding

This work was supported by National Natural Science Foundation of China (No. 81974080, 82170640), Natural Science Foundation of Hunan Province (No. 2022JJ30954). Wang Bao-En Liver Fibrosis Research Fund (No. 2021039). Fundamental Research Funds for the Central Universities of Central South University (No. 2022ZZTS0853, 2021ZZTS0343).

Acknowledgments

We acknowledge TCGA and GEO databases for providing their platforms and contributors for uploading their meaningful datasets.

Conflict of interest

The authors declare that the research was conducted in the absence of any commercial or financial relationships that could be construed as a potential conflict of interest.

Publisher's note

Supplementary material

The Supplementary Material for this article can be found online at: https://www.frontiersin.org/articles/10.3389/fgene.2022.1021473/full#supplementary-material

References

Aran, D., Sirota, M., and Butte, A. J. (2015). Systematic pan-cancer analysis of tumour purity. *Nat. Commun.* 6, 8971. doi:10.1038/ncomms9971

Armaghany, T., Wilson, J. D., Chu, Q., and Mills, G. (2012). Genetic alterations in colorectal cancer. *Gastrointest. Cancer Res.* 5 (1), 19–27.

Arnold, A., Imada, E. L., Zhang, M. L., Edward, D. P., Marchionni, L., and Rodriguez, F. J. (2020). Differential gene methylation and expression of HOX transcription factor family in orbitofacial neurofibroma. *Acta Neuropathol. Commun.* 8 (1), 62. doi:10.1186/s40478-020-00940-7

Bolouri, H. (2015). Network dynamics in the tumor microenvironment. *Semin. Cancer Biol.* 30, 52–59. doi:10.1016/j.semcancer.2014.02.007

Bragazzi, N. L., and Sellami, M. (2021). Cancer bioenergetics as emerging holistic cancer theory: The role of metabolic fluxes and transport proteins involved in metabolic pathways in the pathogenesis of malignancies. State-of-the-art and future prospects. *Adv. Protein Chem. Struct. Biol.* 123, 27–47. doi:10.1016/bs.apcsb.2020.09.001

Butler, M., Pongor, L., Su, Y. T., Xi, L., Raffeld, M., Quezado, M., et al. (2020). MGMT status as a clinical biomarker in glioblastoma. *Trends Cancer* 6 (5), 380–391. doi:10.1016/j.trecan.2020.02.010

Cantile, M., Cindolo, L., Napodano, G., Altieri, V., and Cillo, C. (2003). Hyperexpression of locus C genes in the HOX network is strongly associated *in vivo* with human bladder transitional cell carcinomas. *Oncogene* 22 (41), 6462–6468. doi:10.1038/sj.onc.1206808

Chan, T. A., Yarchoan, M., Jaffee, E., Swanton, C., Quezada, S. A., Stenzinger, A., et al. (2019). Development of tumor mutation burden as an immunotherapy biomarker: Utility for the oncology clinic. *Ann. Oncol.* 30 (1), 44–56. doi:10.1093/annonc/mdy495

Chang, L., Chang, M., Chang, H. M., and Chang, F. (2018). Microsatellite instability: A predictive biomarker for cancer immunotherapy. *Appl. Immunohistochem. Mol. Morphol.* 26 (2), e15–e21. doi:10.1097/PAI.0000000000000575

Chen, J., Cheng, G. H., Chen, L. P., Pang, T. Y., and Wang, X. L. (2013). Prediction of chemotherapeutic response in unresectable non-small-cell lung cancer (NSCLC) patients by 3-(4, 5-dimethylthiazol-2-yl)-5-(3-carboxymethoxyphenyl)-2- (4-sulfophenyl)-2H-tetrazolium (MTS) assay. *Asian pac. J. Cancer Prev.* 14 (5), 3057–3062. doi:10.7314/apjcp.2013.14.5.3057

Frankel, T., Lanfranca, M. P., and Zou, W. (2017). The role of tumor microenvironment in cancer immunotherapy. *Adv. Exp. Med. Biol.* 1036, 51–64. doi:10.1007/978-3-319-67577-0_4

Fusco, M. J., West, H. J., and Walko, C. M. (2021). Tumor mutation burden and cancer treatment. *JAMA Oncol.* 7 (2), 316. doi:10.1001/jamaoncol.2020.6371

Gajewski, T. F., and Schumacher, T. (2013). Cancer immunotherapy. *Curr. Opin. Immunol.* 25 (2), 259–260. doi:10.1016/j.coi.2013.03.008

Gehring, W. J., and Hiromi, Y. (1986). Homeotic genes and the homeobox. *Annu. Rev. Genet.* 20, 147–173. doi:10.1146/annurev.ge.20.120186.001051

Georgakopoulos-Soares, I., Koh, G., Momen, S. E., Jiricny, J., Hemberg, M., and Nik-Zainal, S. (2020). Transcription-coupled repair and mismatch repair contribute towards preserving genome integrity at mononucleotide repeat tracts. *Nat. Commun.* 11 (1), 1980. doi:10.1038/s41467-020-15901-w

Goodman, A. M., Kato, S., Bazhenova, L., Patel, S. P., Frampton, G. M., Miller, V., et al. (2017). Tumor mutational burden as an independent predictor of response to immunotherapy in diverse cancers. *Mol. Cancer Ther.* 16 (11), 2598–2608. doi:10.1158/1535-7163.MCT-17-0386

Gravitz, L. (2013). Cancer immunotherapy. *Nature* 504 (7480), S1. doi:10.1038/504S1a

Hause, R. J., Pritchard, C. C., Shendure, J., and Salipante, S. J. (2016). Classification and characterization of microsatellite instability across 18 cancer types. *Nat. Med.* 22 (11), 1342–1350. doi:10.1038/nm.4191

Jiang, T., Chen, X., Su, C., Ren, S., and Zhou, C. (2020). Pan-cancer analysis of ARID1A alterations as biomarkers for immunotherapy outcomes. *J. Cancer* 11 (4), 776–780. doi:10.7150/jca.41296

Junttila, M. R., and de Sauvage, F. J. (2013). Influence of tumour microenvironment heterogeneity on therapeutic response. *Nature* 501 (7467), 346–354. doi:10.1038/nature12626

Kalantari Khandani, N., Ghahremanloo, A., and Hashemy, S. I. (2020). Role of tumor microenvironment in the regulation of PD-L1: A novel role in resistance to cancer immunotherapy. *J. Cell. Physiol.* 235 (10), 6496–6506. doi:10.1002/jcp.29671

Kim, S., Sundaresan, V., Zhou, L., and Kahveci, T. (2016). Integrating domain specific knowledge and network analysis to predict drug sensitivity of cancer cell lines. *PLoS One* 11 (9), e0162173. doi:10.1371/journal.pone.0162173

Leyten, G. H., Hessels, D., Smit, F. P., Jannink, S. A., de Jong, H., Melchers, W. J., et al. (2015). Identification of a candidate gene panel for the early diagnosis of prostate cancer. *Clin. Cancer Res.* 21 (13), 3061–3070. doi:10.1158/1078-0432.CCR-14-3334

Li, B., Chan, H. L., and Chen, P. (2019). Immune checkpoint inhibitors: Basics and challenges. *Curr. Med. Chem.* 26 (17), 3009–3025. doi:10.2174/0929867324666170804143706

Liberzon, A., Subramanian, A., Pinchback, R., Thorvaldsdottir, H., Tamayo, P., and Mesirov, J. P. (2011). Molecular signatures database (MSigDB) 3.0. *Bioinformatics* 27 (12), 1739–1740. doi:10.1093/bioinformatics/btr260

Linnebacher, M., and Maletzki, C. (2012). Tumor-infiltrating B cells: The ignored players in tumor immunology. *Oncoimmunology* 1 (7), 1186–1188. doi:10.4161/onci.20641

Locy, H., de Mey, S., de Mey, W., De Ridder, M., Thielemans, K., and Maenhout, S. K. (2018). Immunomodulation of the tumor microenvironment: Turn foe into friend. *Front. Immunol.* 9, 2909. doi:10.3389/fimmu.2018.02909

Luo, Z., and Farnham, P. J. (2020). Genome-wide analysis of HOXC4 and HOXC6 regulated genes and binding sites in prostate cancer cells. *PLoS One* 15 (2), e0228590. doi:10.1371/journal.pone.0228590

McKinney, J. A., Wang, G., Mukherjee, A., Christensen, L., Subramanian, S. H. S., Zhao, J., et al. (2020). Distinct DNA repair pathways cause genomic instability at alternative DNA structures. *Nat. Commun.* 11 (1), 236. doi:10.1038/s41467-019-13878-9

Miller, G. J., Miller, H. L., van Bokhoven, A., Lambert, J. R., Werahera, P. N., Schirripa, O., et al. (2003). Aberrant HOXC expression accompanies the malignant phenotype in human prostate. *Cancer Res.* 63 (18), 5879–5888.

Newman, A. M., Liu, C. L., Green, M. R., Gentles, A. J., Feng, W., Xu, Y., et al. (2015). Robust enumeration of cell subsets from tissue expression profiles. *Nat. Methods* 12 (5), 453–457. doi:10.1038/nmeth.3337

O'Connell, E., Reynolds, I. S., McNamara, D. A., Prehn, J. H. M., and Burke, J. P. (2020). Microsatellite instability and response to neoadjuvant chemoradiotherapy in rectal cancer: A systematic review and meta-analysis. *Surg. Oncol.* 34, 57–62. doi:10.1016/j.suronc.2020.03.009

Ohtani, H. (2007). Focus on TILs: Prognostic significance of tumor infiltrating lymphocytes in human colorectal cancer. *Cancer Immun.* 7, 4.

Omatu, T. (1999). Overexpression of human homeobox gene in lung cancer A549 cells results in enhanced motile and invasive properties. *Hokkaido Igaku Zasshi.* 74 (5), 367–376.

Passaro, A., Stenzinger, A., and Peters, S. (2020). Tumor mutational burden as a pan-cancer biomarker for immunotherapy: The limits and potential for convergence. *Cancer Cell* 38 (5), 624–625. doi:10.1016/j.ccell.2020.10.019

Pham, T. H., Park, H. M., Kim, J., Hong, J. T., and Yoon, D. Y. (2020). STAT3 and p53: Dual target for cancer therapy. *Biomedicines* 8 (12), E637. doi:10.3390/biomedicines8120637

Qureshi, M. A., Khan, S., Tauheed, M. S., Syed, S. A., Ujjan, I. D., Lail, A., et al. (2020). Pan-cancer multiomics analysis of TC2N gene suggests its important role(s) in tumourigenesis of many cancers. *Asian pac. J. Cancer Prev.* 21 (11), 3199–3209. doi:10.31557/APJCP.2020.21.11.3199

Rouce, R. H., Shaim, H., Sekine, T., Weber, G., Ballard, B., Ku, S., et al. (2016). The TGF-β/SMAD pathway is an important mechanism for NK cell immune evasion in childhood B-acute lymphoblastic leukemia. *Leukemia* 30 (4), 800–811. doi:10.1038/leu.2015.327

Sabari, J. K., Leonardi, G. C., Shu, C. A., Umeton, R., Montecalvo, J., Ni, A., et al. (2018). PD-L1 expression, tumor mutational burden, and response to immunotherapy in patients with MET exon 14 altered lung cancers. *Ann. Oncol.* 29 (10), 2085–2091. doi:10.1093/annonc/mdy334

Siegel, R. L., Miller, K. D., Fuchs, H. E., and Jemal, A. (2021). Cancer statistics, 2021. *Ca. Cancer J. Clin.* 71 (1), 7–33. doi:10.3322/caac.21654

Srivastava, S., and Hanash, S. (2020). Pan-cancer early detection: Hype or hope? *Cancer Cell* 38 (1), 23–24. doi:10.1016/j.ccell.2020.05.021

Subramanian, A., Tamayo, P., Mootha, V. K., Mukherjee, S., Ebert, B. L., Gillette, M. A., et al. (2005). Gene set enrichment analysis: A knowledge-based approach for interpreting genome-wide expression profiles. *Proc. Natl. Acad. Sci. U. S. A.* 102 (43), 15545–15550. doi:10.1073/pnas.0506580102

Sung, H., Ferlay, J., Siegel, R. L., Laversanne, M., Soerjomataram, I., Jemal, A., et al. (2021). Global cancer statistics 2020: GLOBOCAN estimates of incidence and mortality worldwide for 36 cancers in 185 countries. *Ca. Cancer J. Clin.* 71 (3), 209–249. doi:10.3322/caac.21660

Szigeti, K. A., Galamb, O., Kalmar, A., Bartak, B. K., Nagy, Z. B., Markus, E., et al. (2018). Role and alterations of DNA methylation during the aging and cancer. *Orv. Hetil.* 159 (1), 3–15. doi:10.1556/650.2018.30927

Tiffen, J., Gallagher, S. J., Filipp, F., Gunatilake, D., Emran, A. A., Cullinane, C., et al. (2020). EZH2 cooperates with DNA methylation to downregulate key tumor suppressors and IFN gene signatures in melanoma. *J. Invest. Dermatol.* 140 (12), 2442–2454. doi:10.1016/j.jid.2020.02.042

Wang, Z., Jensen, M. A., and Zenklusen, J. C. (2016). A practical guide to the cancer genome atlas (TCGA). *Methods Mol. Biol.* 1418, 111–141. doi:10.1007/978-1-4939-3578-9_6

Yang, W., Soares, J., Greninger, P., Edelman, E. J., Lightfoot, H., Forbes, S., et al. (2013). Genomics of drug sensitivity in cancer (GDSC): A resource for therapeutic biomarker discovery in cancer cells. *Nucleic Acids Res.* 41, D955–D961. Database issue. doi:10.1093/nar/gks1111

Yang, W., Zhang, W., and Wang, X. (2017). Post-translational control of ABA signalling: The roles of protein phosphorylation and ubiquitination. *Plant Biotechnol. J.* 15 (1), 4–14. doi:10.1111/pbi.12652

Yoshihara, K., Shahmoradgoli, M., Martinez, E., Vegesna, R., Kim, H., Torres-Garcia, W., et al. (2013). Inferring tumour purity and stromal and immune cell admixture from expression data. *Nat. Commun.* 4, 2612. doi:10.1038/ncomms3612

Yuan, H., Yan, M., Zhang, G., Liu, W., Deng, C., Liao, G., et al. (2019). CancerSEA: A cancer single-cell state atlas. *Nucleic Acids Res.* 47 (D1), D900–D908. doi:10.1093/nar/gky939

Glossary

ACC Adrenocortical carcinoma

BLCA Bladder urothelial carcinoma

BRCA Breast invasive carcinoma

CESC Cervical squamous cell carcinoma and endocervical adenocarcinoma

CHOL Cholangiocarcinoma

COAD Colon adenocarcinoma

DLBC Lymphoid neoplasm diffuse large B-cell lymphoma

ESCA Esophageal carcinoma

GBM Glioblastoma multiforme

HNSC Head and neck squamous cell carcinoma

KICH Kidney chromophobe

KIRC Kidney renal clear cell carcinoma

KIRP Kidney renal papillary cell carcinoma

LAML Acute myeloid leukemia

LGG Brain lower grade glioma

LIHC Liver hepatocellular carcinoma

LUAD Lung adenocarcinoma

LUSC Lung squamous cell carcinoma

MESO Mesothelioma

OV Ovarian serous cystadenocarcinoma

PAAD Pancreatic adenocarcinoma

PCPG Pheochromocytoma and paraganglioma

PRAD Prostate adenocarcinoma

READ Rectum adenocarcinoma

SARC Sarcoma

SKCM Skin cutaneous melanoma

STAD Stomach adenocarcinoma

TGCT Testicular germ cell tumors

THCA Thyroid carcinoma

THYM Thymoma

UCEC Uterine corpus endometrial carcinoma

UVM Uveal melanoma

frontiers | Frontiers in Genetics

TYPE Original Research
PUBLISHED 06 October 2022
DOI 10.3389/fgene.2022.1025970

OPEN ACCESS

EDITED BY
Jiao Hu,
Central South University, China

REVIEWED BY
Yongbiao Huang,
Huazhong University of Science and Technology, China
Huaide Qiu,
Nanjing Medical University, China

*CORRESPONDENCE
Qiming Gong,
15610398015@163.com

†These authors have contributed equally to this work

SPECIALTY SECTION
This article was submitted to Cancer Genetics and Oncogenomics, a section of the journal Frontiers in Genetics

RECEIVED 23 August 2022
ACCEPTED 21 September 2022
PUBLISHED 06 October 2022

CITATION
Guo Z, Liu F and Gong Q (2022), Integrative pan-cancer landscape of MMS22L and its potential role in hepatocellular carcinoma. *Front. Genet.* 13:1025970. doi: 10.3389/fgene.2022.1025970

Integrative pan-cancer landscape of MMS22L and its potential role in hepatocellular carcinoma

Zhiting Guo[1†], Fahui Liu[2†] and Qiming Gong[3*]

[1]College of Biological Science and Engineering, Fuzhou University, Fuzhou, China, [2]Department of Medical Biochemistry and Cell Biology, Institute of Biomedicine, University of Gothenburg, Gothenburg, Sweden, [3]Department of Nephrology, Affiliated Hospital of Youjiang Medical University for Nationalities, Baise, Guangxi, China

Methyl methanesulfonate-sensitivity protein 22-like (MMS22L) is crucial in protecting genome integrity during DNA replication by preventing DNA damage and maintaining efficient homologous recombination. However, the role of MMS22L in human cancers remains unclear. Here, we reported the landscape of MMS22L using multi-omics data and identified the relationship between the MMS22L status and pan-cancer prognosis. In addition, the correlation of MMS22L mRNA expression levels with tumor mutational burden, microsatellite instability, homologous recombination deficiency, and loss of heterozygosity in pan-cancer was also described in this study. Furthermore, this study was the first to characterize the relationship between mRNA expression of MMS22L and immune cell infiltration in the tumor microenvironment in human cancer. Concurrently, this study explored the crucial role of MMS22L in different immunotherapy cohorts through current immunotherapy experiments. Eventually, we investigated the role of MMS22L in hepatocellular carcinoma (HCC). The results demonstrated that MMS22L is widely expressed in multiple HCC cell lines, and our results emphasized that MMS22L was involved in HCC progression and affects the prognosis of patients with HCC through multiple independent validation cohorts. Collectively, our findings reveal the essential role of MMS22L as a tumor-regulating gene in human cancers while further emphasizing its feasibility as a novel molecular marker in HCC. These findings provide an essential reference for the study of MMS22L in tumors.

KEYWORDS

MMS22L, pan-cancer, prognosis, immunotherapy, hepatocellular carcinoma

Abbreviations: TMB, tumor mutational burden; MSI, microsatellite instability; HRD, homologous recombination deficiency; LOH, loss of heterozygosity; TCGA, The Cancer Genome Atlas; GEO, gene expression omnibus; ICGC, International Cancer Genome Consortium; CNV, copy number variation; GSEA, gene set enrichment analysis; NR, nonresponse; R, response; HR, homologous recombination; OS, overall survival; DSS, disease-specific survival; DFI, disease-free interval; PFI, progression-free interval.

Introduction

Methyl methanesulfonate-sensitivity protein 22-like (MMS22L) is widely known for its essential role in DNA replication, which involves the formation of the MMS22L-TONSL protein complex (Duro et al., 2010; Saredi et al., 2016). This complex protects DNA molecules in the replication phase and assists in the necessary DNA damage repair by participating in homologous recombination (HR). Since tumor cells divide and differentiate significantly more frequently than normal cells, they have a longer "sensitive period" and a great demand for DNA damage repair (Miller et al., 2019). Therefore, cancer cell DNA is more fragile than normal cell DNA, especially during division, thereby requiring more protection. This finding suggests that MMS22L may serve as a new drug target for blocking DNA repair in cancer cells. The interaction between MMS22L and NFKBIL2 has been proposed as another mechanism for participating in the NFKB pathway in cancer cells (Nguyen et al., 2012), further identifying it as a promising target for cancer therapy. Therefore, these findings suggest that the activity of MMS22L or its complexes involved in tumor cell proliferation appears to be essential in tumorigenesis.

Although MMS22L is an attractive target for cancer therapy, its application in tumor therapy still faces numerous problems. Some studies have demonstrated the complex role of MMS22L in different types of tumors. MMS22L, for instance, was detected in lung cancers as an oncogene involved in tumor proliferation and metastasis (Nguyen et al., 2012). Conversely, a lower expression of MMS22L was associated with worse clinical outcomes in esophageal squamous cell carcinoma, suggesting MMS22L is a tumor suppressor (Luo et al., 2021). Concurrently, many reports described that MMS22L affected the prognosis of patients by regulating drug sensitivity during treatment (Liu et al., 2021). Altogether, these results suggest that the roles of MMS22L in different tumors are diverse and complex and suggest that MMS22L may be a promising target for tumor therapy. However, tumor heterogeneity limits our knowledge about the role of MMS22L in human tumors. Therefore, a comprehensive understanding of the molecular characterization and clinical relevance of MMS22L in human cancer is urgent. Understanding the aberrant expression and genomic alterations of MMS22L may help to clarify its role in cancer prognosis and treatment.

This study presents a relatively comprehensive assessment of MMS22L in pan-cancer using public repository data. The results of this study demonstrate the status of MMS22L and its association with prognostic data and genomic heterogeneity of tumor patients. In addition, we are the first to analyze the association of MMS22L with the immune system in pan-cancer and its role in immunotherapy. Further, by combining multi-cohorts and molecular biology experiments, this study identifies the vital role and clinical significance of MMS22L in hepatocellular carcinoma (HCC). Overall, this study is the first to reveal the landscape of MMS22L in pan-cancer and preliminarily explores the potential role of MMS22L in HCC. These findings demonstrate the potential value of MMS22L in cancer and lay the foundation for developing MMS22L in clinical applications.

Materials and methods

Data source

The UCSC Xena database (https://xenabrowser.net/datapages/) was used to download the gene expression data and corresponding clinical information of The Cancer Genome Atlas (TCGA) and Genotype-Tissue Expression (GTEx). Copy number variation (CNV) data was processed through GISTIC2.0, and single-nucleotide variants (SNV) data were also downloaded. cBioPortal (http://cbioportal.org) was used to visualize the frequency of genomic alterations of MMS22L in 33 cancer types. The Human Protein Atlas (https://www.proteinatlas.org/) database was used to confirm MMS22L protein localization at the cellular level. MMS22L protein interaction information was obtained from ComPPI database (http://comppi.linkgroup.hu). Abbreviations for cancers mentioned in this study are shown in Supplementary Table S1. The expression level of MMS22L in different immunotherapy cohorts, the relationship between MMS22L expression and prognosis of patients with immunotherapy, and MMS22L expression and drug sensitivity were analyzed using the Biomarker Exploration of Solid Tumors (BEST) web server (https://rookieutopia.com/). To further explore the effect of MMS22L in HCC, four microarray data of patients with HCC, including GSE25097, GSE22058, GSE36376, and GSE54236, were downloaded from the Gene Expression Omnibus (GEO). RNA sequencing (RNA-seq) data of ICGC-LIRI-JP were downloaded from the International Cancer Genome Consortium (ICGC) portal (https://dcc.icgc.org/projects/LIRI-JP). In addition, RNA-Seq data of the LIHC-CN cohort was obtained from a previous study (Gao et al., 2019).

Cell culture and RT-qPCR

Huh-7, 7721, MHCC97H, SK, and LO2 cells were cultured in Dulbecco's Modified Eagle Medium (DMEM) media supplemented with 10% fetal bovine serum (FBS, Gibco) at 37 °C with 5% CO_2. SNU398 and SNU449 cells were cultured in 1640 media supplemented with 10% FBS (Gibco) at 37°C with 5% CO_2. Hep3B and HepG2 cells were cultured in Minimum Essential Medium (MEM) media supplemented with 10% FBS (Gibco) at 37 °C with 5% CO_2. For RT-qPCR experiments, Trizol reagent (Thermo Fisher Scientific) and RNeasy Lipid Tissue Kit (QIAGEN) were used to isolate total RNA according to the manufacturer's instructions, and cDNA was synthesized using

reverse transcriptase (Promega). The sequences of primers used in this study are listed in Supplementary Table S2. Sangon Biotech, China, synthesized all primers.

Protein extraction and western blotting

All cells were lysed in RIPA buffer (Sigma-Aldrich) containing a 1% protease inhibitor cocktail (Thermo Fisher Scientific) and phosphatase inhibitor cocktail (Thermo Fisher Scientific). The MMS22L protein and anti-beta actin were separated using 10% SDS–PAGE and transferred to polyvinylidene difluoride membranes. After blocking the membranes with 5% BSA in 1 × PBST buffer (10 mM phosphate buffer, 2.7 mM KCl, 137 mM NaCl, 0.05% Tween-20; pH 7.4) at room temperature for 1h, the membranes were separately incubated overnight with MMS22L recombinant monoclonal antibody (1:1,500; ab181047, Abcam) and anti-beta actin (1:1,500; ab8227, Abcam) at 4°C. The membranes were washed with 1 × PBST buffer three times to remove the unbound protein.

Survival analysis of MMS22L in pan-cancer

A sample barcode was used to merge CNV and clinical survival data for MMS22L in pan-cancer. Tumor samples were divided into wild-type (WT), amplification (Amp.), and deletion (Dele). groups. Log-rank tests were performed to evaluate the survival difference between groups. The SNV data and clinical survival data were merged by sample barcode for survival analysis of MMS22L in pan-cancer studies. Tumor samples were divided into mutant groups when the specific genes in these samples were mutated (deleterious mutants). Cox proportional hazards models and log-rank tests were used to evaluate the survival difference between WT and mutant groups. For survival analysis of MMS22L mRNA expression in pan-cancer, mRNA expression and survival data were merged by sample barcode, and the median value of MMS22L was used to divide tumor samples into high and low expression groups. Next, we used the R package survival to fit the survival time and survival status within the two groups. Cox proportional hazards models and log-rank tests were used to analyze the correlation between mRNA expression of MMS22L with overall survival (OS), disease-specific survival (DSS), disease-free interval (DFI), and progression-free interval (PFI) in pan-cancer.

Analysis of genomic heterogeneity

Homologous recombination deficiency (HRD) data (Thorsson et al., 2018), microsatellite instability (MSI) scores (Bonneville et al., 2017), and loss of heterozygosity (LOH) data (Thorsson et al., 2018) were collected from previous studies. SNV data processed by MuTect2 were from Genomic Data Commons (GDC) (https://portal.gdc.cancer.gov/). With the R package "maftools", the tumor mutational burden (TMB) value was calculated for each tumor.

Gene set enrichment analysis

To determine the pathways associated with MMS22L, for each tumor type, samples were divided into the top 30% and bottom 30% groups based on the expression level of MMS22L. The hallmark gene set (h.all.v7.2. symbols) was downloaded from MSigDB (https://www.gsea-msigdb.org/gsea/msigdb/). Then, the gene set enrichment analysis (GSEA) was performed using R software.

Correlation analysis of MMS22L and immune cell infiltration

The correlation between MMS22L mRNA expression and immune cell infiltration in pan-cancer was downloaded from the TIMER2 database (http://timer.cistrome.org/). Nineteen immune cells, including B cells, cancer-associated fibroblasts, $CD4^+$ T cells, $CD8^+$ T cells, myeloid dendritic cells, endothelial cells, eosinophils, gamma delta T cells, hematopoietic stem cells, macrophages, mast cells, myeloid-derived suppressor cells, monocytes, neutrophils, natural killer (NK) cells, NK T cells, common myeloid progenitors, regulatory T cells, and follicular helper T cells, were incorporated in the present study.

Statistical analysis

In addition to the aforementioned bioinformatic tools, GraphPad Prism 9.0 and R software (4.2.1, www.r-project.org) were used to perform analyses in this study. Comparisons between continuous variables were made using Wilcoxon rank-sum test. The association between two continuous variables was assessed using Spearman's rank correlation. $p < 0.05$ was considered statistically significant in this study.

Result

Basic information about MMS22L in pan-cancer

To gain a basic understanding of MMS22L in pan-cancer, we used the TCGA and GTEx databases to evaluate the expression level of MMS22L in cancer compared with that in normal tissues.

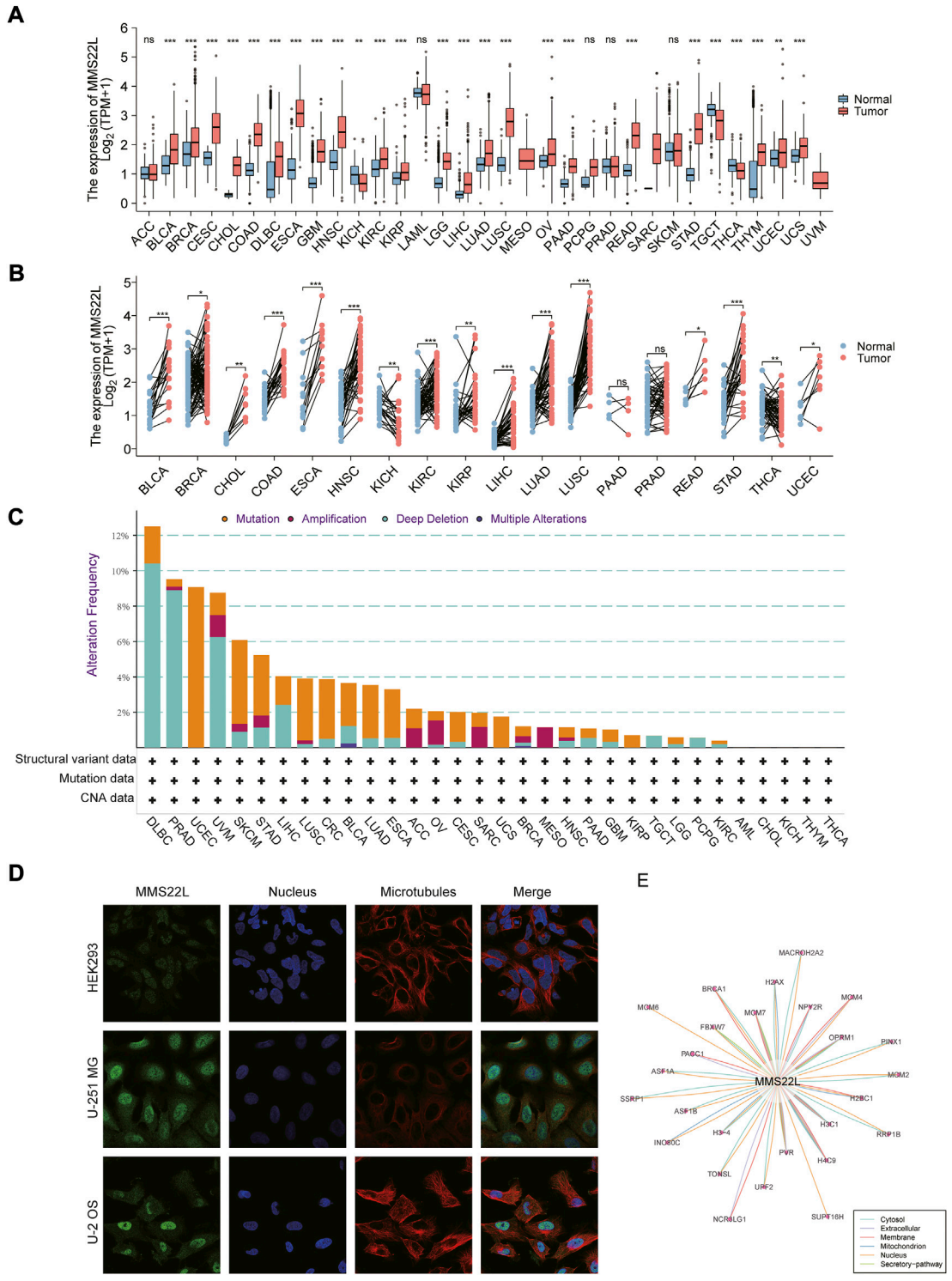

FIGURE 1
Basic information about methyl methanesulfonate-sensitivity protein 22-like (MMS22L) in pan-cancer. **(A)** Differential expression of MMS22L based on The Cancer Genome Atlas and Genotype-Tissue Expression databases in pan-cancer. **(B)** Paired analysis of MMS22L expression in pan-cancer. **(C)** The landscape of MMS22L genomic alterations in pan-cancer according to the cBioPortal database. **(D)** Immunofluorescence images depicting localization information of MMS22L protein in HEK 293, U-2 OS, and U251 MG cell lines. **(E)** Protein-protein interaction network formed by MMS22L. ns, $p \geq 0.05$; *, $p < 0.05$; **, $p < 0.01$; ***, $p < 0.001$.

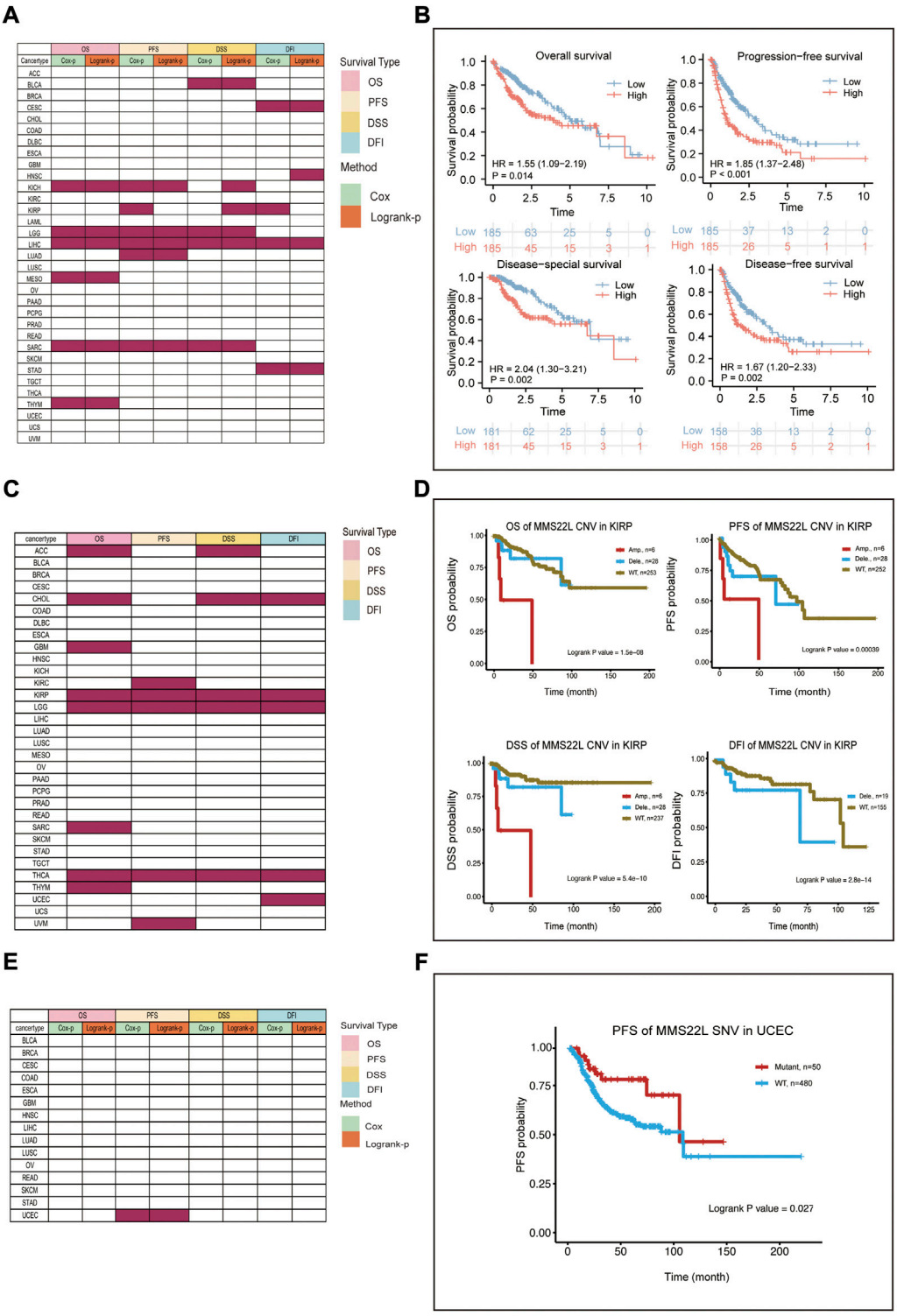

FIGURE 2
Survival landscape of methyl methanesulfonate-sensitivity protein 22-like (MMS22L) in pan-cancer. **(A)** Summary of the correlation between mRNA expression of MMS22L with OS, DSS, DFI, and PFI based on the univariate Cox regression and log-rank tests in pan-cancer. **(B)** High mRNA expression of MMS22L was associated with worse outcomes in patients with HCC. **(C)** Summary of the correlation between the copy number variation status of MMS22L using OS, DSS, DFI, and PFI based on the log-rank tests. **(D)** Amplification of MMS22L is associated with a worse prognosis in kidney renal papillary cell carcinoma. **(E)** Summary of the correlation between the single-nucleotide variant status of MMS22L and OS, DSS, PFI, and DFI based on the univariate Cox regression and log-rank tests. **(F)** Patients with mutated MMS22L had a better prognosis of progression-free survival in uterine corpus endometrial carcinoma.

High expression levels of MMS22L were detected in most cancer types, including BLCA, BRCA, CESC, CHOL, COAD, DLBC, ESCA, GBM, HNSC, KIRC, KIRP, LGG, LIHC, LUAD, LUSC, OV, PAAD, READ, STAD, THYM, UCEC, UCS. The expression levels of MMS22L in TGCT, THCA, and KICH were lower than in normal tissues (Figure 1A). The results of the paired analysis showed that MMS22L still had significant differences among BLCA, BRCA, CHOL, COAD, ESCA, HNSC, KIRC, KIRP, LIHC, LUAD, LUSC, READ, STAD, UCEC, TGCT, and KICH (Figure 1B). Analysis of genomic alterations in MMS22L showed that there was no universal alteration of MMS22L in pan-cancer. DLBC was the most commonly altered cancer type, and among the mutant types was primarily deep deletion, which occurred in approximately 10% of DLBC patients. It is noteworthy that somatic mutation was the only genomic event in UCEC (Figure 1C). Images captured with immunofluorescence showed that MMS22L protein was predominantly localized and distributed in the nucleus of HEK293, U-251 MG, and U-2 OS tumor cell lines (Figure 1D). Analysis of protein-protein interaction networks revealed that proteins closely related to MMS22L and their subcellular localization were distributed in the cytosol, mitochondrion, extracellular membrane, nucleus, and secretory pathway (Figure 1E).

Correlation of MMS22L with survival in different omics pan-cancer data

We further analyzed the association of data from different omics with four different clinical prognostic outcomes in pan-cancer. The specific analysis is indicated in Supplementary Table S3. Specifically, the expression level of MMS22L was significantly correlated with the prognosis of KICH, LGG, LIHC, MESO, SARC, and THYM (Figure 2A). Among them, we found that only in LIHC was the expression level of MMS22L significantly associated with the four clinical outcomes using two different methods. We further visualized the correlation of MMS22L expression with different clinical outcomes, and the results showed that a higher expression of MMS22L was associated with a worse prognosis in patients with HCC (Figure 2B). The CNV level of MMS22L was associated with overall survival (OS) in adrenocortical carcinoma (ACC), CHOL, GBM, KIRP, LGG, SARC, THYM, and THCA (Figure 2C). Meanwhile, the expression of MMS22L was correlated with KIRC, KIRP, LGG, THCA, and UVM. It was evident that the expression of MMS22L in KIRP, LGG, and THCA was associated with all four outcomes. We further visualized the relationship between MMS22L CNV in KIRP and the four types of clinical outcomes. The analysis showed that patients with wild-type MMS22L showed better survival in all clinical outcomes in KIRP (Figure 2D). Finally, we analyzed the association of the SNV status of MMS22L with patient prognosis. We observed that only mutations of MMS22L were associated with the survival of patients with UCEC (Figure 2E). Furthermore, mutations of MMS22L were tightly associated with better progression-free survival of patients with UCEC (Figure 2F).

Functional analysis of MMS22L in pan-cancer

To elucidate the potential mechanism of action of MMS22L, we further analyzed the pathways involved in MMS22L using the GSEA function in pan-cancer (Figure 3A). The analysis showed that pathways including mitotic spindle, G2M checkpoint, and E2F targets were significantly activated in the MMS22L high expression group in pan-cancer. The above results suggested that MMS22L played a key role in the cell cycle in human tumors, which might be one of the key factors for MMS22L to affect tumor evolution. In addition, we noticed that immune pathways, such as TNFα-signaling through NF-kB, inflammatory response, IFN-α response, and IFN-γ response were significantly activated in GBM in the MMS22L low expression group. Conversely, these pathways were significantly activated in the MMS22L high expression group in THCA. These results suggest that the role of MMS22L in pathways involved in immune responses differed across tumor types.

Correlation analysis of MMS22L with genomic heterogeneity in pan-cancer

We further explored the relationship between MMS22L expression and genomic heterogeneity. Genomic heterogeneity has been increasingly reported to be related to numerous genes, although unclear. The relationship between various types of genomic heterogeneity, including TMB, MSI, HRD, and LOH and MMS22L expression in pan-cancer are still unclear. After integrating TMB data and MMS22L expression in pan-cancer, the TMB of 11 types of tumors (LUAD, COAD, READ, STES, KIPAN, STAD, prostate adenocarcinoma (PRAD), pheochromocytoma and paraganglioma (PCPG), ACC, and KICH) were positively related to MMS22L expression. However, the TMB of KIRP was negatively correlated with MMS22L expression (Figure 4A). The MSI scores were closely related to 15 types of tumors. CESC, COAD, COADREAD, STES, SARC, STAD, KIRC, LUSC, and READ were positively related to MMS22L expression (Figure 4B). In addition to TMB and MSI, the relationship between HRD data and the expression of MMS22L is also presented in Figure 4C. A significant correlation was observed in 20 tumors, with a significant positive correlation in 18 tumors (GBMLGG, LGG, LUAD, BRCA, STES, SARC, KIRP, KIPAN, HNSC, LUSC, LIHC, MESO, PAAD, OV, BLCA, ACC, KICH, and CHOL), and a negative correlation in two tumors (THYM and UVM). Finally,

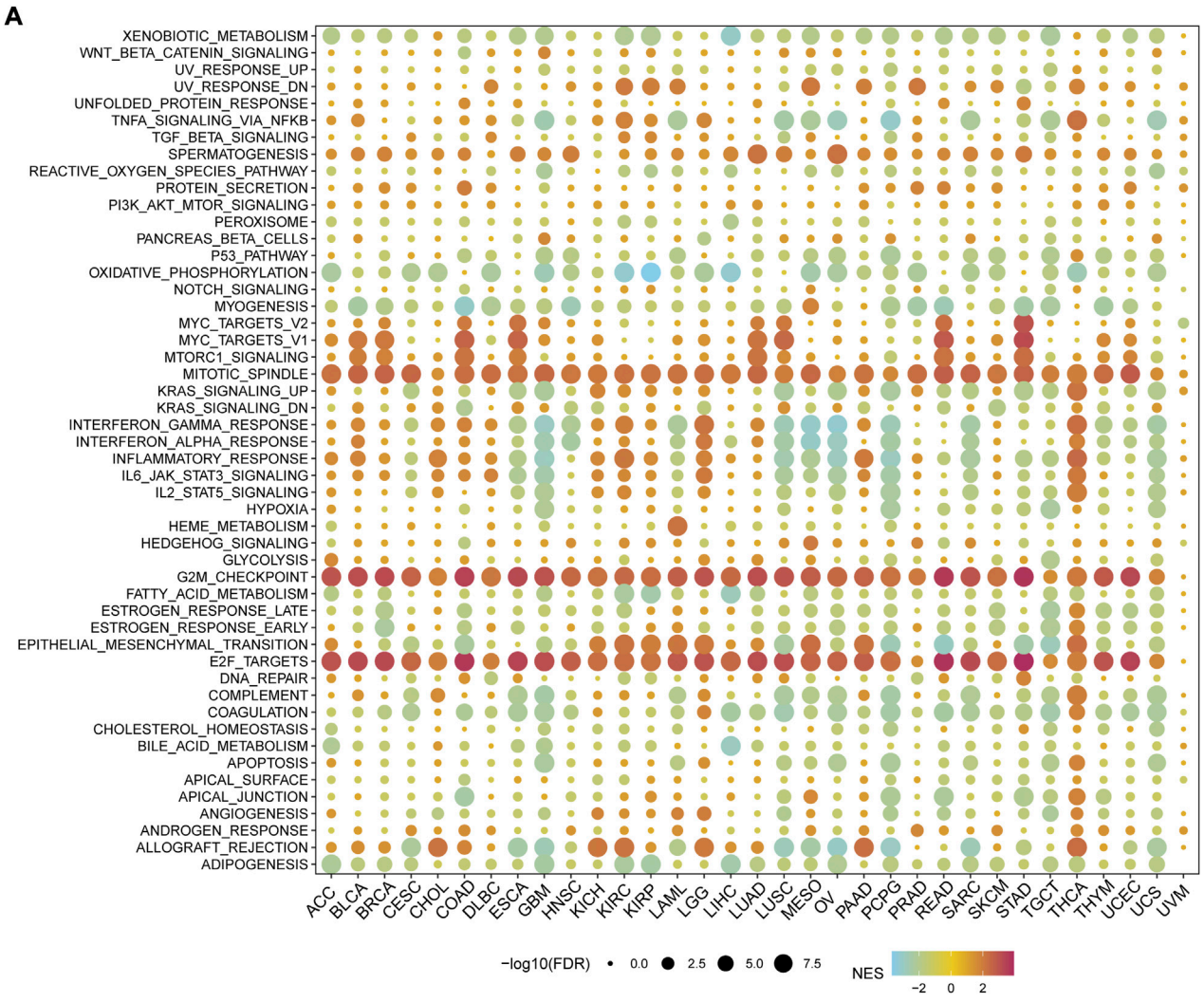

FIGURE 3
Functional analysis of methyl methanesulfonate-sensitivity protein 22-like (MMS22L) in pan-cancer. **(A)** Enrichment analysis for hallmark gene sets between high- and low- MMS22L expression groups.

the correlation between LOH data and MMS22L expression was analyzed. In contrast, 12 types of cancers (GBMLGG, LGG, LUAD, BRCA, STES, SARC, KIRP, HNSC, LUSC, LIHC, OV, and BLCA) in which MMS22L expression was positively related to HRD had a significant positive correlation. However, there was a significant negative correlation among the three tumors, such as KIPAN, KIRC, and UVM (Figure 4D).

MMS22L and immune cells in pan-cancer

In order to confirm the relationship between MMS22L expression and cancer immunity, we examined the correlation between MMS22L expression and the infiltration of immune cells in pan-cancer using the TIMER2 database (Figure 5A). The results indicated that MMS22L was positively associated with the infiltration levels of B cells, cancer-associated fibroblasts (CAF), $CD4^+$ T cells, $CD8^+$ T cells, dendritic cells, endothelial cells (Endo), macrophages, mast cells, myeloid-derived suppressor cells (MDSC), monocytes, neutrophils, NK cells, common lymphoid progenitor cells (CLP), T follicular helper cells (Tfh), and Tregs in the majority of these common cancers. In contrast, MMS22L was negatively associated with the infiltration levels of eosinophils (Eos), HSC, and NKT. In addition, it was also significant that almost all types of cancers were positively

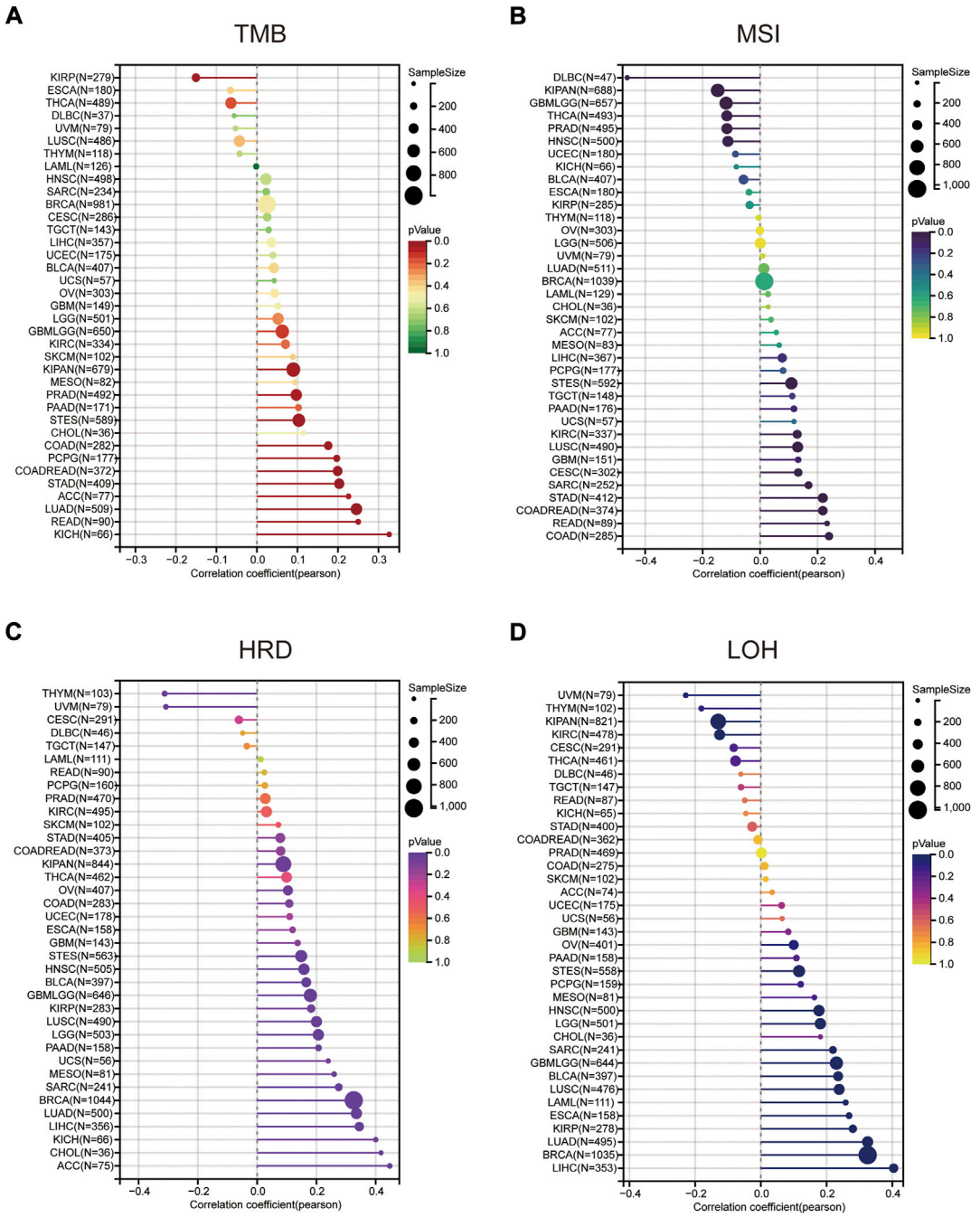

FIGURE 4
The correlation between methyl methanesulfonate-sensitivity protein 22-like (MMS22L) expression and genomic heterogeneity in pan-cancer. **(A)** Spearman correlation analysis of tumor mutational burden and MMS22L mRNA expression. **(B)** Spearman correlation analysis of microsatellite instability and MMS22L mRNA expression. **(C)** Spearman correlation analysis of homologous recombination deficiency and MMS22L mRNA expression. **(D)** Spearman correlation analysis of loss of heterozygosity and MMS22L mRNA expression.

associated with MDSC and neutrophils. Our results indicated that MMS22L is associated with diverse cancers and may affect the effectiveness of therapy by associating with immune cells.

Immunotherapy analyses of MMS22L

The previous analysis showed that MMS22L had different immunoregulatory functions in different tumor types and

10.3389/fgene.2022.1025970

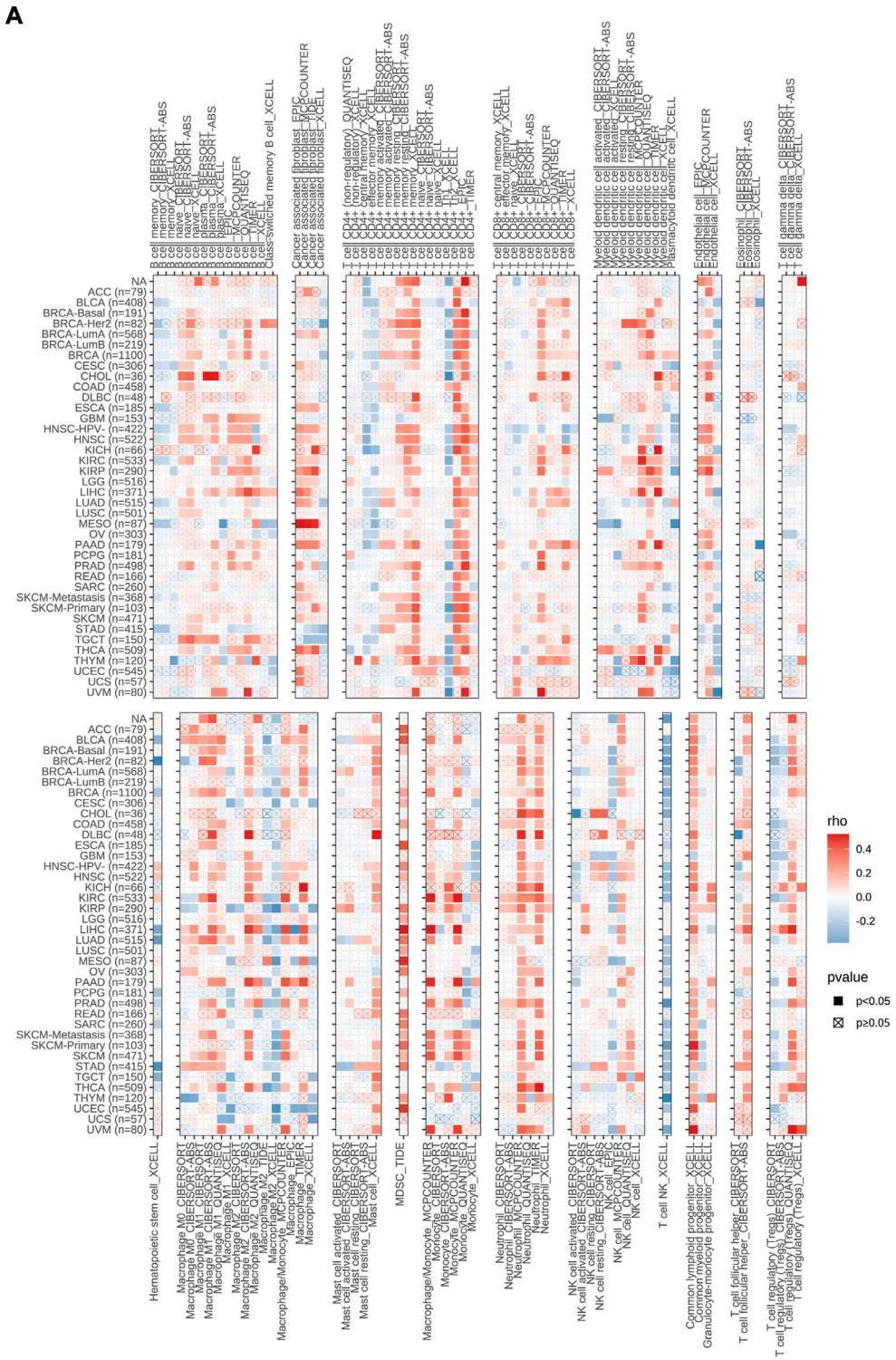

FIGURE 5
Associations of methyl methanesulfonate-sensitivity protein 22-like (MMS22L) expression with immune infiltration in pan-cancer. **(A)** The correlations of MMS22L mRNA expression and immune cell infiltration across human cancers according to the TIMER2.0 database.

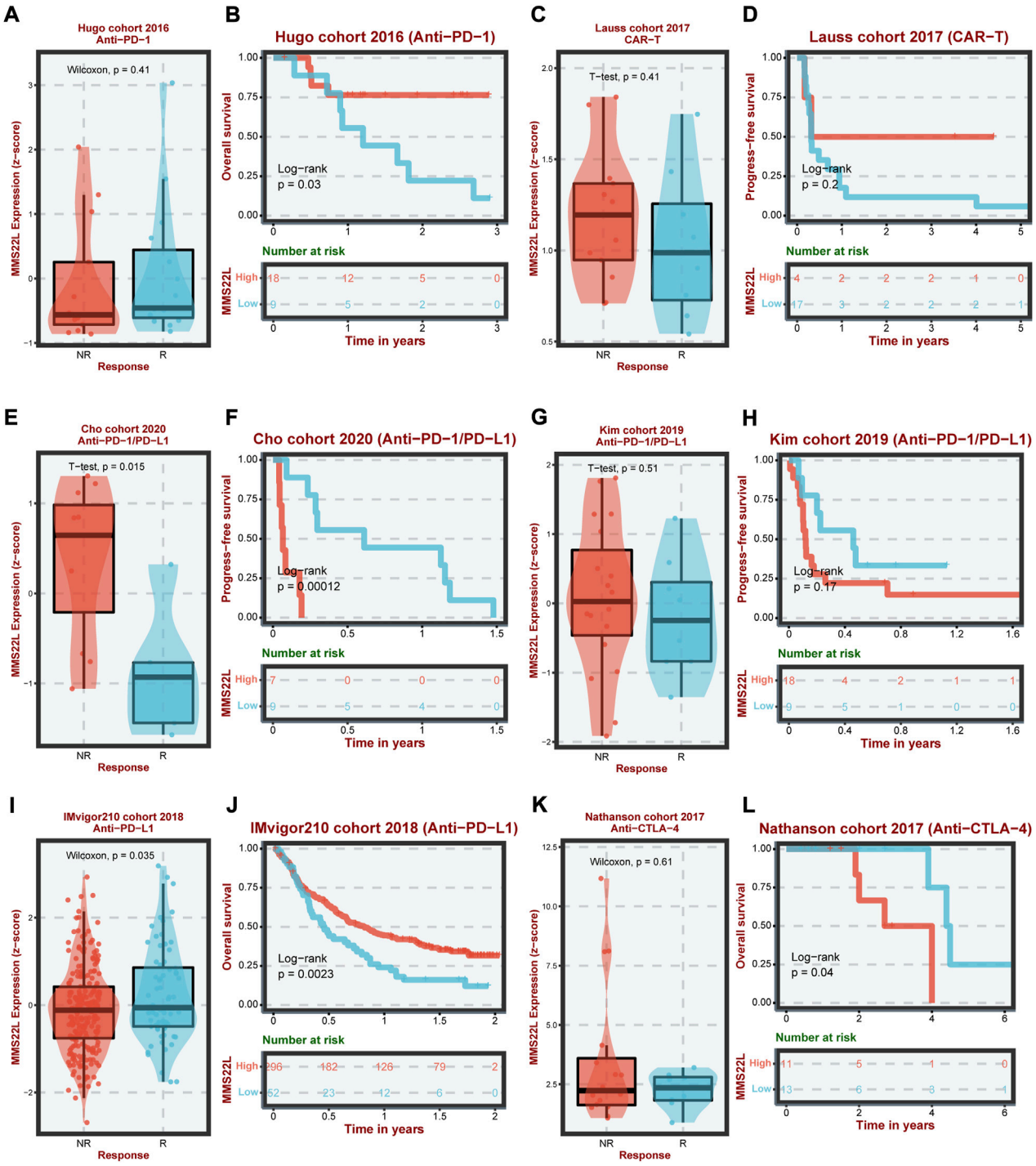

FIGURE 6
Analysis of methyl methanesulfonate-sensitivity protein 22-like (MMS22L) in cancer immunotherapy in different cohorts. The difference in MMS22L expression between the corresponding group and the non-corresponding group and its relationship with the prognosis of patients in Hugo **(A,B)**, Lauss **(C,D)**, Cho **(E,F)**, Kim **(G,H)**, IMvigor210 **(I,J)**, and Nathanson **(K,L)** cohorts.

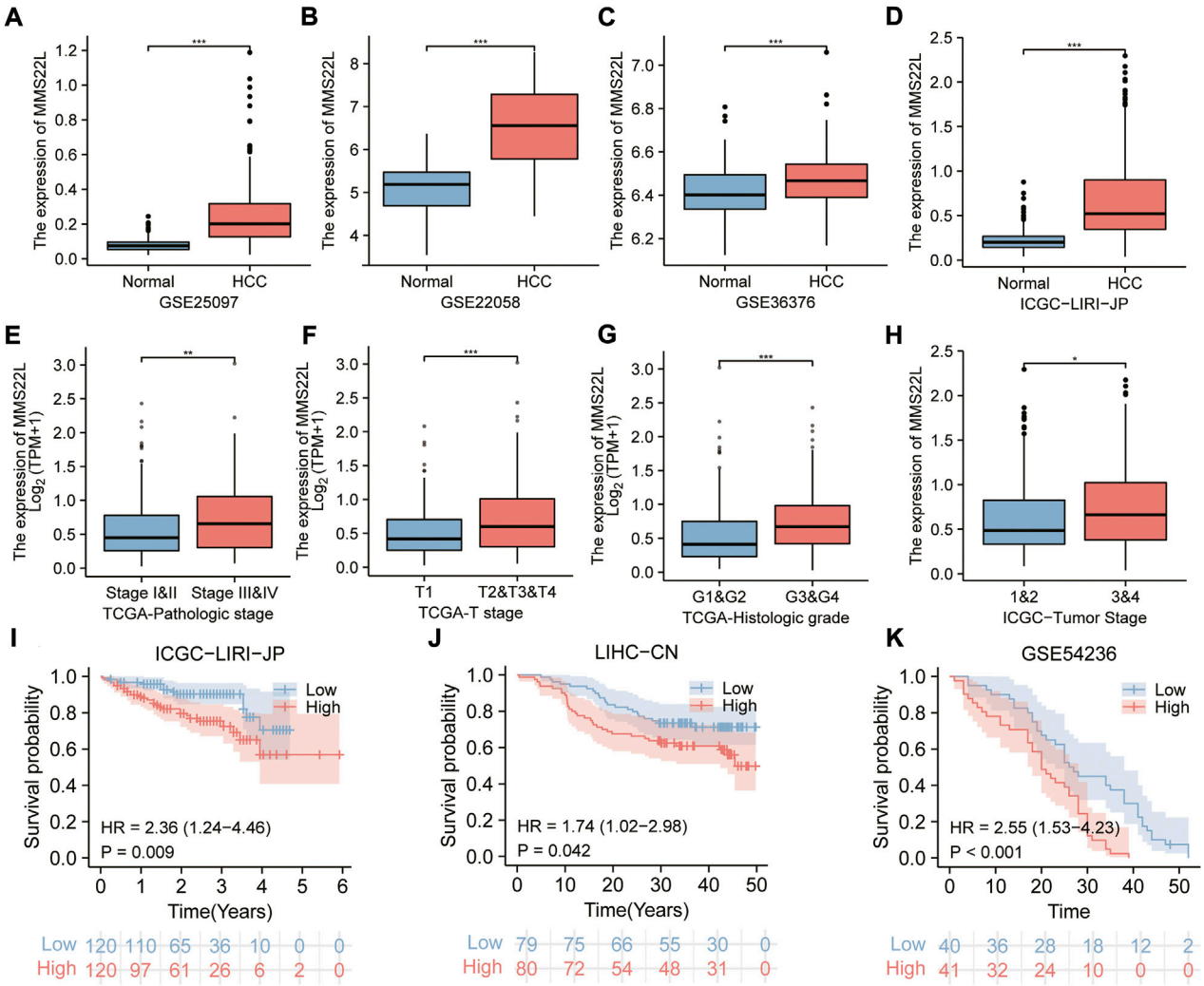

FIGURE 7
The correlation of methyl methanesulfonate-sensitivity protein 22-like (MMS22L) expression with clinical parameters in hepatocellular carcinoma (HCC). **(A–D)** Boxplot for multiple HCC cohorts showing the higher mRNA expression of MMS22L in tumor tissues than in non-tumor tissues. **(E–H)** The elevated level of MMS22L expression is associated with a higher degree of malignancy in HCC. **(I–K)** The Kaplan–Meier curves for MMS22L in the ICGC-LIRI-JP **(I)**, LIHC-CN **(J)**, and GSE54236 **(K)** cohorts. *, $p < 0.05$; **, $p < 0.01$; ***, $p < 0.001$.

correlated with immune cells in the tumor microenvironment. Therefore, we analyzed the expression of MMS22L in six different immunotherapy cohorts and its correlation with patient prognosis (Figures 6A–L). The analytical results showed that in the Cho cohort 2020, the expression level of MMS22L in the nonresponse (NR) group was significantly higher than that in the response (R) group, and the higher expression of MMS22L was significantly associated with a worse prognosis of patients (Figures 6E,F). Conversely, in the IMvigor210 cohort, the expression level of MMS22L in the R group was significantly higher than that in the NR group. Patients with higher levels of MMS22L showed a better clinical outcome (Figures 6I,J). However, MMS22L expression levels did not differ significantly in other immunotherapy cohorts' responses and prognostic outcomes. These results demonstrated the feasibility of MMS22L as an immunotherapy marker. These results further suggested that our focus on heterogeneity among different tumor types might help us to better understand the differences in the effects of immunotherapy among different tumor types.

Clinical relevance of MMS22L in HCC

The previous analysis demonstrated that MMS22L was an important risk factor for HCC. Therefore, we identified HCC as a representative cancer type for subsequent analysis. Using

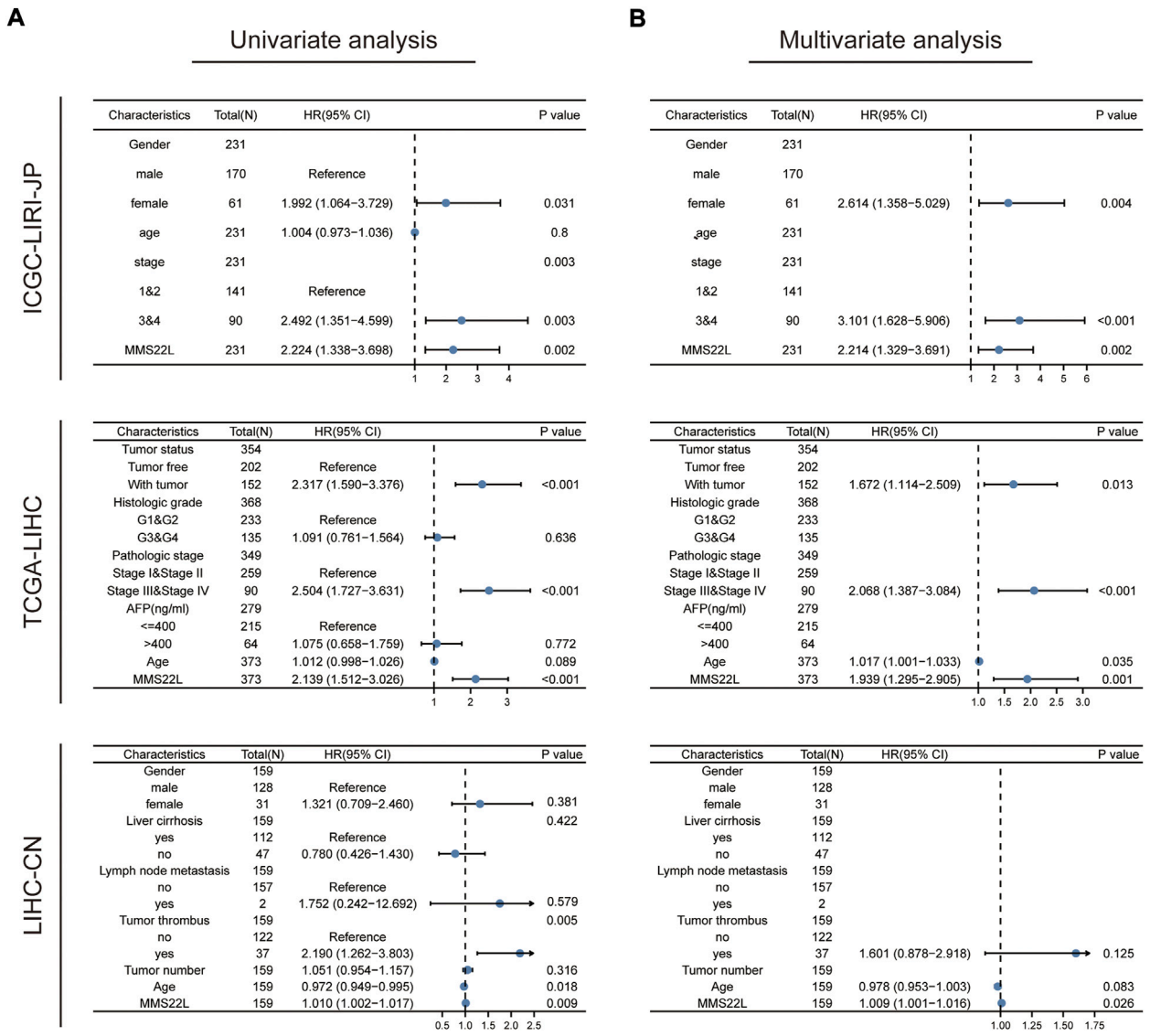

FIGURE 8
Validation of the independency of methyl methanesulfonate-sensitivity protein 22-like (MMS22L) for prediction of overall survival in patients with HCC. **(A,B)** Univariate and multivariate cox regression analysis validated that MMS22L was an independent predictor for OS in TCGA-LIHC, ICGC-LIRI-JP, and LIHC-CN cohorts.

different clinical cohorts, we further explored the relationship between MMS22L expression levels and HCC. The expression level of MMS22L in tumor tissues was significantly higher than that in adjacent normal tissues in different HCC cohorts (Figures 7A–D). In addition, the expression level of MMS22L was higher in patients with higher HCC grades, suggesting that MMS22L participated in the clinical process and related to the malignancy of patients with HCC (Figures 7E–H). Kaplan-Meier curves for OS also showed that patients with higher expression of MMS22L had a worse OS than those with low expression of MMS22L in three different cohorts (Figures 7I,J). These results suggest an important role of MMS22L in HCC. We also detected the mRNA expression levels of MMS22L in HCC cell lines (7721, Hep3B, MHCC97H, SNU398, HepG2, Huh-7, SK, and SNU449 cells) and normal hepatocytes (LO2). The results showed that MMS22L expression in SNU398 was the highest among all these HCC cell lines, while it was lowest in HepG2 (Supplementary Figure S1). However, the expression of MMS22L was higher in all eight HCC cell lines than in LO2. Next, we analyzed the expression level of MMS22L in the protein of 9 cell lines and found that MMS22L expression was the highest in the LO2 cell and the lowest in the HepG2 cell (Supplementary

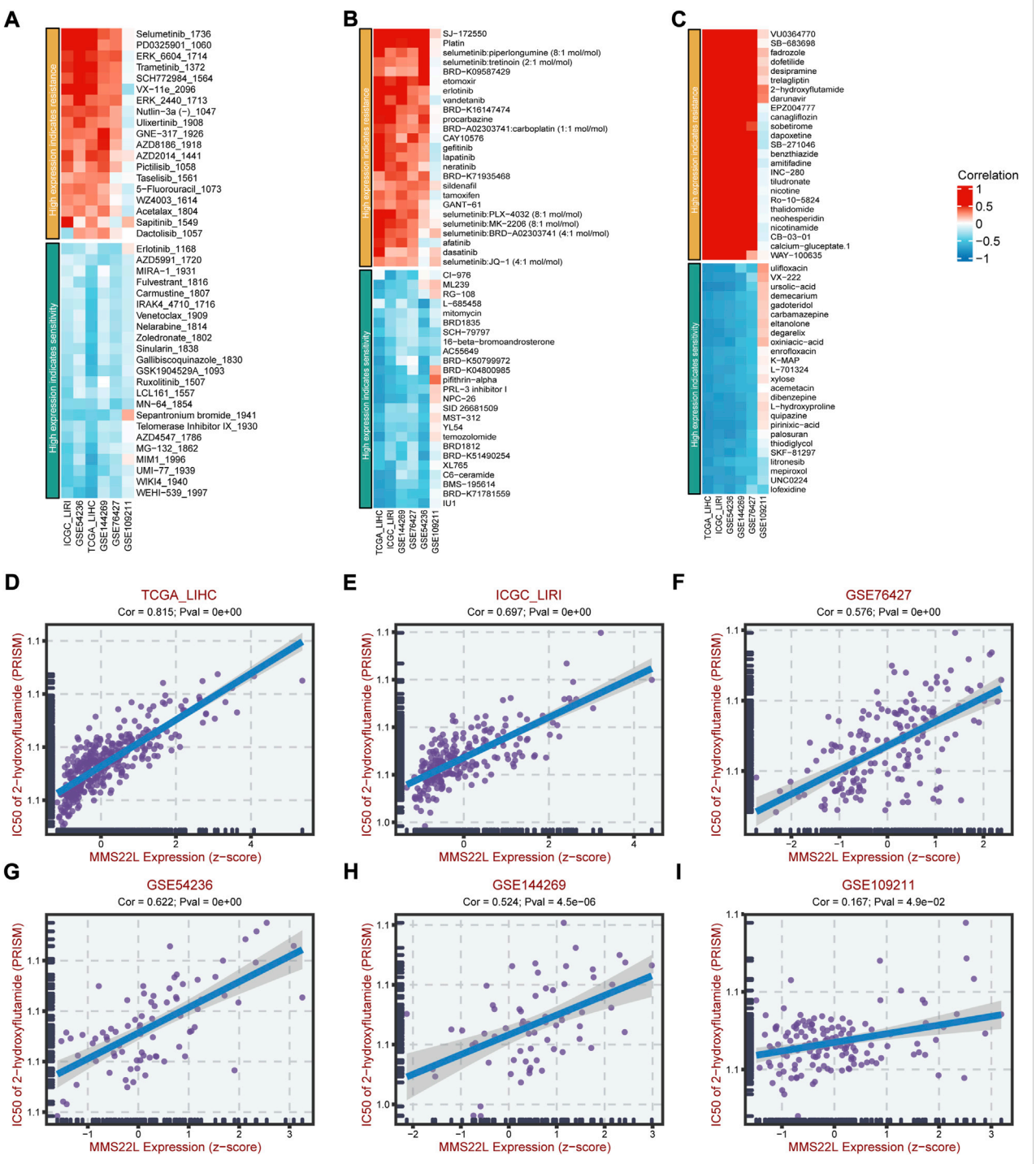

FIGURE 9
The association of methyl methanesulfonate-sensitivity protein 22-like (MMS22L) expression with drug sensitivity in hepatocellular carcinoma (HCC). **(A)** Relation of MMS22L expression with drug sensitivity in multiple HCC cohorts according to the GDSC2 database. **(B)** Relation of MMS22L expression with drug sensitivity in multiple HCC cohorts according to the CTRP database. **(C)** Relation of MMS22L expression with drug sensitivity in multiple HCC cohorts according to the PRISM database. **(D–I)** The correlation of MMS22L expression and 2-hydroxyflutamide sensitivity (IC50) in TCGA-LIHC **(D)**, ICGC-LIRI **(E)**, GSE76427 **(F)**, GSE54236 **(G)**, GSE144269 **(H)** and GSE109211 **(I)** according to the PRISM database.

Figure S2). Except for LO2 cell, MMS22L expression was similar in mRNA level and protein level. These results show that MMS22L expression differed in mRNA and protein levels in HCC cell lines.

MMS22L for prediction of OS

We explored the role of MMS22L as a predictor to validate the independency of OS in patients with HCC. Univariate and multivariate cox regression analyses were used to evaluate whether MMS22L was an independent predictor of OS in TCGA-LIHC, ICGC-LIRI-JP, and LIHC-CN cohorts. As shown in Figures 8A,B, MMS22L was an independent predictor of OS in these three cohorts, which means that MMS22L played an important role in the survival of patients with HCC.

MMS22L expression and drug sensitivity

Since drug resistance has been reported to have a strong relationship with various cancers and affects the prognosis and survival of cancer patients, we further studied the clinical manifestations of MMS22L in HCC. We further studied the relationship between MMS22L expression and drug resistance in HCC. We analyzed the correlation between the MMS22L high expression group and the drug resistance and sensitivity to different drugs in three databases, GDSC2, CTRP, and PRISM, in six HCC cohorts. The results showed that in these three databases, particularly PRISM, the high expression of MMS22L positively correlated with the drug resistance to most chemotherapeutic drugs. On the contrary, the high expression of MMS22L was highly negatively correlated with drug sensitivity, which indicated that the high expression of MMS22L might be the reason for the low sensitivity of HCC cells to certain chemotherapeutic drugs, thus affecting the prognosis and survival of patients (Figures 9A–C). Next, we tested the drug 2-hydroxyflutamide, which showed a high correlation with MMS22L expression in the six cohorts, and the results indicated that the IC50 value of this drug was highly correlated with MMS22L expression in all six cohorts (Figures 9D–I). This showed that MMS22L might be a potential target to improve the suppression of HCC.

Discussion

MMS22L is widely expressed in human tumor tissues and plays different roles in the occurrence and development of various cancers, thus highlighting the possibility of MMS22L as a potential target for cancer therapy. Previous reports mainly identified MMS22L as a potential oncogene, which enhanced its nuclear localization and stability by binding to NFKBIL2 to promote tumor cell growth (Nguyen et al., 2012). Another study reported that MMS22L promoted tumor progression as a biomarker of breast cancer bone metastasis (Savci-Heijink et al., 2016). Nevertheless, not all reports suggested that MMS22L functioned as a cancer-promoting factor, promoting the occurrence and development of cancer. Recent studies have shown that low expression of MMS22L is associated with poor survival and lymph node metastasis and enhances tumor cell migration in ESCC (Luo et al., 2021), suggesting the feasibility of MMS22L as a tumor suppressor gene. However, the function of MMS22L in the majority of human tumors is yet to be thoroughly investigated. Bioinformatics analysis has made the understanding of high-throughput data completer and more strengthened the current understanding of tumor diseases (He et al., 2021; Qiu et al., 2021; Shen et al., 2022). In the current study, we characterized the landscape of MMS22L in pan-cancer through a comprehensive analysis of public repository data. We characterized the hallmark of MMS22L and preliminarily explored the potential mechanism of action of MMS22L and its association with the prognosis of tumor patients, immune cell infiltration, and genomic heterogeneity in pan-cancer. Concomitantly, the evaluation effect of MMS22L in immunotherapy was also shown in this study. More importantly, we identified the feasibility of MMS22L as a molecular marker in HCC by analyzing multiple HCC cohorts. These results described the critical role of MMS22L in human cancers while highlighting the feasibility of MMS22L as a potential therapeutic target for HCC. Altogether, these findings provide useful insights into the value of MMS22L in human cancer therapy.

It is well known that DNA replication plays an irreplaceable role during the cell division process. In humans, genome duplication largely depends on HR (Lopes et al., 2010). Although previous studies have reported that MMS22L is crucial in mediating HR and affecting genome duplication (Saredi et al., 2016), its expression pattern in tumors and its genomic mutational signature remain uncharacterized. In the present study, we first analyzed the landscape characteristics of MMS22L in pan-cancer. Our findings showed that MMS22L had a broad expression pattern in most tumor types and was abnormally expressed in most tumor tissues, indicating the potential of MMS22L as a tumor marker. Next, since the prognosis of tumor patients remains the most concerning issue in cancer research, some studies have characterized the critical role of MMS22L in tumors and its relationship with prognosis. In different omics data, the description of the survival correlation between MMS22L and patients with cancer is still lacking. Therefore, we further explored the association of MMS22L with clinical outcomes. Overall, the effects of MMS22L on the prognosis of patients with different tumor types at different molecular levels were significantly different. At the transcriptional level, the mRNA expression levels of MMS22L appeared to play completely different roles in different tumors. In previous studies, a higher expression of MMS22L in tumor tissues of ESCC was associated with better survival. However, no correlation was shown in our study, and this difference may be

due to the insufficient sample size and esophageal cancer histological type in other studies. At the genomic DNA level, MMS22L with deletion or amplification in CNV was associated with worse OS. Previous studies have speculated that MMS22L mutations caused genomic instability and promoted certain types of ovarian and breast cancer (Piwko et al., 2016); however, our data suggested that patients with MMS22L mutations had a better prognosis than patients with wild-type MMS22L in UCEC. We believe that this does not contradict our observations. In normal cells, aberrant alterations of MMS22L lead to genomic instability and malignant transformation. However, in tumor cells, MMS22L mutations persist throughout tumor development. Since tumor cells divide significantly more frequently than normal cells and have a great demand for DNA damage repair, MMS22L mutations may limit the ability of the tumor to replicate, thereby inhibiting tumor progression. In addition, lack or inhibition of DNA damage repair can increase the sensitivity of tumor cells to DNA-damaging drugs and thus help overcome chemoresistance. Nonetheless, these results suggested that MMS22L produced in molecular modification events at different genetic levels had different prognostic effects on patients with different types of tumors. An in-depth analysis of different omics can help us better judge the prognosis of tumor patients.

The previous analytical results suggested that MMS22L played an essential role in tumor progression and prognosis; however, its mechanism of action remains unclear. Abnormal expression of proto-oncogenes or tumor suppressor genes at the transcriptional level has been widely reported as a key factor in tumor activation in previous studies. Therefore, we grouped tumor samples according to MMS22L mRNA expression levels and performed GSEA analysis to explore the role and potential mechanism of MMS22L in pan-cancer. GSEA results suggested that MMS22L was closely associated with activating cell cycle-related processes in tumors, including mitosis, cellular G2M checkpoints, and targeting the transcription factor E2F. These results suggested an important effect of MMS22L on cell proliferation; however, these results were expected since previous results had shown MMS22L as a key factor in the occurrence of HR events in cells. As an essential factor of cell proliferation and division, it is understandable that MMS22L participates in cell cycle regulation. Overall, these results also further affirm the reliability of the analytical results of this study. However, as mentioned in the results, we observed significant but conflicting effects of MMS22L on specific tumor immune response pathways in different cancers. These results also suggested that MMS22L plays a role in immune regulation in some specific tumor types. However, further research is needed to determine whether MMS22L performs these functions.

MMS22L has been widely reported to play an important role in the HR repair. However, since aberrant alterations in HR-related genes lead to an increased susceptibility to cancer, HR repair deficiency has been observed in nearly all cancer types (van Wilpe et al., 2021). Furthermore, although HRD promotes short-term benefits by increasing tumor sensitivity to chemotherapy, all patients eventually develop resistance to these therapies. Therefore, it is necessary to identify treatment options with more durable efficacy. HRD tumors are thought to be more immunogenic and, therefore, more amenable to treatment with checkpoint inhibitors. Concurrently, a previous study also showed that MMS22L might encode a cancer-testis antigen since the cancer-testis antigen is strongly expressed in tumors and has strong immunogenicity and antigen specificity. Therefore, its importance in tumor immunotherapy has gradually gained attention. These shreds of evidence point to the possibility of MMS22L assisting immunotherapy. Previous studies and reports on MMS22L and immune cells in the tumor microenvironment are still rare. Therefore, in this study, we first explored the correlation between the expression level of MMS22L and immune cell infiltration in the human tumor microenvironment and further compared the role of MMS22L in different immunotherapy cohorts through existing clinical studies. Similarly, and consistent with previous functional analyses, MMS22L exhibited conflicting responses in different immunotherapy cohorts. These disparate results might be due to the different genomic compositions of tumors or the different immune microenvironments between different tumor types. In addition, since cancer-testis antigens can induce specific cellular and humoral immune responses, there are currently two different strategies for using cancer-testis antigens as tumor immunotherapy targets: one is to directly enhance cancer-testis antigen-specific T lymphocytes, known as adoptive T-cell therapies (Xia et al., 2018; Zhang and Wang, 2019), and the other is to introduce other cancer-testis antigens to promote immune recognition and enhance anti-tumor immune responses (Dreno et al., 2018; Palata et al., 2020). Although this study showed some associations between MMS22L and immune cell infiltration, it still seemed insufficient to explain the direct impact of MMS22L on immunotherapy. We believe that introducing other cancer-testis antigens is likely to be an important way for MMS22L to participate in immunotherapy. Concomitantly, previous studies have described MMS22L in detail as an important member of the protein interaction network. Therefore, we believe that the role of tumor vaccine after introducing other cancer-testis antigens is likely to be the fundamental role of MMS22L in tumor immunotherapy. Overall, on the one hand, these results suggest that previous studies using a single immunotherapy cohort to evaluate potential markers may have certain limitations in understanding the role of tumor markers in immunotherapy. On the other hand, these results suggest a possible link between MMS22L and tumor immunotherapy. Targeting MMS22L may contribute to the development of tumor vaccines.

HCC, the most common type of liver cancer, has an increasing incidence worldwide (Carcinoma, 2021). The application of targeted drugs, such as sorafenib and combination therapeutic approaches, has brought hope for the treatment of patients with HCC (Llovet et al., 2008; Bruix et al., 2017; El-Khoueiry et al., 2017) however, it remains significant to identify effective prognostic markers and further

improve clinical outcomes. MMS22L mRNA expression levels are significantly associated with patients' prognoses in previous results. However, the clinicopathological significance of MMS22L in HCC remains unknown, and no studies have elucidated the role of abnormal expression of MMS22L mRNA in developing HCC. Therefore, our study further selected the role of MMS22L in HCC for further analysis. It can be seen that, as the degree of malignancy increased, MMS22L expression increased in HCC. Concurrently, the analytical results of multiple independent cohorts showed that MMS22L was highly expressed in HCC tissues, and these high expressions were significantly associated with patients' poor prognoses. Further univariate and multivariate Cox regression analytical results also proved that MMS22L was an independent factor affecting the prognosis of patients with HCC. These results further confirm the reliability of the findings of this study. To further determine the practical application value of MMS22L in clinical treatment, this study analyzed the relationship between MMS22L expression and drug sensitivity. The role of MMS22L as a drug sensitivity regulator has been reported in various tumors. Reducing drug resistance and increasing drug sensitivity are of great significance as key issues in current clinical treatment. In this study, we focused on the significant association between the drug sensitivity of 2-hydroxyflutamide and MMS22L in HCC. The effect of 2-hydroxyflutamide as an antiandrogen has been reported in previous studies. Meanwhile, the use of antiandrogens to treat HCC patients has been extensively reported (Zhang et al., 2021). However, the related results are controversial. *In vitro* studies have shown that the antiandrogens cyproterone acetate and flutamide have inhibitory effects on androgen-induced HCC cell growth (Koch et al., 2015; Chen et al., 2021). In contrast, large clinical trials with leuprolide and flutamide (antiandrogens) have failed to improve patient survival (GdEedTdC, 2004). These results suggest that the effects of androgens or antiandrogens on the progression of HCC are yet to be further explored. The clinical application of targeted androgens in the treatment of HCC is feasible; however, there are still some limitations. In this study, a high expression of MMS22L resulted in resistance to 2-hydroxyflutamide, suggesting that targeting MMS22L may be a strategy to improve the current androgen-targeted suppression of HCC. These results provide a reference research direction for MMS22L; however, the actual role of MMS22L still needs to be explored by further experiments.

Although this study characterizes the role of MMS22L in pan-cancer and reveals an important role of MMS22L in HCC, there are inevitably some limitations in this study. The pan-cancer data in this study is dominated by the TCGA dataset, which is systematically biased. Furthermore, although we used as many cohorts as possible to elucidate the important role of MMS22L in HCC, expanding the cohort or in-depth mechanistic experiments may help us better understand the role of MMS22L in HCC. To our knowledge, this is the first study to provide a comprehensive description of MMS22L and preliminarily demonstrate its association with important research data in various tumors. It also demonstrates the potential mechanism of MMS22L in pan-cancer and its potential function in predicting immunotherapy response. Furthermore, MMS22L plays a key role in tumor progression and is associated with poor prognosis in patients with HCC, highlighting the therapeutic and diagnostic potential of MMS22L in HCC. We hope this pan-cancer analysis of MMS22L will help guide basic, translational, and clinical research targeting MMS22L in human cancers.

Data availability statement

The original contributions presented in the study are included in the article/Supplementary Material further inquiries can be directed to the corresponding author.

Author contributions

ZG, FL, and QG designed the research. ZG and FL performed the research and analyzed the data. ZG and FL drafted the paper. ZG and QG revised the paper. All authors contributed to the article and approved the submitted version.

Acknowledgments

We thank Bullet Edits Limited for the linguistic editing and proofreading of the manuscript.

Conflict of interest

The authors declare that the research was conducted in the absence of any commercial or financial relationships that could be construed as a potential conflict of interest.

Publisher's note

Supplementary material

The Supplementary Material for this article can be found online at: https://www.frontiersin.org/articles/10.3389/fgene.2022.1025970/full#supplementary-material

References

Bonneville, R., Krook, M. A., Kautto, E. A., Miya, J., Wing, M. R., Chen, H-Z., et al. (2017). Landscape of microsatellite instability across 39 cancer types. *JCO Precis. Oncol.* (1), 17.00073. doi:10.1200/po.17.00073

Bruix, J., Qin, S., Merle, P., Granito, A., Huang, Y-H., Bodoky, G., et al. (2017). Regorafenib for patients with hepatocellular carcinoma who progressed on sorafenib treatment (resorce): A randomised, double-blind, placebo-controlled, phase 3 trial. *Lancet* 389 (10064), 56–66. doi:10.1016/S0140-6736(16)32453-9

Carcinoma, Hepatocellular (2021). *Nat. Rev. Dis. Prim.* 7 (1), 7. doi:10.1038/s41572-021-00245-6

Chen, C-S., Gao, G-L., Ho, D-R., Lin, C-Y., Chou, Y-T., Chen, S-C., et al. (2021). Cyproterone acetate acts as a disruptor of the aryl hydrocarbon receptor. *Sci. Rep.* 11 (1), 5457. doi:10.1038/s41598-021-84769-7

Dreno, B., Thompson, J. F., Smithers, B. M., Santinami, M., Jouary, T., Gutzmer, R., et al. (2018). Mage-A3 immunotherapeutic as adjuvant therapy for patients with resected, mage-A3-positive, stage iii melanoma (derma): A double-blind, randomised, placebo-controlled, phase 3 trial. *Lancet. Oncol.* 19 (7), 916–929. doi:10.1016/S1470-2045(18)30254-7

Duro, E., Lundin, C., Ask, K., Sanchez-Pulido, L., MacArtney, T. J., Toth, R., et al. (2010). Identification of the mms22l-tonsl complex that promotes homologous recombination. *Mol. Cell* 40 (4), 632–644. doi:10.1016/j.molcel.2010.10.023

El-Khoueiry, A. B., Sangro, B., Yau, T., Crocenzi, T. S., Kudo, M., Hsu, C., et al. (2017). Nivolumab in patients with advanced hepatocellular carcinoma (checkmate 040): An open-label, non-comparative, phase 1/2 dose escalation and expansion trial. *Lancet* 389 (10088), 2492–2502. doi:10.1016/S0140-6736(17)31046-2

Gao, Q., Zhu, H., Dong, L., Shi, W., Chen, R., Song, Z., et al. (2019). Integrated proteogenomic characterization of hbv-related hepatocellular carcinoma. *Cell* 179 (2), 561–577. doi:10.1016/j.cell.2019.08.052

GdEedTdC, Hépatocellulaire (2004). Randomized trial of leuprorelin and flutamide in male patients with hepatocellular carcinoma treated with tamoxifen. *Hepatology* 40 (6), 1361–1369. doi:10.1002/hep.20474

He, Y., Ye, Y., Tian, W., and Qiu, H. (2021). A novel lncrna panel related to ferroptosis, tumor progression, and microenvironment is a robust prognostic indicator for glioma patients. *Front. Cell Dev. Biol.* 9, 788451. doi:10.3389/fcell.2021.788451

Koch, D. C., Jang, H. S., O'Donnell, E. F., Punj, S., Kopparapu, P. R., Bisson, W. H., et al. (2015). Anti-androgen flutamide suppresses hepatocellular carcinoma cell proliferation via the aryl hydrocarbon receptor mediated induction of transforming growth factor-ß1. *Oncogene* 34 (50), 6092–6104. doi:10.1038/onc.2015.55

Liu, Y., Wu, H., Luo, T., Luo, Q., Meng, Z., Shi, Y., et al. (2021). The sox9-mms22l Axis promotes oxaliplatin resistance in colorectal cancer. *Front. Mol. Biosci.* 8, 646542. doi:10.3389/fmolb.2021.646542

Llovet, J. M., Ricci, S., Mazzaferro, V., Hilgard, P., Gane, E., Blanc, J-F., et al. (2008). Sorafenib in advanced hepatocellular carcinoma. *N. Engl. J. Med.* 359 (4), 378–390. doi:10.1056/NEJMoa0708857

Lopes, A., Amarir-Bouhram, J., Faure, G., Petit, M-A., and Guerois, R. (2010). Detection of novel recombinases in bacteriophage genomes unveils Rad52, Rad51 and Gp2.5 remote homologs. *Nucleic Acids Res.* 38 (12), 3952–3962. doi:10.1093/nar/gkq096

Luo, Q., He, W., Mao, T., Leng, X., Wu, H., Li, W., et al. (2021). Mms22l expression as a predictive biomarker for the efficacy of neoadjuvant chemoradiotherapy in oesophageal squamous cell carcinoma. *Front. Oncol.* 11, 711642. doi:10.3389/fonc.2021.711642

Miller, A. L., Fehling, S. C., Garcia, P. L., Gamblin, T. L., Council, L. N., van Waardenburg, R. C. A. M., et al. (2019). The bet inhibitor Jq1 attenuates double-strand break repair and sensitizes models of pancreatic ductal adenocarcinoma to parp inhibitors. *eBioMedicine* 44, 419–430. doi:10.1016/j.ebiom.2019.05.035

Nguyen, M. H., Ueda, K., Nakamura, Y., and Daigo, Y. (2012). Identification of a novel oncogene, Mms22l, involved in lung and esophageal carcinogenesis. *Int. J. Oncol.* 41 (4), 1285–1296. doi:10.3892/ijo.2012.1589

Palata, O., Podzimkova Hradilova, N., Mysiková, D., Kutna, B., Mrazkova, H., Lischke, R., et al. (2020). Detection of tumor antigens and tumor-antigen specific T cells in nsclc patients: Correlation of the quality of T cell responses with nsclc subtype. *Immunol. Lett.* 219, 46–53. doi:10.1016/j.imlet.2020.01.001

Piwko, W., Mlejnkova, L. J., Mutreja, K., Ranjha, L., Stafa, D., Smirnov, A., et al. (2016). The mms22l–tonsl heterodimer directly promotes rad51-dependent recombination upon replication stress. *EMBO J.* 35 (23), 2584–2601. doi:10.15252/embj.201593132

Qiu, H., Tian, W., He, Y., Li, J., He, C., Li, Y., et al. (2021). Integrated analysis reveals prognostic value and immune correlates of Cd86 expression in lower grade glioma. *Front. Oncol.* 11, 654350. doi:10.3389/fonc.2021.654350

Saredi, G., Huang, H., Hammond, C. M., Alabert, C., Bekker-Jensen, S., Forne, I., et al. (2016). H4k20me0 marks post-replicative chromatin and recruits the tonsl–mms22l DNA repair complex. *Nature* 534 (7609), 714–718. doi:10.1038/nature18312

Savci-Heijink, C. D., Halfwerk, H., Koster, J., and van de Vijver, M. J. (2016). A novel gene expression signature for bone metastasis in breast carcinomas. *Breast Cancer Res. Treat.* 156 (2), 249–259. doi:10.1007/s10549-016-3741-z

Shen, W., Song, Z., Zhong, X., Huang, M., Shen, D., Gao, P., et al. (2022). Sangerbox: A comprehensive, interaction-friendly clinical bioinformatics analysis platform. *iMeta* 1 (3), e36. doi:10.1002/imt2.36

Thorsson, V., Gibbs, D. L., Brown, S. D., Wolf, D., Bortone, D. S., Ou Yang, T-H., et al. (2018). The immune landscape of cancer. *Immunity* 48 (4), 812–830. doi:10.1016/j.immuni.2018.03.023

van Wilpe, S., Tolmeijer, S. H., Koornstra, R. H. T., de Vries, I. J. M., Gerritsen, W. R., Ligtenberg, M., et al. (2021). Homologous recombination repair deficiency and implications for tumor immunogenicity. *Cancers* 13 (9), 2249. doi:10.3390/cancers13092249

Xia, Y., Tian, X., Wang, J., Qiao, D., Liu, X., Xiao, L., et al. (2018). Treatment of metastatic non-small cell lung cancer with ny-eso-1 specific tcr engineered-T cells in a phase I clinical trial: A case report. *Oncol. Lett.* 16 (6), 6998–7007. doi:10.3892/ol.2018.9534

Zhang, H., Spencer, K., Burley, S. K., and Zheng, X. F. S. (2021). Toward improving androgen receptor-targeted therapies in male-dominant hepatocellular carcinoma. *Drug Discov. Today* 26 (6), 1539–1546. doi:10.1016/j.drudis.2021.02.001

Zhang, J., and Wang, L. (2019). The emerging world of tcr-T cell trials against cancer: A systematic review. *Technol. Cancer Res. Treat.* 18, 1533033819831068. doi:10.1177/1533033819831068

frontiers | Frontiers in Genetics

TYPE Original Research
PUBLISHED 02 November 2022
DOI 10.3389/fgene.2022.1047481

OPEN ACCESS

EDITED BY
Rui Cao,
Capital Medical University, China

REVIEWED BY
Jiayan Chen,
Fudan University, China
Qingbo Huang,
People's Liberation Army General Hospital, China
Wei Zhai,
Shanghai Jiao Tong University, China

*CORRESPONDENCE
Zhenyu Ou,
ouzhenyu1@163.com
Yu Cui,
cuiyeyu@126.com

SPECIALTY SECTION
This article was submitted to Cancer Genetics and Oncogenomics, a section of the journal Frontiers in Genetics

RECEIVED 18 September 2022
ACCEPTED 11 October 2022
PUBLISHED 02 November 2022

CITATION
Li H, Hu J, Zu X, Chen M, Chen J, Zou Y, Deng R, Qin G, Li W, Tang J, Deng D, Liu J, Cheng C, Cui Y and Ou Z (2022), A novel signature to predict the neoadjuvant chemotherapy response of bladder carcinoma: Results from a territory multicenter real-world study. *Front. Genet.* 13:1047481. doi: 10.3389/fgene.2022.1047481

A novel signature to predict the neoadjuvant chemotherapy response of bladder carcinoma: Results from a territory multicenter real-world study

Huihuang Li[1,2], Jiao Hu[1,2], Xiongbing Zu[1,2], Minfeng Chen[1,2], Jinbo Chen[1,2], Yihua Zou[3], Ruoping Deng[4], Gang Qin[4], Wenze Li[5], Jiansheng Tang[6], Dingshan Deng[1,2], Jinhui Liu[1,2], Chunliang Cheng[1,2], Yu Cui[1,2]* and Zhenyu Ou[1,2]*

[1]Department of Urology, Xiangya Hospital, Central South University, Changsha, China, [2]National Clinical Research Center for Geriatric Disorders, Xiangya Hospital, Central South University, Changsha, China, [3]Department of Urology, The First People's Hospital of Chenzhou, Chenzhou, China, [4]Department of Urology, The Central Hospital of Yongzhou, Yongzhou, China, [5]Department of Urology, The First People's Hospital of Xiangtan City, Xiangtan, China, [6]Department of Urology, Affiliated Hospital of Xiangnan University, Chenzhou, China

Background: Although neoadjuvant chemotherapy (NAC) has become the standard treatment option for muscle invasive bladder carcinoma (MIBC), its application is still limited because of the lack of biomarkers for NAC prediction.

Methods: We conducted a territory multicenter real-world study to summarize NAC practice in China and its associated clinicopathologic variables with NAC response. Then, we developed and validated a robust gene-based signature for accurate NAC prediction using weighted correlation network analysis (WGCNA), the least absolute shrinkage and selector operation (LASSO) algorithm, a multivariable binary logistic regression model, and immunohistochemistry (IHC).

Results: In total, we collected 69 consecutive MIBC patients treated with NAC from four clinical centers. The application of NAC in the real world was relatively safe, with only two grade IV and seven grade III AEs and no treatment-related deaths being reported. Among these patients, 16 patients gave up surgery after NAC, leaving 53 patients for further analysis. We divided them into pathological response and non-response groups and found that there were more patients with a higher grade and stage in the non-response group. Patients with a pathological response could benefit from a significant overall survival (OS) improvement. In addition, univariate and multivariate logistic analyses indicated that tumor grade and clinical T stage were both independent factors for predicting NAC response. Importantly, we developed and validated a five-gene-based risk score for extremely high predictive accuracy for NAC response.

Conclusion: NAC was relatively safe and could significantly improve OS for MIBC patients in the real-world practice. Our five-gene-based risk score could guide personalized therapy and promote the application of NAC.

KEYWORDS

bladder carcinoma, neoadjuvant chemotherapy, pathological response, personalized therapy, risk score

Introduction

Bladder carcinoma (BLCA) is one of the most commonly diagnosed carcinomas and a major cause of death globally (Siegel et al., 2019). For muscle invasive bladder carcinoma (MIBC), cisplatin-based neoadjuvant chemotherapy (NAC) plus radical cystectomy (RC) is becoming the standard treatment option (Witjes et al., 2020). Several randomized clinical trials (RCTs) have demonstrated that NAC significantly increased the overall survival (OS) rates compared to RC alone, and this result was also supported by a meta-analysis (Grossman et al., 2003; Advanced Bladder Cancer Meta-analysis Collaboration, 2005; Griffiths et al., 2011; Kitamura et al., 2014). Specifically, patients who achieve a pathologic response (downstaging to ≤ pT1 at cystectomy) after NAC have a strong trend of better OS and disease-specific survival (DSS) (Grossman et al., 2003). However, not all MIBC patients could benefit from NAC, and this fact largely limits the application of NAC (Rosenblatt et al., 2012). In fact, only 30–40% of patients can achieve a pathologic response after NAC, and the remaining patients have even worse survival outcomes than RC alone (Bhindi et al., 2017; Lyon et al., 2019). To avoid chemotherapy-related toxicity and delay radical surgery, identifying which patients could benefit from NAC is vital for the treatment of MIBC.

There are some available reports about biomarkers predictive of response to NAC in MIBC. The most commonly reported is the association between mutation of DNA damage repair (DDR) genes and response to NAC, including *ATM*, *RB1*, *FANCC*, *ERCC2*, and *FGFR3* (Plimack et al., 2015; Liu et al., 2016; Yang et al., 2018; Motterle et al., 2020). Molecular subtypes of MIBC are also commonly reported. Basal tumors are characterized by aggressiveness and a better response to NAC, while p53-like tumors are characterized by resistance to NAC (Choi et al., 2014). Other biomarkers include a 12- and a 14-gene-based prediction scoring system developed by a small number of patients (Takata et al., 2005; Kato et al., 2011). However, none of these reports have been translated into clinical applications partly because of low predictive accuracy and complex detection methods. In this study, we conducted a retrospective collection from multicenter databases of patients treated with NAC and summarized their clinicopathologic features and chemotherapy-related toxicity. Importantly, we developed and validated an NAC prediction scoring system for convenient clinical application.

Materials and methods

Patient selection

We conducted a retrospective collection from multicenter databases for consecutive MIBC patients treated with NAC from 2017 to 2021. Ethical approval was obtained from each center, including Xiangya Hospital, the First People's Hospital of Chenzhou, the Central Hospital of Yongzhou, and the First People's Hospital of Xiangtan City. All the patients included had histologically proven bladder carcinoma and clinical stage T2-T4 N0-2 M0 disease and were then followed for at least two cycles of NAC. We obtained written informed consent from each patient included and registered this study on the Chinese Clinical Trial Registry (http://www.chictr.org.cn/index.aspx), registration number (ChiCTR2100047632).

Treatment choices

Chemotherapy regimens and number of cycles were administered based on clinical practice and guidelines at the discretion of clinicians. Specifically, most patients received three cycles of cisplatin and gemcitabine. Day 1: cisplatin (70 mg/m^2) and gemcitabine (1,000 mg/m^2) administered intravenously (IV). Day 8: gemcitabine (1,000 mg/m^2) IV; this was repeated every 3 weeks. For patients with renal insufficiency (creatinine clearance <60 ml/min), carboplatin-based therapy was administered. After NAC cycles, all patients were recommended to undergo RC and lymphadenectomy unless they refused strongly. In addition, there were some patients who responded well to NAC only receiving transurethral resection of bladder tumor (TURBT) because of a strong willingness of bladder sparing. For these patients, complete TURBT and radiography were performed to confirm non-muscle invasiveness. Urinary diversions after RC included ileal conduit and cutaneous ureterostomy. The decision on which diversion was to be used was mainly based on patients' performance status (PS) and the preferences of the patients and surgeons.

Outcome measurement

Response to NAC was defined based on the pathological stage at RC. Patients without residual MIBC (downstaging to ≤

pT1) were defined as having a pathological response, while the remaining patients were defined as having a pathological non-response (≥pT2). For patients who received TURBT only, we regarded all of them as pathological responses after confirming non-muscle invasiveness by complete TURBT and radiography. Chemotherapy-related toxicity was assessed using the acute and subacute toxicities of the anti-cancer drug indexing table (WHO). OS was calculated from the initial day of NAC administration to death from any cause. We censored patients at the last follow-up time, 1 December 2021.

Sources of public databases

GSE69795 (GPL14951) (McConkey et al., 2016) and GSE52219 (GPL14951) (Choi et al., 2014) are two public datasets containing MIBC patients treated with NAC. We downloaded these two datasets using the "GEOquery" R package and transformed the gene symbols using the corresponding platform "GPL14951." There were 61 samples in GSE69795, of which only 38 patients had detailed response information. We excluded the remaining 23 patients and took the 38 patients for further analysis. For GSE52219, there were 23 patients with detailed response information, and we included all of them for analysis.

Coexpression module networks

We used the "WGCNA" R package to generate a coexpression module network and selected the gene modules with the closest relationship with NAC therapy response. As reported in our previous study (Li et al., 2021), we first filtered out the bad genes and samples using microarray data from GSE69795. Then, we calculated the connection strength and built a scale-free network based on the filtered genes and samples. We set the degree of independence as 0.85 and chose the most suitable soft power value. We developed scale-free gene coexpression networks based on the selected soft power value and selected the module that had the closest relationship with NAC therapy response. The genes in this module were selected to build a risk score for predicting NAC response.

Immunohistochemistry and scoring

Pretreatment formalin-fixed paraffin-embedded (FFPE) MIBC tissues were collected from the Department of Pathology, Xiangya Hospital, and then, IHC was conducted, as described in our previous study (Hu et al., 2020). The anti-CEP83 antibody (PA5-113541, Invitrogen) was used. The H-score system, which integrates the staining intensity and percentage of positive cells, was adopted to evaluate the IHC score (Budwit-Novotny et al., 1986). For staining intensity, a score of 0 indicated no staining, a score of 1 indicated weak staining (faint yellow), a score of 2 indicated moderate staining (pale brown), and a score of 3 indicated strong staining (brown). For the percentage of positive cells, a score of 1 for samples with <25% positive cells, a score of 2 for samples with 25–49% positive cells, a score of 3 for samples with 50–74% positive cells, and a score of 4 for samples with ≥75% positive cells were determined. Then, the IHC score was determined by multiplying the intensity score and the percentage score. Two independent pathologists reviewed the IHCs.

Statistical analysis

We expressed the continuous variables as the mean (range) and compared them by t-test or the Mann–Whitney U test. Dichotomous variables were compared using Pearson's chi-squared test or Fisher's exact test implemented in the "gmodels" R package. The significance of each clinical variable for NAC response was assessed using univariate logistic regression analysis, and only the variables associated with NAC response with a p-value less than 0.1 were included for multivariate analysis. Both univariate and multivariate logistic regression analyses were conducted using the "glm" function. Survival curves were compared using the log-rank test and plotted using the Kaplan–Meier method. We used the least absolute shrinkage and selector operation (LASSO) algorithm to further narrow down the genes selected in the weighted correlation network analysis (WGCNA) step. We then developed a risk score for predicting NAC response using the multivariable binary logistic regression model in the "glm" function: risk score = Σβi*RNAi. The predictive accuracy for NAC response was quantified using receiver operating characteristic (ROC) curves implemented in the "pROC" R package. $p < 0.05$ was regarded as statistically significant, and all analyses were two-sided and conducted by R software (4.0.3).

Results

Patient characteristics

To show the real-world practice of NAC for MIBC from 2017 to 2021 in China, we collected all 70 consecutive MIBC patients treated with chemotherapy before RC from Xiangya Hospital, the First People's Hospital of Chenzhou, the Central Hospital of Yongzhou, and the First People's Hospital of Xiangtan City. One patient received only one cycle of NAC and was excluded, leaving 69 patients for further analysis. None of these patients received adjuvant therapy. The clinicopathologic variables of all the patients are reported in Supplementary Table S1. All patients were in good PS with an

TABLE 1 Comparison of baseline clinicopathologic variables between neoadjuvant chemotherapy (NAC) response and non-response groups.

	Responder, n = 25	Non-responder, n = 28	p-value
Age (years), median (range)	60.0 (30–80)	62.3 (45–79)	0.42
Gender, n (%)	—	—	0.10
Male	24 (96.0%)	22 (78.6%)	—
Female	1 (4.00%)	6 (21.4%)	—
BMI (kg/m2), median (range)	22.5 (16–28.2)	22.0 (15.2–28.9)	0.57
Smoking status, n (%)	—	—	0.10
Non-smokers	7 (28.0%)	14 (50.0%)	—
Smokers	18 (72.0%)	14 (50.0%)	—
Hematuresis, n (%)	—	—	0.10
No	1 (4.00%)	6 (21.4%)	—
Yes	24 (96.0%)	22 (78.6%)	—
History of NMIBC, n (%)	—	—	1.00
No	21 (84.0%)	23 (82.1%)	—
Yes	4 (16.0%)	5 (17.9%)	—
Hydronephrosis, n (%)	—	—	0.26
No	18 (72.0%)	16 (57.1%)	—
Yes	7 (28.0%)	12 (42.9%)	—
NLR, median (range)	3.53 (1.20–11.5)	3.33 (1.10–9.18)	0.76
Pathological type, n (%)	—	—	0.49
Pure urothelial carcinoma	25 (100%)	26 (92.9%)	—
Mixed tumors	0 (0%)	2 (7.14%)	—
Pathological grade	—	—	0.03
Low	10 (40.0%)	4 (14.3%)	—
High	15 (60.0%)	24 (85.7%)	—
T stage	—	—	0.001
T2	14 (56.0%)	4 (14.3%)	—
T3/T4	11 (44.0%)	24 (85.7%)	—
N stage	—	—	0.47
N0	22 (88.0%)	22 (78.6%)	—
N+	3 (12.0%)	6 (21.4%)	—

BMI, body mass index; NMIBC, non-muscle invasive bladder carcinoma; NLR, neutrophil-to-lymphocyte ratio; mixed tumors, urothelial carcinoma mixed with squamous and sarcomatoid carcinoma cells.

Eastern Cooperative Oncology Group (ECOG) score of 0 or 1. Most of the patients were pathologically diagnosed with pure urothelial carcinoma (92.8%), while the remaining patients had mixed tumors (7.25%), including urothelial carcinoma mixed with squamous and sarcomatoid carcinoma cells. The clinical T stage of all the patients ranged from T2 to T4. For patients with clinical N stage of N1 and N2, we rearranged them as clinical lymph node-positive patients (N+, 15.9%). Two patients received an NAC program of gemcitabine and carboplatin because of renal insufficiency, while all of the remaining patients received a cisplatin-based NAC program. All patients were recommended to undergo RC and lymphadenectomy after NAC. Unfortunately, 16 patients (23.2%) gave up treatment because of economic reasons or a lack of confidence in curing. Eight patients received TURBT (11.6%) or partial cystectomy (1.45%) because of a strong willingness of bladder sparing.

The primary objective of this study was pathological response. We defined patients without residual MIBC (downstaging to ≤ pT1) as having a pathological response (response group), while the remaining patients (≥pT2) were defined as having a pathological non-response (non-response group). For patients who received TURBT only, we regarded all of them as pathological responses after confirming non-muscle invasiveness by complete TURBT and radiography. For one patient who received partial cystectomy, we included him into a non-response group based on persistent muscle invasiveness at partial cystectomy. As shown in Table 1, there were 25 patients in the NAC response group and 28 patients in the NAC non-response group. Among these 53 patients, 42 patients were successfully followed up. Patients in the response group exhibited a significantly higher overall survival outcome than those in the non-response group (Figure 1, p = 0.039). There was no significant difference between these two groups for the majority of

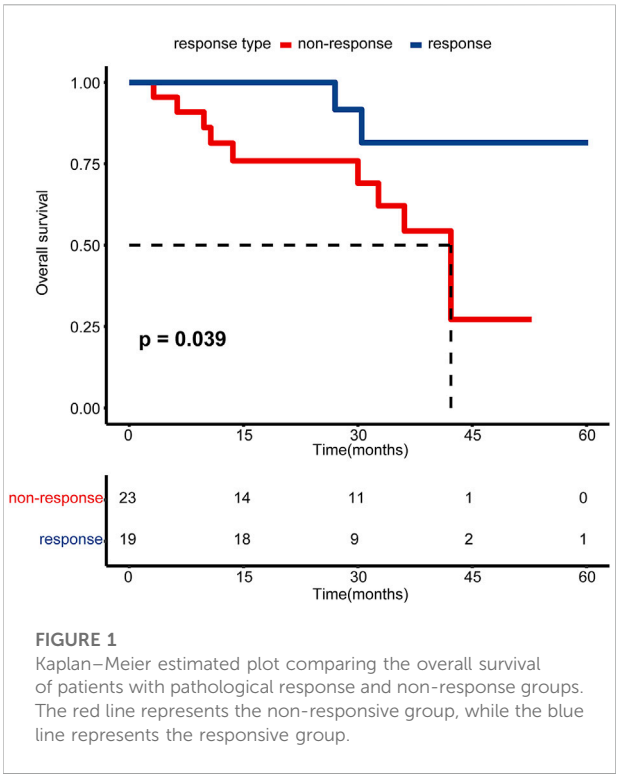

FIGURE 1
Kaplan–Meier estimated plot comparing the overall survival of patients with pathological response and non-response groups. The red line represents the non-responsive group, while the blue line represents the responsive group.

clinicopathologic variables, including age, sex, body mass index (BMI), smoking status, history of hematuresis, history of non-muscle invasive bladder carcinoma (NMIBC), hydronephrosis, the neutrophil-to-lymphocyte ratio (NLR), the pathological type, and N stage (Table 1). For pathological grade and clinical T stage, there were significantly more patients with higher grade (85.7% vs. 60.0%, p = 0.03) and stage (85.7% vs. 44.0%, p = 0.001) in the NAC non-response group (Table 1).

Treatment and safety

Supplementary Table S2 shows the summarized adverse events (AEs) of all the patients. For grade III–IV events, only two patients reported grade IV anemia, and five and two patients reported grade III anemia and decreased white blood cells, respectively. There were no other grade III–IV events reported. Other grade I–II AEs could recover after simple symptomatic treatment, and no patient delayed surgery because of these AEs.

Pretreatment factors for predicting NAC response

The results of univariate and multivariate logistic analysis results are reported in Table 2. The results are presented as odds ratios (ORs, 95% CIs). All the baseline clinicopathologic variables were included in univariate logistic analysis except the pathological type because there were no patients with mixed tumors in the NAC response group (Table 1). All the remaining variables except pathological grade and clinical T stage had no significant association with NAC response. Higher grade (0.25, 95% CI 0.06–0.89, p = 0.04) and clinical T stage (0.13, 95% CI 0.03–0.46, p = 0.003) were significantly associated with NAC non-response. In addition, higher grade (0.14, 95% CI 0.02–0.69, p = 0.03) and clinical T stage (0.16, 95% CI 0.03–0.61, p = 0.01) remained independent factors in multivariate logistic analysis (Table 2).

Development and validation of an NAC-predicting risk score

Microarray data on 38 patients from GSE69795 were used to build a gene coexpression network to find the module with the closest relationship to NAC response (Supplementary Figure S1A). Clinicopathologic variables from GSE69795 included age, PS score, lymphovascular infiltration (LVI), clinical stage, and NAC response (Supplementary Figure S1A). Setting the scale-free R^2 as 0.85, we selected 6 as the soft threshold value to build the scale-free network (Supplementary Figure S1B). Twenty-nine modules were identified, and the green module had the closest relationship (R = 0.36, p = 0.02) with NAC response (Supplementary Figures S1C,D). There were 1819 genes in the green module, and all the genes were significantly coexpressed (cor = 0.45, p < 0.001, Supplementary Figure S1E). Using the LASSO algorithm, we identified five candidate genes, including *TMEM69*, *OR6W1P*, *CNNM1*, ***CEP83***, and *ACTC1*, according to lambda by one standard error (0.22) (Supplementary Figures S2A,B). An NAC-predicting risk score was then developed using a multivariable binary logistic regression model: risk score = 0.01*TMEM69 + 2.25*OR6W1P-0.67*CNNM1+5.68*CEP83-0.21*ACTC1. A higher risk score was associated with a higher NAC response rate. The predictive accuracy was extremely high in the GSE69795 cohort, with an area under the curve (AUC) index of 0.96 (Figure 2A). Importantly, this risk score could be validated in GSE52219 (AUC: 0.72, Figure 2B), indicating satisfactory predictive accuracy. In addition, this risk score could also predict the OS of patients in GSE69769 (p < 0.0001, Figure 3A), although this value was not statistically significant in GSE52219 partly because of the small sample size (p = 0.82, Figure 3B).

As *CEP83* possessed the highest β value in this risk score, we further evaluated the association between NAC response and CEP83 only. To our surprise, *CEP83* possessed relatively satisfactory predictive accuracy for NAC response, with AUCs of 0.84 and 0.63 in GSE69795 (Supplementary Figure S3A) and GSE52219 (Supplementary Figure S3B), respectively. We collected 28 pretreatment FFPE samples

TABLE 2 Univariate and multivariate logistic analysis results of variables associated with neoadjuvant chemotherapy (NAC) response.

	Univariate		Multivariate	
Variable	**OR (95% CI)**	**p-value**	**OR (95% CI)**	**p-value**
Age (years)	0.98 (0.92–1.03)	0.45	—	—
Gender				
Female	Reference	—	Reference	—
Male	6.55 (1.01–128.8)	0.09	11.6 (0.91–406.1)	0.10
BMI	1.06 (0.88–1.28)	0.56	—	—
Smoking status				
Non-smokers	Reference	—	—	—
Smokers	2.57 (0.84–8.44)	0.11	—	—
Hematuresis				
No	Reference	—	Reference	—
Yes	6.55 (1.01–128.8)	0.09	7.36 (0.56–288.7)	0.20
History of NMIBC				
No	Reference	—	—	—
Yes	0.88 (0.19–3.74)	0.86	—	—
Hydronephrosis				
No	Reference	—	—	—
Yes	0.52 (0.16–1.61)	0.26	—	—
NLR	1.04 (0.81–1.34)	0.75	—	—
Pathological grade				
Low	Reference	—	Reference	—
High	0.25 (0.06–0.89)	0.04	0.14 (0.02–0.69)	0.03
T stage				
T2	Reference	—	Reference	—
T3/T4	0.13 (0.03–0.46)	0.003	0.16 (0.03–0.61)	0.01
N stage				
N0	Reference	—	—	—
N+	0.50 (0.10–2.15)	0.37	—	—

OR, odds ratio; CI, confidence interval; BMI, body mass index; NMIBC, non-muscle invasive bladder carcinoma; NLR, neutrophil-to-lymphocyte ratio.

and validated the predictive value of *CEP83* using IHC. Figures 4A,B show representative images of *CEP83* staining. The predictive value of *CEP83* for NAC response was successfully validated in our own IHC cohort (AUC: 0.84, Figure 4C). This result could largely simplify the predictive system for NAC.

Discussion

For the treatment of MIBC, RC and lymphadenectomy have remained the gold standard for the last 3 decades. Since 1999, the Medical Research Council (MRC) has performed a randomized phase III trial, comparing the efficacy of cystectomy and/or radiotherapy with or without three prior cycles of cisplatin, methotrexate, and vinblastine (CMV). This trial concluded that NAC could contribute to a significant 16% reduction in death for patients with MIBC (International collaboration of trialists, 1999; Griffiths et al., 2011). Meanwhile, the Southwest Oncology Group (SWOG)-8710 trial demonstrated that NAC therapy combined with methotrexate, vinblastine, doxorubicin, and cisplatin (MVAC) was associated with a significantly improved survival benefit (Grossman et al., 2003). Based on these two RCTs, NAC plus RC is becoming the standard treatment option for MIBC. The underlying mechanism was that NAC could eradicate micrometastatic disease and downstage the primary MIBC tumor (Buttigliero et al., 2017). However, despite this level 1 evidence, the actual adoption of NAC for MIBC is slow and unsatisfactory, with only 1.4%–20.9% of patients receiving NAC even in contemporary cohorts (Keegan et al., 2014; Kim et al., 2015; Reardon et al., 2015). The proportions of elderly patients, poor PS, multiple comorbidities, and renal insufficiency could be the reasons

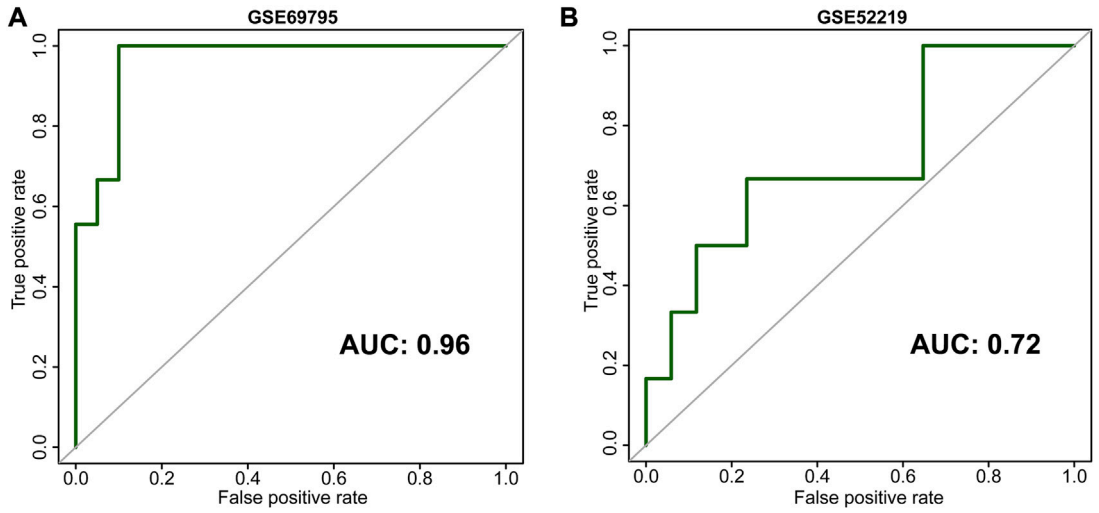

FIGURE 2
Receiver operating characteristic curves (ROCs) of our development [**(A)**, GSE69795] and validation [**(B)**, GSE52219] cohorts.

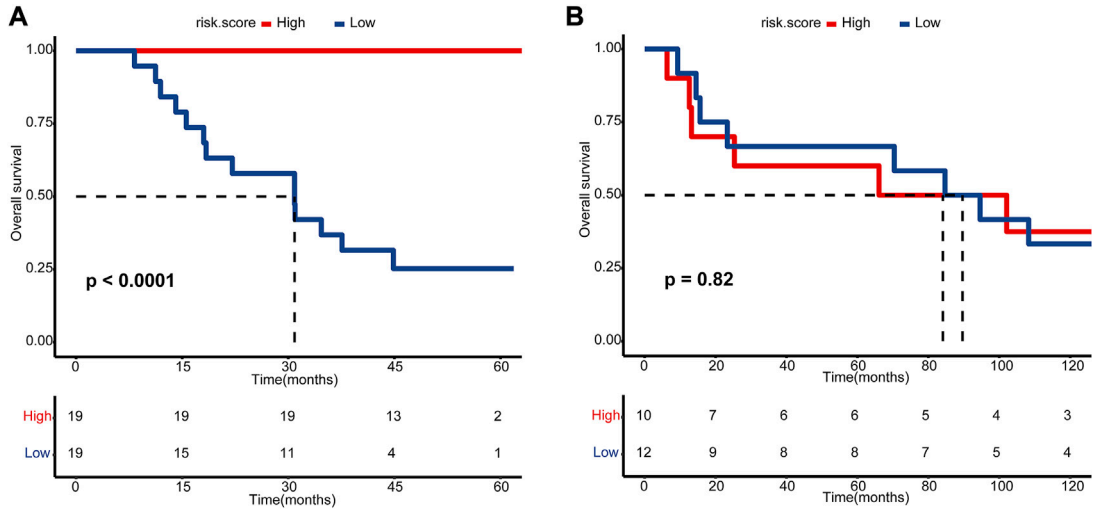

FIGURE 3
Kaplan–Meier estimated plot comparing the overall survival of patients with high- and low-risk score groups. **(A)** GSE69795 and **(B)** GSE52219. The red line represents the high-risk score group, while the blue line represents the low-risk score group.

for the low utilization of NAC (Anan et al., 2017), and patients with these features might be excluded from RCT trials. Therefore, we conducted this research to summarize the real-world practice of NAC in China for the first time. Although we set no strict rules for patient inclusion, all the patients we included were in good PS with an ECOG score of 0 or 1. For the fear of renal insufficiency, only two patients (3%) received an NAC program of gemcitabine and carboplatin because of renal insufficiency. Both patients remained muscle invasive in RC, indicating the lower effectiveness of carboplatin. In addition, the side effects of NAC were acceptable, with only two grade Ⅳ and seven grade Ⅲ AEs reported. No treatment-related deaths or delays in surgery proved that NAC was relatively safe in the real-world practice. Unfortunately, only a small portion (46%, 23/50) of patients achieved a pathologic response from NAC. Additionally, 16 patients (24.2%, 16/66) gave up radical treatment because of economic reasons or a lack of confidence in

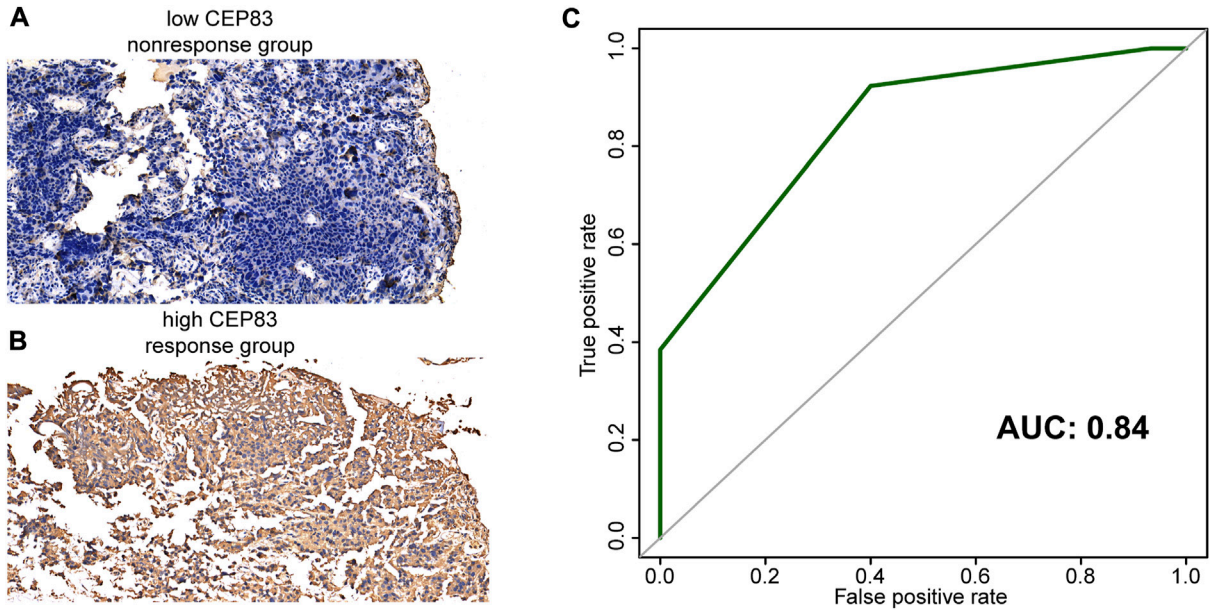

FIGURE 4
Representative images of CEP83 staining. **(A)** Negative staining (no response group). **(B)** Positive staining (response group). **(C)** Receiver operating characteristic curves (ROCs) of CEP83 in our IHC cohort.

curing. These two facts again emphasize the importance of NAC as a predictive biomarker.

Some studies reported an association between clinicopathologic variables and NAC response. Boeri et al. reported that current smokers and previous smokers had four and two times the risk of non-response to NAC, respectively (Boeri et al., 2019). However, Kim et al. concluded that there was no relationship between smoking and NAC response (Kim et al., 2014). For urothelial carcinoma mixed with other tumors, Kaimakliotis et al. reported that NAC could contribute to equal oncological outcomes for patients with pure urothelial carcinoma or mixed tumors (Kaimakliotis et al., 2016). Unfortunately, we could only determine that there was no difference in the pathological type between responders and non-responders and could not calculate the relationship between the pathological type and NAC response because of the small sample size. Interestingly, a high neutrophil-to-lymphocyte ratio (NLR) was related to worse OS and poorer response to NAC (Gondo et al., 2012; Buisan et al., 2017). We did not draw this conclusion in our study, and this may need further research in the future. Lyon et al. stratified patients receiving NAC into low- and high-risk groups based on clinicopathologic variables including hydronephrosis, LVI, variant histology, and clinical T stage (Lyon et al., 2019). In our study, we found that higher tumor grade and clinical stage were both significantly associated with NAC non-response, indicating that tumor grade might also be included as a variable factor for stratifying patients in the future. Although fewer patients with a higher clinical T stage (cT3 or cT4) achieved a pathologic response, we should not exclude them from lifesaving NAC as RC alone cannot cure them because of extravesical invasion. Therefore, we further explored the gene-based predicting signature for NAC.

The major mechanism of cisplatin is to cause DNA damage, affect cell survival, and induce apoptosis. As a result, the association between mutation of DDR genes and response to NAC is widely reported (Motterle et al., 2020). Plimack et al. reported that genomic mutations of ATM, RB1, and FANCC were associated with response and OS after cisplatin-based NAC (Plimack et al., 2015). Somatic mutation of *ERCC2*, another DDR gene, was found to be correlated with a complete pathologic response in the study of Van Allen et al. (2014) and validated in Liu et al. (2016). However, another study found that the association between ERCC2 missense mutations and pathologic response did not reach statistical significance, while only ERBB2 mutations were significantly related to response (Groenendijk et al., 2016). Another focus is molecular subtypes and NAC response. Patients with MIBC can be generally divided into basal/squamous (characterized by squamous features) and luminal (characterized by papillary features) subtypes based on gene expression profiling (Motterle et al., 2020). Choi et al. divided patients into basal, luminal, and p53-like subtypes and found that basal tumors are characterized by aggressiveness and a better response to NAC, while p53-like tumors are characterized by resistance to NAC (Choi et al., 2014). However, all these reports have not translated into clinical applications partly because of inconsistent results, unsatisfactory predictive accuracy, or complex detection methods. Based on the gene expression profiles of 27 patients with MIBC, Takata et al. developed and validated a 14-gene-based signature for NAC prediction (Takata et al., 2005). In addition, Kato et al. developed

a signature for accurate NAC prediction consisting of 12 "predictive" genes (Kato et al., 2011). In our study, we developed (38 patients) and validated (23 patients) a five-gene-based gene signature for extremely accurate prediction with AUC scores of 0.96 and 0.72, respectively. For routine clinical application, detection of a five-gene-based signature is much easier and convenient for MIBC patients planning to receive NAC therapy, and our findings led to the achievement of "personalized therapy". Solmi et al. reported for the first time that TMEM69 could be a biomarker for the metastasis of colon cancer (Solmi et al., 2006). Cyclin M (CNNM) families were vital factors in maintaining cellular and body magnesium (Mg^{2+}) homeostasis (Giménez-Mascarell et al., 2019). For CNNM1, it was reported that CNNM1 could be regulated by SNHG7 and miR-9-5p to promote the progression of hepatocellular carcinoma (Xie et al., 2020). Moreover, ACTC1 was reported to be a novel marker for prognosis of bladder cancer (Liu et al., 2021). We further narrowed down this five-gene-based signature to *CEP83* for convenient clinical application. As a protein-coding gene, *CEP83* was reported to be associated with nephronophthisis, and we found it was related to NAC response for the first time (Failler et al., 2014).

Limitations to our study: First, this is a retrospective study with a small sample size, and there were some patients with missing data. It is impossible to carry out some deep analyses, such as subgroup survival analysis, and this fact may indicate bias in our study. However, to the best of our knowledge, this is the first real-world NAC practice from China, and our study has a complementary effect on RCTs. Second, although our risk score exhibited an accurate predictive value for NAC in the development and validation cohorts, its predictive value should be further validated in larger prospective clinical trials.

Conclusion

NAC was relatively safe and could significantly improve the overall survival for MIBC patients in the real-world practice. Our five-gene-based risk score could guide personalized therapy and promote the application of NAC. The *CEP83* expression exhibited an extremely important value for NAC response prediction.

Data availability statement

The original contributions presented in the study are included in the article/Supplementary Material; further inquiries can be directed to the corresponding author.

Ethics statement

The studies involving human participants were reviewed and approved by the Ethics Committee of the Xiangya Hospital of Central South University, the First People's Hospital of Chenzhou, the Central Hospital of Yongzhou, and the First People's Hospital of Xiangtan City. The patients/participants provided their written informed consent to participate in this study.

Author contributions

HL, XZ, MC, and JC performed analyses and drafted the manuscript. HL, JL, CC, and DD searched and downloaded the original datasets from GEO datasets. HL, YZ, RD, GQ, WL, JT, and JL contributed to data collection and statistical analyses. HL, ZO, MC, YC, and JC edited the pictures. ZO and YC conceived and supervised the study. All authors contributed to writing the manuscript. All authors reviewed and approved the final manuscript.

Funding

This work was supported by the National Natural Science Foundation of China (81873626, 81902592, 82070785, and 81770705), the Hunan Natural Science Foundation (2020JJ5916, 2020JJ5884 and 2021JJ40975), and the Hunan Province Young Talents Program (2021RC3027).

Acknowledgments

The authors sincerely thank all participants in the study.

Conflict of interest

The authors declare that the research was conducted in the absence of any commercial or financial relationships that could be construed as a potential conflict of interest.

Publisher's note

Supplementary material

The Supplementary Material for this article can be found online at: https://www.frontiersin.org/articles/10.3389/fgene.2022.1047481/full#supplementary-material

References

Advanced Bladder Cancer (ABC) Meta-analysis Collaboration (2005). Neoadjuvant chemotherapy in invasive bladder cancer: Update of a systematic review and meta-analysis of individual patient data advanced bladder cancer (ABC) meta-analysis collaboration. *Eur. Urol.* 48 (2), 202–205. doi:10.1016/j.eururo.2005.04.006

Anan, G., Hatakeyama, S., Fujita, N., Iwamura, H., Tanaka, T., Yamamoto, H., et al. (2017). Trends in neoadjuvant chemotherapy use and oncological outcomes for muscle-invasive bladder cancer in Japan: A multicenter study. *Oncotarget* 8 (49), 86130–86142. doi:10.18632/oncotarget.20991

Bhindi, B., Frank, I., Mason, R. J., Tarrell, R. F., Thapa, P., Cheville, J. C., et al. (2017). Oncologic outcomes for patients with residual cancer at cystectomy following neoadjuvant chemotherapy: A pathologic stage-matched analysis. *Eur. Urol.* 72 (5), 660–664. doi:10.1016/j.eururo.2017.05.016

Boeri, L., Soligo, M., Frank, I., Boorjian, S. A., Thompson, R. H., Tollefson, M., et al. (2019). Cigarette smoking is associated with adverse pathological response and increased disease recurrence amongst patients with muscle-invasive bladder cancer treated with cisplatin-based neoadjuvant chemotherapy and radical cystectomy: A single-centre experience. *BJU Int.* 123 (6), 1011–1019. doi:10.1111/bju.14612

Budwit-Novotny, D. A., McCarty, K. S., Cox, E. B., Soper, J. T., Mutch, D. G., Creasman, W. T., et al. (1986). Immunohistochemical analyses of estrogen receptor in endometrial adenocarcinoma using a monoclonal antibody. *Cancer Res.* 46 (10), 5419–5425.

Buisan, O., Orsola, A., Areal, J., Font, A., Oliveira, M., Martinez, R., et al. (2017). Low pretreatment neutrophil-to-lymphocyte ratio predicts for good outcomes in patients receiving neoadjuvant chemotherapy before radical cystectomy for muscle invasive bladder cancer. *Clin. Genitourin. Cancer* 15 (1), 145–151. e2. doi:10.1016/j.clgc.2016.05.004

Buttigliero, C., Tucci, M., Vignani, F., Scagliotti, G. V., and Di Maio, M. (2017). Molecular biomarkers to predict response to neoadjuvant chemotherapy for bladder cancer. *Cancer Treat. Rev.* 54, 1–9. doi:10.1016/j.ctrv.2017.01.002

Choi, W., Porten, S., Kim, S., Willis, D., Plimack, E. R., Hoffman-Censits, J., et al. (2014). Identification of distinct basal and luminal subtypes of muscle-invasive bladder cancer with different sensitivities to frontline chemotherapy. *Cancer Cell* 25 (2), 152–165. doi:10.1016/j.ccr.2014.01.009

Failler, M., Gee, H. Y., Krug, P., Joo, K., Halbritter, J., Belkacem, L., et al. (2014). Mutations of CEP83 cause infantile nephronophthisis and intellectual disability. *Am. J. Hum. Genet.* 94 (6), 905–914. doi:10.1016/j.ajhg.2014.05.002

Giménez-Mascarell, P., González-Recio, I., Fernández-Rodríguez, C., Oyenarte, I., Müller, D., Martínez-Chantar, M. L., et al. (2019). Structural insights into the intracellular region of the human magnesium transport mediator CNNM4. *Int. J. Mol. Sci.* 20 (5), E6279. doi:10.3390/ijms20246279

Gondo, T., Nakashima, J., Ohno, Y., Choichiro, O., Horiguchi, Y., Namiki, K., et al. (2012). Prognostic value of neutrophil-to-lymphocyte ratio and establishment of novel preoperative risk stratification model in bladder cancer patients treated with radical cystectomy. *Urology* 79 (5), 1085–1091. doi:10.1016/j.urology.2011.11.070

Griffiths, G., Hall, R., Sylvester, R., Raghavan, D., and Parmar, M. K. (2011). International phase III trial assessing neoadjuvant cisplatin, methotrexate, and vinblastine chemotherapy for muscle-invasive bladder cancer: Long-term results of the BA06 30894 trial. *J. Clin. Oncol.* 29 (16), 2171–2177. doi:10.1200/jco.2010.32.3139

Groenendijk, F. H., de Jong, J., Fransen van de Putte, E. E., Michaut, M., Schlicker, A., Peters, D., et al. (2016). ERBB2 mutations characterize a subgroup of muscle-invasive bladder cancers with excellent response to neoadjuvant chemotherapy. *Eur. Urol.* 69 (3), 384–388. doi:10.1016/j.eururo.2015.01.014

Grossman, H. B., Natale, R. B., Tangen, C. M., Speights, V. O., Vogelzang, N. J., Trump, D. L., et al. (2003). Neoadjuvant chemotherapy plus cystectomy compared with cystectomy alone for locally advanced bladder cancer. *N. Engl. J. Med.* 349 (9), 859–866. doi:10.1056/NEJMoa022148

Hu, J., Li, H., He, T., Deng, H., Gong, G., Cui, Y., et al. (2020). A nomogram incorporating PD-L1, NLR, and clinicopathologic features to predict inguinal lymph node metastasis in penile squamous cell carcinoma. *Urol. Oncol.* 38 (7), e19–e641. doi:10.1016/j.urolonc.2020.04.015

International collaboration of trialists (1999). Neoadjuvant cisplatin, methotrexate, and vinblastine chemotherapy for muscle-invasive bladder cancer: A randomised controlled trial. *Lancet* 354 (9178), 533–540.

Kaimakliotis, H. Z., Monn, M. F., Cho, J. S., Pedrosa, J. A., Hahn, N. M., Albany, C., et al. (2016). Neoadjuvant chemotherapy in urothelial bladder cancer: Impact of regimen and variant histology. *Future Oncol.* 12 (15), 1795–1804. doi:10.2217/fon-2016-0056

Kato, Y., Zembutsu, H., Takata, R., Miya, F., Tsunoda, T., Obara, W., et al. (2011). Predicting response of bladder cancers to gemcitabine and carboplatin neoadjuvant chemotherapy through genome-wide gene expression profiling. *Exp. Ther. Med.* 2 (1), 47–56. doi:10.3892/etm.2010.166

Keegan, K. A., Zaid, H. B., Patel, S. G., and Chang, S. S. (2014). Increasing utilization of neoadjuvant chemotherapy for muscle-invasive bladder cancer in the United States. *Curr. Urol. Rep.* 15 (4), 394. doi:10.1007/s11934-014-0394-5

Kim, P. H., Kent, M., Zhao, P., Sfakianos, J. P., Bajorin, D. F., Bochner, B. H., et al. (2014). The impact of smoking on pathologic response to neoadjuvant cisplatin-based chemotherapy in patients with muscle-invasive bladder cancer. *World J. Urol.* 32 (2), 453–459. doi:10.1007/s00345-013-1128-x

Kim, S. H., Seo, H. K., Shin, H. C., Chang, S. J., Yun, S., Joo, J., et al. (2015). Trends in the use of chemotherapy before and after radical cystectomy in patients with muscle-invasive bladder cancer in korea. *J. Korean Med. Sci.* 30 (8), 1150–1156. doi:10.3346/jkms.2015.30.8.1150

Kitamura, H., Tsukamoto, T., Shibata, T., Masumori, N., Fujimoto, H., Hirao, Y., et al. (2014). Randomised phase III study of neoadjuvant chemotherapy with methotrexate, doxorubicin, vinblastine and cisplatin followed by radical cystectomy compared with radical cystectomy alone for muscle-invasive bladder cancer: Japan clinical Oncology group study JCOG0209. *Ann. Oncol.* 25 (6), 1192–1198. doi:10.1093/annonc/mdu126

Li, H., Hu, J., Yu, A., Othmane, B., Guo, T., Liu, J., et al. (2021). RNA modification of N6-methyladenosine predicts immune phenotypes and therapeutic opportunities in kidney renal clear cell carcinoma. *Front. Oncol.* 11, 642159. doi:10.3389/fonc.2021.642159

Liu, D., Plimack, E. R., Hoffman-Censits, J., Garraway, L. A., Bellmunt, J., Van Allen, E., et al. (2016). Clinical validation of chemotherapy response biomarker ERCC2 in muscle-invasive urothelial bladder carcinoma. *JAMA Oncol.* 2 (8), 1094–1096. doi:10.1001/jamaoncol.2016.1056

Liu, Z., Xu, L., Lin, Y., Hong, H., Wei, Y., Ye, L., et al. (2021). Identification of biomarkers related to prognosis of bladder transitional cell carcinoma. *Front. Genet.* 12, 682237. doi:10.3389/fgene.2021.682237

Lyon, T. D., Frank, I., Sharma, V., Shah, P. H., Tollefson, M. K., Thompson, R. H., et al. (2019). A risk-stratified approach to neoadjuvant chemotherapy in muscle-invasive bladder cancer: Implications for patients classified with low-risk disease. *World J. Urol.* 37 (8), 1605–1613. doi:10.1007/s00345-018-2551-9

McConkey, D. J., Choi, W., Shen, Y., Lee, I. L., Porten, S., Matin, S. F., et al. (2016). A prognostic gene expression signature in the molecular classification of chemotherapy-naïve urothelial cancer is predictive of clinical outcomes from neoadjuvant chemotherapy: A phase 2 trial of dose-dense methotrexate, vinblastine, doxorubicin, and cisplatin with bevacizumab in urothelial cancer. *Eur. Urol.* 69 (5), 855–862. doi:10.1016/j.eururo.2015.08.034

Motterle, G., Andrews, J. R., Morlacco, A., and Karnes, R. J. (2020). Predicting response to neoadjuvant chemotherapy in bladder cancer. *Eur. Urol. Focus* 6 (4), 642–649. doi:10.1016/j.euf.2019.10.016

Plimack, E. R., Dunbrack, R. L., Brennan, T. A., Andrake, M. D., Zhou, Y., Serebriiskii, I. G., et al. (2015). Defects in DNA repair genes predict response to neoadjuvant cisplatin-based chemotherapy in muscle-invasive bladder cancer. *Eur. Urol.* 68 (6), 959–967. doi:10.1016/j.eururo.2015.07.009

Reardon, Z. D., Patel, S. G., Zaid, H. B., Stimson, C. J., Resnick, M. J., Keegan, K. A., et al. (2015). Trends in the use of perioperative chemotherapy for localized and locally advanced muscle-invasive bladder cancer: A sign of changing tides. *Eur. Urol.* 67 (1), 165–170. doi:10.1016/j.eururo.2014.01.009

Rosenblatt, R., Sherif, A., Rintala, E., Wahlqvist, R., Ullén, A., Nilsson, S., et al. (2012). Pathologic downstaging is a surrogate marker for efficacy and increased survival following neoadjuvant chemotherapy and radical cystectomy for muscle-invasive urothelial bladder cancer. *Eur. Urol.* 61 (6), 1229–1238. doi:10.1016/j.eururo.2011.12.010

Siegel, R. L., Miller, K. D., and Jemal, A. (2019). Cancer statistics. *Cancer J. Clin.* 69 (1), 7–34. doi:10.3322/caac.21551

Solmi, R., Ugolini, G., Rosati, G., Zanotti, S., Lauriola, M., Montroni, I., et al. (2006). Microarray-based identification and RT-PCR test screening for epithelial-specific mRNAs in peripheral blood of patients with colon cancer. *BMC cancer* 6, 250. doi:10.1186/1471-2407-6-250

Takata, R., Katagiri, T., Kanehira, M., Tsunoda, T., Shuin, T., Miki, T., et al. (2005). Predicting response to methotrexate, vinblastine, doxorubicin, and cisplatin neoadjuvant chemotherapy for bladder cancers through genome-wide gene

expression profiling. *Clin. Cancer Res.* 11 (7), 2625–2636. doi:10.1158/1078-0432.Ccr-04-1988

Van Allen, E. M., Mouw, K. W., Kim, P., Iyer, G., Wagle, N., Al-Ahmadie, H., et al. (2014). Somatic ERCC2 mutations correlate with cisplatin sensitivity in muscle-invasive urothelial carcinoma. *Cancer Discov.* 4 (10), 1140–1153. doi:10.1158/2159-8290.Cd-14-0623

Witjes, J. A., Babjuk, M., Bellmunt, J., Bruins, H. M., De Reijke, T. M., De Santis, M., et al. (2020). EAU-ESMO consensus statements on the management of advanced and variant bladder cancer-an international collaborative multistakeholder effort(†): Under the auspices of the EAU-ESMO guidelines committees. *Eur. Urol.* 77 (2), 223–250. doi:10.1016/j.eururo.2019.09.035

Xie, Y., Wang, Y., Gong, R., Lin, J., Li, X., Ma, J., et al. (2020). SNHG7 facilitates hepatocellular carcinoma occurrence by sequestering miR-9-5p to upregulate CNNM1 expression. *Cancer biother. Radiopharm.* 35 (10), 731–740. doi:10.1089/cbr.2019.2996

Yang, Z., Zhang, R., Ge, Y., Qin, X., Kang, X., Wang, Y., et al. (2018). Somatic FGFR3 mutations distinguish a subgroup of muscle-invasive bladder cancers with response to neoadjuvant chemotherapy. *EBioMedicine* 35, 198–203. doi:10.1016/j.ebiom.2018.06.011

frontiers | Frontiers in Genetics

TYPE Original Research
PUBLISHED 08 November 2022
DOI 10.3389/fgene.2022.1047326

OPEN ACCESS

EDITED BY
Rui Cao,
Affiliated Beijing Friendship Hospital, Capital Medical University, China

REVIEWED BY
Yi Zhang,
Xuzhou Medical University, China
Weiqiang Zhao,
Wexner Medical Center, The Ohio State University, United States

*CORRESPONDENCE
Chenjiao Yao,
yaochenjiao@csu.edu.cn

†These authors have contributed equally to this work and share first authorship

SPECIALTY SECTION
This article was submitted to Cancer Genetics and Oncogenomics, a section of the journal Frontiers in Genetics

RECEIVED 18 September 2022
ACCEPTED 24 October 2022
PUBLISHED 08 November 2022

CITATION
Cheng J, Li Q, Xiao S, Nie L, Liao J, Jiang Q, Xiang B, Zhang H, Jiang Y and Yao C (2022), The advanced lung cancer inflammation index predicts chemotherapy response and infection risk in multiple myeloma patients receiving induction chemotherapy. *Front. Genet.* 13:1047326. doi: 10.3389/fgene.2022.1047326

The advanced lung cancer inflammation index predicts chemotherapy response and infection risk in multiple myeloma patients receiving induction chemotherapy

Jie Cheng[1†], Qianyuan Li[1†], Sheng Xiao[1†], Lu Nie[1], Jianping Liao[1], Qingjie Jiang[1], Biyu Xiang[1], Hongfei Zhang[1], Yanhong Jiang[1] and Chenjiao Yao[1,2*]

[1]The Third Xiangya Hospital of Central South University, Changsha, China, [2]The First Affiliated Hospital of Hainan Medical University, Haikou, China

Objective: This study aims to determine the clinical significance of the advanced lung cancer inflammation index (ALI) in predicting prognosis, chemotherapy response, and infection risk in newly diagnosed multiple myeloma (MM) patients receiving induction therapy.

Methods: A retrospective analysis of the clinical characteristics and laboratory data of 111 newly diagnosed MM patients from the Haematology Department of the Third Xiangya Hospital of Central South University from January 2014 to March 2020 was performed. We first determined the relationship between ALI and overall survival (OS), as well as clinical and laboratory parameters. Second, predictive factors for chemotherapy response were analysed by univariate and multivariate regression analyses. Third, univariate regression analysis of risk factors was performed using infection as the evaluable outcome.

Results: Of the 111 evaluable patients, the low ALI group (<32.7) exhibited significantly poorer survival than the high ALI group (51 months versus 77 months). Multivariable analysis showed that advanced age, chemotherapy response and serum calcium level were independent prognostic factors for OS. Better chemotherapy efficacy in the high ALI group (89.3%) than in the low ALI group (42.2%) ($p < 0.001$) was noted. Multivariate analysis suggested that only ALI [HR: 0.110, 95% CI (0.035–0.350), $p = 0.000$] is an independent predictive factor in evaluating the efficiency of induction chemotherapy. Forty patients (36.04%) presented with infection after induction chemotherapy. Univariate analysis suggested that low ALI and abnormal renal function increase risk of infection in newly diagnosed MM patients.

Conclusion: Our study confirmed that ALI is not only a prognostic biomarker for newly diagnosed patients, but also predicts chemotherapy efficacy in newly diagnosed MM patients receiving induction therapy.

KEYWORDS

advanced lung cancer inflammation index, multiple myeloma, chemotherapy response, infection, overall survival (OS)

Introduction

Multiple myeloma (MM) is the second most common malignant tumour of the haematological system, accounting for 1% of haematological tumours (Raab et al., 2009; Palumbo and Anderson, 2011). Revised International Staging System (R-ISS) and the Durie-Salmon (D&S) staging system have been established to predict survival based on prognostic classification of MM patients (Boyd et al., 2012; Palumbo et al., 2015). Induction therapy is the most crucial treatment in newly diagnosed multiple myeloma (NDMM) patients, and bortezomib (PI) and dexamethasone (VD) remain the current standard of care. The recently updated 2021 EHA-ESMO clinical practice guidelines recommend the use of either lenalidomide-VD (VRD) or daratumumab-thalidomide-VD (Dara-VTD) as first-line options for transplant-eligible NDMM patients; when not available, thalidomide-VD (VTD) or cyclophosphamide-VD (VCD) are acceptable alternatives (Bazarbachi et al., 2022). The majority of MM patients are in a refractory or relapsed state (Röllig et al., 2015). Clinical evidence confirms that infections represent a major cause of morbidity and mortality in patients with MM, especially for those with severe infection, pneumonia, and neutropenia in relapsed/refractory settings (Blimark et al., 2015; Balmaceda et al., 2021). In NDMM patients admitted for the first time, risk of infection correlates with poor prognosis, particularly in those with ISS stage III or low haemoglobin levels (Lin et al., 2020). MM patients with a risk of infection and complications are recommended to receive optimal preventive strategies (Bladé and Rosiñol, 2005; Raje et al., 2022). Additionally, biological mechanism research has demonstrated that the proinflammatory cytokine interleukin (IL)-18 is involved in tumour-promoting inflammation, and its high expression suggessts poor overall survival in MM (Nakamura et al., 2018). All of these results indicate that inflammatory markers have potential as prognostic markers (Hanahan and Weinberg, 2011). The inflammation-based neutrophil-to-lymphocyte ratio (NLR) has been demonstrated to be a prognostic biomarker, with higher NLR indicating poorer prognosis in MM patients, as demonstrated by meta-analysis (Mu et al., 2018). Similarly, the advanced lung cancer inflammation index (ALI), which is a modification of NLR that includes albumin (ALB) and body mass index (BMI), has been developed and demonstrated to be a prognostic marker of poor survival in several cancers, including non-small cell lung cancer (NLSCL) (Jafri et al., 2013). ALI also represents a simple tool to predict immunotherapy efficacy in patients with advanced NSCLC treated with PD-L1 inhibitors alone, and the ALI score has a stronger predictive effect than NLR, the PD-L1 tumour proportion score and other biomarkers (Shiroyama et al., 2018; Mountzios et al., 2021). Therefore, ALI, which is calculated based on body composition, nutrition, and systemic inflammation, may represent a comprehensive indicator for predicting prognosis of NDMM patients. Although ALI reflects the systemic inflammation and cachexia provoked by cancer, its prognostic and predictive value in NDMM patients is unknown. We hypothesized that low ALI is associated with poor survival and can predict chemotherapy efficacy in NDMM patients. We also sought to evaluate the predictive capacity of ALI on the overall incidence of infection in patients receiving induction chemotherapy.

Materials and methods

Patients and methods

This was a single-centre, observational, retrospective study. Our study collected data for 111 MM patients at the Department of Haematology, Third Xiangya Hospital, Central South University from January 2014 to March 2020 under approval of the Institutional Review Board of Third Xiangya Hospital, Central South University (No. 22081). We then collected clinical data and performed classification according to ISS staging standards and the DS staging system. Abnormal secretion of clonal immunoglobulins was classified into the following categories: IgG, IgD, IgM, IgE, double clonal, kappa, and lambda light chain or nonsecreting types. NDMM patients were treated consecutively with bortezomib-based triplet regimens, consisting of proteasome inhibitor (PI) bortezomib plus dexamethasone (VD) backbone, with the addition of a third agent, such as thalidomide (VTD), cyclophosphamide (VCD), lenalidomide (VRD) or doxorubicin (PAD). The number of induction cycles varied from 4 to 6. The curative effect was evaluated according to the traditional efficacy standard of International Myeloma Working Group in 2016 (Kumar et al., 2016). Complete remission in a strict sense (SCR), complete remission (CR), very good partial remission (VGPR), and partial remission (PR) are regarded as effectively curative effects; stable disease (SD) and progressive disease (PD) are regarded as ineffective curative effects. In addition, patients who meet any of the following conditions after initial diagnosis of chemotherapy should be judged as having complicated infection: 1) continuous fever for more than 2 days (axillary temperature greater than 38°C), and fever caused by blood transfusion or related drugs should be excluded; 2) exact clinical symptoms and/or signs of infection, such as bladder irritation, frequent micturition and urgent micturition or signs, such as tenderness of the ureter point when urinary system infection occurs; and 3) exact imaging-related examinations and/

or aetiological evidence suggesting the existence of infected foci. The exclusion criteria were as follows: 1) acute or chronic inflammation at the time of initial diagnosis; 2) a history of blood system diseases and malignant tumours; 3) immune disease, such as inflammatory bowel disease, Sjogren's syndrome, or rheumatoid arthritis; 4) complication of acute and chronic hepatitis or liver disease; 5) complication of severe damage to the functions of other important organs except the kidneys; 6) indicators, such as height and weight, not recorded at the time of admission; 7) relevant biochemical tests not completed within 48 h after admission; and 8) treatment discontinuation or incomplete clinical data.

Data were collected retrospectively from the electronic medical records. Weight, height, neutrophil, lymphocyte, and ALB (g/dl) data were collected at baseline before chemotherapy administration. BMI was calculated by dividing weight (kg) by height (m) squared. The neutrophil-to-lymphocyte ratio (NLR) was computed as the absolute neutrophil count divided by the absolute lymphocyte count. We calculated the advanced lung cancer inflammation index (ALI) as follows: ALI = BMI ×ALB/NLR.

Statistical methods

The $\chi 2$ test or Fisher's exact test was used to determine the significance of differences between discrete variables. Significant variables in univariate analysis were included in binary multivariate logistic analysis. A receiver operating characteristic curve (ROC) was used to determine specificity and sensitivity. Univariate and multivariate analyses were performed using the Cox proportional risk regression model to evaluate prognostic factors and their impact on OS. Associations between ALI and OS were analysed using Kaplan–Meier survival curve estimates and compared using the log-rank test. The statistical analysis was performed using SPSS version 26.0, and $p < 0.05$ was considered statistically significant.

Results

Patient characteristics

Overall, we analysed 111 patients with NDMM at first hospitalization (66 males and 45 females). The average age was 58 years (44–75), and 39.6% of the patients were ≥60 years. A total of 49 patients (44.1%) had MM of the IgG type, 27% had the IgA type, and 18% had the λ light chain type. In total, 10.8% of the patients were classified with other types (κ light chain type and IgD type or others). Based on the Durie-Salmon scale, four patients were at stage I, 12 at stage II, and 95 at stage III. In total, 90 patients had normal renal function, whereas 21 had abnormal renal function. Based on the International Staging System (ISS) scale, 12 patients were at stage I, 28 at stage II, and 71 at stage III. All patients received two cycles of induction chemotherapy, and curative effects were evaluated. In total, the response in 78 patients was considered effective, whereas the response was classified as ineffective in 33 patients.

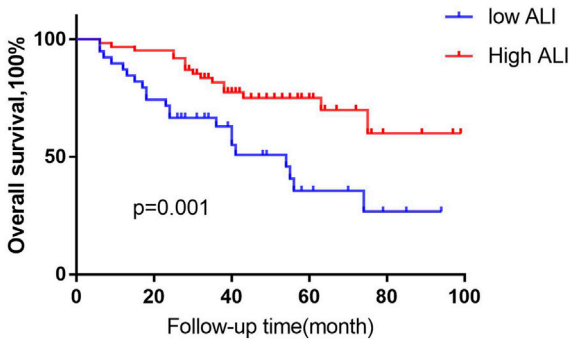

FIGURE 1
Kaplan-Meier analysis of OS based on ALI status. Using the X-tile program, an optimal cut-off value for ALI of 32.7 was determined. We defined MM patients the high- ALI group, (n = 66 cases) and the low -ALI group, (n = 45). Low-ALI patients with MM were significantly correlated with poor prognosis compared with high-ALI patients with respect to overall survival (OS; p = 0.001, log-rank test).

Overall survival

We first analysed the association between ALI and patient prognosis. Using the X-tile program (Camp et al., 2004), an optimal cut-off value for ALI of 32.7 was determined. All cases were categorized into the following two groups: a high ALI group (n = 66 cases) and a low ALI group (n = 45). Patients in the low ALI group had significantly poorer survival than those in the high ALI group (51 months versus 77 months, p = 0.001, Figure 1). Univariate analyses showed that OS correlated with NLR, abnormal renal function, advanced age (>60 years), ß 2-MG level, ISS stage, chemotherapy efficacy, and serum calcium level. Multivariable analyses showed that advanced age, chemotherapy response, and serum calcium were independent prognostic factors for OS (Table 1).

Characteristics of laboratory results and the response to chemotherapy

Next, we analysed the relationship between ALI and patient characteristics as well as laboratory parameters. Table 2 shows that no differences in age, sex, disease classification, plasma cell

TABLE 1 Cox regression analysis of predictive factors for overall survival in patients with MM (n = 111).

Clinical characteristic	Univariate		Multivariate	
	HR (95% CI)	p-value	HR (95% CI)	p-value
Age (years)	0.440 (0.220, 0.843)	0.013*	0.300 (0.143, 0.631)	0.002*
Gender	0.686 (0.359, 1.311)	0.254		
Classification of disease	0.750 (0.381, 1.474)	0.403		
ISS stage	0.303 (0.107, 0.857)	0.024*	0.308 (0.300, 3.171)	0.322
DS stage	0.712 (0.217, 2.332)	0.574		
Renal function	2.167 (1.102, 4.263)	0.025*	0.675 (0.310, 1.472)	0.323
Plasma cell ratio	0.857 (0.453, 1.690)	0.692		
β2-MG(mg/L)	0.305 (0.138, 0.671)	0.003*	0.565 (0.158, 2.023)	0.381
Hb(g/L)	2.38 (0.995, 5.728)	0.051		
Chemotherapy response	2.05 (1.067, 3.951)	0.031*	2.199 (1.010, 4.788)	0.047*
ALB	1.062 (0.557, 2.025)	0.855		
Chemotherapy regimens	1.96 (0.972, 3.962)	0.060		
NLR	2.006 (1.030, 3.905)	0.041*	0.596 (0.247, 1.435)	0.248
ALI	0.362 (0.189, 0.696)	0.002*	1.192 (0.484, 2.937)	0.703
PLT	0.988 (0.502, 1.944)	0.972		
Ca	2.055 (1.010, 4.181)	0.047*	0.748 (0.337, 1.661)	0.047*

$p < 0.05$.

ratio, ISS stage, DS stage, haemoglobin level, or ß 2-MG level were noted between the two groups. However, abnormal renal function and increased serum calcium were significantly associated with the low ALI group. Better chemotherapy efficacy was observed in the high ALI group (89.3%) than in the low ALI group (42.2%) ($p < 0.001$), but there was no significant difference between the high ALI group and the low ALI group in whether bortezomib was used ($p > 0.05$). In univariate analyses, abnormal renal function, lower ALI, and high NLR level was related to poor chemotherapy efficiency, but multivariate analysis suggested that only ALI [HR: 0.110, 95% CI (0.035–0.350), $p = 0.000$] was an independent predictive factor in evaluating the efficiency of induction chemotherapy (Table 3). We compared the predictive value of NLR, ALB, and ALI in patients with MM treated with chemotherapy. The areas under the ROC curves of NLR, ALB, and ALI were calculated (Figure 2), and ALI and NLR were significantly associated with OS. Notably, based on ROC curve analyses, ALI was identified as a more powerful prognostic marker than NLR and ALB.

Risk of infection in newly-diagnosed multiple myeloma patients receiving induction therapy

Among the MM patients, 40 (36.04%) presented with infection after induction chemotherapy. The most common site of infection was the respiratory system (32 cases, 80%), followed by the digestive system (3, 7.5%) and the urinary system (2, 5%). In addition, three patients (7.5%) had more than one site of infection. Univariate analysis suggested that ALI and abnormal renal function were significant in predicting infection in NDMM patients (Table 4).

Discussion

The ALI score, comprising BMI, ALB, and NLR, reflects inflammatory immunity and nutritional status. In this study, advanced age, chemotherapy response and serum calcium were independent prognostic factors for OS. Regarding the prognostic potential of ALI in MM patients, a lower ALI score reduced OS, indicating that ALI can serve as an outcome biomarker (Jafri et al., 2013; Park et al., 2017; Mandaliya et al., 2019; Kusunoki et al., 2020; Yin et al., 2021). Similar research has reported that ALI is a predictive marker for PD-L1 inhibitor monotherapy and has stronger predictive ability compared with other analysed parameters, such as NLR and PD-L1 TPS (Mountzios et al., 2021), which have also been confirmed as predictors of OS in NDMM patients treated with bortezomib-based regimens (Romano et al., 2017; Zhou et al., 2018). A retrospective single-centre study in China showed that age, haemoglobin, ALB, serum calcium, β2-MG, LDH, CRP, the ratio of plasma cells and the percentage of abnormal plasma cells in bone marrow were all independent prognostic factors for OS, which is different from our results (Qian et al., 2017). However, the

TABLE 2 Baseline clinical characteristics according to the ALI.

Clinical characteristic	Total	ALI group		χ^2	*p*
		High (*n* = 66)	Low (*n* = 45)		
Age (years)				0.004	0.949
<60	67	40 (60.6)	27 (0.0)		
≥60	44	26 (39.4)	18 (40.0)		
Gender				0.240	0.624
Male	66	38 (57.6)	28 (62.2)		
Female	45	28 (42.4)	17 (37.8)		
Classification of disease				0.000	0.991
IgG+IgA	79	47 (71.2)	32 (71.1)		
Other types	32	19 (28.8)	13 (28.9)		
ISS stage				1.628	0.431
I	12	8 (12.1)	4 (8.9)		
II	28	19 (28.8)	9 (20.0)		
III	71	39 (59.1)	32 (71.1)		
DS stage				1.873	0.392
I	4	3 (4.6)	1 (2.2)		
II	12	9 (13.6)	3 (6.7)		
III	95	54 (81.8)	4 (91.1)		
Renal function				10.251	0.001*
Normal	90	60 (91.0)	30 (66.7)		
Abnormal	21	6 (9.0)	15 (33.3)		
Plasma cell ratio				1.631	0.202
<30%	66	36 (54.5)	30 (66.7)		
≥30%	45	30 (45.5)	15 (33.3)		
β2-MG(mg/L)				1.822	0.177
<5.5	63	34 (51.5)	29 (64.4)		
≥5.5	48	32 (48.5)	16 (35.6)		
Hb(g/L)				1.610	0.204
<100	79	44 (66.7)	35 (77.8)		
≥100	32	22 (33.3)	10 (22.2)		
Calcium (mmol/L)				3.917	0.048*
<2.75	89	57 (86.3)	32 (71.1)		
≥2.75	22	9 (13.6)	13 (28.9)		
Albumin				0.535	0.464
<35	57	32 (48.5)	25 (55.6)		
≥35	54	34 (51.5)	20 (44.4)		

$p < 0.05$.

strict inclusion criteria for NDMM patients potentially led to sample selection bias. In addition, the sample size of our study was relatively small, which might also lead to bias in our results. Renal dysfunction is an important characteristic of MM, and the development of renal dysfunction is a negative prognostic factor for MM patients undergoing induction chemotherapy (Li et al., 2021). Our study suggests that low ALI is positively associated with renal dysfunction. Kidney damage often manifests as proteinuria and hypoproteinaemia (Pei et al., 1992), which reduce ALB and result in low ALI. Therefore, ALI also represents a potential negative prognostic factor for patients with MM.

Chemotherapy response is an important prognostic factor in NDMM patients receiving bortezomib-based therapy. Based on univariate analyses, we found that abnormal renal function, high NLR, and lower ALI level are related to poor chemotherapy efficiency. Chen's research demonstrated that renal function is associated with a high incidence of chemotherapy-related

TABLE 3 Univariate analysis and multivariate analysis of the response to chemotherapy.

Clinical characteristic	Univariate		Multivariate	
	χ^2	*p*-value	HR (95% CI)	*p*-value
Age (years)	0.026	0.873		
Gender	0.781	0.377		
Classification of disease	0.055	0.814		
ISS stage	0.200	0.905		
DS stage	3.055	0.217		
Renal function	3.968	0.046*	1.248 (0.401,3.882)	0.702
Plasma cell ratio	0.026	0.873		
β2-MG(mg/L)	0.688	0.407		
Hb(g/L)	1.328	0.249		
ALB	0.192	0.661		
Chemotherapy regimens	3.248	0.072		
NLR	11.197	0.001*	1.430 (0.450,4.539)	0.544
ALI	28.499	0.000*	0.110 (0.035,0.350)	0.000*
PLT	0.481	0.488		
Ca	0.079	0.778		

$p < 0.05$.

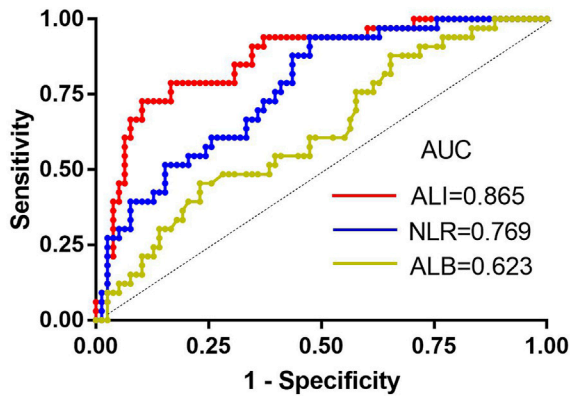

FIGURE 2
The receiver-operating characteristic (ROC) curves for ALI, ALB, and NLR. AUC, area under the curve; ALI, advanced lung cancer inflammation index; NLR, neutrophil-to-lymphocyte ratio; ALB, albumin.

toxicities in metastatic colorectal cancer and even decreases the efficacy of chemotherapy (Chen et al., 2015), which is consistent with our research. In addition, a signature consisting of 11 cytokine genes in the lung environment is able to predict lymph node metastasis and prognosis of lung adenocarcinoma based on IL-8 and TNFα as the top two genes for predicting prognosis (Seike et al., 2007). IL-8 was originally described as a monocyte-derived neutrophil chemotactic factor (MNDCF) that specifically attracts neutrophils (Mukaida et al., 1998), which explains why the NLR value is increased in tumour cells. Hirahara et al. (2019) evaluated the relationship between tumour response and NLR/PLR and found that the score can serve as a new blood predictor of tumour response and prognosis. As discussed above, NLR is related to renal function, and the ALI index is calculated from the NLR value. Therefore, ALI is extremely closely related to the efficacy of chemotherapy. This finding is consistent with our multivariate result that ALI is an independent predictor of chemotherapy effect. Moreover, based on ROC analysis, ALI outperformed other biomarkers of chemotherapy response, including NLR and ALB (Szudy-Szczyrek et al., 2020).

Given that NDMM patients have a high risk of infections at first admission, especially infections with Epstein–Barr virus (EBV), hepatitis B virus (HBV) and *Escherichia coli* (Lin et al., 2020), we excluded MM patients with concurrent infection from this study. Interestingly, our results highlight that ALI is not only an independent predictive marker of chemotherapy efficacy but also a predictor of susceptibility to infection in NDMM patients during induction chemotherapy. Our study also showed that patients with lower ALI may be more susceptible to infectious complications after receiving induction chemotherapy. Some studies have shown that renal impairment is a risk factor for infections in the early phase of MM or in NDMM patients receiving bortezomib-based induction chemotherapy (Sørrig et al., 2019; Soekojo et al., 2020). We also found that renal failure is a significant risk factor for NDMM patients. Therefore, the presence of low ALI and renal dysfunction may be of greater practical value in predicting infection for MM patients without

TABLE 4 Univariate analysis of infection after chemotherapy in patients with MM.

Risk factors	Group		χ^2	*p*
	Infected (*n* = 40)	Uninfected (*n* = 71)		
Age (years)			0.003	0.954
<60	24 (60.0)	43 (60.6)		
≥60	16 (40.0)	28 (39.4)		
Gender			0.100	0.752
Male	23 (57.5)	43 (60.6)		
Female	17 (42.5)	28 (39.4)		
Classification of disease			1.221	0.269
IgG+IgA	28 (70.0)	51 (71.8)		
Other types	12 (30.0)	20 (28.2)		
ISS stage			2.529	0.282
I	2 (5.0)	10 (14.1)		
II	12 (30.0)	16 (22.5)		
III	26 (65.0)	45 (63.4)		
DS stage			3.271	0.195
I	0 (0)	4 (5.6)		
II	6 (15.0)	6 (8.4)		
III	34 (85.0)	61 (86)		
Renal function			5.006	0.025*
Normal	28 (70)	62 (87.3)		
Abnormal	12 (30)	9 (12.7)		
Plasma cell ratio			0.240	0.624
<30%	25 (62.5)	41 (57.7)		
≥30%	15 (37.5)	30 (42.3)		
β2-MG(mg/L)			1.381	0.240
<3.5	26 (65.0)	38 (53.5)		
≥3.5	14 (35.0)	33 (46.5)		
Hb(g/L)			0.447	0.504
<100	30 (75)	49 (69)		
≥100	10 (25)	22 (31)		
Calcium (mmol/L)				
<2.75	32 (80.0)	57 (80.3)	0.001*	0.097
≥2.75	8 (20.0)	14 (19.7)		
Albumin				
<35	21 (52.5)	36 (50.7)	0.033	0.856
≥35	19 (47.5)	35 (49.3)		
ALI				
<32.7	22 (55.0)	23 (32.4)	5.424	0.020*
≥32.7	18 (45.0)	48 (67.6)		
NLR				
<2.0	16 (40.0)	38 (53.5)	1.872	0.171
≥2.0	24 (60.0)	33 (50.7)		
Chemotherapy regimens			3.795	0.051
Contains bortezomib	36 (90.0)	53 (74.6)		
Does not contain	4 (10.0)	18 (25.3)		
PLT			0.724	0.395
<150	12 (30.0)	27 (38)		
≥150	28 (70.0)	44 (62)		

$p < 0.05$.

comorbidities at admission. On the other hand, patients with lower ALI may have a higher NLR value, which may indicate lymphocytopaenia and worse inflammatory immunity and nutritional status (Hirahara et al., 2019), which are significant risk factors for NDMM patients. The incidence of infection after chemotherapy in MM patients is 36.04%, and pulmonary infection is most common, which is consistent with existing research results (O'Brien et al., 2003). Based on data on antimyeloma therapy in previous studies, chemotherapy can increase the risk of bacterial infection, and bortezomib can increase that of influenza infection (Nucci and Anaissie, 2009; Teh et al., 2015). However, we found that chemotherapeutic regimens, including bortezomib, did not increase the risk of infection, which is not consistent with existing research (Nucci and Anaissie, 2009). This finding may be due to our inclusion criteria of MM patients without the presence of comorbidities or multiple organ dysfunctions.

In conclusion, our study confirms that ALI is not only a prognostic biomarker for patients newly diagnosed with MM but also predicts the efficacy of chemotherapy in NDMM patients receiving bortezomib-based therapy. Importantly, those with abnormal renal function have poorer prognosis and are more susceptible to serious infection complications. Therefore, ALI can be adapted in clinical practice to stratify MM patients for future trials. Furthermore, large-scale multicentre prospective studies are required to completely validate our findings.

Data availability statement

The raw data supporting the conclusion of this article will be made available by the authors, without undue reservation.

Ethics statement

This study involving human participants was approved by the Ethics Committee of the Third Xiangya Hospital, Central South University (No. 22081).

Author contributions

CY contributed to the conception and design of the study. JC and QL performed the statistical analysis and SX wrote the article. LN, JL, BX contributed to data collection. YJ, HZ, QJ contributed to manuscript revision. All authors contributed to the study conception and design.

Funding

This research was supported by a grant from the Key Research and Development program of Hainan Province (ZDYF2020135) and Changsha Natural Science Foundation (kq2202427).

Acknowledgments

The authors would like to thank the Third Xiangya Hospital of Central South University for its support.

Conflict of interest

The authors declare that the research was conducted in the absence of any commercial or financial relationships that could be construed as a potential conflict of interest.

Publisher's note

References

Balmaceda, N., Aziz, M., Chandrasekar, V. T., McClune, B., Kambhampati, S., Shune, L., et al. (2021). Infection risks in multiple myeloma: A systematic review and meta-analysis of randomized trials from 2015 to 2019. *BMC Cancer* 21 (1), 730. doi:10.1186/s12885-021-08451-x

Bazarbachi, A. H., Al Hamed, R., Malard, F., Bazarbachi, A., Harousseau, J. L., and Mohty, M. (2022). Induction therapy prior to autologous stem cell transplantation (ASCT) in newly diagnosed multiple myeloma: An update. *Blood Cancer J.* 12 (3), 44. doi:10.1038/s41408-019-0205-9

Bladé, J., and Rosiñol, L. (2005). Renal, hematologic and infectious complications in multiple myeloma. *Best. Pract. Res. Clin. Haematol.* 18 (4), 635–652. doi:10.1016/j.beha.2005.01.013

Blimark, C., Holmberg, E., Mellqvist, U. H., Landgren, O., Björkholm, M., Hultcrantz, M., et al. (2015). Multiple myeloma and infections: A population-based study on 9253 multiple myeloma patients. *Haematologica* 100 (1), 107–113. doi:10.3324/haematol.2014.107714

Boyd, K. D., Ross, F. M., Chiecchio, L., Dagrada, G. P., Konn, Z. J., Tapper, W. J., et al. (2012). A novel prognostic model in myeloma based on co-segregating adverse FISH lesions and the ISS: Analysis of patients treated in the MRC myeloma IX trial. *Leukemia* 26 (2), 349–355. doi:10.1038/leu.2011.204

Camp, R. L., Dolled-Filhart, M., and Rimm, D. L. (2004). X-Tile: A new bio-informatics tool for biomarker assessment and outcome-based cut-point optimization. *Clin. Cancer Res.* 10 (21), 7252–7259. doi:10.1158/1078-0432.CCR-04-0713

Chen, J., Wang, X. T., Luo, P. H., and He, Q. J. (2015). Effects of unidentified renal insufficiency on the safety and efficacy of chemotherapy for metastatic colorectal cancer patients: A prospective, observational study. *Support. Care Cancer* 23 (4), 1043–1048. doi:10.1007/s00520-014-2461-3

Hanahan, D., and Weinberg, R. A. (2011). Hallmarks of cancer: The next generation. *Cell.* 144 (5), 646–674. doi:10.1016/j.cell.2011.02.013

Hirahara, T., Arigami, T., Yanagita, S., Matsushita, D., Uchikado, Y., Kita, Y., et al. (2019). Combined neutrophil-lymphocyte ratio and platelet-lymphocyte ratio predicts chemotherapy response and prognosis in patients with advanced gastric cancer. *BMC Cancer* 19 (1), 672. doi:10.1186/s12885-019-5903-y

Jafri, S. H., Shi, R., and Mills, G. (2013). Advance lung cancer inflammation index (ALI) at diagnosis is a prognostic marker in patients with metastatic non-small cell lung cancer (NSCLC): A retrospective review. *BMC Cancer* 13, 158. doi:10.1186/1471-2407-13-158

Kumar, S., Paiva, B., Anderson, K. C., Durie, B., Landgren, O., Moreau, P., et al. (2016). International Myeloma Working Group consensus criteria for response and minimal residual disease assessment in multiple myeloma. *Lancet. Oncol.* 17 (8), e328–e346. doi:10.1016/S1470-2045(16)30206-6

Kusunoki, K., Toiyama, Y., Okugawa, Y., Yamamoto, A., Omura, Y., Ohi, M., et al. (2020). Advanced lung cancer inflammation index predicts outcomes of patients with colorectal cancer after surgical resection. *Dis. Colon Rectum* 63 (9), 1242–1250. doi:10.1097/DCR.0000000000001658

Li, S., Gong, T., Kou, C., Fu, A., Bolanos, R., and Liu, J. (2021). Clinical outcomes associated with chronic kidney disease in elderly medicare patients with multiple myeloma. *Clin. Lymphoma Myeloma Leuk.* 21 (6), 401–412.e24. doi:10.1016/j.clml.2021.01.015

Lin, C., Shen, H., Zhou, S., Liu, M., Xu, A., Huang, S., et al. (2020). Assessment of infection in newly diagnosed multiple myeloma patients: Risk factors and main characteristics. *BMC Infect. Dis.* 20 (1), 699. doi:10.1186/s12879-020-05412-w

Mandaliya, H., Jones, M., Oldmeadow, C., and Nordman, II (2019). Prognostic biomarkers in stage IV non-small cell lung cancer (NSCLC): Neutrophil to lymphocyte ratio (NLR), lymphocyte to monocyte ratio (LMR), platelet to lymphocyte ratio (PLR) and advanced lung cancer inflammation index (ALI). *Transl. Lung Cancer Res.* 8 (6), 886–894. doi:10.21037/tlcr.2019.11.16

Mountzios, G., Samantas, E., Senghas, K., Zervas, E., Krisam, J., Samitas, K., et al. (2021). Association of the advanced lung cancer inflammation index (ALI) with immune checkpoint inhibitor efficacy in patients with advanced non-small-cell lung cancer. *ESMO Open* 6 (5), 100254. doi:10.1016/j.esmoop.2021.100254

Mu, S., Ai, L., Fan, F., Sun, C., and Hu, Y. (2018). Prognostic role of neutrophil-lymphocyte ratio in multiple myeloma: A dose-response meta-analysis. *Onco. Targets. Ther.* 11, 499–507. doi:10.2147/OTT.S153146

Mukaida, N., Harada, A., and Matsushima, K. (1998). Interleukin-8 (IL-8) and monocyte chemotactic and activating factor (MCAF/MCP-1), chemokines essentially involved in inflammatory and immune reactions. *Cytokine Growth Factor Rev.* 9 (1), 9–23. doi:10.1016/s1359-6101(97)00022-1

Nakamura, K., Kassem, S., Cleynen, A., Chrétien, M. L., Guillerey, C., Putz, E. M., et al. (2018). Dysregulated IL-18 is a Key driver of immunosuppression and a possible therapeutic target in the multiple myeloma microenvironment. *Cancer Cell.* 33 (4), 634–648. e5. doi:10.1016/j.ccell.2018.02.007

Nucci, M., and Anaissie, E. (2009). Infections in patients with multiple myeloma in the era of high-dose therapy and novel agents. *Clin. Infect. Dis.* 49 (8), 1211–1225. doi:10.1086/605664

O'Brien, S. N., Blijlevens, N. M., Mahfouz, T. H., and Anaissie, E. J. (2003). Infections in patients with hematological cancer: Recent developments. *Hematol. Am. Soc. Hematol. Educ. Program* 2003, 438–472. doi:10.1182/asheducation-2003.1.438

Palumbo, A., and Anderson, K. (2011). Multiple myeloma. *N. Engl. J. Med.* 364 (11), 1046–1060. doi:10.1056/NEJMra1011442

Palumbo, A., Avet-Loiseau, H., Oliva, S., Lokhorst, H. M., Goldschmidt, H., Rosinol, L., et al. (2015). Revised international staging system for multiple myeloma: A report from international myeloma working group. *J. Clin. Oncol.* 33 (26), 2863–2869. doi:10.1200/JCO.2015.61.2267

Park, Y. H., Yi, H. G., Lee, M. H., Kim, C. S., and Lim, J. H. (2017). Prognostic value of the pretreatment advanced lung cancer inflammation index (ALI) in diffuse large B cell lymphoma patients treated with R-CHOP chemotherapy. *Acta Haematol.* 137 (2), 76–85. doi:10.1159/000452991

Pei, Y., Cattran, D., and Greenwood, C. (1992). Predicting chronic renal insufficiency in idiopathic membranous glomerulonephritis. *Kidney Int.* 42 (4), 960–966. doi:10.1038/ki.1992.374

Qian, J., Jin, J., Luo, H., Jin, C., Wang, L., Qian, W., et al. (2017). Analysis of clinical characteristics and prognostic factors of multiple myeloma: A retrospective single-center study of 787 cases. *Hematology* 22 (8), 472–476. doi:10.1080/10245332.2017.1309493

Raab, M. S., Podar, K., Breitkreutz, I., Richardson, P. G., and Anderson, K. C. (2009). Multiple myeloma. *Lancet* 374 (9686), 324–339. doi:10.1016/S0140-6736(09)60221-X

Raje, N. S., Anaissie, E., Kumar, S. K., Lonial, S., Martin, T., Gertz, M. A., et al. (2022). Consensus guidelines and recommendations for infection prevention in multiple myeloma: A report from the international myeloma working group. *Lancet. Haematol.* 9 (2), e143–e161. doi:10.1016/S2352-3026(21)00283-0

Röllig, C., Knop, S., and Bornhäuser, M. (2015). Multiple myeloma. *Lancet* 385 (9983), 2197–2208. doi:10.1016/S0140-6736(14)60493-1

Romano, A., Laura Parrinello, N., Cerchione, C., Letizia Consoli, M., Parisi, M., Calafiore, V., et al. (2017). The NLR and LMR ratio in newly diagnosed MM patients treated upfront with novel agents. *Blood Cancer J.* 7 (12), 649. doi:10.1038/s41408-017-0019-6

Seike, M., Yanaihara, N., Bowman, E. D., Zanetti, K. A., Budhu, A., Kumamoto, K., et al. (2007). Use of a cytokine gene expression signature in lung adenocarcinoma and the surrounding tissue as a prognostic classifier. *J. Natl. Cancer Inst.* 99 (16), 1257–1269. doi:10.1093/jnci/djm083

Shiroyama, T., Suzuki, H., Tamiya, M., Tamiya, A., Tanaka, A., Okamoto, N., et al. (2018). Pretreatment advanced lung cancer inflammation index (ALI) for predicting early progression in nivolumab-treated patients with advanced non-small cell lung cancer. *Cancer Med.* 7 (1), 13–20. doi:10.1002/cam4.1234

Soekojo, C. Y., Low, J. Z., Oh, J., Ooi, M., De Mel, S., and Chng, W. J. (2020). Bacterial infection among patients with multiple myeloma treated with bortezomib-based induction therapy: Real-world experience in an asian cancer center. *Clin. Lymphoma Myeloma Leuk.* 20 (4), e165–e170. doi:10.1016/j.clml.2019.12.024

Sørrig, R., Klausen, T. W., Salomo, M., Vangsted, A., and Gimsing, P. (2019). Risk factors for infections in newly diagnosed multiple myeloma patients: A Danish retrospective nationwide cohort study. *Eur. J. Haematol.* 102 (2), 182–190. doi:10.1111/ejh.13190

Szudy-Szczyrek, A., Mlak, R., Mielnik, M., Szczyrek, M., Nowaczyńska, A., Homa-Mlak, I., et al. (2020). Prognostic value of pretreatment neutrophil-to-lymphocyte and platelet-to-lymphocyte ratios in multiple myeloma patients treated with thalidomide-based regimen. *Ann. Hematol.* 99 (12), 2881–2891. doi:10.1007/s00277-020-04092-5

Teh, B. W., Worth, L. J., Harrison, S. J., Thursky, K. A., and Slavin, M. A. (2015). Risks and burden of viral respiratory tract infections in patients with multiple myeloma in the era of immunomodulatory drugs and bortezomib: Experience at an Australian cancer hospital. *Support. Care Cancer* 23 (7), 1901–1906. doi:10.1007/s00520-014-2550-3

Yin, C., Toiyama, Y., Okugawa, Y., Omura, Y., Kusunoki, Y., Kusunoki, K., et al. (2021). Clinical significance of advanced lung cancer inflammation index, a nutritional and inflammation index, in gastric cancer patients after surgical resection: A propensity score matching analysis. *Clin. Nutr.* 40 (3), 1130–1136. doi:10.1016/j.clnu.2020.07.018

Zhou, X., Wang, J., Xia, J., Cheng, F., Mao, J., Zhu, J., et al. (2018). Evaluation of neutrophil-to-lymphocyte ratio in newly diagnosed patients receiving bortezomib-based therapy for multiple myeloma. *Cancer Biomark.* 22 (1), 43–48. doi:10.3233/CBM-170795

frontiers | Frontiers in Genetics

TYPE Original Research
PUBLISHED 01 December 2022
DOI 10.3389/fgene.2022.1065546

OPEN ACCESS

EDITED BY
Rui Cao,
Affiliated Beijing Friendship Hospital, Capital Medical University, China

REVIEWED BY
Lianchun Wang,
University of South Florida, United States
Xuhao Ni,
Sun Yat-sen University, China

*CORRESPONDENCE
Yunxia Lv,
83394045@qq.com
Guancheng Liu,
liuguanchengxy@163.com
Gengming Cai,
cgmkgx@hotmail.com

SPECIALTY SECTION
This article was submitted to Cancer Genetics and Oncogenomics, a section of the journal Frontiers in Genetics

RECEIVED 09 October 2022
ACCEPTED 18 November 2022
PUBLISHED 01 December 2022

CITATION
Wei M, Tian Y, Lv Y, Liu G and Cai G (2022), Identification and validation of a prognostic model based on ferroptosis-associated genes in head and neck squamous cancer.
Front. Genet. 13:1065546.
doi: 10.3389/fgene.2022.1065546

Identification and validation of a prognostic model based on ferroptosis-associated genes in head and neck squamous cancer

Ming Wei[1], Yongquan Tian[1], Yunxia Lv[2]*, Guancheng Liu[3]* and Gengming Cai[4]*

[1]Department of Otolaryngology Head and Neck Surgery, Xiangya Hospital, Central South University, Changsha, China, [2]Department of Thyroid Surgery, The Second Affiliated Hospital to Nanchang University, Nanchang, China, [3]Department of Otolaryngology Head and Neck Surgery, Affiliated Hospital of Guilin Medical University, Guilin, China, [4]Department of Otolaryngology Head and Neck Surgery, First Affiliated Hospital of Quanzhou, Fujian Medical University, Quanzhou, China

Ferroptosis is that under the action of ferrous iron or ester oxygenase, unsaturated fatty acids highly expressed on the cell membrane are catalyzed to undergo lipid peroxidation, thereby inducing cell death. In this study, we used ferroptosis marker genes to identify 3 stable molecular subtypes (C1, C2, C3) with distinct prognostic, mutational, and immune signatures by consensus clustering; TP53, CDKN2A, etc. Have higher mutation frequencies in the three subtypes. C3 has a better prognosis, while the C1 subtype has a worse prognosis. WGCNA is used to identify molecular subtype-related gene modules.After filting, we obtained a total of 540 genes related to the module feature vector (correlation>0.7).We performed univariate COX regression analysis on these genes, and identified a total of 97 genes ($p < 0.05$) that had a greater impact on prognosis, including 8 ''Risk" and 89 ''Protective" genes. After using lasso regression, we identified 8 genes (ZNF566, ZNF541, TMEM150C, PPAN, PGLYRP4, ENDOU, RPL23 and MALSU1) as ferroptosis-related genes affecting prognosis. The ferroptosis prognosis-related risk score (FPRS) was calculated for each sample in TCGA-HNSC dataset. The results showed that FPRS was negatively correlated with prognosis.The activated pathways in the PFRS-high group mainly include immune-related pathways and invasion-related pathways. We assessed the extent of immune cell infiltration in patients in our TCGA-HNSC cohort by using the expression levels of gene markers in immune cells. The FPRS-high group had a higher level of immune cell infiltration. We found that the expression of immune checkpoints was significantly up-regulated in the FPRS-low group and the FPRS-high group had a higher probability of immune escape and a lower probability of benefiting from immunotherapy. In this work,

Abbreviations: HNSC, Head and Neck Squamous Cancer; TCGA, The Cancer Genome Atlas; WGCNA, Weighted Gene Co-expression Network Analysis; FPRS, Ferroptosis Prognosis-related Risk Score; CNV, Copy Number Variation; SNV, Simple Nucleotide Variation; RNA-seq, Transcriptome expression data; GEO, Gene Expression Omnibus database; OS, Overall Survival; ICB, Immune Checkpoint Blockade; TAF, Tumor-associated Fibroblasts; MDSCs, Myeloid-derived Suppressor Cells; TAM, Tumor-associated Macrophages; GSEA, Gene Set Enrichment Analysis.

we constructed a scoring Ferroptosis-related prognostic model that can well reflect risk and positive factors for prognosis in patients with head and neck squamous cell carcinoma. It can be used to guide individualized adjuvant therapy and chemotherapy for patients with head and neck cancer. Therefore, it has a good survival prediction ability and provides an important reference for clinical treatment.

KEYWORDS

hNSC, risk score, prognostic model, predicting survival, ferroptosis-associated genes

1 Introduction

There are about 600,000 new cases of head and neck malignant tumors every year, and more than 60% of these cases are insidious (Chen et al., 2016; Miller et al., 2016). Although great progress has been made in multidisciplinary treatment in head and neck malignant tumors, 5-year survival rate has not improved significantly, only 40%–50% (Siegel et al., 2011). It is an important means to further understand the molecular mechanism of head and neck tumors and explore new molecular targets such as early diagnosis, prognosis evaluation, and targeted therapy.

Ferroptosis is an iron-dependent, different from apoptosis, necrosis, cell autophagy, a novel form of programmed cell death (Dixon et al., 2014; Stockwell, 2022). The main mechanism of ferroptosis is that under the action of ferrous iron or ester oxygenase, unsaturated fatty acids highly expressed on the cell membrane are catalysed to undergo lipid peroxidation, thereby inducing cell death (Stockwell, 2022). Induction of ferroptosis has received increasing attention as a potential tumor treatment option (Lin et al., 2020). Recent studies have found that many tumor suppressors exert some of their tumor suppressor functions by inducing ferroptosis (Jiang et al., 2015; Chu et al., 2019). p53 inhibits the expression of solute carrier family 7 member 11 (SLC7A11) (Jiang et al., 2015). p53 also causes ALOX12-dependent cell death that is inhibited by ferrostatin-1 and involves the expression of the ferroptosis marker gene Ptgs2 (Chu et al., 2019).

It also reported that the loss of ferroptosis can drive tumorigenesis (Wu et al., 2021). Wang et al. found that CD8 + T cells could drive ferroptosis (Wang et al., 2019). Therefore, activating $CD8^+$ T through immune checkpoint blockade therapy to drive ferroptosis to selectively kill tumor cell are obviously beneficial to the improvement of prognosis (Sanmamed and Chen, 2018). Epithelial-mesenchymal transition (EMT) plays an important role in invasion and metastasis, with adverse effects on prognosis. Recent studies have shown that ferroptosis inducers are associated with mesenchymal or metastatic properties of cancer cells and that inhibition of E-cadherin or induction of EMT may contribute to enhanced ferroptosis (Hangauer et al., 2017; Viswanathan et al., 2017; Wu et al., 2019). Inhibition of ferroptosis is an important mechanism of drug resistance in tumor therapy. Inhibition of GPX4 is a well-known method of inducing ferroptosis. Traditional chemotherapeutic drugs inhibit ferroptosis by upregulating GPX4 and X_{c-} system, leading to chemoresistance. However, when some classic chemotherapy drugs are used in combination with ferroptosis inducers, the anticancer effect will be enhanced (Yu et al., 2015). Therefore, ferroptosis can be regarded as an important factor affecting prognosis.

In this study, we used ferroptosis marker genes to identify stable molecular subgroups by consensus clustering type, and further compare the pathway characteristics and immune characteristics between the subtypes. We identified genes associated with the ferroptosis prognostic score by WGCNA and lasso, and further, we constructed a clinical prognostic model of ferroptosis-related prognostic risk score (FPRS). To further improve the prognostic model and survival prediction, we adopted a decision tree model to combine FPRS with clinicopathological features to construct a nomogram for risk assessment of head and neck cancer patients.

2 Materials and methods

2.1 Date set

We downloaded the HNSC RNA-seq data from the Cancer Genome Atlas public data portal, which finally included a total of 499 primary tumor samples after filtering. The expression data of GSE65858 and GSE42743 were obtained from the Gene Expression Omnibus database. After filtering, 253 and 104 head and neck cancer samples, respectively, were included in the analysis. In this study, we used TCGA-HNSC data as the training set and GSE65858 and GSE42743 datasets as independent validation sets. At the same time, we also downloaded a group of head and neck cancer immunotherapy data GSE78220 as risk mode of immunotherapy response prediction. Here, the ferroptosis-related genes are derived from the FerrDb database, with a total of 259 genes.

2.2 Data preprocessing

Perform the following steps to preprocess the RNA-seq data of TCGA: 1)Remove the samples without clinical follow-up

information; 2) Remove the samples without survival time; 3) Remove the samples without Status; 4) Convert Ensembl to Gene symbol; 5) Take the median value for expressions with multiple Gene Symbols; Do the following steps to preprocess the GEO data: For the GEO dataset, we downloaded the annotation information of the corresponding chip platform, mapped probes to genes according to the annotation information, and removed probes that matched one probe to multiple genes. When multiple probes matched a gene, the median was taken as the gene expression value. Various datasets and samples showed in such as attachments * .exp.txt, * .cli.txt.

2.3 Molecular typing of ferroptosis-related genes

Consensus clustering (ConsensusClusterPlus) was used to construct a consistency matrix and cluster the samples (PMID: 20427518). Using the expression data of ferroptosis -related genes, the molecular subtypes of the samples were obtained. We utilized the pam algorithm and "1-Pearson correlation" as the metric distance and performed 500 bootstraps, each bootstraps process including 80% of the training set patients. The number of clusters was set from 2 to 10, and the optimal classification was determined by calculating the consistency matrix and the consistency cumulative distribution function to obtain the molecular subtypes of the samples.

2.4 Construction of weighted gene Co-expression network

Gene co-expression networks were constructed using weighted gene co-expression network analysis (WGCNA) (PMID: 19114008). First, to construct the gene expression similarity matrix, we calculated the absolute value of Pearson's correlation coefficient between genes i and j using the equation:

$$S_{ij} = \left|\left(1 + cor\left(x_i + y_i\right)\right)\right|/2$$

where i and j represent the expression of genes i and j, respectively. Further, the gene expression similarity matrix was transformed into an adjacency matrix. β is a soft-thresholding parameter and represents Pearson's correlation coefficient b for each pair of genes [PMID: 17090670]. This step strengthens the strong correlation and weakens the weak correlation from the index level

$$a_{ij} = \left|\left(1 + \mathrm{cor}\left(x_i + y_i\right)\right)/2\right|^{\beta}$$

The representative genes in each module are called characteristic vector genes, referred to as ME, which represent the overall level of gene expression within the module

$$ME = \mathrm{princomp}\left(x_{ij}^{q}\right)$$

where i represents the gene in modulus q, and j represents the microarray sample in modulus q. We used Pearson's correlation for the expression profiles of the genes in all samples, and the ME expression profiles of the signature vector genes to gauge the identity of that gene in the module. We called this module membership (MM)

$$MM_i^q = \mathrm{cor}\left(x_i, ME^q\right)$$

where ME represents the expression profile of gene i.

2.5 Construction of the FPRS scoring system to evaluate head and neck cancer samples

(1) Molecular subtype -related modules, where we performed WGCNA analysis using the entire expression profile of TCGA-HNSC, we identified the most relevant modules for molecular subtypes as key modules;
(2) Further, we extracted the genes in the key modules, and selected the genes whose correlation with the module feature vector was greater than 0.7 and had a significant prognosis as the genes related to the ferroptosis phenotype;
(3) The number of genes was further reduced by the method of lasso regression, and the genes related to the prognosis of ferroptosis were obtained;
(4) FPRS scoring system construction. We calculated the FPRS score of each patient using the following formula: FPRS = Σβ i ×Exp i), where i refers to the gene expression level of the ferroptosis prognosis-related gene signature, and β is the Cox regression coefficient of the corresponding gene. According to the best cut-off value of FPRS obtained by the R package survminer, the patients were divided into high and low risk groups of FPRS, the survival curve was drawn by the Kaplan-Meier method for prognostic analysis, and the log-rank test was used to determine the significance of the difference.

2.6 Prediction of responsiveness to immunotherapy

We used the TIDE algorithm to verify the effect of IMS on the prediction of clinical responsiveness to ICIs. The TIDE algorithm is a computational method for predicting ICB responsiveness using gene expression profiling [PMID: 30127393]. The TIDE algorithm evaluated three cell types that limit T cell infiltration in tumors, including the M2 subtype of tumor-associated fibroblasts (TAF), myeloid-derived suppressor cells (MDSCs), and tumor-associated macrophages (TAM), and two different mechanisms of tumor immune escape, including the dysfunction score of tumor-infiltrating cytotoxic T lymphocytes (CTLs) (dysfunction)

and the rejection score of CTLs by immunosuppressive factors (exclusion).

2.7 Gene set enrichment analysis

To study the pathways of different biological processes in different molecular subtypes, we used GSEA for pathway analysis, here we used all candidate gene sets in the Hallmark database [PMID: 26771021] for GSEA.

2.8 Calculation of invasive abundance of TME cells

We used the CIBERSORT algorithm (https://cibersort.stanford.edu/) to quantify the relative abundance of 22 immune cells in head and neck cancer. At the same time, we also used ESTIMATE software to calculate the proportion of immune cells.

2.9 Real-time PCR

We used TRIzol to obtain total RNA from fresh human head and neck squamous cell carcinoma tissues and paracancerous tissues, and then reverse transcribed into cDNA. The human tissues got from the patients consented to this study during the time of surgery from January 2020 to December 2020 in Quanzhou First Hospital Affiliated to Fujian Medical University. It is considered by the Ethic Committee of the Quanzhou First Hospital Affiliated to Fujian Medical University. Ethics Committee agrees the program to carry out as planned [No. (2019) 109]. The Quantitative real-time PCR was performed on an ABI 7900 system (Takara, Dalian, China) with SYBR Green using SYBR Green RT-PCR Assay (Takara, Dalian, China) and normalized to GAPDH. The following primers were used for PCR: ZNF566, forward primer: 5′-ctcgacatcacagaattcaca c-3′; and reverse primer: 5′-tctgatgtcgagtgaagtttga-3′; TMEM150C, forward primer, 5′-gagaccagcctgaccaatgtgaag-3′ and reverse primer, 5′-ctgcctccgcctcctgagtag-3′; ENDOU, forward primer, 5′-ttacagtcacatctcgccttta-3′ and reverse primer, 5′-ggagtagagtgcaaactcaaac-3′. MALSU1, forward primer, 5′-ttctacccgacacttacatgccatgand-3′ and reverse primer, 5′-ccacgcacagccagtcatcag-3′.

2.10 Statistical analysis

Statistical analysis was performed using GraphPad Prism 5 and R software (version 3.6.3). Data in the figures are shown as mean ± SD. To compare the expression of tissues Student's *t*-test was used. To obtain a correlation with the prognosis of head and neck cancer univariate cox analysis was performed using the coxph function in R. The survival curve was drawn by the Kaplan-Meier method for prognostic analysis, and the log-rank test was used to determine the significance of the difference. Statistical significance was set at $p < 0.05$.

3 Results

3.1 Molecular typing based on ferroptosis-related genes

We extracted the expression levels of ferroptosis-related genes from the expression profile matrix of TCGA-HNSC. Then we got 47 genes after performed a univariate cox analysis using the coxph function in R to obtain a correlation with the prognosis of head and neck cancer ($p < 0.05$) (tcga.ferroptosis.genes.cox.sig.txt). Next we clustered 499 HNSC samples based on the 47 prognostic-related ferroptosis-related genes through ConsensusClusterPlus, determined the optimal number of clusters according to the cumulative distribution function (CDF). And we observed that, the CDF Delta area curve has relatively stable clustering results (Figures 1A,B) when Cluster is selected as 3. Finally we choose $k = 3$ to obtain three molecular subtypes (Figure 1C; tcga.subtype.txt). Further analysis of the prognostic characteristics of these three molecular subtypes, we observed that they have significant prognostic differences as shown in Figure 1D. In general, the C3 subtype has a better prognosis, while the C1 subtype has a poor prognosis. The mortality rate of patients with C1 subtype was significantly higher than that of C3 subtype Figure 1E.

In addition, same method was used to perform molecular typing on the GSE65858 microarray data, and we observed that there were also significant differences in the prognosis of these three types of molecular typing as shown in Figures 1F,G, which is consistent with the training set.

3.2 Clinicopathological features between molecular subtypes

We further explored the differences in clinicopathological characteristics between different molecular subtypes in the TCGA-HNSC cohort. Here, we compared the distribution of different clinical features in the three molecular subtypes we defined to see if the clinical features are different in different subtypes. As shown in Figure 2A, it was found that: there were no significant differences between M Stage, age, alcohol consumption and smoking history. However, there were significant differences between C1 and C3 subtypes in terms of T Stage, and between C2 and C3 subtypes in terms of N Stage. And there are significant differences between subtypes C1 and C2 in terms of Stage, and between subtypes C1 and C3 in terms of Grade, and between subtypes C1 and C2 in terms of gender. In

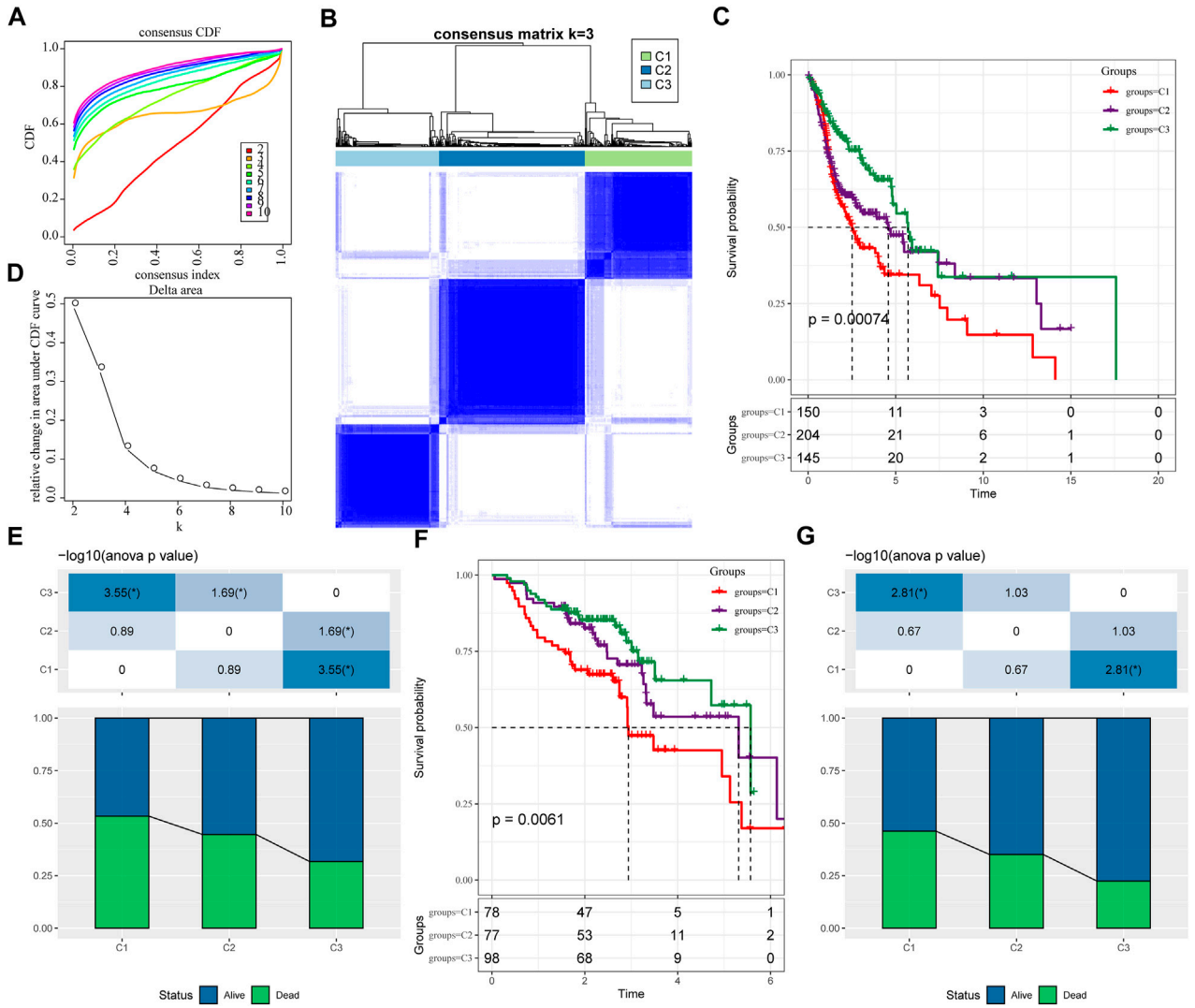

FIGURE 1
Molecular typing based on ferroptosis-related genes. **(A)** the cumulative distribution function (CDF) curve of TCGA-HNSC cohort sample; **(B)** the CDF Delta area curve of TCGA-HNSC cohort sample. Delta area curve of consensus clustering, indicating the relative change in area under the CDF curve for each category number k compared with k−1. The horizontal axis represents the category number k and the vertical axis represents the relative change in area under CDF curve; **(C)** Consensus heat map of sample clustering when k = 3; **(D)** Prognosis of three subtypes Relational Kaplan-Meier curve. **(E)** In TCGA-HNSC Differences in survival status of different subtypes; **(F)** the differences in prognosis of three molecular subtypes in GSE65858 cohort; **(G)** Differences in survival status of different subtypes in GSE65858. The lower half is the proportion, and the upper half is the statistical significance of the distribution difference between the two pairs—log10 (p-value).

addition, we also compared the clinicopathological characteristics of different molecular subtypes in the GSE65858 cohort as shown in Figure 2B.

3.3 Mutational signatures between molecular subtypes

We further explored differences in genomic alterations between different molecular subtypes in the TCGA cohort. Compared with the C3 subtype, the C1 subtype showed higher Aneuploidy Score (Kruskal-Wallis test, p = 5e-05), Homologous Recombination Defects (Kruskal-Wallis test, p = 3.5e-07), Fraction Altered (Kruskal-Wallis test, p = 1.1e-06), Number of Segments (Kruskal-Wallis test, p = 3.3e-08) and Tumor Mutation Burden (Kruskal-Wallis test, p = 0.0016) (Figure 3A). In addition, we also analyzed the correlation between gene mutation and copy number variation and molecular subtype, and found that there was a significant correlation between subtype and gene mutation. Some

FIGURE 2
Clinicopathological features between molecular subtypes. **(A)** Clinicopathological characteristics of molecular subtypes of the TCGA-HNSC cohort; **(B)** Clinicopathological characteristics of molecular subtypes of the GSE65858 cohort; the lower half is the proportion, and the upper half is the distribution difference between the pairwise statistically significant-log10 (*p*-value).

common genes TP53, CDKN2A, etc. Have higher mutation frequencies in the three subtypes. In terms of copy number variation, the C1 subtype has a higher overall copy number amplification than the C3 subtype, while the C3 subtype has an overall higher copy number deletion than the C1 subtype (Figure 3B).

3.4 WGCNA analysis identifies molecular subtype-associated gene modules

We used the R software package WGCNA to identify gene modules related to molecular subtypes. Specifically, samples were firstly clustered to filt for co-expression modules. The clustering results of the samples are shown in Figure 4A. The study shows that the co-expression network conforms to the scale-free network, that is, the logarithm log(k) of a node with a degree of connection k is negatively correlated with the logarithm log (P(k)) of the probability of the node appearing, and the correlation coefficient is greater than 0.85. To ensure that the network is scale-free, we choose β = 9 (Figures 4B,C). The next step is to convert the expression matrix into an adjacency matrix, and then convert the adjacency matrix into a topology matrix. Based on TOM, we use the average-linkage hierarchical clustering method to cluster genes according to the standard of hybrid dynamic shear tree. And set the minimum number of genes for each gene network module is 30. After using the dynamic shearing method to determine the gene modules, we calculate the eigengenes of each module in turn, then perform cluster analysis on the modules, merge the modules with closer distances into a new module, and set height = 0.3, deepSplit = 2, minModuleSize = 30. A total of 39 modules (Figure 4D) were

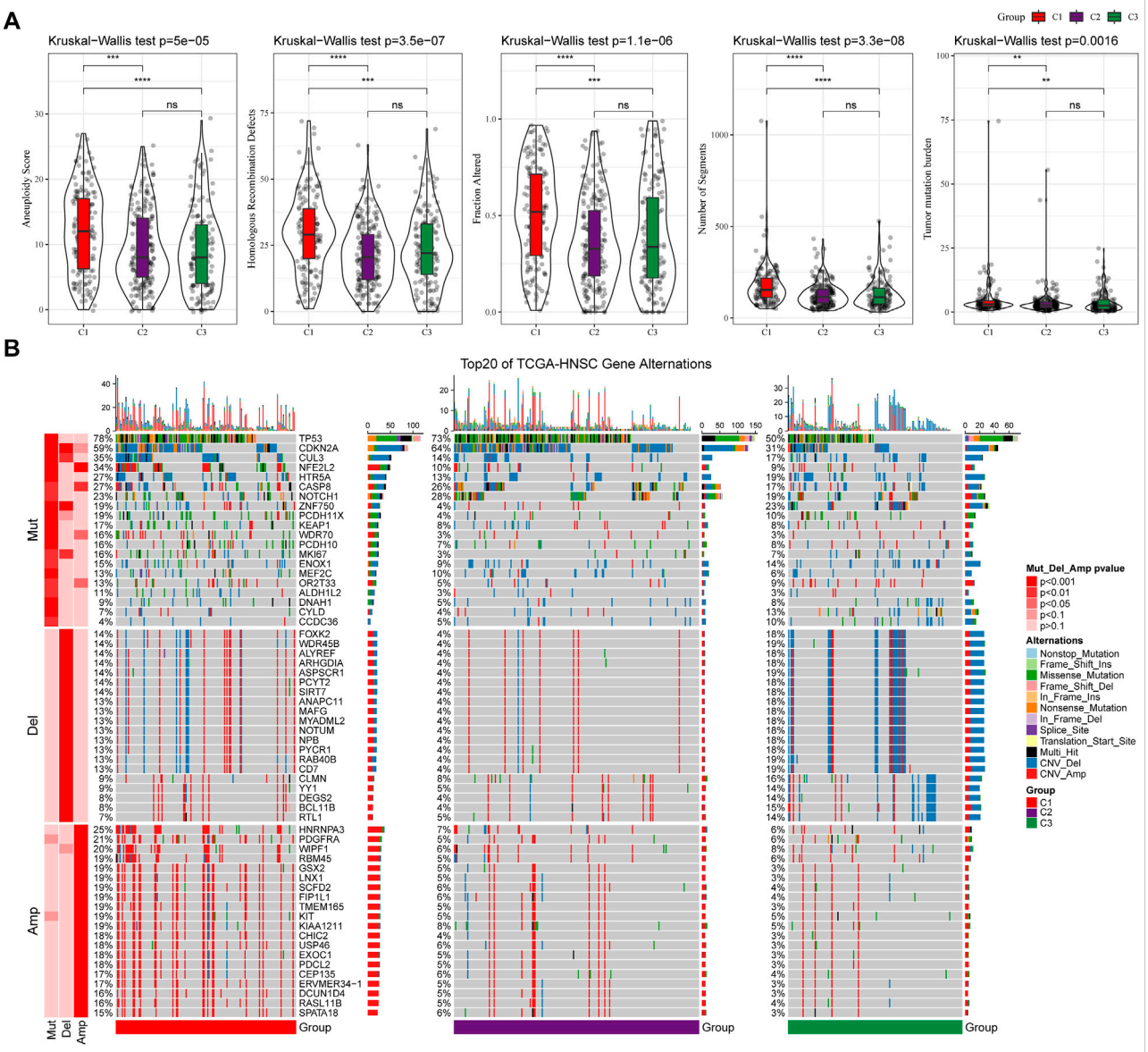

FIGURE 3
Genomic alterations in molecular subtypes of the TCGA cohort. **(A)** Comparison of Homologous Recombination Defects, Aneuploidy Score, Fraction Altered, Number of Segments and Tumor Mutation Burden among different molecular subtypes in TCGA cohort; **(B)** Somatic mutation and copy number variation analysis of different molecular subtypes in TCGA cohort (Fisher's test). *$p < 0.05$; **$p < 0.01$; ***$p < 0.001$; and ****$p < 0.0001$.

obtained. It should be pointed out that the grey module is a set of genes that cannot be aggregated into other modules. The gene statistics of each module are shown in Figure 4E, and the genes in the modules are shown in tcga.wgcna.module.genes.txt.

Further, we analyzed the correlation of each module with molecular subtypes as shown in Figure 4F.

It can be seen that there is a significant positive correlation between the brown module and the C1 subtype, the tan module and the C2 subtype, and the middlenightblue module and the C2 subtype. There are highly positively correlated between the module membership (MM) and gene significance (GS) of genes within the brown module (r = 0.53, P < 1e-5, Figure 4G), the tan module ($r = 0.25$, $P <$ 1e-5, Figure 4H), and the middlenightblue module ($r = 0.72$, $P <$ 1e-5, Figure 4I). Further, we used the R software package clusterProfiler to enrich the genes in the brown, tan and middlenightblue modules. The enrichment results are shown in tcga.XXX.enrich.txt.

It was found that the middlenightblue module significantly enriched Estrogen signaling pathway, Ether lipid metabolism,

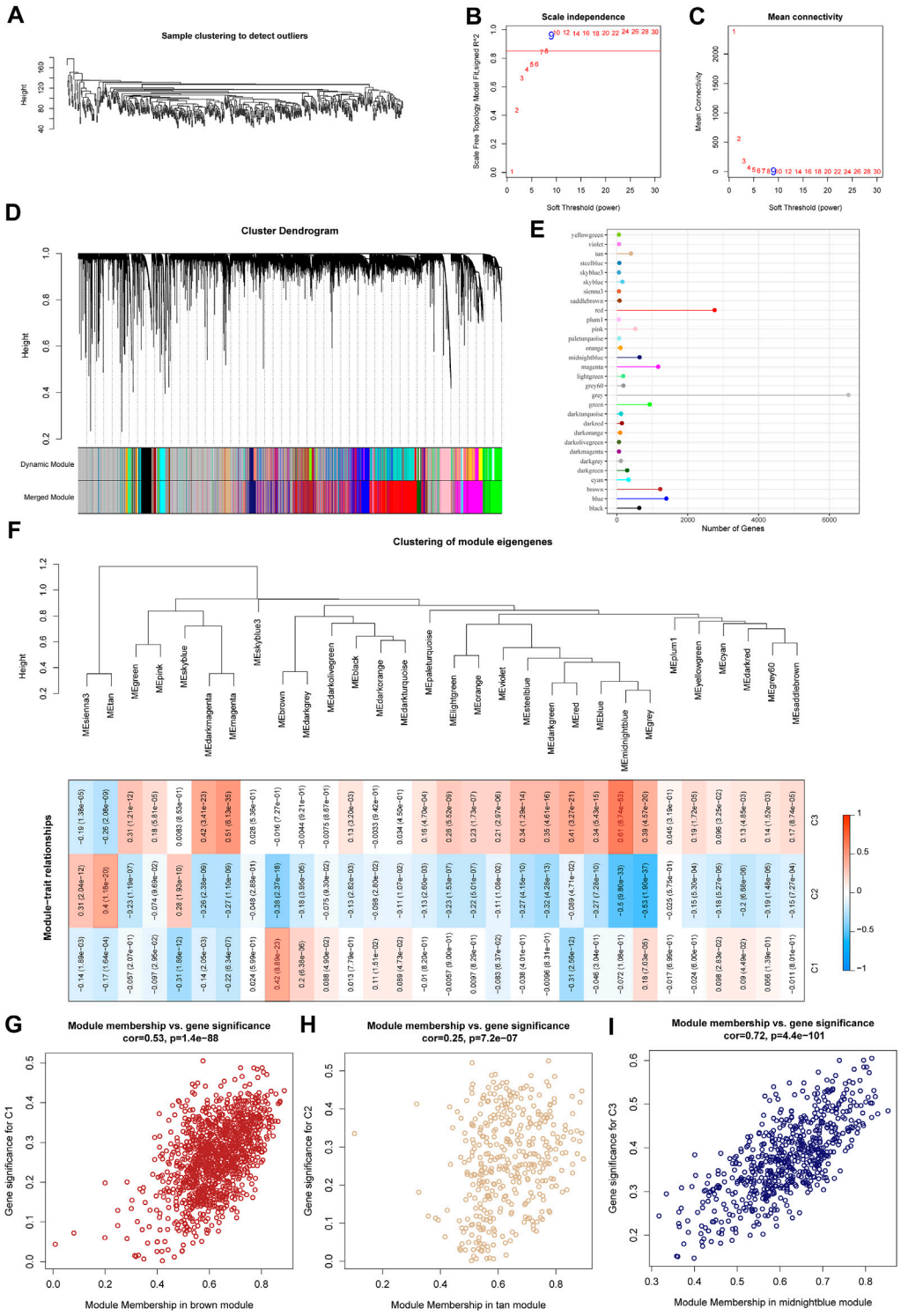

FIGURE 4
WGCNA analysis identifies molecular subtype-associated gene modules. **(A)** Clustering tree of each sample; **(B)** Analysis of the scale-free fit index for various soft-thresholding powers (β). **(C)** Analysis of the mean connectivity for various soft-thresholding powers. **(D)** Dendrogram of all differentially expressed genes/lncRNAs clustered based on a dissimilarity measure (1-TOM); **(E)** statistics of the number of genes in each module; **(F)** correlation between the module eigenvectors of each module and clinical information; **(G)** Scatter diagram for module membership vs. gene significance for C1 in the brown module; **(H)** Scatter diagram for module membership vs. gene significance for C2 in the tan module; **(I)** Scatter diagram for module membership vs. gene significance for C3 in the middlenightblue module.

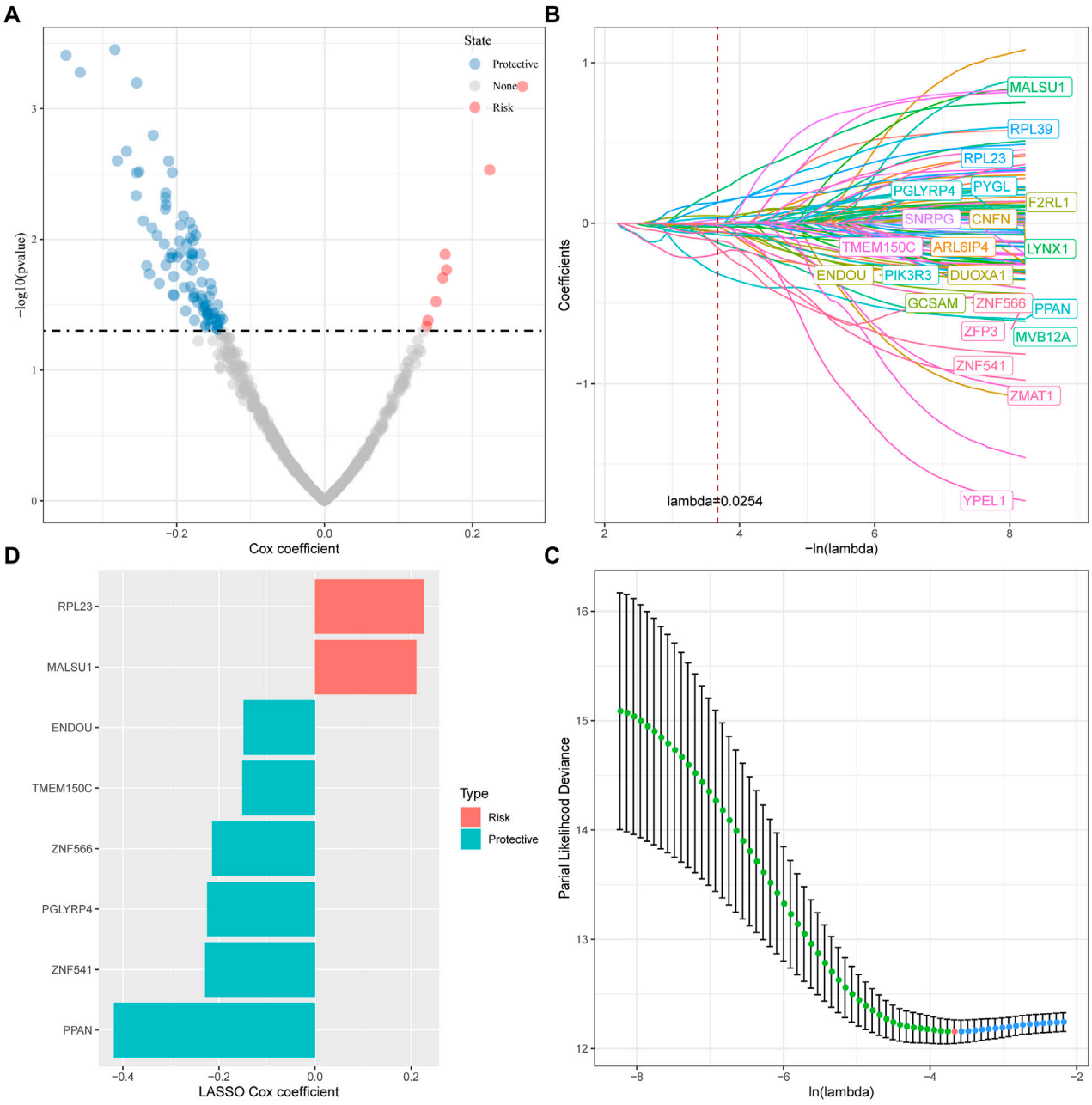

FIGURE 5
Determination of ferroptosis phenotype-related genes. **(A)** A total of promising candidates were identified through the correlation analysis of the gene expression and the Module Membership; **(B)** The trajectory of each independent variable with lambda; **(C)** Confidence interval under lambda; **(D)** Distribution of LASSO coefficients of the ferroptosis-related prognostic gene signature.

alpha-Linolenic acid metabolism, Linoleic acid metabolism and other pathways (Supplementary Figure S1C), and the gene enrichment results in brown and tan modules are shown in Supplementary Figures S1A,B. The brown, tan and middlenightblue modules with high positive correlation in typing were regarded as the key gene modules related to molecular typing.

3.5 Determination of ferroptosis phenotype-related genes

For the genes in the brown, tan and middlenightblue modules identified by WGCNA that are significantly related to molecular subtypes, we first filtered out the genes that are significantly related to the module eigenvectors. Here we select

the genes with a correlation coefficient >0.7. After filting, we obtained a total of 540 genes related to the module feature vector (correlation>0.7). The correlation results showed in brown.cor.txt, tan.cor.txt and midnightblue.cor.txt. Further, we aimed at these Univariate COX regression analysis of genes identified 97 genes that had a greater impact on prognosis ($p < 0.0\ 5$), including 8 risk and 89 protective genes (Figure 5A). Taking it a step further, we compressed these 97 genes in the TCGA-HNSC dataset using lasso regression to reduce the number of genes for the risk model. The Lasso (Least absolute shrinkage and selection operator) method is a compression estimation (Tibshirani, 1996). It obtains a more refined model by constructing a penalty function, so that it compresses some coefficients and sets some coefficients to zero. Therefore, the advantage of subset shrinkage is retained, and it is a biased estimation for processing data with complex collinearity, which can realize the selection of variables at the same time as parameter estimation, and better solve the multicollinearity problem in regression analysis.

Here, we performed lasso cox regression using the R package glmnet. First, the change trajectory of each independent variable is analyzed as shown in Figure 5B. It can be seen that with the gradual increase of lambda, the number of independent variable coefficients tending to 0 also gradually increases. We use 10 -fold cross-validation for the model. Construct and analyze the confidence interval under each lambda as shown in Figure 5C. It can be seen from the figure that the model is optimal when lambda = 0.0254. For this reason, we choose 22 genes when lambda = 0.0254 as the next step target gene. Further, based on the 22 genes in the lasso analysis results, we used stepwise multivariate regression analysis, and the stepwise regression used the AIC Akaike Information Criterion, which considered the statistical fit of the model and the number of parameters used for fitting, stepAIC in the MASS package. The method starts with the most complex model and deletes one variable in turn to reduce the AIC. The smaller the value, the better the model, which means that the model obtains sufficient fit with fewer parameters. Ultimately, we identified 8 genes as ferroptosis-related genes affecting prognosis, as shown in Figure 5D.

3.6 Establishment and validation of clinical prognostic model

Next, the FPRS for each sample was calculated and normalized according to the formula defined by our sample ferroptosis score. The FPRS distribution of patients in the training set TCGA-HNSC cohort is shown in Figure 6A, which suggests that high FPRS samples have poorer prognosis.The low expression of ZNF566, ZNF541, TMEM150C, PPAN, PGLYRP4, and ENDOU is associated with high risk, which is a protective factor. While the high expression of RPL23 and MALSU1 genes is associated with high risk, which is a risk factor. Further, we used the R software package timeROC to carry out the ROC analysis of the prognostic classification of FPRS. We analyzed the 1-year, 3-year, 5-year prognosis prediction classification efficiency is shown in Figure 6B, from which we can see that the model has a higher area under the AUC line. Finally, we classify the FPRS score greater than 0 as high risk, and the FPRS score less than or equal to 0 as low Risk. And we draw the KM curve, as shown in Figure 6C, there is a very significant difference between the high and low FPRS groups ($p < 0.0001$). 249 samples were divided into the high FPRS group, and 250 samples were divided into the low FPRS group. Patients with higher FPRS exhibited worse overall survival in the training cohort (Figure 6C). To confirm the robustness of ferroptosis-related gene signature clinical prognostic model predictions, we performed validation in two independent head and neck cancer cohorts, and we calculated the FPRS scores of patients in the same way. Seeing that in the validation cohort we observed similar results to the training set, with high FPRS having a worse prognosis and low FPRS having a better prognosis (Figures 6D–G).

3.7 FPRS scores on different clinicopathological features and different molecular subtypes

By comparing the distribution of FPRS among clinicopathological groups, we found that higher TNM stage means higher FPRS (Figure 7A). And we also found no significant difference in FPRS between ages (Figure 7A). At the same time, we compared the differences of FPRS among molecular subtypes and found that the FPRS of the C1 subtype with poor prognosis had the highest FPRS score, while the C3 molecular subtype with better prognosis had the lowest FPRS (Figure 7B).

3.8 Mutation signatures between FPRS groups

We further explored differences in genomic alterations between different FPRS subgroups in the TCGA cohort. Compared with the FPRS-low group, the FPRS-high group showed higher Aneuploidy Score (wilcox. test, $p = 0.0019$), Homologous Recombination Defects (wilcox. test, $p = 0.026$), Fraction Altered (wilcox. test, $p = 0.0034$), and Number of Segments (wilcox. test, $p = 0.00016$) (Figure 8A). At the same time, we also analyzed the correlation between FPRS and Homologous Recombination Defects, Aneuploidy Score, Fraction Altered, Number of Segments, and Tumor mutation burden, and found that FPRS was significantly positively correlated with Aneuploidy Score ($p = 0.001$), Fraction Altered ($p = 0.006$), and Tumor Mutation Burden ($p = 0.032$) (Figure 8B). In addition, we also analyzed the correlation between gene mutation and copy

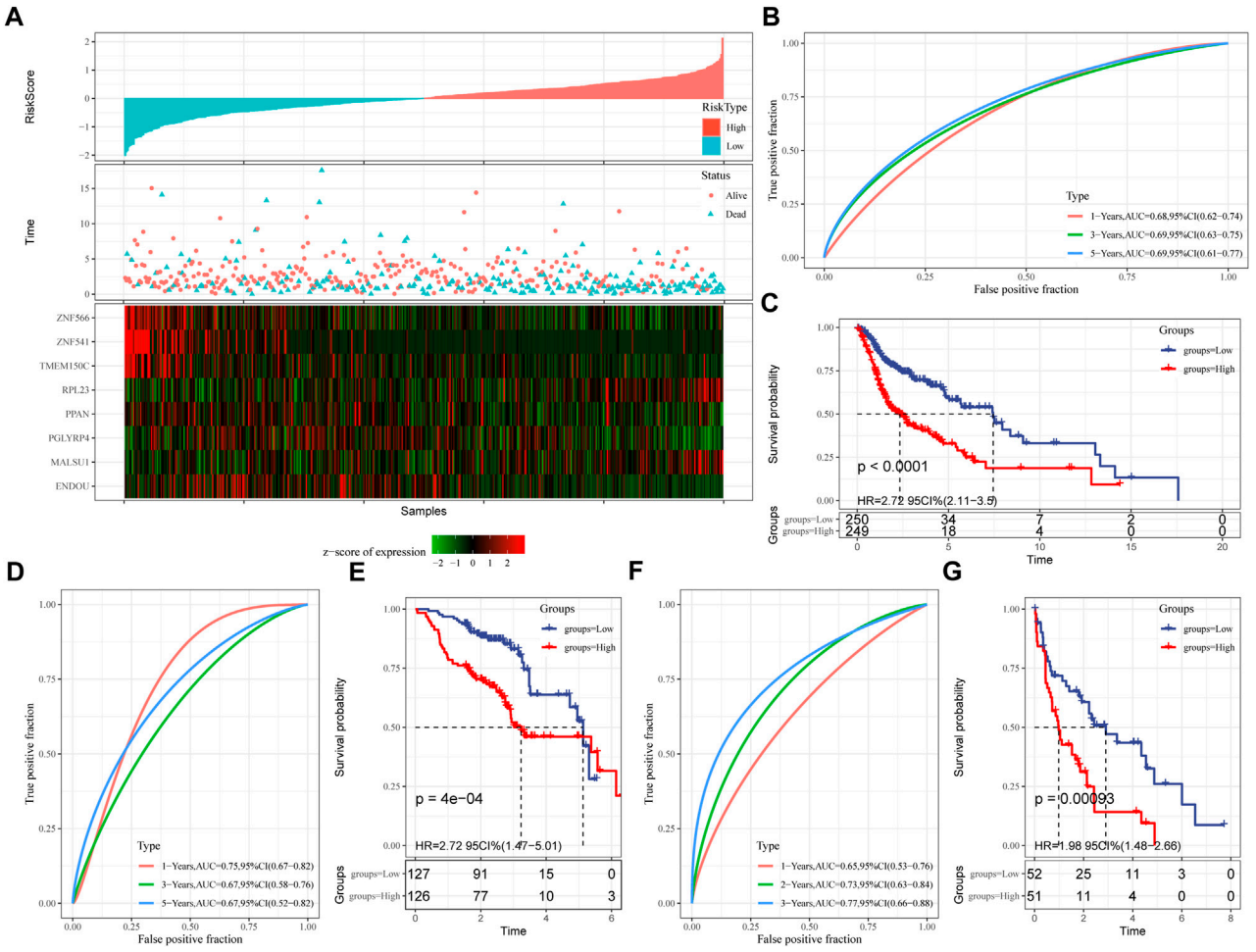

FIGURE 6
Establishment and validation of clinical prognostic model. **(A)** FPRS in TCGA-HNSC data set, survival time and survival status and expression of ferroptosis-related prognostic genes; **(B)** ROC curve and AUC of FPRS classification in TCGA-HNSC data set; **(C)** FPRS in TCGA- KM survival curve distribution in HNSC dataset; **(D,E)** ROC curve and KM survival curve of FPRS in GSE65858 cohort; **(F,G)** ROC curve and KM survival curve of FPRS in GSE 42743 cohort.

number variation and molecular subtype, and found that there was a significant correlation between subtype and gene mutation. The common TP53 was mutated at a higher frequency in both subtypes. In terms of copy number variation, the copy number deletion in the FPRS-low group was generally higher than that in the FPRS-high group, while the copy number amplification was lower than that in the FPRS-high group (Figure 8C).

3.9 Path characteristics between FPRS packets

In order to observe the relationship between FPRS and biological function in different, we selected the gene expression profiles corresponding to the head and neck cancer samples in the TCGA-HNSC cohort using the R software package GSVA to perform a single-sample GSEA analysis (ssgsea). The ssGSEA score of each function corresponding to each sample is obtained after calculating the different functions of each sample. And the correlation between these functions and FPRS is further calculated, and the function with a correlation greater than 0.4 is selected (Figure 9A). It can be seen that 13 of pathways was positively correlated with the FPRS of the samples, and 8 pathways were negatively correlated with the FPRS. Among them, the metabolism-related pathway KEGG_PROTEIN_EXPORT, KEGG_ GLYCOSAMINOGLYCAN _ BIOSYNTHESIS_CHONDROITIN_SULFATE, KEGG_GALAC TOSE_METABOLISM, KEGG_NICOTINATE_AND_NICOTIN

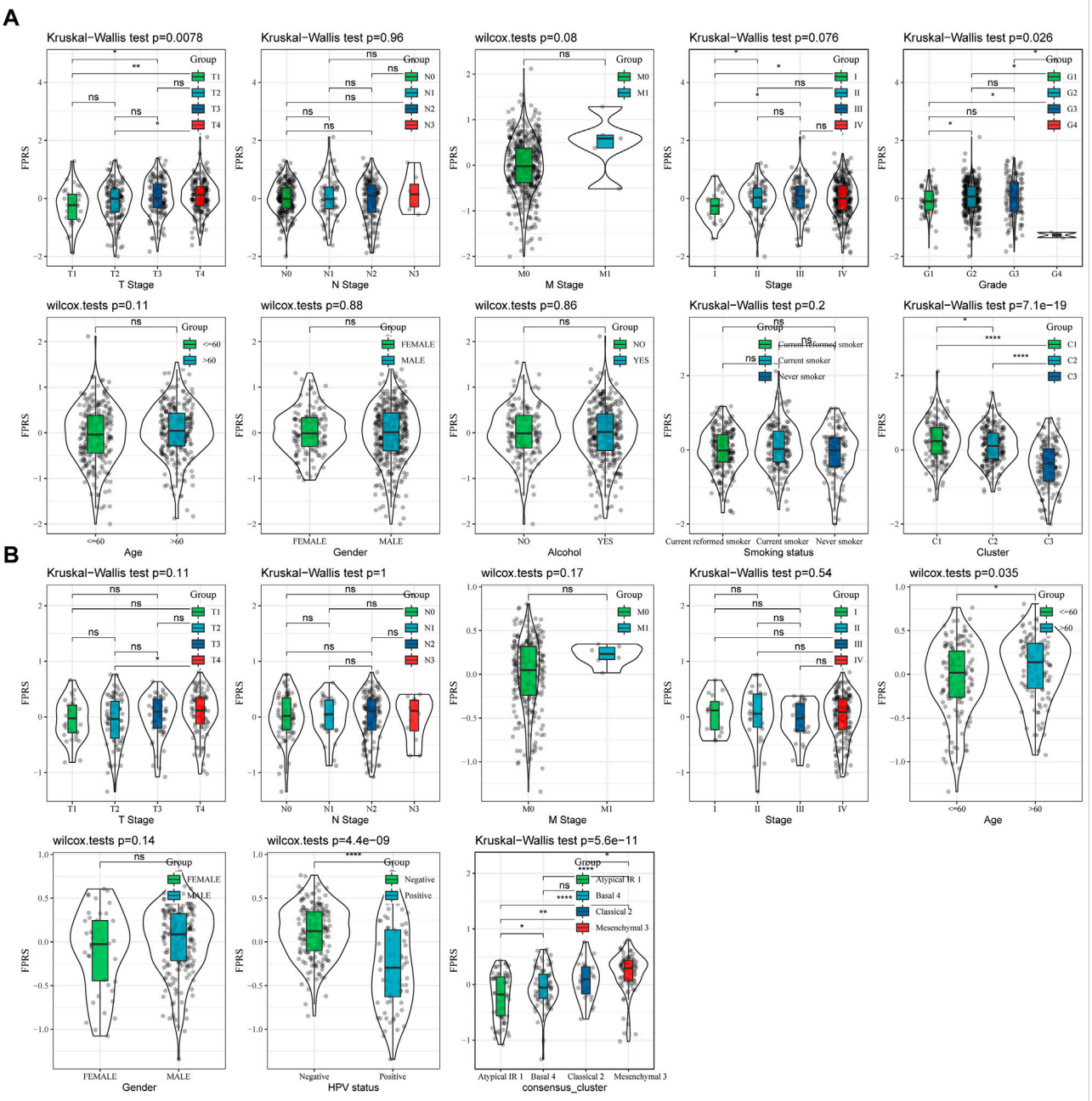

FIGURE 7
FPRS scores on different clinicopathological features and different molecular subtypes. **(A)** Differences in FPRS between different clinicopathological groups in TCGA-HNSC cohort; **(B)** Differences in FPRS between different clinicopathological groups in GSE65858 cohort.

AMIDE_ METABOLISM, KEGG_PURINE_METABOLISM showed a significant positive correlation with FPRS. Next, we analyzed whether there are differentially activated pathways in different FPRS groupings. To identify these pathways, we performed Gene Set Enrichment Analysis (GSEA) using all candidate gene sets in the Hallmark database [PMID: 26771021], where we defined FDR < 0.05 as significant enrichment as shown in Figure 9B. It can be seen that compared with PFRS-low in TCGA-HNSC cohort, 20 pathways were activated in PFRS-high, 4 pathways were inhibited, and 28 pathways were significantly enriched in GSE65858 cohort. Overall, the activated pathways in the PFRS-high group mainly included immune-related pathways such as INFLAMMATORY_RESPONSE, COMPLEMENT, etc., and the invasion-related pathways such as

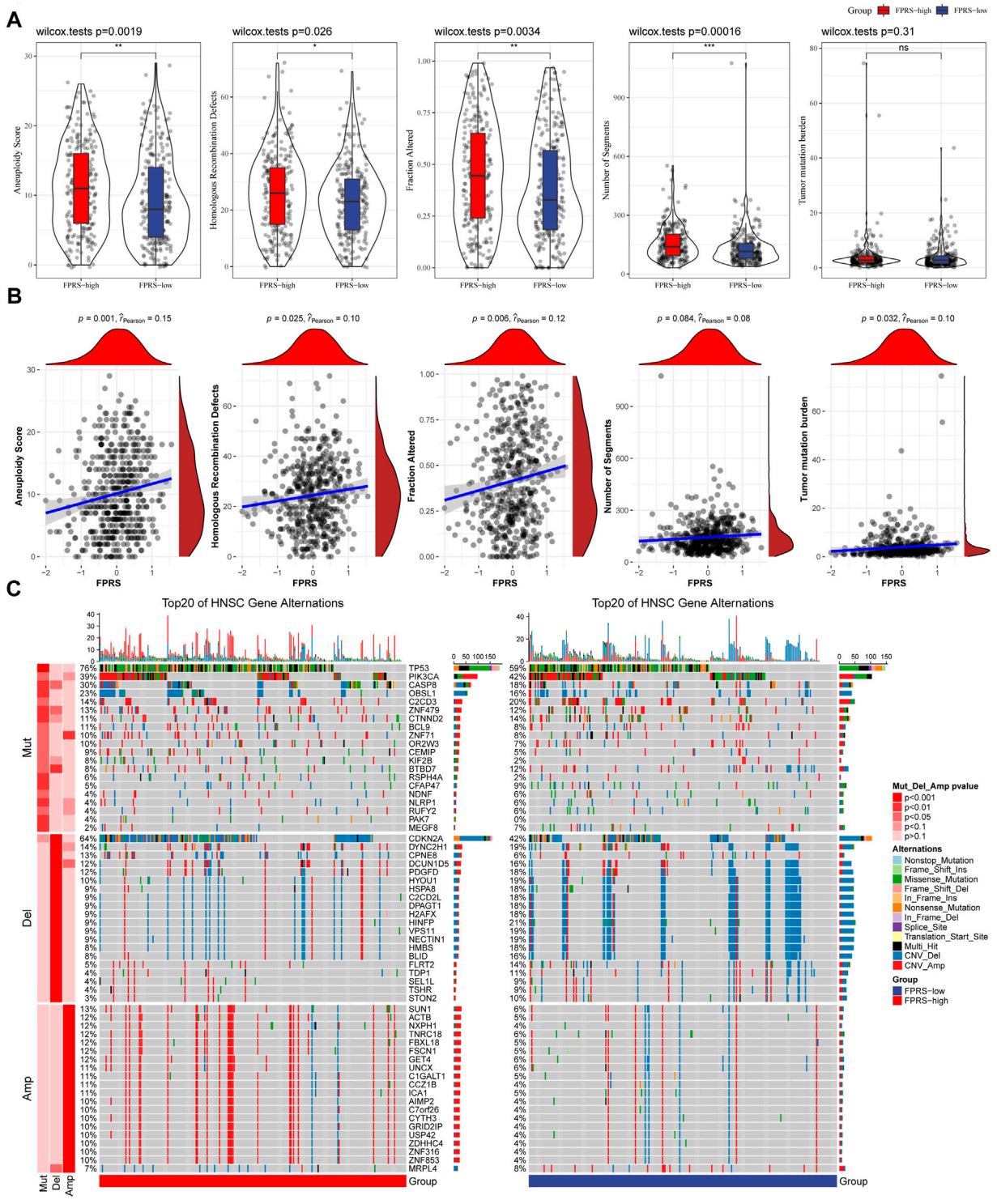

FIGURE 8
Differences inFPRS groupings of the TCGA cohort. **(A)** Compare the differences in Homologous Recombination Defects, Aneuploidy Score, Fraction Altered, Number of Segments and Tumor mutation burden in different FPRS groups of the TCGA cohort; **(B)** FPRS and Homologous Recombination Defects, Aneuploidy Score, Fraction Altered, Number of Segments and Tumor mutation Correlation between burden; **(C)** Somatic mutation and copy number variation analysis (Fisher test) of FPRS groupings in the TCGA cohort. *$p < 0.05$; **$p < 0.01$; ***$p < 0.001$; and ****$p < 0.0001$.

FIGURE 9
Path characteristics between FPRS packets. **(A)** Correlation analysis results between KEGG pathways with FPRS correlation greater than 0.3 and FPRS; **(B)** a heatmap demonstrating normalized enrichment scores (NESs) of Hallmark pathways calculated by comparing FPRS-high with FPRS-low (with a false discovery rate (FDR) of < 0.05).

EPITHELIAL_MESENCHYMAL_TRANSITION, ANGIOGENESIS, TNFA_SIGNALING_*VIA*_NFKB, etc. were significantly enriched in the FPRS-high group as shown in Figure 8B. Overall, the activation of immune-related pathways and the activation of invasion -related pathways in the FPRS-high group may be potential factors for the poor prognosis of FPRS-high.

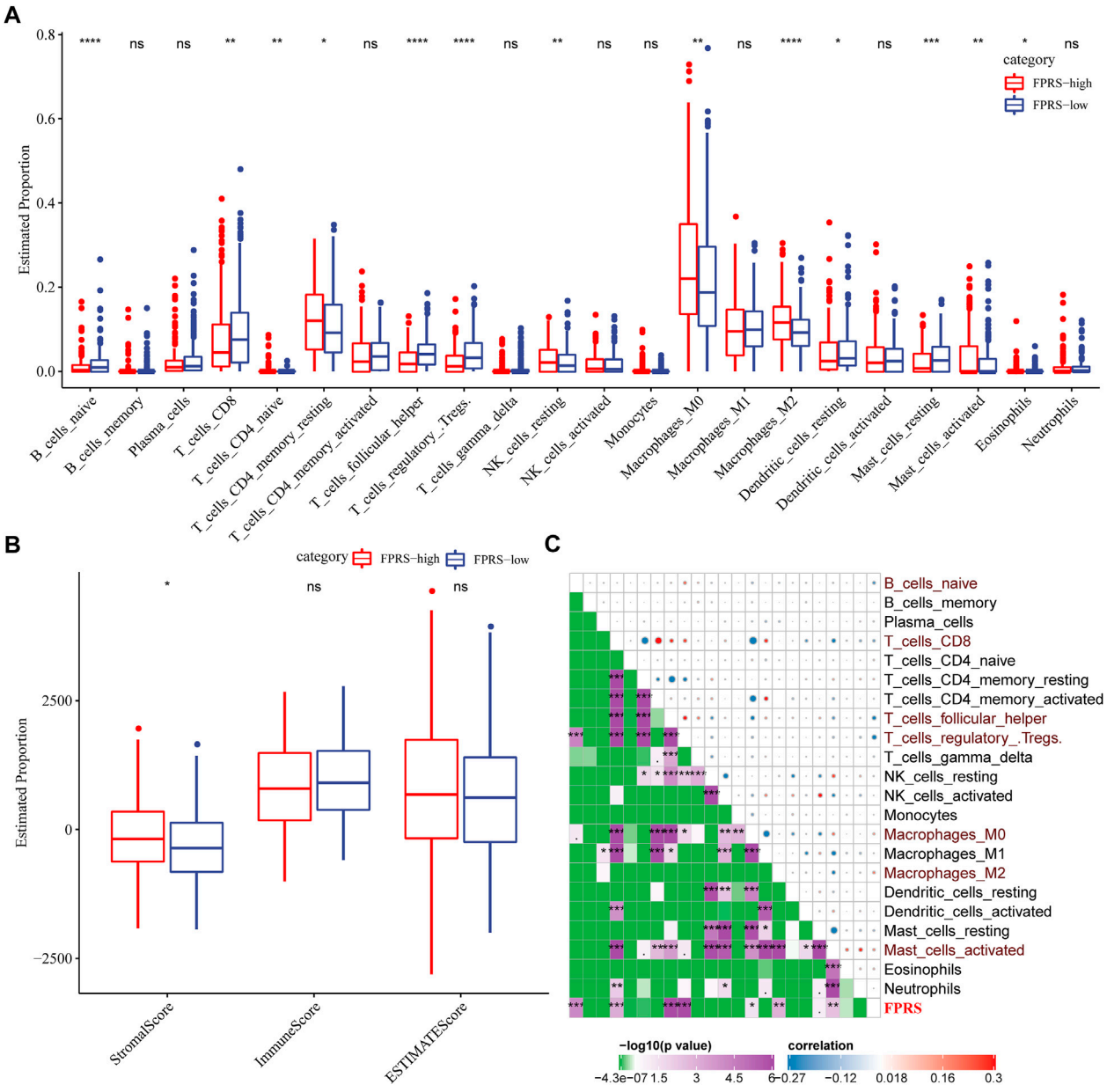

FIGURE 10
Immune signatures between FPRS subgroups. **(A)** The proportion of immune cell components in the TCGA- HNSC cohort; **(B)** The proportion of immune cell components in the TCGA-HNSC cohort calculated by ESTIMATE software; **(C)** The correlation analysis of 22 immune cell components and FPRS.

3.10 Immune signatures between FPRS subgroups

To further elucidate the differences in the immune microenvironment of patients in the FPRS cohort, we assessed the extent of immune cell infiltration in patients in our TCGA-HNSC cohort by using the expression levels of gene markers in immune cells, we first employed CIBERSORT to calculate 22 The relative abundance of immune cells is shown in Figure 10A, and it can be observed that B_cells_naive, T_cells_CD8, T_cells_follicular_helper, T_cells_regulatory_.Tregs. are significantly enriched in the FPRS-low group. At the same time, we also used ESTIMATE to evaluate the infiltration of immune cells, as shown in Figure 10B. It can be seen that the ImmuneScore in the FPRS-low group was slightly higher than that in the FPRS-high group, with higher immune cell

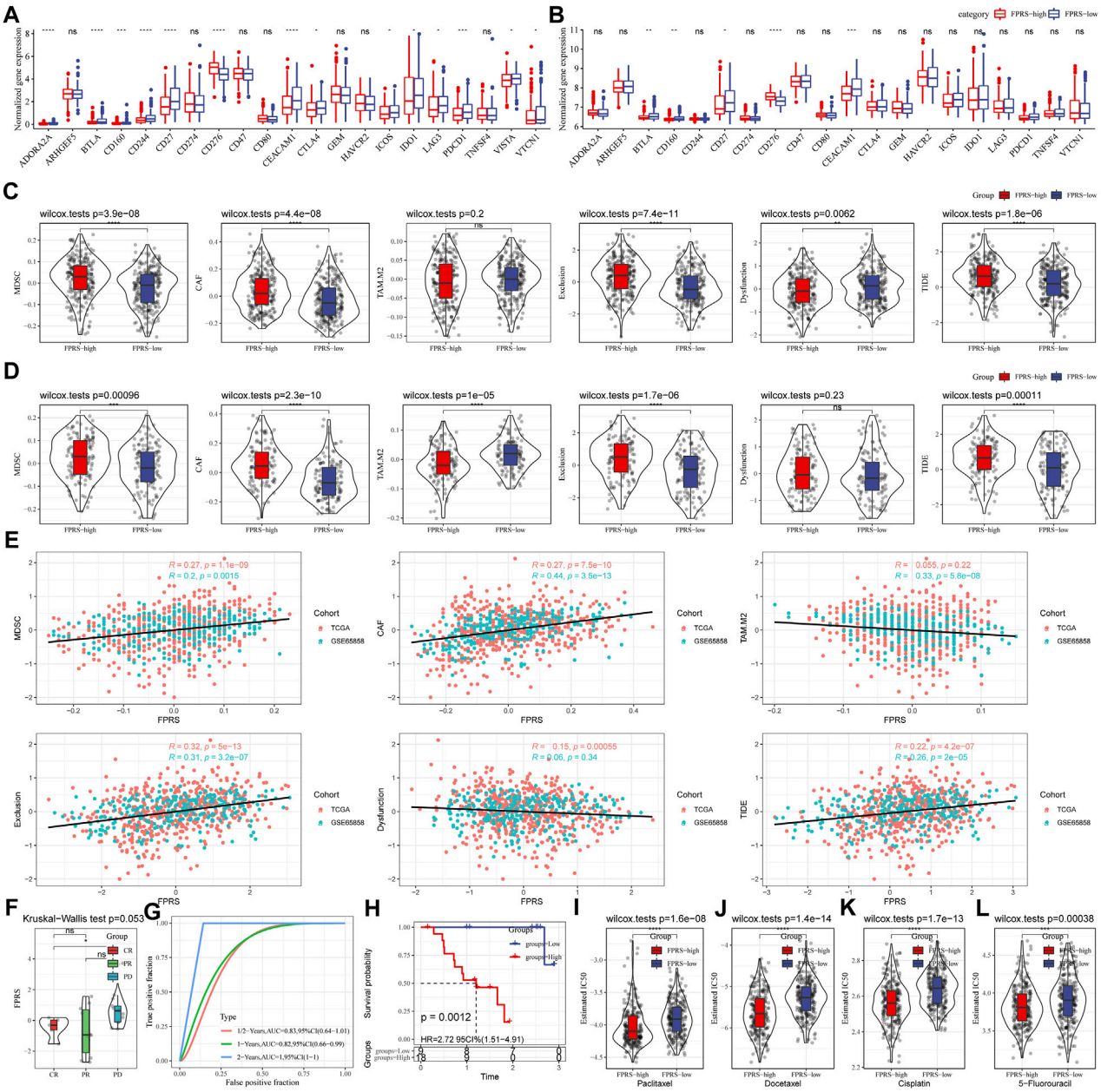

FIGURE 11
Differences in immunotherapy/chemotherapy between FPRS groups. **(A)** Differentially expressed immune checkpoints between different groups in the TCGA-HNSC cohort; **(B)** Differentially expressed immune checkpoints between different groups in the GSE65858 cohort; **(C)** TIDE between different groups in the TCGA-HNSC cohort Differences in analysis results; **(D)** Differences in TIDE analysis results between different groups in the GSE65858 cohort; **(E)** Correlation between TIDE scores and FPRS scores; **(F)** Differences in FPRS for different clinical response status to immunotherapy in the GSE78220 cohort; **(G)** ROC curve and AUC of FRPS classification; **(H)** KM survival curve distribution of FPRS; **(I–L)**: The box plots of the estimated IC50 for Paclitaxel, Docetaxel, Cisplatin and 5−Fluorouracil in TCGA−HNSC.

infiltration. Further, we analyzed the relationship between FPRS and 22 immune cell components, and found that FPRS was significantly negatively correlated with B_cells_naive, T_cells_CD8, T_cells_follicular_helper, T_cells_regulatory_.Tregs., and significantly positively correlated with Macrophages_M2, Mast_cells_activated.

3.11 Differences in immunotherapy/chemotherapy between FPRS groups

Further, we analyzed whether there were differences in response to immunotherapy between the FPRS groups. First, we compared whether there are differences in the expression of

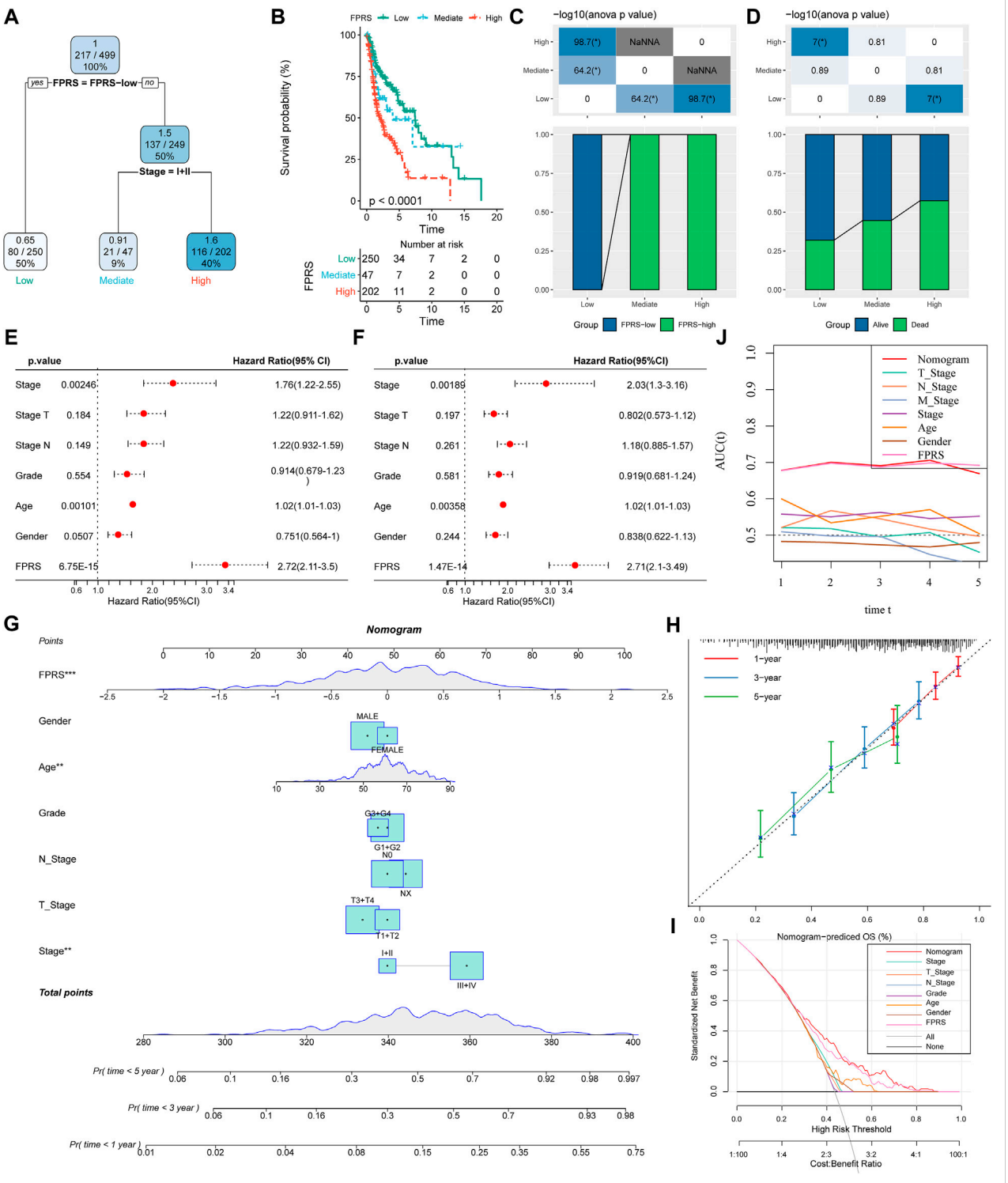

FIGURE 12
FPRS combined with clinicopathological features to further improve prognostic models and survival prediction. **(A)** Patients with full-scale annotations including FPRS, stage, gender and age were used to build a survival decision tree to optimize risk stratification; **(B)** Significant differences of overall survival were observed among the three risk subgroups; **(C,D)** Comparative analysis between different groups; **(E,F)** univariate and multivariate Cox analysis of FPRS and clinicopathological characteristics; **(G)** nomogram model; **(H)** 1, 3, and 5-year calibration curve of nomogram; **(I)** Decision curve of nomogram; **(J)** Compared with other clinicopathological features, the nomogram exhibited the most powerful capacity for survival prediction.

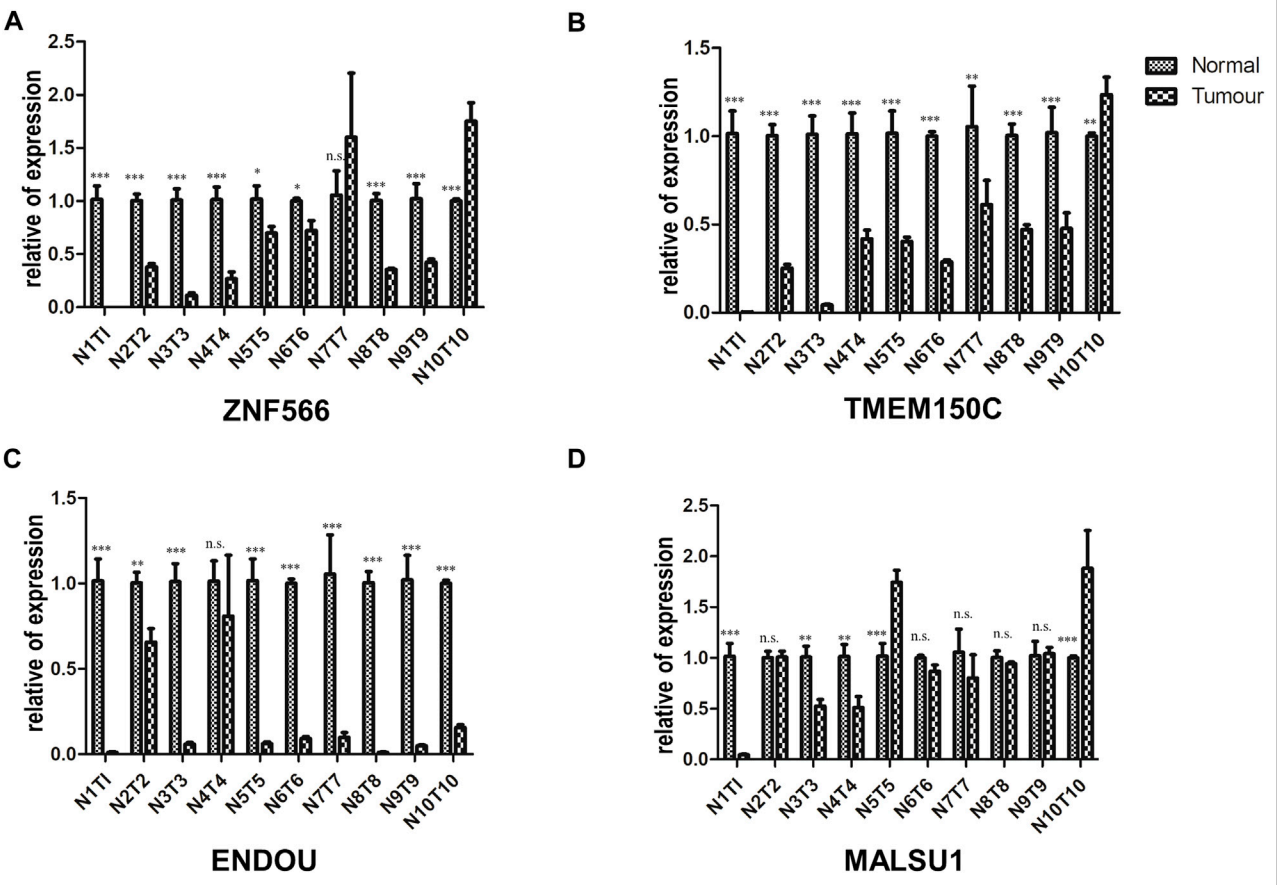

FIGURE 13
Validation of the 4 ferroptosis-related genes in HNSC tissues. RT-qPCR detecting the mRNA expression levels of **(A)** ZNF566, **(B)** TMEM150C, **(C)** ENDOU, **(D)** MALSU1 in the tumor tissue and adjacent tissue of HNSCC patients and normal tissues HNSCC patients*$p < 0.05$; **$p < 0.01$; ***$p < 0.001$.

immune checkpoints between FPRS groups. Here, our immune checkpoints come from the database HisgAtlas [PMID: 31725860]. The results are shown in Figures 11A,B. Most immune checkpoint genes were differentially expressed in FPRS groups. Combining the expression of immune checkpoints in the two cohorts, we found that immune checkpoints such as BTLA, CD160, CD27, and CEACAM1 were significantly up-regulated in the FPRS-low group as shown in Figures 11A,B. Further, we analyzed the differences in immunotherapy among different FPRS groups. Here, we used TIDE (http://tide.dfci.harvard.edu/) software to assess the potential clinical effects of immunotherapy in our defined FPRS high and low groups. The higher the TIDE prediction score, the higher the possibility of immune escape, and the lower the possibility of patients benefiting from immunotherapy. As shown in Figure 11C, we can find that the FPRS-high group has the highest TIDE score in the TCGA-HNSC cohort. It suggesting that the FPRS-high group has a higher possibility of immune escape and is less likely to benefit from immunotherapy. At the same time, we also compared the differences in the predicted T cell dysfunction score and T cell exclusion score among different metabolite subtypes in the TCGA-HNSC cohort, as shown in Figure 11C. And it can be found that the FPRS-high subtype has the highest MDSC, CAF and Exclusion. A similar result was observed in the GSE65858 cohort as shown in Figure 11D.

In addition, we also analyzed the correlation between FPRS score and TIDE score, and found that there was a significant positive correlation between FPRS score and TIDE score (Figure 11E). Further, we included a set of immunotherapy data GSE78220 (anti-PD-1), and calculated the FPRS scores of the samples in the same way, and found that there were differences in the FPRS scores of different clinical response states of immunotherapy in the GSE78220 data set. The FPRS score of patients with response to immunotherapy was lower than that of patients with PD and SD response status (Figure 11F). At the same time, we also found that our clinical prognostic model had stable performance in the two

immunotherapy cohorts, with better classification efficiency for prognosis prediction at 6 months, 1 year, and 2 years and with higher AUC area below the line (Figure 11G). There was a significant difference in prognosis between the high and low FPRS groups (Figure 11H). In addition, we also analyzed the response of FPRS subgroups to traditional chemotherapy drugs Paclitaxel, Docetaxel, Cisplatin and 5-Fluorouracil in the TCGA-HNSC cohort, and found that FPRS-high was more sensitive to these four drugs as shown in Figures 11I–L.

3.12 FPRS combined with clinicopathological features to further improve prognostic models and survival prediction

Here, we constructed a decision tree based on age, gender, T stage, N Stage, Stage, Grade, and FPRS of head and neck cancer patients in the TCGA-HNSC cohort. The results showed that only FPRS and Stage were left in the decision tree and determined three distinct risk subgroups (Figure 12A). Among them, FPRS is the most powerful parameter, followed by the stage. Here, we defined patients with low FPRS as the low risk group, while the intermediate risk group was labeled with low FPRS and Stage low and the high risk group was labeled with high FPRS and Stage high. There were significant differences in overall survival between the three risk subgroups as shown in Figure 12B. The patients in the high risk group and the intermediate risk group were all FPRS-high patients, while the patients in the low risk group were all FPRS-low patients as shown in Figure 12C. In addition, we also found that the high risk group and the intermediate risk group were the proportion of patients in the Dead group was significantly higher than that in the intermediate risk and low risk groups as shown in Figure 12D. Univariate and multivariate Cox regression analysis of FPRS and clinicopathological features showed FPRS to be the most significant prognostic factor (Figures 12E,F).

In order to quantify the risk assessment and survival probability of patients with head and neck cancer, we combined FPRS and other clinicopathological features to establish a nomogram as shown in Figure 12G. From the model results, it can be seen that FPRS has the greatest impact on survival rate prediction. Further, we use the calibration curve (Calibration curve) to evaluate the prediction accuracy of the model, as shown in Figure 12H. It can be observed that the predicted calibration curves of the three calibration points at 1, 3, and 5 years are nearly coincident with the standard curve, which suggests that the nomogram has a good Predictive performance. In addition, we also used DCA (Decision curve) to evaluate the reliability of the model. It can be observed that the benefits of FPRS and nomogram are significantly higher than those of extreme curves. Compared with other clinicopathological characteristics, both nomogram and FPRS show the strongest survival predictive power is shown in Figures 12I,J.

3.13 Validation of the 4 ferroptosis-related genes in HNSC tissues

We validated the mRNA expression levels of the 4 ferroptosis-related genes (ZNF566, TMEM150C, ENDOU, MALSU1) in the tumor tissue and adjacent tissue of 10 HNSCC patients by RT-qPCR. The results showed that in most patients ZNF566 (8/10, 80%, Figure 13A), TMEM150C (9/10, 90%, Figure 13B), ENDOU (8/10, 80%, Figure 13C) were all significantly decrease in HNSCC tissues than in normal tissues ($p < 0.005$). There was no statistical difference in the expression of MALSU1 (Figure 13D).

4 Discussion

Identification of key biomarkers to assess tumor prognosis raises implications for early tumor diagnosis, treatment regimen selection, and cancer prevention (Economopoulou et al., 2019). The prognosis of patients with head and neck cancer is related to many factors, such as age, smoking, gender, TNM stage, stage, drug sensitivity, immune cell infiltration, etc (Zhang et al., 2020; Zhang et al., 2021; Yao et al., 2022). In this work, we got 47 ferroptosis-related genes to obtain a correlation with the prognosis of head and neck cancer patients from the FerrDb database. We identified three stable molecular subtypes (C1, C2, C3) through these genes in TCGA-HNSC cohort. These subtypes are also validated in GSE65858 microarray data. These subtypes did not differ significantly in M Stage, age, alcohol consumption and smoking history. C1 subtype, which has a worst prognosis, has higher tumor mutational burden than other subtypes. In many cancer types, high tumor mutational burden (TMB) is associated with longer survival after immune checkpoint inhibitor (ICI) therapy. While in patients not receiving ICI therapy, higher TMB is associated with worse survival (Valero et al., 2021). Some common genes TP53, CDKN2A, etc. Have higher mutation frequencies in the three subtypes. Recent study had reported a variant of p53 at codon 47 (S47) found in African-descent populations, which alters the ability of p53 to induce cell death and suppress tumor formation (Jennis et al., 2016). This variant leads to accumulation of GSH and CoA (Leu et al., 2019).

To evaluate head and neck cancer samples we construction of the FPRS scoring system. Patients with higher FPRS exhibited worse overall survival. We observed the similar results after validating two independent head and neck cancer cohorts, which confirmed the robustness of ferroptosis-related gene signature clinical prognostic model predictions. The FPRS of the C1 subtype with poor prognosis had the highest FPRS score,

while the C3 molecular subtype with better prognosis had the lowest FPRS. FPRS-high group has a higher possibility of immune escape and is less likely to benefit from immunotherapy, which lead to worse prognosis.

The low expression of ZNF566, ZNF541, TMEM150C, PPAN, PGLYRP4, and ENDOU is considered high risk, predicts a worse prognosis. This is generally consistent with the trend we showed in our clinical sample validation. In most validated samples ZNF566, TMEM150C, ENDOU were all significantly decrease in tumor tissues than in normal tissues. ZNF566 plays a central role in heart regeneration and repair through epithelial to mesenchymal transitions (EMT) (Xin et al., 2013; von Gise and Pu, 2012). Considering that EMT is highly correlated with tumor metastasis, it has an important impact on prognosis. CircZNF566 is highly expressed in hepatoma cells and tissues and positively correlated with poor prognosis (Li et al., 2020). This suggests a complex role of ZNF566 in different tissues. ZNF541 mediates chromatin remodeling and is associated with histone hypoacetylation, normally expressed in germ cells (Choi et al., 2008). The U.S. Food and Drug Administration approved histone deacetylase inhibitors for PTCL (O'Connor et al., 2014). TMEM150C (Tentonin 3) was identified as a cation channel activated by mechanical stimulation with unique slow inactivation kinetics and is a molecular component that helps sense changes in dynamic arterial pressure in baroreceptors (Hong et al., 2016; Lu et al., 2020). In pancreatic β-cells TMEM150C is highly expressed, which regulates glucose-stimulated insulin secretion *in vivo* (Wee et al., 2021). Human PPAN localizes to the nucleolus and mitochondria, and PPAN knockdown triggers a p53-independent nucleolar stress response that ultimately leads to mitochondrial apoptosis (Olausson et al., 2012). PPAN knockdown is also associated with mitochondrial damage and stimulation of autophagy (Dannheisig et al., 2019). ENDOU (PP11) was detected in 66.7% of analyzed mucinous cystadenocarcinomas, 57.1% of serous cystadenocarcinomas, but not in normal ovaries, 47% of breast cancers and 38% of all testicular and gastric cancers (Inaba et al., 1980; Inaba et al., 1981; Inaba et al., 1982).

In this work, we constructed a scoring Ferroptosis-related prognostic model that can well reflect risk and positive factors for prognosis in patients with head and neck squamous cell carcinoma. It can be used to guide individualized adjuvant therapy and chemotherapy for patients with head and neck cancer. Therefore, it has a good survival prediction ability and provides an important reference for clinical treatment. Undoubtedly, our prognostic model is limited by the use of public databases. More *in vitro* and *in vivo* studies and clinical research were need to validate the clinical utility of this model.

Data availability statement

The datasets presented in this study can be found in online repositories. The names of the repository/repositories and accession number(s) can be found in the article/Supplementary Material.

Ethics statement

The studies involving human participants were reviewed and approved by the Ethic Committee of the Quanzhou First Hospital Affiliated to Fujian Medical University. The patients/participants provided their written informed consent to participate in this study.

Author contributions

MW performed the data analysis; MW, GL, and YT prepared all the figures; GC and YL wrote the article. All authors have read and approved the final manuscript.

Funding

The work was supported by The Natural Science Foundation of China (No. 82204879) and The Natural Science Foundation of Fujian Provincial Department of Science and Technology (No. 2020J011281).

Acknowledgments

We thank TCGA for providing the data.

Conflict of interest

The authors declare that the research was conducted in the absence of any commercial or financial relationships that could be construed as a potential conflict of interest.

Publisher's note

Supplementary material

The Supplementary Material for this article can be found online at: https://www.frontiersin.org/articles/10.3389/fgene.2022.1065546/full#supplementary-material

References

Chen, W., Zheng, R., Baade, P. D., Zhang, S., Zeng, H., Bray, F., et al. (2016). Cancer statistics in China, 2015. *Ca. Cancer J. Clin.* 66, 115–132. doi:10.3322/caac.21338

Choi, E., Han, C., Park, I., Lee, B., Jin, S., Choi, H., et al. (2008). A novel germ cell-specific protein, SHIP1, forms a complex with chromatin remodeling activity during spermatogenesis. *J. Biol. Chem.* 283, 35283–35294. doi:10.1074/jbc.M805590200

Chu, B., Kon, N., Chen, D., Li, T., Liu, T., Jiang, L., et al. (2019). ALOX12 is required for p53-mediated tumour suppression through a distinct ferroptosis pathway. *Nat. Cell. Biol.* 21, 579–591. doi:10.1038/s41556-019-0305-6

Dannheisig, D. P., Beck, E., Calzia, E., Walther, P., Behrends, C., and Pfister, A. S. (2019). Loss of Peter Pan (PPAN) affects mitochondrial homeostasis and autophagic flux. *Cells* 8, 894. doi:10.3390/cells8080894

Dixon, S. J., Patel, D. N., Welsch, M., Skouta, R., Lee, E. D., Hayano, M., et al. (2014). Pharmacological inhibition of cystine–glutamate exchange induces endoplasmic reticulum stress and ferroptosis. *elife* 3, e02523. doi:10.7554/eLife.02523

Economopoulou, P., De Bree, R., Kotsantis, I., and Psyrri, A. (2019). Diagnostic tumor markers in head and neck squamous cell carcinoma (HNSCC) in the clinical setting. *Front. Oncol.* 9, 827. doi:10.3389/fonc.2019.00827

Hangauer, M. J., Viswanathan, V. S., Ryan, M. J., Bole, D., Eaton, J. K., Matov, A., et al. (2017). Drug-tolerant persister cancer cells are vulnerable to GPX4 inhibition. *Nature* 551, 247–250. doi:10.1038/nature24297

Hong, G.-S., Lee, B., Wee, J., Chun, H., Kim, H., Jung, J., et al. (2016). Tentonin 3/TMEM150c confers distinct mechanosensitive currents in dorsal-root ganglion neurons with proprioceptive function. *Neuron* 91, 708–710. doi:10.1016/j.neuron.2016.07.019

Inaba, N., Ishige, H., Ijichi, M., Satoh, N., Ohkawa, R., Sekiya, S., et al. (1982). Immunohistochemical detection of pregnancy-specific protein (SP1) and placenta-specific tissue proteins (PP5, PP10, PP11 and PP12) in ovarian adenocarcinomas. *Oncodev. Biol. Med.* 3, 379–389.

Inaba, N., Renk, T., Daume, E., and Bohn, H. (1981). Ectopic production of placenta-"specific" tissue proteins (PP5 and PP11) by malignant breast tumors. *Arch. Gynecol.* 231, 87–90. doi:10.1007/BF02110028

Inaba, N., Renk, T., Wurster, K., Rapp, W., and Bohn, H. (1980). Ectopic synthesis of pregnancy specific β1-glycoprotein (SP1) and placental specific tissue proteins (PP5, PP10, PP11, PP12) in nontrophoblastic malignant tumours possible markers in oncology. *Klin. Wochenschr.* 58, 789–791. doi:10.1007/BF01478287

Jennis, M., Kung, C.-P., Basu, S., Budina-Kolomets, A., Julia, I., Leu, J., et al. (2016). An African-specific polymorphism in the TP53 gene impairs p53 tumor suppressor function in a mouse model. *Genes Dev.* 30, 918–930. doi:10.1101/gad.275891.115

Jiang, L., Kon, N., Li, T., Wang, S.-J., Su, T., Hibshoosh, H., et al. (2015). Ferroptosis as a p53-mediated activity during tumour suppression. *Nature* 520, 57–62. doi:10.1038/nature14344

Leu, J. I.-J., Murphy, M. E., and George, D. L. (2019). Mechanistic basis for impaired ferroptosis in cells expressing the African-centric S47 variant of p53. *Proc. Natl. Acad. Sci. U. S. A.* 116, 8390–8396. doi:10.1073/pnas.1821277116

Li, S., Weng, J., Song, F., Li, L., Xiao, C., Yang, W., et al. (2020). Circular RNA circZNF566 promotes hepatocellular carcinoma progression by sponging miR-4738-3p and regulating TDO2 expression. *Cell. Death Dis.* 11, 452–520. doi:10.1038/s41419-020-2616-8

Lin, X., Ping, J., Wen, Y., and Wu, Y. (2020). The mechanism of ferroptosis and applications in tumor treatment. *Front. Pharmacol.* 11, 1061. doi:10.3389/fphar.2020.01061

Lu, H.-J., Nguyen, T.-L., Hong, G.-S., Pak, S., Kim, H., Kim, H., et al. (2020). Tentonin 3/TMEM150C senses blood pressure changes in the aortic arch. *J. Clin. Invest.* 130, 3671–3683. doi:10.1172/JCI133798

Miller, K. D., Siegel, R. L., Lin, C. C., Mariotto, A. B., Kramer, J. L., Rowland, J. H., et al. (2016). Cancer treatment and survivorship statistics. *Ca. Cancer J. Clin.* 66, 271–289. doi:10.3322/caac.21349

O'Connor, O. A., Bhagat, G., Ganapathi, K., Pedersen, M. B., D'Amore, F., Radeski, D., et al. (2014). Changing the paradigms of treatment in peripheral T-cell lymphoma: From biology to clinical practice. *Clin. Cancer Res.* 20, 5240–5254. doi:10.1158/1078-0432.CCR-14-2020

Olausson, K. H., Nistér, M., and Lindström, M. S. (2012). p53-dependent and-independent nucleolar stress responses. *Cells* 1, 774–798. doi:10.3390/cells1040774

Sanmamed, M. F., and Chen, L. (2018). A paradigm shift in cancer immunotherapy: From enhancement to normalization. *Cell.* 175, 313–326. doi:10.1016/j.cell.2018.09.035

Siegel, R., Ward, E., Brawley, O., and Jemal, A. (2011). Cancer statistics, 2011: The impact of eliminating socioeconomic and racial disparities on premature cancer deaths. *Ca. Cancer J. Clin.* 61, 212–236. doi:10.3322/caac.20121

Stockwell, B. R. (2022). Ferroptosis turns 10: Emerging mechanisms, physiological functions, and therapeutic applications. *Cell.* 185, 2401–2421. doi:10.1016/j.cell.2022.06.003

Tibshirani, R. (1996). Regression shrinkage and selection via the lasso. *J. R. Stat. Soc. Ser. B Methodol.* 58, 267–288. doi:10.1111/j.2517-6161.1996.tb02080.x

Valero, C., Lee, M., Hoen, D., Wang, J., Nadeem, Z., Patel, N., et al. (2021). The association between tumor mutational burden and prognosis is dependent on treatment context. *Nat. Genet.* 53, 11–15. doi:10.1038/s41588-020-00752-4

Viswanathan, V. S., Ryan, M. J., Dhruv, H. D., Gill, S., Eichhoff, O. M., Seashore-Ludlow, B., et al. (2017). Dependency of a therapy-resistant state of cancer cells on a lipid peroxidase pathway. *Nature* 547, 453–457. doi:10.1038/nature23007

von Gise, A., and Pu, W. T. (2012). Endocardial and epicardial epithelial to mesenchymal transitions in heart development and disease. *Circ. Res.* 110, 1628–1645. doi:10.1161/CIRCRESAHA.111.259960

Wang, W., Green, M., Choi, J. E., Gijón, M., Kennedy, P. D., Johnson, J. K., et al. (2019). CD8+ T cells regulate tumour ferroptosis during cancer immunotherapy. *Nature* 569, 270–274. doi:10.1038/s41586-019-1170-y

Wee, J., Pak, S., Kim, T., Hong, G.-S., Lee, J. S., Nan, J., et al. (2021). Tentonin 3/TMEM150C regulates glucose-stimulated insulin secretion in pancreatic β-cells. *Cell. Rep.* 37, 110067. doi:10.1016/j.celrep.2021.110067

Wu, J., Minikes, A. M., Gao, M., Bian, H., Li, Y., Stockwell, B. R., et al. (2019). Intercellular interaction dictates cancer cell ferroptosis via NF2–YAP signalling. *Nature* 572, 402–406. doi:10.1038/s41586-019-1426-6

Wu, W., Li, D., Feng, X., Zhao, F., Li, C., Zheng, S., et al. (2021). A pan-cancer study of selenoprotein genes as promising targets for cancer therapy. *BMC Med. Genomics* 14, 78–14. doi:10.1186/s12920-021-00930-1

Xin, M., Olson, E. N., and Bassel-Duby, R. (2013). Mending broken hearts: Cardiac development as a basis for adult heart regeneration and repair. *Nat. Rev. Mol. Cell. Biol.* 14, 529–541. doi:10.1038/nrm3619

Yao, S., Yin, X., Chen, T., Chen, W., Zuo, H., Bi, Z., et al. (2022). Exploring ALDH2 expression and immune infiltration in HNSC and its correlation of prognosis with gender or alcohol intake. *Sci. Rep.* 12, 2504–2513. doi:10.1038/s41598-022-06244-1

Yu, Y., Xie, Y., Cao, L., Yang, L., Yang, M., Lotze, M. T., et al. (2015). The ferroptosis inducer erastin enhances sensitivity of acute myeloid leukemia cells to chemotherapeutic agents. *Mol. Cell. Oncol.* 2, e1054549. doi:10.1080/23723556.2015.1054549

Zhang, X., Shi, M., Chen, T., and Zhang, B. (2020). Characterization of the immune cell infiltration landscape in head and neck squamous cell carcinoma to aid immunotherapy. *Mol. Ther. Nucleic Acids* 22, 298–309. doi:10.1016/j.omtn.2020.08.030

Zhang, Y., Chen, K., Li, L., Mao, W., Shen, D., Yao, N., et al. (2021). CCR4 is a prognostic biomarker and correlated with immune infiltrates in head and neck squamous cell carcinoma. *Ann. Transl. Med.* 9, 1443. doi:10.21037/atm-21-3936

frontiers | Frontiers in Genetics

TYPE Original Research
PUBLISHED 04 January 2023
DOI 10.3389/fgene.2022.1100317

OPEN ACCESS

EDITED BY
Rui Cao,
Affiliated Beijing Friendship Hospital, Capital Medical University, China

REVIEWED BY
Fahui Liu,
University of Gothenburg, Sweden
Shenglin Gao,
Changzhou No.2 People's Hospital, China

*CORRESPONDENCE
Junbin Yuan,
dabing7220@126.com
Longxiang Wu,
wulongxiang1123@126.com

†These authors have contributed equally to this work

SPECIALTY SECTION
This article was submitted to Cancer Genetics and Oncogenomics, a section of the journal Frontiers in Genetics

RECEIVED 16 November 2022
ACCEPTED 08 December 2022
PUBLISHED 04 January 2023

CITATION
Deng H, Deng D, Qi T, Liu Z, Wu L and Yuan J (2023), An IFN-γ-related signature predicts prognosis and immunotherapy response in bladder cancer: Results from real-world cohorts.
Front. Genet. 13:1100317.
doi: 10.3389/fgene.2022.1100317

An IFN-γ-related signature predicts prognosis and immunotherapy response in bladder cancer: Results from real-world cohorts

Hao Deng[1,2†], Dingshan Deng[1,2†], Tiezheng Qi[3], Zhi Liu[1,2], Longxiang Wu[1,2*] and Junbin Yuan[1,2*]

[1]Department of Urology, Xiangya Hospital, Central South University, Changsha, China, [2]National Clinical Research Center for Geriatric Disorders, Xiangya Hospital, Central South University, Changsha, China, [3]Xiangya School of Medicine, Central South University, Changsha, China

Bladder cancer (BLCA) is featured with high incidence and mortality. Whether the IFN-γ signaling could be used as an immunotherapy determinant for BLCA has not been fully confirmed. In this study, the transcriptome data and clinical information of BLCA samples were collected from The Cancer Genome Atlas (TCGA). Besides, four immunotherapy cohorts including IMvigor210 cohort, Gide cohort, Van Allen cohort, and Lauss cohort were collected. The Xiangya real-world cohort was used for independent validation. An IFN-γ-related signature was developed and validated in BLCA for predicting prognosis, mutation, tumor microenvironment status, and immunotherapy response. This is the first study focusing on the comprehensive evaluation of predictive values on the IFN-γ-related signature in BLCA. The potential clinical application of the IFN-γ-related signature was expected to be further validated with more prospective clinical cohorts.

KEYWORDS

bladder cancer, immunotherapy, IFN-γ, prognosis, real-world cohort study

Introduction

Bladder cancer (BLCA) is recognized as one of the most common and heterogeneous urinary carcinomas worldwide (Antoni et al., 2017; Sung et al., 2021). Clinical data ceaselessly confirmed a high incidence and mortality in BLCA patients (Martinez Rodriguez et al., 2017). Thus, for decades, urologists have explored the mysteries of bladder cancer in hope of getting optimal solutions for precision BLCA treatments. Despite surgeries, radiotherapy, neoadjuvant or adjuvant chemotherapy and targeted therapy, BLCA patients still suffer (Antoni et al., 2017; Lenis et al., 2020). Most suffering patients are not sensitive to the current and mainstream treatment methods according to poor clinical outcomes (Lenis et al.,

2020; Patel et al., 2020). Therefore, inventing new medical tools and treatment modalities for BLCA patients are urgently needed.

Cancer immunotherapy is a relatively burgeoning section in the field of cancer treatment, providing opportunities for alleviating, even curing BLCA patients (Pettenati and Ingersoll, 2018; Lenis et al., 2020). The immune checkpoint blockade (ICB), considered as the main direction of immunotherapy development, has been observed effective survival benefits in solid cancers, including BLCA (Rosenberg et al., 2016). Further from the cellular and molecular level, the ICB response rate mainly depends on the BLCA tumor microenvironment (TME) (Petitprez et al., 2020; Cao et al., 2021; Marin-Acevedo et al., 2021). TME is chiefly composed of cancer cells and immune cells, with other cell subsets and extracellular matrix as well (Hinshaw and Shevde, 2019). However, a malignant BLCA TME generally leads ICB moving towards failure. Potential mechanisms influencing ICB could be including the exhaustion and senescence of CD8 T cells in TME (Lian et al., 2020; Zhang et al., 2021); the huge secretion immunosuppressive factors (Metelli et al., 2018; Lecker et al., 2021). Besides, high tumor mutation burden (TMB), which could represent a high level of neoantigen, is a prominent characteristic of BLCA indicating a potential immunogenic microenvironment (Kandoth et al., 2013). Even though the response of patients with high TMB to ICB is considered heterogeneous, in BLCA, TMB is acknowleged to be a potential indicator reflecting ICB response efficiency (Chan et al., 2019; Liu et al., 2019). However, only a minor patients received ICB therapy achieved ideal outcomes. Therefore, exploring novel biomarkers for distinguishing specific groups of BLCA patients with an inflamed TME is necessary for increasing the ICB response rates.

IFN-γ signaling has been well-recognized as a critical mediator of tumor cell immunogenicity, which could help promote recognize and eliminate tumor cells (Dighe et al., 1994). IFN-γ expression has been proven to potentially predict clinical outcomes for multiple cancer types (Fridman et al., 2012), and is associated with mortality and disease risk of BLCA as well (Gillezeau et al., 2022). Besides, IFN-γ-induced was reported to up-regulate PD-ECGF/TP and enhance the cytotoxicity of 5-fluorouracil and 5′-deoxy-5-fluorouridine in BLCA (Li et al., 2002). Notably, IFN-γ-induced cytotoxicity has been revealed as a biomarker of resistance in BLCA (Green et al., 2021). However, whether the IFN-γ signaling could be used as an immunotherapy determinant for BLCA has not been fully confirmed.

In this study, an IFN-γ-related signature was developed in BLCA for predicting prognosis, mutation, tumor microenvironment, and immunotherapy. To date, we come first to comprehensively evaluate the predictive values of IFN-γ-related signature in BLCA.

Materials and methods

Data collection and procession

The transcriptome data and clinical information of BLCA samples were collected from The Cancer Genome Atlas (TCGA). The FPKM values of the raw matrix were transformed into TPM values for follow-up studies. The TCGA BLCA dataset included 403 BLCA samples and 19 normal samples. Four immunotherapy cohorts were collected, including IMvigor210 (248 samples), Gide (32 samples), Van Allen (42 samples) and Lauss (25 samples). Besides, the copy number variation (CNV) data of BLCA samples in the TCGA BLCA dataset, processed with GISTIC 2.0, were downloaded from the UCSC Xena data portal (http://xena.ucsc.edu/). Drug information, including 184 common anticancer drugs and the corresponding target genes were collected from the DrugBank database (www.drugbank.ca).

The Xiangya real-world cohort

According to our previous studies, the Xiangya real-world cohort was based on BLCA samples after surgical resections in the Xiangya Hospital, Central South University. The Xinagya real-world cohort, already uploaded with the number as GSE188715, included 57 BLCA samples sequenced by the BGISEQ-500 platform (BGI-Shenzhen, China) (Liu et al., 2021a; Hu et al., 2021). The TPM values of the raw matrix were used for the follow-up analysis.

Development of the IFN-γ-related signature in TCGA BLCA cohort

IFN-γ related genes have never been systematically summarized as a list. Originally, we collected IFN-γ-related genes from previous studies as comprehensively as possible (Gao et al., 2016; Hu et al., 2020). The least absolute shrinkage and selector operation (LASSO) regression analysis was first performed on these genes for dimension reduction. Each gene can be regarded as a factor, and factors which contribute relatively less to final outcomes of the analysis were assigned the value zero. Remaining factors, genes with non-zero coefficients, were ultimately selected for multivariable Cox regression analysis and used as variables to construct the IFN-γ-related signature. The formula is as follows: Risk score = $\sum IFNi*RNAi$, where IFNi is the coefficient of the genes and RNAi is the expression value of the genes in multivariable Cox regression analysis. To evaluate the performance of the IFN-γ-related signature, we simultaneously perform the time-dependent receiver operating characteristic (ROC) and calibration curves using

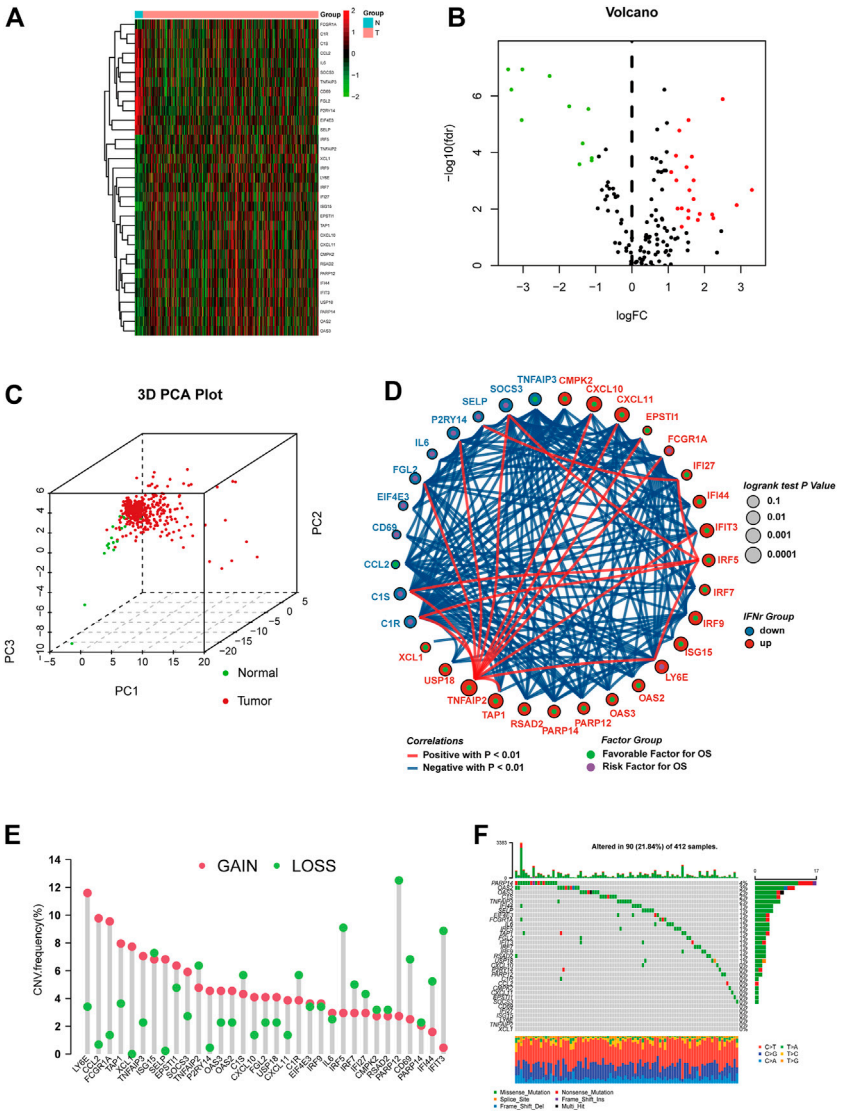

FIGURE 1
The expression pattern of the IFN-γ-related genes in the TCGA BLCA dataset. **(A)** Heatmap depicting the expression differences of the IFN-γ-related genes between BLCA samples and normal samples. **(B)** Volcano plot for the expression differences of the IFN-γ-related genes between BLCA samples and normal samples. **(C)** 3D PCA plot depicting the expression differences of the IFN-γ-related genes between BLCA samples and normal samples. **(D)** Correlations between the IFN-γ-related genes. The size of the circle, calculated by the log-rank test and ranging from .1 to .0001, represents the prognosis of each gene. Green dots represent favorable factors, while purple dots represent risk factors. The color of the lines represents the correlation between the IFN-γ-related genes. Blue represents a negative correlation, and red represents a positive correlation. **(E)** The CNV frequency of the IFN-γ-related genes. The column represents the count, and the color represents gains or losses. Red represents gains, and blue represents losses. **(F)** The mutation frequency of the IFN-γ-related genes. The upper bar plot represents TMB. The number on the right represents the mutation frequency in each IFN-γ-related gene. The right bar plot represents the proportion of each variant type.

the R package "timeROC" in the TCGA BLCA cohort, Xiangya real-world cohort, and IMvigor210 cohort.

Development of a nomogram

The univariate and multivariate Cox regression analyses were adopted to filtrate independent prognostic factors from clinicopathologic characteristics and the IFN-γ-related signature. After analyzing results, prognostic factors in univariate Cox analysis were screened and integrated to construct a nomogram. The performance of the nomogram was evaluated by the time-dependent ROC and calibration curves using the R package "timeROC" in the TCGA BLCA dataset and the Xiangya real-world cohort.

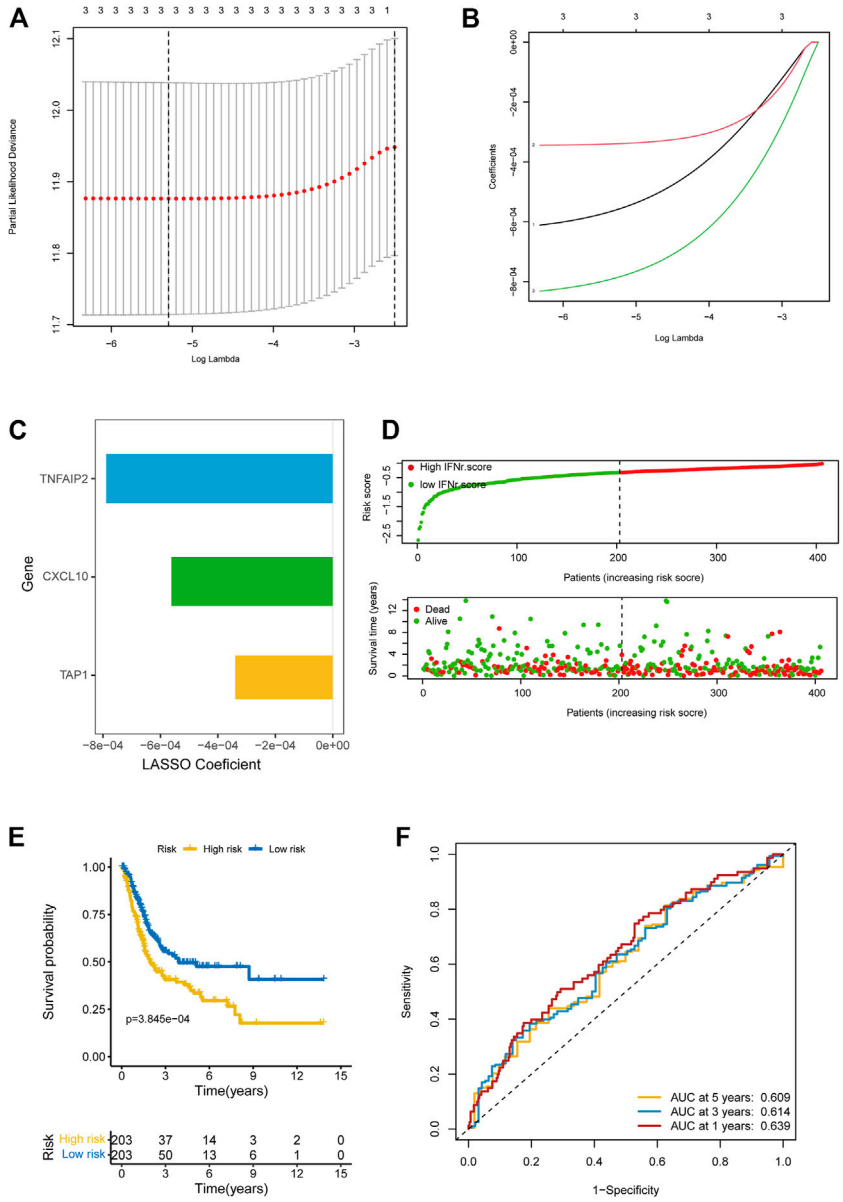

FIGURE 2
Development of the IFN-γ-related signature in the TCGA BLCA dataset. **(A)** The partial likelihood deviance of the IFN-γ-related genes in LASSO regression analysis. **(B)** The coefficients of the IFN-γ-related genes in LASSO regression analysis. **(C)** The coefficients of the IFN-γ-related genes in LASSO regression analysis. **(D)** The distribution of the IFN-γ-related signature in BLCA samples. **(E)** The survival curves of the two IFN-γ-related signature score groups. **(F)** 1-year, 3-year, and 5-year ROC of the IFN-γ-related signature.

The mutation landscape of the IFN-γ-related signature

The mutation landscape of the IFN-γ-related signature was visualized based on CNV data using the R package "maftools." Somatic mutation data of BLCA samples in the TCGA BLCA dataset was used to calculate the tumor mutation burden (TMB).

The immunological characteristics of the IFN-γ-related signature

In our previous studies, relevant immunological characteristics and algorithms in the TME were described in detail (Liu et al., 2021a; Hu et al., 2021). The cancer immunity cycle is composed of seven key steps: the release and presentation of cancer cell antigens (Steps 1 and 2), the priming and activation

of the immune system (Step 3), then the trafficking and infiltration of immune cells into tumors (Steps 4 and 5), finally recognizing and killing cancer cells by T cells (Steps 6 and 7) (26). The cancer immunity cycle and immune infiltrating cells involved were quantified using the single-sample gene-set enrichment analysis (ssGSEA) in BLCA samples.

Drug sensitivity and immunotherapy response prediction within the IFN-γ-related signature

We calculated the sensitivity of anticancer drugs using data downloaded from the DrugBank. The predictive value of the IFN-γ-related signature for the immunotherapy was validated in three immunotherapy cohorts, namely the Gide, Van Allen, and Lauss.

Statistical analysis

Correlation coefficients were determined by the Spearman and distance correlation analyses. Normally distributed continuous variables between the two groups were compared using the *t*-test, while the non-normally ones between the two groups were compared using the Mann-Whitney *U* test instead. Chi-square or Fisher exact tests were used for comparison between categorical variables. The "survcutpoint" function from the R package "survminer" for the maximum rank statistic was used to determine the optimal cutoff value of the IFN-γ-related signature. The survival curves were generated using the Kaplan-Meier method, while the statistical significance was determined using the log-rank test. The threshold of significance was set at $p < .05$, and all statistical tests were two-sided. R project (version 3.6.3, http://www.r-project.org) was used for all analyses.

Results

The expression pattern of the IFN-γ-related genes in the TCGA BLCA dataset

Differential analysis performed on the IFN-γ-related genes between BLCA samples and normal samples was shown in Figures 1A, B. Both sample sets (the BLCA set and normal one) could be clearly separated by IFN-γ-related genes (Figure 1C). Correlations between every two IFN-γ-related genes were shown in Figure 1D, in which 22 IFN-γ-related genes were favorable factors, while the remaining 11 were risk factors. The CNV frequency of IFN-γ-related genes was shown in Figure 1E. Roughly a half of the genes showed CNV loss, while the other half reversed. The mutation frequency of the IFN-γ-related genes was shown in Figure 1F, in which PARP14, OAS2, OAS3, C1S, and TNFAIP3 were the top five mutated IFN-γ-related genes.

Development of the IFN-γ-related signature in the TCGA BLCA dataset

We successfully reduced the dimension of IFN-γ-related genes using LASSO regression analysis (Figure 2A). The coefficients of the IFN-γ-related genes in LASSO regression analysis were shown in Figure 2B. TNFAIP2, CXCL10, and TAP1 were finally included for the multivariable Cox regression analysis. Figure 2C displayed the coefficients of these three genes. The distribution of the IFN-γ-related signature in BLCA samples was shown in Figure 2D. BLCA patients with high IFN-γ-related signature scores were associated with decreased survival time (Figure 2E). The accuracy of the signature in predicting 1-year, 3-year, and 5-year OS was .609, .614, and .639 respectively (Figure 2F).

Development of a nomogram

Univariate Cox regression analysis was performed on clinical characters including the IFN-γ-related signature in the TCGA BLCA cohort. Results revealed that the age, tumor stage, TN grading system, and the IFN-γ-related signature were independent prognostic factors (Figure 3A). Multivariate Cox regression analysis was ultimately performed likewise in the TCGA BLCA dataset, in which age and the IFN-γ-related signature were independent prognostic factors (Figure 3B). Nomogram was constructed based on clinical factors including the IFN-γ-related signature in the TCGA BLCA dataset (Figure 3C).1-year, 3-year, and 5-year ROC of the nomogram in the TCGA BLCA dataset had respective values of .72, .71, and .74 (Figure 4A). 1-year, 3-year, and 5-year calibration curves of the nomogram in the TCGA BLCA dataset were shown in Figure 4B. 1-year, 3-year, and 5-year ROC of the nomogram in the Xiangya real-world cohort had values of .82, .87, and .86 (Figure 4C). 1-year, 3-year, and 5-year calibration curves of the nomogram in the Xiangya real-world cohort were shown in Figure 4D.

The mutation landscape of the IFN-γ-related signature in the TCGA BLCA dataset

TP53, TTN, KMT2D, MUC16, and KDM6A were the top five mutated genes in the high IFN-γ-related signature score

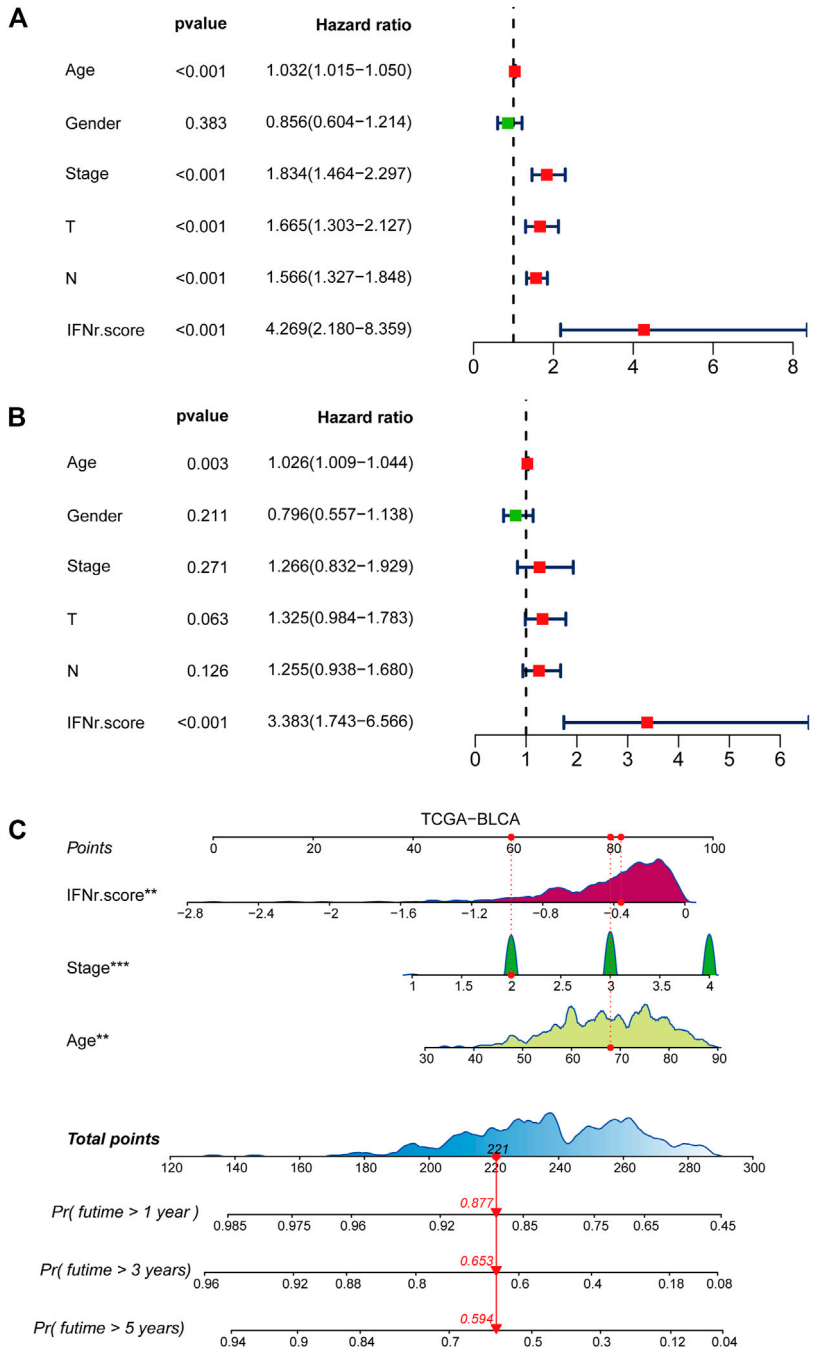

FIGURE 3
Development of a nomogram. **(A)** Univariate Cox regression analysis on the clinical factors including the IFN-γ-related signature in the TCGA BLCA dataset. **(B)** Multivariate Cox regression analysis on the clinical factors including the IFN-γ-related signature in the TCGA BLCA dataset. **(C)** Nomogram based on clinical factors including the IFN-γ-related signature in the TCGA BLCA dataset.

group (Figure 5A). TTN, TP53, MUC16, KMT16, and ARID1A were the top five mutated genes in the low IFN-γ-related signature score group (Figure 5B). The high IFN-γ-related signature score group was significantly associated with a lower TMB level (Figure 5C). However, there was no significant correlation between the MANTIS score and the IFN-γ-related signature (Figure 5D).

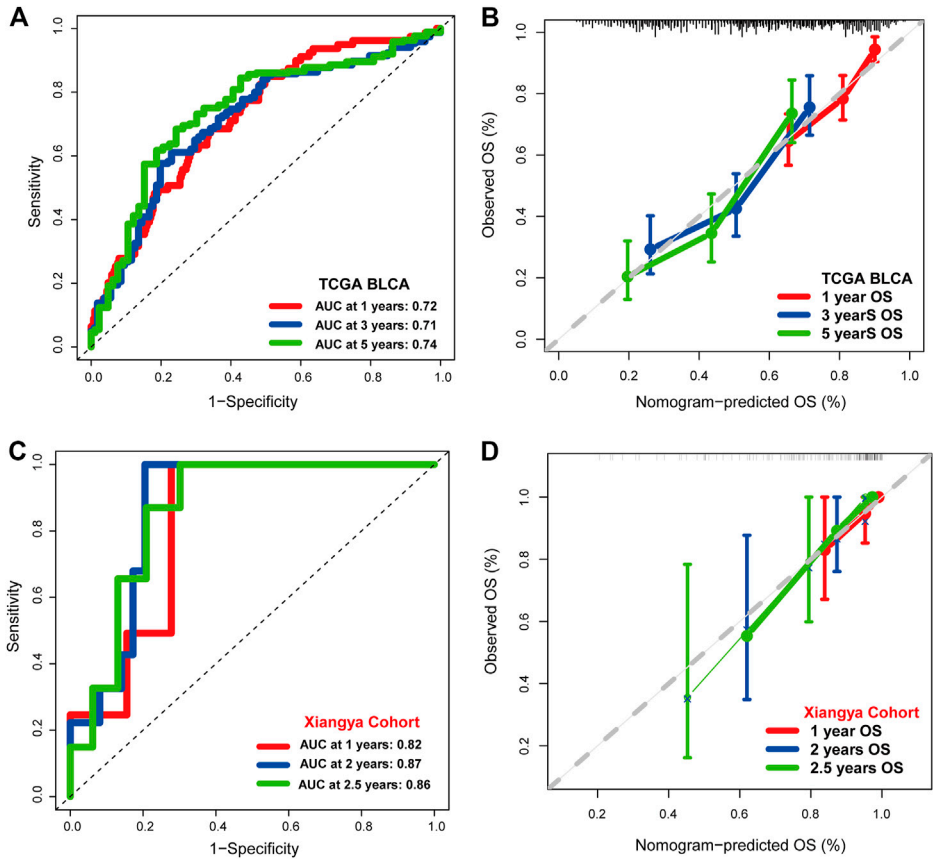

FIGURE 4
The prognostic value of the nomogram. **(A)** 1-year, 3-year, and 5-year ROC of the nomogram in the TCGA BLCA dataset. **(B)** 1-year, 3-year, and 5-year calibration curves of the nomogram in the TCGA BLCA dataset. **(C)** 1-year, 3-year, and 5-year ROC of the nomogram in the Xiangya real-world cohort. **(D)** 1-year, 3-year, and 5-year calibration curves of the nomogram in the Xiangya real-world cohort.

The immunological characteristics of the IFN-γ-related signature in the TCGA BLCA dataset

As was shown in Figure 6A, low IFN-γ-related signature scores significantly indicated some cancer immunity cycles including T cell recruiting, Th 1 cell recruiting, and macrophage recruiting. Besides, the low IFN-γ-related signature scores were generally associated with immune infiltrating cells including activated CD4 cells, activated CD8 cells, and natural killer T cells (Figure 6B). Correlations between the IFN-γ-related signature and each stroma-activated pathway were shown in Figure 6C. Immunotherapy-predicted pathways were relatively more active in the low IFN-γ-related signature score group (Figure 6D). We divided TCGA samples into different binary groups according to the sex and stage. Results of validating our IFN-γ signature in female and male groups, high stage and low stage groups proved the conclusion as expected (Supplementary Figure S1–S4).

The immunological characteristics of the IFN-γ-related signature in the Xiangya real-world cohort

BLCA patients with a high IFN-γ-related signature score were associated with shorter survival time (Figure 7A). 1-year, 3-year, and 5-year ROC of the IFN-γ-related signature had values of .84, .66, and .66, respectively (Figure 7B). The signature also showed negative correlation with multiple immune checkpoint molecules, including CD274, LAG3, CTLA4, PDCD1, and HAVCR2 (Figure 7C). As expected, the signature was negatively associated with cancer immunity cycles, including T cell recruiting, Th 1 cell recruiting, and macrophage recruiting (Figure 7D). The IFN-γ-related signature was

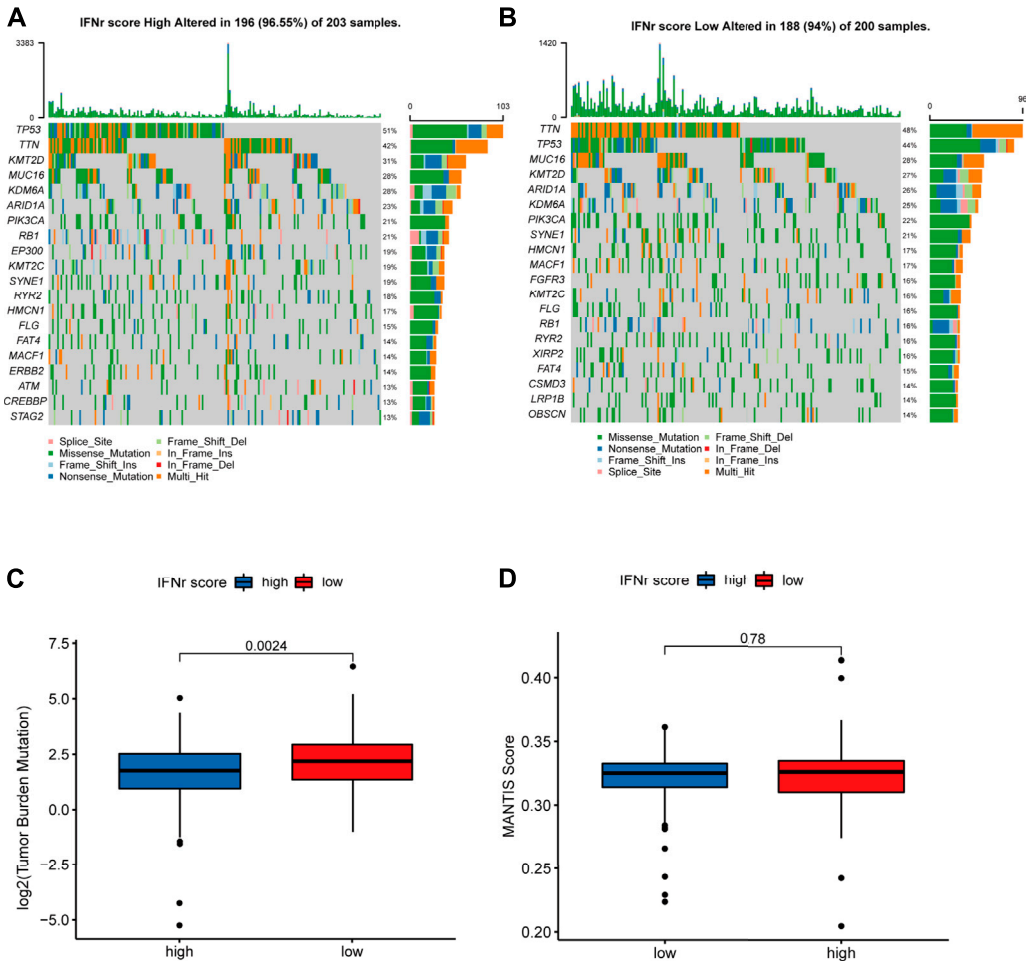

FIGURE 5
The mutation landscape of the IFN-γ-related signature in the TCGA BLCA dataset. **(A)** The top-ranked mutated genes in the high IFN-γ-related signature score group. **(B)** The top-ranked mutated genes in the low IFN-γ-related signature score group. **(C)** The TMB levels in the two IFN-γ-related signature score groups. **(D)** The MANTIS score in the two IFN-γ-related signature score groups.

negatively associated with immunotherapy-predicted pathways, including APM signal, microRNAs in cancer, mismatch repair, cell cycle, and p53 signaling pathway (Figure 7D). In addition, the low signature score group was generally significantly associated with immune infiltrating cells, including activated CD4 cells, activated CD8 cells, and natural killer T cells (Figure 7E).

The immunological characteristics of the IFN-γ-related signature in the IMvigor210 cohort

BLCA patients with high IFN-γ-related signature scores were associated with decreased survival time (Figure 8A). 1-year, 3-year, and 5-year ROC of the IFN-γ-related signature had values of .74, .59, and .6 (Figure 8B). The IFN-γ-related signature was negatively associated with multiple immune checkpoint molecules, including CD274, LAG3, CTLA4, PDCD1, and HAVCR2 (Figure 8C). The IFN-γ-related signature was negatively associated with cancer immunity cycles, including T cell recruiting, Th 1 cell recruiting, and macrophage recruiting (Figure 8D). The IFN-γ-related signature was negatively associated with immunotherapy-predicted pathways, including APM signal, microRNAs in cancer, mismatch repair, cell cycle, and p53 signaling pathway (Figure 8D). In addition, the low IFN-γ-related signature scores were generally significantly associated with immune infiltrating cells, including activated CD4 cells, activated CD8 cells, and natural killer T cells (Figure 8E).

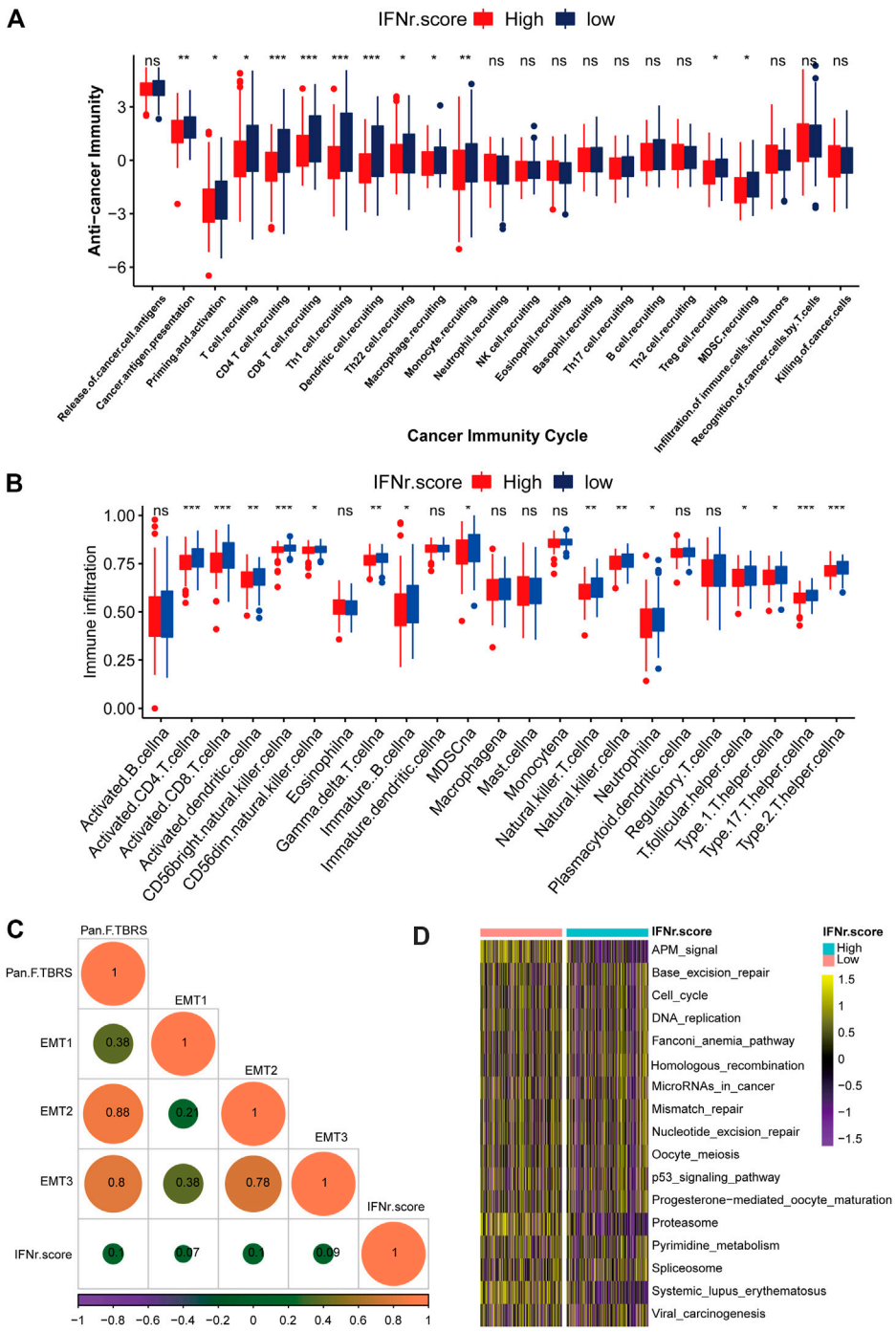

FIGURE 6
The immunological characteristics of the IFN-γ-related signature in the TCGA BLCA dataset. **(A)** Cancer immunity cycles between the two IFN-γ-related signature score groups. **(B)** Immune infiltrating cells between the two IFN-γ-related signature score groups. **(C)** Correlations between the IFN-γ-related signature and stroma-activated pathways. **(D)** Immunotherapy-predicted pathways between the two IFN-γ-related signature score groups. The left bar represents log10 *p*-values, the red bar represents activated pathways, and the blue bar represents inhibited pathways. (ns, Not Significant; *$p < .05$; **$p < .01$; ***$p < .001$; ****$p < .0001$).

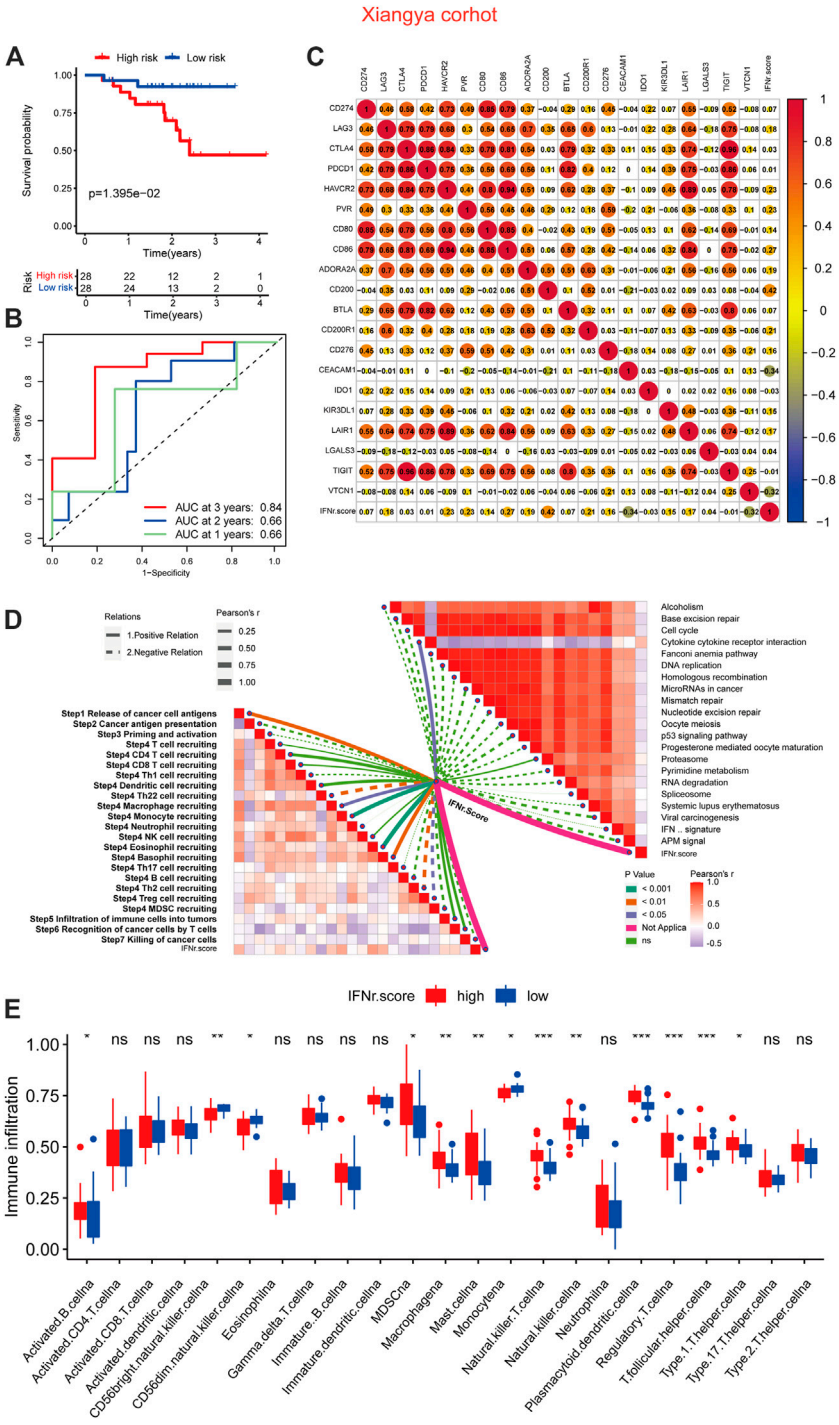

FIGURE 7
The immunological characteristics of the IFN-γ-related signature in the Xiangya real-world cohort. **(A)** The survival curves of the two IFN-γ-related signature score groups. **(B)** 1-year, 3-year, and 5-year ROC of the IFN-γ-related signature. **(C)** Correlations between the IFN-γ-related signature and immune checkpoint molecules. **(D)** Correlations between the IFN-γ-related signature and cancer immunity cycles and immunotherapy-predicted pathways. **(E)** Correlations between the IFN-γ-related signature and immune infiltrating cells.

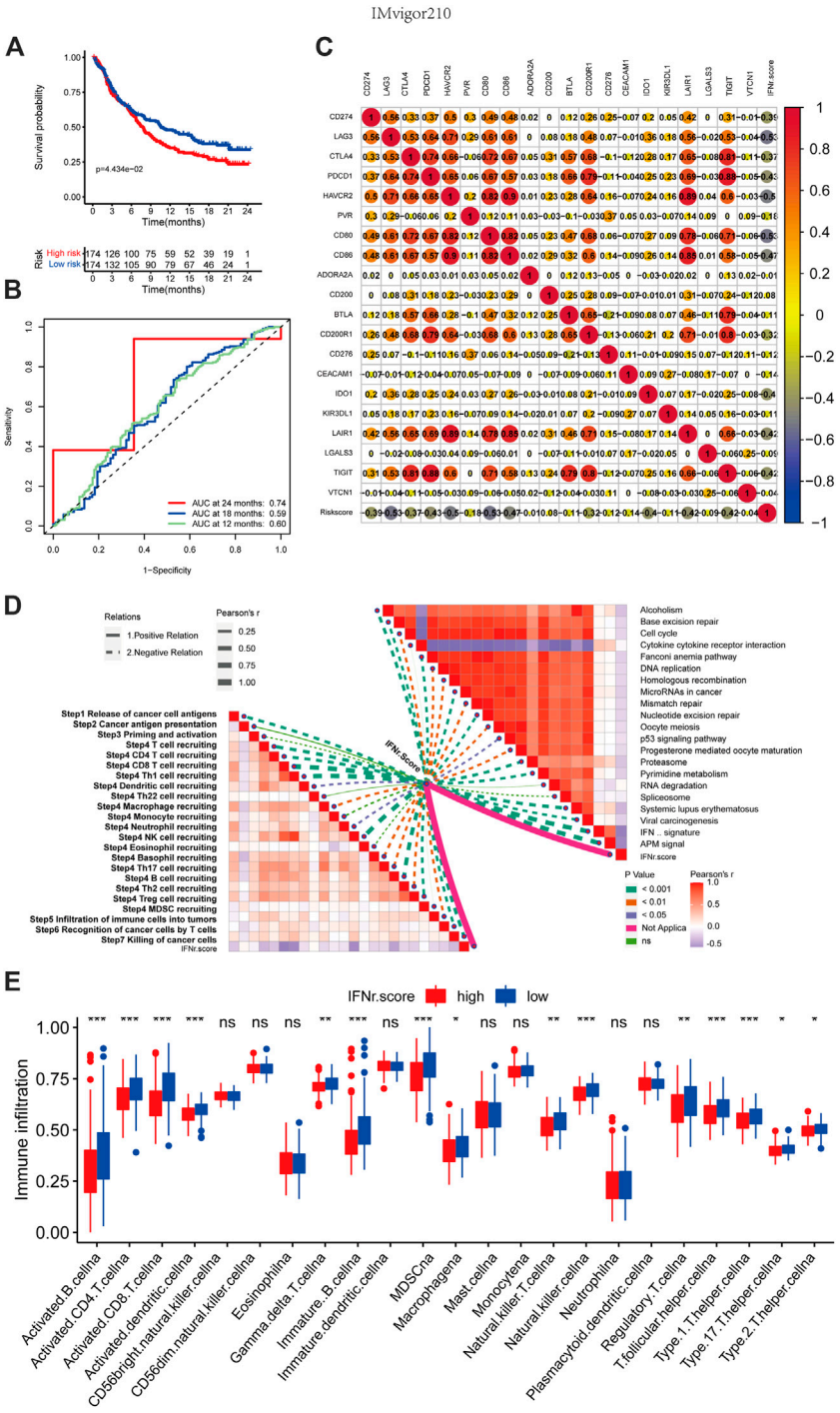

FIGURE 8
The immunological characteristics of the IFN-γ-related signature in the IMvigor210 cohort. **(A)** The survival curves of the two IFN-γ-related signature score groups. **(B)** 1-year, 3-year, and 5-year ROC of the IFN-γ-related signature. **(C)** Correlations between the IFN-γ-related signature and immune checkpoint molecules. **(D)** Correlations between the IFN-γ-related signature and cancer immunity cycles and immunotherapy-predicted pathways. **(E)** Correlations between the IFN-γ-related signature and immune infiltrating cells.

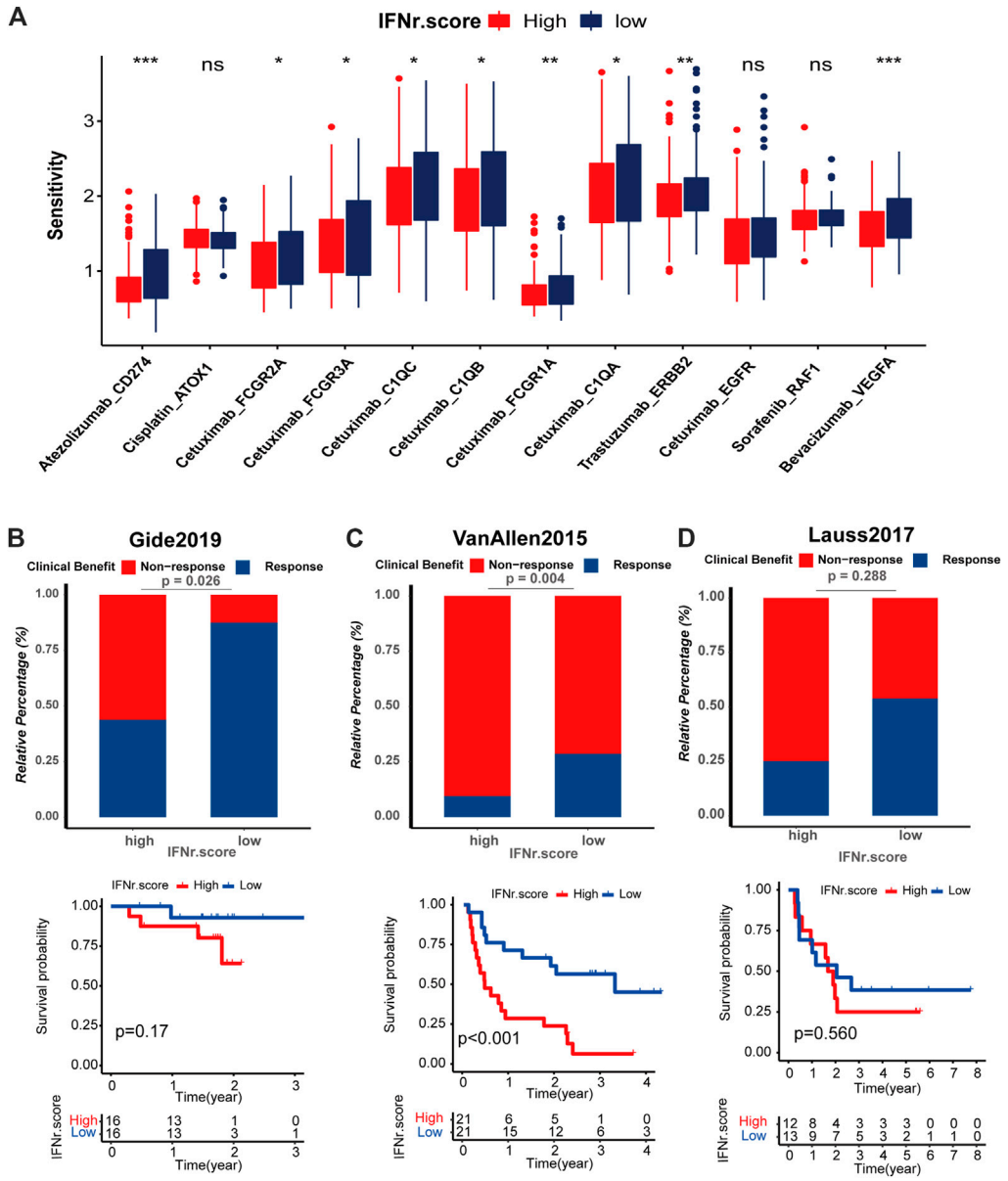

FIGURE 9
Drug prediction and immunotherapy response prediction of the IFN-γ-related signature. **(A)** The sensitivity of the anticancer drugs in the two IFN-γ-related signature score groups. The predictive value of the IFN-γ-related signature for the immunotherapy was validated in three immunotherapy cohorts, including. **(B–D)** Response of melanoma patients with high and low IFN-γ-related signature scores to ICB in Gide, Van Allen and Lauss respectively.

Drug prediction and immunotherapy response prediction of the IFN-γ-related signature

We predicted the sensitivity of BLCA patients to common drugs. Atezolizumab_CD274, Cetuximab_FCGR2A, Cetuximab_FCGR3A, Cetuximab_C1QC, Cetuximab_C1QB, Cetuximab_FCGR1A, Cetuximab_G1QA, Trastuzumab_ERBB2, and Bevacizumab_VEGFA had significantly lower drug sensitivity in the high IFN-γ-related signature score group (Figure 9A). Likewise, melanoma patients with high IFN-γ-related signature scores were less likely to respond to ICB (Figures 9B–D). Notably, melanoma patients with high IFN-γ-related signature scores were associated with decreased survival time (Figure 9C).

Discussion

Increasing evidence constantly confirmed that IFN-γ plays a critical role in the tumorigenicity and immunogenicity of various cancers (Jorgovanovic et al., 2020; Stifter et al., 2020). Specially, IFN-γ is a cytokine that physiologically promotes innate and adaptive immune responses, while preventing the development of primary and transplanted tumors (Burke and Young, 2019). However, the potential roles of IFN-γ in the prognosis and especially in the TME of BLCA remain unclear. Recently, mining markers precisely predicting prognosis and survival in cancers based on large-scale bioinformatic analysis has received much more attention in the big data era than ever before. Several markers have been proven robust in predicting survival outcomes and immunotherapy responses (Zhang et al., 2022a; Zhang et al., 2022b). Thus, we aimed to explore the predictive value of IFN-γ and its related genes in BLCA using comprehensive bioinformatics on internal datasets and external real-world validation cohort.

Our study originally proved that most IFN-γ-related genes were risk factors in BLCA.

After summarizing IFN-γ-related genes, a corresponding signature was successfully developed in TCGA BLCA cohort. The predictive signature consisted of three genes, namely TNFAIP2, CXCL10, and TAP1. From with, TNFAIP2, a primary response gene of TNFα, is highly expressed in immune cells and the urinary bladder cells (Jia et al., 2016; Niwa et al., 2019). TNFAIP2 has been reported to promote proliferation, angiogenesis, migration, and invasion of cancer (Jia et al., 2018). CXCL10, CXCL9, CXCL11/CXCR3 is an important axis for immune activation, which is necessary for developing novel cancer therapy (Tokunaga et al., 2018). In addition, a significantly negative correlation between TAP1 and survival in breast, lung, liver, and ovarian cancer is revealed (Tabassum et al., 2021).

The IFN-γ-related signature could predict the survival outcomes of BLCA patients in the TCGA BLCA dataset, Xiangya real-world cohort and IMvigor210 cohort. Cox regression analysis determined that the signature was an independent prognostic factor as age, tumor stage, and TN grading system in the predictive nomogram. The constructed nomogram performs robustly in predicting the survival outcomes of BLCA patients. As generally agreed, the TNM staging system is the most widely accepted and most commonly used system for BLCA (Adsay et al., 2012). The IFN-γ-related signature showed sensationally superior performance compared to the TNM staging system regarding predicting the prognosis of BLCA patients. TP53 is an important tumor suppressor gene that is frequently mutated in cancer (Donehower et al., 2019). While MUC16 and TTN genes mutation were previously reported to correlate with prognosis, tumor mutation burden, and immunotherapy efficacy in cancers (Yang et al., 2020). KMT2D deficiency was found to impair super-enhancers to confer a glycolytic vulnerability in lung cancer (Alam et al., 2020). KDM6A-ARHGDIB axis could block metastasis of BLCA by inhibiting Rac1 (Liu et al., 2021b). In accordance with these findings, TP53, TTN, KMT2D, MUC16, and KDM6A were the top five mutated genes in the high IFN-γ-related signature score group.

The core part of immunotherapy is to help the immune system recognize and destroy tumor cells through enhancing the reaction of immune cells to present tumor antigens (Frankel et al., 2017). TME, composed of cancer cells, non-cancerous cells (mainly immune infiltrating cells), and secreted cytokines, has emerged as a promising mediator for immunotherapy (Bejarano et al., 2021). An immune hot TME, which is infiltrated by more immune cells, is more likely to present a better ICB response (Wang et al., 2022). The IFN-γ-related signature was negatively associated with cancer immunity cycles, immunotherapy-predicted pathways, and immune infiltrating cells in the TCGA BLCA dataset, Xiangya real-world cohort, and IMvigor210 cohort. As the most important determinant for ICB, immune checkpoint molecules have been widely studied in the past few decades. CD274, LAG3, CTLA4, PDCD1, and HAVCR2 have been the most promising immune checkpoint molecules with satisfying results in clinical trials (Wang et al., 2022). As expected, the IFN-γ-related signature was negatively associated with multiple immune checkpoint molecules, including CD274, LAG3, CTLA4, PDCD1, and HAVCR2. Besides, the high IFN-γ-related signature score group was significantly associated with a lower TMB level. These results indicate potential lower response rates in BLCA patients with high IFN-γ-related signature scores. The direct immunotherapy response prediction of the IFN-γ-related signature in Gide, Van Allen, and Lauss cohorts proved this finding. Furthermore, IFN-γ-related signature could predict drug sensitivity of Atezolizumab_CD274, Cetuximab_FCGR2A, Cetuximab_FCGR3A, Cetuximab_C1QC, Cetuximab_C1QB, Cetuximab_FCGR1A, Cetuximab_G1QA, Trastuzumab_ERBB2, and Bevacizumab_VEGFA.

To sum up, an IFN-γ-related signature was developed in BLCA for predicting prognosis, mutation, tumor microenvironment, and immunotherapy. The potential clinical application of the IFN-γ-related signature is expected to be further validated by more clinical cohorts.

Data availability statement

The datasets presented in this study can be found in online repositories. The names of the repository/repositories and accession number(s) can be found in the article/Supplementary Material.

Ethics statement

The studies involving human participants were reviewed and approved by the Ethics Committee of the Xiangya Hospital of Central South University. The patients/participants provided their written informed consent to participate in this study. The animal

study was reviewed and approved by the Ethics Committee of the Xiangya Hospital of Central South University. Written informed consent was obtained from the individual(s) for the publication of any potentially identifiable images or data included in this article.

Author contributions

Conception and design: LW, JY, HD, and DD. Provision of study materials or patients: TQ and ZL. Collection and assembly of data: TQ and ZL. Data analysis and interpretation: HD, DD, TQ, and ZL. Manuscript writing: HD, DD, TQ, ZL, LW, and JY. Final approval of manuscript: All authors.

Funding

This work was supported by the grants from the Natural Science Foundation of Hunan Province (2021JJ31122).

Acknowledgments

We sincerely thank all participants in the study.

Conflict of interest

The authors declare that the research was conducted in the absence of any commercial or financial relationships that could be construed as a potential conflict of interest.

Publisher's note

Supplementary material

The Supplementary Material for this article can be found online at: https://www.frontiersin.org/articles/10.3389/fgene.2022.1100317/full#supplementary-material

SUPPLEMENTARY FIGURE S1
Exploring correlations between the IFN-γ score and TME characteristics in female group. **(A)** Differences in cancer immune cycle activity between high-risk and low-risk groups. **(B)** Correlation between the score and the infiltration of different immune cells. **(C)** Relationship between the TIS and the IFN-γ score. **(D)** Correlation between the IFN-γ score and various common ICB response pathways. **(E)** Correlation between the IFN-γ score and immune checkpoints.

SUPPLEMENTARY FIGURE S2
Exploring correlations between the IFN-γ score and TME characteristics in male group.

SUPPLEMENTARY FIGURE S3
Exploring correlations between the IFN-γ score and TME characteristics in high stage group.

SUPPLEMENTARY FIGURE S4
Exploring correlations between the IFN-γ score and TME characteristics in low stage group.

References

Adsay, N. V., Bagci, P., Tajiri, T., Oliva, I., Ohike, N., Balci, S., et al. (2012). Pathologic staging of pancreatic, ampullary, biliary, and gallbladder cancers: Pitfalls and practical limitations of the current AJCC/UICC TNM staging system and opportunities for improvement. *Semin. Diagn Pathol.* 29, 127–141. doi:10.1053/j.semdp.2012.08.010

Alam, H., Tang, M., Maitituoheti, M., Dhar, S. S., Kumar, M., Han, C. Y., et al. (2020). KMT2D deficiency impairs super-enhancers to confer a glycolytic vulnerability in lung cancer. *Cancer Cell* 37, 599–617. doi:10.1016/j.ccell.2020.03.005

Antoni, S., Ferlay, J., Soerjomataram, I., Znaor, A., Jemal, A., and Bray, F. (2017). Bladder cancer incidence and mortality: A global overview and recent trends. *Eur. Urol.* 71, 96–108. doi:10.1016/j.eururo.2016.06.010

Bejarano, L., Jordao, M. J. C., and Joyce, J. A. (2021). Therapeutic targeting of the tumor microenvironment. *Cancer Discov.* 11, 933–959. doi:10.1158/2159-8290.cd-20-1808

Burke, J. D., and Young, H. A. (2019). IFN-Γ: A cytokine at the right time, is in the right place. *Semin. Immunol.* 43, 101280. doi:10.1016/j.smim.2019.05.002

Cao, R., Yuan, L., Ma, B., Wang, G., and Tian, Y. (2021). Tumour microenvironment (TME) characterization identified prognosis and immunotherapy response in muscle-invasive bladder cancer (MIBC). *Cancer Immunol. Immunother.* 70, 1–18. doi:10.1007/s00262-020-02649-x

Chan, T. A., Yarchoan, M., Jaffee, E., Swanton, C., Quezada, S. A., Stenzinger, A., et al. (2019). Development of tumor mutation burden as an immunotherapy biomarker: Utility for the oncology clinic. *Ann. Oncol.* 30, 44–56. doi:10.1093/annonc/mdy495

Dighe, A. S., Richards, E., Old, L. J., and Schreiber, R. D. (1994). Enhanced *in vivo* growth and resistance to rejection of tumor cells expressing dominant negative IFN gamma receptors. *Immunity* 1, 447–456. doi:10.1016/1074-7613(94)90087-6

Donehower, L. A., Soussi, T., Korkut, A., Liu, Y., Schultz, A., Cardenas, M., et al. (2019). Integrated analysis of TP53 gene and pathway alterations in the cancer Genome Atlas. *Cell Rep.* 28, 3010–1384 e5. doi:10.1016/j.celrep.2019.08.061

Frankel, T., Lanfranca, M. P., and Zou, W. (2017). The role of tumor microenvironment in cancer immunotherapy. *Adv. Exp. Med. Biol.* 1036, 51–64. doi:10.1007/978-3-319-67577-0_4

Fridman, W. H., Pages, F., Sautes-Fridman, C., and Galon, J. (2012). The immune contexture in human tumours: Impact on clinical outcome. *Nat. Rev. Cancer* 12, 298–306. doi:10.1038/nrc3245

Gao, J., Shi, L. Z., Zhao, H., Chen, J., Xiong, L., He, Q., et al. (2016). Loss of IFN-gamma pathway genes in tumor cells as a mechanism of resistance to anti-CTLA-4 therapy. *Cell* 167, 397–404. doi:10.1016/j.cell.2016.08.069

Gillezeau, C., Movva, N., van Gerwen, M., Rabon-Stith, K., Shire, N., Brohawn, P. Z., et al. (2022). Interferon gamma expression and mortality in unselected cohorts of urothelial bladder cancer patients. *PLoS One* 17, e0271339. doi:10.1371/journal.pone.0271339

Green, J. L., Osterhout, R. E., Klova, A. L., Merkwirth, C., McDonnell, S. R. P., Zavareh, R. B., et al. (2021). Molecular characterization of type I IFN-induced cytotoxicity in bladder cancer cells reveals biomarkers of resistance. *Mol. Ther. Oncolytics* 23, 547–559. doi:10.1016/j.omto.2021.11.006

Hinshaw, D. C., and Shevde, L. A. (2019). The tumor microenvironment innately modulates cancer progression. *Cancer Res.* 79, 4557–4566. doi:10.1158/0008-5472.CAN-18-3962

Hu, B., Wei, Q., Li, X., Ju, M., Wang, L., Zhou, C., et al. (2020). Development of an IFNγ response-related signature for predicting the survival of cutaneous melanoma. *Cancer Med.* 9, 8186–8201. doi:10.1002/cam4.3438

Hu, J., Yu, A., Othmane, B., Qiu, D., Li, H., Li, C., et al. (2021). Siglec15 shapes a non-inflamed tumor microenvironment and predicts the molecular subtype in bladder cancer. *Theranostics* 11, 3089–3108. doi:10.7150/thno.53649

Jia, L., Shi, Y., Wen, Y., Li, W., Feng, J., and Chen, C. (2018). The roles of TNFAIP2 in cancers and infectious diseases. *J. Cell Mol. Med.* 22, 5188–5195. doi:10.1111/jcmm.13822

Jia, L., Zhou, Z., Liang, H., Wu, J., Shi, P., Li, F., et al. (2016). KLF5 promotes breast cancer proliferation, migration and invasion in part by upregulating the transcription of TNFAIP2. *Oncogene* 35, 2040–2051. doi:10.1038/onc.2015.263

Jorgovanovic, D., Song, M., Wang, L., and Zhang, Y. (2020). Roles of IFN-γ in tumor progression and regression: A review. *Biomark. Res.* 8, 49. doi:10.1186/s40364-020-00228-x

Kandoth, C., McLellan, M. D., Vandin, F., Ye, K., Niu, B., Lu, C., et al. (2013). Mutational landscape and significance across 12 major cancer types. *Nature* 502, 333–339. doi:10.1038/nature12634

Lecker, L. S. M., Berlato, C., Maniati, E., Delaine-Smith, R., Pearce, O. M. T., Heath, O., et al. (2021). TGFBI production by macrophages contributes to an immunosuppressive microenvironment in ovarian cancer. *Cancer Res.* 81, 5706–5719. doi:10.1158/0008-5472.can-21-0536

Lenis, A. T., Lec, P. M., Chamie, K., and Mshs, M. D. (2020). Bladder cancer: A review. *Jama* 324, 1980–1991. doi:10.1001/jama.2020.17598

Li, G., Kawakami, S., Kageyama, Y., Yan, C., Saito, K., and Kihara, K. (2002). IFN gamma-induced up-regulation of PD-ECGF/TP enhances the cytotoxicity of 5-fluorouracil and 5'-deoxy-5-fluorouridine in bladder cancer cells. *Anticancer Res.* 22, 2607–2612.

Lian, J., Yue, Y., Yu, W., and Zhang, Y. (2020). Immunosenescence: A key player in cancer development. *J. Hematol. Oncol.* 13, 151. doi:10.1186/s13045-020-00986-z

Liu, L., Bai, X., Wang, J., Tang, X. R., Wu, D. H., Du, S. S., et al. (2019). Combination of TMB and CNA stratifies prognostic and predictive responses to immunotherapy across metastatic cancer. *Clin. Cancer Res.* 25, 7413–7423. doi:10.1158/1078-0432.CCR-19-0558

Liu, L., Cui, J., Zhao, Y., Liu, X., Chen, L., Xia, Y., et al. (2021). KDM6A-ARHGDIB axis blocks metastasis of bladder cancer by inhibiting Rac1. *Mol. Cancer* 20, 77. doi:10.1186/s12943-021-01369-9

Liu, Z., Qi, T., Li, X., Yao, Y., Othmane, B., Chen, J., et al. (2021). A novel TGF-β risk score predicts the clinical outcomes and tumour microenvironment phenotypes in bladder cancer. *Front. Immunol.* 12, 791924. doi:10.3389/fimmu.2021.791924

Marin-Acevedo, J. A., Kimbrough, E. O., and Lou, Y. (2021). Next generation of immune checkpoint inhibitors and beyond. *J. Hematol. Oncol.* 14, 45. doi:10.1186/s13045-021-01056-8

Martinez Rodriguez, R. H., Buisan Rueda, O., and Ibarz, L. (2017). Bladder cancer: Present and future. *Med. Clin. Barc.* 149, 449–455. doi:10.1016/j.medcli.2017.06.009

Metelli, A., Salem, M., Wallace, C. H., Wu, B. X., Li, A., Li, X., et al. (2018). Immunoregulatory functions and the therapeutic implications of GARP-TGF-β in inflammation and cancer. *J. Hematol. Oncol.* 11, 24. doi:10.1186/s13045-018-0570-z

Niwa, N., Tanaka, N., Hongo, H., Miyazaki, Y., Takamatsu, K., Mizuno, R., et al. (2019). TNFAIP2 expression induces epithelial-to-mesenchymal transition and confers platinum resistance in urothelial cancer cells. *Lab. Invest* 99, 1702–1713. doi:10.1038/s41374-019-0285-y

Patel, V. G., Oh, W. K., and Galsky, M. D. (2020). Treatment of muscle-invasive and advanced bladder cancer in 2020. *CA Cancer J. Clin.* 70, 404–423. doi:10.3322/caac.21631

Petitprez, F., Meylan, M., de Reyniès, A., Sautès-Fridman, C., and Fridman, W. H. (2020). The tumor microenvironment in the response to immune checkpoint blockade therapies. *Front. Immunol.* 11, 784. doi:10.3389/fimmu.2020.00784

Pettenati, C., and Ingersoll, M. A. (2018). Mechanisms of BCG immunotherapy and its outlook for bladder cancer. *Nat. Rev. Urol.* 15, 615–625. doi:10.1038/s41585-018-0055-4

Rosenberg, J. E., Hoffman-Censits, J., Powles, T., van der Heijden, M. S., Balar, A. V., Necchi, A., et al. (2016). Atezolizumab in patients with locally advanced and metastatic urothelial carcinoma who have progressed following treatment with platinum-based chemotherapy: A single-arm, multicentre, phase 2 trial. *Lancet* 387, 1909–1920. doi:10.1016/S0140-6736(16)00561-4

Stifter, K., Krieger, J., Ruths, L., Gout, J., Mulaw, M., Lechel, A., et al. (2020). IFN-γ treatment protocol for MHC-I(lo)/PD-L1(+) pancreatic tumor cells selectively restores their TAP-mediated presentation competence and CD8 T-cell priming potential. *J. Immunother. Cancer* 8, e000692. doi:10.1136/jitc-2020-000692

Sung, H., Ferlay, J., Siegel, R. L., Laversanne, M., Soerjomataram, I., Jemal, A., et al. (2021). Global cancer statistics 2020: GLOBOCAN estimates of incidence and mortality worldwide for 36 cancers in 185 countries. *CA Cancer J. Clin.* 71, 209–249. doi:10.3322/caac.21660

Tabassum, A., Samdani, M. N., Dhali, T. C., Alam, R., Ahammad, F., Samad, A., et al. (2021). Transporter associated with antigen processing 1 (TAP1) expression and prognostic analysis in breast, lung, liver, and ovarian cancer. *J. Mol. Med. Berl.* 99, 1293–1309. doi:10.1007/s00109-021-02088-w

Tokunaga, R., Zhang, W., Naseem, M., Puccini, A., Berger, M. D., Soni, S., et al. (2018). CXCL9, CXCL10, CXCL11/CXCR3 axis for immune activation - a target for novel cancer therapy. *Cancer Treat. Rev.* 63, 40–47. doi:10.1016/j.ctrv.2017.11.007

Wang, Y., Zhang, H., Liu, C., Wang, Z., Wu, W., Zhang, N., et al. (2022). Immune checkpoint modulators in cancer immunotherapy: Recent advances and emerging concepts. *J. Hematol. Oncol.* 15, 111. doi:10.1186/s13045-022-01325-0

Yang, Y., Zhang, J., Chen, Y., Xu, R., Zhao, Q., and Guo, W. (2020). MUC4, MUC16, and TTN genes mutation correlated with prognosis, and predicted tumor mutation burden and immunotherapy efficacy in gastric cancer and pan-cancer. *Clin. Transl. Med.* 10, e155. doi:10.1002/ctm2.155

Zhang, H., Zhang, N., Wu, W., Zhou, R., Li, S., Wang, Z., et al. (2022). Machine learning-based tumor-infiltrating immune cell-associated lncRNAs for predicting prognosis and immunotherapy response in patients with glioblastoma. *Brief. Bioinform* 23, bbac386. doi:10.1093/bib/bbac386

Zhang, J., He, T., Xue, L., and Guo, H. (2021). Senescent T cells: A potential biomarker and target for cancer therapy. *EBioMedicine* 68, 103409. doi:10.1016/j.ebiom.2021.103409

Zhang, N., Zhang, H., Wu, W., Zhou, R., Li, S., Wang, Z., et al. (2022). Machine learning-based identification of tumor-infiltrating immune cell-associated lncRNAs for improving outcomes and immunotherapy responses in patients with low-grade glioma. *Theranostics* 12, 5931–5948. doi:10.7150/thno.74281

frontiers | Frontiers in Genetics

TYPE Original Research
PUBLISHED 05 January 2023
DOI 10.3389/fgene.2022.1082654

OPEN ACCESS

EDITED BY
Jiao Hu,
Xiangya Hospital, Central South University, China

REVIEWED BY
Jian Kang,
Northeastern University, China
Zhixiang Yu,
Fourth Military Medical University, China
Xiaokang Zhang,
Beijing Tiantan Hospital, Capital Medical University, China

*CORRESPONDENCE
Jie Luan,
luanjieplastic@126.com
Su Fu,
doctorsufu@163.com

†These authors have contributed equally to this work and share last authorship

SPECIALTY SECTION
This article was submitted to Cancer Genetics and Oncogenomics, a section of the journal Frontiers in Genetics

RECEIVED 28 October 2022
ACCEPTED 15 December 2022
PUBLISHED 05 January 2023

CITATION
Hou X, Luan J and Fu S (2023), Multi-functional gene ZNF281 identified as a molecular biomarker in soft tissue regeneration and pan-cancer progression. *Front. Genet.* 13:1082654.
doi: 10.3389/fgene.2022.1082654

Multi-functional gene ZNF281 identified as a molecular biomarker in soft tissue regeneration and pan-cancer progression

Xueying Hou, Jie Luan*† and Su Fu*†

Breast Plastic and Reconstructive Surgery Center, Plastic Surgery Hospital, Chinese Academy of Medical Sciences, Peking Union Medical College, Beijing, China

Regeneration and tumorigenesis are indicated as related processes, while regeneration leads to life and the outcome of tumorigenesis is death. Here, we show the upregulation of *zfp281* (zinc finger 281) in our adipose *de novo* regeneration model through RNA-seq analysis. Then, we validated the upregulation of zfp281 in adipose regeneration *via* immunofluorescence. Following that, we found that *ZNF281* (the human homolog of *Zfp281*) was upregulated in most types of cancer and related to worse prognosis in 10 tumors. We further investigated the role of *ZNF281* in cervical squamous cell carcinoma and endocervical adenocarcinoma (CESC), pancreatic adenocarcinoma (PAAD), and stomach adenocarcinoma (STAD) and confirmed the high accuracy in the clinical diagnostic feature. Beyond that, based on these three types of cancers, we analyzed the *ZNF281*-related tumor immune infiltration and DNA methylation sites and finally built risk prediction models for future disease diagnosis. Taken together, our findings provide new insights into the dual role of *ZNF281*, and we found that it was a potential biomarker for regeneration and tumor prognosis.

KEYWORDS

ZNF281, regeneration, tumorigenesis, biomarker, pan-cancer

1 Introduction

Regeneration is characterized by the process of restoring homeostasis when organs sense the signals of damage, and this renewal process is orchestrated by a complex network of gene regulation and cellular processes (Chargé and Rudnicki, 2004; Gurtner et al., 2008; Gray et al., 2018). Like wound healing, regeneration proceeds through several overlying statuses, including inflammation (Eming et al., 2017), tissue reconstruction (Ghuman et al., 2016), and remodeling (Kim et al., 2018). All along the regeneration process, specific signals induce cellular proliferation in a finite number of cells, and finally, termination signals are released to avoid dysregulated proliferation, which causes tumorigenesis. Interestingly, increasing evidence indicates that regeneration and tumorigenesis are regulated by the same molecular pathways, and they may be recognized as related processes (Beachy et al., 2004; Schäfer and Werner, 2008; Cernaro et al., 2012; Jung et al., 2021). Thus, it is intriguing and significant to understand the link between regeneration and tumorigenesis.

ZNF281 (zinc finger protein 281) plays a role in the regulation of embryonic stem cell (ESC) differentiation and is very important in maintaining cellular stemness (An integrated encyclopedia of DNA, 2012; Pieraccioli et al., 2018). Knock-out of ZNF281 induces

multipotent stem cell differentiation to osteogenic lineage (Seo et al., 2013). Moreover, epithelial-to-mesenchymal transition (EMT) is activated by ZNF281 in colon cancer cells through the regulation of SNAI1 and other EMT-related gene expressions (Hahn et al., 2013). We identified transcription factor *zfp28*1, the human homolog of which is *ZNF281*, upregulated in a mice adipose regeneration model through RNA-seq. However, the role of ZNF281 in the regeneration program and tumorigenesis is largely unveiled.

In this study, we present findings that implicate ZNF281 as a promising biomarker in regeneration and multiple cancers. We applied basic fibroblast growth factor (bFGF) *via* controlled release of decellularized cells to induce adipocyte regeneration in C57BL/6N mice, and this model has been proven efficient in inducing adipogenesis (Zhang et al., 2016). In addition to mRNA upregulation of *zfp281*, histological analysis also validated the higher expression of zfp281 in the regeneration group. Furthermore, for a more complex and systematic understanding of *ZNF281* in tumors, the expression level of *ZNF281* was also investigated in pan-cancer and an upregulated phenomenon in most tumors compared to their related normal tissues and adjacent tissues was observed. Next, *ZNF281* expression was found in 10 types of human cancer related to worse prognosis considering overall survival (OS); however, in kidney renal papillary cell carcinoma (KIRP), higher *ZNF281* expression was related to a better prognosis, and this may due to the complexity and heterogeneity in cancer. Then, in three types of cancer, cervical squamous cell carcinoma and endocervical adenocarcinoma (CESC), pancreatic adenocarcinoma (PAAD), and stomach adenocarcinoma (STAD), *ZNF281* was confirmed as a good prognostic molecular marker considering the high accuracy in the clinical diagnostic feature. After that, we applied single-sample Gene Set Enrichment Analysis (ssGSEA) and found a positive relation between *ZNF281* and T-cell activation in these three tumors. Then, we screened DNA methylation sites. The least absolute shrinkage and selection operator (LASS)) builds on linear regression by increasing the penalty term (lambda × absolute slope value) to reduce the overfitting of the model and improve the generalization ability of the model (Zhang et al., 2020). Statistical analysis using the LASSO technique allowed the prediction of cancer with high sensitivity and specificity (Zhang et al., 2017). Finally, we established risk prediction models based on *ZNF281*-related lncRNAs for future disease diagnosis using the LASSO technique. In conclusion, our data focused on the dual role of ZNF281 and showed that it was a potential biomarker for regeneration and might also be functional in the diagnosis and clinical prediction of multiple types of cancer.

2 Materials and methods

2.1 Preparation of decellularized adipose-derived matrix loaded with bFGF

The procedure of decellularizing adipose tissues was accomplished following our previous protocols (Tang et al., 2022). All protocols reported in this study complied with ethical regulations for work with human subjects, and the study protocol was approved by the Plastic Surgery Hospital Ethics Committee (No. ZX 201843). Briefly, human lipoaspirate from healthy women under liposuction was obtained at the Chinese Academy of Medical Sciences & Peking Union Medical College Plastic Surgery Hospital. The mixture was allowed to stand for 10–15 min; then, the upper oil and lower bloody fluids were removed. After several cycles of washing in distilled water, three freeze–thaw cycles (−80°C–37°C, 2 h each) were performed. Then, the samples were homogenized using the A11 Basic Analytical Mill (IKA, Germany) three times (28,000 rpm, 1 min each). Followed by centrifugation and removal of oil, the milky suspension was agitated in hypotonic (0.5 M NaCl, 4 h) and hypertonic solutions (1 M NaCl, 4 h). After overnight washing in distilled water, samples were soaked in 1% Triton X-100 solution, and the solution was changed three times a day for 48 h. The white floc-like precipitate was washed again in distilled water (30 min, three times), and then, 99.9% isopropanol was used for further lipid removal. After the final three repeated cycles of washing with distilled water (30 min each) and three times of agitation in 70% ethanol (30 min each) for disinfection, DAM was placed in phosphate-buffered saline (PBS) (HyClone) containing 1% penicillin–streptomycin (HyClone) at 4°C for storage.

In this study, we applied heparin cross-linking of DAM for the loading of bFGF following the previously described methods (Wissink et al., 2001; Zhang et al., 2016), the sustained releasing bFGF of which was <70% of the loaded bFGF over a period of 10 days. For loading bFGF, 250 mg wet weight DAM was mixed in 500 μL normal saline containing 2 μg/ml bFGF, and DAM was scissor-minced thoroughly. The bFGF dose has been reported as the optimal concentration for inducing adipose *in situ* regeneration (Hiraoka et al., 2006).

2.2 *In vivo* experiments

All animal model studies were approved in advance by the Animal Ethics Committee at the Chinese Academy of Medical Sciences & Peking Union Medical College and performed following the Animal Ethics Committee's guidelines. Female eight-week-old C57BL/6 N mice were used for injecting the bFGF-loaded DAM mixture. As a control group, heparinized DAM mixed with PBS was used. The volume of suspension was 200 μL per site of injection ($n \geq 5$ for each group). The animals were sacrificed at 1, 2, 3, and 12 weeks, and the samples were obtained for RNA-seq and histological analysis.

2.3 mRNA-Seq assay

Total RNA extracts were acquired from implanted mouse tissues of bFGF-loaded DAM and DAM at 1 week using the MagBeads Total RNA Extraction Kit (Cat#T02-096) according to the manufacturer's instructions, and RNA integrity was checked with the RNA integrity number (RIN) by using a bioanalyzer (Agilent Technologies, US). RNA purification was performed by using the RNAClean XP kit (Cat A63987, USA) and RNase-Free DNase Set (Cat#79254, QIAGEN, Germany). After the quality control of RNA, the sequencing libraries were constructed. After library inspection using the Qubit fluorometer and Agilent 4200, the libraries were sequenced with the Illumina NovaSeq 6,000 sequencing platform, and the PE150 mode was selected. All the data were analyzed in R 3.6.4, and the R package DESeq2 was used for differential expression significance analysis. For filtrating differential expressed genes, the absolute value of log2(fold change) was selected above 2, and the p value was less than 0.05.

2.4 Histological analysis and immunofluorescence staining

After 24–48 h fixation (4% formalin), the samples retrieved from the animals were dehydrated and embedded in paraffin (Leica) for routine sectioning. The sections underwent deparaffinization and rehydration, and then, antigen retrieval was processed in a microwave in citric acid (Solarbio). After washing with PBS, slides were blocked with 5% goat serum for half an hour at 37°C, and overnight incubation with the primary antibody at 4°C was performed. Secondary immunofluorescent-tagged antibodies were used to incubate slides for 1 hour at 37°C for signal amplification. The following antibodies were used for immunofluorescence: mouse monoclonal IgG2a κ ZNF281 antibody (1:100, Cat. No. sc-166933, Santa Cruz), rabbit polyclonal perilipin-1 antibody (1:100, Cat. No. ab3526, Abcam), CoraLite 488-conjugated goat anti-rabbit IgG (H + L) (1:100, Cat. No. SA00013-2, Proteintech), and CoraLite 594-conjugated goat anti-mouse IgG (H + L) (1:100, Cat.No. SA00013-3, Proteintech). The nuclei were stained with DAPI (Invitrogen). Single-channel and merge images were generated in Photoshop.

2.5 Analysis of *ZNF281* expression in normal tissues and pan-cancer

The mRNA expression level of *ZNF281* in normal tissues was analyzed in the Human Protein Atlas (HPA) online platform (https://www.proteinatlas.org/) (Sjöstedt et al., 2020; Karlsson et al., 2021). Based on the HPA RNA-seq data and scRNA-seq data, we displayed the tissue/cell distribution of *ZNF281*, especially in normal adipose tissues. The data of RNA-seq and related clinical information were acquired from The Cancer Genome Atlas (TCGA) and the Genotype-Tissue Expression (GTEx) database using USCS Xena (http://xena.ucsc.edu/) on 16 August 2022 (Vivian et al., 2017). The data of cancer involves adrenal cortical carcinoma (ACC), bladder urothelial carcinoma (BLCA), breast-invasive carcinoma (BRCA), CESC, cholangiocarcinoma (CHOL), colon adenocarcinoma (COAD), lymphoid neoplasm diffuse large B-cell lymphoma (DLBC), esophageal carcinoma (ESCA), glioblastoma multiforme (GBM), head and neck squamous cell carcinoma (HNSC), kidney chromophobe (KICH), kidney renal clear cell carcinoma (KIRC), KIRP, acute myeloid leukemia (LAML), brain lower grade glioma (LGG), liver hepatocellular carcinoma (LIHC), lung adenocarcinoma (LUAD), lung squamous cell carcinoma (LUSC), ovarian serous cystadenocarcinoma (OV), PAAD, pheochromocytoma and paraganglioma (PCPG), prostate adenocarcinoma (PRAD), rectum adenocarcinoma (READ), skin cutaneous melanoma (SKCM), STAD, testicular germ cell tumors (TGCT), thyroid carcinoma (THCA), thymoma (THYM), uterine corpus endometrial carcinoma (UCEC), and uterine carcinosarcoma (UCS). All the data were analyzed in R 3.6.4, and the visualization was completed with the R package ggplot2. The statistical method used was the Mann–Whitney *U* test, and when $p < 0.05$, the difference was considered to reach statistical significance.

2.6 Survival analysis

The survival curve (also known as the Kaplan–Meier curve) can describe the survival of each group of patients. Based on the median expression of *ZNF281* or model risk scores, patients could be subdivided into the high-expression group and the low-expression group. The survminer R package was used for visualization, and the survival R package was used for the statistical analysis of survival data. OS was set as the survival outcome.

2.7 Receiver operating characteristic curve

The receiver operating characteristic (ROC) curve is a comprehensive index reflecting the sensitivity and specificity of continuous variables, and the composition method reflects the correlation between sensitivity and specificity. When the expression of a molecule is a trend to promote the occurrence of events, the area under the curve (AUC) of this molecule will be >0.5, and the closer the AUC approaches 1, the better the prediction performance. When the expression of a molecule is contrary to the trend of event occurrence, the molecule will be <0.5, and the closer the AUC is to 0, the more accurate the prediction performs. In brief, the point closest to the top left of the curve is the critical value with the highest sensitivity and specificity on the ROC curve. The larger the area under the curve, the higher the diagnostic accuracy. The R package pROC was used in the ROC analysis, and the ggplot2 R package was applied to visualize results (Robin et al., 2011). The expression level of *ZNF281* was used as the input in ROC analysis in 30 types of cancer. To proceed with further analysis, we selected tumors for which *ZNF281* might be recognized as a risk factor based on differential analysis, OS, ROC, and AUC; then, CESC, PAAD, and STAD were selected.

2.8 Single-sample Gene Set Enrichment Analysis

As an extension of Gene Set Enrichment Analysis (GSEA), single-sample Gene Set Enrichment Analysis calculates separate enrichment scores for each pairing of a sample and gene set. Gene markers for 24 immune cells were obtained from an article, and the classification and description of specific cells are shown in Bindea et al. (2013). Then, the procedures of ssGSEA were performed by the R package GSVA (version: 1.34.0) (Hänzelmann et al., 2013). Then, the relationship between the ssGSEA scores of 24 immune cells and *ZNF281* expression in CESC, PAAD, and STAD was calculated by Spearman correlation analysis.

2.9 *ZNF281*-associated DNA methylation sites

The correlation between the beta value of methylation sites within 5000bp upstream and downstream of the transcription start site (TSS) and the expression level of *ZNF281* was calculated. Spearman correlation analysis was included. The stat R package was used. DNA methylation sites with *p* value less than 0.05 and Spearman correlation coefficient greater than 0.3 were selected.

2.10 Screening *ZNF281*-related genes

In CESC, PAAD, and STAD, we investigated the correlation between other genes and *ZNF281* expression *via* Spearman and Pearson correlation analyses. To find genes with statistical

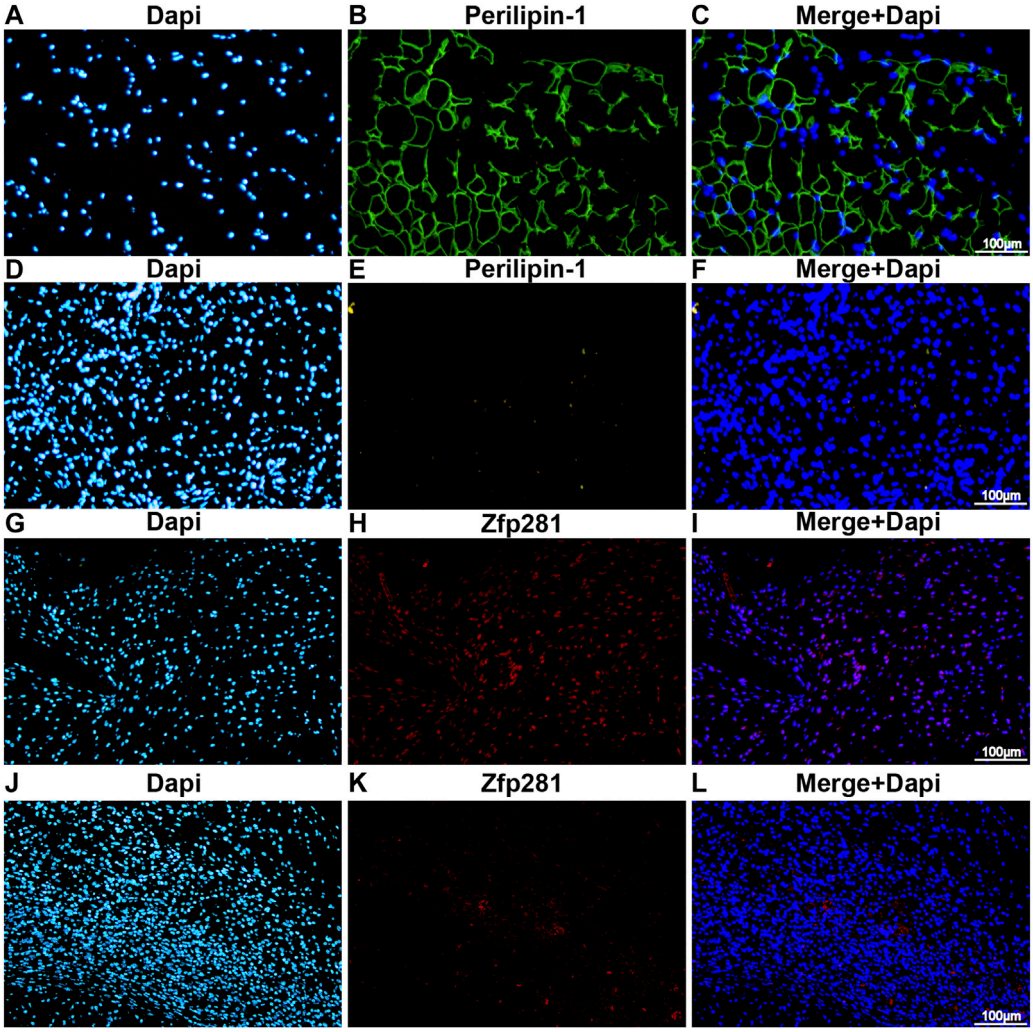

FIGURE 1
Zfp281 is upregulated at an early stage in adipose *de novo* regeneration tissues. **(A–F)** Immunofluorescence staining of perilipin-1 in bFGF-loaded DAM **(A–C)** and DAM-injected mouse tissuees **(D–F)** at 12 weeks; **(G–L)** immunofluorescence staining of zfp281 in bFGF-loaded DAM **(G–I)** and DAM-injected mouse tissues **(J–L)** at 1 week. Perilippin-1 is labeled in green. Zfp281 is Labeled in red. Nuclei are labeled with DAPI in blue.

significance, *P* (Spearman) and *p* (Pearson) less than 0.05 were selected as the basic screening rule. Genes with correlation coefficient (Cor) more than 0.55 or less than −0.55 for both Spearman and Pearson analyses in CESC and STAD were screened. For PAAD, the absolute value of Cor (Spearman) was filtered over 0.7 and the absolute value of Cor (Pearson) was filtered over 0.6. This procedure was achieved *via* the stat R package.

2.11 Least absolute shrinkage and selection operator

The expression of *ZNF281*-related genes was selected as the input in LASSO. In the process of ten-fold cross validation, the seed number was set as 2021. The screening threshold of the model coefficients was selected as lambda. min. According to the selected genes by LASSO, we built the risk models in CESC, PAAD, and STAD. Also, the LASSO coefficients were used to calculate the risk scores with the expression of genes in models. The glmnet and survival R packages were used.

2.12 Time-dependent receiver operating characteristic curve

Time-dependent receiver operating characteristic (tdROC) curve analysis was mainly used to analyze the predictive efficacy of one continuous variable in predicting outcomes related to time. The tdROC was used to complete the analysis, and ggplot2 was used to visualize the results. Also, the tdROC results of the expression of *ZNF281* at 1, 3, and 5 years were calculated.

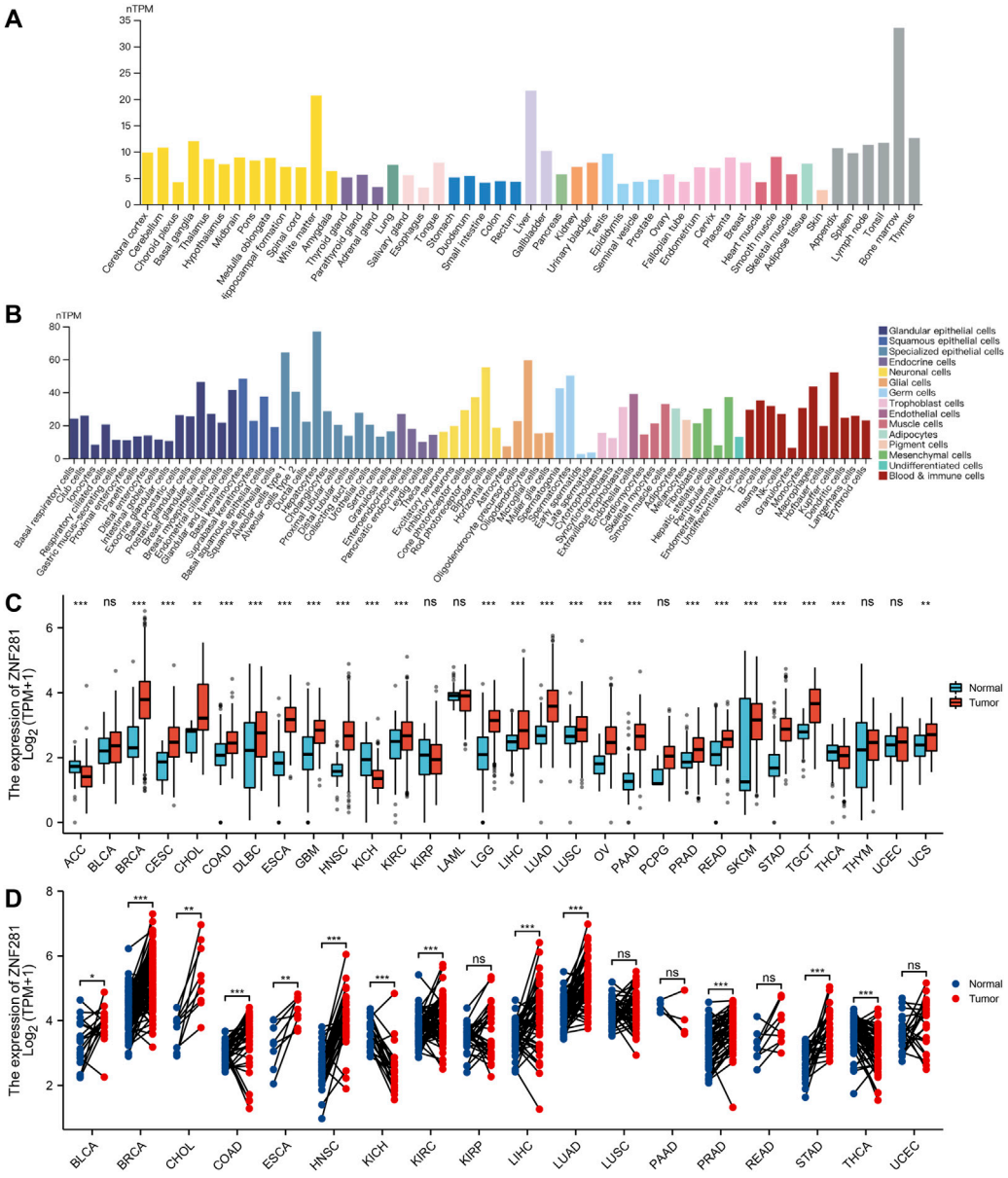

FIGURE 2
Expression levels of *ZNF281* were higher in tumors and normal tissues. **(A)** *ZNF281* expression in normal tissues, **(B)** *ZNF281* expression in single-cell types, **(C)** *ZNF281* expression was upregulated in most types of cancers than normal tissues, combining the data of TCGA and the GTEx database, and **(D)** *ZNF281* expression in TCGA tumors and adjacent normal tissues (*$p < 0.05$, **$p < 0.01$, and ***$p < 0.001$).

3 Results

3.1 New adipose formation and concomitant *zfp281* expression upregulated at an early stage

The differential gene expression of RNA-seq is displayed in Supplementary Figure S1A, and a significant fold difference in *zfp281* is shown between the two groups. Compared to the control group (Figures 1D–F), samples derived from bFGF-loaded DAM (Figures 1A–C) showed a significant adipose regeneration phenomenon. Moreover, zfp281 expression in the early stage (1 week) was validated higher in the bFGF-loaded DAM group (Figures 1G–L).

3.2 Gene expression in normal tissues and pan-cancer

As shown in Figures 2A, B, we found *ZNF281* was highly expressed in the bone marrow, followed by the liver and white matter. Moreover, the cell type that expressed the highest level of *ZNF281* is hepatocytes. In adipose tissues (Supplementary Figure S2B), a cluster of macrophages express the highest amount of *ZNF281* mRNA. We compared *ZNF281* expression levels across 30 types of tumors and relevant normal tissues. In most types of cancers, *ZNF281* was expressed significantly higher in tumors (Figures 2C, D). However, *ZNF281* was less expressed in three types of tumors compared to corresponding normal tissues, including ACC, KICH, and THCA. By integrating data from the GTEx database,

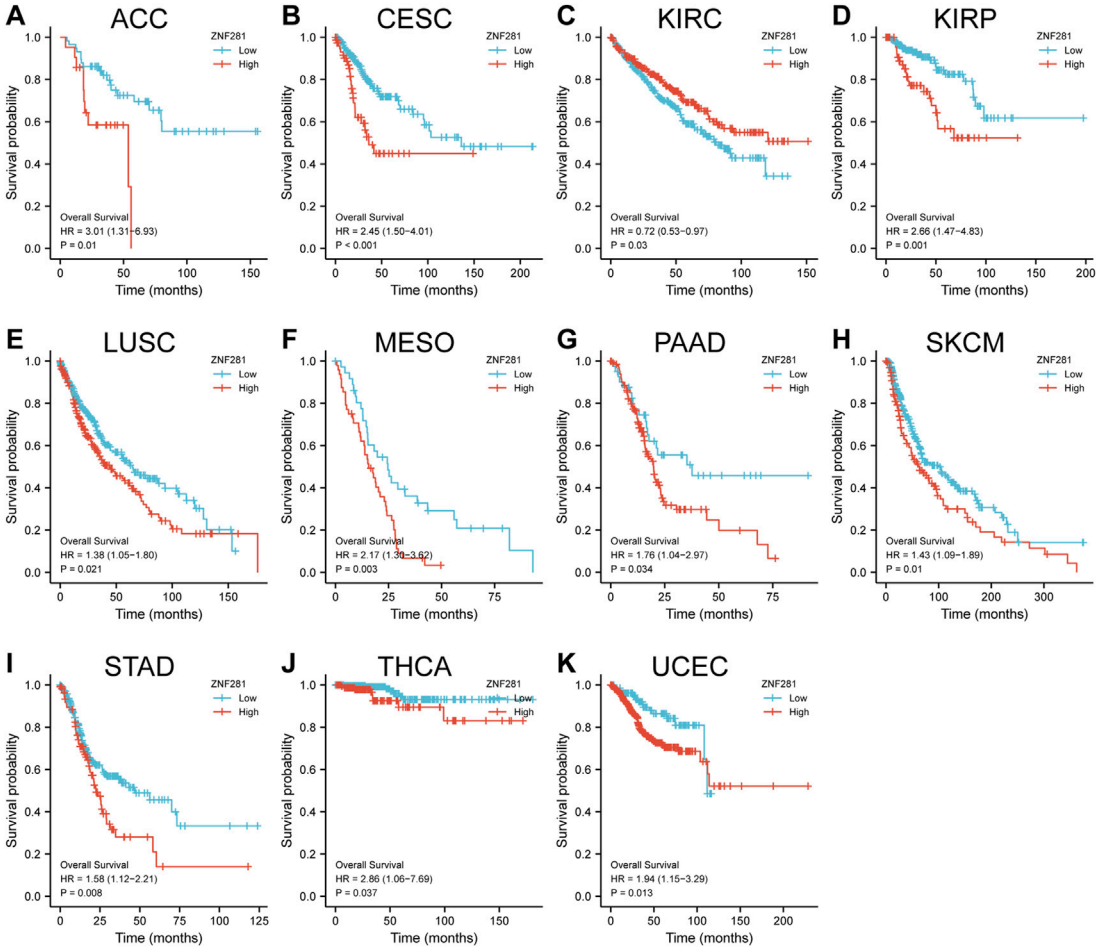

FIGURE 3
Correlations between the *ZNF281* expression and prognosis (OS) of patients in different cancers. **(A)** ACC, **(B)** CESC, **(C)** KIRC, **(D)** KIRP, **(E)** LUSC, **(F)** MESO, **(G)** PAAD, **(H)** SKCM, **(I)** STAD, **(J)** THCA, and **(K)** UCEC.

we compared the *ZNF281* expression levels in cancer and their normal adjacent tissues, and *ZNF281* was significantly expressed higher in 11 cancer types, including BLCA, BRCA, CHOL, COAD, ESCA, HNSC, KIRC, LIHC, LUAD, PRAD, and STAD. Meanwhile, in KICH and THCA, *ZNF281* was downregulated in cancer.

3.3 Higher expression of *ZNF281* in a variety of tumors suggests a poorer prognosis

According to the results of survival analyses (Figure 3), patients with *ZNF281* expression above the median value had worse OS in ACC ($p = 0.01$, HR = 3.01), CESC ($p < 0.001$, HR = 2.45), KIRP ($p = 0.001$, HR = 2.66), LUSC ($p = 0.021$, HR = 1.38), MESO ($p = 0.003$, HR = 2.17), PAAD ($p = 0.034$, HR = 1.76), SKCM ($p = 0.01$, HR = 1.43), STAD ($p = 0.008$, HR = 1.58), THCA ($p = 0.037$, HR = 2.86), and UCEC ($p = 0.013$, HR = 1.94). However, patients with lower *ZNF281* expression levels based on the median value showed the worst prognosis in KIRC ($p = 0.03$, HR = 0.72). However, in the other types of cancer, *ZNF281* was not related to prognosis, and the results are shown in Supplementary Figure S2.

3.4 *ZNF281* has good diagnostic efficacy in CESC, STAD, and PAAD

According to ROC analysis, *ZNF281* showed a good diagnostic ability in differentiating tumors from benign tissues in CESC (Figure 4A, AUC = 0.794), STAD (Figure 4B, AUC = 0.946), and PAAD (Figure 4C, AUC = 0.917). The ROC analysis in the other types of tumors is shown in Supplementary Figure S3.

3.5 ZNF281 is mainly related to the activation of the T-cell family

As shown in Figure 4D, *ZNF281* was positively correlated to the levels of Th2 cells, eosinophils, T gamma delta cells, T effector memory cells, and T helper cells in CESC. Also, according to Figure 4E, more expressions of *ZNF281* indicated more levels of neutrophils, T helper cells, Th1 cells, macrophages, and Th2 cells in PAAD. In STAD (Figure 4F), the levels of *ZNF281* were associated with the content of T central memory cells, macrophages, T helper cells, Th1 cells, and T effector memory cells.

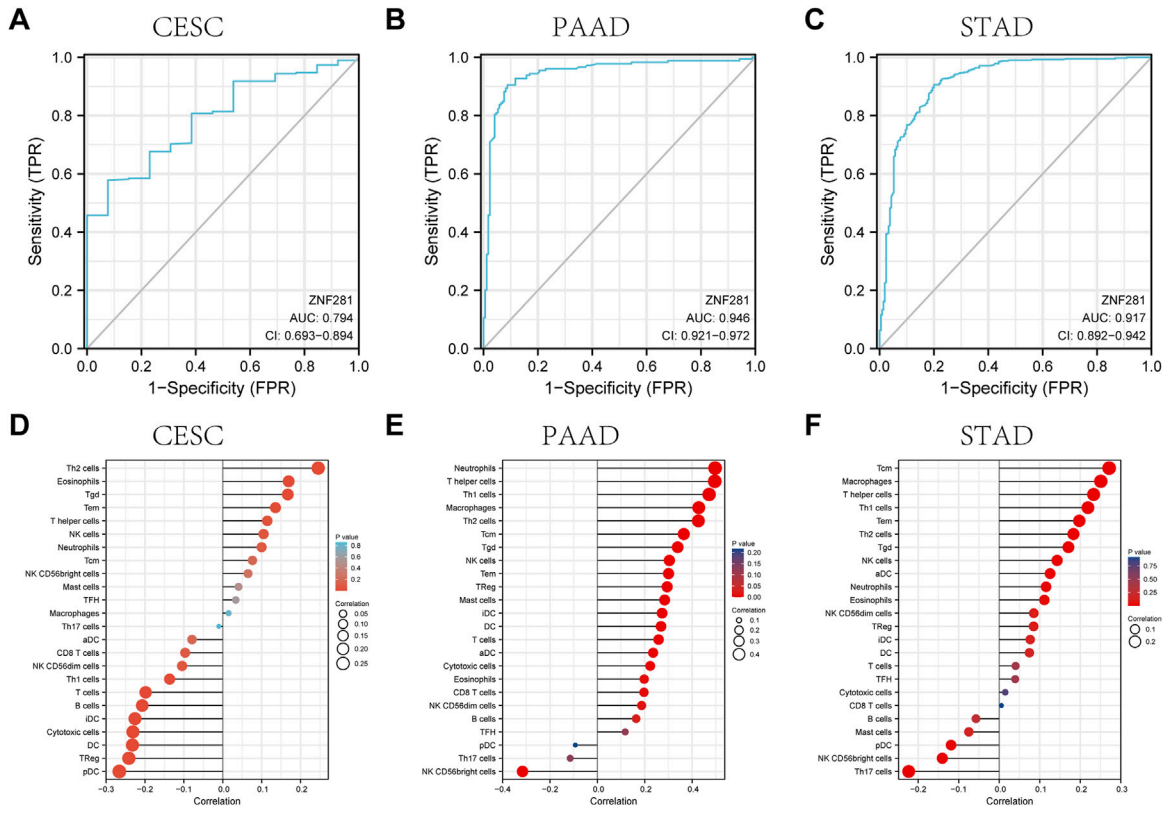

FIGURE 4
ROC curve and the relationship with immune cell infiltration for *ZNF281* in CESC, PAAD, and STAD. **(A)** ROC curve for *ZNF281* in CESC, **(B)** ROC curve for *ZNF281* in PAAD, and **(C)** ROC curve for ZNF281 in STAD. **(D)** Immune infiltration analysis for *ZNF281* in CESC, **(E)** immune infiltration analysis for *ZNF281* in PAAD, and **(F)** immune infiltration analysis for *ZNF281* in STAD.

3.6 Two DNA methylation sites in the TSS region of *ZNF281* may regulate its transcription activity in PAAD

Methylation is mainly carried out through DNA methyltransferase to add methyl groups to DNA and to affect the DNA transcription process without changing the DNA sequence. Based on the screening conditions of $p < 0.05$ and Spearman correlation coefficient >0.3, two DNA methylation sites (cg03559467: correlation coefficient = −0.303, $p < 0.001$ and cg25841477: correlation coefficient = −0.334, $p < 0.001$) might be related to the transcription of *ZNF281* in PAAD (Figures 5E, G). However, the transcriptional regulation of *ZNF281* did not seem to be related to DNA methylation in STAD and CESC (Figure 5).

3.7 Three lncRNA prognostic models based on ZNF281-correlated genes were constructed in CESC, PAAD, and STAD

We screened 129 lncRNA coding genes in CESC (Supplementary Table S1), 63 lncRNA coding genes in PAAD (Supplementary Table S2), and 41 lncRNA coding genes in STAD (Supplementary Table S3) associated with the *ZNF281* level. The expression of these selected lncRNA coding genes was used as the input to train the prognostic models in CESC, PAAD, and STAD. As shown in Figures 6A–C, each point in the figure represented the mean value of likelihood deviation corresponding to each lambda in the process of cross validation, and the error line represents the corresponding error situation. In general, a smaller likelihood deviation value corresponds to a better model, which corresponds to the lambda. min value. According to the lambda. min value, genes in the final models were selected and their coefficients are shown in Figures 6D–F. The risk score can be calculated as follows: CESC: risk score = BOLA3-AS1 × 0.048 + AC139887.2 × 0.024 + NADK2-AS1 × 0.081 + NKILA × 0.130 + LINC01719 × 0.417 + AC022784.5 × 0.068 + AP001094.2 × 0.103 + AL365436.2 × 0.083; PAAD: risk score = AC099850.3 × 0.139 + AP003119.3 × 0.133 + AC112721.2 × 0.129 + AC073046.1 × 0.032—HCG18 × 0.073; and STAD: risk score = ERICD × 0.573 + AC105036.3 × 0.272 + ZNF8-ERVK3-1 × 0.226 + NKILA × 0.166 + PTOV1-AS1×0.132 + AC005332.6 × 0.124 + AP000759.1 × 0.114 + STARD4-AS1 × 0.070 + LINC00205 × 0.019—AC092171.2 × 0.013—AC107068.1 × 0.276—AL355574 × 0.288—LINC00630 × 0.367. The higher risk score is related to a worse prognosis. As shown in Figures 6G–I, patients with higher risk scores presented worse OS in CESC ($p < 0.001$, HR = 2.79), PAAD ($p < 0.001$, HR = 2.23), and STAD ($p < 0.001$, HR = 2.19). Furthermore, these three lncRNA prognostic models for CESC, PAAD, and STAD exhibited good predictive ability for PFI at 1, 3, and 5 years (Figures 6J–L).

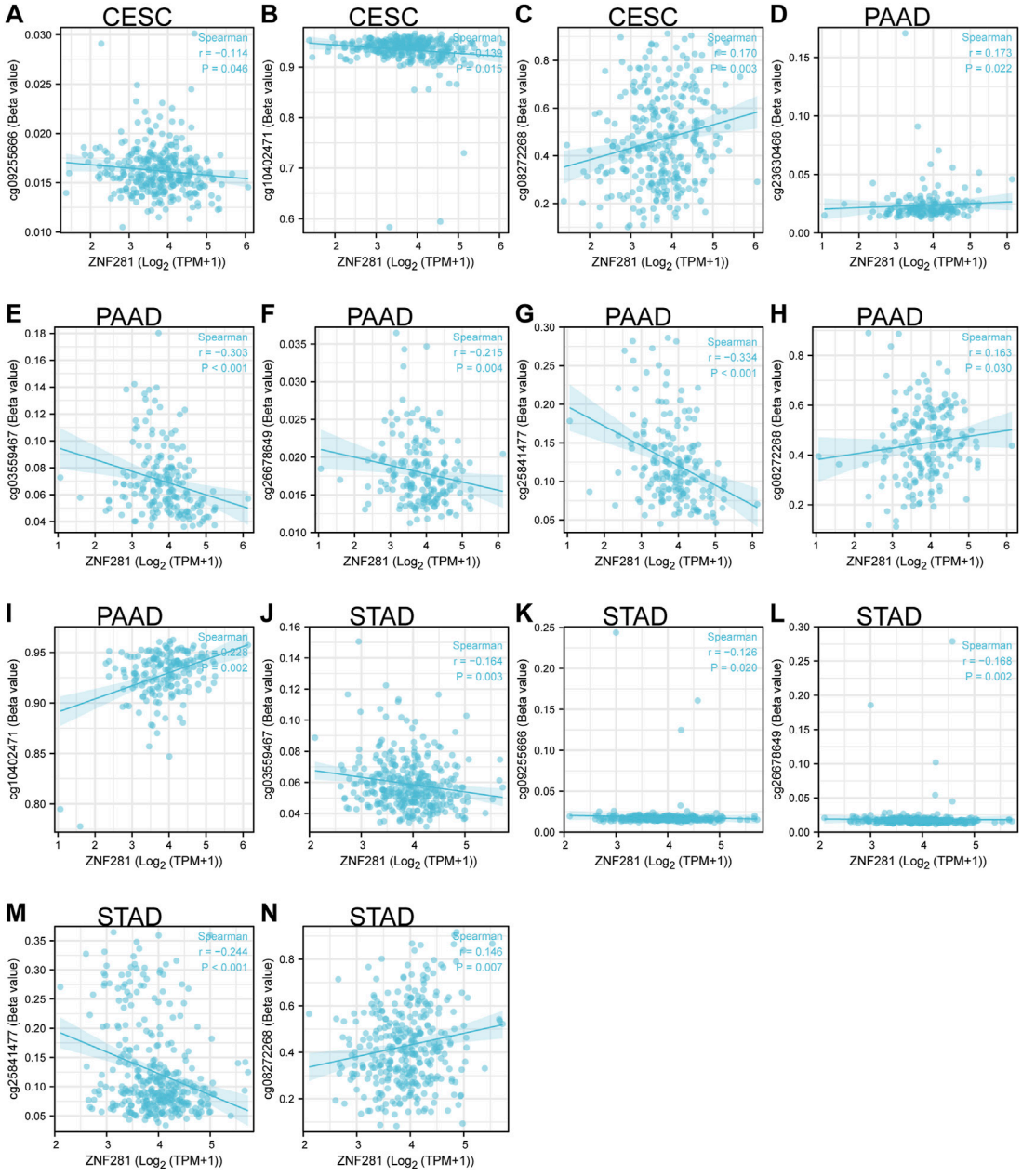

FIGURE 5
ZNF281-associated DNA methylation sites in CESC, PAAD, and STAD. **(A–C)** Methylation sites in the TSS region of *ZNF281* in CESC, **(D–I)** methylation sites in the TSS region of *ZNF281* in CESC, and **(J–N)** methylation sites in the TSS region of *ZNF281* in CESC.

4 Discussion

We hypothesized that ZNF281 (zfp281 in *Mus musculus*) would be a potential biomarker in some forms of regeneration and tumorigenesis, which share similar molecular pathways. We first detected the upregulation of *zfp281* in *de novo* adipogenesis through RNA-seq and then validated the histological expression in the early stage of the adipose regeneration model. Through literature review, we found that ZNF281 was related to the tumor development and progression mechanism, such as EMT (Hahn et al., 2013; Pierdomenico et al., 2018; Sadłecki et al., 2019; Xue et al., 2019). Considering the heterogeneity and complexity of tumors, we analyzed the *ZNF281* expression in pan-cancer and related normal tissues using RNA-seq data from TCGA and GTEx and found the upregulation of *ZNF281* in most types of cancer. Moreover, the *ZNF281* expression level was related to worse prognosis in 10 types of cancer. However, in KIRC, higher expression of *ZNF281* was expected to have survival benefits given the OS analysis. Further investigation indicated *ZNF281* had good prognostic value in CESC, PAAD, and STAD. Also, certain types of T-cell activation were positively correlated to the *ZNF281* expression. In addition, we explored two DNA methylation sites in the TSS region of *ZNF281* that may regulate its transcription activity in PAAD and could be targeted when treating PAAD. Finally, we

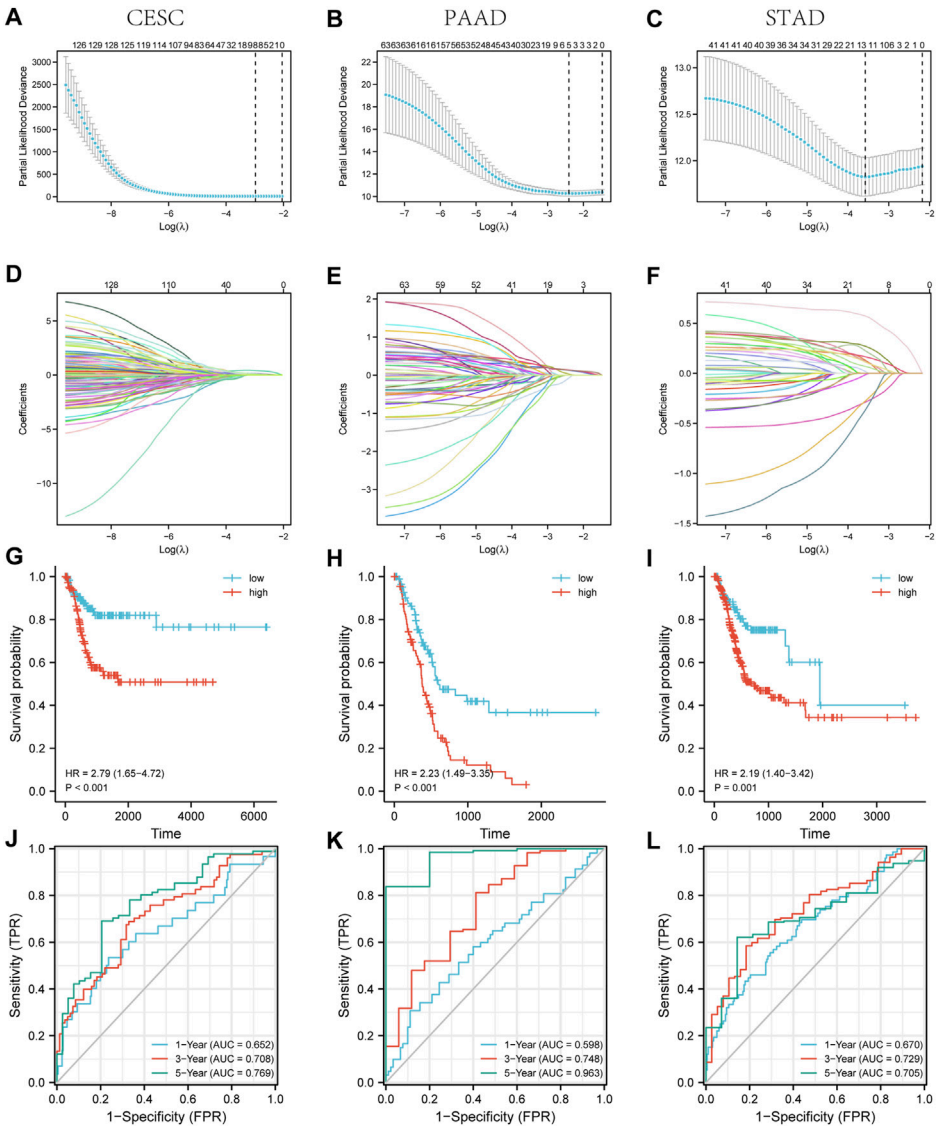

FIGURE 6
Three lncRNA prognostic models associated with *ZNF281* showed good accuracy in predicting the prognosis of patients in CESC, PAAD, and STAD. **(A–C)** Cross validation based on C-index to determine the best choice of genes in the prediction models. **(D–F)** Genes in the different choices of models and their corresponding coefficients based on different lambda values. **(G–I)** According to prediction models, the relationship between the survival outcome and risk levels of patients. **(J–L)** The tdROC curve of 1, 3, and 5 years verified the efficacy of prediction models. **(A,D,G,J)** CESC, **(B,E,H,K)** PAAD, and **(C,F,I,L)** STAD.

established clinical prognostic models based on *ZNF281*-related lncRNA in CESC, PAAD, and STAD.

ZNF281 has also shown its role in regeneration regulation. Zhou et al. (2017) found ZNF281 enhances cardiac reprogramming and upregulation of ZNF281 significantly activated genes related to myogenesis, muscle contraction, and heart processes. As a strong activator in cardiac reprogramming, ZNF281 promotes cardiac regeneration by working on GATA4, which represents an important cardiogenic transcription factor (Lalit et al., 2017; Stone et al., 2019), and works against inflammatory reactions, which inhibits cardiac reprogramming. Here, we hypothesized three possible explanations for elevated zfp281 at the early stages of adipose regeneration. First, that might be the result of environmental response to regeneration signals, which promotes cell proliferation and migration. A mesenchymal-like program as negative feedback is exerted by the environment to keep homeostasis, and then, the expression of zfp281 might be upregulated (Kciuk et al., 2022; Nobre et al., 2022). Second, ZNF281 might promote regeneration by activating EMT-related pathways (Hahn et al., 2013). EMT is divided into three different subtypes: type-1 EMT, type-2 EMT, and type-3 EMT. Type-2 EMT is correlated to the wound healing process, tissue regeneration, and organ fibrosis (Oh et al., 2018; Aharonov et al., 2020; Klatt Shaw et al., 2021; Marconi et al., 2021). Activation of EMT has been linked to the acquisition of both normal and neoplastic stem cells, which might lead to regeneration and carcinogenesis, respectively (Lambert and Weinberg, 2021). Finally, ZNF281 has been recognized as a direct participant in DNA damage response and repair (DRR), and the

upregulation of DDR-related molecules reduces tumor immunogenicity and then causes neoplastic cells to escape from the immune system (Nicolai et al., 2020a). A similar mechanism may also exist in regenerating cells.

ZNF281 inhibits the differentiation of neurons, and higher expression was proven related to a worse prognosis in neuroblastoma (Pieraccioli et al., 2018). Moreover, ZNF281 is mainly expressed in poorly differentiated cells and tissues, and accompanying differentiating process, the expression level of ZNF281 was downregulated. Nicolai et al. (2020b) proposed that ZNF281 directly inhibits muscle differentiation promoted by microRNA-1. Furthermore, they validated the higher expression of ZNF281 in certain types of soft-tissue sarcoma, such as rhabdomyosarcoma and leiomyosarcoma tumors. In our research, we found that ZNF281 was expressed higher in most tumors than in the corresponding normal tissues. Moreover, reduced survival expectations were observed in high ZNF281 cancer. These findings can also be explained by EMT and DDR mechanisms, which are related to metastasis and immune escape of tumors. Beyond that, we validated the good prognostic value of ZNF281 in CESC, STAD, and PAAD and finally established risk prediction models based on ZNF281-related molecules for future clinical diagnosis and treatment.

Sharing common molecular pathways, more and more evidence indicates that regeneration and carcinogenesis are related processes, although accompanying diverse outcomes are life and death (Ewerbeck et al., 1985; Sarig and Tzahor, 2017). In this context, the activity of ZNF281 might be recognized as a potential biomarker for regeneration and cancer. However, there are still some limitations. First, the risk model does not apply an external database to verify its effectiveness. Second, extensive further work is required to understand the mechanism that how ZNF281 is regulated in the specific regeneration-promoted environment and how ZNF281, in turn, regulates regeneration. Further interactions between regeneration and tumorigenesis should also be uncovered in future scientific research. Moreover, in this study, we utilized shallow machine learning to build the risk model other than deep learning, which is more flexible.

Data availability statement

The datasets presented in this study can be found in online repositories. The names of the repository/repositories and accession number(s) can be found in the article/Supplementary Material.

Ethics statement

The studies involving human participants were reviewed and approved by the Plastic Surgery Hospital Ethics Committee. The patients/participants provided their written informed consent to participate in this study. The animal study was reviewed and approved by the Plastic Surgery Hospital Ethics Committee.

Author contributions

JL and SF conceptualized and designed the study. XH performed the experimental studies and analyzed the data in consultation with SF. XH wrote the manuscript with editorial feedback provided by JL and SF.

Funding

This work was supported by the CAMS Innovation Fund for Medical Sciences (2021-2M-1-052) and the Key projects of medical school development of Shijingshan district (20078).

Conflict of interest

The authors declare that the research was conducted in the absence of any commercial or financial relationships that could be construed as a potential conflict of interest.

Publisher's note

Supplementary material

The Supplementary Material for this article can be found online at: https://www.frontiersin.org/articles/10.3389/fgene.2022.1082654/full#supplementary-material

References

Aharonov, A., Shakked, A., Umansky, K. B., Savidor, A., Genzelinakh, A., Kain, D., et al. (2020). ERBB2 drives YAP activation and EMT-like processes during cardiac regeneration. *Nat. Cell Biol.* 22 (11), 1346–1356. Epub 2020/10/14PubMed PMID: 33046882. doi:10.1038/s41556-020-00588-4

An integrated encyclopedia of DNA (2012). An integrated encyclopedia of DNA elements in the human genome. *Nature* 489 (7414), 57–74. doi:10.1038/nature11247

Beachy, P. A., Karhadkar, S. S., and Berman, D. M. (2004). Tissue repair and stem cell renewal in carcinogenesis. *Nature* 432 (7015), 324–331. Epub 2004/11/19PubMed PMID: 15549094. doi:10.1038/nature03100

Bindea, G., Mlecnik, B., Tosolini, M., Kirilovsky, A., Waldner, M., Obenauf, A. C., et al. (2013). Spatiotemporal dynamics of intratumoral immune cells reveal the immune landscape in human cancer. *Immunity* 39 (4), 782–795. Epub 2013/10/22PubMed PMID: 24138885. doi:10.1016/j.immuni.2013.10.003

Cernaro, V., Lacquaniti, A., Donato, V., Fazio, M. R., Buemi, A., and Buemi, M. (2012). Fibrosis, regeneration and cancer: What is the link? *Nephrol. Dial. Transpl.* 27 (1), 21–27. Epub 2011/11/22PubMed PMID: 22102616. doi:10.1093/ndt/gfr567

Chargé, S. B., and Rudnicki, M. A. (2004). Cellular and molecular regulation of muscle regeneration. *Physiol. Rev.* 84 (1), 209–238. Epub 2004/01/13PubMed PMID: 14715915. doi:10.1152/physrev.00019.2003

Eming, S. A., Wynn, T. A., and Martin, P. (2017). Inflammation and metabolism in tissue repair and regeneration. *Science* 356 (6342), 1026–1030. Epub 2017/06/10PubMed PMID: 28596335. doi:10.1126/science.aam7928

Ewerbeck, V., Bolkenius, M., Braun, A., and Brandeis, W. E. (1985). Bone tumors and tumor-like changes in the neonatal period and in infancy. *Z Orthop. Ihre Grenzgeb* 123 (6), 918–928. Epub 1985/11/01PubMed PMID: 3832678. doi:10.1055/s-2008-1044780

Ghuman, H., Massensini, A. R., Donnelly, J., Kim, S. M., Medberry, C. J., Badylak, S. F., et al. (2016). ECM hydrogel for the treatment of stroke: Characterization of the host cell infiltrate. *Biomaterials* 91, 166–181. Epub 2016/04/01PubMed PMID: 27031811; PubMed Central PMCID: PMCPMC4893791. doi:10.1016/j.biomaterials.2016.03.014

Gray, N., Le Bot, N., and Heemels, M. T. (2018). Regeneration. *Nature* 557 (7705), 321. Epub 2018/05/17PubMed PMID: 29765125. doi:10.1038/d41586-018-05155-4

Gurtner, G. C., Werner, S., Barrandon, Y., and Longaker, M. T. (2008). Wound repair and regeneration. *Nature* 453 (7193), 314–321. Epub 2008/05/16PubMed PMID: 18480812. doi:10.1038/nature07039

Hahn, S., Jackstadt, R., Siemens, H., Hünten, S., and Hermeking, H. (2013). SNAIL and miR-34a feed-forward regulation of ZNF281/ZBP99 promotes epithelial-mesenchymal transition. *Embo J.* 32 (23), 3079–3095. Epub 2013/11/05PubMed PMID: 24185900; PubMed Central PMCID: PMCPMC3844956. doi:10.1038/emboj.2013.236

Hänzelmann, S., Castelo, R., and Guinney, J. (2013). Gsva: Gene set variation analysis for microarray and RNA-seq data. *BMC Bioinforma.* 14 (1), 7. doi:10.1186/1471-2105-14-7

Hiraoka, Y., Yamashiro, H., Yasuda, K., Kimura, Y., Inamoto, T., and Tabata, Y. (2006). *In situ* regeneration of adipose tissue in rat fat pad by combining a collagen scaffold with gelatin microspheres containing basic fibroblast growth factor. *Tissue Eng.* 12 (6), 1475–1487. Epub 2006/07/19PubMed PMID: 16846345. doi:10.1089/ten.2006.12.1475

Jung, Y. S., Stratton, S. A., Lee, S. H., Kim, M. J., Jun, S., Zhang, J., et al. (2021). TMEM9-v-ATPase activates wnt/β-catenin signaling via APC lysosomal degradation for liver regeneration and tumorigenesis. *Hepatology* 73 (2), 776–794. Epub 2020/05/08PubMed PMID: 32380568; PubMed Central PMCID: PMCPMC7647947. doi:10.1002/hep.31305

Karlsson, M., Zhang, C., Méar, L., Zhong, W., Digre, A., Katona, B., et al. (2021). A single-cell type transcriptomics map of human tissues. *Sci. Adv.* 7 (31), eabh2169. Epub 2021/07/30PubMed PMID: 34321199; PubMed Central PMCID: PMCPMC8318366. doi:10.1126/sciadv.abh2169

Kciuk, M., Gielecińska, A., Kołat, D., Kałuzińska, Ż., and Kontek, R. (2022). Cancer-associated transcription factors in DNA damage response. *Biochim. Biophys. Acta Rev. Cancer* 1877 (4), 188757. Epub 2022/07/06PubMed PMID: 35781034. doi:10.1016/j.bbcan.2022.188757

Kim, G. H., Uriel, N., and Burkhoff, D. (2018). Reverse remodelling and myocardial recovery in heart failure. *Nat. Rev. Cardiol.* 15 (2), 83–96. Epub 2017/09/22PubMed PMID: 28933783. doi:10.1038/nrcardio.2017.139

Klatt Shaw, D., Saraswathy, V. M., Zhou, L., McAdow, A. R., Burris, B., Butka, E., et al. (2021). Localized EMT reprograms glial progenitors to promote spinal cord repair. *Dev. Cell* 56 (5), 613–626.e7. e7. Epub 2021/02/21PubMed PMID: 33609461; PubMed Central PMCID: PMCPMC8044706. doi:10.1016/j.devcel.2021.01.017

Lalit, P. A., Rodriguez, A. M., Downs, K. M., and Kamp, T. J. (2017). Generation of multipotent induced cardiac progenitor cells from mouse fibroblasts and potency testing in *ex vivo* mouse embryos. *Nat. Protoc.* 12 (5), 1029–1054. Epub 2017/04/21PubMed PMID: 28426026; PubMed Central PMCID: PMCPMC5693216. doi:10.1038/nprot.2017.021

Lambert, A. W., and Weinberg, R. A. (2021). Linking EMT programmes to normal and neoplastic epithelial stem cells. *Nat. Rev. Cancer* 21 (5), 325–338. Epub 2021/02/07PubMed PMID: 33547455. doi:10.1038/s41568-021-00332-6

Marconi, G. D., Fonticoli, L., Rajan, T. S., Pierdomenico, S. D., Trubiani, O., Pizzicannella, J., et al. (2021). Epithelial-mesenchymal transition (EMT): The type-2 EMT in wound healing, tissue regeneration and organ fibrosis. *Cells* 10 (7), 1587. Epub 2021/07/03PubMed PMID: 34201858; PubMed Central PMCID: PMCPMC8307661. doi:10.3390/cells10071587

Nicolai, S., Mahen, R., Raschellà, G., Marini, A., Pieraccioli, M., Malewicz, M., et al. (2020). ZNF281 is recruited on DNA breaks to facilitate DNA repair by non-homologous end joining. *Oncogene* 39 (4), 754–766. Epub 2019/10/02PubMed PMID: 31570788; PubMed Central PMCID: PMCPMC6976523. doi:10.1038/s41388-019-1028-7

Nicolai, S., Pieraccioli, M., Smirnov, A., Pitolli, C., Anemona, L., Mauriello, A., et al. (2020). ZNF281/Zfp281 is a target of miR-1 and counteracts muscle differentiation. *Mol. Oncol.* 14 (2), 294–308. Epub 2019/11/30PubMed PMID: 31782884; PubMed Central PMCID: PMCPMC6998661. doi:10.1002/1878-0261.12605

Nobre, A. R., Dalla, E., Yang, J., Huang, X., Wullkopf, L., Risson, E., et al. (2022). ZFP281 drives a mesenchymal-like dormancy program in early disseminated breast cancer cells that prevents metastatic outgrowth in the lung. *Nat. Cancer* 3, 1165–1180. Epub 2022/09/02PubMed PMID: 36050483. doi:10.1038/s43018-022-00424-8

Oh, S. H., Swiderska-Syn, M., Jewell, M. L., Premont, R. T., and Diehl, A. M. (2018). Liver regeneration requires Yap1-TGFβ-dependent epithelial-mesenchymal transition in hepatocytes. *J. Hepatol.* 69 (2), 359–367. Epub 2018/05/15PubMed PMID: 29758331; PubMed Central PMCID: PMCPMC6349217. doi:10.1016/j.jhep.2018.05.008

Pieraccioli, M., Nicolai, S., Pitolli, C., Agostini, M., Antonov, A., Malewicz, M., et al. (2018). ZNF281 inhibits neuronal differentiation and is a prognostic marker for neuroblastoma. *Proc. Natl. Acad. Sci. U. S. A.* 115 (28), 7356–7361. Epub 2018/06/27PubMed PMID: 29941555; PubMed Central PMCID: PMCPMC6048510. doi:10.1073/pnas.1801435115

Pierdomenico, M., Palone, F., Cesi, V., Vitali, R., Mancuso, A. B., Cucchiara, S., et al. (2018). Transcription factor ZNF281: A novel player in intestinal inflammation and fibrosis. *Front. Immunol.* 9, 2907. Epub 2019/01/09PubMed PMID: 30619271; PubMed Central PMCID: PMCPMC6297801. doi:10.3389/fimmu.2018.02907

Robin, X., Turck, N., Hainard, A., Tiberti, N., Lisacek, F., Sanchez, J. C., et al. (2011). pROC: an open-source package for R and S+ to analyze and compare ROC curves. *BMC Bioinforma.* 12, 77. Epub 2011/03/19PubMed PMID: 21414208; PubMed Central PMCID: PMCPMC3068975. doi:10.1186/1471-2105-12-77

Sadłecki, P., Grabiec, M., Grzanka, D., Jóźwicki, J., Antosik, P., and Walentowicz-Sadłecka, M. (2019). Expression of zinc finger transcription factors (ZNF143 and ZNF281) in serous borderline ovarian tumors and low-grade ovarian cancers. *J. Ovarian Res.* 12 (1), 23. Epub 2019/03/20PubMed PMID: 30885238; PubMed Central PMCID: PMCPMC6423742. doi:10.1186/s13048-019-0501-9

Sarig, R., and Tzahor, E. (2017). The cancer paradigms of mammalian regeneration: Can mammals regenerate as amphibians? *Carcinogenesis* 38 (4), 359–366. Epub 2017/03/24PubMed PMID: 28334384. doi:10.1093/carcin/bgw103

Schäfer, M., and Werner, S. (2008). Cancer as an overhealing wound: An old hypothesis revisited. *Nat. Rev. Mol. Cell Biol.* 9 (8), 628–638. Epub 2008/07/17PubMed PMID: 18628784. doi:10.1038/nrm2455

Seo, K. W., Roh, K. H., Bhandari, D. R., Park, S. B., Lee, S. K., and Kang, K. S. (2013). ZNF281 knockdown induced osteogenic differentiation of human multipotent stem cells *in vivo* and *in vitro*. *Cell Transpl.* 22 (1), 29–40. Epub 2012/09/12PubMed PMID: 22963690. doi:10.3727/096368912x654948

Sjöstedt, E., Zhong, W., Fagerberg, L., Karlsson, M., Mitsios, N., Adori, C., et al. (2020). An atlas of the protein-coding genes in the human, pig, and mouse brain. *Science* 367 (6482), eaay5947. Epub 2020/03/07PubMed PMID: 32139519. doi:10.1126/science.aay5947

Stone, N. R., Gifford, C. A., Thomas, R., Pratt, K. J. B., Samse-Knapp, K., Mohamed, T. M. A., et al. (2019). Context-specific transcription factor functions regulate epigenomic and transcriptional dynamics during cardiac reprogramming. *Cell Stem Cell* 25 (1), 87–102. e9. Epub 2019/07/05PubMed PMID: 31271750; PubMed Central PMCID: PMCPMC6632093. doi:10.1016/j.stem.2019.06.012

Tang, W., Qi, J., Wang, Q., Qu, Y., Fu, S., and Luan, J. (2022). Investigating the adipogenic effects of different tissue-derived decellularized matrices. *Front. Bioeng. Biotechnol.* 10, 872897. Epub 2022/05/03PubMed PMID: 35497363; PubMed Central PMCID: PMCPMC9046558. doi:10.3389/fbioe.2022.872897

Vivian, J., Rao, A. A., Nothaft, F. A., Ketchum, C., Armstrong, J., Novak, A., et al. (2017). Toil enables reproducible, open source, big biomedical data analyses. *Nat. Biotechnol.* 35 (4), 314–316. Epub 2017/04/12PubMed PMID: 28398314; PubMed Central PMCID: PMCPMC5546205. doi:10.1038/nbt.3772

Wissink, M. J., Beernink, R., Pieper, J. S., Poot, A. A., Engbers, G. H., Beugeling, T., et al. (2001). Binding and release of basic fibroblast growth factor from heparinized collagen matrices. *Biomaterials* 22 (16), 2291–2299. Epub 2001/07/18PubMed PMID: 11456069. doi:10.1016/s0142-9612(00)00418-x

Xue, Y. B., Ding, M. Q., Xue, L., and Luo, J. H. (2019). CircAGFG1 sponges miR-203 to promote EMT and metastasis of non-small-cell lung cancer by upregulating ZNF281 expression. *Thorac. Cancer* 10 (8), 1692–1701. Epub 2019/06/28PubMed PMID: 31243884; PubMed Central PMCID: PMCPMC6669801. doi:10.1111/1759-7714.13131

Zhang, E., Hou, X., Hou, B., Zhang, M., and Song, Y. (2020). A risk prediction model of DNA methylation improves prognosis evaluation and indicates gene targets in prostate cancer. *Epigenomics* 12 (4), 333–352. Epub 2020/02/07PubMed PMID: 32027524. doi:10.2217/epi-2019-0349

Zhang, J., Rector, J., Lin, J. Q., Young, J. H., Sans, M., Katta, N., et al. (2017). Nondestructive tissue analysis for *ex vivo* and *in vivo* cancer diagnosis using a handheld mass spectrometry system. *Sci. Transl. Med.* 9 (406), eaan3968. Epub 2017/09/08PubMed PMID: 28878011; PubMed Central PMCID: PMCPMC5830136. doi:10.1126/scitranslmed.aan3968

Zhang, S., Lu, Q., Cao, T., and Toh, W. S. (2016). Adipose tissue and extracellular matrix development by injectable decellularized adipose matrix loaded with basic fibroblast growth factor. *Plast. Reconstr. Surg.* 137 (4), 1171–1180. Epub 2016/03/29PubMed PMID: 27018672. doi:10.1097/prs.0000000000002019

Zhou, H., Morales, M. G., Hashimoto, H., Dickson, M. E., Song, K., Ye, W., et al. (2017). ZNF281 enhances cardiac reprogramming by modulating cardiac and inflammatory gene expression. *Genes Dev.* 31 (17), 1770–1783. Epub 2017/10/07PubMed PMID: 28982760; PubMed Central PMCID: PMCPMC5666675. doi:10.1101/gad.305482.117

frontiers | Frontiers in Genetics

TYPE Original Research
PUBLISHED 09 January 2023
DOI 10.3389/fgene.2022.1087938

OPEN ACCESS

EDITED BY
Jiao Hu,
Central South University, China

REVIEWED BY
Anna M. Eiring,
Texas Tech University Health Sciences Center El Paso, United States
Jingfeng Zhou,
Shenzhen University, China

*CORRESPONDENCE
Chun Chen,
chenchun@mail.sysu.edu.cn

SPECIALTY SECTION
This article was submitted to Cancer Genetics and Oncogenomics, a section of the journal Frontiers in Genetics

RECEIVED 02 November 2022
ACCEPTED 23 December 2022
PUBLISHED 09 January 2023

CITATION
Liu Y, Zhang J, Du Z, Huang J, Cheng Y, Yi W, Li T, Yang J and Chen C (2023), Comprehensive analysis of *PTPN* family expression and prognosis in acute myeloid leukemia.
Front. Genet. 13:1087938.
doi: 10.3389/fgene.2022.1087938

Comprehensive analysis of *PTPN* family expression and prognosis in acute myeloid leukemia

Yong Liu[1], Jing Zhang[2], Zefan Du[1], Junbin Huang[1], Yucai Cheng[1], Wenfang Yi[1], Tianwen Li[1], Jing Yang[1] and Chun Chen[1]*

[1]Division of Hematology/Oncology, Department of Pediatrics, The Seventh Affiliated Hospital of Sun Yat-Sen University, Shenzhen, China, [2]Department of Breast and Thyroid Surgery, Guangzhou Women and Children's Medical Center, Guangzhou, China

Background: Tyrosyl phosphorylation is carried out by a group of enzymes known as non-receptor protein tyrosine phosphatases (PTPNs). In the current investigation, it is hoped to shed light on the relationships between the expression patterns of *PTPN* family members and the prognosis of acute myeloid leukemia (AML).

Methods: *PTPN* expression was examined using GEPIA and GEO databases. To investigate the connection between *PTPN* expression and survival in AML patients, we downloaded data from the Broad TCGA Firehose and Clinical Proteomic Tumor Analysis (CPTAC) of the Cancer Genome Atlas (TCGA). We used quantitative real-time PCR (qRT-PCR) to confirm that essential genes were performed in clinical samples and cell lines. We then used western blot to verify that the genes expressed in the above databases were positive in normal tissues, AML patient samples, and AML cell lines. Next, we investigated associations between genome-wide expression profiles and *PTPN6* expression using the GEO datasets. We investigated the interactive exploration of multidimensional cancer genomics using the cBioPortal datasets. Using the DAVID database, a study of gene ontology enrichment was performed. The protein-protein interaction (PPI) network was created using the STRING portal, and the gene-gene interaction network was performed using GeneMANIA.

Results: Data from GEO and GEPIA revealed that most *PTPN* family members were linked to AML. Patients with leukemia have elevated levels of several *PTPN* members. All of the AML patients' poor overall survival (OS, $p < .05$) was significantly linked with higher expression of *PTPN1*, *PTPN6*, and *PTPN7*. Additionally, clinical samples showed that the expression of *PTPN 6*, *PTPN 7*, *PTPN 13*, and *PTPN 14* was higher than normal in AML patients ($p = .0116$, $p = .0034$, $p = .0092$, and $p = .0057$, respectively) and AML cell lines ($p = .0004$, $p = .0035$, $p = .0357$, and $p = .0177$, respectively). Western blotting results showed that the expression of *PTPN6* in AML samples and AML cell lines was significantly higher than that in normal control samples.

Conclusion: Differentially expressed PTPN family members were found in AML. The prognosis of patients and *PTPN* gene expression were shown to be correlated. *PTPN6* is one of these members and may be used as an AML diagnostic and prognostic marker.

KEYWORDS

PTPNs, AML, bioinformatics, prognosis, biomarker, expression level

Introduction

The most prevalent kind of acute leukemia in adults and the cause of the most significant number of leukemia-related fatalities each year in the United States is acute myeloid leukemia (AML), a heterogeneous hematologic malignancy characterized by the clonal growth of myeloid blasts in peripheral blood, bone marrow, and other organs (Tallman et al., 2019). In 2022, it is predicted that 20,050 people will be diagnosed with AML, and 11,540 people will pass away from the condition (Siegel et al., 2022). Despite improvements in AML treatment, such as the introduction of chemotherapy and other successful targeted medicines over the previous few decades, the 5-years relative survival rate increased from 6.2% in the mid- 1970s to 30% for those diagnosed from 2009 to 2015 (Lai et al., 2019). However, there are significant restrictions in the prognosis predicted by the existing biomarkers because of the clinical and molecular heterogeneity of AML (Patel et al., 2012). Therefore, it is vital to find reliable biomarkers that will allow for an earlier diagnosis and better, more specialized therapy of AML.

Complex phosphorylation and dephosphorylation networks are created when kinases and phosphatases, which carry out phosphorylation and dephosphorylation, are linked by their shared substrates or direct interactions. These networks are essential for controlling cellular functions (Li et al., 2013). Protein tyrosine phosphatases (PTPs) are a group of enzymes that catalyze the dephosphorylation of tyrosine residues (Chen et al., 2020). One hundred three genes encode PTPs, which are organized into four primary superfamily classes. The Human Genome Organization's Nomenclature Committee has given each PTP member an official gene name (Ogino et al., 2007). There are 17 non-receptor PTPs in Class I of the most prominent family, known as PTPN, with a number, according to the literature (Alonso et al., 2004). More and more evidence points to the possibility that protein tyrosine kinases (PTKs) and protein tyrosine phosphatases (PTPNs) collaborate to control a wide range of cellular processes, including immune response, migration, metabolism, and proliferation and differentiation (Tonks, 2013; Yu and Zhang, 2018). The *PTPN* family numbers significantly influence various disorders, according to numerous research that has already been published. For instance, *PTPN22* restricts T-cell receptor-induced proliferation. It hinders naive T-cell activation and effector cell responses in response to low-affinity antigens (Salmond et al., 2015), and *PTPN12* expression is elevated in both stomach adenocarcinoma and cancer (Chen et al., 2020). Additionally, one study indicates that the deletion of *PTPN2* may enhance the therapeutic effectiveness of CAR-T cells in the treatment of breast cancer (Wiede et al., 2020). The cell cycle, apoptosis, and metastasis are all heavily regulated by *PTPN2*, which is a significant predictor of the prognosis of pancreatic cancer (Kuang et al., 2022). The *PTPN* genes are generally a promising prognostic and therapeutic target for cancer therapy due to this evidence. However, the distinct roles of *PTPN* family genes in AML have yet to be understood entirely.

Therefore, discovering oncogenes or tumor suppressors mediated by *PTPN* as potential pathways for predicting biomarkers may offer novel therapeutic approaches for treating AML. The difficulty comes from the fact that most *PTPN* genes' variances in transcriptional levels, prognostic values, molecular roles, and biological processes have not yet been thoroughly understood in the context of AML disease. In order to thoroughly investigate the association between *PTPN* subtypes and the pathogenesis and progression of AML, we combed through some widely used databases as part of this work to further our understanding of AML.

Materials and methods

Ethics statement

The Seventh Affiliated Hospital of Sun Yat-Sen University's Academic Committee approved this study, which was carried out following the guidelines outlined in the Declaration of Helsinki. Each patient signed informed consent. Since all the datasets were taken from published works, it was verified that written informed consent had been obtained for every one of them.

Download and expression analysis of microarray data

The GEO database (http://www.ncbi.nlm.nih.gov/geo) is a public functional genomics data repository that downloads the GSE149237 microarray dataset (Jäger et al., 2021). This dataset was obtained by comparing five healthy HSPCs sequenced and compared to eight AML patient samples, and the study was conducted with GPL20301 Illumina HiSeq 4000 sequencing platform. Then, we performed a classification analysis on the mRNA expression values of the target genes. The filter conditions are p-value <0.05 and the absolute value of the difference (| log2 (Fold Change) |) > 1.

Download the data set GSE37642 and its corresponding platform file GPL96 (Affymetrix Human Genome U133A Array). The GSE37642 data set based on the GPL96 platform contains a total of 422 tissue samples (bone marrow mononuclear cells) of AML patients, and clinical information such as survival time, survival status, and whether *PTPN6* mutations occur in the samples are extracted.

GEPIA dataset

GEPIA (Gene Expression Profiling Interactive Analysis) is a newly created interactive web server for evaluating the RNA sequencing expression data of 9,736 tumors and 8,587 normal samples from projects like the Genotype-Tissue Expression (GTEx) and the Cancer Genome Atlas (TCGA), using a regular processing pipeline. (http://gepia.cancer-pku.cn/). Customizable features offered by GEPIA include dimensionality reduction analysis, similar gene discovery, patient survival analysis, profiling based on cancer kinds or pathological stages, tumor or normal differential expression analysis, patient survival analysis, and similar gene detection (Tang et al., 2017).

LinkedOmics dataset

In the software ecosystem, LinkedOmics (http://www.linkedomics.orglogin.php) is a brand-new and unique tool for

sharing data from extensive cancer omics initiatives. To reduce duplication of effort, which is concentrated on the detection and interpretation of attribute connections, preprocessed and normalized data from the Clinical Proteomic Tumor Analysis (CPTAC) data portal and the Broad TCGA Firehose are used, completing the work of the already-existing cancer data portals (Vasaikar et al., 2018).

Cell lines and cell culture

Four AML cells, HL-60, KG-1, THP-1, and MOLM-13, were purchased from American Type Culture Collection (Rockville, MD). HL-60 and KG-1 were cultured in IMDM medium (Invitrogen, Shanghai, China) supplemented with 20% fetal bovine serum (Biological Industries, Kibbutz Beit Haemek, Israel) and 100 units/ml penicillin and streptomycin. THP-1 and MOLM-13 were cultured in RPMI medium (Invitrogen, Shanghai, China) supplemented with 10% fetal bovine serum (Biological Industries, Kibbutz Beit Haemek, Israel) and 100 units/ml penicillin and streptomycin. Cells were incubated at 37°C in a humidified atmosphere of 95% air and 5% CO_2, as described previously (Jin et al., 2015). The cells were confirmed to be mycoplasma-free routinely.

RNA extraction, reverse transcription and quantitative real-time polymerase chain reaction (qRT-PCR)

To verify the expression of crucial genes in clinical samples and cell lines, we further verified the expression level of essential genes in blood monocytes of four newly diagnosed patients with AML (confirmed by WHO-AML criteria, excluding AML-M3 cases. Not receive treatment was received) and four AML cell lines (HL-60, KG-1, THP-1, and MOLM-13) using qPCR. Peripheral blood monocytes from four anonymous healthy volunteers were used as control samples.

According to g Trizol reagent and the manufacturer's instructions, total RNA was extracted from cultivated cells (Takara Bio, Kusatsu, Japan). The expression of the indicated genes was examined using SYBR Premix Ex Taq TM II and PCR detection equipment from Bio-Rad in Hercules, California, United States. A quick all-in-one RT-Kit was used to create the cDNA (ES Science Biotech). The internal control gene GAPDH's transcript levels were used to standardize transcription levels. The supplementary table displays the order of the primers. Triplicate analyses of each RNA sample were carried out.

Reagents and antibodies

PTPN6 (Rabbit, 3759) and PTPN14 (Rabbit, 13,808) antibody was from Cell Signaling Technology (Beverly, MA). Antibodies against β-actin were from Sigma-Aldrich (Mouse, A5441, Shanghai, China). Antibodies against PTPN1(Goat, AF3954) was from Novus Biologicals (Littleton, CO). Antibodies against PTPN7(Goat, AF3954) was from Novus Biologicals (Littleton, CO). Antibodies against PTPN13 (Rabbit, PA5-72907) were from Thermo-Fisher Scientific (Shanghai, China). The fluorescent-conjugated secondary antibodies anti-mouse and anti-rabbit IgG were from LI-COR Biotechnology (Nebraska, United States).

For western blotting assays, whole cell lysates were prepared in RIPA buffer (1 × PBS, 1% NP-40, .5% sodium deoxycholate, .1% SDS) supplemented with 10 mmol/L β-glycerophosphate, 1 mmol/L sodium orthovanadate, 10 mmol/L NaF, 1 mmol/L phenylmethylsulfonyl fluoride, and 1 × Roche complete Mini protease inhibitor cocktail (Roche, Indianapolis, IN) (Jin et al., 2017). The cytosolic fractionations for cytochrome c detection were prepared with digitonin extraction buffer (10 mmol/L PIPES pH 6.8, .015% digitonin, 300 mmol/L sucrose, 100 mmol/L NaCl, 3 mmol/L MgCl2, 5 mmol/L EDTA, and 1 mmol/L phenylmethylsulfonyl fluoride) as described previously (Jin et al., 2017). Protein samples were separated by SDS-PAGE and transferred to nitrocellulose membranes, which were then incubated with the primary antibodies. After incubation with appropriate secondary antibodies, the membranes were scanned by the Odyssey infrared imaging system (LI-COR, Lincoln, Nebraska).

TCGA data and the cBioPortal

The cBioPortal (http://www.cbioportal.org/) for cancer genomics is an open-access and open-source platform developed for the interactive study of multidimensional cancer genomics datasets (Cerami et al., 2012). It supports and maintains data about non-synonymous mutations, DNA copy-numbers, mRNA and microRNA expression, protein-level and phosphoprotein levels, DNA methylation, and de-identified clinical data. We may compute mRNA expression z-scores (RNA Seq V2 RSEM), PTPN family gene correlations, and the frequency of gene modifications using the web tool cBioPortal.

GO and PPI analysis for the function and interaction of PTPN family

Enrichment analysis of gene ontology (GO) of *PTPN* genes was explored using the Database for Annotation, Visualization and Integrated Discovery (DAVID; v.6.8; https://david.ncifcrf.gov/home.jsp; accessed on 20 November 2019) (Chandrasekharan et al., 2013). The gene-gene interaction network was structured using the Gene Multiple Association Network Integration Algorithm (GeneMANIA; https://www.genemania.org/; accessed on 21 November 2019) (Warde-Farley et al., 2010) and the search tool for the Retrieval of Interacting Genes Database (STRING v.10.0; https://string-db.org/; accessed on 23 November 2019) was used to create a protein-protein interaction (PPI) network (Szklarczyk et al., 2017).

Statistical analysis

Utilizing the software packages R Studio (R version 4.0.2) and GraphPad Prism 8.3, statistical analysis and visualization were carried out (GraphPad Software, Inc., La Jolla, CA, United States). Single

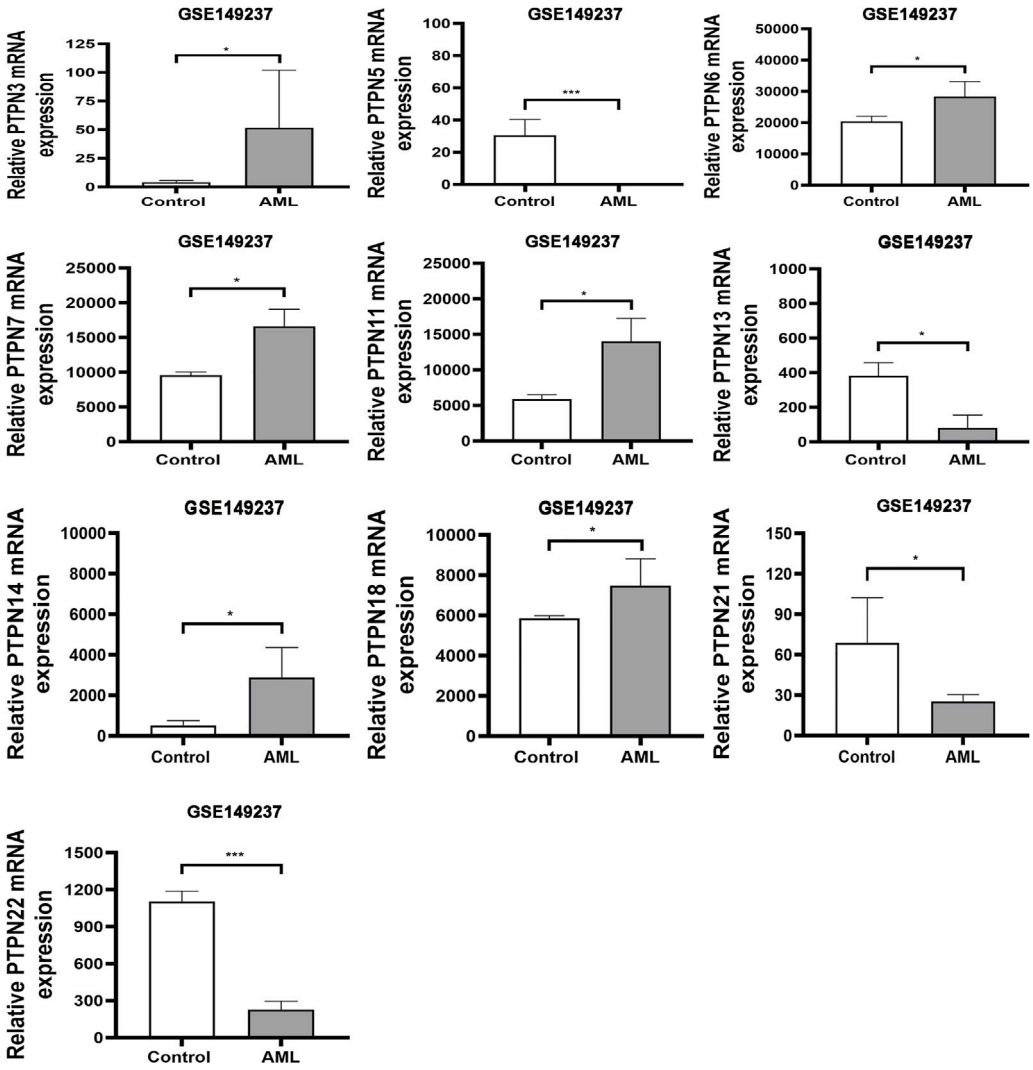

FIGURE 1
In the GSE149237 microarray dataset, there were differential transcript levels of the PTPN gene in AML and healthy control samples. The filter conditions are p-value <0.05 and the absolute value of the difference (| log2 (Fold Change) |) > 1.

e-variable Cox proportional regression models and two-way ANOVA analysis were employed to examine the overall survival and mRNA expression datasets. An illustration of the prognosis was a Kaplan-Meier survival curve. We compared variations in central gene expression levels using two-way ANOVA analysis. Statistical significance was set at as < .05.

Results

Transcriptional level of *PTPNs* in patients with AML in the GEO database

The human genome contains *PTPN* genes, which have been found. We compared the transcriptional expression of the PTPN genes in tumorigenic and healthy control samples using the GSE149237 microarray dataset. GEO analysis revealed that the mRNA expression level of *PTPN3*, *PTPN6*, *PTPN7*, *PTPN11*, *PTPN14*, and *PTPN18*, was upregulated in AML patients compared with normal controls (p < .05, Figure 1). However, the expression levels of *PTPN5*, *PTPN13*, *PTPN21*, and *PTPN22* were lower in AML patients (p < .05, Figure 1). While others, such as *PTPN1*, *PTPN2*, *PTPN9*, *PTPN12*, *PTPN20*, and *PTPN23*, showed no difference between AML and normal samples (p > .05, Supplementary Figure S1).

The mRNA levels of *PTPNs* in AML samples and normal samples in the GEPIA

Database

In order to compare the mRNA expression of *PTPN* factors in leukemia and normal samples, we used the GEPIA (Gene Expression Profiling Interactive Analysis) dataset (http://gepia.

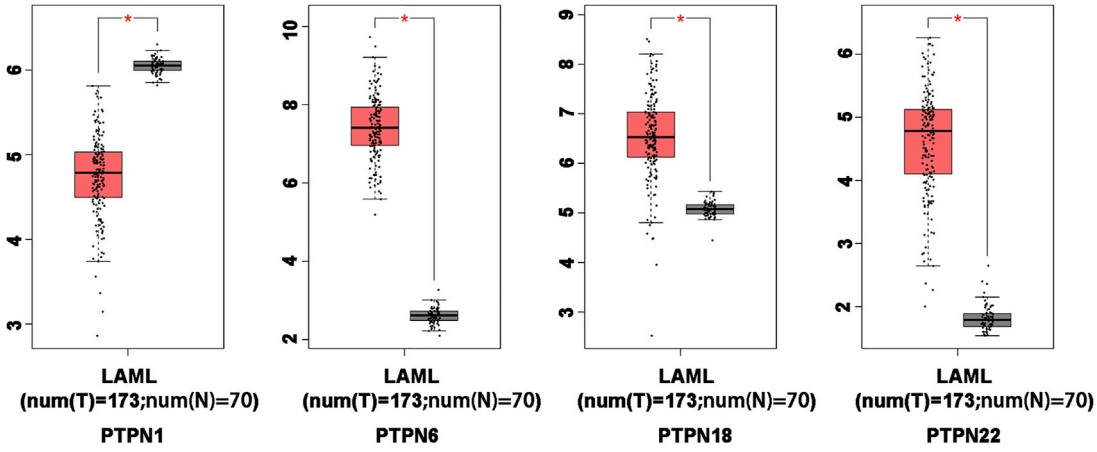

FIGURE 2
Differentially expressed PTPN genes in AML and healthy control samples in the GEPIA database. The filter conditions are *p*-value <0.05 and the absolute value of the difference (| log2 (Fold Change) |) > 1.

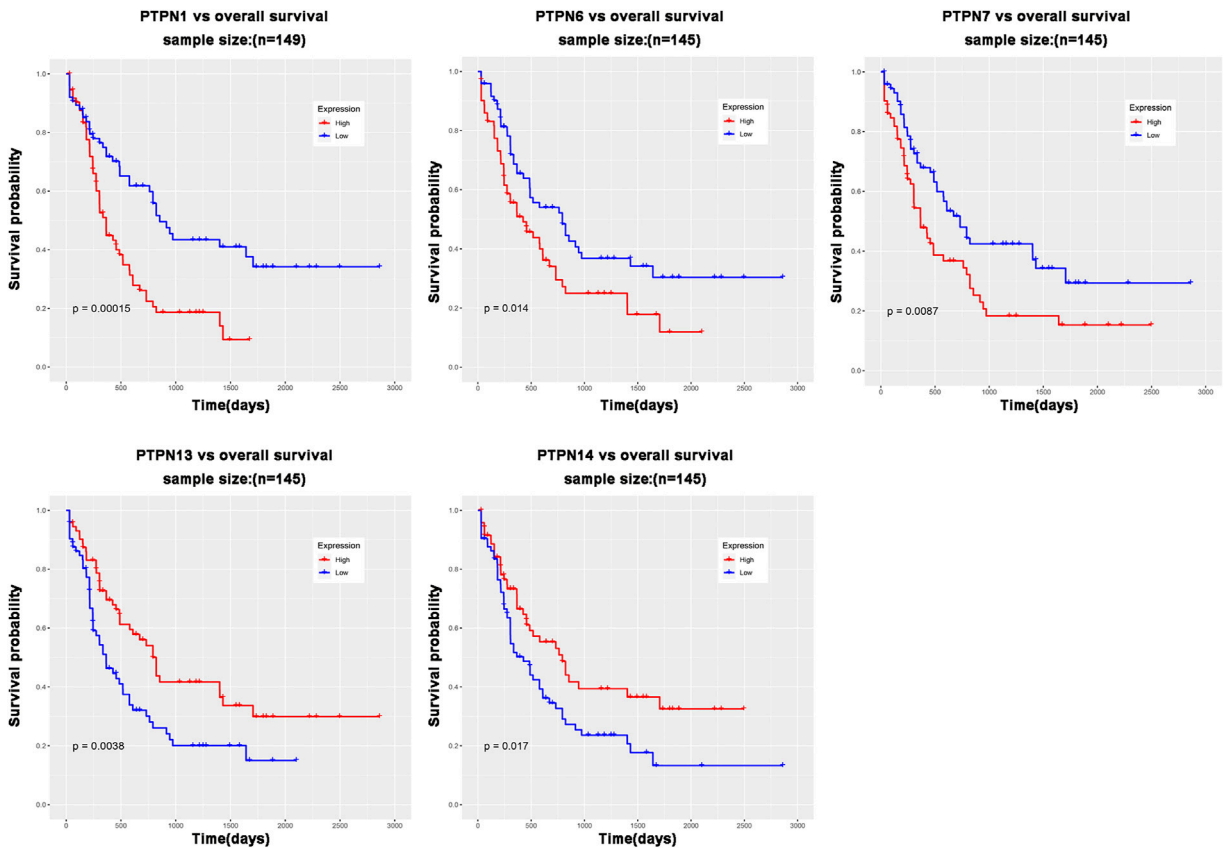

FIGURE 3
PTPN genes whose expression level is related to patient prognosis in AML patients.

cancer-pku.cn/). The findings showed that *PTPN6, PTPN18*, and *PTPN22* had higher expression levels in leukemia than in normal blood samples, while *PTPN1* had a lower expression level in the former than the latter (Figure 2). However, there was no discernible difference in the expression levels of *PTPN2, PTPN3, PTPN4, PTPN5, PTPN7, PTPN9, PTPN*

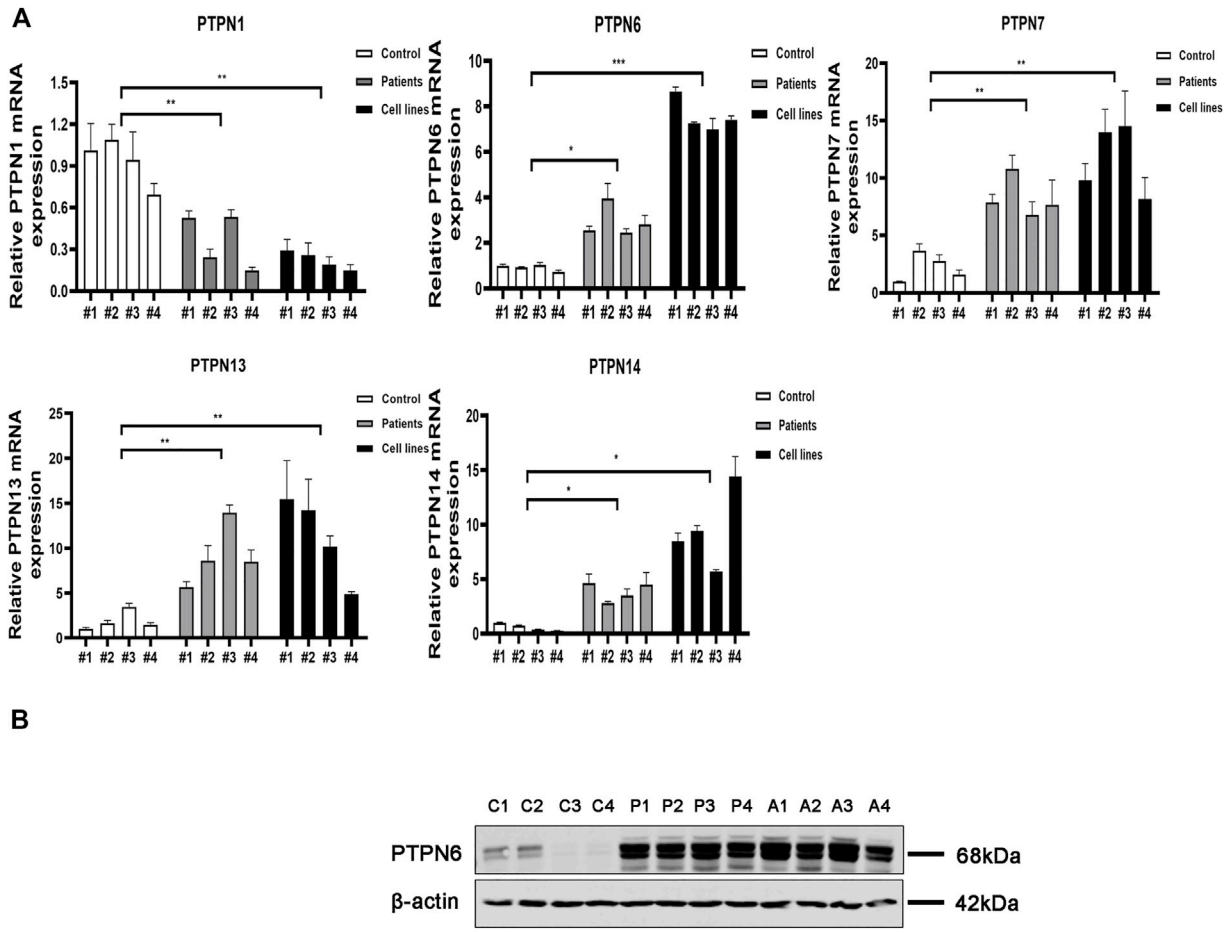

FIGURE 4
Relative mRNA and protein expression of the PTPN gene in AML samples and AML cell lines and normal controls were detected by qRT-PCR and western blotting. **(A)** Relative mRNA expression of PTPN gene in AML samples and AML cell lines and normal healthy controls detected by qRT-PCR. **(B)** Protein expression levels of PTPN6 in AML samples and AML cell lines and normal healthy controls detected by western blotting. Note: C1-C4 represent 4 normal controls, P1-P4 control 4 AML clinical samples, A1-A4 represent 4 AML cell lines including HL-60, KG-1, THP-1, and MOLM-13.

11, *PTPN12*, *PTPN13*, *PTPN14*, *PTPN20*, *PTPN21*, and *PTPN23* (Supplementary Figure S2).

Relationship between the mRNA level of *PTPNs* and the prognosis of patients with leukemia

The role of *PTPN* genes in AML patients' survival was the subject of our further research. We conducted a prognostic analysis of *PTPN* genes in patients with AML using the LinkedOmics database. The results of the study showed that there was a significant correlation between poor overall survival (OS, $p < .05$, Figure 3) and increased expression levels of *PTPN1*, *PTPN6*, and *PTPN7* in all AML patients, but was associated with low expression of *PTPN13* and *PTPN14* (OS, $p < .05$, Figure 3). However, there were no significantly different in the expression levels of *PTPN2*, *PTPN3*, *PTPN4*, *PTPN5*, *PTPN9*, *PTPN11*, *PTPN12*, *PTPN18*, *PTPN20*, *PTPN21*, *PTPN22*, and *PTPN23* (Supplementary Figure S3). *PTPN1*, *PTPN6*, and *PTPN7* overexpression may indicate a poor prognosis for AML.

Clinical samples were used to verify the mRNA and protein levels of *PTPNs* in AML and normal samples

We next carried out qRT-PCR experiments utilizing clinical samples and cell lines to confirm further the expression level of *PTPNs* mRNA in AML. According to the findings, the expression of *PTPN 6*, *PTPN 7*, *PTPN 13*, and *PTPN 14* was higher in AML patients ($p = .0116$, $p = .0034$, $p = .0092$, and $p = .0057$, respectively) and AML cell lines ($p = .0004$, $p = .0035$, $p = .0357$, and $p = .0177$, respectively) than in normal individuals. The expression level of *PTPN1* was, however, lower in AML patients ($p = .0094$) and AML cell lines ($p = .0013$) (Figure 4A). However, there were no significantly different in the expression levels of *PTPN2*, *PTPN3*, *PTPN4*, *PTPN5*, *PTPN9*, *PTPN11*, *PTPN12*, *PTPN18*, *PTPN20*, *PTPN21*, *PTPN22*, and *PTPN23* (Supplementary Figure S4A).

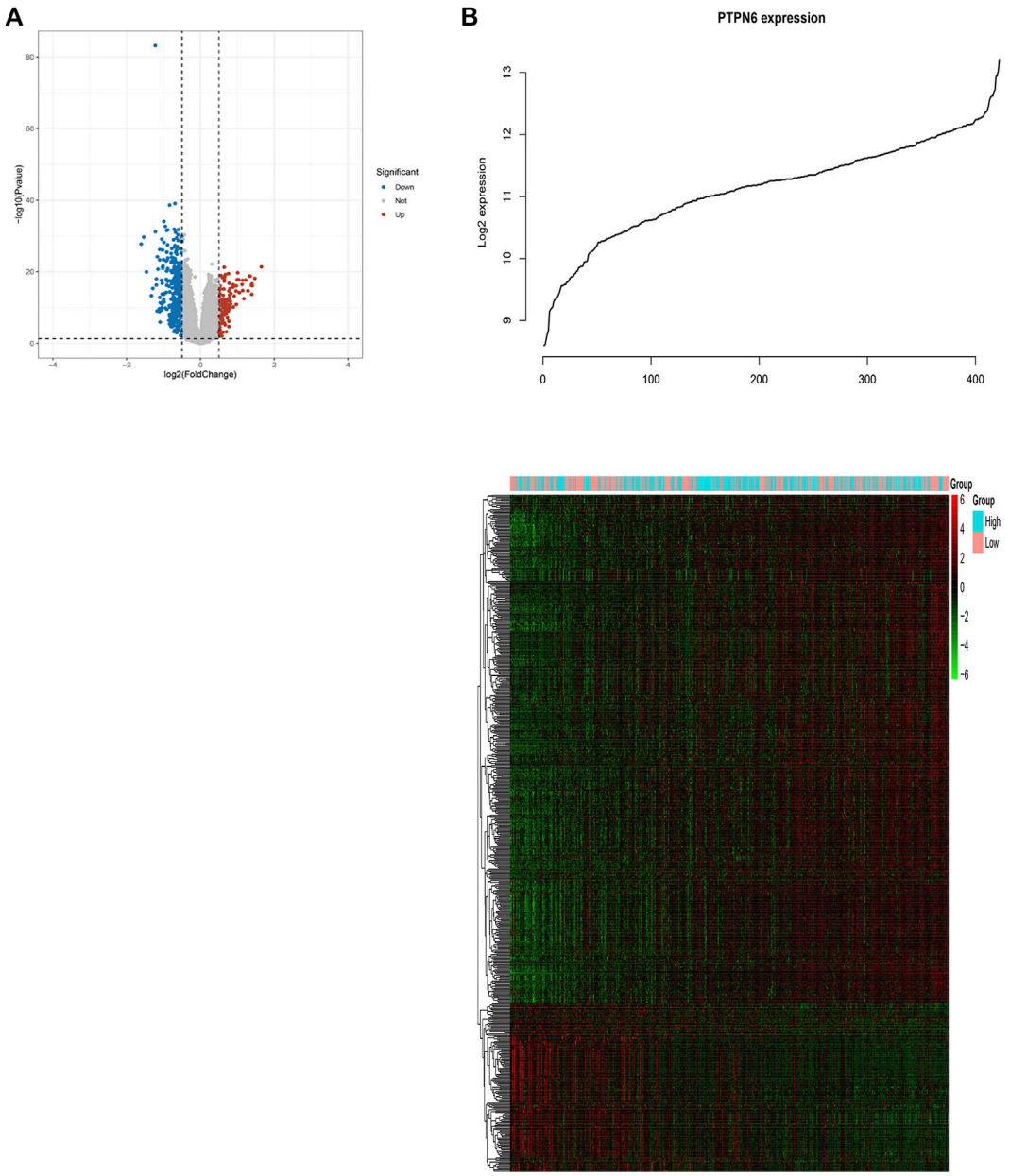

FIGURE 5
Genome-wide genes associated with PTPN6 expression. **(A)** Volcano plot of differential gene profiles between PTPN6 high and PTPN6 low. **(B)** Expression heatmap of PTPN6-associated genes. The top curve shows PTPN6's expression distribution of 156 CN-AML samples.

According to the results of GEO, GEPIA, LinkedOmics, and qRT-PCR, only *PTPN6* expression was increased in AML patients in all major databases and qRT-PCR, and the results were consistent with each other. Next, we explored the protein expression of PTPN 1, PTPN6, PTPN 7, PTPN 13, and PTPN 14 in normal controls, clinical AML patients, and AML cell lines. The results of western blotting assays showed that the expression of PTPN6 in AML patient samples and AML cell lines was significantly higher than that in normal controls (Figure 4B). However, the expression levels of PTPN1, PTPN7, PTPN13 and PTPN14 were not different among AML patient samples, AML cell lines and normal controls (Supplementary Figure S4B).

Associations between genome-wide expression profiles and *PTPN6* expression

In order to further study the biological role of *PTPN6* in leukemogenesis, the gene expression profile related to *PTPN6* was obtained based on the analysis of GSE dataset 37,642. As a result, 128 upregulated genes and 390 downregulated genes were identified as being significantly associated with the expression of *PTPN6* (fdr-adjusted $p < .05$ and FC > 1.5 or FC < 1/1.5, Figure 5A). In addition, we also presented these differentially expressed genes as a heat map (Figure 5B). The upregulated genes include: 1) Genes related to leukemia (such as *HHEX, NET1*), tumor-promoting factors (such as *CDK6, HOX* family genes), tyrosine kinase genes (*c-KIT, GRB10*); 2)

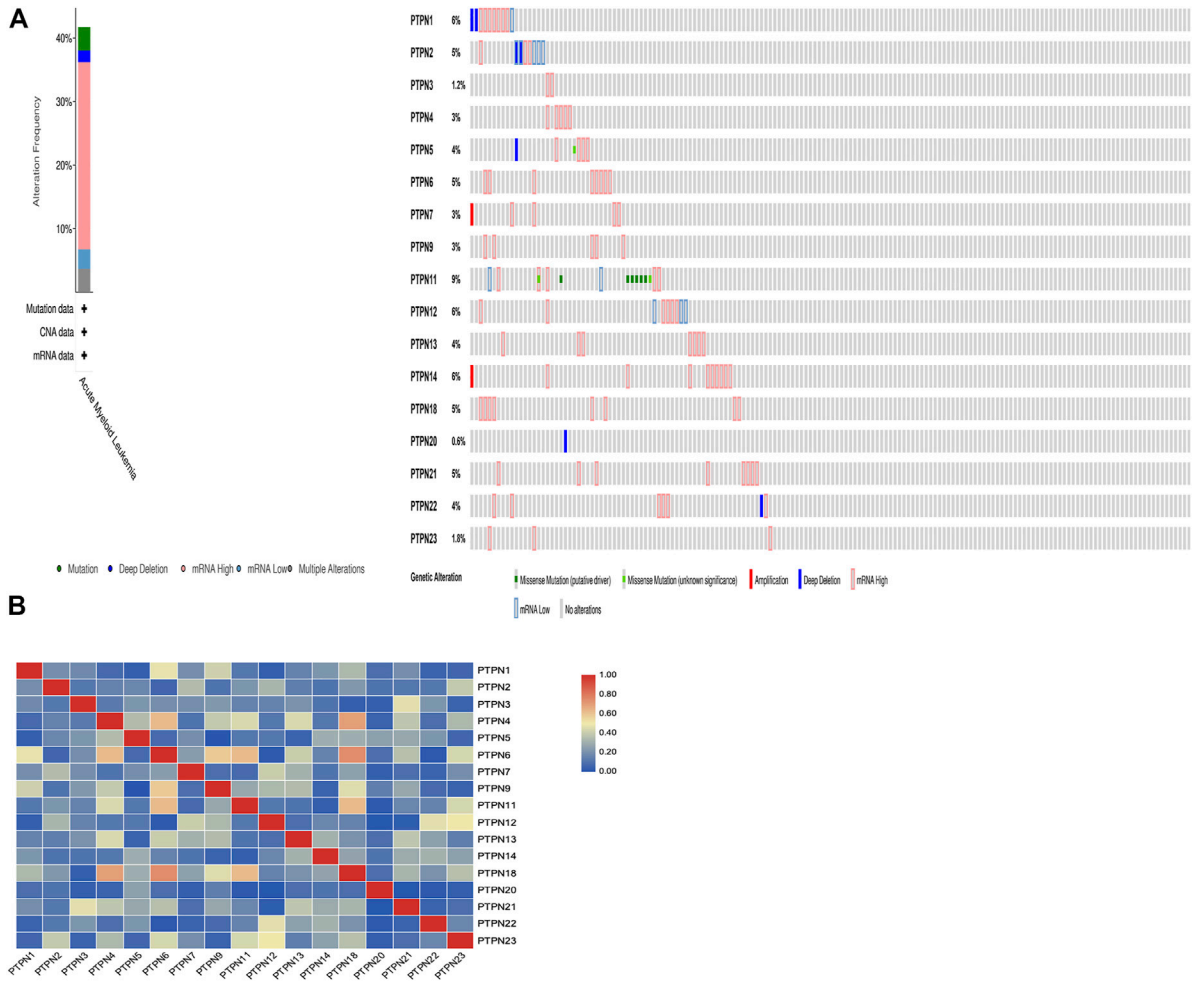

FIGURE 6
Genetic alteration and correlations of PTPN genes in AML. **(A)** Genetic alteration of PTPN gene in AML. **(B)** Genetic correlations of PTPN genes in AML.

Prognosis-related genes (such as *WT1, CXXC5, MSI2*, etc.); 3) *CD34* (a marker of hematopoietic progenitor cells); 4) AML drug resistance-related genes (such as *IGFBP2 and ABCC1*). Downregulated genes include: 1) Immune system activators, such as *CD86*; 2) blood tumor suppressors *ID2* and *KLF4*; 3) *CEBPB*, *CEBPB* is a *BCR/ABL* negative regulator gene, which can inhibit the proliferation of BCR/ABL-positive cells, and promote cell differentiation.

Genetic alterations and correlations of *PTPN* genes in AML

We gathered details on genetic changes to the PTPN genes and determined any gene-to-gene correlations using the online resource cBioPortal and the "TCGA, Firehose Legacy" database for AML. In 68/163 (42%) patient samples with AML, *PTPN* genes were changed (Figure 6A). Mutation, deep deletion, mRNA overexpression, mRNA down-expression, and numerous alterations were among the several genetic alterations. The percentage of genetic alterations in *PTPN* family members for leukemia varied from .6% to 9% for individual genes based on the TCGA, Firehose Legacy dataset (*PTPN1*, 6%; *PTPN2*, 5%; *PTPN3*, 1.2%; *PTPN4*, 3%; *PTPN5*, 4%; *PTPN6*, 5%; *PTPN7*, 3%; *PTPN9*, 3%; *PTPN11*, 9%; *PTPN12*, 6%; *PTPN13*, 4%; *PTPN14*, 6%; *PTPN18*, 5%; *PTPN20*, .6%; *PTPN21*, 5%; *PTPN22*, 4%; *PTPN23*, 1.8%; Figure 6A). In addition, cBioPortal was used to investigate the expression of *PTPN* genes in AML [using mRNA sequencing (RNA-seq) version V2 RSEM], and the relationships between certain *PTPN* genes (including Pearson's correlation) were calculated. Except for *PTPN1* and *PTPN22*, the findings showed a significant positive correlation between any two *PTPN* family gene members (Pearson = .00952, p = .905) (Figure 6B).

Function and interaction of *PTPN* family genes

The three main categories of GO analysis were molecular function groups, cellular component groups, and biological process groups. Figure 7A displays the top five enriched categories for each group as determined by the analysis results. GO analysis revealed that most PTPN proteins were associated with the cytoplasm. Protein dephosphorylation and protein tyrosine phosphatase activity were the main targets of *PTPN* genes' actions. The KEGG pathway enriched 11 genes using the David online platform. JAK-STAT signaling

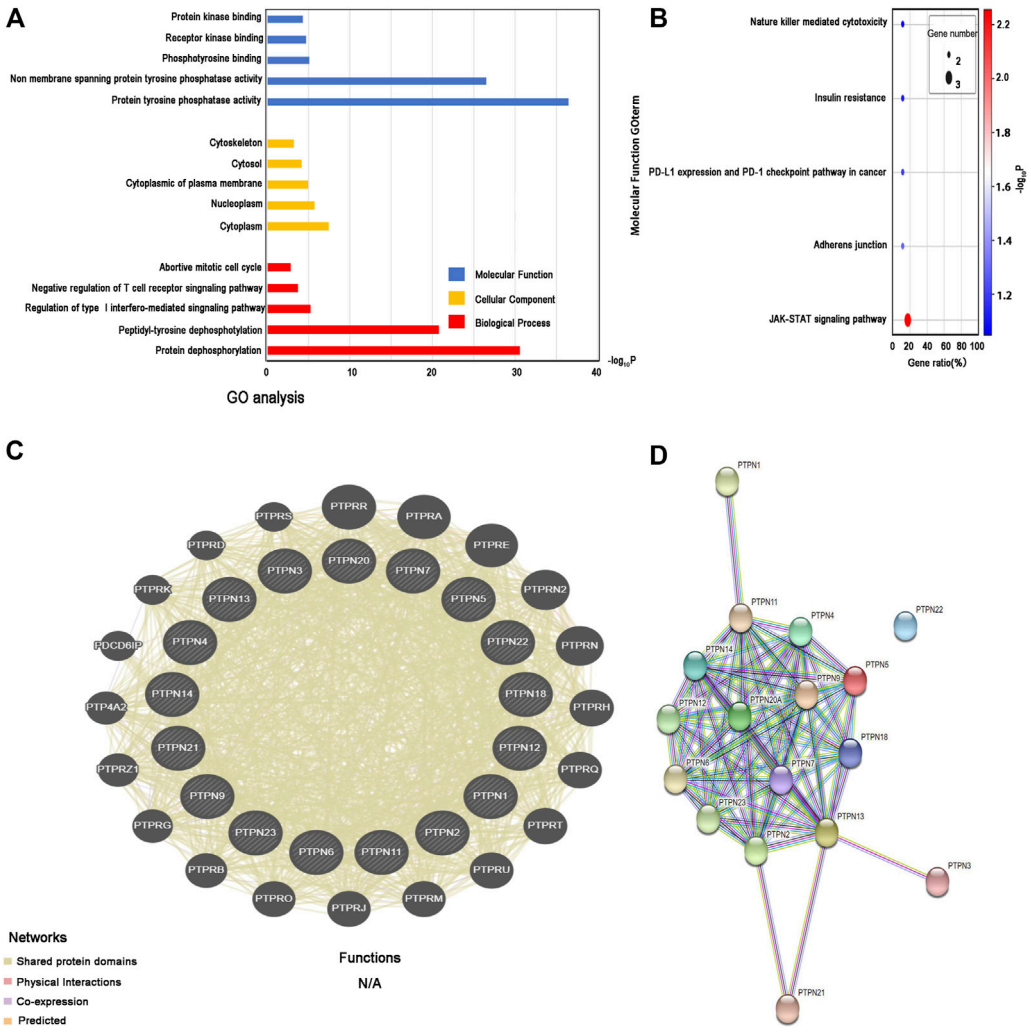

FIGURE 7
Enrichment and correlation analysis among PTPN family genes. **(A)** GO analysis of PTPN family genes. The top five enriched categories for Molecular Function, Cellular Component, and Biological Process were showed. **(B)** KEGG pathway analysis of PTPN family genes, top five KEGG pathway category were showed. **(C)** Gene–gene interaction network among PTPN gene family members. **(D)** Protein–protein interaction network among PTPN gene family members.

pathway, Adherens junction, PD-L1 expression, and PD-1 checkpoint pathway in cancer, as well as insulin resistance and natural killer cell-mediated cytotoxicity, were the principal pathways associated with the eleven genes (Figure 7B). To further understand the relationships between colocalization, shared protein domains, co-expression, prediction, and pathways, interaction analysis of *PTPN* genes at the gene level was carried out using GeneMANIA (Figure 7C). The STRING protein-protein interaction network analysis revealed that the connections between the members of the *PTPN* gene family were complex (Figure 7D).

Discussion

According to the Global Burden of Disease study, acute myeloid leukemia (AML) is the deadliest form of leukemia in the world, with 147,000 fatalities attributed to it in 2019 (Fitzmaurice et al., 2019; GBD 2019 Diseases and Injuries Collaborators, 2020) AML is linked to 40% of leukemia-related mortality in the United States and around the world, but only about 30% of leukemia occurrences (Siegel et al., 2021). AML incidence has increased more during the previous 10 years than chronic lymphocytic leukemia (CLL) (34% vs 25%), acute lymphoblastic leukemia (ALL) (22%), and chronic myeloid leukemia (13%), in part due to population expansion and aging as well as an increase in the standardized incidence rate (Cao et al., 2021). Therefore, it is noteworthy and crucial for AML that new biological therapeutic targets are found.

Together with protein-tyrosine kinases, PTPN regulates tyrosine phosphorylation and dephosphorylation in cellular signal transmission. They are essential members of the protein tyrosine phosphatases family (Tonks, 2006). Numerous studies have examined the relationships between specific *PTPN* family members and various neoplasms (Chen et al., 2020; Mitra and Ayyannan, 2020). To date, no report has provided an overview of the connections between *PTPN* family genes and human leukemia. In this study, *PTPN* gene expression patterns were illustrated for the first time,

and it was also shown how the *PTPN* family of genes and AML diagnosis and prognosis are related. This information gave genes clearer understanding of the clinical value of all the *PTPN* genes in human leukemia.

We investigated the level of PTPN gene expression in AML using GEO database and the online databases GEPIA, Next, we used the LinkedOmics database to explore the relationship between the *PTPN* family's expression and AML patients' survival. Then we validated our findings using qRT-PCR. As a result of the high levels of expression of numerous *PTPN* family members in human AML discovered in our study, *PTPNs* may 1 day be used as an AML diagnostic biomarker. However, there is much debate about the expression of the *PTPN* family in AML and normal samples. The expression level of *PTPN1* in AML mice is significantly lower than in normal mice, and myeloid-specific deficiency of *PTPN1* can promote the development of AML (Le Sommer et al., 2018). In the GSE149237 microarray, there was no difference in the expression of *PTPN1* in AML and normal samples. In contrast to the GEPIA database and RT-PCR, which revealed the opposite findings. This suggests that the expression and role of *PTPN1* in AML are still controversial, and further studies are needed to explore and clarify. *PTPN2* is frequently absent in adult and pediatric T-ALL patients, but the expression level of *PTPN1* does not correlate with patient prognosis (Alcantara et al., 2019). Similar to our findings, *PTPN2* expression did not differ between AML and normal samples and was not associated with patient prognosis. *PTPN3* is an oncoprotein with a poor prognosis and can promote cell invasion and proliferation in biliary cancer (Wang et al., 2018). *PTPN4* is highly expressed in AML and can guide the classification of AML (Kabir et al., 2013). *PTPN5* act as a tumor suppressor in breast cancer (Palaniappan et al., 2018), but previous studies have not found differences in the expression of *PTPN5* between AML and normal samples. Our findings demonstrated that, *PTPN3, PTPN4*, and *PTPN5* were not differentially expressed in AML and normal blood, and there was no correlation between their expression levels and patient survival. Several transmembrane receptors' intracellular signaling is modulated by *PTPN6* (SHP-1). When SHP-1 expression and activity are reduced, JAK kinase activity is raised, which causes aberrant cell proliferation (Wu et al., 2003). Activation of *PTPN6* (SHP-1) recruits CAMK1 to mediate self-renewal of AML (Hao et al., 2021). Compared to samples from AML patients and AML cell lines, the expression of *PTPN6* was significantly lower in our study's normal samples (whether in GEO and GEPIA databases or RT-PCR and western blotting results). Further evidence that *PTPN6* can be employed as a marker for the diagnosis and prognosis of AML comes from the substantial correlation between the high expression of *PTPN6* and the poor survival of AML patients. Cytoplasmic protein tyrosine phosphatase PTPN7, sometimes referred to as hematopoietic PTP, was first cloned from human T-cells. Since PTPN7 dephosphorylated ERK, T-cell activation was decreased in T cells derived from *PTPN7*-KO mice, as seen by the hyperphosphorylation of ERK on those cells (Inamdar et al., 2019). Our results from GEO and RT-PCR showed that *PTPN7* expression was lower in normal samples than in AML patients. However, the GEPIA results showed no statistically significant difference between the two. In contrast, the cytoplasmic PTP PTPN9 is broadly distributed in the tissues of the brain, leukocytes, endocrine cells, and other cells (Wang et al., 2019). PTPN11 is involved in many signal transduction functions necessary for normal hematopoiesis, and mutations in *PTPN11* can mediate the development of AML and are associated with poor prognosis (Alfayez et al., 2021). *PTPN12* is highly expressed in AML samples (Arora et al., 2012). Our results showed that in the GSE149237 microarray dataset, the expression of *PTPN11* was higher in AML than in normal controls, but in the GEPIA database, there was no difference between the two. The expression of *PTPN9* and *PTPN12* did not differ between AML patients and normal controls, neither in the GEO nor the GEPIA database. Transcription levels of *PTPN13* are abnormally elevated in myeloid malignancies (Mundle et al., 1999). *PTPN14* is now considered a tumor suppressor, but its expression and role in AML have not been studied and reported (Au et al., 2010). Our results showed the opposite. In the analysis of the GEO database, *PTPN13* was higher in AML than normal controls, while *PTPN14* was the utter opposite. In contrast, GEPIA results showed *PTPN13* and *PTPN14* expression in AML and normal controls with no difference. RT-PCR results showed that the expression of *PTPN13* and *PTPN14* was higher in AML and AML cell lines than in the control group. Only brain tissues express *PTPN20* (Xia et al., 2018), and overexpression of *PTPN21* promotes the proliferation of ALL cells by activating the mitogen-activated protein kinase (MAPK) signaling pathway (Wang et al., 2020). In our study, *PTPN20* expression did not differ between AML and normal samples. However, the expression results of *PTPN21* in AML and normal samples in the GSE149237 microarray dataset and GEPIA database were inconsistent. *PTPN23* is required for AML cell survival (Zhang et al., 2017). However, our results showed that normal samples had higher expression levels of *PTPN23* than AML samples. Furthermore, the expression of *PTPN23* in AML patients was not associated with the prognosis of the patients. Combined with the GSE149237 microarray dataset, GEPIA database, LinkedOmics database, RT-PCR, and western blotting results. *PTPN6* can be used as a marker for the diagnosis and prognosis of AML. However, further research and testing are needed to determine its association with AML risk.

Significant genomic genes of genetic alterations include changing the genetic code, inducing gene disruptions, and producing phenotypic differences (Egger et al., 2004; Zhou et al., 2016; Wu and Xu, 2020). An abnormal expression and *PTPN* dysfunction in AML can result from altered *PTPN* genes' chromosomal structure. In our study, 68/163 (42%) of the patient samples with AML had *PTPN* gene alterations, which included mutations, deep deletions, mRNA overexpression, mRNA down-expression, and multiple alterations. *PTPN11* mutations are frequently associated with acute myelomonocytic/monocytic leukemia subtypes, and *PTPN11* is associated with lower rates of complete remission and shorter overall survival (Alfayez et al., 2021). Our study shows that *PTPN11* has the highest probability of mutation, followed by *PTPN1, PTPN12, PTPN12*, and *PTPN6*. These results suggest that high genetic alterations in the *PTPN* gene are related to the development of AML.

GO analysis in this study showed that the PTPN protein was primarily related with the cytoplasm. The primary functions of *PTPN* genes, which have been extensively documented in various publications, are protein tyrosine phosphatase activity and dephosphorylation. *PTPN11* contains two N-terminal Src homology 2 (SH2) domains, a protein tyrosine phosphatase (PTP) catalytic domain, and a COOH terminus. *PTPN11* further contributes to the transformation of AML by encoding a ubiquitously expressed cytoplasmic phosphatase SHP2, which mediates cellular responses to hormones and cytokines (Stasik et al., 2021). Additionally, the outcomes of interaction network analysis at the gene and protein levels

further suggested extensive interactions between *PTPN* members and other genes. However, few studies have examined interactions between *PTPN* members in AML. According to one investigation, the dephosphorylation of IRF3 at Y245 is mediated by a protein that both *PTPN1* and *PTPN2* target (Xia et al., 2019). By dephosphorylating protein tyrosine kinases unique to lymphocytes, *PTPN2* and *PTPN22* have been found to affect T-cell receptor signaling (Cloutier and Veillette, 1999; Wiede et al., 2011). Multiple studies showed that PTPN5 and PTPN7 might bind to and inactivate the mitogen-activated protein kinases Erk2 and P38, which could negatively influence cell proliferation and differentiation (Francis et al., 2011; Francis et al., 2013; Francis et al., 2014). It has been noted that diffuse large B-cell lymphomas are prevented from progressing by the hypermethylation of the *PTPN6* and *PTPN13* promoters (Wang et al., 2016). In our study, the prognosis of patients with AML was related to *PTPN6, PTPN7, PTPN13*, and *PTPN13*. Therefore, *PTPN* members have the potential to play the role of numerous diseases, including AML, *via* consortium processes.

Our results demonstrate the expression status and prognostic value of *PTPN* members in AML. The results showed the differential expression of some *PTPN* members and their correlation with the prognosis of AML. These members' samples from healthy people had significantly lower levels of *PTPN6* expression than samples from AML patients. Furthermore, patients with AML had significantly worse survival rates when their PTPN6 expression was higher. *PTPN6* may be employed as a diagnostic and prognostic marker for AML, according to our findings. To further develop the therapeutic applicability of PTPNs, further well-designed studies are required to explain the importance of our findings.

Data availability statement

The datasets presented in this study can be found in online repositories. The names of the repository/repositories and accession number(s) can be found in the article/Supplementary Material.

Ethics statement

The studies involving human participants were reviewed and approved by Academic Committee of Seventh Affiliated Hospital of Sun Yat-Sen University. The patients/participants provided their written informed consent to participate in this study.

Author contributions

CC designed the paper. YL and CC are responsible for the conceptualization of the paper. CC performed the formal analysis. YL and CC wrote and corrected the manuscript. All authors contributed to the article and approved the submitted version.

Acknowledgments

We thank Sanming Project of Medicine in Shenzhen (No. SZSM202011004) to support the design of the study, Shenzhen Healthcare Research Project (Grant No. SZLY2018001), and Shenzhen Science and Technology Innovation Commission (JCYJ20180307150419435 and JCYJ20210324123004011) to support the manuscript preparation and publication.

Conflict of interest

The authors declare that the research was conducted in the absence of any commercial or financial relationships that could be construed as a potential conflict of interest.

Publisher's note

Supplementary material

The Supplementary Material for this article can be found online at: https://www.frontiersin.org/articles/10.3389/fgene.2022.1087938/full#supplementary-material

References

Alcantara, M., Simonin, M., Lhermitte, L., Touzart, A., Dourthe, M. E., Latiri, M., et al. (2019). Clinical and biological features of PTPN2-deleted adult and pediatric T-cell acute lymphoblastic leukemia. *Blood Adv.* 3 (13), 1981–1988. doi:10.1182/bloodadvances.2018028993

Alfayez, M., Issa, G. C., Patel, K. P., Wang, F., Wang, X., Short, N. J., et al. (2021). The Clinical impact of PTPN11 mutations in adults with acute myeloid leukemia. *Leukemia* 35 (3), 691–700. doi:10.1038/s41375-020-0920-z

Alonso, A., Sasin, J., Bottini, N., Friedberg, I., Friedberg, I., Osterman, A., et al. (2004). Protein tyrosine phosphatases in the human genome. *Cell* 117 (6), 699–711. doi:10.1016/j.cell.2004.05.018

Arora, D., Köthe, S., van den Eijnden, M., Hooft van Huijsduijnen, R., Heidel, F., Fischer, T., et al. (2012). Expression of protein-tyrosine phosphatases in acute myeloid leukemia cells: FLT3 ITD sustains high levels of DUSP6 expression. *Cell Commun. Signal* 10 (1), 19. doi:10.1186/1478-811X-10-19

Au, A. C., Hernandez, P. A., Lieber, E., Nadroo, A. M., Shen, Y. M., Kelley, K. A., et al. (2010). Protein tyrosine phosphatase PTPN14 is a regulator of lymphatic function and choanal development in humans. *Am. J. Hum. Genet.* 87 (3), 436–444. doi:10.1016/j.ajhg.2010.08.008

Cao, W., Chen, H. D., Yu, Y. W., Li, N., and Chen, W. Q. (2021). Changing profiles of cancer burden worldwide and in China: A secondary analysis of the global cancer statistics 2020. *Chin. Med. J. Engl.* 134 (7), 783–791. doi:10.1097/CM9.0000000000001474

Cerami, E., Gao, J., Dogrusoz, U., Gross, B. E., Sumer, S. O., Aksoy, B. A., et al. (2012). The cBio cancer genomics portal: An open platform for exploring multidimensional cancer genomics data. *Cancer Discov.* 2 (5), 401–404. doi:10.1158/2159-8290.CD-12-0095

Chandrasekharan, U. M., Dechert, L., Davidson, U. I., Waitkus, M., Mavrakis, L., Lyons, K., et al. (2013). Release of nonmuscle myosin II from the cytosolic domain of tumor necrosis factor receptor 2 is required for target gene expression. *Sci. Signal* 6 (284), ra60. doi:10.1126/scisignal.2003743

Chen, J., Zhao, X., Yuan, Y., and Jing, J. J. (2020). The expression patterns and the diagnostic/prognostic roles of PTPN family members in digestive tract cancers. *Cancer Cell Int.* 20, 238. doi:10.1186/s12935-020-01315-7

Cloutier, J. F., and Veillette, A. (1999). Cooperative inhibition of T-cell antigen receptor signaling by a complex between a kinase and a phosphatase. *J. Exp. Med.* 189 (1), 111–121. doi:10.1084/jem.189.1.111

Egger, G., Liang, G., Aparicio, A., and Jones, P. A. (2004). Epigenetics in human disease and prospects for epigenetic therapy. *Nature* 429 (6990), 457–463. doi:10.1038/nature02625

Fitzmaurice, C., Abate, D., Abbasi, N., Abbastabar, H., Abd-Allah, F., Abdel-Rahman, O., et al. (2019). Global, regional, and national cancer incidence, mortality, years of life lost, years lived with disability, and disability-adjusted life-years for 29 cancer groups, 1990 to 2017: A systematic analysis for the global burden of disease study. *JAMA Oncol.* 5 (12), 1749–1768. doi:10.1001/jamaoncol.2019.2996

Francis, D. M., Koveal, D., Tortajada, A., Page, R., and Peti, W. (2014). Interaction of kinase-interaction-motif protein tyrosine phosphatases with the mitogen-activated protein kinase ERK2. *PLoS One* 9 (3), e91934. doi:10.1371/journal.pone.0091934

Francis, D. M., Różycki, B., Koveal, D., Hummer, G., Page, R., and Peti, W. (2011). Structural basis of p38α regulation by hematopoietic tyrosine phosphatase. *Nat. Chem. Biol.* 7 (12), 916–924. doi:10.1038/nchembio.707

Francis, D. M., Kumar, G. S., Koveal, D., Tortajada, A., Page, R., and Peti, W. (2013). The differential regulation of p38α by the neuronal kinase interaction motif protein tyrosine phosphatases, a detailed molecular study. *Structure* 21 (9), 1612–1623. doi:10.1016/j.str.2013.07.003

GBD 2019 Diseases and Injuries Collaborators (2020). Global burden of 369 diseases and injuries in 204 countries and territories, 1990-2019: A systematic analysis for the global burden of disease study 2019. *Lancet* 396, 1204–1222. doi:10.1016/S0140-6736(20)30925-9

Hao, F., Wang, C., Sholy, C., Cao, M., and Kang, X. (2021). Strategy for leukemia treatment targeting SHP-1, 2 and SHIP. *Front. Cell Dev. Biol.* 9, 730400. doi:10.3389/fcell.2021.730400

Inamdar, V. V., Reddy, H., Dangelmaier, C., Kostyak, J. C., and Kunapuli, S. P. (2019). The protein tyrosine phosphatase PTPN7 is a negative regulator of ERK activation and thromboxane generation in platelets. *J. Biol. Chem.* 294 (33), 12547–12554. doi:10.1074/jbc.RA119.007735

Jäger, P., Geyh, S., Twarock, S., Cadeddu, R. P., Rabes, P., Koch, A., et al. (2021). Acute myeloid leukemia-induced functional inhibition of healthy CD34+ hematopoietic stem and progenitor cells. *Stem Cells* 39 (9), 1270–1284. doi:10.1002/stem.3387

Jin, Y., Cao, Q., Chen, C., Du, X., Jin, B., and Pan, J. (2015). Tenovin-6-mediated inhibition of SIRT1/2 induces apoptosis in acute lymphoblastic leukemia (ALL) cells and eliminates ALL stem/progenitor cells. *BMC Cancer* 15, 226. doi:10.1186/s12885-015-1282-1

Jin, B., Wang, C., Li, J., Du, X., Ding, K., and Pan, J. (2017). Anthelmintic niclosamide disrupts the interplay of p65 and FOXM1/β-catenin and eradicates leukemia stem cells in chronic myelogenous leukemia. *Clin. Cancer Res.* 23 (3), 789–803. doi:10.1158/1078-0432.CCR-16-0226

Kabir, N. N., Rönnstrand, L., and Kazi, J. U. (2013). Deregulation of protein phosphatase expression in acute myeloid leukemia. *Med. Oncol.* 30 (2), 517. doi:10.1007/s12032-013-0517-8

Kuang, W., Wang, X., Ding, J., Li, J., Ji, M., Chen, W., et al. (2022). PTPN2, A key predictor of prognosis for pancreatic adenocarcinoma, significantly regulates cell cycles, apoptosis, and metastasis. *Front. Immunol.* 13, 805311. doi:10.3389/fimmu.2022.805311

Lai, C., Doucette, K., and Norsworthy, K. (2019). Recent drug approvals for acute myeloid leukemia. *J. Hematol. Oncol.* 12 (1), 100. doi:10.1186/s13045-019-0774-x

Le Sommer, S., Morrice, N., Pesaresi, M., Thompson, D., Vickers, M. A., Murray, G. I., et al. (2018). Deficiency in protein tyrosine phosphatase PTP1B shortens lifespan and leads to development of acute leukemia. *Cancer Res.* 78 (1), 75–87. doi:10.1158/0008-5472.CAN-17-0946

Li, X., Wilmanns, M., Thornton, J., and Köhn, M. (2013). Elucidating human phosphatase-substrate networks. *Sci. Signal* 6 (275), rs10. doi:10.1126/scisignal.2003203

Mitra, R., and Ayyannan, S. R. (2020). Small-molecule inhibitors of Shp2 phosphatase as potential chemotherapeutic agents for glioblastoma: A minireview. *ChemMedChem* 16, 777–787. doi:10.1002/cmdc.202000706

Mundle, S. D., Mativi, B. Y., Bagai, K., Feldman, G., Cheema, P., Gautam, U., et al. (1999). Spontaneous down-regulation of Fas-associated phosphatase-1 may contribute to excessive apoptosis in myelodysplastic marrows. *Int. J. Hematol.* 70 (2), 83–90.

Ogino, S., Gulley, M. L., den Dunnen, J. T., and Wilson, R. B. (2007). Standard mutation nomenclature in molecular diagnostics: Practical and educational challenges. *J. Mol. Diagn* 9 (1), 1–6. doi:10.2353/jmoldx.2007.060081

Palaniappan, M., Edwards, D., Creighton, C. J., Medina, D., and Conneely, O. M. (2018). Reprogramming of the estrogen responsive transcriptome contributes to tamoxifen-dependent protection against tumorigenesis in the p53 null mammary epithelial cells. *PLoS One* 13 (3), e0194913. doi:10.1371/journal.pone.0194913

Patel, J. P., Gönen, M., Figueroa, M. E., Fernandez, H., Sun, Z., Racevskis, J., et al. (2012). Prognostic relevance of integrated genetic profiling in acute myeloid leukemia. *N. Engl. J. Med.* 366 (12), 1079–1089. doi:10.1056/NEJMoa1112304

Salmond, R. J., Brownlie, R. J., and Zamoyska, R. (2015). Multifunctional roles of the autoimmune disease-associated tyrosine phosphatase PTPN22 in regulating T cell homeostasis. *Cell Cycle* 14 (5), 705–711. doi:10.1080/15384101.2015.1007018

Siegel, R. L., Miller, K. D., Fuchs, H. E., and Jemal, A. (2021). Cancer statistics, 2017. *CA Cancer J. Clin.* 71 (1), 7–30. doi:10.3322/caac.21387

Siegel, R. L., Miller, K. D., Fuchs, H. E., and Jemal, A. (2022). Cancer statistics, 2016. *CA Cancer J. Clin.* 72 (1), 7–30. doi:10.3322/caac.21332

Stasik, S., Eckardt, J. N., Kramer, M., Röllig, C., Krämer, A., Scholl, S., et al. (2021). Impact of PTPN11 mutations on clinical outcome analyzed in 1529 patients with acute myeloid leukemia. *Blood Adv.* 5 (17), 3279–3289. doi:10.1182/bloodadvances.2021004631

Szklarczyk, D., Morris, J. H., Cook, H., Kuhn, M., Wyder, S., Simonovic, M., et al. (2017). The STRING database in 2017: Quality-controlled protein-protein association networks, made broadly accessible. *Nucleic Acids Res.* 45 (D1), D362–D368. doi:10.1093/nar/gkw937

Tallman, M. S., Wang, E. S., Altman, J. K., Appelbaum, F. R., Bhatt, V. R., Bixby, D., et al. (2019). Acute myeloid leukemia, version 3.2019, NCCN clinical practice guidelines in oncology. *J. Natl. Compr. Canc Netw.* 17 (6), 721–749. doi:10.6004/jnccn.2019.0028

Tang, Z., Li, C., Kang, B., Gao, G., Li, C., and Zhang, Z. (2017). Gepia: A web server for cancer and normal gene expression profiling and interactive analyses. *Nucleic Acids Res.* 45 (W1), W98–W102. doi:10.1093/nar/gkx247

Tonks, N. K. (2006). Protein tyrosine phosphatases: From genes, to function, to disease. *Nat. Rev. Mol. Cell Biol.* 7 (11), 833–846. doi:10.1038/nrm2039

Tonks, N. K. (2013). Protein tyrosine phosphatases--from housekeeping enzymes to master regulators of signal transduction. *Febs J.* 280 (2), 346–378. doi:10.1111/febs.12077

Vasaikar, S. V., Straub, P., Wang, J., and Zhang, B. (2018). LinkedOmics: Analyzing multi-omics data within and across 32 cancer types. *Nucleic Acids Res.* 46 (D1), D956–D63. doi:10.1093/nar/gkx1090

Wang, W., Wang, J., Li, Z., Zhu, M., Zhang, Z., Wang, Y., et al. (2016). Promoter hypermethylation of PTPL1, PTPN6, DAPK, p16 and 5-azacitidine inhibits growth in DLBCL. *Oncol. Rep.* 35 (1), 139–146. doi:10.3892/or.2015.4347

Wang, Y., Su, Y., Ji, Z., and Lv, Z. (2018). High expression of PTPN3 predicts progression and unfavorable prognosis of glioblastoma. *Med. Sci. Monit.* 24, 7556–7562. doi:10.12659/MSM.911531

Wang, D., Cheng, Z., Zhao, M., Jiao, C., Meng, Q., Pan, H., et al. (2019). PTPN9 induces cell apoptosis by mitigating the activation of Stat3 and acts as a tumor suppressor in colorectal cancer. *Cancer Manag. Res.* 11, 1309–1319. doi:10.2147/CMAR.S187001

Wang, H., Zhu, N., Ye, X., Wang, L., Wang, B., Shan, W., et al. (2020). PTPN21-CDSlong isoform inhibits the response of acute lymphoblastic leukemia cells to NK-mediated lysis via the KIR/HLA-I axis. *J. Cell Biochem.* 121 (5-6), 3298–3312. doi:10.1002/jcb.29601

Warde-Farley, D., Donaldson, S. L., Comes, O., Zuberi, K., Badrawi, R., Chao, P., et al. (2010). The GeneMANIA prediction server: Biological network integration for gene prioritization and predicting gene function. *Nucleic Acids Res.* 38, W214–W220. doi:10.1093/nar/gkq537

Wiede, F., Shields, B. J., Chew, S. H., Kyparissoudis, K., van Vliet, C., Galic, S., et al. (2011). T cell protein tyrosine phosphatase attenuates T cell signaling to maintain tolerance in mice. *J. Clin. Invest.* 121 (12), 4758–4774. doi:10.1172/JCI59492

Wiede, F., Lu, K. H., Du, X., Liang, S., Hochheiser, K., Dodd, G. T., et al. (2020). PTPN2 phosphatase deletion in T cells promotes anti-tumour immunity and CAR T-cell efficacy in solid tumours. *Embo J.* 39 (2), e103637. doi:10.15252/embj.2019103637

Wu, C., Sun, M., Liu, L., and Zhou, G. W. (2003). The function of the protein tyrosine phosphatase SHP-1 in cancer. *Gene* 306, 1–12. doi:10.1016/s0378-1119(03)00400-1

Wu, Y., and Xu, Y. (2020). Integrated bioinformatics analysis of expression and gene regulation network of COL12A1 in colorectal cancer. *Cancer Med.* 9 (13), 4743–4755. doi:10.1002/cam4.2899

Xia, C. Q., Han, K., Qi, Y., Zhang, Y., and Yu, D. J. (2018). A self-training subspace clustering Algorithm under low-rank representation for cancer classification on gene expression data. *IEEE/ACM Trans. Comput. Biol. Bioinform.* 15 (4), 1315–1324. doi:10.1109/TCBB.2017.2712607

Xia, T., Yi, X. M., Wu, X., Shang, J., and Shu, H. B. (2019). PTPN1/2-mediated dephosphorylation of MITA/STING promotes its 20S proteasomal degradation and attenuates innate antiviral response. *Proc. Natl. Acad. Sci. U. S. A.* 116 (40), 20063–20069. doi:10.1073/pnas.1906431116

Yu, Z. H., and Zhang, Z. Y. (2018). Regulatory mechanisms and novel therapeutic targeting strategies for protein tyrosine phosphatases. *Chem. Rev.* 118 (3), 1069–1091. doi:10.1021/acs.chemrev.7b00105

Zhang, S., Fan, G., Hao, Y., Hammell, M., Wilkinson, J. E., and Tonks, N. K. (2017). Suppression of protein tyrosine phosphatase N23 predisposes to breast tumorigenesis via activation of FYN kinase. *Genes Dev.* 31 (19), 1939–1957. doi:10.1101/gad.304261.117

Zhou, S., Treloar, A. E., and Lupien, M. (2016). Emergence of the noncoding cancer genome: A target of genetic and epigenetic alterations. *Cancer Discov.* 6 (11), 1215–1229. doi:10.1158/2159-8290.CD-16-0745

frontiers | Frontiers in Genetics

TYPE Original Research
PUBLISHED 18 January 2023
DOI 10.3389/fgene.2022.1065424

OPEN ACCESS

EDITED BY
Rui Cao,
Capital Medical University, China

REVIEWED BY
Qiaqia Li,
Sun Yat-sen University Cancer Center (SYSUCC), China
Qi Liu,
Sir Run Run Shaw Hospital, China
Yixin Tong,
University of Freiburg Medical Center, Germany

*CORRESPONDENCE
Xuanzi Yi,
xuanziyi22@gmail.com

SPECIALTY SECTION
This article was submitted to Cancer Genetics and Oncogenomics, a section of the journal Frontiers in Genetics

RECEIVED 09 October 2022
ACCEPTED 05 December 2022
PUBLISHED 18 January 2023

CITATION
Cheng X and Yi X (2023), RNA modification writers pattern in relation to tumor microenvironment and prognosis in prostate cancer. *Front. Genet.* 13:1065424. doi: 10.3389/fgene.2022.1065424

RNA modification writers pattern in relation to tumor microenvironment and prognosis in prostate cancer

Xu Cheng[1] and Xuanzi Yi[2]*

[1]Department of Urology, Xiangya Hospital, Central South University, Changsha, China, [2]Department of General Practice, The Third-Xiangya Hospital, Central South University, Changsha, China

Background: RNA modifications are important in the study of epigenetic regulatory mechanisms in immune responses and tumorigenesis. When RNA writers are mutated or disrupted in expression, the genes associated with the pathways they modify are also disrupted and can activate or repress related pathways, affecting tumorigenesis and progression. However, the potential role of RNA writers in prostate cancer is unclear.

Methods: Based on data from three datasets, we describe 26 RNA writers that mediate gene expression and genetic mutation in prostate cancer and assess their expression patterns in 948 prostate cancer samples. Using principal component analysis algorithms, the RM Score was developed to quantify the RNA modification patterns of specific tumors.

Results: Two different categories were determined by unsupervised clustering methods, and survival analysis showed significant differences in OS prognosis between these two categories. Differentially expressed genes between the different categories were detected and the RNA writers-mediated scoring model RM_Score were constructed based on this. Also, the RM_Score was analyzed in relation to clinical characteristics, immune infiltration level, drug response, and efficacy of chemotherapy and immunotherapy. Those results confirm that multilayer alterations in epitope-modified RNA writers are associated with patient prognosis and with immune cell infiltration characteristics. Finally, we examined differentially expressed mRNA, lncRNA and miRNA between high and low RM_Score groups, based on which a ceRNA regulatory network was constructed.

Conclusion: This work is a comprehensive analysis of modified writers in prostate cancer and identified them to have a role in chemotherapy and immunotherapy.

Abbreviations: APA, Alternative polyadenylation; M1A, N1-methyladenosine; A-to-I, Adenosine-to-inosine; BCa, Breast cancer; CNV, Copy number variation; DEGs, Differentially expressed genes; GEO, Gene Expression Omnibus; GSVA, Gene set variation analysis; HR, Hazard ratios; ICB, Immunological checkpoint blockade; PC, Prostate cancer; m6A, N6-methyladenosine; PCA, Principal component analysis; ssGSEA, Single-sample gene-set enrichment analysis; TCGA, The Cancer Genome Atlas; TME, Tumor microenvironment.

KEYWORDS

prostate cancer, RNA modification writers, immunotherapy, RM_score, prognosis

Introduction

In the male population worldwide, prostate cancer is the most common malignancy, and there is no effective treatment for advanced prostate cancer, particularly metastatic prostate cancer and castration-resistant prostate cancer (CRPC) (Siegel et al., 2021).% (Small and de Bono, 2011; Emmanuel et al., 2014; Royce et al., 2017).

In genetics, epigenetics is the study of stable and heritable phenotypes caused by changes in chromosomal sequence that do not alter gene sequences. In recent years, an increasing number of studies have demonstrated that RNA modification is a critical mechanism of epigenetic regulation and is involved in both physiological processes and disease development (Mo et al., 2014; Li et al., 2020; Ma et al., 2020; Yuan et al., 2020).

To fully understand the importance of post-transcriptional modifications, there is a need to explore the crosstalk between different patterns of these alterations. A few studies on *p*Ca have emphasized the importance of RNA alteration in carcinogenesis (Cai et al., 2019; Chen et al., 2021a). The majority of studies have concentrated on a limited number of genes, whereas RNA modification "writers" may form an important and complex network of cellular regulation in PC (Zhang et al., 2016; Zhang et al., 2020; Zhao et al., 2020), and an understanding of this network may provide important insights into the mechanisms behind PC tumorigenesis.

In this study, we explored genomic alterations in PC samples from the Gene Expression Omnibus (GEO) and The Cancer Genome Atlas (TCGA) cohorts and assessed patterns of RNA modifications. We found that RNA modification patterns were not only associated with infiltration of multiple immune cell types and clinical features, but also with AR pathway activation. Next, based on differentially expressed genes (DEGs) in the RNA modification pattern, we developed an RNA modification score (RM_Score) model of "writers" to quantify the efficacy of "writers" in individual patients. Finally, we assessed its therapeutic value in targeted therapies and immunotherapy and constructed a RM_Score-based CeRNA network.

Methods

Prostate cancer datasets source and preprocessing

The workflow of our study was shown in Supplementary Figure S1. Public gene-expression date and full clinical annotation were searched in the Cancer Genome Atlas (TCGA) database and Gene Expression Omnibus (GEO). Patients without survival information were removed from further evaluation. In total, two eligible PC cohorts (GSE70770, GSE116918) AND TCGA-PRAD (The Cancer Genome Atlas- Prostate Adenocarcinoma) were gathered in this study for further analysis. For microarray data, the normalized matrix files were directly downloaded. As to datasets in TCGA, RNA sequencing data (FPKM value) of gene expression and sample CNV information for prostate cancer samples were downloaded from the UCSC xena database (https://xenabrowser.net/datapages/), clinical information was downloaded using the R package cgdsr (version: 1.3.0), and mutation data was downloaded using the R package TCGAbiolinks (version: 2.16.4). It was then merged with the GSE70770 and GSE116918 chip expression data and batch effects from non-biological technical biases were corrected using the "ComBat" algorithm of sva package. (Version: 3.36.0) (Leek et al., 2012). In addition, copy number variation information for other tumors was downloaded using the R package TCGAmutations (version: 0.3.0).

The immunotherapy dataset for bladder cancer was downloaded using the R package IMvigor210CoreBiologies (version: 1.0.0)[15]. AS to chemotherapy datasets for breast cancer and advanced urothelial tumors (GSE25066 and GSE111636), the normalized matrix files were directly downloaded from GEO.

Clustering expression pattern of 26 RNA modification "writers"

Cluster analysis of RNA-modified "writers" in 984 prostate cancer samples was performed using an unsupervised clustering algorithm. 7 m6A modification enzymes (METTL3, METTL14, WTAP, RBM15, RBM15B, ZC3H13, and KIAA1429), 4 m1A modification enzymes (TRMT61A, TRMT61B, TRMT10C, and TRMT6), 12 APA modification enzymes (CPSF1-4, CSTF1/2/3, PCF11, CFI, CLP1, NUDT21, and PABPN1), and 3 A- (ADAR, ADARB1, and ADARB2). Unsupervised clustering was used to identify robust prostate cancer clustering (Hartigan et al., 1979). For the preceding steps, we utilized the Consensus-Clusterplus package (version 1.52.0) (Wilkerson and Hayes, 2010) and conducted 1,000 repetitions to ensure the classification's stability.

Identification of differentially expressed genes (DEGs) between RNA modification distinct phenotypes

To identify RNA modification "writers"-related genes, we classified patients into two distinct m6A modification patterns based on the expression of 26 RNA modification "writers". The

empirical Bayesian approach of limma R package was applied to determine DEGs between different modification patterns. The criteria for determining DEGs was set as adjusted p-value <0.05 and |logFC|>0.58.

Gene set variation analysis (GSVA) and estimation of TME cell infiltration

To study the differences of RNA modification patterns in biological processes, we used "GSVA" R package (version: 1.36.3) to conduct GSVA enrichment analysis (Hänzelmann et al., 2013). The gene set "c2. cp.kegg.v7.4" and "h.all.v7.4" for GSVA analysis was downloaded from the MSigDB database (https://www.gsea-msigdb.org/gsea/index.jsp, V7.4). The clusterProfiler R Package was used to functionally annotate 26 RNA modification enzyme genes (Yu et al., 2012).

To assess the proportion of 28 immune cell species in different subpopulations (data source: https://www.cell.com/cms/10.1016/j.celrep.2016.12.019/attachment/f353dac9-4bf5-4a52-bb9a-775e74d5e968/mmc3. xlsx), we obtained the degree of infiltration of 28 immune cell species using the ssGSEA (single sample gene set enrichment analysis) analysis in the R package GSVA (Charoentong et al., 2017).

Generation of RM_Score

To quantify the RNA modification patterns of individual tumor, we constructed a set of scoring system to evaluate the RNA modification pattern of individual patients with prostate cancer—the RM_Score (Zeng et al., 2019). The procedures for establishment of RM_Score were as follows:

First, the DEGs identified from distinct RNA modification clusters were normalized across all PC samples, and the overlap genes were extracted. Using an unsupervised clustering method for analyzing overlap DEGs, the patients were divided into multiple groups for further examination. The consensus clustering algorithm was used to determine the number and stability of gene clusters. Then, using the univariate Cox regression model, we performed prognostic analysis on each gene in the signature. The significant prognostic genes were isolated for further analysis. Then, using principal component analysis (PCA), we constructed a gene signature relevant to m6A. Components 1 and 2 were both chosen to serve as signature scores.

Calculation of TME cell invasion abundance

To quantify the relative abundance of 22 types of immune cells in colorectal cancer, we used CIBERSORT algorithm (https://cibersort.stanford.edu/) (Becht et al., 2016): the input mixture matrix is our gene expression matrix, the input is a gene signature reference for 22 immune cell types from Newman et al. (Newman et al., 2015), 100 times for permutation test, and RNA-seq data without quantile normalization, whereas microarray data with quantile normalization.

Correlation between RM_Score and other related biological processes

In a study by Mariathasan et al., they constructed a set of gene sets that primarily contained genes associated with biological processes such as 1) immune-checkpoint; 2) antigen processing machinery; 3) CD8 T-effector signature; 4) epithelial-mesenchymal transition (EMT) markers including EMT1, EMT2 and EMT3; 5) Angiogenesis signature; 7) pan-fibroblast TGFb response signature (Pan-F-TBRS); 8) WNT targets; 9) DNA damage repair; 10) mismatch repair; 11) Nucleotide excision repair; 12) DNA replication; 13) Antigen processing and presentation. We quantified these biological functions in each sample using GSVA analysis to calculate an Enrichment score (ES), which further revealed links between samples with high and low RM_Score groupings and a few relevant biological pathways (Mariathasan et al., 2018).

Association analysis of RM_Score and stromal score, immune score, estimate score, tumor purity

Immune scores, stromal scores, and tumor purity were calculated by R package estimate (version 1.0.13) based on specific gene expression profiles of immune and stromal cells by entering the gene expression profiles of the samples.

Association analysis of RM_Score and drug sensitivity

Approximately 1,000 transcription profiles for cancer cell lines were obtained from Genomics of Drug Sensitivity in Cancer (GDSC) (Yang et al., 2013), available at (http://www.cancerrxgene.org/downloads) (Adams et al., 2007). We calculated the correlation between drug sensitivity and RM_Score using Spearman correlation analysis, where |Rs| > 0. 35 and p 0.05 were considered significant correlations.

ceRNA regulatory network construction

Differential miRNA, lncRNA, mRNA between RM_Score high and low risk groupings were identified by R package limma,

where mRNA, miRNA, lncRNA screening criteria are |logFC| >0.58, $p < 0.05$, and miRNA-miRNA relationship pairs were downloaded from the miRTarBase database (http://mirtarbase.mbc.nctu.edu.tw/php/index.php), miRDB database and TargetScan database (http://www.targetscan.org/vert_72/)to download miRNA-miRNA targeting relationships, and then screened for mRNA_miRNA relationship pairs that were included in at least two sets of databases.

lncRNA-miRNA targeting relationships were downloaded from the TargetScan database (http://www.targetscan.org/vert_72/) to identify lncRNAs that have interactions with the above screened miRNAs. mRNA-miRNA-lncRNA networks were constructed by Cytoscape.

Statistical analysis

Spearman and distance correlation were used to calculate the RNA modification "writers" expression correlation coefficient. The Wilcoxon test was utilized to evaluate the differences. Utilizing the receiver operating characteristic (ROC) curve, the model's validity was determined.

On the basis of the correlation between RM Score and patient survival, the servicer package was utilized to establish the survival information cutoff point for each dataset. To reduce the calculated batch effect, the "surv-cutpoint" function was used to dichotomize RM Score, and all potential cutting points were repeatedly tested to determine the maximum rank statistic. Patients were then divided into the RM Score-high group and the RM Score-low group based on the maximum selected log-rank statistic. The Kaplan-Meier method was used to generate survival curves for prognostic analysis, and the log-rank test was applied to determine the significance of the differences. Utilizing a univariate Cox regression model, the hazard ratio (HR) between differentially expressed genes and "writers" was calculated. To determine whether RM Score is an independent predictor, we perform a multivariate Cox regression model analysis with age, gender, and stage as independent variables. All statistical analyses were two-sided, and p 0.05 was considered statistically significant.

Results

Landscape of genetic variation of 26 RNA modification "writers" in prostate cancer

The current study included 26 RNA modification "writers" (Supplementary Table S1), including three A-I modification "writers" seven m6A modification "writers" four m1A modification "writers" and twelve APA modification "writers."

To determine the genetic changes in RNA modification writers in pan-cancer, the prevalence of non-silent somatic mutations in 26 writers was evaluated. The mutation frequency of RNA writers was relatively low in the PRAD, PCPG, and UVM cohorts of the TCGA, while it was relatively high in the COAD cohort (Supplementary Figure S2A). Only 33 (29.46%) of the 484 PRAD samples contained mutations of RNA modification "writers" (Figure 1A). ZC3H13 had the highest mutation frequency (1%), followed by PCF11 and RBM15, whereas PABPN1 and NUDT21 did not exhibit any mutations in PRAD samples. PRAD patients with mutations of these "writers" showed a trend of longer overall survival rate than those without mutations though the difference showed non-statistically significant (Supplementary Figure S2B). Enrichment analysis' Gene Set Variation Analysis (GSVA) was used to compare the signature gene sets of the "writers" mutation group and the non-mutation group. Myogenesis, Inflammatory response, and other pathways are upregulated in the mutation group, whereas MYC target and androgen response are downregulated. (Supplementary Figure S2D).

We then examined somatic copy number variation (CNV) of these writers in prostate cancer and found that KIAA1429 and CPSF1 had a widespread frequency of copy number variation (CNV) gain (Figure 1B). We defined patients with CNV or SNP as the mutation group and the rest of the samples as the non-mutation group, then went for further survival analysis. The overall survival of the mutant group was significantly lower than that of the non-mutant group. (Figure 1C).

To determine whether these genetic variations influenced the expression of RNA writers in PC patients, we compared the mRNA changes of regulators between paired normal and PC samples and found that the expression of most RNA writers was significantly elevated in PC (Figures 1D–G). Additionally, the analysis revealed that RNA authors with CNV gain were expressed at a higher level in cancer tissues (Figures 1D–G). RNA modification "writers" with CNV gain (e.g., CPSF1 and TRMT10C) were significantly more prevalent in PC tissues than in normal prostate tissue, indicating that CNV may be a regulator factor for "writer" mRNA expression. However, a subset of "writer" cells exhibited upregulated mRNA expression and a high frequency of CNV loss. To investigate the discrepancy between CNV values and mRNA expression in tumor samples, we divided the PC cohort into four groups based on their CNV values, which included CNV gain, CNV loss, and non-significant CNV alteration. Then, we compared the "writer" mRNA expression between these groups (Supplementary Figure S2C). In fact, patients with CNV gain exhibited higher expression levels than patients with CNV loss in these "writers." CNV changes could not fully explain the differential expression of "writers" between tumor and normal tissues, as tumorigenesis is a complex process. Although many of the detected expression changes of "writers" can be explained by copy number variants (CNVs), CNVs are not the only factor that regulates mRNA expression. In addition to DNA methylation and transcription factors, additional factors can regulate gene expression.

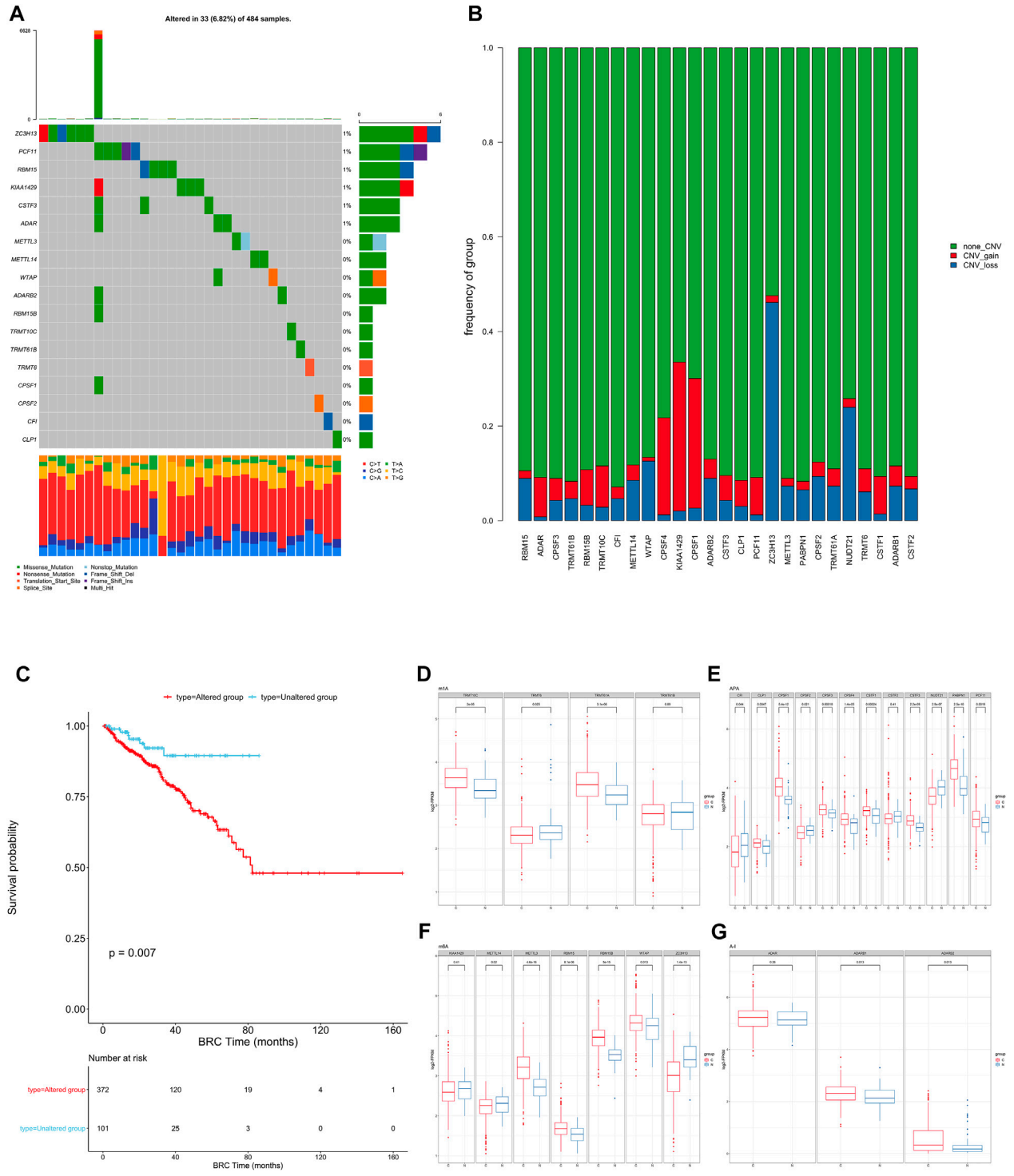

FIGURE 1
(A) The mutation frequency of RNA modification "writers" in 484 patients from the TCGA cohort. Each column represents individual patients. The upper bar graph shows TMB; the number on the right indicates the mutation frequency in each "writer". The right bar graph shows the proportion of each variant type. The stacked bar graph below shows the fraction of conversions in each sample. **(B)** Bar graphs showing the frequency of CNV gain (red), loss (blue) and non CNV (green) of RNA modification "writers" in the TCGA-PRAD cohort. The height of each bar represents the alteration frequency. **(C)** Kaplan-Meier curves show overall survival of patients with (red) or without (blue) mutations in RNA modification "writers" in the TCGA-PRAD cohort. The grouping of PC samples is indicated at the bottom of the chart. $P < 0.05$ in the two-sided log-rank test was considered statistically significant. **(D–G)**. Box plots show the expression distribution of 26 "writers" of 4 types of RNA modification between paired normal (blue) and cancer (red) tissues. The boxes indicate the median ±1 quartile, with the whiskers extending from the hinge to the smallest or largest value within 1.5× IQR from the box boundaries.

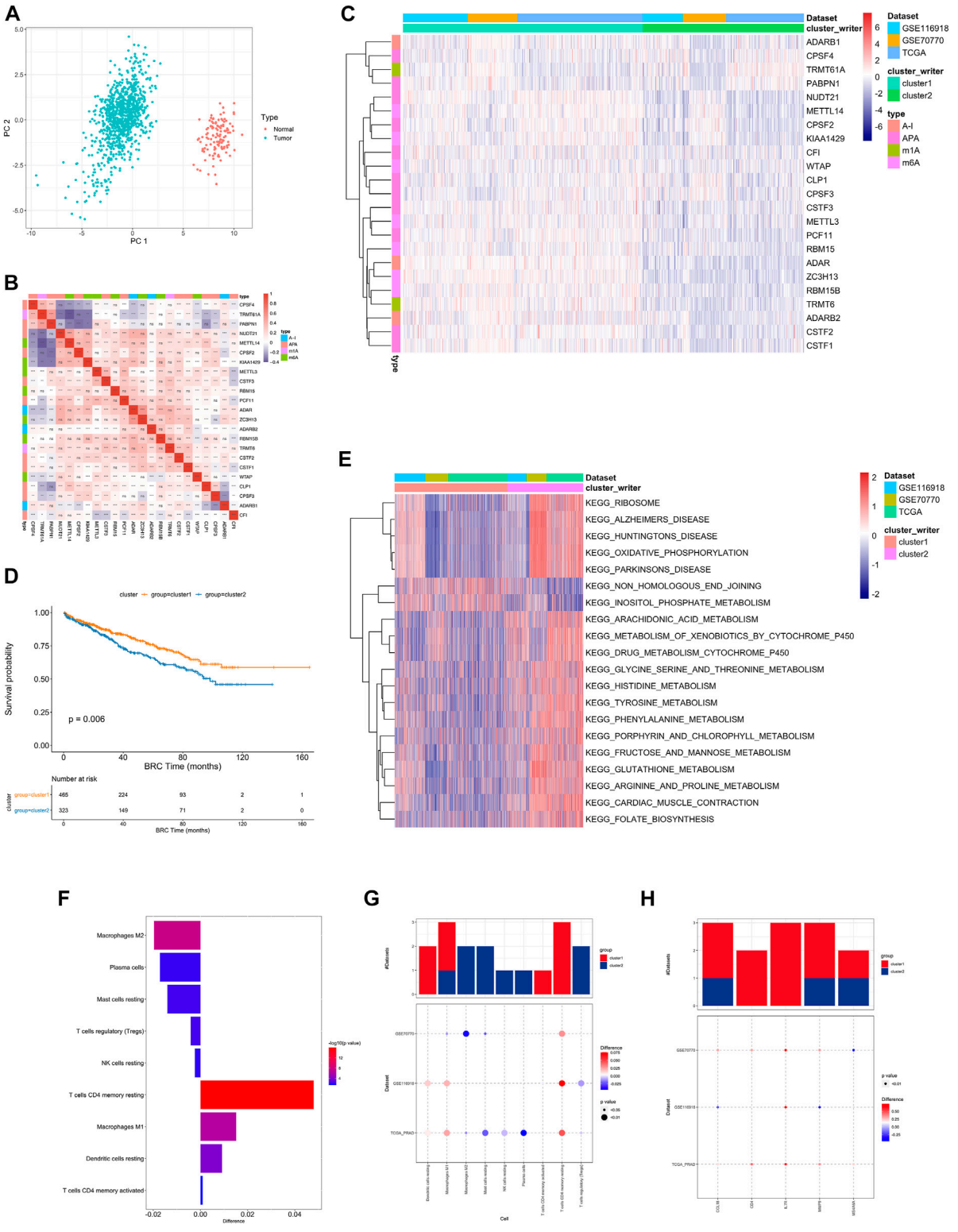

FIGURE 2
(A) PCA analysis of RNA writers between normal (red dot) and tumor (green) samples. **(B)** The difference in the relative abundance of immune cell infiltration in TME between RNA modification Cluster_1 and RNA modification Cluster_2 was calculated by the CIBERSORT algorithm. Difference >0 indicates that the immune cells were enriched in RNA modification Cluster_1, and the column color represents the statistical significance of the difference. **(C)** Heatmap shows a positive (red) and negative (blue) correlation among RNA modification "writers" in PC. *$p <$
(*Continued*)

FIGURE 2 (Continued)
0.05, **p < 0.01, and ***p < 0.001, as determined by the Spearman correlation analysis. **(D)** Kaplan-Meier curves compare overall survival between two RNA modification patterns, Cluster_1 (red) and Cluster_2 (blue), in all patients. The grouping of samples is shown at the bottom of the chart. P < 0.05 in the two-sided log-rank test was considered statistically significant. **(E)** Unsupervised clustering of 26 RNA modification "writers". The clusters of PC cohorts and RNA modification types were used as sample annotations. Red, high expression of "writers"; blue, low expression. **(F)** Heatmap visualizing the GSVA enrichment analysis shows the activation states of biological pathways in distinct RNA modification patterns. Red, activated pathways; blue, inhibited pathways. The names of PC cohorts were used as sample annotations. **(G,H)**. The difference of immune cell infiltration **(G)** and expression of macrophage M2 and T cells CD4 memory resting marker genes **(H)** between RNA modification patterns. The upper bar graph shows the number of datasets that differ significantly between Cluster_1 and Cluster_2. The color of the bubble below the graph indicates the difference in each of the distinct GEO datasets, and 0the bubble size indicates the statistical significance of the difference. Difference >0 indicates that the infiltration of immune cells **(G)** or expression of macrophage M2 and T cells CD4 memory resting marker genes **(H)** were higher in RNA modification Cluster 1.

This suggests that the mutation of "writer" including CNV and SNP, has potential role in the tumorigenesis and development of PC.

Distinct patterns of RNA modification "writers" associated with cancer hallmarks and immune infiltration

A total of 948 prostate cancer samples and 125 control samples were selected for further analysis from three databases (TCGA, GSE116918, GSE70770) to obtain a more comprehensive understanding of the expression patterns of writers involved in tumorigenesis in prostate cancer.

First, the distribution of the studied RNA writers in the genes were showed (Supplementary Figure S3A, Supplementary Table S7). PCA analysis of cancer and normal samples using these genes can clearly distinguish cancer samples from healthy control samples (Figure 2A).

Univariate Cox regression was performed on RNA writers and the samples were divided into two categories based on median gene expression values. 6 RNA writers were found to be associated with prostate cancer prognosis, including CPSF3, CSTF1, etc. (Supplementary Figure S1D, Supplementary Table S8).

A pairwise correlation was calculated between the expression of 26 writers in PC, and positive correlations were more common than negative correlations (Figure 2B). There was a significant correlation not only between the expression of RNA modification "writers" in the same category, but also among different types of modification writers.

In addition, we also performed consistent clustering of RNA writers expression profiles and presented the results in a network plot, which is shown in Supplementary Figure S3C The genes with black dots were positively correlated with prognosis and those with green dots were negatively correlated with prognosis, and the RNA writers gene regulatory network in this figure depicts the correlation between these genes interactions and the regulators with prognosis (Supplementary Table S9).

Based on the expression profiles of 23 selected RNA modification "writers" (Supplementary Table S12), we classified patients with qualitatively different RNA modification patterns using Consensus Clustering. According to unsupervised clustering, 567 patients from the combined datasets were assigned to Cluster_1, whereas 381 patients were assigned to Cluster_2 (Figure 2C). A prognostic analysis of RNA modification patterns revealed that Cluster_1 showed a marked survival advantage (Figure 2D, log-rank test, p = 0.006). An analysis of GSVA enrichment (Supplementary Table S13) was performed to determine the biological significance of these distinct RNA modification patterns. Cluster_1 was enriched in steroid hormone biosynthesis and prostate cancer pathways. Cluster_2 was enriched in ribosome, oxidative phosphorylation, and drug metabolism cytochrome P450 (Figure 2E).

Infiltrating immune cells from TMEs have been linked to RNA modification in numerous studies. Thus, we investigated the function of "writers" in TME. To determine the type of immune cells found in tumors, we used the CIBERSORT deconvolution algorithm, based on support vector regression, to compare immune cell types among RNA modification patterns (Supplementary Table S10). A significant correlation between CFI expression and dendritic cell resting was found, while a significant correlation between CPSF3 expression and plasma cells was found (Supplementary Figure S3B).

There were also significant differences in TME cell infiltration between the two RNA modification clusters (Figure 2F). We observed that Macrophages M1 and resting DCs were significantly higher in Cluster_1, whereas M2 macrophages, TREGs, and NK cells were significantly higher in Cluster_2 (Figures 2G,H). Accordingly, a comparison of the expression of macrophage markers in Cluster_1 and Cluster_2 indicated that M2 macrophage marker genes and T cell CD4 memory resting genes were significantly upregulated in Cluster_1 (Figure 2H). As a result, RNA modification patterns affected the degree of infiltration by certain immune cell types but did not alter the types of immune cells infiltrating the cells.

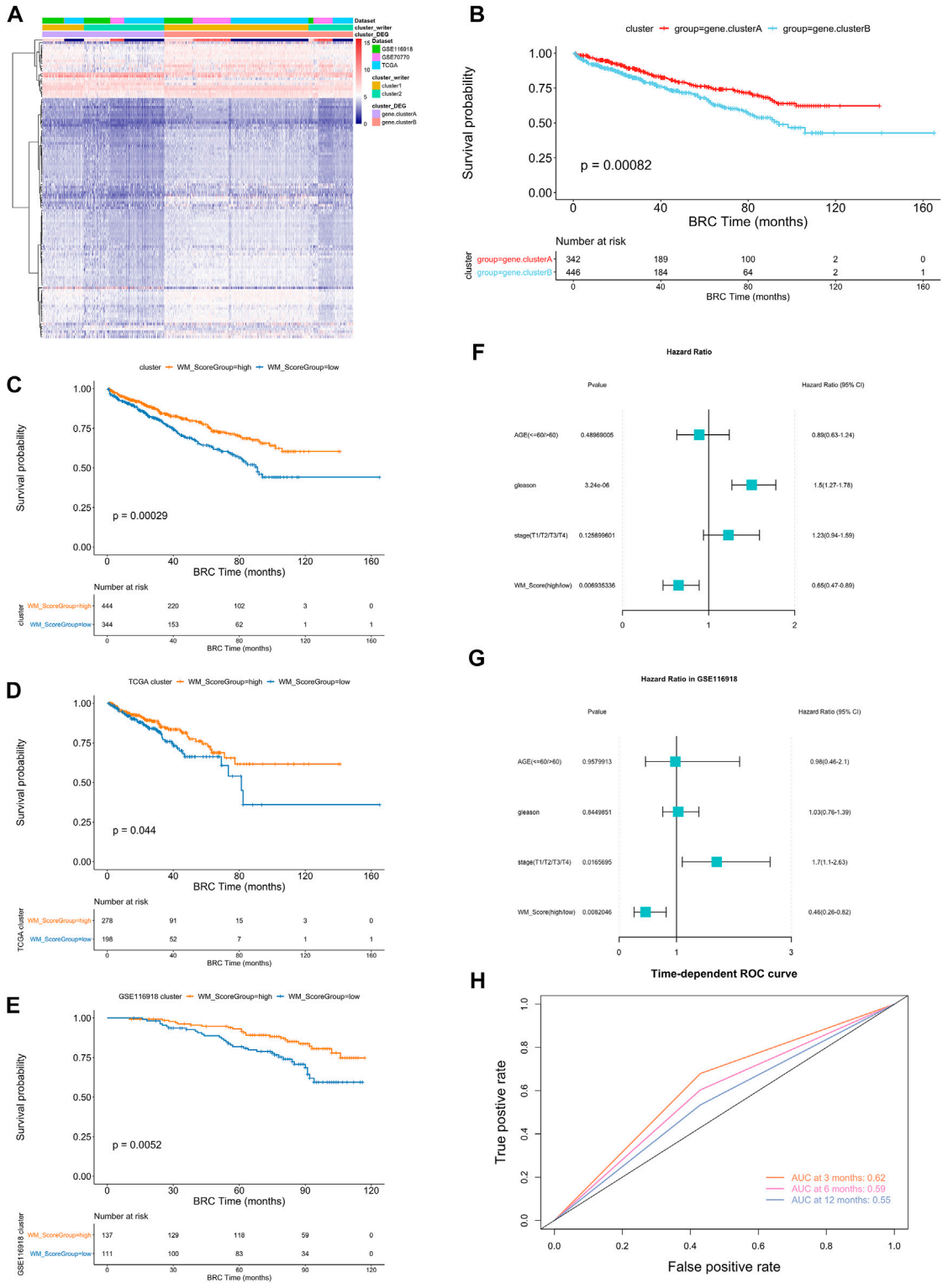

FIGURE 3
(A) Unsupervised clustering of the RNA modification phenotype-related genes. The names of those 3 PC cohorts were used as sample annotations. Red, high expression of phenotype-related genes; blue, low expression. **(B)** Kaplan-Meier curves comparing overall survival between two DEG clusters, gene. cluster_A (red) and gene. cluster_B (blue), in the 3 PC cohort. The grouping of PC samples is shown under the Kaplan-Meier plot. $P < 0.05$ in the two-sided log-rank test was considered statistically significant. **(C–E)** Kaplan-Meier curves show overall survival in WM_ Score-high (red) and -low (blue) in all samples **(C)**, TCGA **(D)** and GSE116918 **(E)**. The grouping of PC samples is shown at the bottom of the chart. $P <$
(*Continued*)

FIGURE 3 (Continued)
0.05 in the two-sided log-rank test was considered statistically significant. **(F–G)**. Multivariate Cox regression model analysis, which included the factors of WM_Score, patient age, Gleason score, TNM status, and patient outcomes in the overall samples **(F)** and GSE116918 **(G)** cohorts. The length of the horizontal line represents the 95% confidence interval (CI) for each group. The vertical dotted line represents the hazard ratio (HR) of all patients shown by the forest plot. **(H)** The predictive value of WM_Score in patients (AUC:0.62, 0.59, and 0.55, 3, 6, 12-month overall survival).

Construction of RNA modification "writer" signature

To further analysis those two RNA modification patterns in the prostate cancer, we identified 116 RNA modification related differential expressed genes and performed enrichment analysis (Figure 3A, Supplementary Table S15, screening criteria were |logFC|>0.58, p-value < 0.05). These differential genes were mainly associated with some metabolic pathways (Supplementary Table S17). To further validate this differential regulation, an unsupervised clustering analysis was performed on these differential genes. This analysis classified patients into two genetic subtypes: gene cluster A and gene cluster B (Supplementary Table S16), and the two subtype clusters showed significant differences in prognosis (Figure 3B).

In order to quantify the RNA modification pattern of individual patients with PC, we constructed a DEGs-based score model based on these phenotype-related genes; this model was referred to as the RM_Score ("Writers" of RNA Modification_Score; see Methods). According to the surv cut point function in the R package survminer, the best threshold points for RM_Score classification was determined (cutoff = 0.0212,004) and the samples were classified into two categories, RM_Score high and RM_Score low (Supplementary Table S19), the RM_Score high and RM_Score low samples were significantly different in prognosis across all samples, RM_Score high (Figure 3C). The similar results are observed in the TCGA (Figure 3D) and GSE116918 (Figure 3E) datasets. And the area under the ROC curve for prediction of survival at 3, 6 and 12 months reached 0.62, 0.59 and 0.55 (Figure 3H). The subtypes obtained from the second clustering analysis also had significantly different RM_Score in the two previous clustering analyses. Based on Wayne diagrams and histograms of frequency distributions (Supplementary Figure S4A–D), A comparison of these three classifications revealed that the latter two classifications were calculated consistently (Supplementary Table S20).

Molecular subtypes and clinical characteristics associated with RM_Score in PC

An analysis of multivariate Cox regression using the patient's clinical characteristics, including age, Gleason score and stage status, was conducted to determine whether the RM_Score could be used as an independent prognostic factor (Figure 3F). The analysis showed that both Gleason and RM_Score were significantly associated with prognosis in the full sample (Figures 4A,B, Supplementary Table S22). A sample of prostate cancer patients from the GSE116918 database was used to validate the reliability of the RM_Score, in which the data set demonstrated a significant correlation between the stage and the RM_Score. (Figure 3G, Supplementary Table S22).

The result of comparison between different subtype and Gleason score in all patients were shown (Figures 4A,B). Also, we compared the variability of RM_score between hormone resistant and sensitive samples in the GSE70770 set and it showed a significant difference in scores between two (Figure 4C). Notably, lower RM_score was found in higher Gleason score group and castration resistant group, which corresponded to the result of the survival analysis in the previous section, i.e., the low RM_score group had a poor prognosis. It is not absolute, however. Figure 4D illustrates the flow of various Gleason scores between RM_score groups for all datasets. Some low Gleason score patients are categorized as low-RM_score groups, whilst some high Gleason score patients are categorized as high RM_score groups.

As to the GSVA analysis, most pathways were up-regulated in RM_score high group, like PI3K, KRAS, MAPL, P53, estrogen response pathway, while androgen response and MYC targets were up-regulated in RM_score low group (Figure 4E).

Using the maftools package, we then analyzed the distribution differences of somatic mutation between low and high RM score in the TCGA-PRAD cohort. As shown in Supplementary Figure S7A,B, the low RM score group had a mutation burden comparable to the high RM score group. The high frequency of mutational load suggests that these genes play a significant role in the development of prostate cancer, despite the absence of a statistically significant difference between the two groups.

Analysis of the relationship between RM_Score and immune infiltration

We used ssGSEA to analyze the differences in immune infiltrating cell types between the RM_Score high and low risk groups (Supplementary Table S25). The results are shown in Figure 5A. However, there is no significant difference in all cell types between RM_score high and low groups, which indicates RNA modification patterns may affect the degree of infiltration but did not alter the types of infiltrating immune cells.

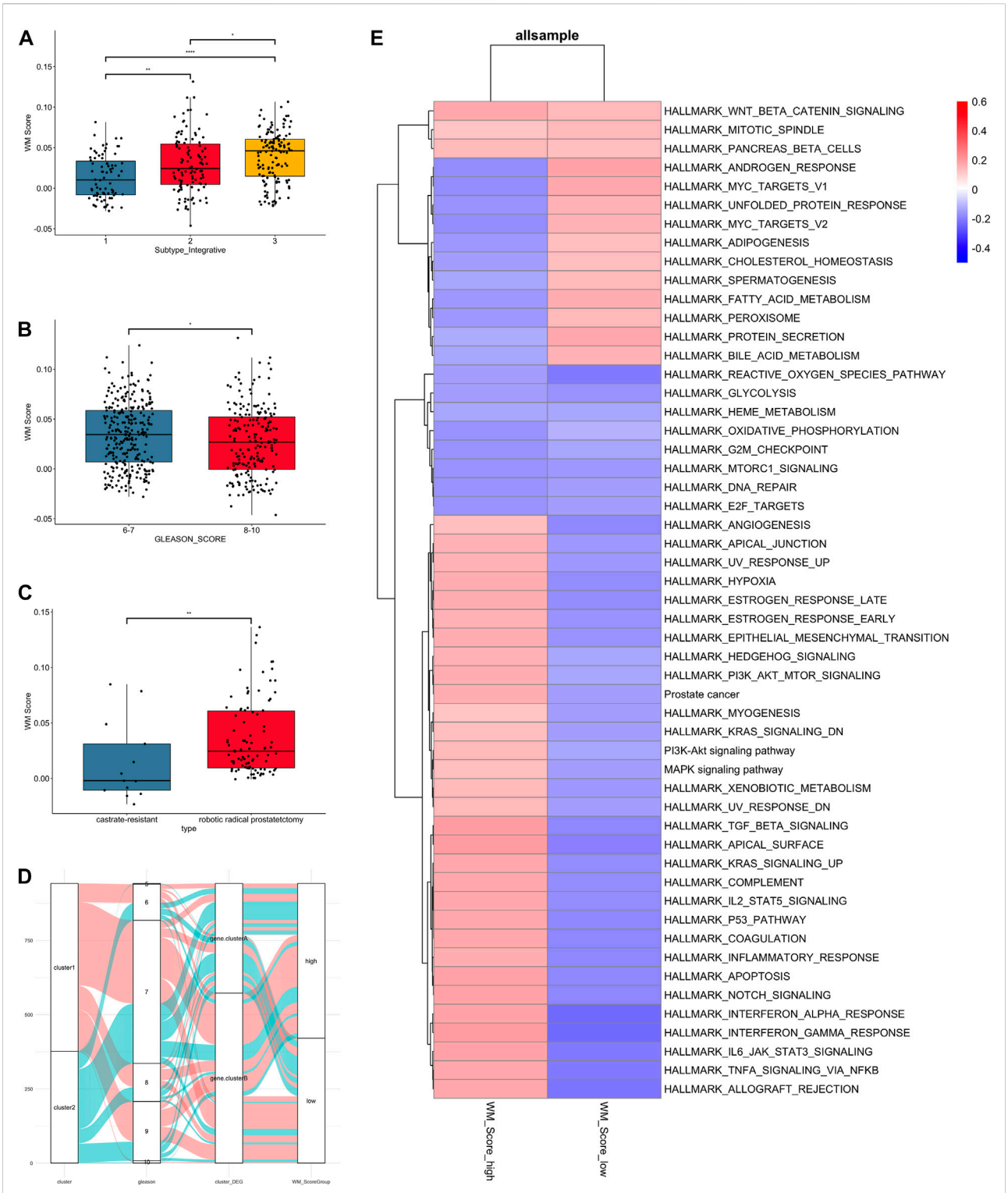

FIGURE 4
Clinical and biological characteristics of PC associated with the WM_Score. **(A)** WM_Score differences among TCGA molecular subtypes of PC in TCGA-RAD datasets. **(B)** Differences in the WM_Score between Gleason score 6-7 (blue) and 8-10 (red) group in the 3 PC cohort. **(C)** Differences in the WM_Score between castrate-resistant (blue) and robotic radical prostatectomy (red) group in the GSE70770 cohort. Wilcoxon test was used to assess the difference. The boxes indicate the median ±1 quartile, with the whiskers extending from the hinge to the smallest or largest value within 1.5× IQR from the box boundaries. **(D)** The Sankey diagram shows the variation in the distribution of samples across these classifications **(E)** Heatmap shows the differences in enrichment in the characteristic signaling pathways of PC subtypes between WM_Score-high and -low groups in all samples. Red, high enrichment score; blue, low enrichment score.

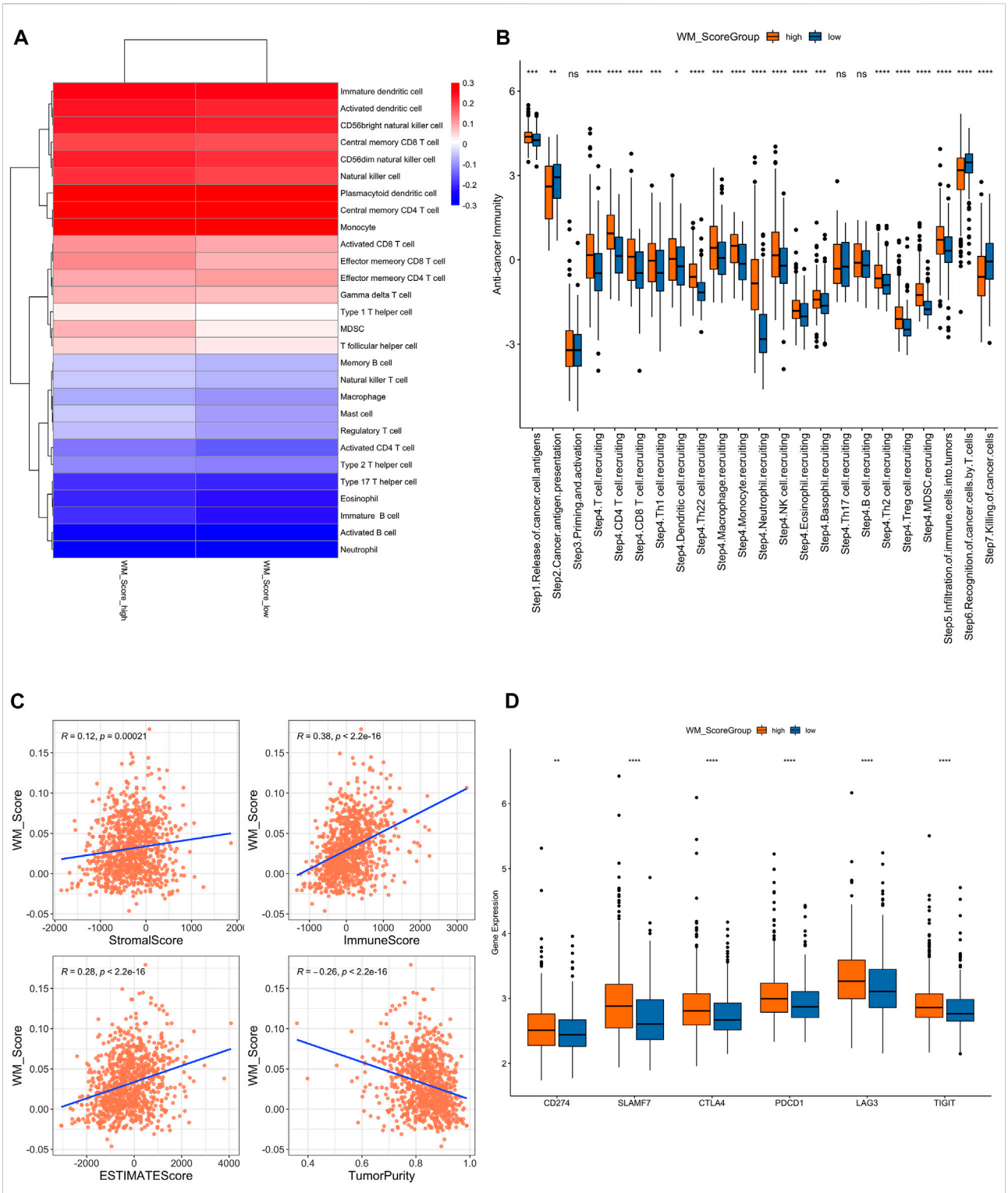

FIGURE 5
(A). Difference of immune cell infiltration in the WM_Score-high/-low. **(B)** Analysis of the difference in anti-tumor immune process activity between high and low risk groups with WM_Score scores. **(C)** Correlation of WM_Score scores with stromal score, immune score, and tumor purity (A: stromal score; **(B)** immune score; **(C)** estimate score; **(D)** tumor purity) by Spearman analysis. **(D)** Gene expression of immune checkpoint expression in WM_Score -high and -low.

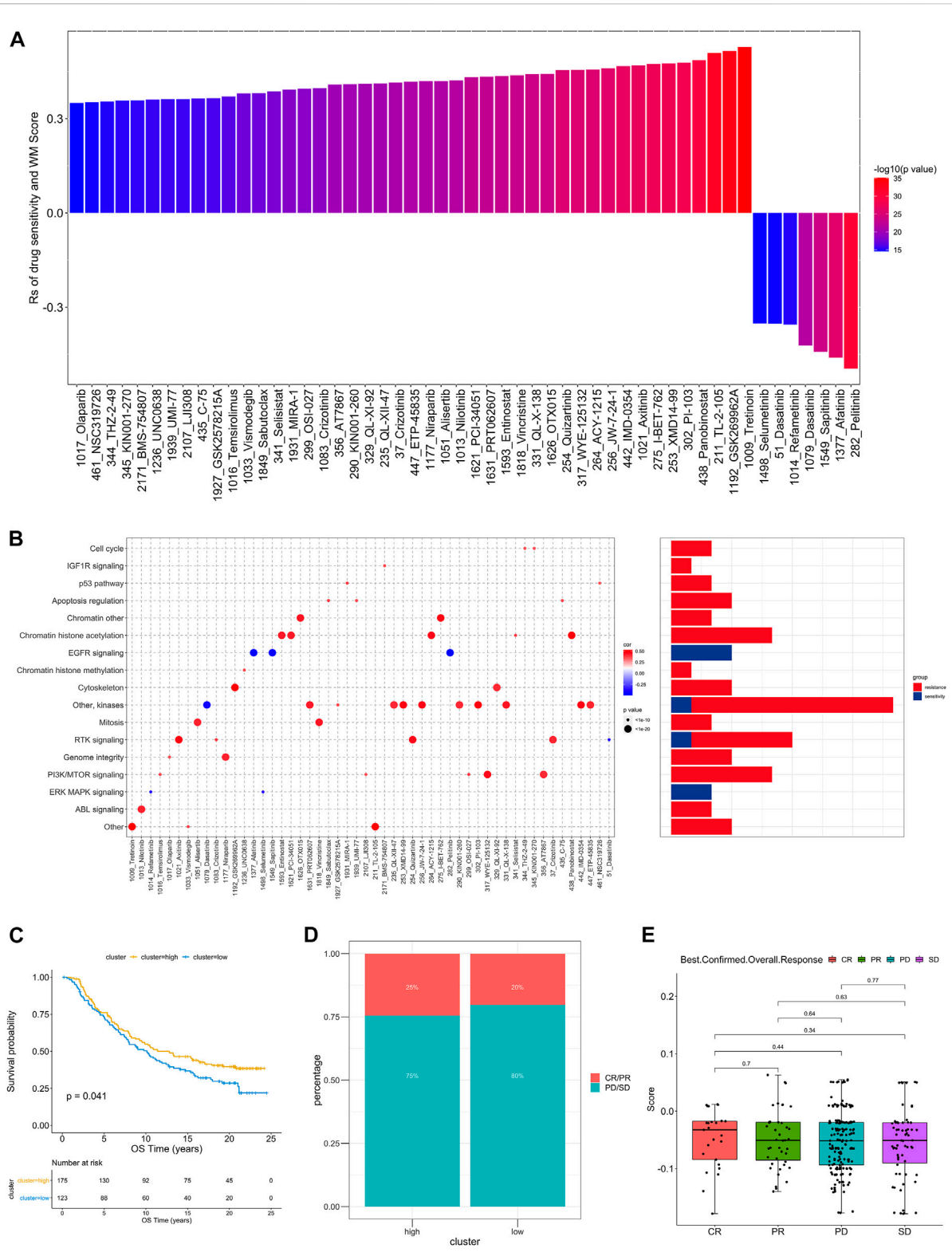

FIGURE 6
The relationship between WM_Score and drug sensitivity and efficacy of immunotherapy. **(A)** The correlation between WM_Score and drug sensitivity evaluated by the Spearman analysis. Each column represents a drug. The color of the column indicates the significance of the correlation. The height of the column indicates the correlation, indicates that WM_Score related to drug resistance (Rs > 0) or drug sensitive (Rs < 0) to WM_Score. **(B)** Signaling pathways targeted by drugs that are resistant (red) or sensitivity (blue) to the WM_Score. Drug names are listed on the

(*Continued*)

FIGURE 6 (Continued)
horizontal axis and the signaling pathway targeted by the drug on the vertical axis. The bar graph on the right shows the number of drugs targeting each signaling pathway. The size of the point indicates the significance of the correlation. **(C)** Kaplan-Meier curves show overall survival in the WM_Score-high (red) and -low (blue) subgroups after the immunotherapy in the IMvigor210 cohort. The grouping of patients is shown at the bottom of the chart. $P < 0.05$ in the two-sided log-rank test was considered statistically significant. **(D)** The proportion of patients in the IMvigor210 cohort with different responses to PD-L1 blockade immunotherapy. The fisher test was used to determine the statistical significance of the difference. SD, stable disease; PD, progressive disease; CR, complete response; PR, partial response. **(E)** The difference in the WM_Score between distinct clinical outcomes of anti-PD-L1 treatment in the IMvigor210 cohort.

We also performed a correlation analysis between RM_Score and stromal score, immune score, and tumor purity (Figure 5C, Supplementary Table S26). The stromal and immune score were proportional to RM_score but tumor purity had negative correlation to RM_score.

We downloaded the results of the TIP analysis of TCGA prostate cancer samples from the TIP (Tracking Tumor Immunophenotype) website (http://biocc.hrbmu.edu.cn/TIP/) and then compared the differences in anti-tumor immune process activity between the high and low RM_Score risk groups. We also analyzed the differential expression of immune checkpoint expression in those two groups. The RM_Score high group showed significantly higher expression levels than the RM_Score low group, as shown in Figure 5B, importantly in step4 T cell recruiting, while the step7 killing of cancer cells are more active in RM_score low group.

Additionally, we examined the differences in immune checkpoint expression between the WM Score high and low score groups. These genes' expression levels varied significantly between the two groups of samples, and they were significantly higher in the WM Score high group than in the WM Score low group (Figure 5D).

The role of RM_Score in drug sensitivity and immunotherapy and chemotherapy efficacy

In order to further understand how the RM_Score affects drug response, we assessed the relationship between the RM_Score and the response to drugs in cancer cell lines. As a result of Spearman correlation analysis, we identified 52 significant correlations between RM_Score and drug sensitivity in the Genomics of Drug Sensitivity in Cancer (GDSC) database (Figure 6A, Supplementary Table S28). Among them, forty-five pairs showed that drug sensitivity correlated with the RM_Score, including the EGFR inhibitor Afatinib ($Rs = -0.26$, $p = 4.12 \times 10–13$). Seven pairs exhibited drug resistance correlated with the RM_Score, including PARP inhibitor Olaparib ($Rs = 0.35$ $p = 2.60E-15$), TKI inhibitor Axitinib ($Rs = 0.47$, $p = 1.04E-27$). A further analysis was conducted to examine the signaling pathways of the genes targeted by these drugs. It was found that drugs whose sensitivity was associated with high RM_Score targeted cell cycle, chromatin, and RTK signaling pathways. In contrast, the drugs associated with low RM Score sensitivity targeted the MAPK and EGFR pathways (Figure 6B). These findings suggest a correlation between RNA modification patterns and drug sensitivity. Thus, the RM Score may serve as a biomarker for determining the most effective treatment strategies.

As the RM_Score appears to be associated with the immune microenvironment of the tumor (Figure 5C), we examined its ability to predict the response of patients to ICB treatment. A total of two immunotherapy cohorts were analyzed in this study. As shown in Figure 6C, the RM_Score high group had significant clinical benefits and a markedly prolonged overall survival in the anti-PD-L1 cohort (IMvigor210). However, there was no significant difference between the 348 IMvigor210 patients' responses to anti-PD-L1 blockers (Figures 6D,E), including complete responses (CR), partial responses (PR), stable diseases (SD), and progressive diseases (PD). As shown in Figure 6E, we didn't observe significant differences between the immune subtypes of IMvigor210, namely "immune inflamed", "immune excluded", and "immune desert". Additionally, TMB and neoantigen burden were similar in groups with low and high RM_Score (Supplementary Figures S4C–E). However, the situation is different in another anti-PD-1 cohort (GSE111636). The RM_score was significantly higher in responder to anti-PD-1 therapy group than progressor group (Figures 7C,D).

The situation is even more interesting in a breast cancer chemotherapy cohort when we tried to better define the role of RM_score in chemotherapy. Unlike the previous prostate cancer cohort and the high-grade uroepithelial cancer cohort (GSE111636), the survival analysis of the breast cancer cohort showed significantly better survival in the low group than in the high group (Figure 7A, $p < 0.0001$). Also, the chemotherapy sensitive group exhibited lower RM_score than insensitive group (Figure 7B, $p = 0.048$).

RM_Score related ceRNA network construction

We then used R package limma to identify RM_Score high and low risk grouping differential miRNAs, lncRNAs, and mRNAs. mRNA, miRNA, and seven differential miRNAs, and 77 differential lncRNAs were screened, respectively (Figures 7E–H, Supplementary Table S30). Then the ceRNA network was constructed by combining the regulatory relationships of the database. The network contained a total of 15 mRNAs, 1 lncRNA and 1 miRNA (Figure 7I).

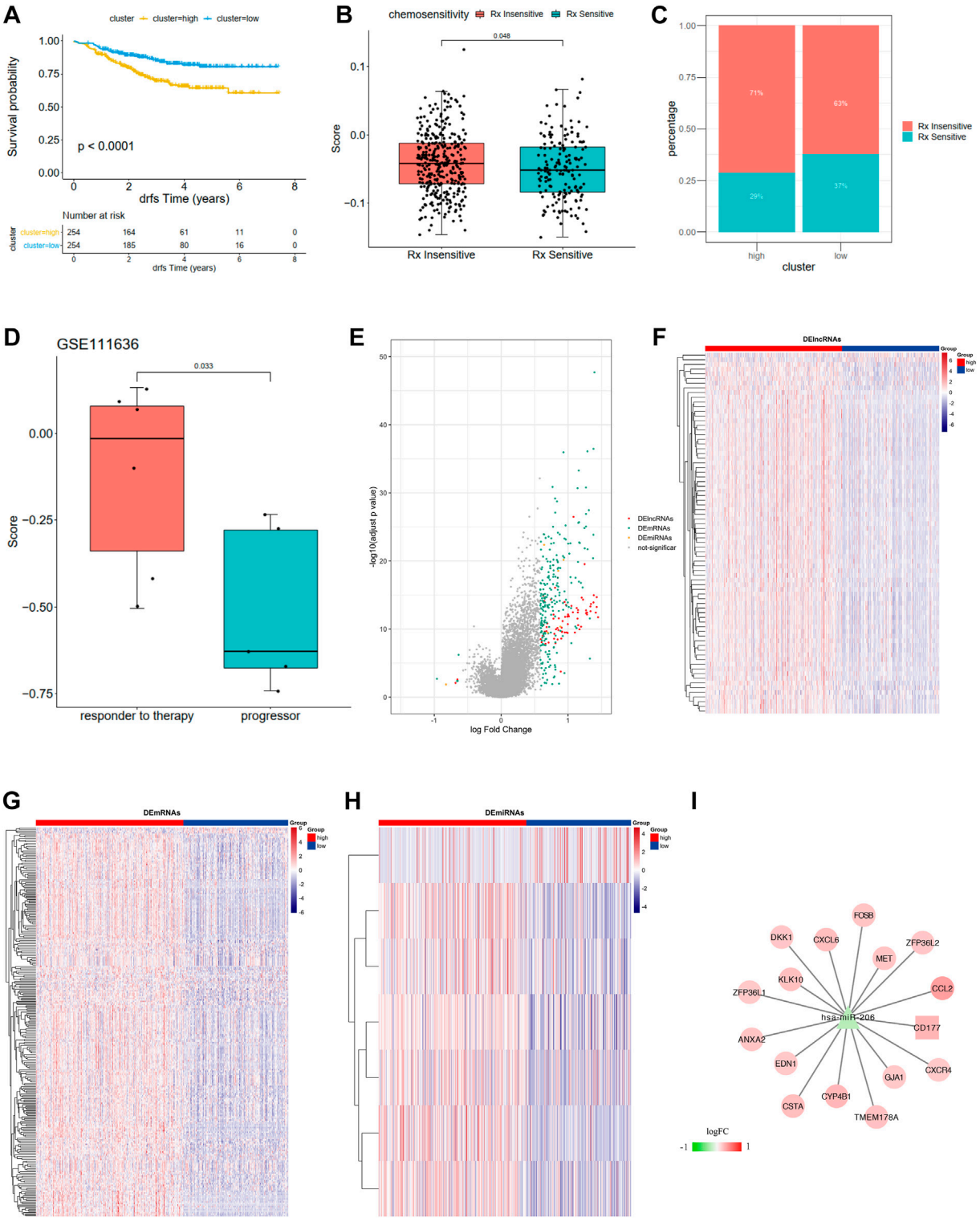

FIGURE 7
(A) Kaplan-Meier curves show overall survival in the WM_Score-high (yellow) and -low (blue) subgroups after the immunotherapy in the GSE25066. The grouping of patients is shown at the bottom of the chart. $P < 0.05$ in the two-sided log-rank test was considered statistically significant. **(B)** The proportion of patients in the GSE25066 with different responses to chemotherapy. The fisher test was used to determine the statistical significance of the difference. **(C)** The difference between distinct between the WM_Score high and low groups in the GSE25066. **(D)** The difference in the WM_Score between distinct clinical outcomes of anti-PD-1 treatment in the GSE111636. **(E–I)** WM_Score -High and -low differential expression of miRNA, lncRNA, mRNA (E: differential volcano map; FGH: differential lncRNA, mRNA, miRNA heat map, respectively) and ceRNA network (I: square is lncRNA, triangle is miRNA, circles are mRNAs).

Discussion

Increasing evidence suggests that RNA modifications play a crucial role in inflammation, innate immunity, and anti-tumor activity by interacting with a variety of "writers." The interrelationships and functions of multiple types of RNA modification "writers" in cancer are not yet fully understood. Here, we reveal the overall variation in RNA modifications at the transcriptional level: m6A, m1A, APA, and A-to-I RNA editing enzymes; and their interrelationship in prostate cancer.

We identified two distinct RNA modification patterns based on 26 RNA modifying enzymes, defined two subtypes of prostate cancer associated with RNA modification, and developed a scoring model, RM Score, to evaluate the effectiveness of RNA modification "writers" in individual patients. Intriguingly, it was associated with a better prognosis in breast cancer but a worse prognosis in prostate and bladder cancer. In addition, the subtype with a high RM Score is distinguished by a significant inhibition of the AR signaling pathway and a significant activation of the estrogen pathway.

In our study, RM_score scores had opposite prognostic predictive effects for two different tumors, the urological cancer and breast cancer. It has been shown that the androgen pathway and estrogen pathway play a different role in these two types of tumors. Several key signaling pathways cross over with the AR pathway, including the PI3K/Akt/mTOR and MAPK pathways, as well as hormone receptors such as the estrogen receptor and human epidermal growth factor receptor 2.

It has been reported that androgens not only increase nAR-positive BCa cell infiltration *via* the classical nAR, but also that DHT and the novel membrane receptor mAR-SLC39A9 may increase migration and infiltration of nAR-negative BCa cells by altering Gαi protein-regulated MAPK/MMP9 intracellular signaling (Chen et al., 2020). Inoue et al. found that AR pathway is involved in the tumor growth modulating ATF2 activity through ERK in bladder cancer cells (Inoue et al., 2018).

Activated AR, on the other hand, inhibited the growth of breast cancers driven by the ER through displacement of the ER and critical transcriptional co-activators from chromatin, which resulted in transcriptional downregulation (Hickey et al., 2021).

RNA modifications and androgen pathway effects have been linked to prostate cancer progression in recent studies. The gradual decrease of METTL14 (methyltransferase like 14) and the increase of ALKBH5 affected the activity of AMPK, causing an inhibition of autophagy and a subsequent suppression of testosterone synthesis in Leydig cells (Chen et al., 2021b). According to other studies, SIAH1 is a tumor suppressor involved in PC pathogenesis by repressing CPSF1-mediated AR-v7 generation and is a key regulatory factor (Xia et al., 2022).

mi206 played a key role in the differentially expressed ceRNA network in high- and low-RM_Score subtypes, and mi206 expression has been reported to be significantly upregulated in the tumor-associated stromal fraction. Nevertheless, mi206 plays a different role in prostate cancer and breast cancer. It has been demonstrated that miR-206 is highly expressed in breast tumors with no estrogen receptor compared with those with estrogen receptor positive breast tumors (Kondo et al., 2008). Specific to ER-negative breast cancer, miR-206 expression is higher than in ER-positive breast cancer (Adams et al., 2007). MiR-206 induces estrogen non-dependent state in MCF-7 cells when forced to express in these cells. Moreover, mi206 is significantly upregulated in prostate cancer, but functions as a tumor suppressor (Goljanek-Whysall et al., 2012; Singh et al., 2013; Walter et al., 2013).

Finally, we demonstrate the potential therapeutic efficacy of RNA modifiers in prostate cancer. According to the RM_Score, resistance to drugs targeting the cell cycle or apoptotic pathways may be associated with resistance to drugs targeting MAPK or EGFR signaling pathways. These findings imply that patients with a higher RM Score may benefit more from drugs that target these signaling pathways than from those that target the cell cycle or apoptotic pathways. By identifying distinct RNA modifications in tumors, our findings expand the scope for personalized chemotherapy and targeted treatment of prostate cancer. Due to the retrospective nature of the cohort and all our results are derived from bioinformatics analyses of publicly available databases, further additional experimental research is required. Still, our findings are supported by multiple independent GEO datasets, demonstrating their validity. Second, based on the expression patterns of 24 writers to represent distinct RNA modification patterns, we divided PC patients into two clusters. Due to the lack of large-scale m6A-seq performed in the PC cohorts, the precise RNA modification landscape is unclear in clinical practice. Due to the lack of available data sets, we only validated a few data sets, including breast cancer and bladder cancer data sets. To draw more precise conclusions, this relationship must be investigated further in a large clinical cohort.

Data availability statement

The original contributions presented in the study are included in the article/Supplementary Material, further inquiries can be directed to the corresponding authors.

Author contributions

XY: Conceptualization, Writing—Reviewing and Editing, Supervision XC: Methodology, Software, Data curation, Writing—Original draft preparation.

Conflict of interest

The authors declare that the research was conducted in the absence of any commercial or financial relationships that could be construed as a potential conflict of interest.

Publisher's note

All claims expressed in this article are solely those of the authors and do not necessarily represent those of their affiliated organizations, or those of the publisher, the editors and the reviewers. Any product that may be evaluated in this article, or claim that may be made by its manufacturer, is not guaranteed or endorsed by the publisher.

Supplementary material

The Supplementary Material for this article can be found online at: https://www.frontiersin.org/articles/10.3389/fgene.2022.1065424/full#supplementary-material

References

Adams, B. D., Furneaux, H., and White, B. A. (2007). The micro-ribonucleic acid (miRNA) miR-206 targets the human estrogen receptor-alpha (ERalpha) and represses ERalpha messenger RNA and protein expression in breast cancer cell lines. *Mol. Endocrinol.* 21, 1132–1147. doi:10.1210/me.2007-0022

Becht, E., Giraldo, N. A., Lacroix, L., Buttard, B., Elarouci, N., Petitprez, F., et al. (2016). Erratum to: Estimating the population abundance of tissue-infiltrating immune and stromal cell populations using gene expression. *Genome Biol.* 17, 249. doi:10.1186/s13059-016-1113-y

Cai, J., Yang, F., Zhan, H., Situ, J., Li, W., Mao, Y., et al. (2019). RNA m(6)A methyltransferase METTL3 promotes the growth of prostate cancer by regulating hedgehog pathway. *Onco. Targets. Ther.* 12, 9143–9152. doi:10.2147/OTT.S226796

Charoentong, P., Finotello, F., Angelova, M., Mayer, C., Efremova, M., Rieder, D., et al. (2017). Pan-cancer immunogenomic analyses reveal genotype-immunophenotype relationships and predictors of response to checkpoint blockade. *Cell Rep.* 18, 248–262. doi:10.1016/j.celrep.2016.12.019

Chen, J., Chou, F., Yeh, S., Ou, Z., Shyr, C., Huang, C., et al. (2020). Androgen dihydrotestosterone (DHT) promotes the bladder cancer nuclear AR-negative cell invasion via a newly identified membrane androgen receptor (mAR-SLC39A9)-mediated Gαi protein/MAPK/MMP9 intracellular signaling. *Oncogene* 39, 574–586. doi:10.1038/s41388-019-0964-6

Chen, Y., Pan, C., Wang, X., Xu, D., Ma, Y., Hu, J., et al. (2021). Silencing of METTL3 effectively hinders invasion and metastasis of prostate cancer cells. *Theranostics* 11, 7640–7657. doi:10.7150/thno.61178

Chen, Y., Wang, J., Xu, D., Xiang, Z., Ding, J., Yang, X., et al. (2021). m6A mRNA methylation regulates testosterone synthesis through modulating autophagy in Leydig cells. *Autophagy* 17, 457–475. doi:10.1080/15548627.2020.1720431

Emmanuel, S. A., Lu, C., Wang, H., Luber, B., Nakazawa, M., Roeser, J. C., et al. (2014). AR-V7 and resistance to enzalutamide and abiraterone in prostate cancer. *N. Engl. J. Med.* 371 (11), 1028–1038. doi:10.1056/NEJMoa1315815

Goljanek-Whysall, K., Pais, H., Rathjen, T., Sweetman, D., Dalmay, T., and Munsterberg, A. (2012). Regulation of multiple target genes by miR-1 and miR-206 is pivotal for C2C12 myoblast differentiation. *J. Cell Sci.* 125, 3590–3600. doi:10.1242/jcs.101758

Hänzelmann, S., Castelo, R., and Guinney, J. G. S. V. A. (2013). Gsva: Gene set variation analysis for microarray and RNA-seq data. *BMC Bioinforma.* 14, 7. doi:10.1186/1471-2105-14-7

Hartigan, J. A., Wong, M. A., and Algorithm, A. S. (1979). Algorithm as 136: A K-means clustering algorithm. *Appl. Stat.* 28, 100. doi:10.2307/2346830

Hickey, T. E., Selth, L. A., Chia, K. M., Laven-Law, G., Milioli, H. H., Roden, D., et al. (2021). The androgen receptor is a tumor suppressor in estrogen receptor-positive breast cancer. *Nat. Med.* 27, 310–320. doi:10.1038/s41591-020-01168-7

Inoue, S., Mizushima, T., Ide, H., Jiang, G., Goto, T., Nagata, Y., et al. (2018). ATF2 promotes urothelial cancer outgrowth via cooperation with androgen receptor signaling. *Endocr. Connect.* 7, 1397–1408. doi:10.1530/EC-18-0364

Kondo, N., Toyama, T., Sugiura, H., Fujii, Y., and Yamashita, H. (2008). miR-206 Expression is down-regulated in estrogen receptor alpha-positive human breast cancer. *Cancer Res.* 68, 5004–5008. doi:10.1158/0008-5472.CAN-08-0180

Leek, J. T., Johnson, W. E., Parker, H. S., Jaffe, A. E., and Storey, J. D. (2012). The sva package for removing batch effects and other unwanted variation in high-throughput experiments. *Bioinformatics* 28, 882–883. doi:10.1093/bioinformatics/bts034

Li, E., Wei, B., Wang, X., and Kang, R. (2020). METTL3 enhances cell adhesion through stabilizing integrin β1 mRNA via an m6A-HuR-dependent mechanism in prostatic carcinoma. *Am. J. Cancer Res.* 10, 1012–1025.

Ma, X.-X., Cao, Z.-G., and Zhao, S.-L. (2020). m6A methyltransferase METTL3 promotes the progression of prostate cancer via m6A-modified LEF1. *Eur. Rev. Med. Pharmacol. Sci.* 24, 3565–3571. doi:10.26355/eurrev_202004_20817

Mariathasan, S., Turley, S. J., Nickles, D., Castiglioni, A., Yuen, K., Wang, Y., et al. (2018). TGFβ attenuates tumour response to PD-L1 blockade by contributing to exclusion of T cells. *Nature* 554, 544–548. doi:10.1038/nature25501

Mo, F., Wyatt, A. W., Sun, Y., Brahmbhatt, S., McConeghy, B. J., Wu, C., et al. (2014). Systematic identification and characterization of RNA editing in prostate tumors. *PLoS ONE* 9, e101431. doi:10.1371/journal.pone.0101431

Newman, A. M., Liu, C. L., Green, M. R., Gentles, A. J., Feng, W., Xu, Y., et al. (2015). Robust enumeration of cell subsets from tissue expression profiles. *Nat. Methods* 12, 453–457. doi:10.1038/nmeth.3337

Royce, T. J., Chen, M. H., Wu, J., Loffredo, M., Renshaw, A. A., Kantoff, P. W., et al. (2017). Surrogate end points for all-cause mortality in men with localized unfavorable-risk prostate cancer treated with radiation therapy vs radiation therapy plus androgen deprivation therapy: A secondary analysis of a randomized clinical trial. *JAMA Oncol.* 3, 652–658. doi:10.1001/jamaoncol.2016.5983

Siegel, R. L., Miller, K. D., Fuchs, H. E., and Jemal, A. Cancer (2021). Cancer statistics, 2021. *Ca. Cancer J. Clin.* 71, 7–33. doi:10.3322/caac.21654

Singh, A., Happel, C., Manna, S. K., Acquaah-Mensah, G., Carrerero, J., Kumar, S., et al. (2013). Transcription factor NRF2 regulates miR-1 and miR-206 to drive tumorigenesis. *J. Clin. Invest.* 123, 2921–2934. doi:10.1172/JCI66353

Small, E. J., and de Bono, J. S. (2011). Prostate cancer: Evolution or revolution? *J. Clin. Oncol.* 29, 3595–3598. doi:10.1200/JCO.2011.37.8653

Walter, B. A., Valera, V. A., Pinto, P. A., and Merino, M. J. (2013). Comprehensive microRNA profiling of prostate cancer. *J. Cancer* 4, 350–357. doi:10.7150/jca.6394

Wilkerson, M. D., and Hayes, D. N. (2010). ConsensusClusterPlus: A class discovery tool with confidence assessments and item tracking. *Bioinformatics* 26(12), 1572–1573. doi:10.1093/bioinformatics/btq170

Xia, L., Han, Q., Duan, X., Zhu, Y., Pan, J., Dong, B., et al. (2022). m^{6}A-induced repression of SIAH1 facilitates alternative splicing of androgen receptor variant 7 by regulating CPSF1. *Mol. Ther. Nucleic Acids* 28, 219–230. doi:10.1016/j.omtn.2022.03.008

Yang, W., Soares, J., Greninger, P., Edelman, E. J., Lightfoot, H., Forbes, S., et al. (2013). Genomics of drug sensitivity in cancer (GDSC): A resource for therapeutic biomarker discovery in cancer cells. *Nucleic Acids Res.* 41, D955–D961. doi:10.1093/nar/gks1111

Yu, G., Wang, L.-G., Han, Y., and He, Q.-Y. (2012). clusterProfiler: an R package for comparing biological themes among gene clusters. *Omics J. Integr. Biol.* 16, 284–287. doi:10.1089/omi.2011.0118

Yuan, Y., Du, Y., Wang, L., and Liu, X. (2020). The M6A methyltransferase METTL3 promotes the development and progression of prostate carcinoma via mediating MYC methylation. *J. Cancer* 11, 3588–3595. doi:10.7150/jca.42338

Zeng, D., Li, M., Zhou, R., Zhang, J., Sun, H., Shi, M., et al. (2019). Tumor microenvironment characterization in gastric cancer identifies prognostic and immunotherapeutically relevant gene signatures. *Cancer Immunol. Res.* 7, 737–750. doi:10.1158/2326-6066.CIR-18-0436

Zhang, D., Hu, Q., Liu, X., Ji, Y., Chao, H. P., Liu, Y., et al. (2020). Intron retention is a hallmark and spliceosome represents a therapeutic vulnerability in aggressive prostate cancer. *Nat. Commun.* 11, 2089. doi:10.1038/s41467-020-15815-7

Zhang, D., Park, D., Zhong, Y., Lu, Y., Rycaj, K., Gong, S., et al. (2016). Stem cell and neurogenic gene-expression profiles link prostate basal cells to aggressive prostate cancer. *Nat. Commun.* 7, 10798. doi:10.1038/ncomms10798

Zhao, S. G., Chen, W. S., Li, H., Foye, A., Zhang, M., Sjöström, M., et al. (2020). The DNA methylation landscape of advanced prostate cancer. *Nat. Genet.* 52 (8), 778–789. doi:10.1038/s41588-020-0648-8

frontiers | Frontiers in Genetics

TYPE Original Research
PUBLISHED 23 January 2023
DOI 10.3389/fgene.2023.1071694

OPEN ACCESS

EDITED BY
Jiao Hu,
Xiangya Hospital, Central South University, China

REVIEWED BY
Aitao Nai,
The First Affiliated Hospital of University of South China, China
Ji-Feng Feng,
University of Chinese Academy of Sciences, China

*CORRESPONDENCE
Tingting Chen,
ctt3034@zcmu.edu.cn

SPECIALTY SECTION
This article was submitted to Cancer Genetics and Oncogenomics, a section of the journal Frontiers in Genetics

RECEIVED 16 October 2022
ACCEPTED 13 January 2023
PUBLISHED 23 January 2023

CITATION
Yao Y, Chen H, Lou M and Chen T (2023), Cuproptosis-related gene FDX1 as a prognostic biomarker for kidney renal clear cell carcinoma correlates with immune checkpoints and immune cell infiltration.
Front. Genet. 14:1071694.
doi: 10.3389/fgene.2023.1071694

Cuproptosis-related gene FDX1 as a prognostic biomarker for kidney renal clear cell carcinoma correlates with immune checkpoints and immune cell infiltration

Yimin Yao[1], Haixin Chen[2], Minjun Lou[1] and Tingting Chen[1]*

[1]Medical Laboratory, The First Affiliated Hospital of Zhejiang Chinese Medical University (Zhejiang Provincial Hospital of Chinese Medicine), Hangzhou, China, [2]The First Clinical Medical College, Zhejiang Chinese Medical University, Hangzhou, China

Background: Kidney renal clear cell carcinoma (KIRC) is not sensitive to radiotherapy and chemotherapy, and only some KIRC patients can benefit from immunotherapy and targeted therapy. Cuproptosis is a new mechanism of cell death, which is closely related to tumor progression, prognosis and immunity. The identification of prognostic markers related to cuproptosis in KIRC may provide targets for treatment and improve the prognosis of KIRC patients.

Methods: Ten cuproptosis-related genes were analyzed for differential expression in KIRC-TCGA and a prognostic model was constructed. Nomogram diagnostic model was used to screen independent prognostic molecules. The screened molecules were verified in multiple datasets (GSE36895 and GSE53757), and in KIRC tumor tissues by RT-PCR and immunohistochemistry (IHC). Clinical correlation of cuproptosis-related independent prognostic molecules was analyzed. According to the molecular expression, the two groups were divided into high and low expression groups, and the differences of immune checkpoint and tumor infiltrating lymphocytes (TILs) between the two groups were compared by EPIC algorithm. The potential Immune checkpoint blocking (ICB) response of high and low expression groups was predicted by the "TIDE" algorithm.

Results: FDX1 and DLAT were protective factors, while CDKN2A was a risk factor. FDX1 was an independent prognostic molecule by Nomogram, and low expressed in tumor tissues compared with adjacent tissues ($p < 0.05$). FDX1 was positively correlated with CD274, HAVCR2, PDCD1LG2, and negatively correlated with CTLA4, LAG3, and PDCD1. The TIDE score of low-FDX1 group was higher than that of high-FDX1 group. The abundance of $CD4^+$ T cells, $CD8^+$ T cells and Endothelial cells in FDX1-low group was lower than that in FDX1-high group ($p < 0.05$).

Conclusion: FDX1, as a key cuproptosis-related gene, was also an independent prognostic molecule of KIRC. FDX1 might become an interesting biomarker and potential therapeutic target for KIRC.

KEYWORDS

cuproptosis-related gene, fdx1, prognostic biomarker, kidney renal clear cell carcinoma, immune checkpoints, immune cell infiltration

Introduction

Renal cell carcinoma (RCC) accounts for about 2% of adult malignant tumors, and kidney renal clear cell carcinoma (KIRC) is the most important pathological type (Hakimi et al., 2016). Advanced RCC patients are not sensitive to radiotherapy and chemotherapy, and about 30% of RCC patients have metastasized at the initial diagnosis (Jakubek et al., 2020). Immunotherapy brings a turning point for advanced RCC patients, which can improve the survival (Li et al., 2020). However, not all RCC patients are effective with existing

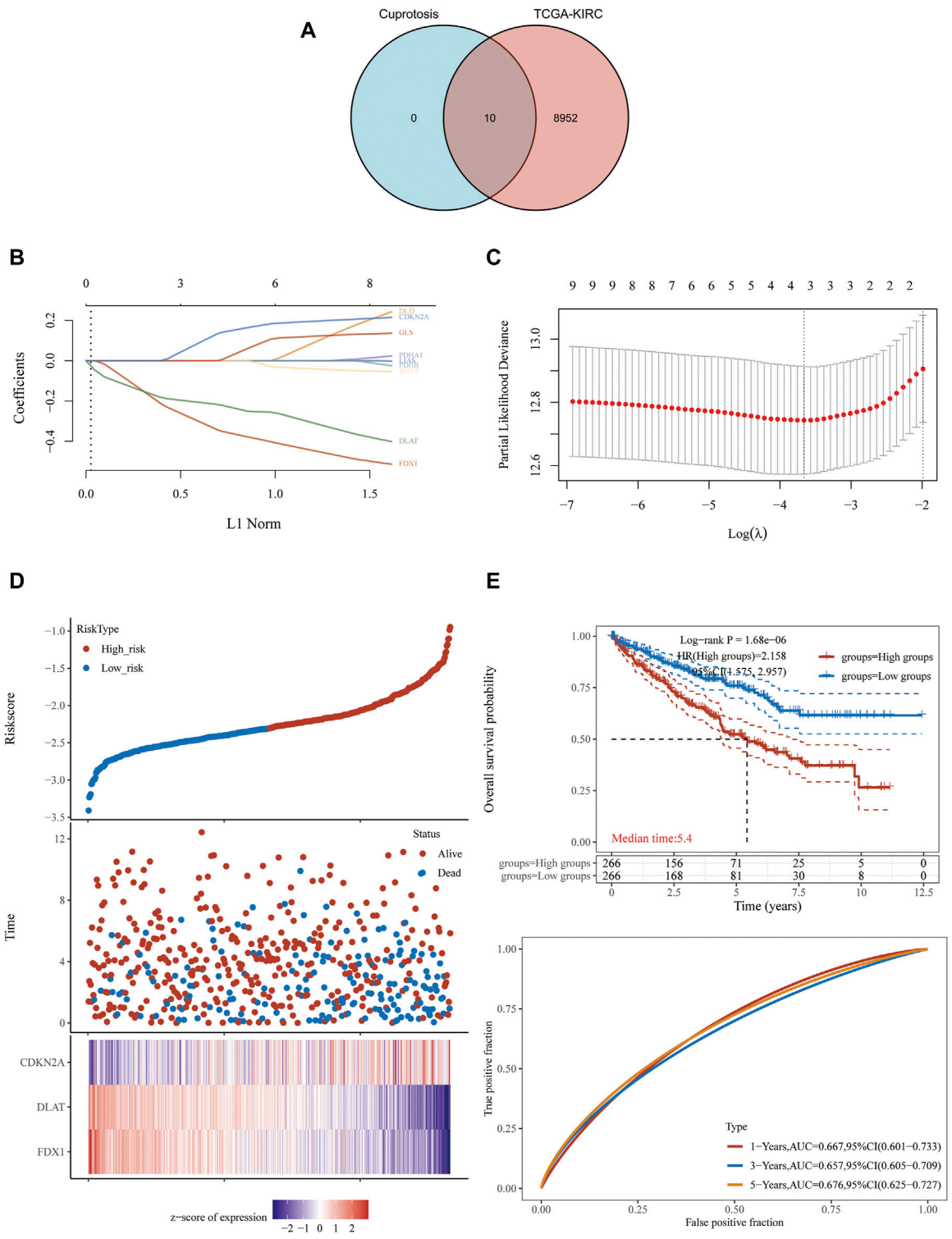

FIGURE 1
FDX1, DLAT and CDKN2A cuproptosis-related genes prognostic model. **(A)** 8,962 potential prognostic molecules of KIRC and 10 cuproptosis-related genes Venn diagram. **(B)** LASSO variable trajectory diagram. **(C)** LASSO coefficient screening diagram. **(D)** The prognostic risk factor graph, red represents high-risk group, blue represents low-risk group. **(E)** Kaplan-Meier survival curve and time dependent ROC.

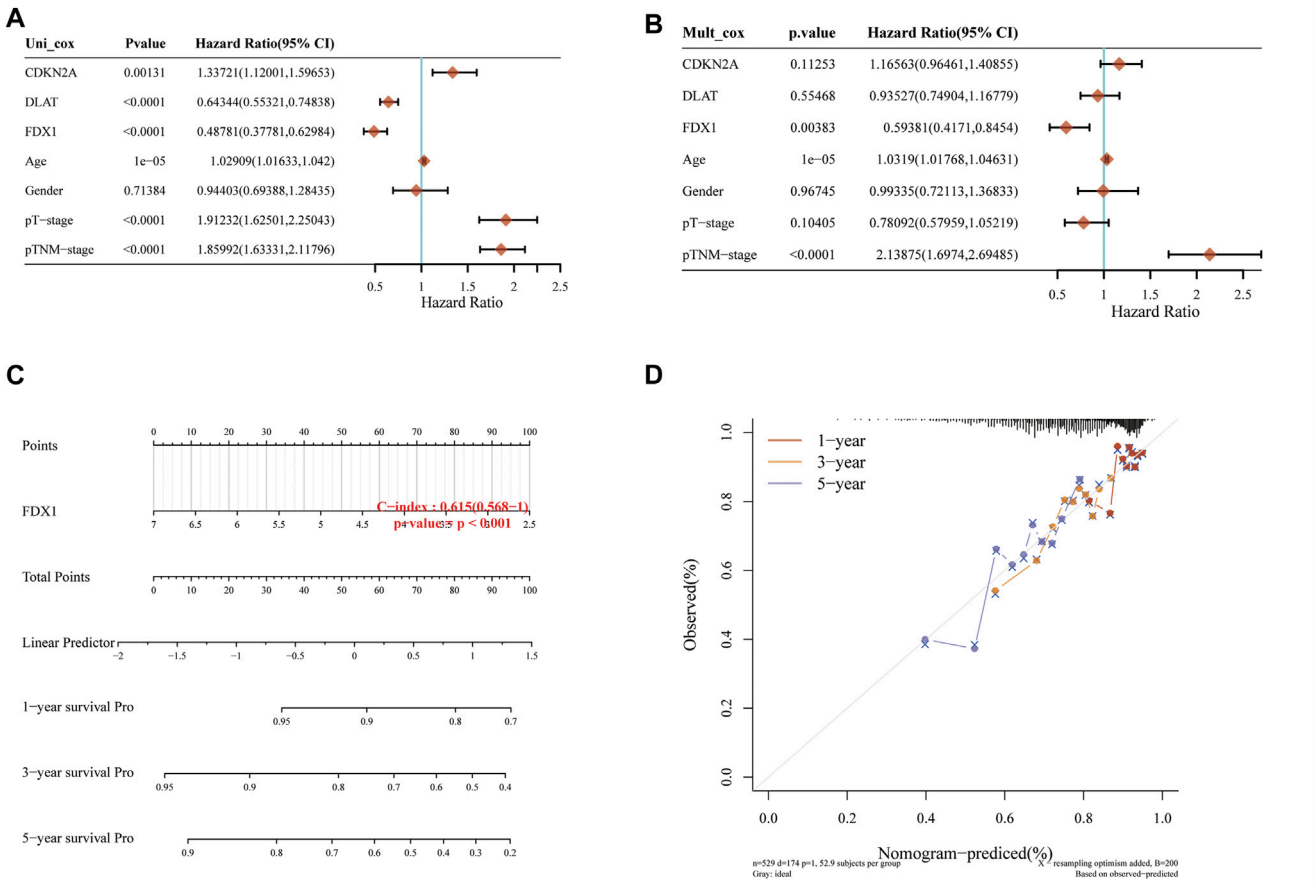

FIGURE 2
Independent prognostic molecules associated with cuproptosis. **(A)** Univariate Cox analysis of cuproptosis-related genes. **(B)** Multivariate Cox analysis of cuproptosis-related genes. **(C)** one, two and three-year overall survival of KIRC patients were predicted by Nomogram. **(D)** Calibration curve of the overall survival Nomogram model in the discovery group.

immunotherapies. How to mine the new key prognostic molecules and develop the corresponding targeted drugs are expected to bring dawn to advanced RCC patients who are ineffective to the existing targeted drugs.

Copper ions, as an important cofactor of many enzymes in the body, participate in oxidative stress, lipid metabolism and energy metabolism (Meydan et al., 2017). It can combine with copper carrier to induce apoptosis (Xiong et al., 2020). The mechanism of cuproptosis is mainly through the combination of copper ions and liposylated protein in the tricarboxylic acid cycle (TCA), which reduces the level of iron sulfur cluster protein, causes cytotoxic stress, and finally leads to cell death (Tsvetkov et al., 2022). Copper ions maintain a steady state in the body. When cuproptosis-related genes mutation or expression change, it can lead to copper ions imbalance and induce a series of diseases (Bao et al., 2022; Wang et al., 2022). Cuproptosis, different from traditional programmed death, has become a hot spot in tumor treatment field in recent years. Some copper chelating agents for tumor treatment, such as tetrathiomolybdate (TM), are in clinical trials (Lopez et al., 2019; Li Y. et al., 2022). In breast cancer and malignant pleural mesothelioma, the copper chelating strategy successfully delayed the progression and metastasis of tumors (Zhou et al., 2019). When using platinum compounds, copper chelators can regulate copper homeostasis and reduce cisplatin resistance (Zhu et al., 2017). Therefore, we explored the key regulatory molecules by studying the cuproptosis-related genes in KIRC, which help to develop new treatment strategies and bring hope to advanced RCC patients. In addition, the unregulation of immune checkpoints can inhibit the anti-tumor function of immune cells, leading to tumor cells escape (Mayadev et al., 2020). Analyzing the relationship between cuproptosis-related genes and immune cell status also help us master the immune statues of KIRC patients, optimize treatment strategies constantly, and prolong the prognosis. Zilong Bian et al. found that cuproptosis-related genes were closely related to the Overall Survival (OS) and Progression-Free-Survival (PFS) in KIRC through the prognostic risk score, and were also related to the immune infiltration and PD-1 expression (Bian et al., 2022). Wangli Mei et al. found the expression of cuproptosis-related genes (ATP7B, DBT, DLAT, LIAS and PDHB) were significantly different between tumor tissues and adjacent tissues, and speculated that these genes might be independent prognostic factors of OS in KIRC (Mei et al., 2022). However, their research was not verified by clinical samples, nor had they excavated the core gene of cuproptosis-related genes in KIRC.

In our study, we analyzed the expression changes of cuproptosis-related genes in KIRC-TCGA database, and constructed the relevant signature. FDX1 was screened as a key cuproptosis-related gene through COX regression analysis and closely related to the prognosis of KIRC. The differential expression of FDX1 was

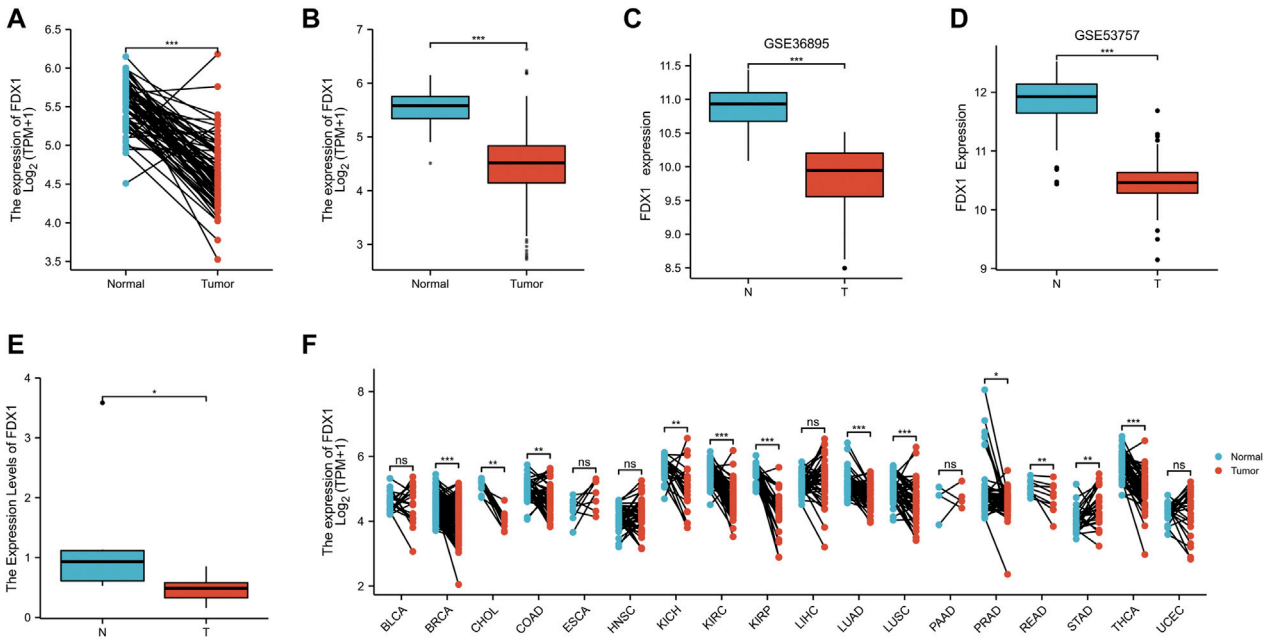

FIGURE 3
The expression difference of FDX1 in KIRC. **(A)** Differential expression of FDX1 in paired samples in TCGA-KIRC database. **(B)** Differential expression of FDX1 in unpaired samples in TCGA-KIRC database. **(C)** Differential expression of FDX1 in GSE36895. **(D)** Differential expression of FDX1 in GSE53757. **(E)** Differential expression of FDX1 between KIRC patients and normal renal tissue by RT-qPCR. **(F)** Differential expression of FDX1 in TCGA pan cancer. NS, $p > .05$; *, $p < .05$; **, $p < .01$; ***, $p < .001$.

verified in clinical tumor tissues by RT-qPCR and immunohistochemistry (IHC). The correlation of FDX1 with immune cell infiltration and immune checkpoints were also analyzed. Finally, we concluded that FDX1 was the key cuproptosis-related gene of KIRC and FDX1 may become a new therapeutic target to improve the prognosis of KIRC patients.

Materials and methods

Data sources

The KIRC-TCGA database (3 May 2022) including clinial information and processed RNA-sequencing expression (level 3) data were downloaded from The Cancer Genome Atlas (TCGA) (https://portal.gdc.com). Seventy-two paracancerous samples and 532 tumor samples were collected to analyze the expression differences and clinical correlation.

GSE36895 (Peña-Llopis et al., 2012) and GSE53757 (von Roemeling et al., 2014) datasets from the Gene Expression Omnibus (GEO) database were downloaded to verify the screened key genes. GSE36895 dataset included 76 samples, of which 52 samples were collected and divided into KIRC group (29 primary tumors samples) and control group (23 normal kidney cortices samples). GSE53757 dataset included 144 samples, of which 72 tumor tissues were defined as KIRC group, and the other 72 normal kidney tissues were defined as control group.

Ten KIRC tissues and six paracancerous tissues from KIRC patients who underwent tumor resection in Zhejiang Province Hospital of Traditional Chinese Medicine were collected for validation. Histological diagnosis and tumor grade were assessed by three experienced pathologists following WHO/ISUP grading of renal clear cell carcinoma. All procedures were approved by the Ethics Committee of our Hospital.

Cuproptosis-related genes were used to constructed prognostic model

Univariate Cox analysis on 532 RNA-seq data from TCGA-KIRC dataset was performed by "survival" R package to gain potential prognostic genes ($p < .05$, coding genes, and the prognosis type was overall survival (OS)). Then, these potential prognostic genes intersected with 10 cuproptosis-related genes (FDX1、LIAS、LIPT1、DLD、DLAT、PDHA1、PDHB、MTF1、GLS and CDKN2A) (Tsvetkov et al., 2022) to obtain cuproptosis-related potential prognostic genes using "ggplot2" R package. LASSO regression analysis was used to reduce the dimension and construct a prognostic model (signature). Potential prognostic genes related to cuproptosis were identified by "glmnet" R package and "survival" R package, and 10 folds cross validation was used.

The "ggplot2" R package was used to evaluate the risk score and grouping of the prognosis model for RNA-seq data and clinical information in TCGA-KIRC dataset. Use "ggplot2" R package and "timeROC" R package to evaluate the area under the characteristic curve and evaluate the predictive ability of the prognosis model. The survival of KIRC patients in high-risk group and low-risk group was analyzed with "survminer" R package and "survival" R package.

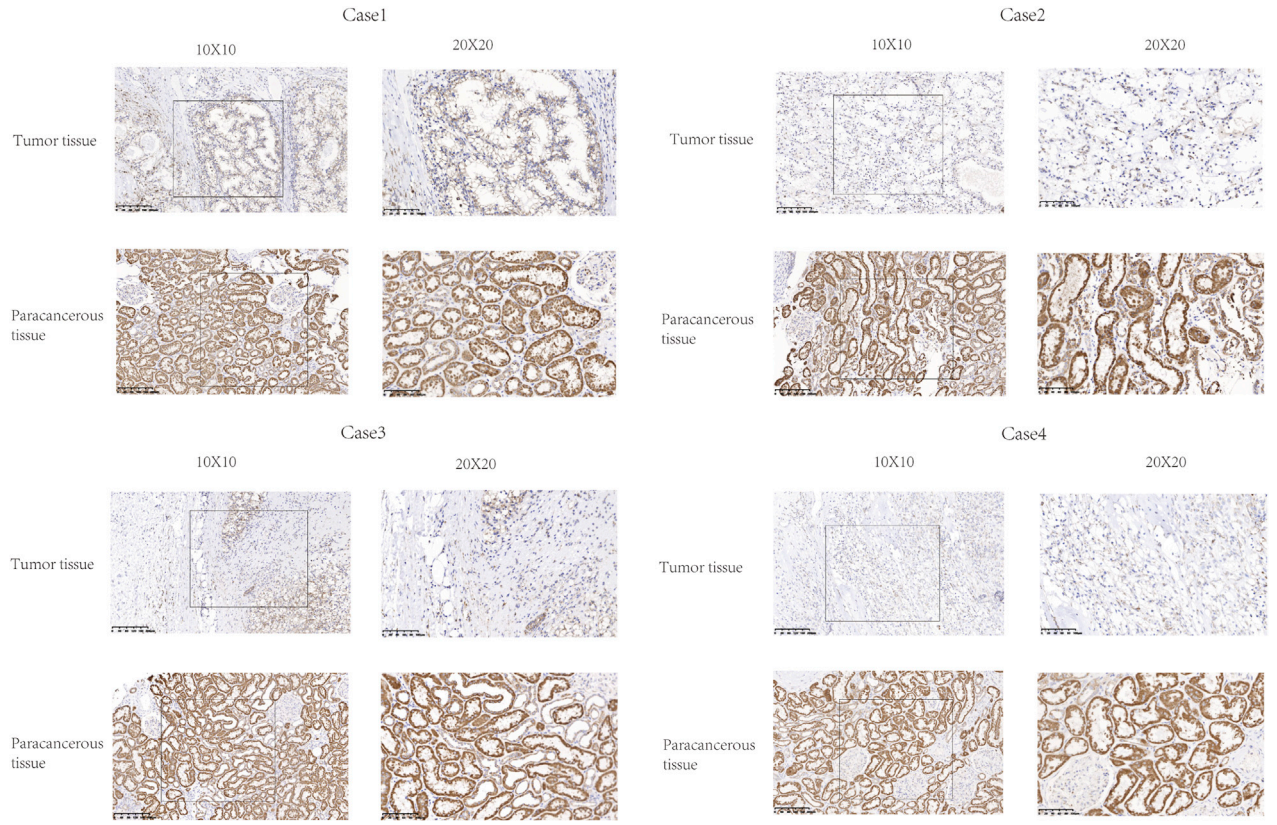

FIGURE 4
Representative images of FDX1 expression in KIRC tissues and their matched paracancerous tissues. Original magnifications ×100 and 400× (inset panels).

Screening of independent prognostic molecules related to cuproptosis (nomogram prognostic model)

Univariate and multivariate cox regression analysis were performed to identify the proper terms to build the Nomogram. The forest was used to show the *p*-value, HR and 95% CI of each variable through "forestplot" R package. Univariate analysis showed differences, which were considered to be related to prognosis, while multivariate analysis also showed differences, which were considered to be independent prognostic factors. A Nomogram was developed based on multivariate cox proportional hazards analysis to predict the 1, 3, 5-year overall recurrence.

The Nomogram provided a graphical representation of the factors which can be used to calculate the risk of recurrence for an individual patient by the points associated with each risk factor through "rms" R package.

Differential expression of cuproptosis-related independent prognostic molecules

The differential expression of cuproptosis-related independent prognostic molecules in TCGA-KIRC was analyzed through "ggplot2" R package. Gene expression profile for cuproptosis-related independent prognostic molecules were downloaded from GSE36895 and GSE53757, boxplots were constructed using "ggplot2" R package to compare the differences between different groups (Gene expression levels of different groups samples were compared using Wilcoxon rank sum test. Significance identification: NS, $p \geq .05$; *, $p < .05$; **, $p < .01$; ***, $p < .001$.

Clinical tissue validation by RT-qPCR and IHC

RNA was extracted from 3 to 5 10 μM thick scrolls obtained from formalin-fixed paraffin embedded (FFPE) tissues using the Spacegen nucleic acid extraction kit (Batch number: HS221121701). CT value was obtained by RT-qPCR, the sequence of the forward primer for FDX1 is TTCAACCTGTCA CCTCATCTTTG, the reverse primer sequence is TGCCAGATC GAGCATGTCATT, and the relative quantitative analysis was carried out by "ggplot2" R package.

KIRC FFPE tissues and paracancerous FFPE tissues were sliced into 4–6 μm sections, and FDX1 florescence intensity was analyzed by IHC. After deparaffinization, rehydration and microwave antigen retrieval, the slides were incubated with ADX (BOSTER, Cat #M04441) antibody at 1:100 dilution at 4°C overnight. Then, the slides were incubated with secondary antibody at room temperature for 30 min and stained with DAB substrate, followed by haematoxylin counterstaining.

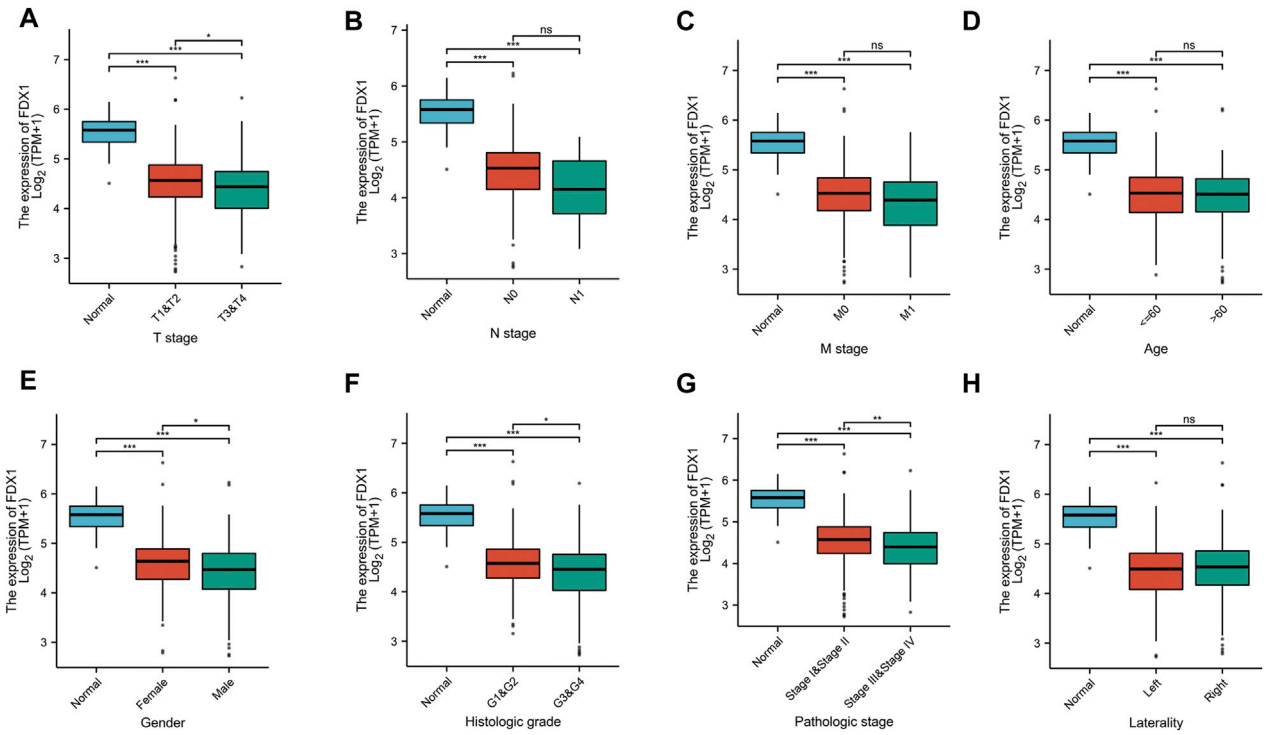

FIGURE 5
The correlation between FDX1 and clinical characteristics in KIRC. **(A)** The correlation between FDX1 and T stage. **(B)** The correlation between FDX1 and N stage. **(C)** The correlation between FDX1 and M stage. **(D)** The correlation between FDX1 and Age. **(E)** The correlation between FDX1 and Gender. **(F)** The correlation between FDX1 and Histologic grade. **(G)** The correlation between FDX1 and Pathologic stage. **(H)** The correlation between FDX1 and Laterality. NS, $p > .05$; *, $p < .05$; **, $p < .01$; ***, $p < .001$.

Clinical correlation of cuproptosis-related independent prognostic molecules

The RNA-seq data and clinical data of 609 samples of TCGA-KIRC were analyzed by "ggplot2" R package to analyze the clinical correlation of independent prognostic molecules related to cuproptosis, including T stage, N stage, M stage, Age, Gender, Pathological stage, Historical grade and Laterality.

Correlation between cuproptosis-related independent prognostic molecules and other cuproptosis-related genes

The selected molecule was an independent prognostic molecule related to cuproptosis. Input the other cuproptosis-related genes in the molecular list. Through the "ggplot2" R package, select the statistical method as Spearman, and perform single gene co-expression analysis on the RNA-seq data of 532 samples of TCGA-KIRC.

In order to further understand the correlation between 10 cuproptosis-related molecules, input 10 cuproptosis-related gene names in the molecular list, and select Spearman correlation analysis method to perform correlation analysis on RNA-seq data of 532 samples of TCGA KIRC through "ggplot2" R package.

Immune checkpoint expression analysis and immune checkpoint blocking (ICB) response

According to the expression of cuproptosis-related independent prognostic key gene, the KIRC samples from KIRC-TCGA database were divided into high and low expression groups. The expression level above the median level was defined as high expression group, and the expression level below the median level was defined as low expression group. Referring to some high-quality literatures, the expression differences of immune checkpoint related genes (SIGLEC15, TIGIT, CD274, HAVCR2, PDCD1, CTLA4, LAG3 and PDCD1LG2) were compared between these two groups by "ggplots2" and "pheatmap" R packages (Ravi et al., 2018; Wang et al., 2019; Zeng et al., 2019; Yi et al., 2020). Spearman's correlation analysis was used to describe the correlation between quantitative variables without normal distribution, and *p*-value less than 0.05 was considered statistically significance.

The overall survival rate was selected as the prognosis type, and Cox regression was selected as the statistical method. The "survminer" package was used for visualization and the "survival" package was used for statistics. The "TIDE" algorithm predicted the potential ICB response of high and low expression groups, "ggplot2" and "ggpubr" packages were used for mapping analysis.

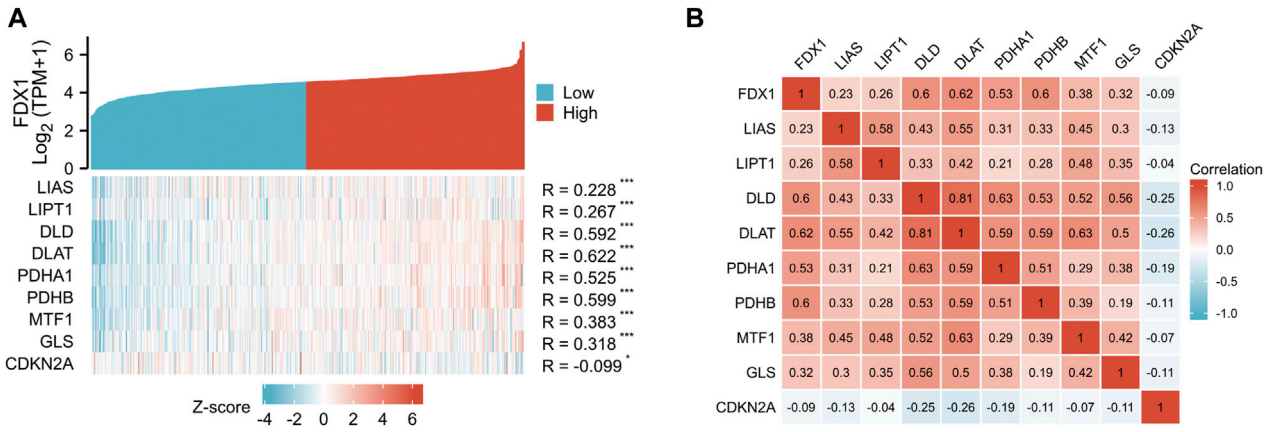

FIGURE 6
Correlation between FDX1 and other nine cuproptosis genes. **(A)** FDX1 and other nine cuproptosis-related molecules co-expression heatmap. **(B)** 10 cuproptosis-related genes correlation heatmap.

Analysis of immune infiltrate

The KIRC samples from KIRC-TCGA were stratified into two groups based on the expression of cuproptosis-related independent prognostic molecule. Immune score evaluation was performed by "immunedeconv" R package using EPIC, data were visualized using "ggplot2" and "pheatmap" R packages. Further survival analysis of immune infiltrating cells was carried out using TIMER2.0 (http://timer.cistrome.org/), a web server designed for comprehensive analysis of tumor-infiltrating immune cells.

EPIC algorithm was used to evaluate the immune infiltration of GSE53575 dataset to further verify the correlation between cuproptosis-related independent prognostic molecule and KIRC immune infiltration. The expression values of EPIC algorithm of immune infiltrating cells B cell, $CD4^+$ T cell, $CD8^+$ T cell, Endothelial cell, Macrophage and NK cell were extracted, and the expression of immune infiltrating cells were analyzed visually through "ggplot2" and "pheatmap" R packages.

R software version

All the analysis methods and R packages were implemented by R (foundation for statistical computing 2020) version 4.0.3. $p < .05$ was considered statistically significant.

Results

FDX1, DLA and CDKN2A cuproptosis-related genes prognostic model (signature)

In order to explore whether cuproptosis-related genes can be used as effective biomarkers to indicate the prognosis of KIRC, we obtained 8,962 potential prognostic molecules of KIRC from KIRC-TCGA database. Then, these 8,962 prognostic molecules were intersected with 10 cuproptosis-related genes (FDX1, LIAS, LIPT1, DLD, DLAT, PDHA1, PDHB, MTF1, GLS and CDKN2A), we found these 10 genes were all in these intersection (Figure 1A).

LASSO regression analysis was used to fit the overall survival of KIRC patients according to the selected 10 potential prognostic genes related to cuproptosis. Key genes will be assigned to a non-zero coefficient and selected to build a prognostic model (signature). Last, we built a prognostic scoring formula: Riskscore = (−0.3336) *FDX1 + (−0.215) *DLAT + (0.1233) *CDKN2A. Three genes in the model were multiplied by a weight. Negative numbers represent protective genes while positive numbers represent risk genes. We concluded that FDX1 and DLAT were protective factors, while CDKN2A was a risk factor. LASSO variable trajectory diagram showed that the selection method L1 norm, at the position of 3, the vertical line cut to the variables with the corresponding coefficient of non-0 were FDX1, DLAT and CDKN2A (Figure 1B).

LASSO coefficient screening diagram indicated that when lambda.min was 3, the partial likelihood deviance was the smallest, and the corresponding model was the better (Figure 1C).

The prognostic risk factor graph showed the Riskscore, survival time and survival status in KIRC-TCGA. The top graph represented the scatter plot of the Riskscore from low to high and the middle figure represented the scatter diagram distribution of survival time and survival state corresponding to Riskscore of different samples. The corresponding death patients in the high-risk area were higher than those in the low-risk area. The bottom figure represented the expression heat map of three molecules including FDX1, DLAT and CDKN2A in the signature.

FDX1 and DLAT were low expression and CDKN2A was high expression under the corresponding high-risk region, FDX1 and DLAT were high expression and CDKN2A was low expression under the corresponding low-risk region (Figure 1D). In the prognostic model, the survival probability of high-risk group and low-risk group was significantly different, and the prognosis of high-risk group was poor through log rank test according to the Kaplan-Meier survival curve [p = 1.68e−06, HR = 2.158, 95%CL (1.575, 2.957)]. The AUC of this prognostic model at 1, 3 and 5 years were .667, .657 and .676, respectively. It indicated that cuproptosis-related genes (FDX1, DLAT and CDKN2A) as predictive prognostic models had good accuracy (Figure 1E).

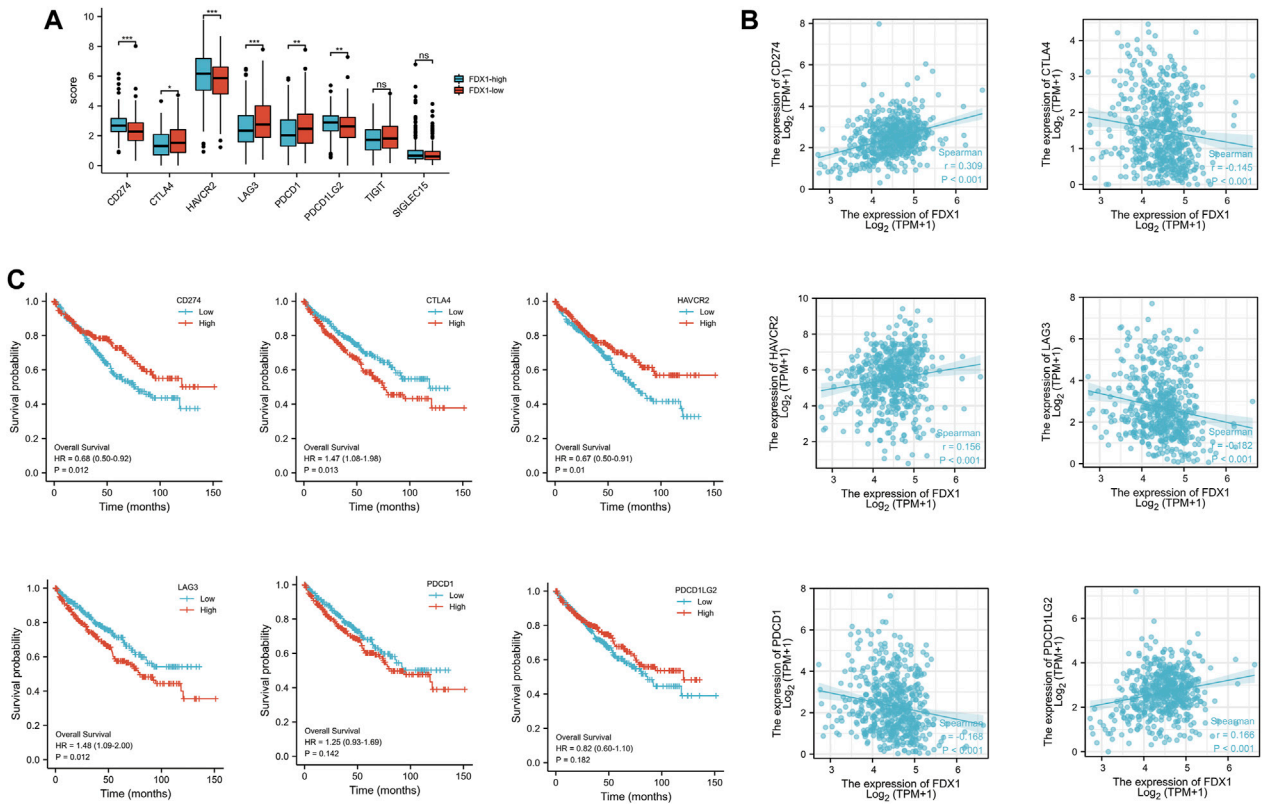

FIGURE 7
The expression and the prognosis analysis of immune checkpoints. **(A)** Expression of immune checkpoint in high and low expression groups of FDX1. **(B)** Scatter plot of immune checkpoint association with FDX1. **(C)** Overall survival curve of immune checkpoints in KIRC patients.

FDX1 is an independent prognostic molecule associated with cuproptosis by Nomogram

Univariate and multivariate Cox regression can identify variables in Nomogram. The prognosis of FDX1 showed significant differences in univariate and multivariate, which indicated that FDX1 was a variable independent of other clinical factors (Figures 2A, B). The total points and 1, 3, 5-year survivals were inversely proportional to the expression of FDX1 (Figures 2C, D). The closer the Nomogram model was to the calibration curve, the better the predicted result of the model.

The expression difference of FDX1 in KIRC

According to Nomogram model, we concluded that FDX1 was an independent prognostic factor of KIRC related to prognosis and survival. In KIRC-TCGA database, the expression of FDX1 was decreased in tumor tissues compared with adjacent tissues ($p < .05$) (Figures 3A, B). In GSE36895 and GSE53757, the expression of FDX1 was also verified to be lower in tumor tissues than in normal renal tissues ($p < .05$) (Figures 3C, D). Consistent with the bioinformatics analysis, our clinical samples showed that FDX1 expression was lower in renal tumor tissues than in adjacent tissues ($p < .05$) (Figure 3E).

The FDX1 expression was further analyzed in Pan cancer in TCGA database, and the FDX1 expression was lower in tumor tissues than in normal tissues in breast cancer (BRCA), Cholangio carcinoma (CHOL), Colon adenocarcinoma (COAD), Kidney Chromophobe (KICH), Kidney renal clear cell carcinoma (KIRC), Kidney renal papillary cell carcinoma (KIRP), Lung Adenocarcinoma (LUAD), Lung Squamous cell carcinoma (LUSC), Prostatic cancer (PRAD), Rectum adenocarcinoma (READ) and Thyroid carcinoma (THCA) ($p < 0.05$). However, FDX1 expression in tumor tissues of Stomach adenocarcinoma (STAD) was higher than in normal tissues ($p < .05$) (Figure 3F).

FDX1 fluorescence intensity in KIRC tissues by IHC

The expression of FDX1 was analyzed by IHC in six KIRC tissues and paired paracancerous tissues. The expression of FDX1 was downregulated in these six tumor tissues compared with the adjacent tissues (Figure 4).

The correlation between FDX1 and clinical characteristics in KIRC

To explore the value of FDX1 in KIRC, we analyzed the correlation between the FDX1 expression and the clinical characteristics of KIRC (T stage, N stage, M stage, Age, Gender, Histologic grade, Pathologic stage, Laterality). T3&T4 was lower than T1&T2, Stage III&Stage IV

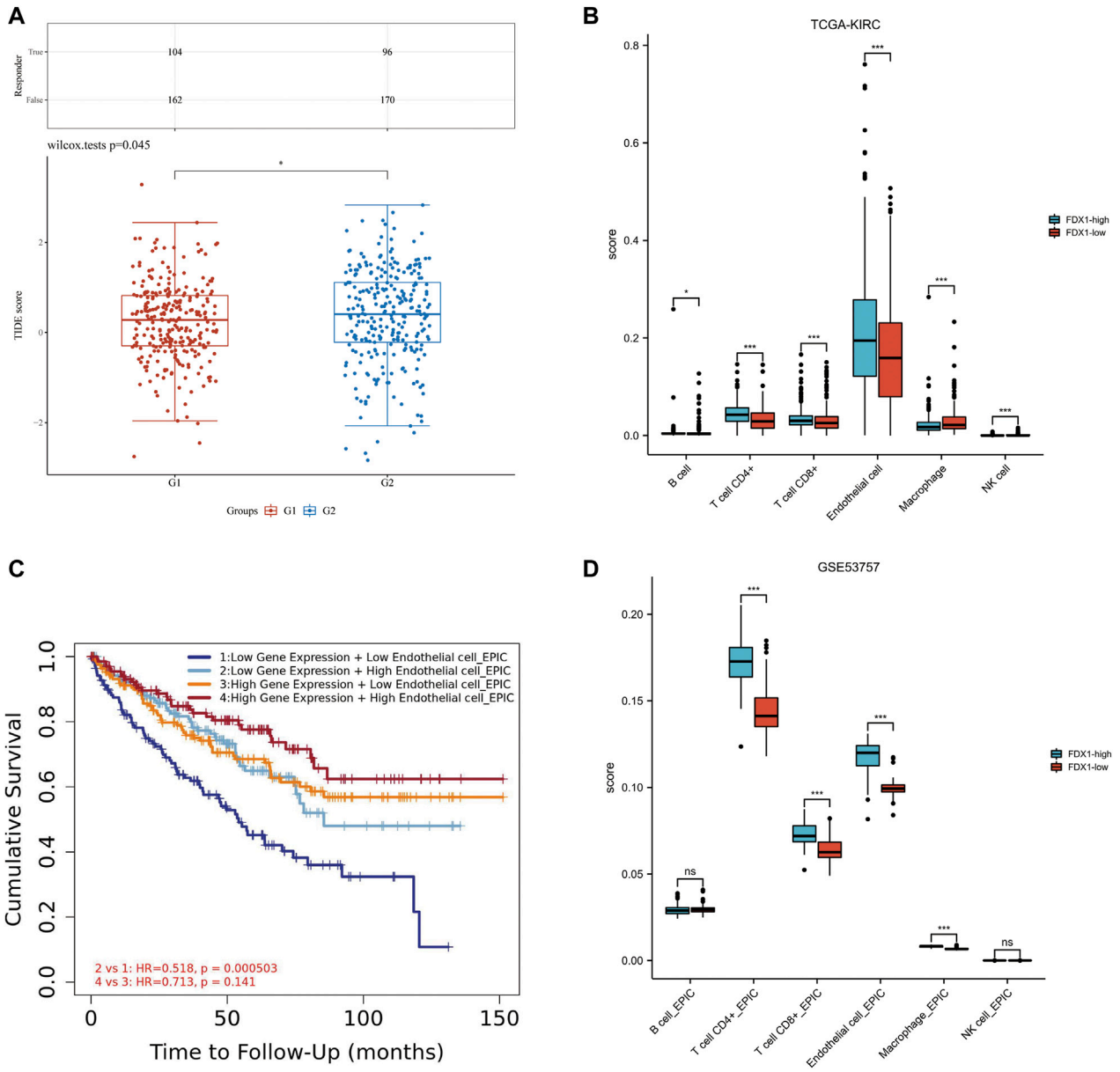

FIGURE 8
Relationship among FDX1 expression, ICB and immune cell infiltration in KIRC. **(A)** Distribution of immune response scores in high and low expression groups of FDX1. **(B)** The abundance of immune cell infiltration in FDX1-low group and FDX1-high group in TCGA-KIRC. **(C)** The Kaplan-Meier curve of Endothelial cells in KIRC. G1 group represented FDX1-high group, G2 group represented FDX1-low group. **(D)** The abundance of immune cell infiltration in FDX1-low group and FDX1-high group in GSE53757.

was lower than Stage I&Stage II, G3&G4 was lower than G1&G2, male was lower than female ($p < .05$). But the years, N stage, M stage, left or right had no statistically significant ($p > .05$) (Figure 5).

Correlation analysis between FDX1 and other cuproptosis-related genes

The coexpression Heatmap of single gene showed that FDX1 expression was correlated with the other nine cuproptosis-related genes in KIRC, and was strongly and positively correctly with DLD, DLAT, PDHA1 and PDHB (Figure 6A). Correlation Heatmap analysis showed that FDX1, DLD, DLAT, PDHA1 and PDHB were positively correlated and the correlation coefficient was greater than .5 (Figure 6B).

Expression of immune checkpoint and prognosis in high and low expression groups of FDX1

KIRC-TCGA database was divided into high expression group and low expression group according to FDX1. Eight immune checkpoints (SIGLEC15, TIGIT, CD274, HAVCR2, PDCD1, CTLA4, LAG3 and

PDCD1LG2) were selected to be analyzed between high and low groups. The expression of CD274, HAVCR2 and PDCD1LG2 in FDX1-low group was lower than that in FDX1-high group ($p < .05$). However, the expression of CTLA4, LAG3 and PDCD1 in FDX1-low group was higher than that in FDX1-high group ($p < .05$) (Figure 7A).

The correlation analysis between FDX1 and immune checkpoint showed that FDX1 was positively correlated with CD274, HAVCR2, PDCD1LG2, and negatively correlated with CTLA4, LAG3, and PDCD1 (Figure 7B). Kaplan-Meier survival curve analysis illustrated that the overall survival (OS) was poor when CTLA1 and LAG3 expression was high, while CD274 and HAVCR2 expression was low (Figure 7C).

Evaluation of immune blocking therapy and immune infiltration

TIDE algorithm was used to predict the potential immunotherapeutic response. TIDE used a set of genes to evaluate two different mechanisms of tumor immune escape, including the dysfunction of tumor infiltrating cytotoxic T lymphocytes (CTLs) and the rejection of CTLs by immunosuppressive factors. High TIDE score predicted poor efficacy of immune checkpoint block therapy and short survival after ICB. The TIDE score of low-FDX1 group was higher than that of high-FDX1 group, indicating that the efficacy of ICB in low-FDX1 group was poor (Figure 8A).

The correlation between FDX1 and immune infiltration was further analyzed. In KIRC-TCGA database and GSE53757 dataset, the abundance of $CD4^+$ T cells, $CD8^+$ T cells and Endothelial cells in FDX1-low group was lower than that in FDX1-high group ($p < 0.05$) (Figures 8B, C). The Kaplan-Meier curve of Endothelial cells in KIRC showed that FDX1 was low expression and low Endothelial cell infiltration, and the cumulative survival was poor (Figure 8D).

Discussion

RCC is one of the top ten cancers with high mortality (Clark et al., 2019). As the main pathological type of RCC, KIRC accounts for more than 80% of RCC (Alsaab et al., 2018). Advanced patients with KIRC are not sensitive to radiotherapy and chemotherapy, and miss the opportunity of surgery because of metastasis (Mu et al., 2020). Targeted therapy can benefit some patients, however, many advanced patients are ineffective to the existing targeted drug (Li et al., 2018). Because KIRC lacks precise targets and therapeutic mechanisms, it is necessary to identify the key molecules that affect the prognosis of KIRC. Targeting these molecules might become a new therapeutic target for KIRC and bring hope to patients with advanced KIRC.

Copper is an essential cofactor for organisms, and excess copper induces cell death if its concentration exceeds the steady-state threshold (Tsvetkov et al., 2022). Cuproptosis is different from the known death mechanism and mainly depends on mitochondrial respiration (Ren et al., 2019). It occurs by direct binding of copper to the fatty acylated components of the TCA cycle, which leads to the aggregation of lipo-acylated proteins, the subsequent loss of iron sulfur cluster proteins, proteotoxic stress and ultimately to cell death (Li S. R. et al., 2022). In some cancer, we found that the content of copper ions in tumor tissues and serum of tumor patients was higher than that of normal people (da Silva et al., 2022). Therefore, we analyzed whether there was differential expression of cuproptosis-related genes in KIRC. In our study, ten cuproptosis-related genes were differentially expressed in tumor tissues of KIRC compared with adjacent tissues ($p < .05$). Through our established prognostic model, we concluded that two protective genes (FDX1 and DLAT) and one pathogenic gene (CDKN2A) were closely related to prognosis. Through univariate and multivariate Cox regression analysis, we concluded that FDX1 was an independent prognostic gene of KIRC. However, the HR of pT-stage in univariate and multivariate Cox regression analysis were inconsistent. We speculated that because pTNM-stage caused a collinearity interference to pT-stage, it was not true that pT-stage was a risk factor of KIRC in univariate Cox regression analysis. FDX1, as a protein coding gene, has been reported to be involved in not only iron death but also cuproptosis (Zhang et al., 2022). FDX1 can regulate glucose, lipid and amino acid metabolism, affect the prognosis of LUAD and may participate in the occurrence and development of polycystic ovary syndrome (PCOS) (Wang et al., 2021; Zhang et al., 2021). Recently, Harvard team found that FDX1 is the key cuproptosis-related gene which encodes Elesclopmol (Tsvetkov et al., 2022). By analyzing the correlation between FDX1 and other cuproptosis-related genes in KIRC, we also found that FDX1 was positively correlated with DLD, DLAT, PDHA1 and PDHB, indicating that FDX1 was a key cuproptosis-related gene. Through bioinformatics and clinical tissues verification, we found that FDX1 was low expressed in tumor tissues of KIRC. In Zhang C's study, they also found that FDX1 was low expressed in tumor tissues of KIRC, and speculated that FDX1might play a role in KIRC as a tumor suppressor gene (Zhang et al., 2022). Zilong Bian's study showed that FDX1 was significantly related to the level of immune infiltration and the expression of programmed cell death protein 1 (PD-1) in KIRC, and they inferred that FDX1 could be used as a potential prognostic predictor for KIRC (Bian et al., 2022). Their researches were consistent with our conclusion, which verified the results of our data mining.

Many studies have shown that FDX1 was closely related to immune regulation in Pan-cancer (Liu, 2022; Zhang et al., 2022). We found that FDX1 was low expressed in KIRC tumor tissues and may be an independent prognostic gene of KIRC. Next, we analyzed the relationship between FDX1 and other eight immune checkpoints (SIGLEC15, TIGIT, CD274, HAVCR2, PDCD1, CTLA4, LAG3 and PDCD1LG2). We concluded that the expressions of CD274, HAVCR2 and PDCD1LG2 were positively correlated with FDX1 in KIRC, while CTLA4, LAG3 and PDCD1 were negatively correlated with FDX1 ($p < .05$). Kaplan-Meier survival curve analysis illustrated that the OS was poor when CTLA1 and LAG3 expression was high, while CD274 and HAVCR2 expression was low. Therefore, the FDX1 expression was positively related with CD274 and HAVCR2 expression, but negatively related with CTLA4 and LAG3 expression, indicating that the OS of KIRC patients was poor.

Immunotherapy can effectively inhibit the progression of KIRC, suggesting that immune cell infiltration may play an important role in the treatment of KIRC. Therefore, we analyzed the relationship between FDX1 and immune infiltration. The tumor infiltrating lymphocytes (TILs) also differentially expressed between low-FDX1

group and high-FDX1 group. Through the TIDE algorithm, the TIDE score in low-FDX1 group was higher than in high-FDX1 group, indicating that the lower the FDX1 expression, the worse the effect of ICB. Interestingly, the abundance of endothelial cells in low-FDX1 group was lower than that in high-FDX1 group ($p < .05$). According to the Kaplan-Meier curve of endothelial cells, the expression of FDX1 was low, the infiltration of endothelial cells was low, and the cumulative survival rate was low. Tumor metastasis depended to a large extent on the rapid and effective escape from the blood flow through the endothelial barrier (Morad et al., 2019). Tumor cell extravasation was similar to leukocyte migration through the endothelium. However, it is still unclear how tumor cells interact with endothelial cells during extravasation and how these processes are regulated. Studies have shown that tumor cells induce programmed necroptosis of endothelial cells, thereby promoting tumor cell extravasation and metastasis (Wettschureck et al., 2019). We inferred that FDX1 may participate in the interaction between tumor cells and endothelial cells, mediate the damage of endothelial cell barrier, and thus lead to tumor invasion and metastasis. Targeting FDX1 mediated cuproptosis of vascular endothelial cells to inhibit metastasis of KIRC may be a promising therapeutic approach.

Cuproptosis status affects treatment options about immunotherapy and targeted therapy for KIRC patients. Some studies revealed that FDX1 can regulate protein lipoylation modification, and high expression of lipoylated protein may become a new direction of tumor therapy (Zhang et al., 2021). According to our model, we found that FDX1 was not only an independent prognostic factor of KIRC, but also can regulate the status of immune cells and the expression of immune checkpoints in the tumor microenvironment (TME). Targeting FDX1 may become a new therapeutic target for KIRC.

However, this study still had some shortcomings. Firstly, we only verified the difference expression of FDX1 in tumor tissues and adjacent tissues of KIRC through clinical samples, and lacked further clinical experiments to verify immune infiltration and TILs. The number of samples we selected was not very large, nor does it cover different stages of KIRC. The insufficient number of samples made it impossible to further verify the prognostic value of FDX1 in KIRC. Secondly, we lack clinical relevance research and cannot analyze it with clinical information. Thirdly, although FDX1 was predicted as an independent prognostic factor of KIRC according to our Nomogram model, other important factors with predictive value were not considered in this study. In the next study, we will select more KIRC samples covering different stages to analyze and verify the regulatory mechanism of cuproptosis-related genes in KIRC, so as to lay a theoretical foundation for later development of targeted drugs.

In conclusion, our study showed that FDX1 was an independent factor affecting the prognosis of KIRC. The FDX1 expression in paired and unpaired tumor samples illustrated that the FDX1 downregulated compared with normal kidney tissues ($p < .05$). There was a significant correlation between FDX1 and immune infiltration in tumor samples of KIRC. The abundance of B cells, CD4 + T cells, CD8 + T cells, endothelial cells and NK cells in low-FDX1 group was lower than that in high-FDX1 group. Kaplan-Meier curve of endothelial cells showed low FDX1 expression and poor cumulative survival. Targeting FDX1 in KIRC may regulate cuproptosis to improve the prognosis of patients. Nevertheless, the specific pathogenesis and molecular targets still need to be further verified.

Conclusion

FDX1, as a key cuproptosis-related gene, was also an independent prognostic molecule of KIRC. It was closely related to immune cell infiltration and immune checkpoint regulation. In KIRC, FDX1 expression was decreased, and targeted regulation of FDX1 expression may be helpful to improve patient prognosis.

Data availability statement

The original contributions presented in the study are included in the article/supplementary material, further inquiries can be directed to the corresponding author.

Ethics statement

The studies involving human participants were reviewed and approved by Zhejiang Province Hospital of Traditional Chinese Medicine. Written informed consent for participation was not required for this study in accordance with the national legislation and the institutional requirements.

Author contributions

HC were responsible for patient enrollment and sample collection according to the inclusion criteria. ML carried out sample detection. YY was responsible for bioinformatics analysis and clinical data analysis. TC was a major contributor in writing the manuscript.

Funding

This work was supported by Zhejiang Medical Science and Technology Project (2022KY223) in the design of this study and collection of data.

Acknowledgments

The authors would like to express their gratitude to HELIX_1110 for the expert linguistic services provided.

Conflict of interest

The authors declare that the research was conducted in the absence of any commercial or financial relationships that could be construed as a potential conflict of interest.

Publisher's note

All claims expressed in this article are solely those of the authors and do not necessarily represent those of their

affiliated organizations, or those of the publisher, the editors and the reviewers. Any product that may be evaluated in this article, or claim that may be made by its manufacturer, is not guaranteed or endorsed by the publisher.

Supplementary Material

The Supplementary Material for this article can be found online at: https://www.frontiersin.org/articles/10.3389/fgene.2023.1071694/full#supplementary-material

References

Alsaab, H. O., Sau, S., Alzhrani, R. M., Cheriyan, V. T., Polin, L. A., Vaishampayan, U., et al. (2018). Tumor hypoxia directed multimodal nanotherapy for overcoming drug resistance in renal cell carcinoma and reprogramming macrophages. *Biomaterials* 183, 280–294. doi:10.1016/j.biomaterials.2018.08.053

Bao, J. H., Lu, W. C., Duan, H., Ye, Y. Q., Li, J. B., Liao, W. T., et al. (2022). Identification of a novel cuproptosis-related gene signature and integrative analyses in patients with lower-grade gliomas. *Front. Immunol.* 13, 933973. doi:10.3389/fimmu.2022.933973

Bian, Z., Fan, R., and Xie, L. (2022). A novel cuproptosis-related prognostic gene signature and validation of differential expression in clear cell renal cell carcinoma. *Genes (Basel)* 13 (5), 851. doi:10.3390/genes13050851

Clark, D. J., Dhanasekaran, S. M., Petralia, F., Pan, J., Song, X., Hu, Y., et al. (2019). Integrated proteogenomic characterization of clear cell renal cell carcinoma. *Cell* 179 (4), 964–983.e31. e931. doi:10.1016/j.cell.2019.10.007

da Silva, D. A., De Luca, A., Squitti, R., Rongioletti, M., Rossi, L., Machado, C. M. L., et al. (2022). Copper in tumors and the use of copper-based compounds in cancer treatment. *J. Inorg. Biochem.* 226, 111634. doi:10.1016/j.jinorgbio.2021.111634

Hakimi, A. A., Reznik, E., Lee, C. H., Creighton, C. J., Brannon, A. R., Luna, A., et al. (2016). An integrated metabolic Atlas of clear cell renal cell carcinoma. *Cancer Cell* 29 (1), 104–116. doi:10.1016/j.ccell.2015.12.004

Jakubek, Y. A., Chang, K., Sivakumar, S., Yu, Y., Giordano, M. R., Fowler, J., et al. (2020). Large-scale analysis of acquired chromosomal alterations in non-tumor samples from patients with cancer. *Nat. Biotechnol.* 38 (1), 90–96. doi:10.1038/s41587-019-0297-6

Li, H., Wang, G., Yu, Y., Jian, W., Zhang, D., Wang, Y., et al. (2018). α-1,2-Mannosidase MAN1C1 inhibits proliferation and invasion of clear cell renal cell carcinoma. *J. Cancer* 9 (24), 4618–4626. doi:10.7150/jca.27673

Li, S. R., Bu, L. L., and Cai, L. (2022a). Cuproptosis: Lipoylated TCA cycle proteins-mediated novel cell death pathway. *Signal Transduct. Target Ther.* 7 (1), 158. doi:10.1038/s41392-022-01014-x

Li, Y., Fang, M., Xu, Z., and Li, X. (2022b). Tetrathiomolybdate as an old drug in a new use: As a chemotherapeutic sensitizer for non-small cell lung cancer. *J. Inorg. Biochem.* 233, 111865. doi:10.1016/j.jinorgbio.2022.111865

Li, Y., Wang, Z., Jiang, W., Zeng, H., Liu, Z., Lin, Z., et al. (2020). Tumor-infiltrating TNFRSF9(+) CD8(+) T cells define different subsets of clear cell renal cell carcinoma with prognosis and immunotherapeutic response. *Oncoimmunology* 9 (1), 1838141. doi:10.1080/2162402x.2020.1838141

Liu, H. (2022). Pan-cancer profiles of the cuproptosis gene set. *Am. J. Cancer Res.* 12 (8), 4074–4081.

Lopez, J., Ramchandani, D., and Vahdat, L. (2019). Copper depletion as a therapeutic strategy in cancer. *Met. Ions Life Sci.* 19. doi:10.1515/9783110527872-018

Mayadev, J. S., Enserro, D., Lin, Y. G., Da Silva, D. M., Lankes, H. A., Aghajanian, C., et al. (2020). Sequential ipilimumab after chemoradiotherapy in curative-intent treatment of patients with node-positive cervical cancer. *JAMA Oncol.* 6 (1), 92–99. doi:10.1001/jamaoncol.2019.3857

Mei, W., Liu, X., Jia, X., Jin, L., Xin, S., Sun, X., et al. (2022). A cuproptosis-related gene model for predicting the prognosis of clear cell renal cell carcinoma. *Front. Genet.* 13, 905518. doi:10.3389/fgene.2022.905518

Meydan, S., Klepacki, D., Karthikeyan, S., Margus, T., Thomas, P., Jones, J. E., et al. (2017). Programmed ribosomal frameshifting generates a copper transporter and a copper chaperone from the same gene. *Mol. Cell* 65 (2), 207–219. doi:10.1016/j.molcel.2016.12.008

Morad, G., Carman, C. V., Hagedorn, E. J., Perlin, J. R., Zon, L. I., Mustafaoglu, N., et al. (2019). Tumor-derived extracellular vesicles breach the intact blood-brain barrier via transcytosis. *ACS Nano* 13 (12), 13853–13865. doi:10.1021/acsnano.9b04397

Mu, L., Guan, B., Tian, J., Li, X., Long, Q., Wang, M., et al. (2020). MicroRNA-218 inhibits tumor angiogenesis of human renal cell carcinoma by targeting GAB2. *Oncol. Rep.* 44 (5), 1961–1970. doi:10.3892/or.2020.7759

Peña-Llopis, S., Vega-Rubín-de-Celis, S., Liao, A., Leng, N., Pavía-Jiménez, A., Wang, S., et al. (2012). BAP1 loss defines a new class of renal cell carcinoma. *Nat. Genet.* 44 (7), 751–759. doi:10.1038/ng.2323

Ravi, R., Noonan, K. A., Pham, V., Bedi, R., Zhavoronkov, A., Ozerov, I. V., et al. (2018). Bifunctional immune checkpoint-targeted antibody-ligand traps that simultaneously disable TGFβ enhance the efficacy of cancer immunotherapy. *Nat. Commun.* 9 (1), 741. doi:10.1038/s41467-017-02696-6

Ren, F., Logeman, B. L., Zhang, X., Liu, Y., Thiele, D. J., and Yuan, P. (2019). X-ray structures of the high-affinity copper transporter Ctr1. *Nat. Commun.* 10 (1), 1386. doi:10.1038/s41467-019-09376-7

Tsvetkov, P., Coy, S., Petrova, B., Dreishpoon, M., Verma, A., Abdusamad, M., et al. (2022). Copper induces cell death by targeting lipoylated TCA cycle proteins. *Science* 375 (6586), 1254–1261. doi:10.1126/science.abf0529

von Roemeling, C. A., Radisky, D. C., Marlow, L. A., Cooper, S. J., Grebe, S. K., Anastasiadis, P. Z., et al. (2014). Neuronal pentraxin 2 supports clear cell renal cell carcinoma by activating the AMPA-selective glutamate receptor-4. *Cancer Res.* 74 (17), 4796–4810. doi:10.1158/0008-5472.Can-14-0210

Wang, J., Sun, J., Liu, L. N., Flies, D. B., Nie, X., Toki, M., et al. (2019). Siglec-15 as an immune suppressor and potential target for normalization cancer immunotherapy. *Nat. Med.* 25 (4), 656–666. doi:10.1038/s41591-019-0374-x

Wang, W., Lu, Z., Wang, M., Liu, Z., Wu, B., Yang, C., et al. (2022). The cuproptosis-related signature associated with the tumor environment and prognosis of patients with glioma. *Front. Immunol.* 13, 998236. doi:10.3389/fimmu.2022.998236

Wang, Z., Dong, H., Yang, L., Yi, P., Wang, Q., and Huang, D. (2021). The role of FDX1 in granulosa cell of Polycystic ovary syndrome (PCOS). *BMC Endocr. Disord.* 21 (1), 119. doi:10.1186/s12902-021-00775-w

Wettschureck, N., Strilic, B., and Offermanns, S. (2019). Passing the vascular barrier: Endothelial signaling processes controlling extravasation. *Physiol. Rev.* 99 (3), 1467–1525. doi:10.1152/physrev.00037.2018

Xiong, Z., Yuan, C., Shi, J., Xiong, W., Huang, Y., Xiao, W., et al. (2020). Restoring the epigenetically silenced PCK2 suppresses renal cell carcinoma progression and increases sensitivity to sunitinib by promoting endoplasmic reticulum stress. *Theranostics* 10 (25), 11444–11461. doi:10.7150/thno.48469

Yi, L., Wu, G., Guo, L., Zou, X., and Huang, P. (2020). Comprehensive analysis of the PD-L1 and immune infiltrates of m(6)A RNA methylation regulators in head and neck squamous cell carcinoma. *Mol. Ther. Nucleic Acids* 21, 299–314. doi:10.1016/j.omtn.2020.06.001

Zeng, D., Li, M., Zhou, R., Zhang, J., Sun, H., Shi, M., et al. (2019). Tumor microenvironment characterization in gastric cancer identifies prognostic and immunotherapeutically relevant gene signatures. *Cancer Immunol. Res.* 7 (5), 737–750. doi:10.1158/2326-6066.Cir-18-0436

Zhang, C., Zeng, Y., Guo, X., Shen, H., Zhang, J., Wang, K., et al. (2022). Pan-cancer analyses confirmed the cuproptosis-related gene FDX1 as an immunotherapy predictor and prognostic biomarker. *Front. Genet.* 13, 923737. doi:10.3389/fgene.2022.923737

Zhang, Z., Ma, Y., Guo, X., Du, Y., Zhu, Q., Wang, X., et al. (2021). FDX1 can impact the prognosis and mediate the metabolism of lung adenocarcinoma. *Front. Pharmacol.* 12, 749134. doi:10.3389/fphar.2021.749134

Zhou, P., Qin, J., Zhou, C., Wan, G., Liu, Y., Zhang, M., et al. (2019). Multifunctional nanoparticles based on a polymeric copper chelator for combination treatment of metastatic breast cancer. *Biomaterials* 195, 86–99. doi:10.1016/j.biomaterials.2019.01.007

Zhu, S., Shanbhag, V., Wang, Y., Lee, J., and Petris, M. (2017). A role for the ATP7A copper transporter in tumorigenesis and cisplatin resistance. *J. Cancer* 8 (11), 1952–1958. doi:10.7150/jca.19029

frontiers | Frontiers in Genetics

TYPE Original Research
PUBLISHED 01 March 2023
DOI 10.3389/fgene.2023.1148437

OPEN ACCESS

EDITED BY
Rui Cao,
Capital Medical University, China

REVIEWED BY
Xu-Sheng Liu,
Hubei University of Medicine, China
Fahui Liu,
University of Gothenburg, Sweden

*CORRESPONDENCE
Dingshan Deng,
dds15116217256@163.com
Yuanqing Dai,
dycooper8828@126.com

†These authors have contributed equally to this work and share first authorship

SPECIALTY SECTION
This article was submitted to Cancer Genetics and Oncogenomics, a section of the journal Frontiers in Genetics

RECEIVED 20 January 2023
ACCEPTED 20 February 2023
PUBLISHED 01 March 2023

CITATION
Liu J, Cheng C, Qi T, Xiao J, Zhou W, Deng D and Dai Y (2023), ACER2 forms a cold tumor microenvironment and predicts the molecular subtype in bladder cancer: Results from real-world cohorts. *Front. Genet.* 14:1148437. doi: 10.3389/fgene.2023.1148437

ACER2 forms a cold tumor microenvironment and predicts the molecular subtype in bladder cancer: Results from real-world cohorts

Jinhui Liu[1,2†], Chunliang Cheng[1,2†], Tiezheng Qi[3], Jiatong Xiao[1,2], Weimin Zhou[1,2], Dingshan Deng[1,2*] and Yuanqing Dai[1,2*]

[1]Department of Urology, Xiangya Hospital, Central South University, Changsha City, China, [2]National Clinical Research Center for Geriatric Disorders, Xiangya Hospital, Central South University, Changsha, China, [3]Xiangya School of Medicine, Central South University, Changsha, China

Background: ACER2 is a critical gene regulating cancer cell growth and migration, whereas the immunological role of ACER2 in the tumor microenvironment (TME) is scarcely reported. Thus, we lucubrate the potential performance of ACER2 in bladder cancer (BLCA).

Methods: We initially compared ACER2 expressions in BLCA with normal urothelium tissues based on data gathered from the Cancer Genome Atlas (TCGA) and our Xiangya cohort. Subsequently, we systematically explored correlations between ACER2 with immunomodulators, anti-cancer immune cycles, tumor-infiltrating immune cells, immune checkpoints and the T-cell inflamed score (TIS) to further confirm its immunological role in BLCA TME. In addition, we performed ROC analysis to illustrate the accuracy of ACER2 in predicting BLCA molecular subtypes and explored the response to several cancer-related treatments. Finally, we validated results in an immunotherapy cohort and Xiangya cohort to ensure the stability of our study.

Results: Compared with normal urinary epithelium, ACER2 was significantly overexpressed in several cell lines and the tumor tissue of BLCA. ACER2 can contribute to the formation of non-inflamed BLCA TME supported by its negative correlations with immunomodulators, anti-cancer immune cycles, tumor-infiltrating immune cells, immune checkpoints and the TIS. Moreover, BLCA patients with high ACER2 expression were inclined to the luminal subtype, which were characterized by insensitivity to neoadjuvant chemotherapy, chemotherapy and radiotherapy but not to immunotherapy. Results in the IMvigor210 and Xiangya cohort were consistent.

Conclusion: ACER2 could accurately predict the TME and clinical outcomes for BLCA. It would be served as a promising target for precision treatment in the future.

KEYWORDS

ACER2, tumor micro environment, bladder cancer, Chemothearpy, Immunothrapy

1 Introduction

Bladder cancer (BLCA) is the second common urinary malignancy with 81,180 new cases each year, and results in 17,100 deaths in United States (Siegel et al., 2022). Despite multiple treatment strategies including surgery, chemotherapy and radiotherapy, have been applied in the present, half of BLCA patients would still relapse or found to be metastasized after the radical cystectomy (Witjes et al., 2021). And the prognosis of metastatic BLCA is still frustrating.

Recently, cancer immunotherapy represented by immune checkpoint blockade (ICB) had gained colossal survival benefits for advanced BLCA (Bellmunt et al., 2017; Powles et al., 2018). However, BLCA varied with significant heterogeneity, thus a portion of patients were observed not to respond to ICB (Rosenberg et al., 2016; Sharma et al., 2017). A main mechanism is that lower neoantigen burden and tumor mutation burden in TME suppresses the response to ICB due to the impair of T-cells to destroy tumor cells (Morad et al., 2021). Besides, tumor microenvironment (TME) was vital for the effect of immunotherapy, in which tumor cells themselves can upregulate the expression of PD-L1 and stimulate the expression of PD-L1 in TME cells, and thus suppresses antitumor immune response of cytotoxic T-cells (Alsaab et al., 2017). ICB inhibited tumor growth by re-invigorating tumor-cytotoxic T-cells. Unfortunately, non-inflamed TME would cause resistance to ICB by some molecules or pathways. Consequently, it was critical to explore new TME state indicators and treatment response biomarkers for BLCA to early screen a suitable group who may respond to ICB.

Alkaline ceramidase 2 (ACER2) was a sphingolipid metabolizing enzyme localized to the Golgi complex, which could convert ceramide to sphingosine *in vivo* (Sun et al., 2010). ACER2 was highly expressed in a majority of human tumor tissues (Xu et al., 2006; Xu et al., 2018a). Accumulated studies have reported that ACER2 was transactivated to mediate the DNA damage response, and regulated autophagy and programmed cell death by increasing the production of reactive oxygen species (ROS) (Xu et al., 2016; Wang et al., 2017; Xu et al., 2018a). Besides, ACER2 was observed to be a crucial biomarker, which contribute to the tumor growth, invasion, and migration in several cancers (Liu et al., 2020; Zhang et al., 2020; Zheng et al., 2022). Considering the effect in the cancer cell apoptosis and proliferation, ACER2 could be served as a potential molecular target for cancer treatment.

However, the immunological role of ACER2 in tumor microenvironment (TME) was rarely reported. Herein, we comprehensively explored the relationship between ACER2 expression and TME in the BLCA. We found that ACER2 promoted the development of a non-inflamed BLCA TME, and had the potential to predict the molecular subtypes of BLCA.

2 Methods

2.1 Data collection and preprocessing

We obtained the mRNA expression data (FPKM) value and corresponding clinicopathologic information of bladder cancer in The Cancer Genome Atlas (TCGA) (https://portal.gdc.cancer.gov/). The cohort comprised 410 BLCA samples and 19 normal urothelium tissues. And then, the FPKM value of TCGA cohort was translated into transcripts per kilobase million (TPM) value before analysis.

The validation cohort was derived from the bladder cancer patients who underwent surgery in Xiangya Hospital. It comprised a total of 57 BLCA cancer samples and 13 normal urothelium tissues. Fresh tissues were collected and stored with liquid nitrogen immediately. First, total RNA was extracted from fresh tissues using TRIzol (Invitrogen, Carlsbad, California, United States). The total RNA was then quantified using NanoDrop and Agilent 2100 biological analyzers (Thermo Fisher Scientific, MA, United States). After constructing the mRNA library, we further purified and fragmented the total RNA into small pieces. After that, we synthesized the first-strand cDNA and the second-strand cDNA, and further amplified by PCR to construct the final library (single-stranded circular DNA). Finally, 57 BLCA samples and 13 normal tissues were qualified and sequenced on the BGISEQ-500 platform (BGI-Shenzhen, China).TPM value was also translated in Xiangya cohort. Besides, the data has been uploaded to the GEO database (GSE188715).

IMvigor210 was an immunotherapy cohort in which BLCA patients received anti-PD-1 therapy. We obtained the mRNA expression data and corresponding clinicopathologic information from http://research-pub.Gene.com/imvigor210corebiologies/based on the Creative Commons 3.0 License.

2.2 Depicting immunological characteristics of TME

The effect of anticancer immunity was highly associated with the expression of immunomodulators, activity of the cancer immunity cycle, infiltration level of tumor infiltrating lymphocytes (TILs), and the expression of inhibitory immune checkpoints in an inflamed tumor microenvironment (TME). We collected the information of 122 immunomodulators in the previous study (Charoentong et al., 2017), and compared differential expression immunomodulators including MHC, receptors, chemokines, and immune stimulators between low and high ACER2 groups. We further explored the effect of ACER2 in impacting cancer immunity cycle in BLCA. The cancer immunity cycle was stepwise events proceed and expand iteratively comprising in 7 critical steps, which determined the fate of tumor cells (Chen and Mellman, 2013). Thereafter, we calculated the correlation between the infiltration level of TILs in TME and ACER2 expression using seven independent algorithms, including Cibersort-ABS, MCP-counter, quanTIseq, TIMER, xCell, TIP, and TISIDB (Newman et al., 2015; Becht et al., 2016; Li et al., 2016; Xu et al., 2018b; Finotello et al., 2019; Ru et al., 2019; Li et al., 2020). The relationships between ACER2 and the corresponding effector genes of these TILs were also analyzed. Moreover, we correlated the ACER2 expression with 22 common immune checkpoint inhibitors (ICIs), such as PD-1, PD-L1, CTLA-4, and LAG-3. Finally, we analyzed the T-cell inflamed score (TIS) and corresponding TIS-related effector genes in the TME, which represented pre-existing cancer immunity and predicted the clinical response of ICB (Ayers et al., 2017).

2.3 Prediction to molecular subtypes and therapeutic response

Consider that BLCA varied with high heterogeneity and differed distinctly in the treatment response and prognosis, several molecular subtype systems of BLCA had been constructed (Sjödahl et al., 2022), including UNC, Baylor, TCGA, MDA, Lund, CIT, and Consensus subtype systems. We used ConsensusMIBC and BLCA subtyping R packages to determine the molecular subtype systems, and depicted the relationship between the specific signatures of molecular subtypes and ACER2 expression (Hu et al., 2021). Receiver operating characteristic (ROC) curves were used for evaluating the accuracy of ACER2 in predicting BLCA molecular subtypes. The difference of neoadjuvant chemotherapy related mutation was evaluated in the high and low ACER2 groups. Subsequently, we explored several therapeutic responses to immunotherapy, targeted therapies and radiotherapy. Finally, drug-target genes were collected and analyzed in the Drug Bank database.

2.4 Real-time quantitative PCR (qPCR)

Bladder cancer and normal bladder cell lines were used to extracted total RNA using cell total RNA isolation kit (Foregene, China) according to manufacturer's protocol. cDNA was synthesized using UeIris II RT-PCR System for First-Strand cDNA Synthesis (US Everbright, China). qRT-PCR was performed using SYBR Green qPCR Master Mix (US Everbright, China) on CFX Connect System (Bio-Rad, United States). Gene expression levels were normalized to the "housekeeping" gene GAPDH. The primers were designed and synthesized by Sangon Biotech (Shanghai, China) and detailed primer sequences were listed below: ACER2: (forward primer: 5′-CCTTTGGGTTCTGATGTGTGCTTTG-3′; reverse primer: 5′-GGA CACTGACCACCACCTTGAAC-3′); GAPDH: (forward primer: 5′-CAAGGCTGTGGGCAAGGTCATC-3′; reverse primer: 5′- GTGTCG CTGTTGAAGTCAGAGGAG-3′).

2.5 Statistical analysis

Pearson or Spearman coefficients was calculated to explore correlations between variables. For variables fitting a normal distribution between binary groups, t-test was used to compare the differences. For categorical variables, chi-squared test or Fisher's exact test was performed. Analyses with two-sided $p = 0.05$ were considered as the threshold of statistical significance. Receiver operating characteristic (ROC) curves were depicted to evaluate the predictive accuracy for molecular subtypes. All the statistical analyses and visualizations were performed in R software, Version: 4.2.2.

3 Result

3.1 Pan-cancer analysis evaluates the immunological role of ACER2

We performed pan-cancer analysis to illustrate the immunological role of ACER2, and screened cancer types which were impacted most by ACER2. Figure 1A revealed the relationship between ACER2 expression and immunomodulators across 37 cancer types. We found that ACER2 was positively associated with multiple immunomodulators in several cancer types, such as THYM, CHOL, ACC, and SARC. Remarkably, we noticed negative correlations in BLCA between ACER2and a majority of immunomodulators including immunomostimulators, MHC, receptors, and chemokines. Likewise, a negative relation was also observed in breast cancer. We then explored the relationship between ACER2 expression and several critical immune checkpoints. Of note, ACER2 expression in BLCA was negatively correlated with four immune checkpoints, namely, PD-L1, PD-1, CTLA-4, and LAG-3 (Figures 1B–E). Besides, we uncovered ACER2 expression in BLCA was negatively associated with the ESTIMATE score, Immune score and Stromal score in TME (Figures 1F–H). In brief, ACER2 was considered potential to be a biomarker to predict the TME status especially in BLCA. High ACER2 expression in BLCA may contribute to the formation of non-inflamed TME, as the result of the reduced level of immunomodulators, immune checkpoints, immune cells, and stromal cells in TME.

3.2 ACER2 is highly expressed in BLCA

We assessed the expression characteristics of ACER2 in BLCA. The qPCR analysis of Xiangya cohort revealed that ACER2 was significantly elevated in tumor tissues ($p = 0.0086$) compared with normal urothelium (Figure 2A). Then we analyzed the differential expression of ACER2 in diverse cell lines. ACER2 was significantly higher expressed in bladder cancer cell lines in comparison to bladder epithelial cell lines (Figure 2B). Besides, single-cell analysis also indicated a higher expression in the malignant epithelial cells (Figure 2C). However, we did not observe the correlations between ACER2 expression and gender, T stage (Figures 2D,E). No significant difference was observed in the disease-specific survival between high- and low-ACER2 ($p = 0.088$) (Figure 2F).

3.3 ACER2 contributes to a non-inflamed TME in BLCA

ACER2 exhibited negative correlations with multiple immunomodulators (Figure 3A). The high ACER2 group had an obvious downregulation of the majority of chemokines including CCL4, CCL3, CCL24, and CCL26. Immunostimulators including CD80, CD86, ICOS, and TNFSF13B were also found negatively correlated with ACER2. Subsequently, four major steps in the anti-cancer immunity cycle were downregulated in the high ACER2 group (Figure 3B), which included the release of cancer cell antigens, priming and activation, immune cells recruiting and killing of cancer cells. Strikingly, we noticed that recruiting of multiple immune cells such as T-cell, $CD8^+$ T-cell, macrophage cell, NK cell, Th1 cell, dendritic cell, neutrophil cell, eosinophil cell, basophil cell, Th17 cell, CD4 T-cell were significantly restrained in the high ACER2 group. It implied the reduction of infiltration levels of effector TILs in the TME.

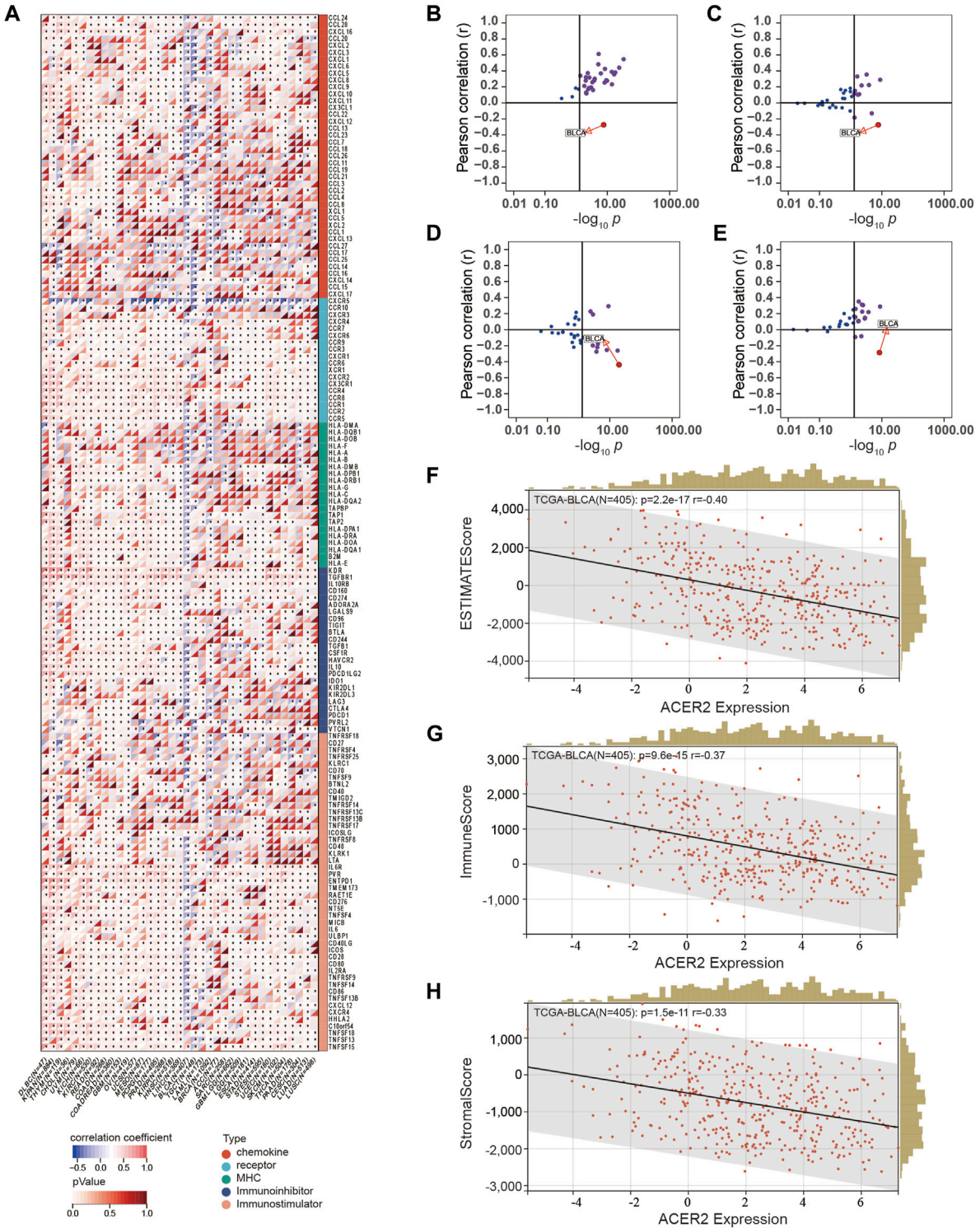

FIGURE 1
Correlations between ACER2 with immunological characteristics in pan-cancers. **(A)** Correlation between ACER2 and 122 immunomodulators (chemokines, receptors, MHC, and immunostimulators). **(B–E)** Correlation between ACER2 and four immune checkpoints, namely, PD-L1, CTLA-4, PD-1, and LAG-3. **(F–H)** Correlation between ACER2 expression and the ESTIMATE score, Immune score and Stromal score in TME.

For further validating the correlation between ACER2 and TILs in the TME, we calculated the infiltration level of TILs using seven independent algorithms. Similarly, ACER2 was negatively correlated with the infiltration level of $CD8^+$ T-cell, macrophage, NK cell, Th1 cell, and dendritic cell (Figure 3C). Likewise, ACER2 was proved to be negatively correlated with the effector genes of TILs (Figure 3D). Moreover, we explored the relation between ACER2 and immune checkpoint inhibitors in the TME.

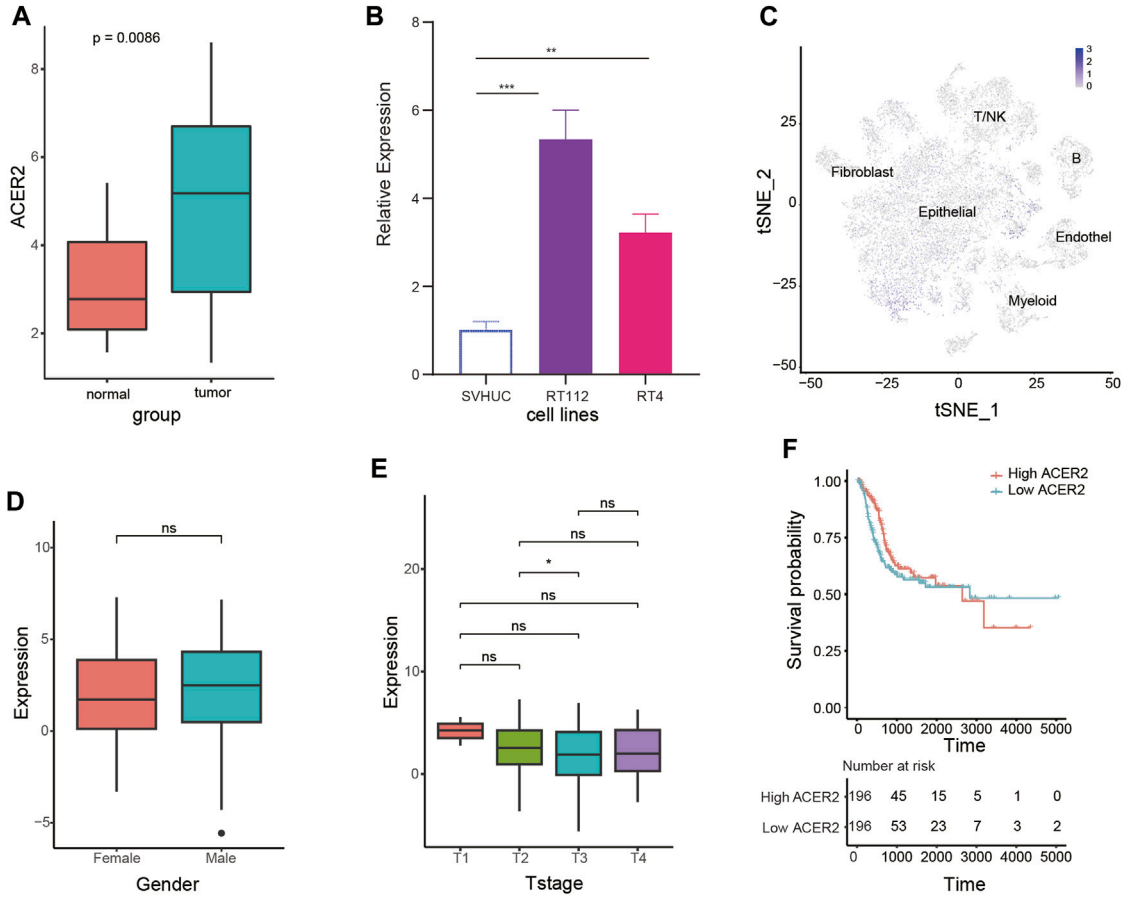

FIGURE 2
Expression characteristics of ACER2 in BLCA. **(A)** Expression analysis of ACER2 in the Xiangya cohort. **(B)** Expression of ACER2 in diverse cell lines. **(C)** Single-cell analysis of ACER2 expression in tumor and normal tissues. **(D, E)** Correlations between ACER2 expression and gender, T stage. **(F)** Kaplan-Meier curve for disease-specific survival by expression of ACER2.

ACER2 was found to be negatively correlated with a majority of usual immune checkpoint inhibitors including PD-L1, PD-1, CTLA-4, LAG-3, TIM-3, and TIGIT (Figure 3E). Finally, we further discovered ACER2 was negatively correlated with the TIS and corresponding TIS-related effector genes (Figures 4A,B). In summary, the results revealed that ACER2 contributed to the formation of non-inflamed TME in BLCA.

3.4 ACER2 predicts molecular subtypes and drug sensitivity

BLCA was a highly heterogeneous malignancy with various molecular subtypes which mainly differed in sensitivity to diverse therapeutic regimens. Therefore, we distinguished BLCA molecular subtypes in the TCGA within ACER2 expression. Figure 4C illustrated patients with low ACER2 expression were more likely to be basal subtype and characterized by basal differentiation, EMT differentiation, immune differentiation, and keratinization. As shown in previous studies, basal subtype was more sensitive to ICB with higher immune infiltration level and pathological response rates, which was consistent to our prior finding (Kamoun et al., 2020; Necchi et al., 2020). Thus, patients with lower ACER2 expression may benefit from ICB. Conversely, individuals with high ACER2 expression were inclined to luminal subtype with urothelial differentiation, Ta pathway, and luminal differentiation. Thereafter, ROC analysis was adopted to evaluate the predictive accuracy of ACER2 for molecular subtypes, and the area under the ROC curves was calculated ranging from 0.77 to 0.93 (Figure 4D).

In order to further explore the correlation between ACER2 with neoadjuvant chemotherapy (NAC), we found that low ACER2 group was more likely to carry neoadjuvant chemotherapy related mutation such as RB1 (23%), ATM (13%), and ERBB2 (10%). We also found that high mutation rates of ATM (12%), RB1 (12%), and ERBB2 (11%) in the high ACER2 group (Figure 4E). Notably, chemotherapy related mutation of RB1 was significantly higher in the low ACER2 group, which implied that tumors with low ACER2 may be more sensitive to NAC. Ulteriorly, we revealed enrichment scores for radiotherapy-predicted pathways and EGFR ligands was higher in the low ACER2 group (Figure 4F). And several enrichment scores for various immunosuppressive oncogenic pathways such as PPARG coexpressed genes, WNT-β-catenin pathway, and IDH1 were significantly higher in high ACER2 group, which also indicated the formation of non-inflamed TME in BLCA. Besides, we used the

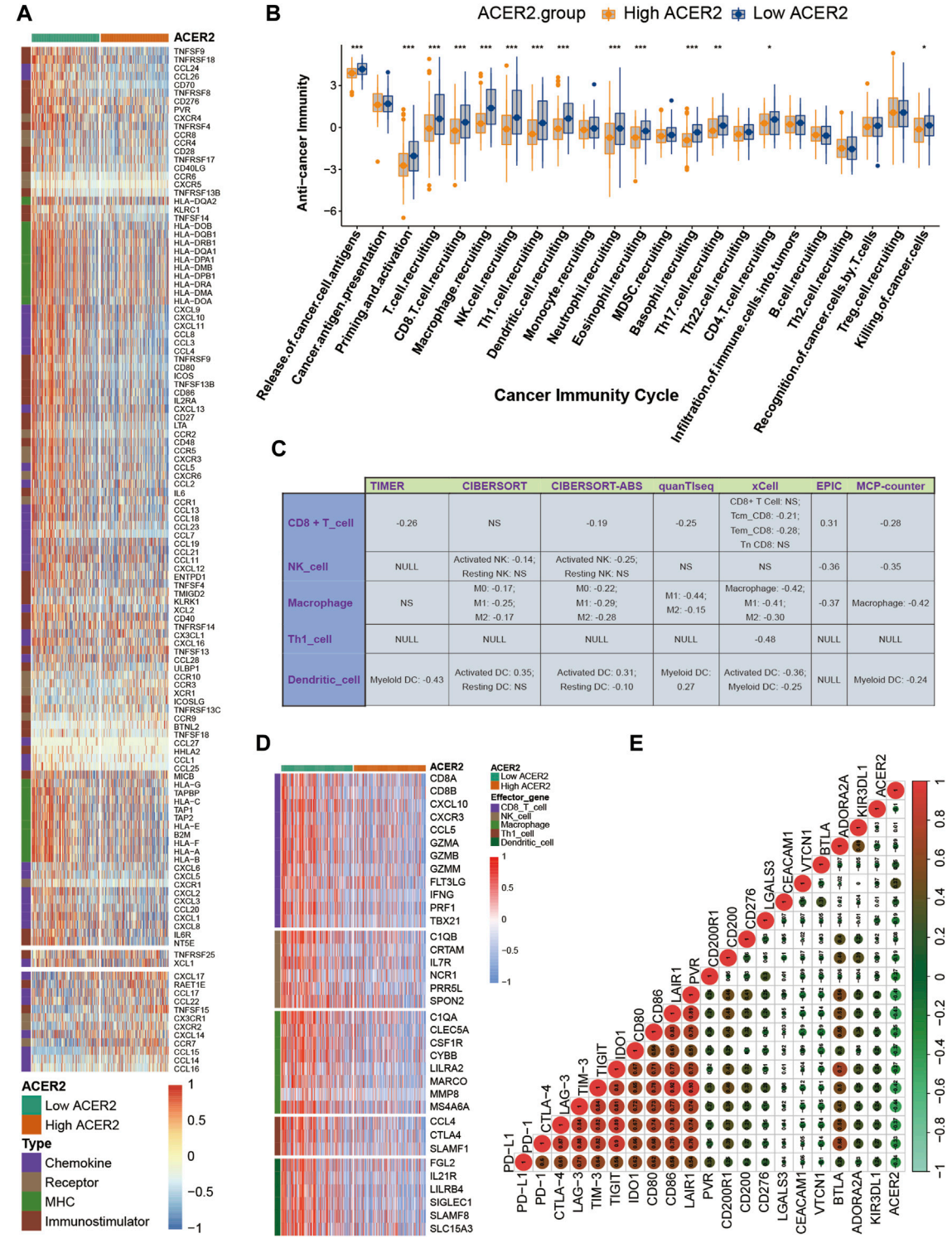

FIGURE 3
ACER2 correlated with the tumor immune microenvironment in BLCA. **(A)** Differential expression of ACER2 between high- and low-ACER2 tissues in BLCA. **(B)** Differential expression of ACER2 among various steps of the anti-tumor immune cycle. **(C)** Correlation between ACER2 and the infiltration levels of five TIICs with various algorithms. **(D)** Differential expression of effector genes of five mentioned TIICs between high- and low-ACER2 tissues in BLCA. **(E)** Correlation betweenACER2 and 20 inhibitory immune checkpoints.

Drugbank database to determine that the low ACER2 group was sensitive to immunotherapy and ERBB therapy, whereas antiangiogenic therapy may be more suitable for high ACER2 group (Figure 4G). Collectively, neoadjuvant chemotherapy, adjuvant chemotherapy, immunotherapy, ERBB therapy could be used for patients with low ACER2.

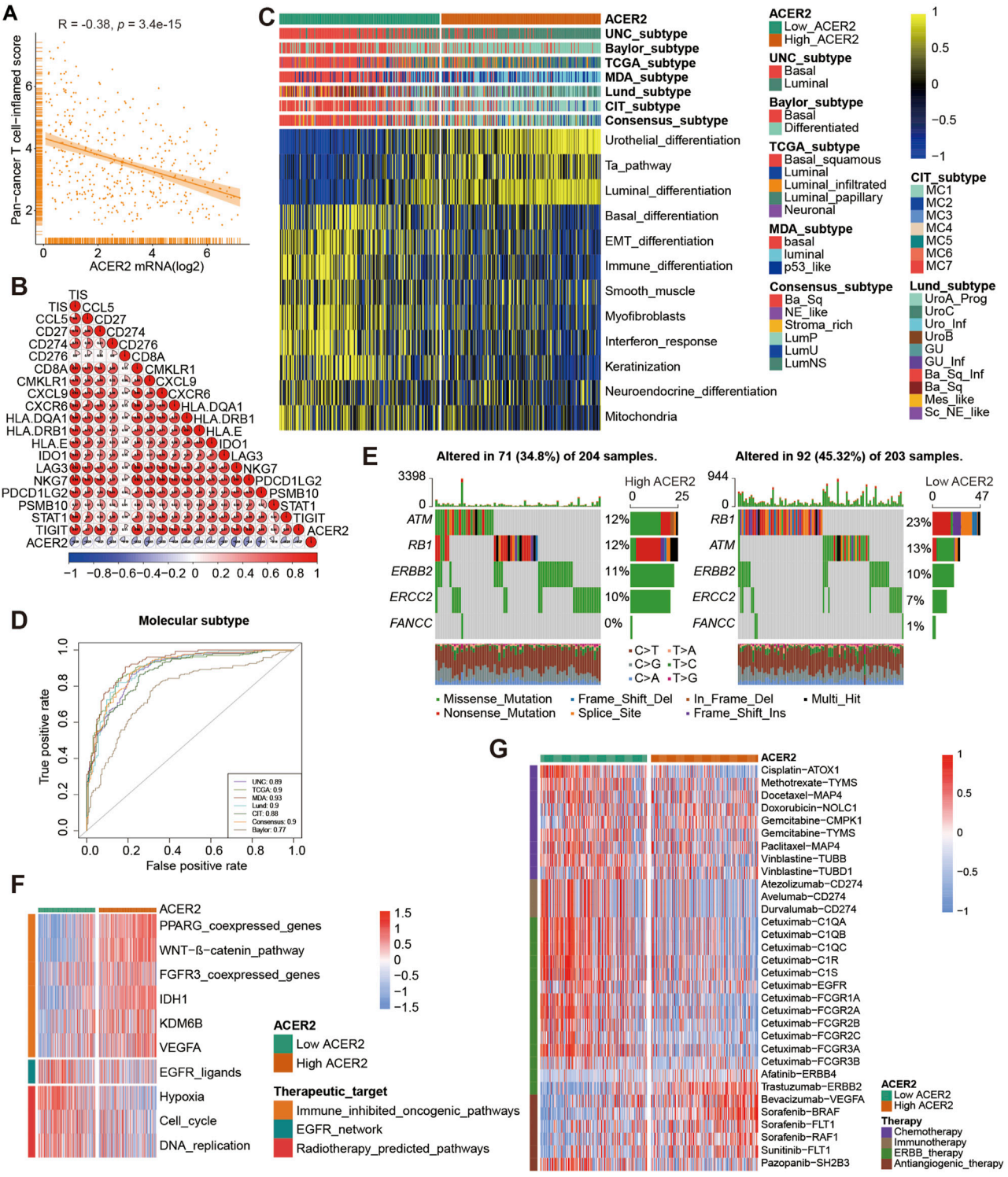

FIGURE 4
ACER2 predicts the molecular subtype and response to several therapies in BLCA. **(A, B)** Correlation between ACER2 with TIS and the corresponding TIS-related effector genes. **(C)** Correlations between ACER2 and molecular subtypes with seven different subtyping systems. **(D)** ROC analysis on the prediction accuracy of ACER2 for molecular subtypes with different systems. **(E)** Mutational profiles of neoadjuvant chemotherapy-related genes in low- and high-ACER2 tissues. **(F)** Correlation between ACER2 and the enrichment scores of therapeutic signatures. **(G)** Correlation between ACER2 and the drug-target genes of various therapies.

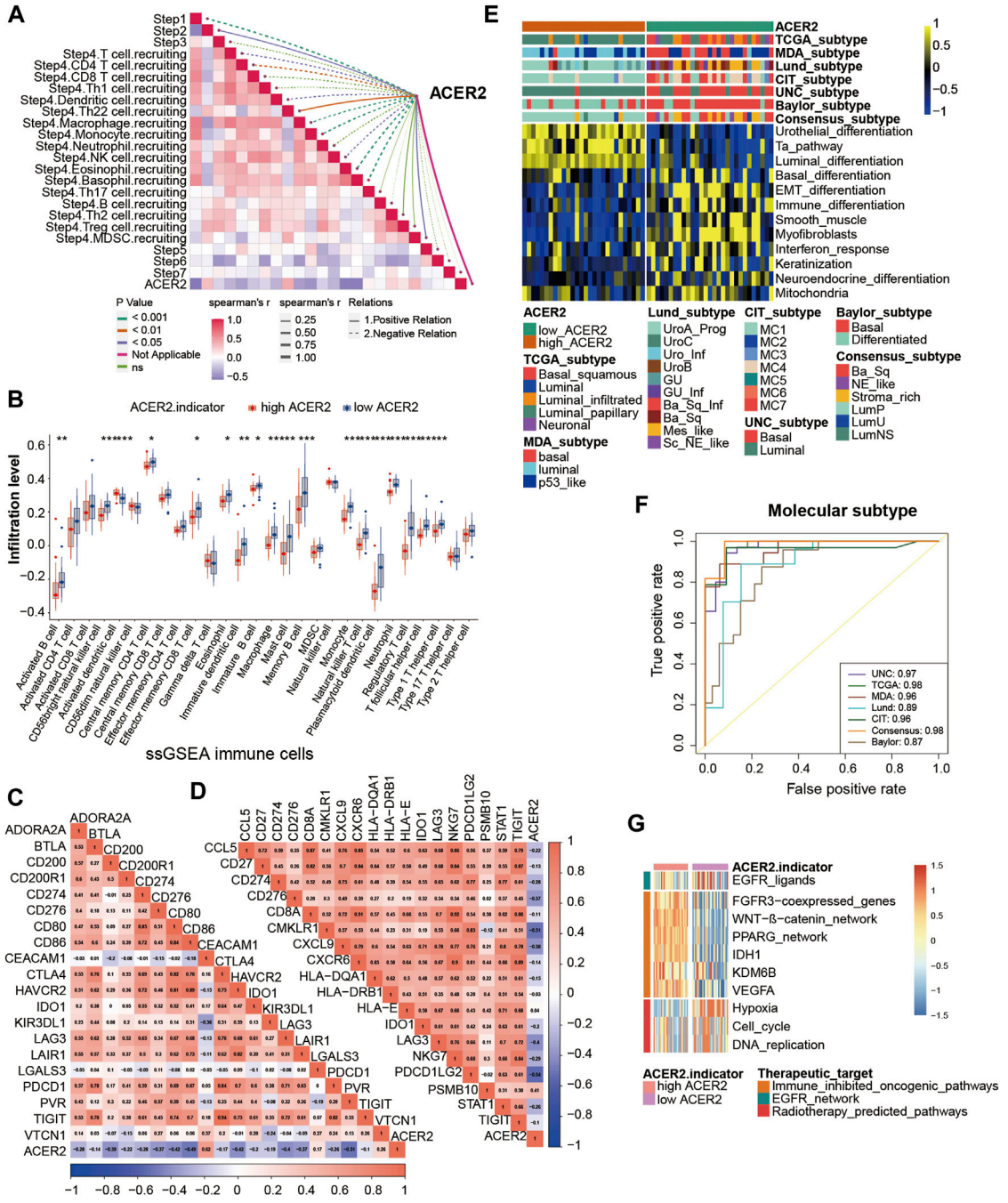

FIGURE 5
Validation of the ACER2 prediction for molecular subtypes and the response to several therapies in the Xiangya cohort. **(A)** Correlations between ACER2 and the process of the anti-cancer immunity cycle. **(B)** Correlations between ACER2 and multiple ssGSEA immune cells. **(C)** Correlations between ACER2 and 20 immune checkpoints. **(D)** Correlation between ACER2 and TIS-related effector genes. **(E)** Correlations between ACER2 and seven molecular subtype systems. **(F)** ACER2 molecular subtype prediction accuracy. **(G)** Correlation between ACER2 and the enrichment scores of therapeutic signatures.

3.5 Validation of the roles of ACER2 in the Xiangya cohort

Thereafter, we further validated the role of ACER2 in Xiangya cohort. ACER2 negatively correlated with the several critical steps of the anti-cancer immune cycles especially including the release of cancer cell antigens, and immune cells recruiting (Figure 5A). Consistently, ACER2 was also negatively associated with multiple ssGSEA immune cells including activated dendritic cell, macrophage cell, natural killer cell, regulatory T-cell, T follicular helper cell (Figure 5B). Subsequently, a negative relationship between ACER2 and immune checkpoints was

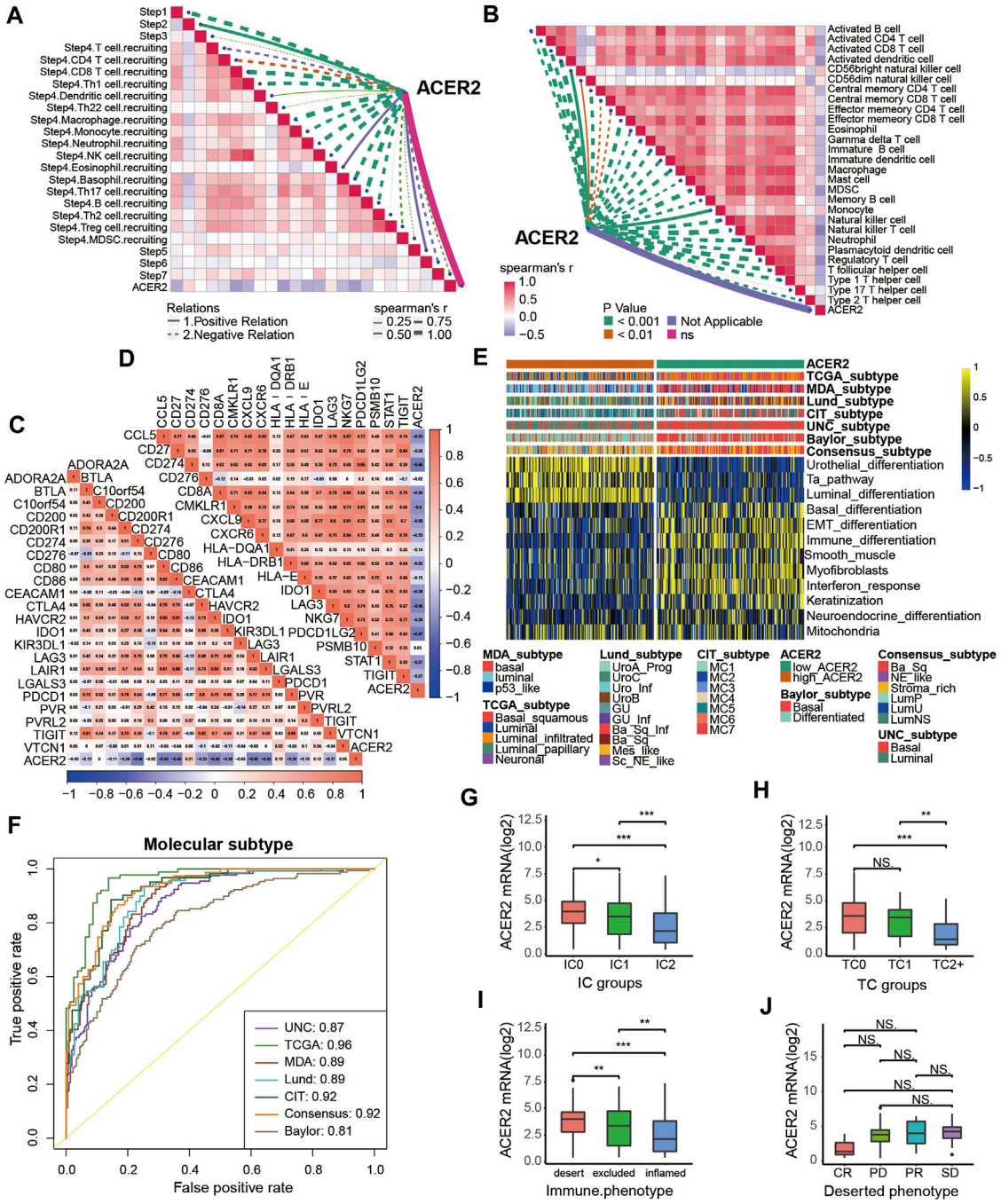

FIGURE 6
Validation of the ACER2 prediction for low immune infiltration and molecular subtypes in the IMvigor210. **(A)** Correlation between ACER2 and the process of the anti-cancer immunity cycle. **(B)** Correlation between ACER2 and several immune-related cells. **(C)** Correlation between ACER2 and ICI effector genes. **(D)** Correlation between ACER2 and TIS-related genes. **(E, F)** Correlations between ACER2 and seven molecular subtype systems and corresponding ROC analysis for prediction accuracy. **(G)** Differential expression of ACER2 in different IC groups. **(H)** Differential expression of ACER2 in different TC groups. **(I)** Differential expression of ACER2 in three immune phenotypes (the desert, excluded, and inflamed). **(J)** Correlation between ACER2 and the clinical response of tumor immunotherapy in the desert group.

observed in Xiangya cohort (Figure 5C). Besides, we confirmed that lower ACER2 was associated with high expression in T-cell inflamed scores effector genes including CD274, LAG-3, and TIGHT (Figure 5D). Consistent with the prediction for subtype in TCGA, high ACER2 group was more likely to be luminal subtype in Xiangya cohort (Figure 5E), and the accuracy of ACER2 in prediction for molecular subtypes was over 0.87 (Figure 5F). Likewise, high ACER2 was more likely to respond to immune inhibited oncogenic therapy (Figure 5G).

3.6 ACER2 predicted clinical response of ICB

We further explored the effect of ACER2 in predicting clinical response to ICB in an immunotherapy cohort, the IMvigor210 cohort, in which patients received anti-PD-1 therapy. In the IMvigor210 cohort, ACER2 was also observed negative correlations with several critical steps of cancer immune cycles (Figure 6A), thus the infiltration level of TILs in TME was downregulated when ACER2 high expressed (Figure 6B). Whereafter, we found that ACER2 was negatively correlated with the expression of several ICI genes and the TIS genes (Figures 6C,D). In addition, high expressions of ACER2 were inclined to the luminal subtype which was consistent with the results captured from the TCCA cohort (Figure 6E). And the area under ROC curves of predictive accuracy for molecular subtypes was calculated ranging from 0.81 to 0.96 (Figure 6F).

In the IMvigor210 cohort, immunohistochemistry (IHC) was performed to detect the PD-L1 expression on immune cells or cancer cells. Based on the PD-L1 expression level, immune cells and cancer cells were classified into three groups. We discovered ACER2 was significantly expressed in the TC0 and IC0 groups (Figures 6G,H), which existed the lowest PD-L1 expression in the immune cells and cancer cells, respectively. And ACER2 was higher expressed in the desert TME compared with inflamed TME (Figure 6I). Moreover, we compared the ACER2 expressions in different clinical responses to ICB. ACER2 expression was lower in patients with desert TME with complete response (CR) compared with partial response (PR), progressive disease (PD), and stable disease (SD). Even so, we did not observe significant difference across these groups (Figure 6J).

4 Discussion

In this study, we uncovered that ACER2 was a potential molecular biomarker to reflect the TME status in diverse cancers especially in BLCA, and contribute to the formation of non-inflamed TME in BLCA. The expression of ACER2 would be a convincing indicator to predict the molecular subtypes. Patients with low ACER2 expression were more likely to be basal subtype, and sensitive to ICB with higher immune infiltration levels. Besides, individuals with lower ACER2 expression were more likely to response to neoadjuvant chemotherapy, adjuvant chemotherapy and ERBB therapy.

Sphingolipid metabolism is mainly induced by ceramidases and plays essential roles in numerous human diseases, including cancer. Ceramidases are a family comprising acid ceramidase, neutral ceramidase, and alkaline ceramidase 1, 2, and 3, which are encoded by ASAH1, ASAH2, ACER1, ACER2 and ACER3, respectively. (Parveen et al., 2019). Ceramidases regulates ceramide catabolism by converting ceramide into sphingosine (SPH). Afterwards, SPH can be further phosphorylated to sphingosine-1 phosphate (S1P). Multiple previous studies revealed ceramide was associated with stress-related cellular responses and apoptosis, and S1P was related to cell proliferation, and tissue regeneration (Perry et al., 1996; Spiegel et al., 1998; Sassoli et al., 2019). The expression of ceramidases balanced the ceramide, SPH, and S1P levels, and substantially contributed to modulation of cell fate (Van Brocklyn and Williams, 2012).

ACER2 was a transcriptional target of p53, and the activation of ACER2 by p53 mediated DNA damage response by increasing the production of ROS (Xu et al., 2016; Xu et al., 2018a). The overexpression of ACER2 in multiple cancer cells regulated proliferation, DNA damage response, programmed cell death, and autophagy. Zhang et al. demonstrated that ACER2 enhanced TIM-mediated promotive effects of cancer cell growth and mitochondrial respiration in ER-positive breast cancer (Zhang et al., 2020). Meanwhile, ACER2 was revealed to promote the growth, invasion, and migration of hepatocellular carcinoma cells (Liu et al., 2020). Whereas, a current investigation revealed a lower ACER2 elevated gastric cancer cell proliferation and migration ability, and thus inhibited apoptosis (Zheng et al., 2022). In our study, we uncovered ACER2 was overexpressed in the tumor tissues and tumor cell lines of BLCA. The relatively higher expression of ACER2 inhibited the killing of tumor cells by decreasing TILs in the TME. Besides, ACER2 was negatively correlated with a majority of common immune checkpoint inhibitors, which restrained the re-invigorating of tumor-cytotoxic T-cells that recognized and eradicated cancer cells. Collectively, ACER2 contributed to the formation of non-inflamed TME in BLCA, hence ACER2 may also contribute to the tumor growth, invasion, metastasis in the BLCA. Unfortunately, we did not observe the difference of ACER2 expression in T stage, prognostic benefit and clinical response to ICB. Although no statistical difference was observed in clinical response to ICB, there was a significant increasing trend. Besides, the insignificance was occurred due to a relatively small sample size, and need to verify in further larger-scale cohorts. Moreover, they would also be partly explained by the dual role of ectopic ACER2 in tumor cell proliferation and death. Xu et al. uncovered that ACER2 promoted the generation of S1P and S1P-mediated cell proliferation and survival, whereas the overexpression of ACER2 may also cause cell growth arrest as the result of an accumulation of sphingosine (Xu et al., 2006). Taken together, we discovered the suppressive immunological role of ACER2 in TME, but precise effects of ACER2 on tumor growth and death were perhaps controlled by multiple factors.

In multiple cancers, S1P produced by ceramidase played a crucial role in tumor growth and resistance to chemotherapy, thus several inhibitors targeting the ceramidase had been developed. Bhabak et al. modified the structural of previous ceramidase inhibitors, and discovered an enhancement of apoptotic cell death in breast cancer cell lines by inhibiting ceramidase (Bhabak et al., 2013). In addition, Carmofur, an ASAH1 inhibitor, was approved to be against colorectal cancer in Japan (Parveen et al., 2019). It indicated inhibition of ceramidases was potential treatment which induced apoptosis, and elevated the response to chemotherapy. Despite up to now there were no inhibitors targeting ACER2, we identified the potential response to drugs based on the ACER2 expression in BLCA. According to the ACER2 expression, BLCA patients could be divided into basal and luminal subtypes. Individuals with lower ACER2 expression were more likely to respond to ICB, chemotherapy, and ERBB therapy which contributed to precision medicine.

The study inevitably existed several limitations. Firstly, all the results were performed based on bioinformatic analyses without *in vivo* or *in vitro* experiments to explore mechanism. Secondly, despite

the result was validated well in our Xiangya cohort, the total sample size (only 57) was an inevitable flaw. Thirdly, we used the median ACER2 mRNA expression as the threshold value to distinguish high or low expression groups without determining the optimal cut-off value. Hence, validation with more data from tumor tissues and experiments are imperatively needed.

5 Conclusion

In summary, we discovered that ACER2 promoted the formation of non-inflamed TME in BLCA which was resistant to cancer immunotherapy. Meanwhile, ACER2 could be used as a convincing indicator to predict the molecular subtypes and indicate sensitive treatment options.

Data availability statement

The original data presented in this study has been uploaded to the GEO database (GSE188715). Further inquiries can be directed to the corresponding authors.

Author contributions

DD and YD: Conceptualization, Resources, Supervision, Writing—Review and Editing. JL and CC: Conceptualization, Methodology, Software, Formal Analysis, Writing—Original Draft. JX, WZ, and TQ: Data Curation, Software, Validation, Writing—Original Draft. All authors: Manuscript writing. All authors contributed to the article and approved the submitted version. All authors agreed to be accountable for all aspects of the work.

Funding

This work was supported by National Natural Science Foundation of China (81873626, 81902592, 82070785).

Acknowledgments

We sincerely thank all participants in the study.

Conflict of interest

The authors declare that the research was conducted in the absence of any commercial or financial relationships that could be construed as a potential conflict of interest.

Publisher's note

References

Alsaab, H. O., Sau, S., Alzhrani, R., Tatiparti, K., Bhise, K., Kashaw, S. K., et al. (2017). PD-1 and PD-L1 checkpoint signaling inhibition for cancer immunotherapy: Mechanism, combinations, and clinical outcome. *Front. Pharmacol.* 8, 561. doi:10.3389/fphar.2017.00561

Ayers, M., Lunceford, J., Nebozhyn, M., Murphy, E., Loboda, A., Kaufman, D. R., et al. (2017). IFN-γ-related mRNA profile predicts clinical response to PD-1 blockade. *J. Clin. Invest.* 127 (8), 2930–2940. doi:10.1172/JCI91190

Becht, E., Giraldo, N. A., Lacroix, L., Buttard, B., Elarouci, N., Petitprez, F., et al. (2016). Estimating the population abundance of tissue-infiltrating immune and stromal cell populations using gene expression. *Genome Biol.* 17 (1), 218. doi:10.1186/s13059-016-1070-5

Bellmunt, J., de Wit, R., Vaughn, D. J., Fradet, Y., Lee, J. L., Fong, L., et al. (2017). Pembrolizumab as second-line therapy for advanced urothelial carcinoma. *N. Engl. J. Med.* 376 (11), 1015–1026. doi:10.1056/NEJMoa1613683

Bhabak, K. P., Kleuser, B., Huwiler, A., and Arenz, C. (2013). Effective inhibition of acid and neutral ceramidases by novel B-13 and LCL-464 analogues. *Bioorg Med. Chem.* 21 (4), 874–882. doi:10.1016/j.bmc.2012.12.014

Charoentong, P., Finotello, F., Angelova, M., Mayer, C., Efremova, M., Rieder, D., et al. (2017). Pan-cancer immunogenomic analyses reveal genotype-immunophenotype relationships and predictors of response to checkpoint blockade. *Cell Rep.* 18 (1), 248–262. doi:10.1016/j.celrep.2016.12.019

Chen, D. S., and Mellman, I. (2013). Oncology meets immunology: The cancer-immunity cycle. *Immunity* 39 (1), 1–10. doi:10.1016/j.immuni.2013.07.012

Finotello, F., Mayer, C., Plattner, C., Laschober, G., Rieder, D., Hackl, H., et al. (2019). Molecular and pharmacological modulators of the tumor immune contexture revealed by deconvolution of RNA-seq data. *Genome Med.* 11 (1), 34. doi:10.1186/s13073-019-0638-6

Hu, J., Yu, A., Othmane, B., Qiu, D., Li, H., Li, C., et al. (2021). Siglec15 shapes a non-inflamed tumor microenvironment and predicts the molecular subtype in bladder cancer. *Theranostics* 11 (7), 3089–3108. doi:10.7150/thno.53649

Kamoun, A., de Reyniès, A., Allory, Y., Sjödahl, G., Robertson, A. G., Seiler, R., et al. (2020). A Consensus molecular classification of muscle-invasive bladder cancer. *Eur. Urol.* 77 (4), 420–433. doi:10.1016/j.eururo.2019.09.006

Li, B., Severson, E., Pignon, J. C., Zhao, H., Li, T., Novak, J., et al. (2016). Comprehensive analyses of tumor immunity: Implications for cancer immunotherapy. *Genome Biol.* 17 (1), 174. doi:10.1186/s13059-016-1028-7

Li, T., Fu, J., Zeng, Z., Cohen, D., Li, J., Chen, Q., et al. (2020). TIMER2.0 for analysis of tumor-infiltrating immune cells. *Nucleic Acids Res.* 48 (W1), W509–w14. doi:10.1093/nar/gkaa407

Liu, B., Xiao, J., Dong, M., Qiu, Z., and Jin, J. (2020). Human alkaline ceramidase 2 promotes the growth, invasion, and migration of hepatocellular carcinoma cells via sphingomyelin phosphodiesterase acid-like 3B. *Cancer Sci.* 111 (7), 2259–2274. doi:10.1111/cas.14453

Morad, G., Helmink, B. A., Sharma, P., and Wargo, J. A. (2021). Hallmarks of response, resistance, and toxicity to immune checkpoint blockade. *Cell* 184 (21), 5309–5337. doi:10.1016/j.cell.2021.09.020

Necchi, A., Raggi, D., Gallina, A., Ross, J. S., Farè, E., Giannatempo, P., et al. (2020). Impact of molecular subtyping and immune infiltration on pathological response and outcome following neoadjuvant pembrolizumab in muscle-invasive bladder cancer. *Eur. Urol.* 77 (6), 701–710. doi:10.1016/j.eururo.2020.02.028

Newman, A. M., Liu, C. L., Green, M. R., Gentles, A. J., Feng, W., Xu, Y., et al. (2015). Robust enumeration of cell subsets from tissue expression profiles. *Nat. Methods* 12 (5), 453–457. doi:10.1038/nmeth.3337

Parveen, F., Bender, D., Law, S. H., Mishra, V. K., Chen, C. C., and Ke, L. Y. (2019). Role of ceramidases in sphingolipid metabolism and human diseases. *Cells* 8 (12), 1573. doi:10.3390/cells8121573

Perry, D. K., Obeid, L. M., and Hannun, Y. A. (1996). Ceramide and the regulation of apoptosis and the stress response. *Trends Cardiovasc Med.* 6 (5), 158–162. doi:10.1016/1050-1738(96)00044-8

Powles, T., Durán, I., van der Heijden, M. S., Loriot, Y., Vogelzang, N. J., De Giorgi, U., et al. (2018). Atezolizumab versus chemotherapy in patients with platinum-treated locally advanced or metastatic urothelial carcinoma (IMvigor211): A multicentre, open-label, phase 3 randomised controlled trial. *Lancet* 391 (10122), 748–757. doi:10.1016/S0140-6736(17)33297-X

Rosenberg, J. E., Hoffman-Censits, J., Powles, T., van der Heijden, M. S., Balar, A. V., Necchi, A., et al. (2016). Atezolizumab in patients with locally advanced and metastatic urothelial carcinoma who have progressed following treatment with platinum-based chemotherapy: A single-arm, multicentre, phase 2 trial. *Lancet* 387 (10031), 1909–1920. doi:10.1016/S0140-6736(16)00561-4

Ru, B., Wong, C. N., Tong, Y., Zhong, J. Y., Zhong, S. S. W., Wu, W. C., et al. (2019). Tisidb: An integrated repository portal for tumor-immune system interactions. *Bioinformatics* 35 (20), 4200–4202. doi:10.1093/bioinformatics/btz210

Sassoli, C., Pierucci, F., Zecchi-Orlandini, S., and Meacci, E. (2019). Sphingosine 1-phosphate (S1P)/S1P receptor signaling and mechanotransduction: Implications for intrinsic tissue repair/regeneration. *Int. J. Mol. Sci.* 20 (22), 5545. doi:10.3390/ijms20225545

Sharma, P., Retz, M., Siefker-Radtke, A., Baron, A., Necchi, A., Bedke, J., et al. (2017). Nivolumab in metastatic urothelial carcinoma after platinum therapy (CheckMate 275): A multicentre, single-arm, phase 2 trial. *Lancet Oncol.* 18 (3), 312–322. doi:10.1016/S1470-2045(17)30065-7

Siegel, R. L., Miller, K. D., Fuchs, H. E., and Jemal, A. (2022). Cancer statistics, 2022. *CA Cancer J. Clin.* 72 (1), 7–33. doi:10.3322/caac.21708

Sjödahl, G., Abrahamsson, J., Bernardo, C., Eriksson, P., Höglund, M., and Liedberg, F. (2022). Molecular subtypes as a basis for stratified use of neoadjuvant chemotherapy for muscle-invasive bladder cancer-A narrative Review. *Cancers (Basel).* 14 (7), 1692. doi:10.3390/cancers14071692

Spiegel, S., Cuvillier, O., Edsall, L., Kohama, T., Menzeleev, R., Olivera, A., et al. (1998). Roles of sphingosine-1-phosphate in cell growth, differentiation, and death. *Biochem. (Mosc)* 63 (1), 69–73.

Sun, W., Jin, J., Xu, R., Hu, W., Szulc, Z. M., Bielawski, J., et al. (2010). Substrate specificity, membrane topology, and activity regulation of human alkaline ceramidase 2 (ACER2). *J. Biol. Chem.* 285 (12), 8995–9007. doi:10.1074/jbc.M109.069203

Van Brocklyn, J. R., and Williams, J. B. (2012). The control of the balance between ceramide and sphingosine-1-phosphate by sphingosine kinase: Oxidative stress and the seesaw of cell survival and death. *Comp. Biochem. Physiol. B Biochem. Mol. Biol.* 163 (1), 26–36. doi:10.1016/j.cbpb.2012.05.006

Wang, Y., Zhang, C., Jin, Y., WangHe, Q., Liu, Z., et al. (2017). Alkaline ceramidase 2 is a novel direct target of p53 and induces autophagy and apoptosis through ROS generation. *Sci. Rep.* 7, 44573. doi:10.1038/srep44573

Witjes, J. A., Bruins, H. M., Cathomas, R., Compérat, E. M., Cowan, N. C., Gakis, G., et al. (2021). European association of urology guidelines on muscle-invasive and metastatic bladder cancer: Summary of the 2020 guidelines. *Eur. Urol.* 79 (1), 82–104. doi:10.1016/j.eururo.2020.03.055

Xu, L., Deng, C., Pang, B., Zhang, X., Liu, W., Liao, G., et al. (2018). Tip: A web server for resolving tumor immunophenotype profiling. *Cancer Res.* 78 (23), 6575–6580. doi:10.1158/0008-5472.CAN-18-0689

Xu, R., Garcia-Barros, M., Wen, S., Li, F., Lin, C. L., Hannun, Y. A., et al. (2018). Tumor suppressor p53 links ceramide metabolism to DNA damage response through alkaline ceramidase 2. *Cell Death Differ.* 25 (5), 841–856. doi:10.1038/s41418-017-0018-y

Xu, R., Jin, J., Hu, W., Sun, W., Bielawski, J., Szulc, Z., et al. (2006). Golgi alkaline ceramidase regulates cell proliferation and survival by controlling levels of sphingosine and S1P. *Faseb J.* 20 (11), 1813–1825. doi:10.1096/fj.05-5689com

Xu, R., Wang, K., Mileva, I., Hannun, Y. A., Obeid, L. M., and Mao, C. (2016). Alkaline ceramidase 2 and its bioactive product sphingosine are novel regulators of the DNA damage response. *Oncotarget* 7 (14), 18440–18457. doi:10.18632/oncotarget.7825

Zhang, S., Huang, P., Dai, H., Li, Q., Hu, L., Peng, J., et al. (2020). TIMELESS regulates sphingolipid metabolism and tumor cell growth through Sp1/ACER2/S1P axis in ER-positive breast cancer. *Cell Death Dis.* 11 (10), 892. doi:10.1038/s41419-020-03106-4

Zheng, J., Jiang, X., Jiang, K., Yan, Y., Pan, J., Liu, F., et al. (2022). miR-196a-5p correlates with chronic atrophic gastritis progression to gastric cancer and induces malignant biological behaviors of gastric cancer cells by targeting ACER2. *Mol. Biotechnol.* [Epub ahead of print]. doi:10.1007/s12033-022-00589-8

frontiers | Frontiers in Genetics

TYPE Original Research
PUBLISHED 15 March 2023
DOI 10.3389/fgene.2023.1151651

OPEN ACCESS

EDITED BY
Rui Cao,
Affiliated Beijing Friendship Hospital, Capital Medical University, China

REVIEWED BY
Nianzeng Xing,
National Urological Cancer Center, China
Yang Yute,
Zhejiang University, China

*CORRESPONDENCE
Chao-Feng Guo,
guochaofeng2016@126.com
Hong-Qi Zhang,
403206@csu.edu.cn

SPECIALTY SECTION
This article was submitted to Cancer Genetics and Oncogenomics, a section of the journal Frontiers in Genetics

RECEIVED 26 January 2023
ACCEPTED 06 March 2023
PUBLISHED 15 March 2023

CITATION
Liang Z-T, Li J-K, Li J, Tang H, Guo C-F and Zhang H-Q (2023), PECAM1 plays a role in the pathogenesis and treatment of bone metastases.
Front. Genet. 14:1151651.
doi: 10.3389/fgene.2023.1151651

PECAM1 plays a role in the pathogenesis and treatment of bone metastases

Zhuo-Tao Liang[1,2], Jia-Ke Li[3], Jiong Li[1,2], Hao Tang[1,2], Chao-Feng Guo[1,2]* and Hong-Qi Zhang[1,2]*

[1]Department of Spine Surgery and Orthopaedics, Xiangya Hospital, Central South University, Changsha, Hunan, China, [2]National Clinical Research Center for Geriatric Disorders, Xiangya Hospital, Central South University, Changsha, Hunan, China, [3]Department of General Surgery, The Third Xiangya Hospital of Central South University, Changsha, China

Bone is the third most common metastatic site for all primary tumors, the common primary focus of bone metastases include breast cancer, prostate cancer, and so on. And the median survival time of patients with bone metastases is only 2–3 years. Therefore, it is urgent to develop new targets to diagnose and treat bone metastases. Based on two data sets GSE146661 and GSE77930 associated with bone metastases, it was found that 209 genes differentially expressed in bone metastases group and control group. PECAM1 was selected as hub-gene for the follow-up research after constructing protein-protein interaction (PPI) network and enrichment analysis. Moreover, q-PCR analysis verified that the expression of PECAM1 decreased in bone metastatic tumor tissues. PECAM1 was believed to be possibly related to the function of osteoclasts, we knocked down the expression of PECAM1 with shRNA in lymphocytes extracted from bone marrow nailed blood. The results indicated that sh-PECAM1 treatment could promote osteoclast differentiation, and the sh-PECAM1-treated osteoclast culture medium could significantly promote the proliferation and migration of tumor cells. These results suggested that PECAM1 may be a potential biomarker for the diagnosis and treatment of bone metastases of tumor.

KEYWORDS

PECAM1, bone metastasis, osteoclast, breast cancer, prostate cancer, biomarker

Introduction

Cancer has been one of the major diseases causing death, with more than 20 million new cases worldwide every year (Sung et al., 2021). Its fatal reason lies that it can leave the primary site of the tumor, and spread to other parts of the body through a complicated process called metastases, and therefore causing the failure of organ function and eventually leading to death. Bone is the third most common site of metastases for all primary tumors (von Moos et al., 2019), and the common primary sites of bone metastases include breast cancer, prostate cancer, and thyroid cancer, in order. It has been reported that more than 70% of breast cancer patients and prostate cancer patients would eventually develop bone metastases (Boxer et al., 1989; Coleman, 2006). The median survival time of patients with bone metastases was only 2–3 years. Therefore, it is urgent to develop new targets to diagnose and treat bone metastases of tumor (Liang et al., 2020).

As a dynamic tissue, bone plays an important role in supporting structure and movement. It is composed of resident cells with different functions. Among these cells, osteoblasts and

osteoclasts are the core, which maintain bone remodeling and absorption (Hofbauer et al., 2014; Sims and Martin, 2014). The physiological variations of bone are strictly regulated, but disease and aging will alter this environment, and provide suitable "soil" for the metastases of a variety of primary tumors. Nevertheless, the specific mechanism of bone metastases still remains to be clarified. Currently, it is believed that the site of bone metastases has abundant circulation of blood. The presence of bone trabeculae, and the alteration of the intracellular microenvironment of bone may also cause the development of bone metastases (Yip et al., 2021). The alteration of microenvironment of cells in bone has always been the research focus on tumor bone metastases.

The most typical example of tumor cells altering the bone environment is the concept of "vicious cycle" proposed by Muddy (Mundy, 1997). This is the first time to point out that tumor cells can stimulate bone cells to secrete various growth factors such as TGF-β and IGF, thus promoting tumor cell colonization and further bone destruction. Herein, osteoclasts act as a major role (Chen et al., 2010). Osteoclasts are large multinucleated syncytial cells formed by the fusion of bone marrow-derived mononuclear cells. Mature osteoclasts attach to the bone surface through actin rings and secrete a variety of proteases to demineralize the bone matrix and degrade proteins to form cavities (Buijs et al., 2011; Suva et al., 2011). While the RANKL/OPG pathway is the key pathway in osteoclast differentiation process, nuclear factor k-B ligand (RANKL) activates NF-κβ to stimulate osteoclast differentiation by combining with RANK, OPG can competitively inhibit this process by combining with RANKL (Kearns et al., 2008). In addition, some factors can also directly induce osteoclast activation, or stimulate adjacent cells to produce RANKL activation, including interleukin-6 (IL-6) (Weilbaecher et al., 2011), IL-11 (Kang et al., 2003), and soluble intercellular adhesion molecule 1 (ICAM-1) (Ell et al., 2013). Some studies demonstrated that tumor cells could directly secrete these factors, thereby activating osteoclast differentiation. Because of the understandings, bisphosphonates have been applied, such as zoledronic acid and denosumab could treat patients with bone metastases or improve their quality of life by targeting osteoclasts to limit bone turnover (D'Oronzo et al., 2019). However, the role of osteoclasts in bone metastases is far from fully understood.

In this study, we selected GSE146661 and GSE77930 data sets from the Gene Expression Omnibus (GEO) database, which were sequencing items related to bone metastases of breast cancer and prostate cancer (the two most common primary lesions of bone metastases cancer). Moreover, various bioinformatics analyses were also performed, so as to explore the gene expression and protein-protein interactions during tumor bone metastases, and to establish new biomarkers for its diagnosis and treatment.

Methods and materials

Dataset inclusion

Gene expression profile data (GSE146661 and GSE77930) were downloaded from GEO (Supplementary Tables S1, S2). Inclusion criteria of gene expression data: 1) the samples used for analysis were the tissues; 2) the experimental group was tumor bone metastases tissues, and the control group was primary focus tissue or other metastatic tissues, and the samples with combined bone metastases should be excluded; 3) complete information could be obtained for analysis; 4) the sample size of each study set was greater than 10. The array data of GSE146661 included 7 cases of breast cancer with bone metastases and 4 cases of primary lesion tissues as the control group, and the array data of GSE77930 included 11 prostate cancer with bone metastases and 15 other prostate cancer metastases as the control group.

Subjects

We recruited five patients with bone metastases and 7 seven patients without tumors as controls (Supplementary Table S3). The inclusion criterion used for the patients are diagnosed by imaging examination which have primary tumor and bone metastases. The inclusion criteria for the control group were sex-matched patients without tumor, including healthy individuals and patients with bone fracture at our medical examination center. The patients in the control group were subjected to a comprehensive examination to confirm that no bone metastases existed.

This study was approved by the Ethics Committee of Xiangya Hospital of Central South University (Reference: 201703358). Informed written consent was given by all the subjects and their legal guardians prior to participation in the study.

Differential gene analysis

Differentially expressed genes (DEGs) between tumor bone metastases samples and control group samples were analyzed using GEO2R (http://www.ncbi.nlm.nih.gov/geo/geo2r). GEO2R is a network tool that can compare and analyze DEGs in samples through GEOquery R packages of Bioconductor project. The adjusted *p*-values and |log2-fold variation| (|log2FC|) values were employed to assess the significance of DEGs, with the threshold set to $|log2FC| > 1$ and the adjusted *p*-values <0.05. Gene ontology (GO) is commonly used for comprehensive evaluation of gene function. Kyoto Encyclopedia of Genes and Genomes (KEGG), a database that annotates the advanced functions of biological systems at the molecular level. Enrichment of DEGs was analyzed and visualized by GOplot package (version 1.0.2) and ggplot2 (version 3.3.3) of R (https://www.r-project.org). The truncation criterion was set to *p*-value less than 0.01.

The protein-protein interaction (PPI) network of DEGs was constructed using the STRING (http://string-db.org/) database (which searched for interacting genes and provided important information about protein-protein interactions (PPI)), and the PPI network was processed and analyzed using Cytoscape (version 3.7.2). The threshold criterion was a composite score≥0.9. The truncation standard was set to *p*-value less than 0.05.

Quantitative real-time polymerase chain reaction (qPCR)

During the operation, 4 cases of bone metastases and 4 cases of control bone tissues without tumor were collected. Informed written consent was given by all the subjects and their legal guardians prior to participation in the study. This study was approved by the Ethics

TABLE 1 Primers for quantitative real-time PCR (qPCR).

Gene		Primer sequences (5′to 3′)
PECAM1	R	ATGGAGCAGGACAGGTTCAGTC
	F	AAGTGGAGTCCAGCCGCATATC
COL3A1	R	TGTGTTTCGTGCAACCATCC
	F	CTTCTCTCCAGCCGAGCTTC
CD4	R	GACGGCAGCCTGACAGTAATGAG
	F	CACAGCGCAGGTGTACTCGCCC
ITGB3	R	GAAGGTAGACGT GGCCTCTTT
	F	CGCTAAATTTGAGGAAGAACG
TLR4	R	CGATGGGAACATTCAGGGCAGAG
	F	ACACATTCATGGAGGCACTGGAAC
RN18s	R	AGAAACGGCTACCACATCCA
	F	CCCTCCAATGGATCCTCGTT

Committee of Xiangya Hospital of Central South University (Reference: 201703358).

Total RNA were extracted from the organization. The experimental method used for qRT-PCR was based on a previously described method (Liang et al., 2019). The primers used in this study were listed in Table 1.

Western blotting (WB)

The experimental method used for WB was based on a previously described method (Liang et al., 2019). The following primary antibodies were used: GAPDH (1:5,000; CST, United States), PECAM1 (1:500; Abcam, United States), RANKL (1:500; Abcam, United States), OPG (1:800; CST, United States). The membranes were subsequently incubated with secondary antibodies (1:10,000, Proteintech, China) at room temperature for 1 h. The results were then detected using the Chemiluminescent Protein Detection Module (Thermo Scientific, United States).

Immunofluorescence (IF)

Cells were placed on slides and fixed with 4% paraformaldehyde for 15 min, incubated with 0.3% triton solution for 10 min, sealed with 5% BSA for 30 min and then incubated with Ki67 (1:500; CST, United States) primary antibody at 4°C overnight. The following morning, the cells were incubated with a fluorescence secondary antibody (1:300, Abcam, United States) at room temperature for 1 h. Images were then acquired by a confocal microscope.

shRNA transfection

First, the cells were seeded into 24-well plates at a density of 1 × 10^4 cells per well. The cells were then transfected with shRNAs using riboFECTTM CP reagent (RiboBio, China) at final shRNA concentrations of 50 nM in accordance with the manufacturer's recommended protocols. The shRNA sequences used to knock-down PECAM1 were: sense 5′-GAAUUCUCGAGACCAGAAUUU and antisense 5′-AUUCUGGUCUCGAGAAUUCUU. Forty-eight hours after transfection, the expression levels of PECAM1 protein were verified by Western blotting (WB).

Scratch assay

HCT116 and SW620 cells were seeded at a density of 1 × 105 cells/well in 24-well plates until they were 90% confluent. Scrape wounds were generated using a 20-μL pipette tip; then, cells were cultured with a serum-free medium for 48 h. Wound closure was monitored and photographed at 0, 24, and 48 h using microscope.

Trap staining

The cells were fixed with 4% paraformaldehyde for 15 min, then 500 uL of sodium nitrite and parafuchsin hydrochloride were mixed evenly, 18 mL of sodium acetate buffer solution was added, and then 1 mL of naphthol AS-BI phosphate solution was added. Afterwards, 0.282 g of potassium sodium tartrate was weighed and finally added, fully dissolved to prepare the working solution. Then the working solution was added dropwise onto the cell climbing sheets. The sheets were incubated at 37°C for 1–2 h, and then washed with distilled water for three times. Subsequently, the cells were stained with hematoxylin staining solution for 1 min, washed with tap water, differentiated with differentiation solution, washed with tap water. And finally the experimental results were observed by microscopy.

Statistical analysis

All data are expressed as mean ± standard deviation (SD). The student's t-test (unpaired or paired) was used to determine the significance of differences between the two groups. Analysis of variance (ANOVA) was used to determine the significance of differences between multiple groups. $p < 0.05$ was considered statistically significant.

Results

Identification of differentially expressed genes in bone metastases

According to the GEO2R analysis, differentially expressed genes (434 in GSE146661 (Supplementary Table S1), 3,196 in GSE77930 (Supplementary Table S2)) were identified after normalization of microarray data (Figures 1A, B). Venn diagram analysis of bioinformatics and evolutionary genomics platforms indicated that a total of 209 common DEGs (cDEGs) were included in the two datasets (Figure 1C; Supplementary Table S4).

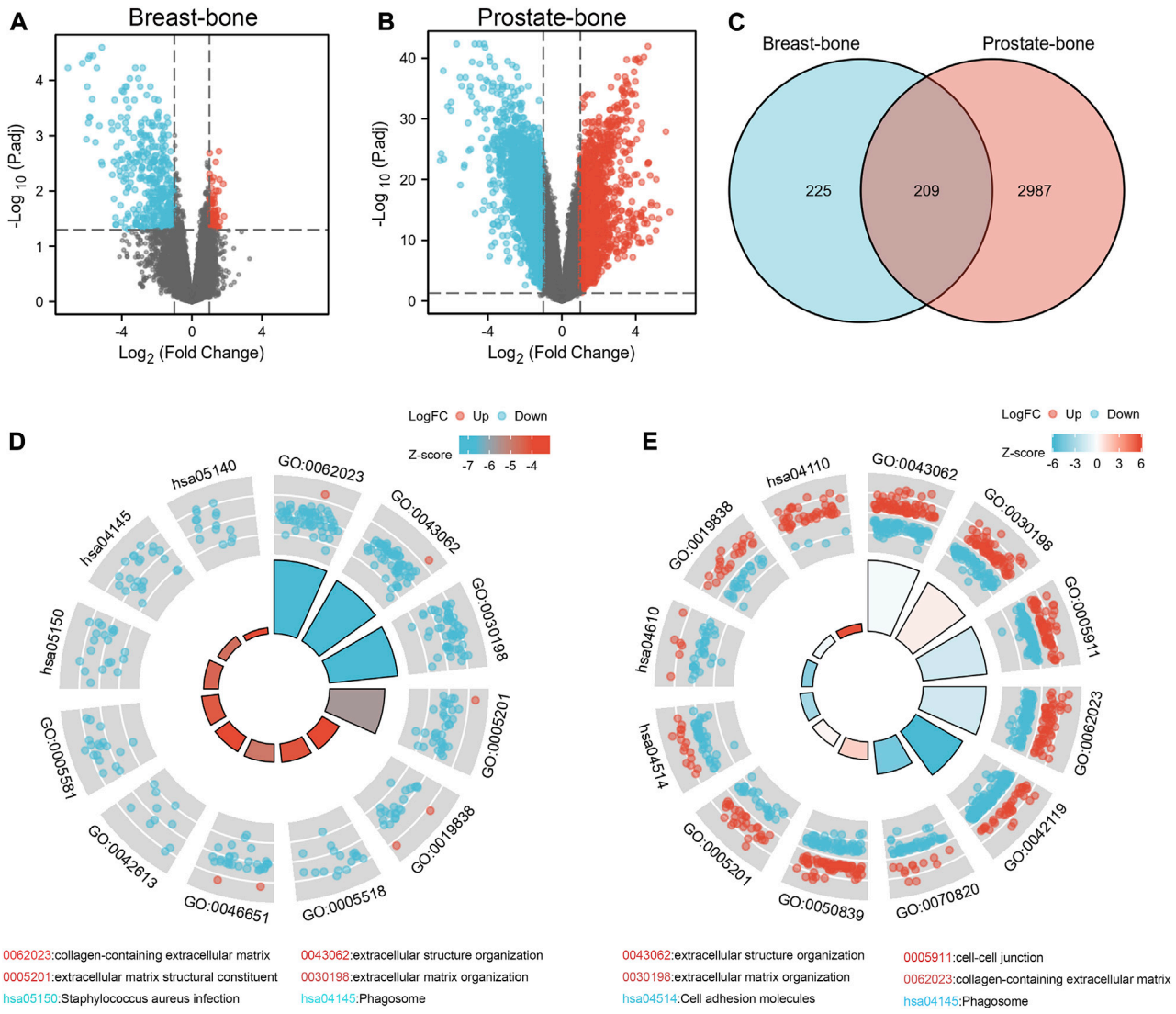

FIGURE 1
Identification and enrichment analysis of DEGs in bone metastases. The volcano map showed 434 DEGs in GSE146661 **(A)** and 3,196 DEGs in GSE77930 **(B)**. 209 DEGs were identified from GSE146661 and GSE77930 **(C)**. GO/KEGG joint enrichment analysis on GSE146661 and GSE77930 indicated that DEGs from GSE146661 and GSE77930 were mainly enriched in extracellular structure organization; extracellular matrix organization; cell-cell junction; cell adhesion and collagen-containing extracellular matrix plate pathways **(D, E)**.

We performed GO/KEGG joint enrichment analysis on GSE146661 and GSE77930 respectively (Supplementary Tables S5, S6). The analysis results indicated that DEGs from GSE146661 and GSE77930 were mainly enriched in extracellular structure organization and extracellular matrix organization in biological process (BP) analysis. In addition, the analysis of cell composition (CC) illustrated that the DEGS of GSE146661 and GSE77930 were mainly enriched in cell-cell junction and collagen-containing extracellular matrix plate. Molecular function (MF) analysis indicated that the DEGS of GSE77930 was mainly enriched in cell adhesion molecule binding and extraceller matrix structural constituent plate. The DEGS of GSE146661 was mainly enriched in the extracellular matrix structural constituent and growth factor binding plate. And KEGG pathway analysis suggested that most of the DEGs in GSE77930 were mainly involved in cell adhesion molecules and complement and coagulation cascades pathway, while most of the DEGs in GSE146661 were mainly involved in *staphylococcus aureus* infection and phagosome pathway (Figures 1D, E). Herein, we found a lot of overlapping parts in the enrichment analysis results of the two gene sets.

Analysis of selected differential expressed genes

And therefore, further KEGG (Figure 2A) and GO (Figure 2B) enrichment analysis of 209 common differentially expressed genes (cDEGs) in the two gene sets was conducted. We attached importance to genes of encoding secretory proteins and cell

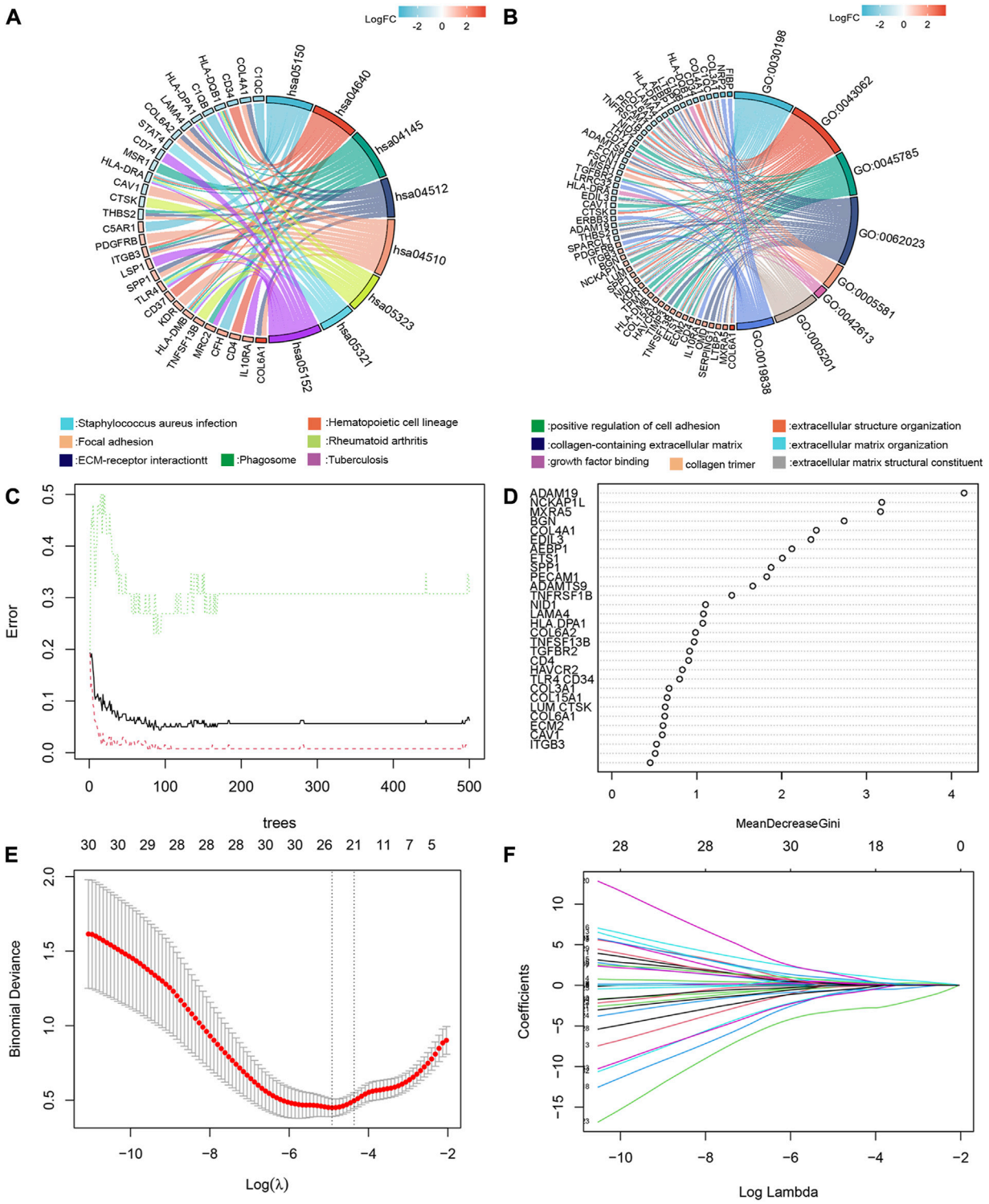

FIGURE 2
GO/KEGG enrichment analysis, random forest algorithm and LASSO regression modeling to screen key gene variables capable of distinguishing bone metastases and controls. KEGG **(A)** and GO **(B)** enrichment analysis of 209cDEGs. **(C)** The out-of-bag (OOB) error rate reached a minimum when the number of trees was equal to 85. **(D)** 28 of 36 genes were selected as important variables *via* random forest algorithm. **(E)** The optimal lambda was determined when the the model reached an optimum. **(F)** LASSO coefficient profiles of the candidate genes for bone metastases.

membrane proteins, which usually played a key role in tumor-bone microenvironment interactions, such as the pathways related to extracellular matrix formation and cell adhesion. We listed these 36 candidate genes in Supplementary Table S7. We also employed a random forest algorithm to screen key gene variables capable of distinguishing bone metastases and controls, with a relative

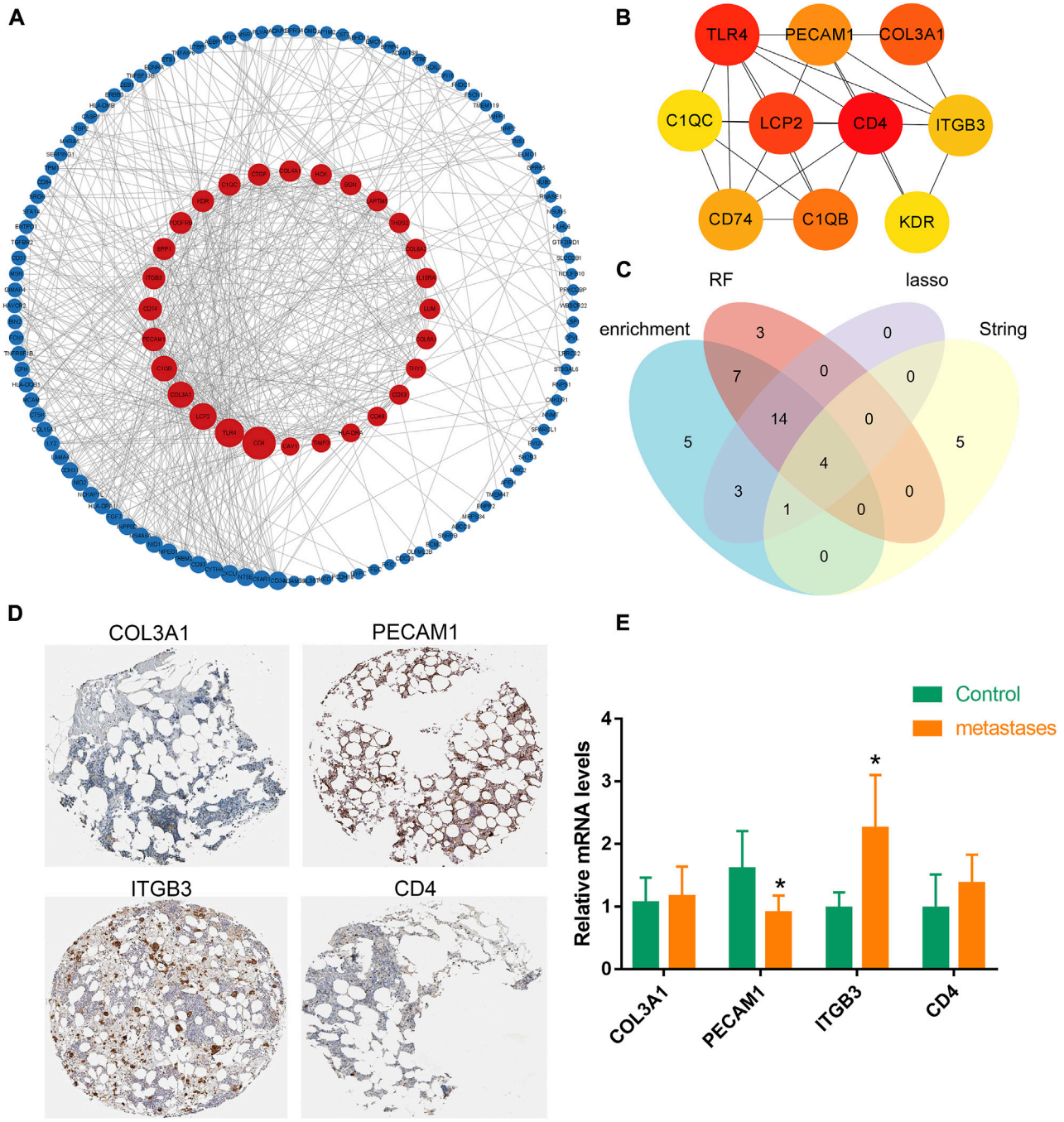

FIGURE 3
Expression of hub-genes in bone. **(A)** A PPI network was generated based on cDEGs using Cytoscape (combined score ≥ 0.9), upregulated genes are marked in dark red; downregulated genes are marked in dark blue. **(B)** The interaction network of the 10 nodes with the highest degree scores. The red, orange, and yellow nodes represented the top 10 hub genes in the network. **(C)** Venn diagram was mapped by the screened gene in PPI and the candidate genes selected by random forest algorithm and LASSO regression modeling, and four overlapped genes were obtained. **(D)** Four hub-genes in bone marrow tissues were verified by THPA database. It was showed high level of PECAM1 and ITGB3 genes in bone marrow, while COL3A1 and CD4 exhibited low level. **(E)** q-PCR results indicated that the expression levels of PECAM1 decreased significantly, but COL3A1; ITGB3 and CD4 had no significant difference in the expression of bone metastases tumor tissues. Data are shown as the mean ± SD, * means p <0.05 vs. the control group.

importance greater than 0.5 as the filtering criterion. The out-of-bag (OOB) error rate reached a minimum when the number of trees was equal to 85 (Figure 2C), and 28 of 36 genes were selected as important variables (Figure 2D). Based on the fivefold cross-validation, the model reached an optimum when lambda was equal to 0.007, containing 21 key gene variables (Figures 2E, F).

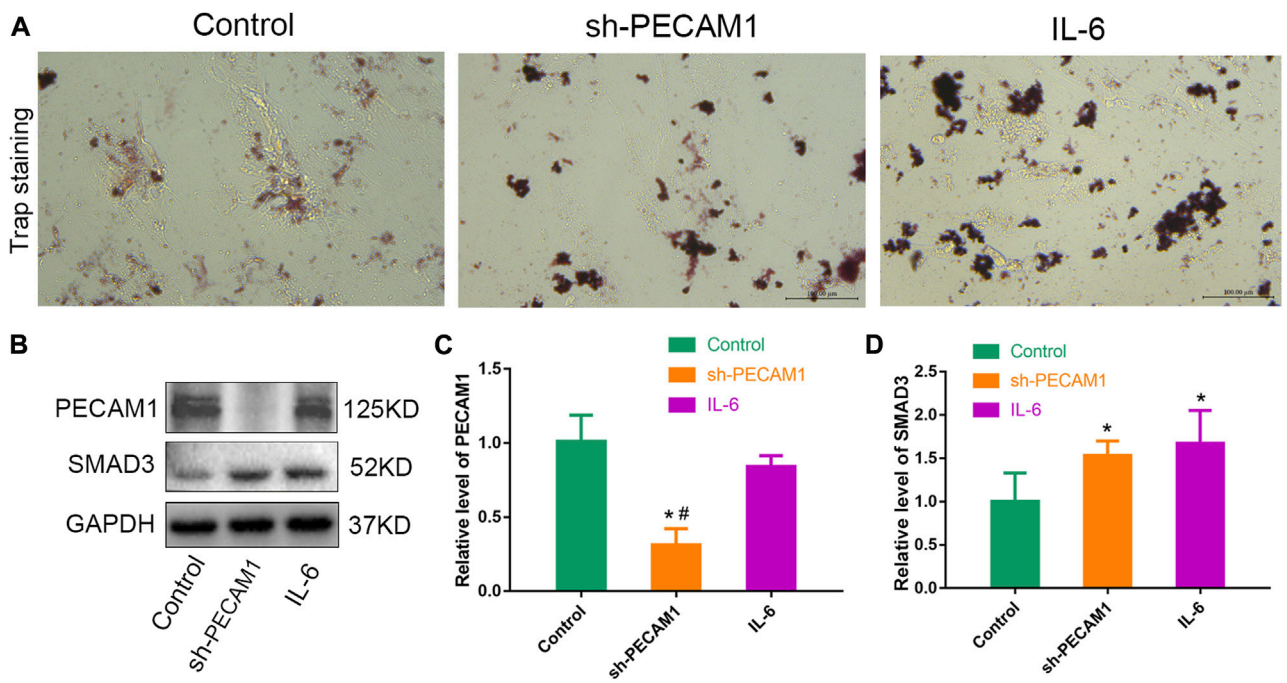

FIGURE 4
Knocking down PECAM1 expression promotes osteoclast differentiation. **(A)** Representative images of trap staining in either control group, sh-PECAM1 treatment group and IL-6 treatment mononuclear macrophages group. **(B–D)** Protein levels of PECAM1 and SMAD3 in either control group, sh-PECAM1 treatment group and IL-6 treatment mononuclear macrophages group. Scale bar, 100 μm. Data are shown as the mean ± SD, * means $p < 0.05$ vs the control group. # means $p < 0.05$ vs the IL-6 treated group.

Protein-protein interaction network construction and analysis of hub-genes

Next, a PPI network was constructed for 209 differential genes obtained in Figure 1C. The PPI network consisted of 136 nodes and 602 edges (Figure 3A). The top ten ranked hub-gene was selected for subsequent in-depth analysis based on the degree value (an indicator representing the importance of each node) as the selection condition (Figure 3B; Supplementary Table S7). After that, Venn diagram was mapped by the screened gene in PPI and the candidate genes selected from enrichment analysis, and four overlapped genes were obtained, namely, Collagen Type III Alpha 1 (COL3A1), platelet/endothelial cell adhesion molecule-1 (PECAM1), β3 integrin (ITGB3), CD4 (Figure 3C). Then, the correlation between these four hub-genes in bone marrow tissue and different cells were further verified by THPA database. It was showed high level of PECAM1 and ITGB3 genes in bone marrow, while COL3A1 and CD4 exhibited low level (Figure 3D). Mononuclear macrophages in bone marrow cavity were the precursor cells of osteoclasts, which could differentiate into osteoclasts after being activated. Meanwhile, we found the list of macrophage-specific marker genes through THPA database. It was demonstrated that PECAM1, CD4 and COL3A1 had certain cell specificity, and they could be used as marker genes of macrophages (Supplementary Figure S1). The mRNA expression levels of these genes were verified in human primary bone metastases tumor tissues and normal bone tissues by q-PCR, and the results indicated that the expression levels of PECAM1 decreased and ITGB3 increased significantly, but COL3A1 and CD4 had no significant difference in the expression of bone metastases tissues (Figure 3E). Eventually, PECAM1 gene was selected for further analysis.

Knocking down PECAM1 expression promotes osteoclast differentiation

In view of the central role of osteoclast in the colonization and proliferation of tumor cells in bone tissue, it is meaningful to explore whether PECAM1 can affect the osteoclast differentiation of mononuclear macrophages. We therefore obtained monocyte macrophages from the nailed blood of human bone marrow, and induced osteoclast differentiation of mononuclear macrophages by using osteoclast differentiation induction medium. We set up three groups, namely, control group, sh-PECAM1 treatment group and IL-6 treatment mononuclear macrophages group. Trap staining results revealed that compared with CT group, knockdown of PECAM1 expression would promote osteoclast differentiation of mononuclear macrophages, and the result was close to that of IL-6 treatment group (Figure 4A). Meanwhile, we also collected the total protein of mononuclear macrophages after 7 days of induced differentiation. The WB test results indicated that the expression of PECAM1 protein significantly decreased in the sh-PECAM1 group, as compared to the other two groups (Figures 4B, C). In addition, the value of the key protein smad3 in the osteoclast differentiation pathway significantly increased in the sh-PECAM1 and IL-6 groups, suggesting that the osteoclast differentiation pathway was activated (Figures 4B, D).

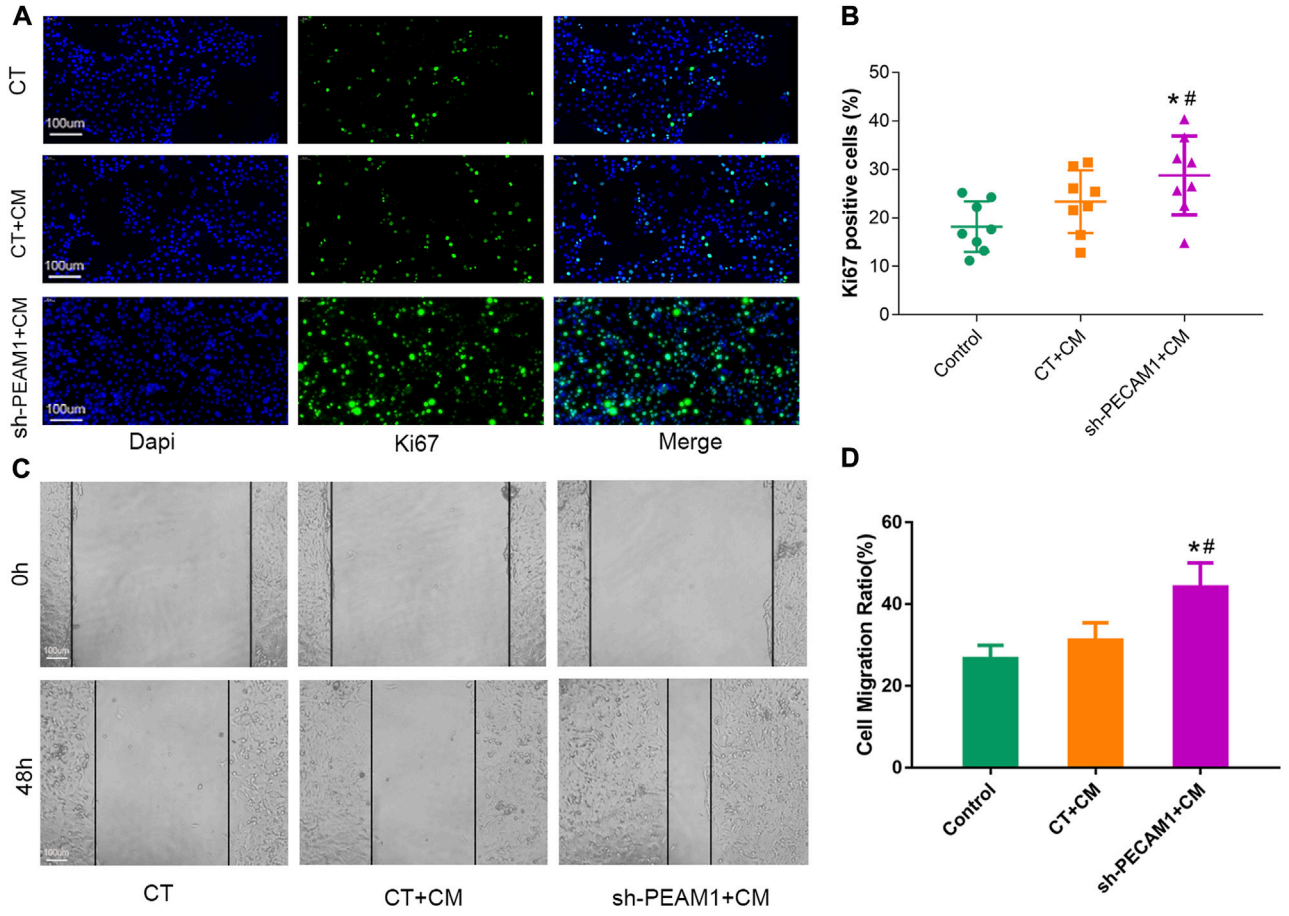

FIGURE 5
sh-PECAM1 treatment of osteoclast conditioned medium could promote tumor cell proliferation and migration. **(A, B)** Representative images of Ki67 immunofluorescence staining 627 in either control; treatment group with untreated osteoclast conditioned medium (CT + CM) and sh-PECAM1 treated osteoclast conditioned medium group (sh-PECAM1+CM). Scale bar, 100 μm. **(C, D)** Representative images of scratch assay in either control; CT + CM and sh-PECAM1+CM group. Scale bar, 100 μm. Data are shown as the mean ± SD, * means $p < 0.05$ vs the control group. # means $p < 0.05$ vs the CT + CM treated group.

sh-PECAM1 treatment of osteoclast conditioned medium could promote tumor cell proliferation and migration

MCF-7 cells (breast cancer cell line) were cultured using different treatments of osteolast conditioned medium to observe their effects on tumor cell proliferation and migration ability. We set up three different subgroups, *viz.* control group without any special treatment (CT), treatment group with untreated osteoclast conditioned medium (CT + CM), sh-PECAM1 treated osteoclast conditioned medium group (sh-PECAM1+CM). Ki67 staining results illustrated that the proliferative capacity of MCF-7 cells in the sh-PECAM1+CM group was significantly higher than that of the other two groups (Figures 5A, B). Moreover, the scratch assay showed that the migration ability of MCF-7 cells in sh-PECAM1+CM group was stronger than that of the other two groups (Figures 5C, D). The above results suggested that sh-PECAM1-treated osteoclast conditioned medium would stimulate the proliferation and migration of tumor cells, therefore creating a more favorable situation for bone metastases of tumors.

Discussion

Bone is one of the most common metastases sites among various tumors, for instance, the most common distant metastases of breast cancer and prostate cancer is bone (Bray et al., 2018). So far, the mechanism of bone metastases of primary tumor remains unclear. Nevertheless, multiple genes and pathways have been confirmed to participate in this process, making the research of bone metastases mechanism be extremely sophisticated. Therefore, it is urgent to improve our understanding of the mechanism of tumor bone metastases. What's more, employing genomics, transcriptomics, proteomics, and metabonomics analysis will be beneficial to develop better diagnosis and treatment strategies based on the identification of new biomarkers (Li et al., 2021).

In the present study, the RNA sequencing studies of prostate cancer and breast cancer bone metastases tissue samples were included for further analysis. Taking the bone metastases tissue as the experimental group, and primary tumor or other metastases sites as the control group, 209 common differentially expressed genes were selected through GEO2R

analysis. It was found that these genes were mainly enriched in extracellular matrix formation, cell adhesion, growth factor binding and other pathways. We focused on some pathways encoding secretory proteins or cell membrane related proteins, because these genes may be involved in intercellular signal transduction. We also constructed a PPI network to further screen the hub-gene. Finally, we obtained four key candidate genes: ITGB3, PECAM1, CD4, and COL3A1. q-PCR results illustrated that the expression of PECAM1 in bone metastases was significantly lower than that of the normal bone tissues and ITGB3 level in bone metastases was significantly higher, while the other two genes had no significant difference. Moreover, based on THPA database analysis, we found that PECAM1 exhibited a higher cell specificity and was one of the marker genes of macrophages (Jackson, 2003). It has been known that osteoclasts were derived from the bone marrow monocyte-macrophage system. Previous works reported that knockdown of PECAM1 expression in mononuclear cells could lead to the enhanced osteoclast differentiation (Wu et al., 2009), which suggested that PECAM1 might regulate bone metastases of tumor by affecting osteoclast differentiation. Tumor bone metastases usually occurred first in the hypervascular axial bone containing red bone marrow, indicating that the slow blood flow in these areas could support the attachment of metastatic tumor cells to the surface of the endosteal membrane (Paget, 1989). Alternatively, anatomical features could not adequately explain the mechanism of metastases. The molecular characteristics of malignant cells (i.e., seeds) and their interaction with the intraosseous microenvironment (soil) played a more important role in promoting tumor metastases and diffusion (Brylka and Schinke, 2019).

Many studies demonstrated that cancer cells stimulated the generation of osteoclasts. In this theory, osteoclasts were often regarded as “bone digesters.” The secondary effects of bone resorption, including the physical space of tumor growth and the degradation of bone matrix to release prototype factors, promote tumor colonization in bone. The histological manifestations of bone metastases could be classified as osteolytic metastases, osteogenic metastases, and mixed metastases, which were based on the variations in osteolysis or sclerosis. Focal bone destruction occurred when osteoclast mediated bone resorption was dominant, resulting in what was described as “punched out” lytic lesions. In contrast, in bone metastases characterized by increased osteoblast activity, the metastatic bone exhibited dense osteosclerotic lesions (Thomas et al., 1999; Yin et al., 2003). Although these phenotypes represented both ends of the spectrum, autopsy studies indicated that the bone metastases in individual patients may be heterogeneous, that was, osteolytic at one site and osteogenic or mixed in another. In fact, most solid tumors metastasized to bone were mixed metastases, such as breast cancer and prostate cancer. This was because after the increase of osteoclast production, it would also release some growth factors, such as osteoblasts deposit growth factors, which promoted the formation of osteoblasts. From the above studies, it could be deduced that osteoblasts undoubtedly play a crucial role in the process of bone metastases of tumors (Nelson et al., 1995; Liu et al., 2004). But the specific mechanisms that mediated tumor bone metastases remain to be further investigated.

In the current status, there are several main directions regarding the regulation of tumor bone metastases by osteoclasts. One is that osteoclasts metabolize bone matrix to release a large amount of calcium ions. Calcium has been proved to support the growth of cancer cells in bone by activating calcium-sensitive receptors on the surface of tumor cells (Roudier et al., 2004). In addition to calcium, bone is also a storehouse of growth factors. Many factors that can promote tumor growth can be released and activated by osteoclasts, such as transforming growth factor-β(TGFβ). The release of these factors would create a vicious cycle, in which, enhanced tumor growth promotes osteolysis, and release additional growth factors, and therefore further aggravating tumor progression (Joeckel et al., 2014). Besides, the immune system in the bone marrow would also inhibit or promote the growth of a variety of cells, which would also affect tumor metastases to bone. It has been known that osteoclasts were derived from monocytes, and RANKL, the most important factor regulating osteoclast function, could be secreted not only by osteocytes, lymphocytes and macrophages (Xiong et al., 2011; Xiong et al., 2015; Brylka and Schinke, 2019). Furthermore, some factors that regulated the homing of immune cells to the action site cold also regulate the colonization of tumor cells (Saxena et al., 2021). Therefore, the regulation of osteoclasts on tumor bone metastases was investigated in the presented work. After knocking down the expression of PECAM1 in human monocytes, it could be found that PECAM1 could promote osteoclast differentiation. And RANKL/OPG, the pathway that stimulated osteoclast formation, was also activated, indicating that PECAM1 may promote osteoclast differentiation by activating the secretion of RANKL. Moreover, the research on the function of osteoclasts on tumor cells is also worth paying attention to. We collected the culture media of osteoclasts after 1 day of culture to treat MCF-7 cells, to investigate the effect of osteoclast culture medium on tumor cells. The results indicated that the osteoclast-conditioned medium could promote the proliferation of MCF-7 cells to a certain extent. Furthermore, it has been found that the osteoclast medium after sh-PECAM1 intervention significantly improved the proliferation and migration ability of tumor cells, and there was a significant difference when compared with the blank control group or the osteoclast media group without special treatment. The results indicated that PECAM1 gene might play a role in promoting osteoclast differentiation and tumor cell proliferation and migration in bone, which provided a new entry point for the diagnosis and treatment of bone metastases of tumor.

There are also some limitations in our study. For example, the gene set and sample size included in the bioinformatics analysis weren’t large. This may be because it is difficult to collect tissues including the primary site, as well as bone metastases and other metastases, resulting in fewer sequencing researches in this field. In the future, we should pay attention to the research trends in this field. And moreover, our own sequencing projects should be carried out to expand and verify the results. In addition, the verification experiment of candidate gene function needs to be further improved to better understand the regulation mode of PECAM1 in the process of tumor bone metastases. Moreover, other genes such as TLR4, CD4, COL3A1, and ITGB3 are also of great research value, and

whether other genes are also involved in the regulation of tumor bone metastases will be investigated in the later studies.

Data availability statement

The datasets presented in this study can be found in online repositories. The names of the repository/repositories and accession number(s) can be found in the article/Supplementary Material.

Ethics statement

The studies involving human participants were reviewed and approved by this study was approved by the Ethics Committee of Xiangya Hospital of Central South University (Reference: 201358). Informed written consent was given by all the subjects and their legal guardians prior to participation in the study. The patients/participants provided their written informed consent to participate in this study.

Author contributions

Conceived and completed the experiment: Z-TL; administrative and financial support: H-QZ and C-FG, manuscript writing: Z-TL; collection and assembly of data: JL and HT; guidance for writing and submission: H-QZ and J-KL; final approval of manuscript: All authors.

Funding

This study was supported by the Natural Science Foundation of China (81772298) and National Natural Science Foundation of China (82170901).

Conflict of interest

The authors declare that the research was conducted in the absence of any commercial or financial relationships that could be construed as a potential conflict of interest.

Publisher's note

All claims expressed in this article are solely those of the authors and do not necessarily represent those of their affiliated organizations, or those of the publisher, the editors and the reviewers. Any product that may be evaluated in this article, or claim that may be made by its manufacturer, is not guaranteed or endorsed by the publisher.

Supplementary material

The Supplementary Material for this article can be found online at: https://www.frontiersin.org/articles/10.3389/fgene.2023.1151651/full#supplementary-material

References

Boxer, D. I., Todd, C. E., Coleman, R., and Fogelman, I. (1989). Bone secondaries in breast cancer: The solitary metastasis. *J. Nucl. Med.* 30, 1318–1320.

Bray, F., Ferlay, J., Soerjomataram, I., Siegel, R. L., Torre, L. A., and Jemal, A. (2018). Global cancer statistics 2018: GLOBOCAN estimates of incidence and mortality worldwide for 36 cancers in 185 countries. *CA Cancer J. Clin.* 68, 394–424. doi:10.3322/caac.21492

Brylka, L. J., and Schinke, T. (2019). Chemokines in physiological and pathological bone remodeling. *Front. Immunol.* 10, 2182. doi:10.3389/fimmu.2019.02182

Buijs, J. T., Stayrook, K. R., and Guise, T. A. (2011). TGF-B in the bone microenvironment: Role in breast cancer metastases. *Cancer Microenviron.* 4, 261–281. doi:10.1007/s12307-011-0075-6

Chen, Y. C., Sosnoski, D. M., and Mastro, A. M. (2010). Breast cancer metastasis to the bone: Mechanisms of bone loss. *Breast Cancer Res.* 12, 215. doi:10.1186/bcr2781

Coleman, R. E. (2006). Clinical features of metastatic bone disease and risk of skeletal morbidity. *Clin. Cancer Res.* 12, 6243s–6249s. doi:10.1158/1078-0432.CCR-06-0931

D'Oronzo, S., Coleman, R., Brown, J., and Silvestris, F. (2019). Metastatic bone disease: Pathogenesis and therapeutic options: Up-date on bone metastasis management. *J. Bone Oncol.* 15, 004. doi:10.1016/j.jbo.2018.10.004

Ell, B., Mercatali, L., Ibrahim, T., Campbell, N., Schwarzenbach, H., Pantel, K., et al. (2013). Tumor-induced osteoclast miRNA changes as regulators and biomarkers of osteolytic bone metastasis. *Cancer Cell.* 24, 542–556. doi:10.1016/j.ccr.2013.09.008

Hofbauer, L. C., Rachner, T. D., Coleman, R. E., and Jakob, F. (2014). Endocrine aspects of bone metastases. *Lancet Diabetes Endocrinol.* 2, 500–512. doi:10.1016/S2213-8587(13)70203-1

Jackson, D. E. (2003). The unfolding tale of PECAM-1. *FEBS Lett.* 540, 7–14. doi:10.1016/s0014-5793(03)00224-2

Joeckel, E., Haber, T., Prawitt, D., Junker, K., Hampel, C., ThüROFF, J. W., et al. (2014). High calcium concentration in bones promotes bone metastasis in renal cell carcinomas expressing calcium-sensing receptor. *Mol. Cancer* 13, 42. doi:10.1186/1476-4598-13-42

Kang, Y., Siegel, P. M., Shu, W., Drobnjak, M., Kakonen, S. M., CordóN-Cardo, C., et al. (2003). A multigenic program mediating breast cancer metastasis to bone. *Cancer Cell.* 3, 537–549. doi:10.1016/s1535-6108(03)00132-6

Kearns, A. E., Khosla, S., and Kostenuik, P. J. (2008). Receptor activator of nuclear factor kappaB ligand and osteoprotegerin regulation of bone remodeling in health and disease. *Endocr. Rev.* 29, 155–192. doi:10.1210/er.2007-0014

Li, N., Liu, M., Cao, X., Li, W., Li, Y., and Zhao, Z. (2021). Identification of differentially expressed genes using microarray analysis and COL6A1 induction of bone metastasis in non-small cell lung cancer. *Oncol. Lett.* 22, 693. doi:10.3892/ol.2021.12954

Liang, Z. T., Li, J., Rong, R., Wang, Y. J., Xiao, L. G., Yang, G. T., et al. (2019). Ghrelin up-regulates cartilage-specific genes via the ERK/STAT3 pathway in chondrocytes of patients with adolescent idiopathic scoliosis. *Biochem. Biophys. Res. Commun.* 518, 259–265. doi:10.1016/j.bbrc.2019.08.044

Liang, Y., Zhang, H., Song, X., and Yang, Q. (2020). Metastatic heterogeneity of breast cancer: Molecular mechanism and potential therapeutic targets. *Semin. Cancer Biol.* 60, 14–27. doi:10.1016/j.semcancer.2019.08.012

Liu, A. Y., Roudier, M. P., and True, L. D. (2004). Heterogeneity in primary and metastatic prostate cancer as defined by cell surface CD profile. *Am. J. Pathol.* 165, 1543–1556. doi:10.1016/S0002-9440(10)63412-8

Mundy, G. R. (1997). Mechanisms of bone metastasis. *Cancer* 80, 1546–1556. doi:10.1002/(sici)1097-0142(19971015)80:8+<1546::aid-cncr4>3.3.co;2-r

Nelson, J. B., Hedican, S. P., George, D. J., Reddi, A. H., Piantadosi, S., Eisenberger, M. A., et al. (1995). Identification of endothelin-1 in the pathophysiology of metastatic adenocarcinoma of the prostate. *Nat. Med.* 1, 944–949. doi:10.1038/nm0995-944

Paget, S. (1989). The distribution of secondary growths in cancer of the breast. 1889. *Cancer Metastases Rev.* 8, 98–101.

Roudier, M. P., Corey, E., True, L. D., Hiagno, C. S., Ott, S. M., and Vessell, R. L. (2004). Histological, immunophenotypic and histomorphometric characterization of prostate cancer bone metastases. *Cancer Treat. Res.* 118, 311–339. doi:10.1007/978-1-4419-9129-4_13

Saxena, Y., Routh, S., and Mukhopadhaya, A. (2021). Immunoporosis: Role of innate immune cells in osteoporosis. *Front. Immunol.* 12, 687037. doi:10.3389/fimmu.2021.687037

Sims, N. A., and Martin, T. J. (2014). Coupling the activities of bone formation and resorption: A multitude of signals within the basic multicellular unit. *Bonekey Rep.* 3, 481. doi:10.1038/bonekey.2013.215

Sung, H., Ferlay, J., Siegel, R. L., Laversanne, M., Soerjomataram, I., Jemal, A., et al. (2021). Global cancer statistics 2020: GLOBOCAN estimates of incidence and mortality worldwide for 36 cancers in 185 countries. *CA Cancer J. Clin.* 71, 209–249. doi:10.3322/caac.21660

Suva, L. J., Washam, C., Nicholas, R. W., and Griffin, R. J. (2011). Bone metastasis: Mechanisms and therapeutic opportunities. *Nat. Rev. Endocrinol.* 7, 208–218. doi:10.1038/nrendo.2010.227

Thomas, R. J., Guise, T. A., Yin, J. J., Elliott, J., Horwood, N. J., Martin, T. J., et al. (1999). Breast cancer cells interact with osteoblasts to support osteoclast formation. *Endocrinology* 140, 4451–4458. doi:10.1210/endo.140.10.7037

Von Moos, R., Costa, L., Gonzalez-Suarez, E., Terpos, E., Niepel, D., and Body, J. J. (2019). Management of bone health in solid tumours: From bisphosphonates to a monoclonal antibody. *Cancer Treat. Rev.* 76, 57–67. doi:10.1016/j.ctrv.2019.05.003

Weilbaecher, K. N., Guise, T. A., and Mccauley, L. K. (2011). Cancer to bone: A fatal attraction. *Nat. Rev. Cancer* 11, 411–425. doi:10.1038/nrc3055

Wu, Y., Tworkoski, K., Michaud, M., and Madri, J. A. (2009). Bone marrow monocyte PECAM-1 deficiency elicits increased osteoclastogenesis resulting in trabecular bone loss. *J. Immunol.* 182, 2672–2679. doi:10.4049/jimmunol.0802398

Xiong, J., Onal, M., Jilka, R. L., Weinstein, R. S., Manolagas, S. C., and O'Brien, C. A. (2011). Matrix-embedded cells control osteoclast formation. *Nat. Med.* 17, 1235–1241. doi:10.1038/nm.2448

Xiong, J., Piemontese, M., Onal, M., Campbell, J., Goellner, J. J., Dusevich, V., et al. (2015). Osteocytes, not osteoblasts or lining cells, are the main source of the RANKL required for osteoclast formation in remodeling bone. *PLoS One* 10, e0138189. doi:10.1371/journal.pone.0138189

Yin, J. J., Mohammad, K. S., KäKöNEN, S. M., Harris, S., Wu-Wong, J. R., Wessale, J. L., et al. (2003). A causal role for endothelin-1 in the pathogenesis of osteoblastic bone metastases. *Proc. Natl. Acad. Sci. U. S. A.* 100, 10954–10959. doi:10.1073/pnas.1830978100

Yip, R. K. H., Rimes, J. S., Capaldo, B. D., Vaillant, F., Mouchemore, K. A., Pal, B., et al. (2021). Mammary tumour cells remodel the bone marrow vascular microenvironment to support metastasis. *Nat. Commun.* 12, 6920. doi:10.1038/s41467-021-26556-6

frontiers | Frontiers in Genetics

TYPE Original Research
PUBLISHED 04 April 2023
DOI 10.3389/fgene.2023.1105900

OPEN ACCESS

EDITED BY
Changsheng Xing,
University of Southern California,
United States

REVIEWED BY
Xin Liu,
University of Southern California,
United States
Laralynne Przybyla,
University of California, San Francisco,
United States
Jianyang Du,
Shandong Provincial Hospital Affiliated to
Shandong First Medical University, China

*CORRESPONDENCE
Bo Ma,
mabo3476@bjsjth.cn
Riyue Yu,
yu-riyue@bjsjth.cn

SPECIALTY SECTION
This article was submitted to Cancer Genetics and Oncogenomics, a section of the journal Frontiers in Genetics

RECEIVED 23 November 2022
ACCEPTED 20 March 2023
PUBLISHED 04 April 2023

CITATION
Ma B and Yu R (2023), Pan-cancer analysis of ADAMs: A promising biomarker for prognosis and response to chemotherapy and immunotherapy. *Front. Genet.* 14:1105900. doi: 10.3389/fgene.2023.1105900

Pan-cancer analysis of ADAMs: A promising biomarker for prognosis and response to chemotherapy and immunotherapy

Bo Ma* and Riyue Yu*

Department of Stomatology, Beijing Shijitan Hospital, Capital Medical University, Beijing, China

Background: Members of a disintegrin and metalloproteinase (ADAM) family play a vital role in cancer development. However, a comprehensive analysis of the landscape of the ADAM family in pan-cancer remains to be performed.

Methods: The correlation of the expression level and prognostic value with ADAMs in a pan-cancer cohort and the relationship between ADAMs and the stemness score, tumour microenvironment (TME), chemotherapy-related drug sensitivity, immune subtype, and immunotherapy outcome were investigated.

Results: ADAMs were differentially expressed between tumour and para-carcinoma tissues in the pan-cancer cohort, and the expression of ADAMs was significantly correlated with patient prognosis. Furthermore, ADAMs were significantly correlated with the stromal score and immune score based on the TME analysis. Additionally, ADAMs were also correlated with DNAss and RNAss in the pan-cancer cohort. On investigating the CellMiner database, ADAMs were revealed to be significantly correlated with the sensitivity of various drugs, including raloxifene and tamoxifen. Moreover, in the IMvigor210 and GSE78220 cohorts, ADAMs were correlated with immunotherapy response and immune activation genes. Furthermore, quantitative real-time polymerase chain reaction (qRT-PCR) and immunohistochemistry (IHC) were utilised to determine the differential level of ADAM9 in cancer and para-carcinoma tissues in patients' samples.

Conclusion: This study elucidates the importance of ADAMs in cancer progression and lays a foundation for further exploration of ADAMs as potential pan-cancer targets.

KEYWORDS

ADAMs, pan-cancer, TME, prognosis, chemotherapy, immunotherapy

1 Introduction

The extracellular matrix (ECM) is a macromolecular structure consisting of the basement membrane (BM) and intercellular substance (Padhi and Nain, 2020). The ECM constitutes a complex network structure that supports and connects tissue structures and regulates tissue formation and cellular physiological activities (Valdoz et al., 2021).

The ECM acts as an important bio-barrier for tumour local or distant metastasis. Tumour cells secrete proteolytic enzymes to degrade the ECM, thereby creating a local lysis zone for cancer cell intravasation and extravasation (Najafi et al., 2019). Generally,

TABLE 1 Chromosome location of ADAMs.

ADAM	Chromosome location
ADAM2	8p11.22
ADAM7	8p21.2
ADAM8	10q26.3
ADAM9	8p11.22
ADAM10	15q21.3
ADAM11	17q21.31
ADAM12	10q26.2
ADAM15	1q21.3
ADAM17	2p25.1
ADAM18	8p11.22
ADAM19	5q33.3
ADAM20	14q24.2
ADAM21	14q24.2
ADAM22	7q21.12
ADAM23	2q33.3
ADAM28	8p21.2
ADAM29	4q34.1
ADAM30	1p12
ADAM32	8p11.22
ADAM33	20p13

cancer cells with a high degree of malignancy have a strong proteolytic effect, which can erode and destroy the membrane and promote metastasis. The enzymes involved in this process are mainly serine proteases, such as plasminogen activator (PA) and metalloproteinase (MP), which include collagenase IV, matrix-degrading enzymes, and hyaluronidase (Mohan et al., 2020). Various secreted proteins, including cross-linkers, modifying enzymes, and proteases and their inhibitors, regulate ECM homoeostasis. Thus, the activation or inhibition of the aforementioned proteins promotes the proliferation and invasion of cancer cells, which suggests their potential as therapeutic targets in cancer treatment (Walker et al., 2018).

In addition to degradation, the turnover of the matrix is also significantly important for ECM homoeostasis (Huang et al., 2021). The substrate turnover of the matrix is regulated by various enzyme families. The "normal" stroma degradation followed by an increase in the stromal turnover of the tumour promotes the replacement by the tumour stroma, reinforces aggressive features, and removes physical barriers (e.g., the basement membrane), consequently favouring the malignancy and metastasis of tumours (Nissen et al., 2019). As an important ligand pool of growth factors, the degradation and turnover of the ECM could activate the binding growth factors and induce intracellular signalling responses. Moreover, the ECM not only includes enzymes such as growth factors, chemokines, and cytokines but also is a repository for inorganic molecules (Girigoswami et al., 2021). During matrix remodelling, divalent cations like calcium ions are activated to facilitate calcium transport, which further induces the activation of matrix metalloproteinases (MMPs), a disintegrin and metalloproteinases (ADAMs), and ADAMs with thrombospondin motifs (ADAMTSs), which constitute the calcium-dependent, zinc-containing thyroxine superfamily endopeptidases (Theret et al., 2021).

The ADAM family can be divided into trans-model ADAM and secretory ADAM components based on structural differences (Saha et al., 2019). The genomic distribution of ADAMs is presented in Table 1. The pre-control region ensures that the metalloprotease domain is inactive, while the catalytic site is activated by the activation of the cysteine switch mechanism. The furin recognition site (RXXR sequence) is located between the pre-control region and the metalloprotease domain, which is involved in the intracellular activation of many ADAM family members in a trans-Golgi network by a furin-like preprotein convertase. The active site of the metalloprotease domain of ADAM molecule with proteolytic activity contains a common "HEXGH" conserved sequence, whose alteration will result in the loss of proteolytic activity (Malemud, 2019). Although the ADAM family has been extensively studied, little is known about the specificity of ADAM substrates, which are hypothesised to be determined by disintegrin and cysteine domains, especially the interaction of a substrate and enzyme (Heib et al., 2020). The main function of ADAM molecules is to mediate "extracellular domain shedding," a post-translational mechanism. ADAMs can induce proteolytic processing to release the membrane-attached proteins and activate the cleaved molecules, which are involved in growth factor signalling, cell migration, cell adhesion, and other aspects (Camodeca et al., 2019). Studies report that ADAM is abnormally upregulated and downregulated in various malignant tumour tissues, such as lung cancer, liver cancer, and colon cancer (Li et al., 2018; Jin et al., 2020; Du et al., 2022). Such abnormal expression promotes the proliferation of tumour cells and participation in tumour angiogenesis by regulating intercellular adhesion and degrading the intercellular substance.

In this study, we aimed to investigate the potential effects and mechanisms of ADAM families for pan-cancer analysis across 33 distinct tumours by integrating bulk RNA-seq, tumour mutation burden (TMB), and clinicopathological parameters in The Cancer Genome Atlas (TCGA) datasets. Moreover, we further used ESTIMATE and CIBERSORT to explore the correlation of ADAMs with immune cell infiltration and TME status. Moreover, the sensitivity of distinct FDA-approved drugs to target cancers was also examined through the CellMiner database. Furthermore, as ADAMs were significantly correlated with TME infiltration, the sensitivity of immune checkpoint inhibitor (ICI)-based immunotherapy and the association between the expression of ADAMs and the outcomes of patients treated with ICIs were explored in IMvigor210 and GSE78220 cohorts, and we found that ADAM19 was strikingly correlated with ICI immunotherapy response. Moreover, we also found that ADAMs, especially ADAM9, were strikingly correlated with the sensitivity of FDA-approved drugs. Considering the correlation of all ADAMs with drug sensitivity and immunotherapy response, we finally verified that ADAMs were significantly associated with all types of cancers and might be the novel targets for chemotherapy and immunotherapy.

2 Materials and methods

2.1 Identification of ADAMs in TCGA pan-cancer cohort

RNA-seq (FPKM) gene expression data were downloaded from the open access database UCSC Xena (http://xena.ucsc.edu) and were transformed into transcripts per kilobase million (Wagner et al., 2012). Clinical information of the samples and pathological information, including immune subtypes and stemness scores (RNA-based, RNAss; DNA methylation, DNAss), for all these cancers were also acquired from UCSC Xena (Miao et al., 2020). For pan-cancer TCGA analysis, a total of 20 ADAM (Supplementary Table S1) expression levels were extracted (Supplementary Table S2), and the differences in para-carcinoma and tumour tissue samples were evaluated using Student's *t*-test. Importantly, the number of normal samples of some cancer types was less than five; hence, these cancer types were excluded to prevent a statistical error. The box plots and heat maps were designed using "ggpubr" and "pheatmap" in R. The ADAM internal correlation was performed using "corrplot" in R.

2.2 Survival analyses of ADAMs in pan-cancers

Kaplan–Meier survival curves and log-rank test (*p*-value cut-off point 0.05) were used for the survival analysis. The cut-off was selected based on the average expression level of ADAMs in each tumour sample, and the patients were divided into high-expression and low-expression groups. Survival curves were plotted using the R packages "survminer" and "survival." Furthermore, Cox analysis was performed to determine the relationship between ADAMs and cancer prognosis. Finally, the forest plot was drawn using the R packages "survival" and "forestplot."

2.3 Correlation of ADAMs with the TME and stemness score in pan-cancers

The stromal scores and immune cell scores were calculated using "ESTIMATE" and "limma" in R for evaluating the stromal cell and immune cell infiltrating levels. Spearman's correlations were used to analyse the correlation between ADAMs and RNAss/DNAss, and the R package "corrplot" was used to visualise the results.

2.4 Correlation of ADAMs with chemotherapy-related drug sensitivity and the immune subtype

We acquired the chemotherapy-related drug sensitivity data from an open access database CellMiner (https://discover.nci.nih.gov/cellminer/loadDownload.do). Moreover, "limma" and "ggplot2" were used for data analysis and visualisation. Th immune subtypes of the samples were acquired from UCSC Xena. Furthermore, the correlation between immune subtypes and ADAMs was analysed by "limma" and "reshape2" in R.

2.5 Correlation of ADAMs and immunotherapy

The immunotherapy data were obtained from the IMvigor210 and GSE78220 datasets. The treatment outcomes are shown in Supplementary Table S3. Visualisation and response analysis of the result were processed using "ggpubr," "ggplot2," and "limma" in R.

2.6 Correlation of ADAM19 with TMB, microsatellite instability, and immune activation-related genes

The TMB and microsatellite instability (MSI) were calculated using TCGA somatic mutation data. A radar legend was established to show the relationship between ADAM19 and the TMB and MSI using Spearman's correlation analysis. Additionally, the co-expression of ADAM19 and immune activation-related genes was further analysed.

2.7 Tissue specimens and immunohistochemistry

We collected 18 paired KIRC and BLCA samples from Beijing Friendship Hospital, Capital Medical University (Beijing, China), between June 2022 and October 2022. The Institutional Research Ethics Committee approved the sample collection (No. 2021-P2-159). All samples were pathologically confirmed to be KIRC or BLCA. The antibody of ADAM9 was acquired from ABclonal (A22058, Wuhan, China).

2.8 Total RNA extraction, reverse transcription, and quantitative real-time polymerase chain reaction

The RNeasy Plus Mini Kits (74136, QIAGEN, Germany) were used to extract the total RNA of the samples. Subsequently, the quality of the extracted RNA was examined using NanoDrop (NP80, Implen, Germany). Following this, the ReverTra Ace qPCR RT Kit (FSQ-201, TOYOBO, Japan) was used for further cDNA synthesis. Finally, reverse and forward primers designed by us and iQ™ SYBR® Green Supermix (1708880, Bio-Rad, United States) were mixed to perform qRT-PCR. The expression of the targeted genes was normalised using the expression of GAPDH (Schmittgen and Livak, 2008).

2.9 Statistical analyses

Statistical significance between two groups was tested using Student's *t*-test. For variables that fall into more than three groups,

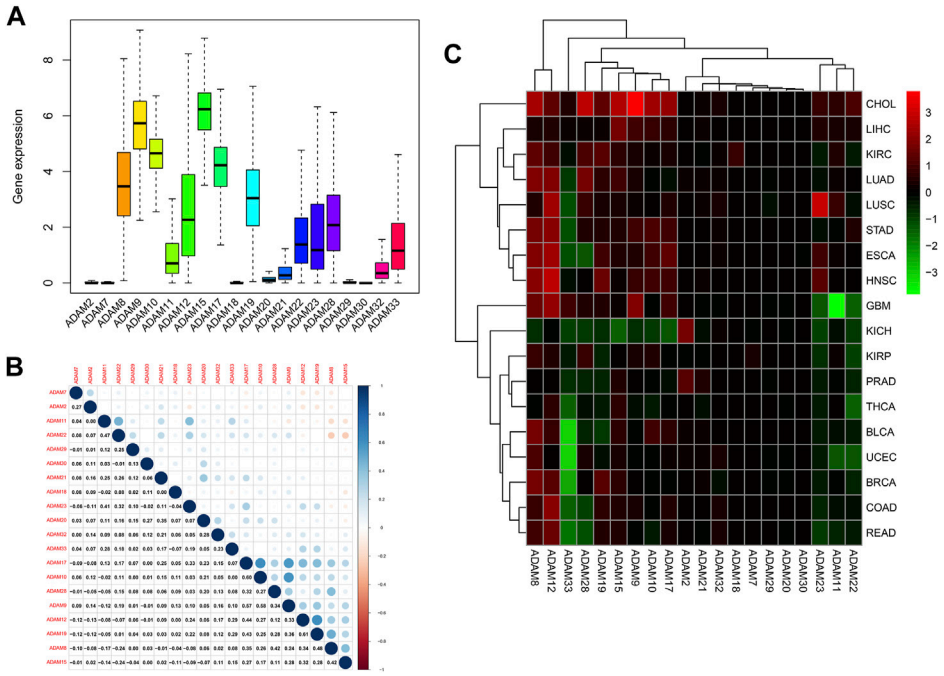

FIGURE 1
Expression levels and correlations of ADAM family genes in different types of cancer in TCGA. **(A)** Over-expression or under-expression of the ADAM family in various types of cancer. **(B)** Expression data from TCGA showing the ADAM family expressed in different types of cancer. The colour of each small rectangle represents high or low expression of ADAM family genes in each cancer. Red and green colours indicate high and low expression, respectively. **(C)** Correlations between ADAM family genes. Blue dots represent positive correlations, and red dots represent negative correlations. ACC, adrenocortical carcinoma; BLCA, bladder urothelial carcinoma; BRCA, breast invasive carcinoma; CESC, cervical squamous cell carcinoma and endocervical adenocarcinoma; CHOL, cholangiocarcinoma; COAD, colon adenocarcinoma; DLBC, diffuse large B-cell lymphoma; ESCA, oesophageal carcinoma; GBM, glioblastoma multiforme; HNSC, head and neck squamous cell carcinoma; KICH, kidney chromophobe; KIRC, kidney renal clear cell carcinoma; KIRP, kidney renal papillary cell carcinoma; LAML, acute myeloid leukaemia; LGG, brain lower-grade glioma; LIHC, liver hepatocellular carcinoma; LUAD, lung adenocarcinoma; LUSC, lung squamous cell carcinoma; MESO, mesothelioma; OV, ovarian serous cystadenocarcinoma; PAAD, pancreatic adenocarcinoma; PRAD, prostate adenocarcinoma; READ, rectum adenocarcinoma; SKCM, skin cutaneous melanoma; STAD, stomach adenocarcinoma; TGCA, testicular germ-cell tumour; THCA, thyroid carcinoma; THYM, thymoma; UCEC, uterine corpus endometrial carcinoma; UVM, uveal melanoma.

a one-way analysis of variance or the Kruskal–Wallis test was used, depending on the type of data. Kaplan–Meier (KM) curves were used to calculate and visualise the survival rates, and the log-rank test was used to test whether differences were significant. Correlation coefficients were calculated using Spearman's correlation analysis. A univariate Cox proportional hazards model was used to determine the timing of the variables and whether they were independent predictors. Statistical significance was set at $p < 0.05$.

3 Results

3.1 The landscape of ADAMs in the pan-cancer cohort

Figure 1A displays the expression of ADAMs in 33 types of cancers. Moreover, a series of genes in ADAMs, namely, ADAM8, ADAM9, ADAM10, ADAM11, ADAM12, ADAM17, ADAM19, ADAM21, ADAM22, ADAM23, ADAM28, ADAM32, and ADAM33, were highly expressed among all types of cancers. Additionally, the correlation between different ADAMs was also explored (Figure 1B), with ADAM8 and ADAM22 exhibiting the most significant positive correlation, whereas ADAM9 and ADAM10/ADAM17 exhibiting the most negative correlation. We further explored the expression of all ADAMs in 33 cancers (Figure 1C). ADAM9 was observed to be highly expressed in CHOL, whereas ADAM33 had a significantly lower expression in pan-cancers, especially in BLCA and UCEC (Figure 1C).

We also extracted the expression of ADAMs in TCGA database using R software, and the resultant expression is presented in Supplementary Table S2. ADAMs were differentially expressed among all cancers and para-carcinoma tissues (Figure 2; Supplementary Figure S1).

3.2 Correlation of ADAMs and prognosis in the pan-cancer cohort

The number of normal samples of some cancer types was less than five in our study; hence, these cancers were excluded to prevent

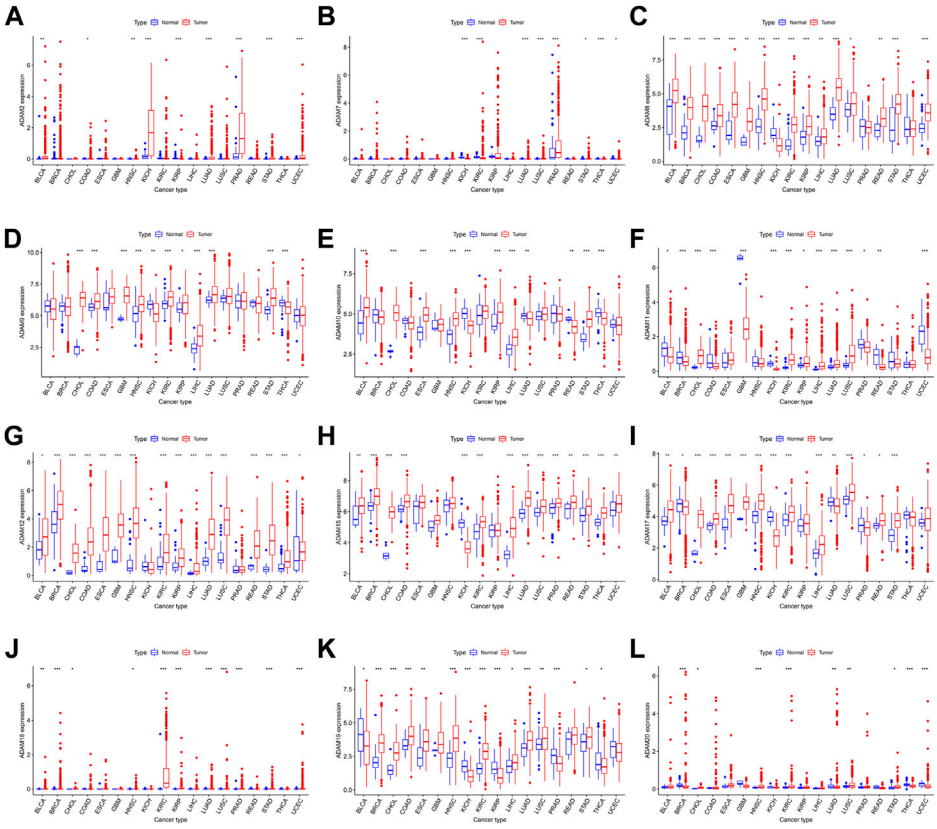

FIGURE 2
ADAM family expression levels in different cancer and para-carcinoma tissues. **(A)** Differential expression of ADAM2, **(B)** differential expression of ADAM7, **(C)** differential expression of ADAM8, **(D)** differential expression of ADAM9, **(E)** differential expression of ADAM10, **(F)** differential expression of ADAM11, **(G)** differential expression of ADAM12, **(H)** differential expression of ADAM15, **(I)** differential expression of ADAM17, **(J)** differential expression of ADAM18, **(K)** differential expression of ADAM19, and **(L)** differential expression of ADAM20. The red rectangle box represents gene expression levels in tumour tissue, and the blue rectangle box represents normal tissue. $*p < 0.05$, $**p < 0.01$, and $***p < 0.001$. Cancer names in red indicate high expression, and cancer names in blue indicate low expression of the corresponding ADAM family gene.

a statistical error, and a total of 28 cancers were contained in this study. We subsequently analysed the correlation between the expression of ADAMs and prognostic data. The Kaplan–Meier survival curves of ADAM9 and ADAM19 are shown in Figure 3, and the *p*-values of the survival analysis of other ADAMs are listed in Supplementary Table S4. Among the analysed ADAMs, ADAM9 had a negative effect on BLCA (N = 406, $p = 0.042$; Figure 3A), CESC (N = 293, $p = 0.009$; Figure 3B), KICH (N = 64, $p = 0.009$; Figure 3C), LGG (N = 524, $p < 0.001$; Figure 3D), LIHC (N = 368, $p < 0.001$; Figure 3E), MESO (N = 84, $p = 0.005$; Figure 3F), PAAD (N = 177, $p < 0.001$; Figure 3G), and THYM (N = 118, $p = 0.019$; Figure 3H). Furthermore, ADAM19 also had a negative effect on ACC (N = 79, $p = 0.028$; Figure 3I), KIRP (N = 286, $p = 0.034$; Figure 3J), LGG (N = 524, $p < 0.001$; Figure 3K), LIHC (N = 368, $p = 0.039$; Figure 3L), MESO (N = 84, $p = 0.002$; Figure 3M), and UVM (N = 80, $p < 0.001$; Figure 3O), while ADAM19 appeared to induce a protective effect on SKCM (N = 457, $p = 0.023$; Figure 3N). Furthermore, we investigated the prognostic risk of ADAMs in pan-cancers using Cox regression analysis, which revealed results consistent with that of the Kaplan–Meier survival curves (Figure 4).

3.3 Association of ADAMs with the TME and stemness score in pan-cancers

We explored the relationship between the expression of ADAMs and the TME in pan-cancers. The immune scores and stromal scores were significantly positively correlated with the expression of ADAMs (Figures 5A, B). Furthermore, significant negative or positive correlations were found between ADAMs and RNAss (Figure 5C). A correlation between ADAMs and DNAss (Figure 5D) was also found in pan-cancers (Supplementary Table S5).

We also revealed the relevance between ADAMs and the stromal score, immune score, stemness score, and ESTIMATE score in certain types of cancer (BLCA and KIRC) (Figures 6, 7; Supplementary Table S6) and found that ADAMs had an extensive correlation with the BLCA and KIRC TME as well as DNAss and RNAss.

3.4 Association of ADAMs with immune subtypes in pan-cancers

Thorsson et al. (2019) put forward six immune subtypes (C1–C6) among 33 pan-cancer types. They performed an

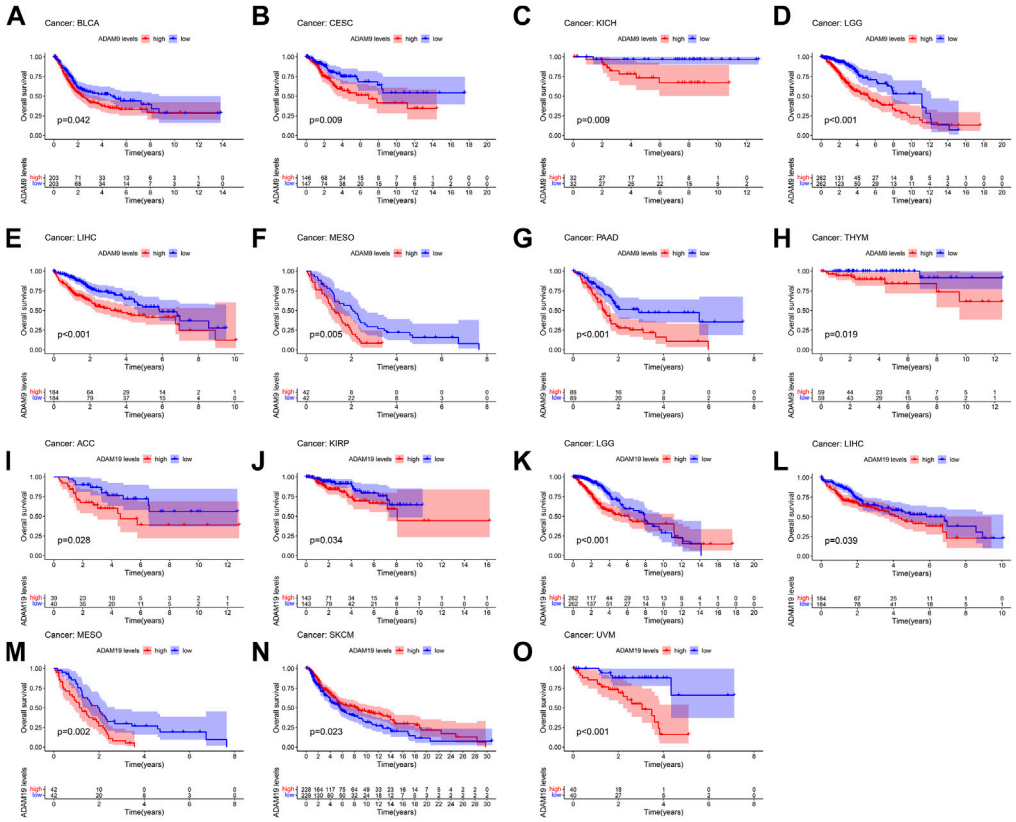

FIGURE 3
Kaplan–Meier survival curve comparison of high/low expression of ADAM family genes in pan-cancer. **(A)** Survival curves of ADAM9 in BLCA (N = 406), **(B)** survival curves of ADAM9 in CESC (N = 293), **(C)** survival curves of ADAM9 in KICH (N = 64), **(D)** survival curves of ADAM9 in LGG (N = 524), **(E)** survival curves of ADAM9 in LIHC (N = 368), **(F)** survival curves of ADAM9 in MESO (N = 84), **(G)** survival curves of ADAM9 in PAAD (N = 177), **(H)** survival curves of ADAM9 in THYM (N = 118), **(I)** survival curves of ADAM19 in ACC (N = 79), **(J)** survival curves of ADAM19 in KIRP (N = 286), **(K)** survival curves of ADAM19 in LGG (N = 524), **(L)** survival curves of ADAM19 in LIHC (N = 368), **(M)** survival curves of ADAM19 in MESO (N = 84), **(N)** survival curves of ADAM19 in SKCM (N = 457), and **(O)** survival curves of ADAM19 in UVM (N = 80).

extensive immunogenomic analysis of over 10,000 tumours, comprising 33 diverse cancer types and utilising data compiled by TCGA. They identified six immune subtypes: IFN-γ-dominant, wound healing, lymphocyte-depleted, inflammatory, TGF-β-dominant, and immunologically quiet, which showed the different characteristics of immune cell infiltration and prognosis. The immune subtypes were significantly associated with tumour prognosis and genetic and immunomodulatory changes. Thus, we further explored the correlation of ADAMs with the immune subtypes and observed that ADAM8, ADAM10, ADAM11, ADAM12, ADAM15, ADAM19, ADAM22, ADAM23, ADAM28, and ADAM33 were differentially expressed in both BRCA and COAD (Figure 8). Additionally, ADAM19 showed a significantly higher expression in C1–C3 of BLCA and KIRC, whereas ADAM8 was highly expressed in C6 of BLCA and KIRC. Moreover, the expression of the ADAM family in C5 was generally lower than that in other immune subtypes in KIRC. Thus, ADAMs were correlated with these immune subtypes (Figure 8), which improved the prognostic value and potential clinical use of ADAMs.

3.5 Association of ADAMs with the outcome of chemotherapy and immunotherapy treatments in the pan-cancer cohort

We extracted drug sensitivity data from the CellMiner database to determine the correlation between ADAMs and drug sensitivity. The top 16 drugs showing sensitivity to ADAMs are shown in Figure 9 and Supplementary Table S7. Notably, ADAM33 was positively correlated with the sensitivity of nelarabine, chelerythrine, fluphenazine, dexamethasone (Decadron), PX-316, asparaginase, fludarabine, and fenretinide (Figures 9A–D, G, J, O, P). Additionally, raloxifene, tamoxifen, and bafetinib were negatively correlated with ADAM9 (Figures 9E, F, M). Furthermore, nelarabine was positively correlated with ADAM22 (Figure 9H); procarbazine and itraconazole shared a positive correlation with ADAM8 (Figures 9K, L); ADAM28 was negatively correlated with ixazomib citrate (Figure 9I); and ADAM17 was negatively correlated with tamoxifen (Figure 9N). ADAM9 was significantly associated with 82 different drug sensitivities, including tamoxifen,

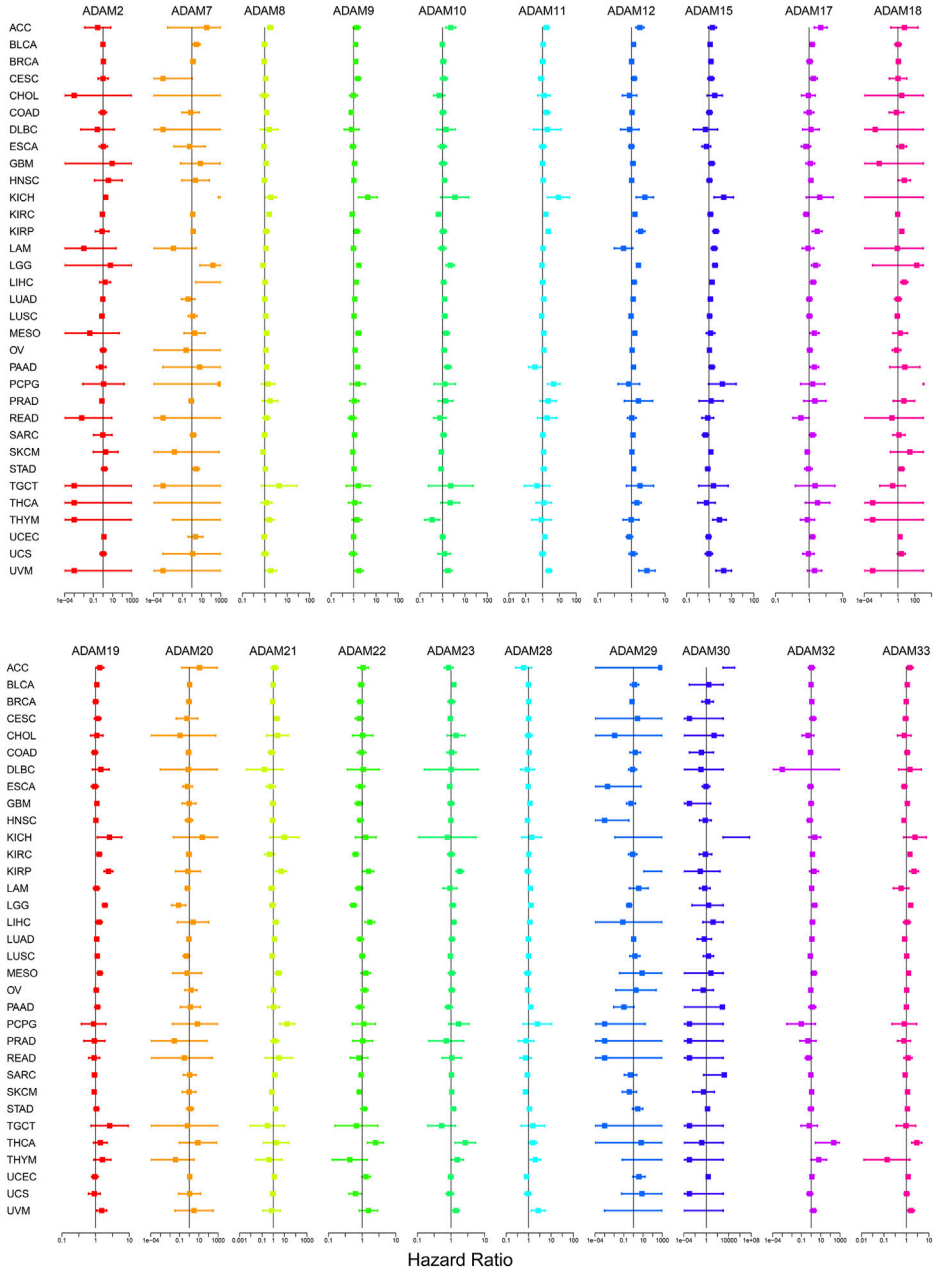

FIGURE 4
Cox regression analysis of the correlation between ADAM family expression and survival. Lines with different colours represent the risk values for different genes within the tumour, with a hazard ratio <1 indicating low risk and a hazard ratio >1 indicating high risk.

cyclophosphamide, oxaliplatin, and bafetinib. Furthermore, ADAM9 showed significantly different expression between tumour and para-carcinoma tissues in KIRC using qRT-PCR analysis (Figure 9Q). The protein expression of ADAM9 in KIRC using immunohistochemistry revealed results consistent with that of qRT-PCR, wherein a significantly higher expression of ADAM9 in tumour tissues was confirmed. However, the differential expression of ADAM9 in BLCA samples was also observed (Supplementary Figure S2).

We further extracted the expression levels of ADAM19 from the GSE78220 (Figure 10A) and IMvigor210 (Figure 10B) datasets and compared the expression with immune response. ADAM19 was significantly negatively correlated with immunotherapy response.

TMB has been recently considered a potential predictive biomarker of immunotherapy (Picard et al., 2020; Jardim et al., 2021; Rizzo et al., 2021). Meanwhile, MSI has also been reported to be correlated with immunotherapy outcomes (Rizzo et al., 2021). The relationship between TMB and ADAM19 expression was explored (Figure 10C;

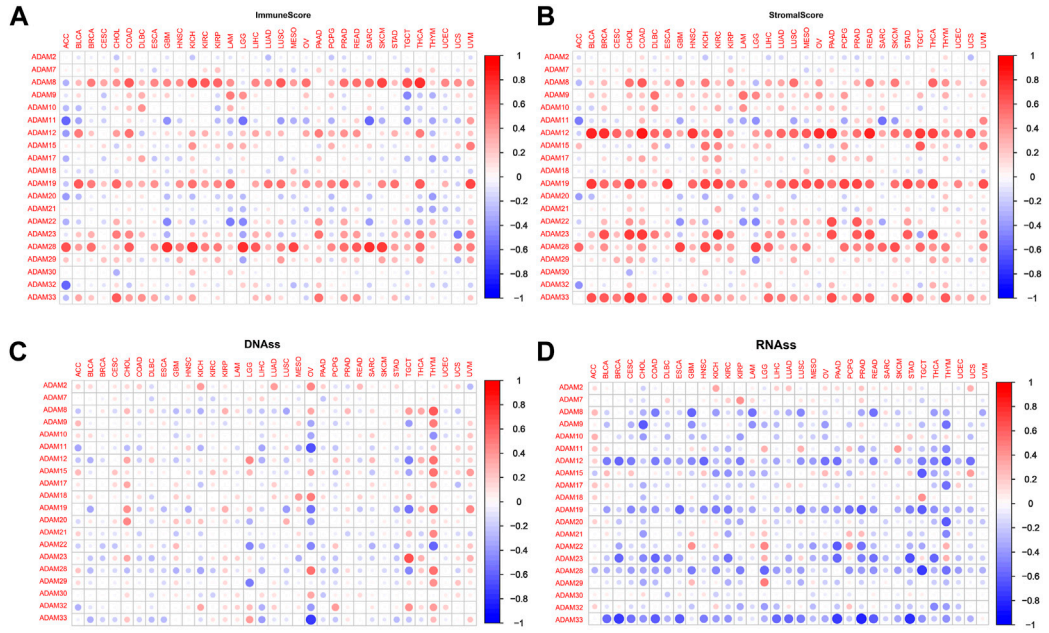

FIGURE 5
Correlation of ADAM family gene expression with the tumour microenvironment and stemness score in pan-cancer. **(A, B)** ADAM family gene expression correlates with various mesenchymal and immune cancer scores. Red dots indicate a positive correlation between tumour gene expression and mesenchymal score, and green dots indicate a negative correlation between tumour gene expression and mesenchymal score. **(C, D)** Correlation of ADAM family expression with RNAss and DNAss in pan-cancer. Red dots indicate a positive correlation between tumour gene expression and immune score, and blue dots indicate a negative correlation between tumour gene expression and immune score.

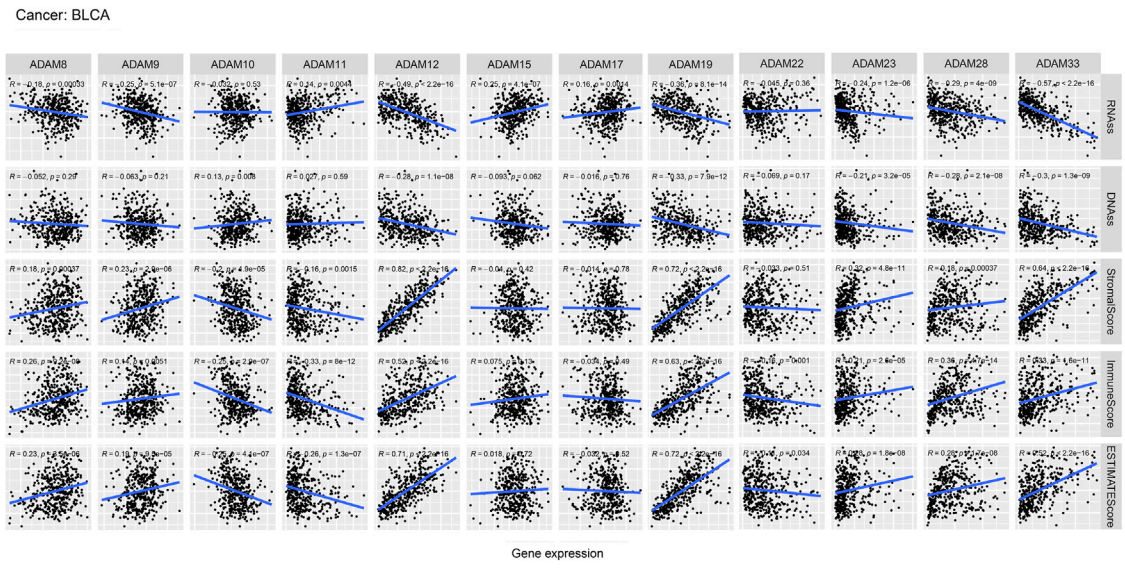

FIGURE 6
Correlation analysis of ADAM family gene expression with RNAss, DNAss, stromal score, immune score, and ESTIMATE score in BLCA.

Supplementary Table S8), and the significant correlation between ADAM19 expression and MSI was detected in various types of cancers, including CHOL, DLBC, ESCA, HNSC, KIRP, LICH, SKCM, STAD, UCEC, and UVM (Figure 10D).

Furthermore, we found the co-expression of immune activation genes and ADAM19 (Figure 10E), revealing a significant correlation of ADAM19 with immune activation genes among almost all 33 types of cancer.

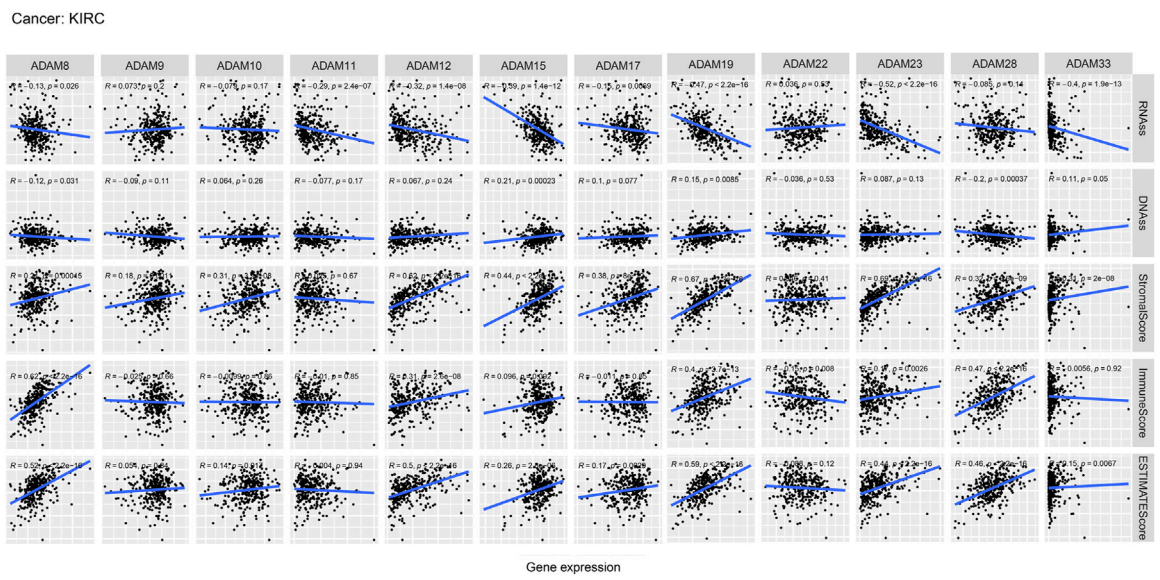

FIGURE 7
Correlation analysis of ADAM family gene expression with RNAss, DNAss, stromal score, immune score, and ESTIMATE score in KIRC.

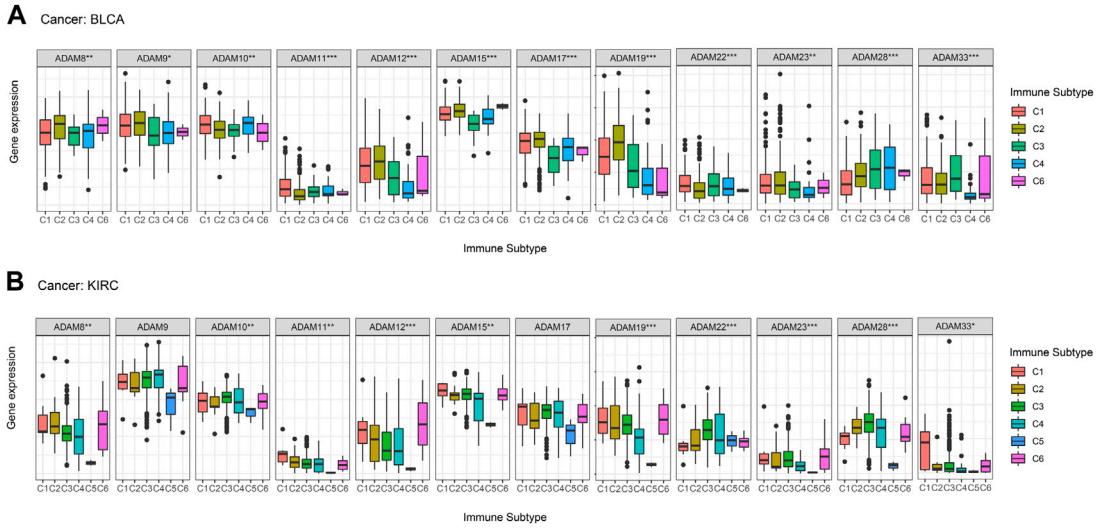

FIGURE 8
Correlation between ADAM family expression and immune subtypes in BLCA and KIRC. **(A)** ADAM family expression in different immune subtypes in BLCA. **(B)** ADAM family expression in different immune subtypes in KIRC. The X-axis represents the immune subtype, and the Y-axis represents gene expression. C1, wound healing; C2, IFN-γ-dominant; C3, inflammatory; C4, lymphocyte-depleted; C5, immunologically quiet; C6, TGF-β-dominant. $p < 0.05$; $^{**}p < 0.01$; $^{***}p < 0.001$.

4 Discussion

Cancer is the leading cause of death globally (Shams-White et al., 2021; Soerjomataram and Bray, 2021). In 2022, approximately 4.82 million new cancer cases and 3.21 million cancer-related deaths have been reported in China (Xia et al., 2022). Since 2000, the number of cancer-related morbidity and mortality along with their incidence has been increasing annually in China (Wei et al., 2020). Accumulating evidence indicated that proteolytic enzymes, such as MMPs and closely related ADAMs and ADAMTSs, play key roles in cancer initiation and progression (Rocks et al., 2008). Wei et al. (2019) reported that the over-expression of ADAM28 in pancreatic cancer was closely correlated with the regulation of gemcitabine resistance. Similarly, Wang et al. (2011) reported that ADAM10 was significantly associated with lymph node and distant

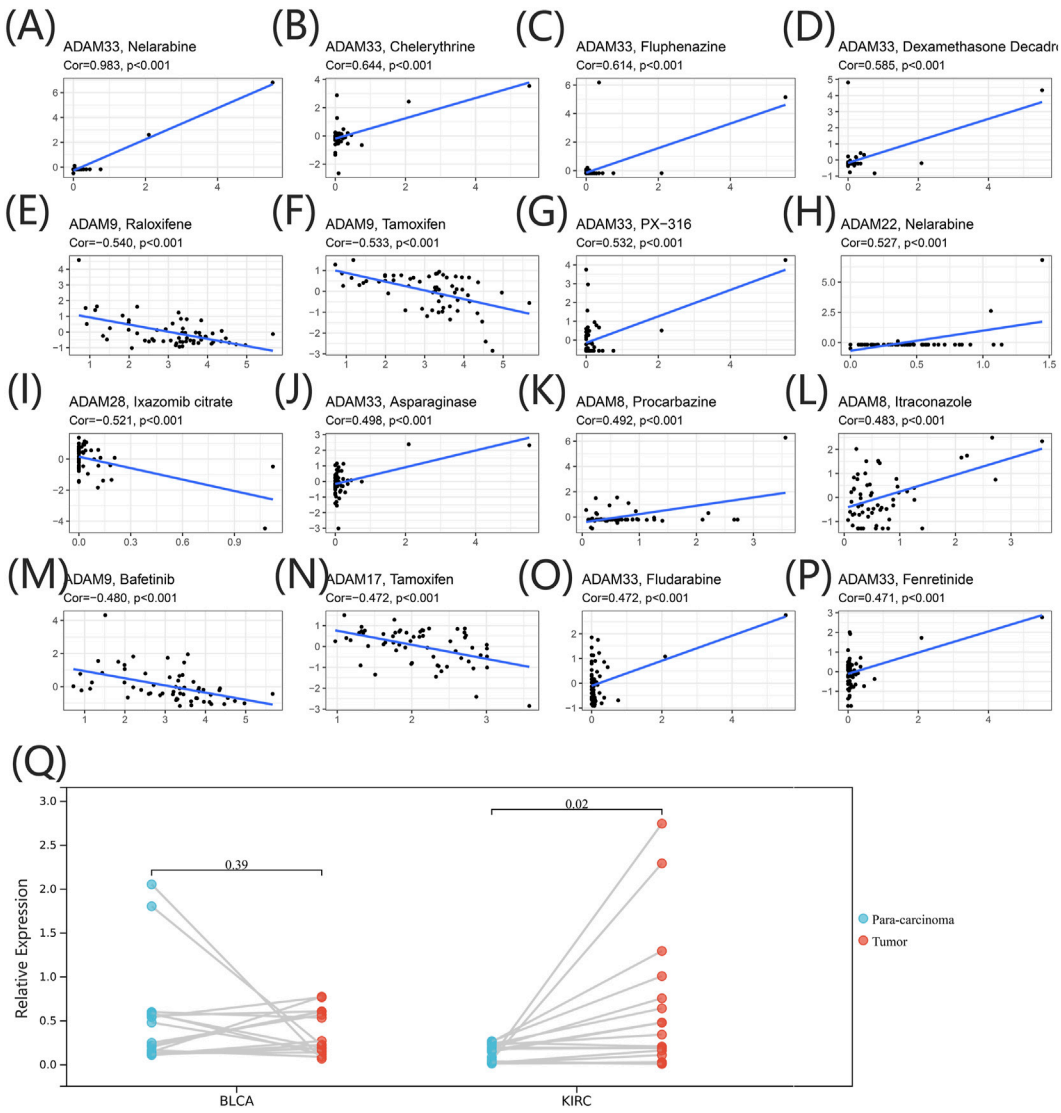

FIGURE 9
(A–P) Drug sensitivity analysis of the ADAM family gene. The X-axis represents the relative sensitivity with certain drugs, and the Y-axis represents the relative expression of ADAMs. **(Q)** Differential expression of ADAM9 in BLCA and KIRC tissues.

metastasis in gastric cancer. In this study, we focused on the pan-cancer analysis of all ADAMs and explored the differential expression of ADAMs in various types of cancer, as shown in Table 1; we found that both ADAM8 and ADAM12 were located at 10q26. In our results, we also found a significant positive correlation between ADAM8 and ADAM12. Similar results were also observed between ADAM21 and ADAM22. Shimura et al. (2015) revealed that urinary MMP-9/NGAL and urinary ADAM12 are potential non-invasive biomarkers for gastric cancer, including early-stage diseases. Xiao et al. (2012) reported that ADAM17 was an important contributor to prostate cancer invasion according to the shedding of the EGFR ligand TGF-α, which subsequently activates the EGFR–MEK–ERK signalling pathway and induces the over-expression of MMP-2 and MMP-9. Furthermore, Karan et al. (2003) indicated that an inverse expression pattern of ADAM17/TACE and TIMP3 and the regulation of ADAMs with DHT could play an important role in the pathogenesis of prostate cancer. Currently, the most specific therapeutic monoclonal antibody against ADAM17 is D1 (A12), which binds to both the catalytic and disintegrin/cysteine-rich domains of ADAM17 (Tape et al., 2011). It has been proven to be effective in ovarian cancer cells (Richards et al., 2012), breast cancer (Caiazza et al., 2015), and head and neck cancer (Huang et al., 2014). Additionally, ADAM inhibitors can also effectively assist the therapeutic effect of existing monoclonal antibodies. ADAM10 inhibitors have been reported to be protective against HER2-positive breast cancers, which are resistant to Herceptin (trastuzumab) (Rimawi et al., 2015).

The role of ADAMs in tumours remains limited, despite the increasing knowledge of the overall role of ADAMs. In our study, significant differential expression of ADAM8, ADAM9, ADAM10,

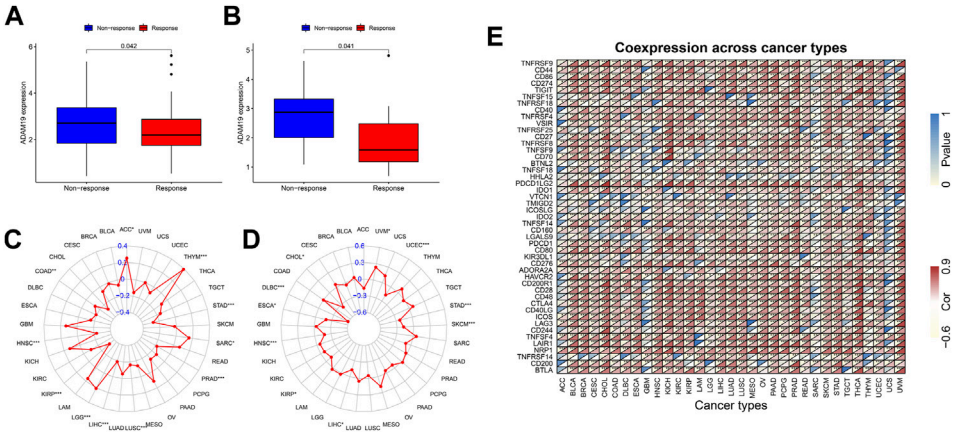

FIGURE 10
Correlation of immunotherapy outcome, TMB, MSI, and immune activation-related genes with the expression of ADAM19. **(A)** Expression levels of ADAM19 in GSE78220. **(B)** Expression levels of ADAM19 in IMvigor210 **(C)** The relationship between TMB and ADAM19 expression **(D)** The relationship between MSI and ADAM19 expression **(E)** Co-expression of immune activation genes with ADAM19.

ADAM11, ADAM12, ADAM15, ADAM17, ADAM19, ADAM22, ADAM23, and ADAM33 was observed among almost all types of cancer. ADAM8 was significantly highly expressed in tumour tissue compared with para-cancerous tissue in all types of cancer, except for KIRC, PRAD, and THCA, indicating ADAM8 could be a significant biomarker for tumours. Notably, the correlation of ADAM8 with tumour progression, metastasis, and chemoresistance in various invasive cancers, including pancreatic cancer (Yu et al., 2019), breast cancer (Conrad et al., 2018), and lung cancer (Ishikawa et al., 2004), has been previously reported. Furthermore, ADAM12 was also generally highly expressed in almost all types of tumour tissues. Wang et al. (2021) reported that ADAM12 inhibition, which was induced by a hypoxia-inducible factor, could effectively downregulate migration and invasion in breast cancer cell lines and also in immuno-deficient mice.

Recently, researchers have been increasingly focusing on the surroundings of solid cancers instead of the tumour itself (Quail and Joyce, 2013; Wu and Dai, 2017; Hinshaw and Shevde, 2019). The surroundings of the cancers are collectively known as the TME which includes immune and stromal cells, and these factors synergistically formed an inflammatory, tumour-promoting, and immuno-suppressive environment which helps cancer cells escape from immune surveillance (Wu and Dai, 2017). In this study, the ESTIMATE algorithm was used to calculate the immune score and stromal score as well as explore the correlation between these scores and ADAM expression. As shown in Figures 5A, B, ADAM8, 19, and 28 showed a significantly positive correlation with both the immune score and stromal score in pan-cancers, indicating that these genes may play an important role in TME development and could be potential immunotherapy targets. Furthermore, we assessed tumour stemness among different ADAMs in cancers using RNAss and DNAss. These results highlighted the negative effect of ADAMs on characterising cancer cells. Furthermore, as shown in Figures 6, 7, a significant positive correlation was observed between ADAM expression, including ADAM8, 9, 12, 19, 23, 28, and 33, whereas ADAM10, 11, and 22 were negatively correlated with the stromal score and immune score.

Although most studies related to ADAM9 focused more on its effect on tumour proliferation, migration, and invasion, various studies have pointed out the value of ADAM9 for tumour drug therapy. In the current study, ADAM9 was significantly associated with 82 different drug sensitivities, including tamoxifen, cyclophosphamide, oxaliplatin, and bafetinib. Liu et al. (2021) revealed that the cisplatin treatment of non-small-cell lung cancer could be promoted by ADAM9 while being negatively regulated by miR-126-5p. Slapak et al. (2021) reported a novel ADAM9-responsive, protease-dependent, drug delivery system for patients with pancreatic ductal adenocarcinoma that can reduce the cytotoxicity of systemic chemotherapy. As for the different results of ADAM9 of PCR and immunohistochemistry in BLCA, it happens occasionally. The transcription and translation of eukaryotic genes were differentially expressed; hence, it is also necessary to determine how the protein level changes.

In terms of cancer treatment, monoclonal antibodies also have their niche population. Monoclonal antibodies have a more specific mode of action and thus cause fewer cytotoxic side effects than low-molecular-weight antibodies. In addition, some monoclonal antibodies can exert anti-cancer activity by inducing antibody-dependent cytotoxicity (Mullooly et al., 2016). Furthermore, in the current study, ADAM19 was negatively correlated with immunotherapy outcomes and strongly correlated with chemotherapy drugs, thus providing a solid theoretical foundation for further research.

5 Conclusion

The expression profile of ADAMs in pan-cancers has been demonstrated to correlate with prognosis, tumour microenvironment, treatment outcome, and stemness score. Furthermore, the expression levels of ADAMs in tumour cells are also related to the efficacy of different chemotherapy-related drugs and their response to immunotherapy. These results thus provide a reference for future research on ADAM family genes as potential pan-cancer targets.

Data availability statement

The datasets presented in this study can be found in online repositories. The names of the repository/repositories and accession number(s) can be found in the article/Supplementary Material.

Ethics statement

The studies involving human participants were reviewed and approved by the Institutional Research Ethics Committee. The clinical specimens were collected with permission from the Institutional Research Ethics Committee (No. 2021-P2-159). The Ethics Committee waived the requirement of written informed consent for participation.

Author contributions

BM and RY made substantial contributions to the conception and design of the research. BM integrated and analysed the data and drafted the manuscript. RY edited the manuscript and provided critical comments. All authors read and approved the final manuscript.

Funding

This work was funded by the Beijing Natural Science Foundation (Grant No. 7194279).

Acknowledgments

The authors are grateful to The Cancer Genome Atlas Research Network for the clinicopathological and genetic alteration data. They are also thankful to the Urology Department of Beijing Friendship Hospital, Capital Medical University, for their contribution in obtaining the tissue samples of BLCA and KIRC. They also thank Bullet Edits Limited for the linguistic editing and proofreading of the manuscript.

Conflict of interest

The authors declare that the research was conducted in the absence of any commercial or financial relationships that could be construed as a potential conflict of interest.

Publisher's note

All claims expressed in this article are solely those of the authors and do not necessarily represent those of their affiliated organizations, or those of the publisher, the editors, and the reviewers. Any product that may be evaluated in this article, or claim that may be made by its manufacturer, is not guaranteed or endorsed by the publisher.

Supplementary material

The Supplementary Material for this article can be found online at: https://www.frontiersin.org/articles/10.3389/fgene.2023.1105900/full#supplementary-material

References

Caiazza, F., McGowan, P. M., Mullooly, M., Murray, A., Synnott, N., O'Donovan, N., et al. (2015). Targeting ADAM-17 with an inhibitory monoclonal antibody has antitumour effects in triple-negative breast cancer cells. *Br. J. Cancer* 112 (12), 1895–1903. doi:10.1038/bjc.2015.163

Camodeca, C., Cuffaro, D., Nuti, E., and Rossello, A. (2019). ADAM metalloproteinases as potential drug targets. *Curr. Med. Chem.* 26 (15), 2661–2689. doi:10.2174/0929867325666180326164104

Conrad, C., Gotte, M., Schlomann, U., Roessler, M., Pagenstecher, A., Anderson, P., et al. (2018). ADAM8 expression in breast cancer derived brain metastases: Functional implications on MMP-9 expression and transendothelial migration in breast cancer cells. *Int. J. Cancer* 142 (4), 779–791. doi:10.1002/ijc.31090

Du, S., Sun, L., Wang, Y., Zhu, W., Gao, J., Pei, W., et al. (2022). ADAM12 is an independent predictor of poor prognosis in liver cancer. *Sci. Rep.* 12 (1), 6634. doi:10.1038/s41598-022-10608-y

Girigoswami, K., Saini, D., and Girigoswami, A. (2021). Extracellular matrix remodeling and development of cancer. *Stem Cell Rev. Rep.* 17 (3), 739–747. doi:10.1007/s12015-020-10070-1

Heib, M., Rose-John, S., and Necroptosis, Adam D. (2020). Necroptosis, ADAM proteases and intestinal (dys)function. *Int. Rev. Cell Mol. Biol.* 353, 83–152. doi:10.1016/bs.ircmb.2020.02.001

Hinshaw, D. C., and Shevde, L. A. (2019). The tumor microenvironment innately modulates cancer progression. *Cancer Res.* 79 (18), 4557–4566. doi:10.1158/0008-5472.CAN-18-3962

Huang, J., Zhang, L., Wan, D., Zhou, L., Zheng, S., Lin, S., et al. (2021). Extracellular matrix and its therapeutic potential for cancer treatment. *Signal Transduct. Target Ther.* 6 (1), 153. doi:10.1038/s41392-021-00544-0

Huang, Y., Benaich, N., Tape, C., Kwok, H. F., and Murphy, G. (2014). Targeting the sheddase activity of ADAM17 by an anti-ADAM17 antibody D1(A12) inhibits head and neck squamous cell carcinoma cell proliferation and motility via blockage of bradykinin induced HERs transactivation. *Int. J. Biol. Sci.* 10 (7), 702–714. doi:10.7150/ijbs.9326

Ishikawa, N., Daigo, Y., Yasui, W., Inai, K., Nishimura, H., Tsuchiya, E., et al. (2004). ADAM8 as a novel serological and histochemical marker for lung cancer. *Clin. Cancer Res.* 10 (24), 8363–8370. doi:10.1158/1078-0432.CCR-04-1436

Jardim, D. L., Goodman, A., de Melo Gagliato, D., and Kurzrock, R. (2021). The challenges of tumor mutational burden as an immunotherapy biomarker. *Cancer Cell* 39 (2), 154–173. doi:10.1016/j.ccell.2020.10.001

Jin, Q., Jin, X., Liu, T., Lu, X., Wang, G., and He, N. (2020). A disintegrin and metalloproteinase 8 induced epithelial-mesenchymal transition to promote the invasion of colon cancer cells via TGF-β/Smad2/3 signalling pathway. *J. Cell Mol. Med.* 24 (22), 13058–13069. doi:10.1111/jcmm.15907

Karan, D., Lin, F. C., Bryan, M., Ringel, J., Moniaux, N., Lin, M. F., et al. (2003). Expression of ADAMs (a disintegrin and metalloproteases) and TIMP-3 (tissue inhibitor of metalloproteinase-3) in human prostatic adenocarcinomas. *Int. J. Oncol.* 23 (5), 1365–1371. doi:10.3892/ijo.23.5.1365

Li, Y. Q., Liu, Y. S., Ying, X. W., Zhou, H. B., Wang, Z., Wu, S. C., et al. (2018). Lentivirus-mediated disintegrin and metalloproteinase 17 RNA interference reversed the acquired resistance to gefitinib in lung adenocarcinoma cells *in vitro*. *Biotechnol. Prog.* 34 (1), 196–205. doi:10.1002/btpr.2564

Liu, B., Wang, R., and Liu, H. (2021). mir-126-5p promotes cisplatin sensitivity of non-small-cell lung cancer by inhibiting ADAM9. *Biomed. Res. Int.* 2021, 6622342. doi:10.1155/2021/6622342

Malemud, C. J. (2019). Inhibition of MMPs and ADAM/ADAMTS. *Biochem. Pharmacol.* 165, 33–40. doi:10.1016/j.bcp.2019.02.033

Miao, Y., Wang, J., Li, Q., Quan, W., Wang, Y., Li, C., et al. (2020). Prognostic value and immunological role of PDCD1 gene in pan-cancer. *Int. Immunopharmacol.* 89, 107080. doi:10.1016/j.intimp.2020.107080

Mohan, V., Das, A., and Sagi, I. (2020). Emerging roles of ECM remodeling processes in cancer. *Semin. Cancer Biol.* 62, 192–200. doi:10.1016/j.semcancer.2019.09.004

Mullooly, M., McGowan, P. M., Crown, J., and Duffy, M. J. (2016). The ADAMs family of proteases as targets for the treatment of cancer. *Cancer Biol. Ther.* 17 (8), 870–880. doi:10.1080/15384047.2016.1177684

Najafi, M., Farhood, B., and Mortezaee, K. (2019). Extracellular matrix (ECM) stiffness and degradation as cancer drivers. *J. Cell Biochem.* 120 (3), 2782–2790. doi:10.1002/jcb.27681

Nissen, N. I., Karsdal, M., and Willumsen, N. (2019). Collagens and Cancer associated fibroblasts in the reactive stroma and its relation to Cancer biology. *J. Exp. Clin. Cancer Res.* 38 (1), 115. doi:10.1186/s13046-019-1110-6

Padhi, A., and Nain, A. S. (2020). ECM in differentiation: A review of matrix structure, composition and mechanical properties. *Ann. Biomed. Eng.* 48 (3), 1071–1089. doi:10.1007/s10439-019-02337-7

Picard, E., Verschoor, C. P., Ma, G. W., and Pawelec, G. (2020). Relationships between immune landscapes, genetic subtypes and responses to immunotherapy in colorectal cancer. *Front. Immunol.* 11, 369. doi:10.3389/fimmu.2020.00369

Quail, D. F., and Joyce, J. A. (2013). Microenvironmental regulation of tumor progression and metastasis. *Nat. Med.* 19 (11), 1423–1437. doi:10.1038/nm.3394

Richards, F. M., Tape, C. J., Jodrell, D. I., and Murphy, G. (2012). Anti-tumour effects of a specific anti-ADAM17 antibody in an ovarian cancer model *in vivo*. *PLoS One* 7 (7), e40597. doi:10.1371/journal.pone.0040597

Rimawi, M. F., Schiff, R., and Osborne, C. K. (2015). Targeting HER2 for the treatment of breast cancer. *Annu. Rev. Med.* 66, 111–128. doi:10.1146/annurev-med-042513-015127

Rizzo, A., Ricci, A. D., and Brandi, G. (2021). PD-L1, TMB, MSI, and other predictors of response to immune checkpoint inhibitors in biliary tract cancer. *Cancers (Basel)* 13 (3), 558. doi:10.3390/cancers13030558

Rocks, N., Paulissen, G., El Hour, M., Quesada, F., Crahay, C., Gueders, M., et al. (2008). Emerging roles of ADAM and ADAMTS metalloproteinases in cancer. *Biochimie* 90 (2), 369–379. doi:10.1016/j.biochi.2007.08.008

Saha, N., Robev, D., Himanen, J. P., and Nikolov, D. B. (2019). ADAM proteases: Emerging role and targeting of the non-catalytic domains. *Cancer Lett.* 467, 50–57. doi:10.1016/j.canlet.2019.10.003

Schmittgen, T. D., and Livak, K. J. (2008). Analyzing real-time PCR data by the comparative C(T) method. *Nat. Protoc.* 3 (6), 1101–1108. doi:10.1038/nprot.2008.73

Shams-White, M. M., Barajas, R., Jensen, R. E., Rotunno, M., Dueck, H., Ginexi, E. M., et al. (2021). Systems epidemiology and cancer: A review of the national institutes of health extramural grant portfolio 2013-2018. *PLoS One* 16 (4), e0250061. doi:10.1371/journal.pone.0250061

Shimura, T., Dagher, A., Sachdev, M., Ebi, M., Yamada, T., Yamada, T., et al. (2015). Urinary ADAM12 and MMP-9/NGAL complex detect the presence of gastric cancer. *Cancer Prev. Res. (Phila).* 8 (3), 240–248. doi:10.1158/1940-6207.CAPR-14-0229

Slapak, E. J., Kong, L., El Mandili, M., Nieuwland, R., Kros, A., Bijlsma, M. F., et al. (2021). ADAM9-Responsive mesoporous silica nanoparticles for targeted drug delivery in pancreatic cancer. *Cancers (Basel)* 13 (13), 3321. doi:10.3390/cancers13133321

Soerjomataram, I., and Bray, F. (2021). Planning for tomorrow: Global cancer incidence and the role of prevention 2020-2070. *Nat. Rev. Clin. Oncol.* 18 (10), 663–672. doi:10.1038/s41571-021-00514-z

Tape, C. J., Willems, S. H., Dombernowsky, S. L., Stanley, P. L., Fogarasi, M., Ouwehand, W., et al. (2011). Cross-domain inhibition of TACE ectodomain. *Proc. Natl. Acad. Sci. U. S. A.* 108 (14), 5578–5583. doi:10.1073/pnas.1017067108

Theret, N., Bouezzedine, F., Azar, F., Diab-Assaf, M., and Legagneux, V. (2021). ADAM and ADAMTS proteins, new players in the regulation of hepatocellular carcinoma microenvironment. *Cancers (Basel)* 13 (7), 1563. doi:10.3390/cancers13071563

Thorsson, V., Gibbs, D. L., Brown, S. D., Wolf, D., Bortone, D. S., Ou Yang, T. H., et al. (2019). The immune landscape of cancer. *Immunity* 51 (2), 411–412. doi:10.1016/j.immuni.2019.08.004

Valdoz, J. C., Johnson, B. C., Jacobs, D. J., Franks, N. A., Dodson, E. L., Sanders, C., et al. (2021). The ECM: To scaffold, or not to scaffold, that is the question. *Int. J. Mol. Sci.* 22, 12690. doi:10.3390/ijms222312690

Wagner, G. P., Kin, K., and Lynch, V. J. (2012). Measurement of mRNA abundance using RNA-seq data: RPKM measure is inconsistent among samples. *Theory Biosci.* 131 (4), 281–285. doi:10.1007/s12064-012-0162-3

Walker, C., Mojares, E., and Del Rio Hernandez, A. (2018). Role of extracellular matrix in development and cancer progression. *Int. J. Mol. Sci.* 19 (10), 3028. doi:10.3390/ijms19103028

Wang, R., Godet, I., Yang, Y., Salman, S., Lu, H., Lyu, Y., et al. (2021). Hypoxia-inducible factor-dependent ADAM12 expression mediates breast cancer invasion and metastasis. *Proc. Natl. Acad. Sci. U. S. A.* 118 (19), e2020490118. doi:10.1073/pnas.2020490118

Wang, Y. Y., Ye, Z. Y., Li, L., Zhao, Z. S., Shao, Q. S., and Tao, H. Q. (2011). ADAM 10 is associated with gastric cancer progression and prognosis of patients. *J. Surg. Oncol.* 103 (2), 116–123. doi:10.1002/jso.21781

Wei, L., Wen, J. Y., Chen, J., Ma, X. K., Wu, D. H., Chen, Z. H., et al. (2019). Oncogenic ADAM28 induces gemcitabine resistance and predicts a poor prognosis in pancreatic cancer. *World J. Gastroenterol.* 25 (37), 5590–5603. doi:10.3748/wjg.v25.i37.5590

Wei, W., Zeng, H., Zheng, R., Zhang, S., An, L., Chen, R., et al. (2020). Cancer registration in China and its role in cancer prevention and control. *Lancet Oncol.* 21 (7), e342–e349. doi:10.1016/S1470-2045(20)30073-5

Wu, T., and Dai, Y. (2017). Tumor microenvironment and therapeutic response. *Cancer Lett.* 387, 61–68. doi:10.1016/j.canlet.2016.01.043

Xia, C., Dong, X., Li, H., Cao, M., Sun, D., He, S., et al. (2022). Cancer statistics in China and United States, 2022: Profiles, trends, and determinants. *Chin. Med. J. Engl.* 135 (5), 584–590. doi:10.1097/CM9.0000000000002108

Xiao, L. J., Lin, P., Lin, F., Liu, X., Qin, W., Zou, H. F., et al. (2012). ADAM17 targets MMP-2 and MMP-9 via EGFR-MEK-ERK pathway activation to promote prostate cancer cell invasion. *Int. J. Oncol.* 40 (5), 1714–1724. doi:10.3892/ijo.2011.1320

Yu, X., Gao, Y., and Zhang, F. (2019). Propofol inhibits pancreatic cancer proliferation and metastasis by up-regulating miR-328 and down-regulating ADAM8. *Basic Clin. Pharmacol. Toxicol.* 125 (3), 271–278. doi:10.1111/bcpt.13224

Frontiers in Genetics

Highlights genetic and genomic inquiry relating to all domains of life

The most cited genetics and heredity journal, which advances our understanding of genes from humans to plants and other model organisms. It highlights developments in the function and variability of the genome, and the use of genomic tools.

Discover the latest Research Topics

See more →

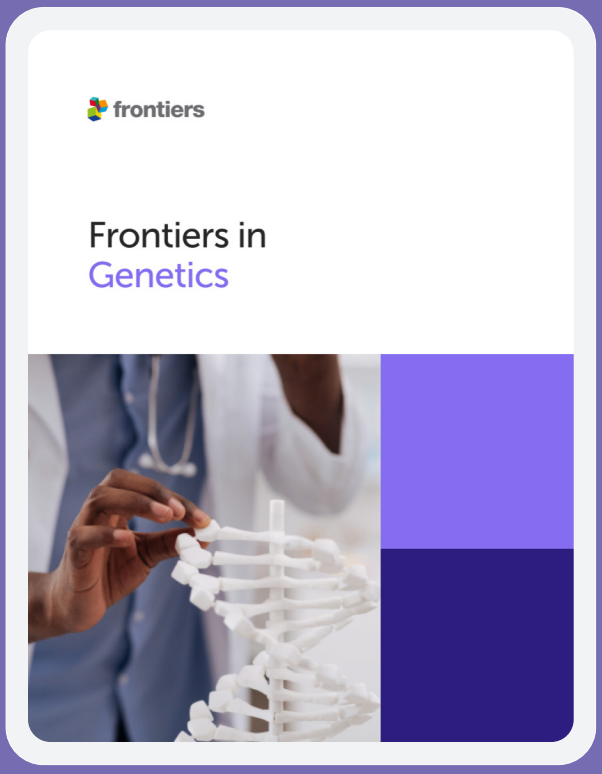

Frontiers

Avenue du Tribunal-Fédéral 34
1005 Lausanne, Switzerland
frontiersin.org

Contact us

+41 (0)21 510 17 00
frontiersin.org/about/contact